

STRUCTURE AND BONDING

135

Series Editor D. M. P. Mingos  
Volume Editor Jianzhuang Jiang

# Functional Phthalocyanine Molecular Materials

 Springer

**135**

**Structure and Bonding**

**Series Editor: D. M. P. Mingos**

**Editorial Board:**

**P. Day · X. Duan · L.H. Gade · K.R. Poeppelmeier  
G. Parkin · J.-P. Sauvage**

For further volumes:

<http://www.springer.com/series/430>

# Structure and Bonding

Series Editor: D. M. P. Mingos

Recently Published and Forthcoming Volumes

## **Functional Phthalocyanine Molecular Materials**

Volume Editor: Jianzhuang Jiang  
Vol. 135, 2010

## **Data Mining in Crystallography**

Volume Editors: Hofmann, D. W. M.,  
Kuleshova, L. N.  
Vol. 134, 2010

## **Controlled Assembly and Modification of Inorganic Systems**

Volume Editor: Wu, X.- T.  
Vol. 133, 2009

## **Molecular Networks**

Volume Editor: Hosseini, M. W.  
Vol. 132, 2009

## **Molecular Thermodynamics of Complex Systems**

Volume Editors: Lu, X., Hu, Y.  
Vol. 131, 2009

## **Contemporary Metal Boron Chemistry I**

Volume Editors: Marder, T. B., Lin, Z.  
Vol. 130, 2008

## **Recognition of Anions**

Volume Editor: Vilar, R.  
Vol. 129, 2008

## **Liquid Crystalline Functional Assemblies and Their Supramolecular Structures**

Volume Editor: Kato, T.  
Vol. 128, 2008

## **Organometallic and Coordination Chemistry of the Actinides**

Volume Editor: Albrecht-Schmitt, T. E.  
Vol. 127, 2008

## **Halogen Bonding**

Fundamentals and Applications  
Volume Editors: Metrangolo, P., Resnati, G.  
Vol. 126, 2008

## **High Energy Density Materials**

Volume Editor: Klapötke, T. H.  
Vol. 125, 2007

## **Ferro- and Antiferroelectricity**

Volume Editors: Dalal, N. S.,  
Bussmann-Holder, A.  
Vol. 124, 2007

## **Photofunctional Transition Metal Complexes**

Volume Editor: V. W. W. Yam  
Vol. 123, 2007

## **Single-Molecule Magnets and Related Phenomena**

Volume Editor: Winpenny, R.  
Vol. 122, 2006

## **Non-Covalent Multi-Porphyrin Assemblies**

Synthesis and Properties  
Volume Editor: Alessio, E.  
Vol. 121, 2006

## **Recent Developments in Mercury Science**

Volume Editor: Atwood, David A.  
Vol. 120, 2006

## **Layered Double Hydroxides**

Volume Editors: Duan, X., Evans, D. G.  
Vol. 119, 2005

## **Semiconductor Nanocrystals and Silicate Nanoparticles**

Volume Editors: Peng, X., Mingos, D. M. P.  
Vol. 118, 2005

# Functional Phthalocyanine Molecular Materials

Volume Editor: Jianzhuang Jiang

With contributions by

Ö. Bekaroğlu · Y. Bian · G. Bottari · X. Cai ·  
G. de la Torre · U. Hahn · N. Ishikawa · J. Jiang ·  
N. Kobayashi · X. Li · Y. Liu · J-Y. Liu · P-C. Lo ·  
Q. Luo · D.K.P. Ng · T. Nyokong · H. Tian · T. Torres ·  
H. Wang · H. Wu · S. Yoshimoto · Y. Zhang

Prof. Dr. Jianzhuang Jiang  
University of Science and Technology Beijing  
Department of Chemistry  
100083 Beijing  
China, People's Republic  
jianzhuang@ustb.edu.cn

and

Shandong University  
Department of Chemistry  
250100 Jinan  
China, People's Republic  
jzjiang@sdu.edu.cn

ISSN 0081-5993 e-ISSN 1616-8550  
ISBN 978-3-642-04751-0 e-ISBN 978-3-642-04752-7  
DOI 10.1007/978-3-642-04752-7  
Springer Heidelberg Dordrecht London New York

Library of Congress Control Number: 2009939119

© Springer-Verlag Berlin Heidelberg 2010

This work is subject to copyright. All rights are reserved, whether the whole or part of the material is concerned, specifically the rights of translation, reprinting, reuse of illustrations, recitation, broadcasting, reproduction on microfilm or in any other way, and storage in data banks. Duplication of this publication or parts thereof is permitted only under the provisions of the German Copyright Law of September 9, 1965, in its current version, and permission for use must always be obtained from Springer. Violations are liable to prosecution under the German Copyright Law.

The use of general descriptive names, registered names, trademarks, etc. in this publication does not imply, even in the absence of a specific statement, that such names are exempt from the relevant protective laws and regulations and therefore free for general use.

*Cover design:* KünkelLopka GmbH, Heidelberg, Germany

Printed on acid-free paper

Springer is part of Springer Science+Business Media ([www.springer.com](http://www.springer.com))

---

## Series Editor

Prof. D. Michael P. Mingos

Principal  
St. Edmund Hall  
Oxford OX1 4AR, UK  
*michael.mingos@st-edmund-hall.oxford.ac.uk*

## Volume Editor

Prof. Dr. Jianzhuang Jiang

University of Science and Technology Beijing  
Department of Chemistry  
100083 Beijing  
China, People's Republic  
*jianzhuang@ustb.edu.cn*

and

Shandong University  
Department of Chemistry  
250100 Jinan  
China, People's Republic  
*jzjiang@sdu.edu.cn*

## Editorial Board

Prof. Peter Day

Director and Fulleren Professor  
of Chemistry  
The Royal Institution of Great Britain  
21 Albermarle Street  
London W1X 4BS, UK  
*pday@ri.ac.uk*

Prof. Xue Duan

Director  
State Key Laboratory  
of Chemical Resource Engineering  
Beijing University of Chemical Technology  
15 Bei San Huan Dong Lu  
Beijing 100029, P.R. China  
*duanx@mail.buct.edu.cn*

Prof. Lutz H. Gade

Anorganisch-Chemisches Institut  
Universität Heidelberg  
Im Neuenheimer Feld 270  
69120 Heidelberg, Germany  
*lutz.gade@uni-hd.de*

Prof. Dr. Kenneth R. Poeppelmeier

Department of Chemistry  
Northwestern University  
2145 Sheridan Road  
Evanston, IL 60208-3133  
USA  
*krp@northwestern.edu*

Prof. Gerard Parkin

Department of Chemistry (Box 3115)  
Columbia University  
3000 Broadway  
New York, New York 10027, USA  
*parkin@columbia.edu*

Prof. Jean-Pierre Sauvage

Faculté de Chimie  
Laboratoires de Chimie  
Organo-Minérale  
Université Louis Pasteur  
4, rue Blaise Pascal  
67070 Strasbourg Cedex, France  
*sauvage@chimie.u-strasbg.fr*

---

## Structure and Bonding

### Also Available Electronically

*Structure and Bonding* is included in Springer's eBook package *Chemistry and Materials Science*. If a library does not opt for the whole package the book series may be bought on a subscription basis. Also, all back volumes are available electronically.

For all customers who have a standing order to the print version of *Structure and Bonding*, we offer the electronic version via SpringerLink free of charge.

If you do not have access, you can still view the table of contents of each volume and the abstract of each article by going to the SpringerLink homepage, clicking on "Chemistry and Materials Science," under Subject Collection, then "Book Series," under Content Type and finally by selecting *Structure and Bonding*.

You will find information about the

- Editorial Board
- Aims and Scope
- Instructions for Authors
- Sample Contribution

at [springer.com](http://springer.com) using the search function by typing in *Structure and Bonding*.

Color figures are published in full color in the electronic version on SpringerLink.

### Aims and Scope

The series *Structure and Bonding* publishes critical reviews on topics of research concerned with chemical structure and bonding. The scope of the series spans the entire Periodic Table and addresses structure and bonding issues associated with all of the elements. It also focuses attention on new and developing areas of modern structural and theoretical chemistry such as nanostructures, molecular electronics, designed molecular solids, surfaces, metal clusters and supramolecular structures. Physical and spectroscopic techniques used to determine, examine and model structures fall within the purview of *Structure and Bonding* to the extent that the focus

is on the scientific results obtained and not on specialist information concerning the techniques themselves. Issues associated with the development of bonding models and generalizations that illuminate the reactivity pathways and rates of chemical processes are also relevant.

The individual volumes in the series are thematic. The goal of each volume is to give the reader, whether at a university or in industry, a comprehensive overview of an area where new insights are emerging that are of interest to a larger scientific audience. Thus each review within the volume critically surveys one aspect of that topic and places it within the context of the volume as a whole. The most significant developments of the last 5 to 10 years should be presented using selected examples to illustrate the principles discussed. A description of the physical basis of the experimental techniques that have been used to provide the primary data may also be appropriate, if it has not been covered in detail elsewhere. The coverage need not be exhaustive in data, but should rather be conceptual, concentrating on the new principles being developed that will allow the reader, who is not a specialist in the area covered, to understand the data presented. Discussion of possible future research directions in the area is welcomed.

Review articles for the individual volumes are invited by the volume editors.

In references *Structure and Bonding* is abbreviated *Struct Bond* and is cited as a journal.

Impact Factor in 2008: 6.511; Section “Chemistry, Inorganic & Nuclear”:  
Rank 2 of 40; Section “Chemistry, Physical”: Rank 7 of 113



# Preface

Phthalocyanines exhibit intriguing physic-chemical properties that render them important as a class of molecular functional materials. In addition to their traditional industrial applications as dyes and pigments, more recently their use as the organic semiconductors, photodynamic therapy medicines, non-linear optical materials, catalysts for the photo oxidation, optical recording materials, and gas sensors attracts great research interests in these tetrapyrrole species. As manifested by the rapidly increasing number of related scientific publications in recent years, great progress has been made in the field of advanced phthalocyanine materials.

Tremendous efforts have been paid toward the development of new phthalocyanine molecular materials as well as toward their applications. Recent emphasis in both academic researches and technical field has been put on the design and synthesis of novel phthalocyanine species, the structure–property relationship, self-assembly properties, molecular electronics and opto-electronics, and dye-sensitized solar cells. Although excellent reviews and monographs about phthalocyanines were published several years ago, it is time to provide a survey of a number of new important developments in this fascinating area of phthalocyanine chemistry. The aim of this book is to bring both the academic and industrial researchers an easy way to the new progress of phthalocyanines made lately in related field.

Nine chapters are included in this volume. The fascinating development in the synthesis of novel phthalocyanine derivatives with near-infrared absorbing and photochromic property is presented at the beginning. Emphasis is on the relationship between the electronic structure and the photochemical- or electrochemical-properties. The following chapters deal with the exciting progress made in the supramolecularly assembled nanostructures and applications of phthalocyanines in photodynamic therapy, molecular magnets, dye-sensitized solar cells, and organic field-effect transistors.

*Jianzhuang Jiang, Beijing and Jinan, China*

# Contents

<b>Functional Phthalocyanines: Synthesis, Nanostructuration, and Electro-Optical Applications</b> .....	1
Gema de la Torre, Giovanni Bottari, Uwe Hahn, and Tomas Torres	
<b>Electronic Spectral and Electrochemical Behavior of Near Infrared Absorbing Metallophthalocyanines</b> .....	45
Tebello Nyokong	
<b>Photochromic Dithienylethene–Phthalocyanines and Their Analogs</b> .....	89
Qianfu Luo, Yi Liu, and He Tian	
<b>Ball-Type Phthalocyanines: Synthesis and Properties</b> .....	105
Özer Bekaroğlu	
<b>Supramolecular Nanostructures of Phthalocyanines and Porphyrins at Surfaces Based on the “Bottom-Up Assembly”</b> .....	137
Soichiro Yoshimoto and Nagao Kobayashi	
<b>Phthalocyanine-Containing Supramolecular Arrays</b> .....	169
Jian-Yong Liu, Pui-Chi Lo, and Dennis K.P. Ng	
<b>Phthalocyanine-Based Magnets</b> .....	211
Naoto Ishikawa	
<b>Phthalocyanines and Their Analogs Applied in Dye-Sensitized Solar Cell</b> .....	229
Xiyou Li, Haixia Wang, and Haixia Wu	
<b>Organic Semiconductors of Phthalocyanine Compounds for Field Effect Transistors (FETs)</b> .....	275
Yuexing Zhang, Xue Cai, Yongzhong Bian, and Jianzhuang Jiang	
<b>Index</b> .....	323

# Functional Phthalocyanines: Synthesis, Nanostructuration, and Electro-Optical Applications

Gema de la Torre, Giovanni Bottari, Uwe Hahn, and Tomas Torres

**Abstract** This overview focuses on the design and preparation of phthalocyanines (Pcs) and covers both fundamental synthetic approaches and more applied research. Thus, different topics including, e.g., the preparation of conjugated assemblies using Pcs as synthetic building blocks, the supramolecular organization of appropriately featured Pc-molecules, and the incorporation of Pcs into dendrimers and polymers, are discussed in this chapter. The second part of the review has been devoted to more technological aspects of these compounds covering Pc-based nanostructures and Pcs as active components of functional devices.

**Keywords** Functional phthalocyanines · Macromolecular structures · Multicomponent assemblies · Nanostructuration · Supramolecular organization

## Contents

1	Introduction .....	2
2	Synthesis of Monofunctionalized Phthalocyanines as Building Blocks for the Preparation of Conjugated Systems/Assemblies .....	3
3	Supramolecular Organization of Phthalocyanines .....	14
4	Phthalocyanine-Based Polymers and Dendrimers .....	20
5	Phthalocyanine-Based Nanostructures .....	24
5.1	Phthalocyanine Adlayers .....	25
5.2	Self-Organization of Phthalocyanines on Surfaces by Solution-Processable Techniques .....	27
5.3	Phthalocyanine-Based Nanowires and Nanoparticles .....	28
5.4	Phthalocyanines as Precursors for the Preparation of Carbon Nanotubes .....	30
5.5	Nanostructuration of Phthalocyanines into Clathrates .....	31
5.6	Supramolecular Interactions of Phthalocyanines with Carbon Nanotubes .....	31

---

G. de la Torre, G. Bottari, U. Hahn and T. Torres (✉)  
Departamento de Química Orgánica, Facultad de Ciencias, Universidad Autónoma de Madrid, Cantoblanco, 28049, Madrid, Spain  
e-mail: tomas.torres@uam.es

6	Phthalocyanines as Active Components of Functional Devices .....	32
6.1	Organic Field Effect Transistors .....	32
6.2	Sensors, Light-Emitting Devices and Optical Information Recording Media .....	33
6.3	Solar Cells Applications .....	34
7	Conclusion .....	36
	References .....	37

## 1 Introduction

Phthalocyanines (Pcs) [1–4] were serendipitously discovered in 1928, and from then on, these synthetic analogues of the naturally occurring porphyrins have been the subject of extensive research in many different fields [5, 6]. Pcs are planar aromatic macrocycles consisting of four isoindole units presenting an 18  $\pi$ -electron aromatic cloud delocalized over an arrangement of alternated carbon and nitrogen atoms. For many years, Pcs have been an important article of trade, i.e., dyestuffs for textiles and inks, as a consequence of their dark green-blue color: their absorption spectra show, in fact, an intense Q-band in the visible region, usually centered at 620–700 nm [7].

More recently, Pcs have emerged as attractive molecular building blocks for their arrangement into molecular materials and nanotechnological devices [8]. To date, Pcs have been successfully incorporated as active components in semiconductor and electrochromic devices, information storage systems, and liquid crystal color displays, among others.

What makes these molecules that outstanding within the fields of materials science and nanotechnology? Besides their electrical properties and their strong absorption in the visible region, Pcs are thermally and chemically stable compounds, and can support intense electromagnetic radiations. Another remarkable feature is their versatility; the two hydrogen atoms of the central cavity can be replaced by more than 70 metals and a variety of substituents can be incorporated, both at the periphery of the macrocycle and/or at the axial positions, thus allowing fine-tuning of the physical properties. Because of the versatile chemistry of Pcs, their assembly into multicomponent photo- and electroactive systems [9] can be easily performed through the linkage with appropriate units, which broadens the applicability of this type of macrocycles, for example in the processing of light into chemical or electrical energy.

The successful incorporation of Pcs into devices requires a fine control of the spatial arrangement of these macrocycles with respect to each other, as an appropriate supramolecular organization of the chromophores allows the expression of their optoelectronic properties to a maximum level. Within this context, in-depth studies on the self-organization of Pcs taking advantage of their intrinsic  $\pi$ - $\pi$  stacking abilities are of superior importance. The incorporation of Pc molecules into macromolecular structures, i.e., dendrimers or polymers, is also worthwhile. Ultimately, the nanostructuring of Pcs, either at surfaces or in three-dimensional

(3-D) objects, allows a fine control of the nanometer-scale morphology, which is a relevant parameter in the fabrication of efficient Pc-based devices.

In this chapter, we intend to revise the most recent contributions to the aforementioned aspects of Pc research. We will describe how the versatile chemistry of Pcs makes possible the preparation of monofunctionalized macrocycles, mainly aimed at preparing multicomponent systems through reaction with other electroactive moieties. The controlled organization of Pcs in solution and the incorporation of these chromophores into macromolecular structures, as well as the preparation of mono-, bi-, and three-dimensional nanostructures, will be the object of study. Finally, some examples of Pc-based devices (solar cells, sensors, transistors, etc.) will also be given as an example of the real applicability of these molecules.

## 2 Synthesis of Monofunctionalized Phthalocyanines as Building Blocks for the Preparation of Conjugated Systems/Assemblies

The synthesis of Pcs usually involves the reaction of either phthalonitrile or diiminoisoindoline precursors that assemble to form the macrocyclic structure [10, 11]. The ring arrangement is thus spanned by four isoindole units that are fused at their 1,3-positions by aza-bridges. Most often this reaction is conducted in the presence of metal ions that perform the function of a template during the ring formation. As a result of the four benzene rings at the periphery of the Pc, chemical alteration of such scaffolds is basically accomplished through synthetic methods that are related to aromatic hydrocarbons. Concerning the modification of Pcs, there is hardly any restriction to the number of functional groups that can be introduced at the periphery of the macrocyclic scaffold.

Among the various strategies for the synthesis of monofunctionalized  $A_3B$ -type Pcs, the approach relying on the statistical reaction of two different phthalonitrile or diiminoisoindoline precursors A and B in ratios of 3:1 equivalents (or a slight excess of A), appears to be the most commonly applied (Fig. 1) [10, 12]. Compound A holds thereby a chemically inert moiety such as, for instance, *tert*-butyl or mono- or dioxyether groups, whereas B imparts the function to be introduced in the Pc scaffold. However, incorporation of chemically inert bulky groups not only enhances the solubility but can also avoid the often observed strong aggregation of Pcs. Moreover, these groups often help to adjust the targeted Pcs properties because of their electron-donating or electron-withdrawing character. In many cases, the presence of such units allows the facile preparation of the desired structure in reasonable yields after separation of the symmetric  $A_4$  and other higher functionalized ( $A_2B_2$ ,  $AB_3$ , etc.) Pc homologs via the usual purification techniques. A special case of this methodology includes the use of phthalonitriles covalently bound to a polymer support [13–17]. Statistical crossover condensation with an excess of the unbound phthalonitrile forms the target structure that can be purified from the byproducts and subsequently be regenerated while cleaving the anchor group from the polymer backbone. Apart from this approach, there exist a few other attempts described in the literature for the construction of such unsymmetrical functionalized macrocyclic

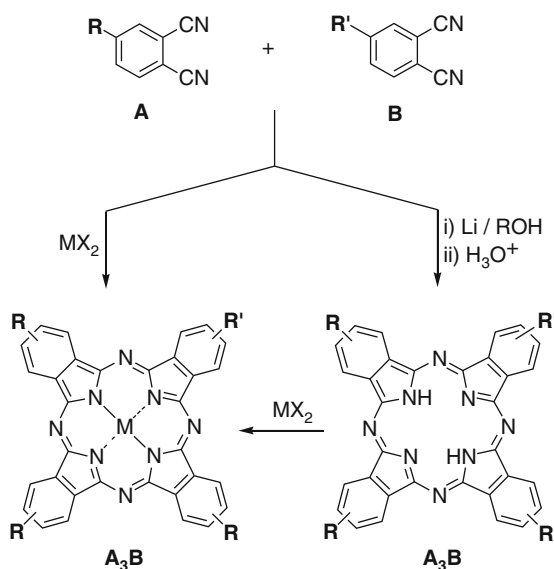


**Fig. 1** General schematic representation of the statistical condensation strategy to the preparation of unsymmetrically substituted  $A_3B$ -type phthalocyanines

structures. For instance, another methodology pursued is the ring opening of subphthalocyanines (subPcs), i.e., the Kobayashi ring expansion reaction [18]. The macrocyclic structure of three isoindoline units that bears a boron atom in its cavity is opened in the presence of a functionalized diiminoisoindoline (Fig. 2a). Thus, the implementation of this functionalized diiminoisoindoline moiety leads to the formation of the desired  $A_3B$ -type Pc. However, this strategy lacks of selectivity and the yields obtained are generally poor. A few recent reports on the employment of this approach toward multicomponent systems deal with structures comprising a Pc and either one or two porphyrins moieties [19, 20]. Another possible method to obtain monofunctionalized Pcs is constituted by the axial modification. Well-known species are for instance Pcs with silicon or ruthenium atoms in the central cavity, in which axial ligands can be introduced (Fig. 2b). Correspondingly, functionalization through axial ligand coordination has been exploited for the fabrication of multicomponent systems as it has been demonstrated recently by various examples. Such entities consist of Pcs that are modified axially among others with, e.g., subPcs [21], porphyrins [22–27], perylenes [28, 29], or fullerenes [30–38]. The employment of the statistical strategy toward non-centrosymmetric, unsymmetrically substituted  $A_3B$ -type Pcs will be described in detail herein in connection with the construction of photoactive and/or electroactive multicomponent assemblies. However, it shall be pointed out that this section does not present an exhausting overview of all such assemblies rather than highlighting the advances made during the recent years.

As already mentioned above, there is almost no restriction with regard to the incorporation of functional groups into the Pc structure. The nature of the introduced

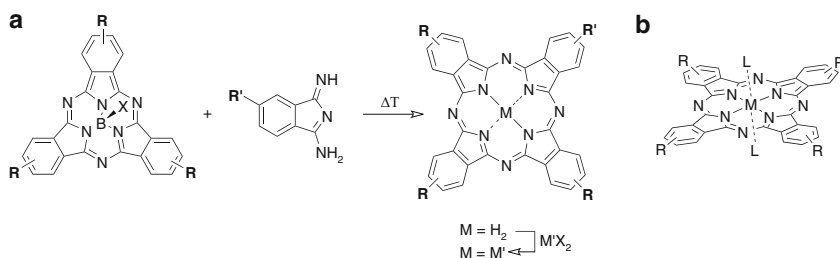


**Fig. 2** (a) Kobayashi ring opening reaction of subphthalocyanines. (b) Schematic structure of a metallophthalocyanine with ligands in axial positions

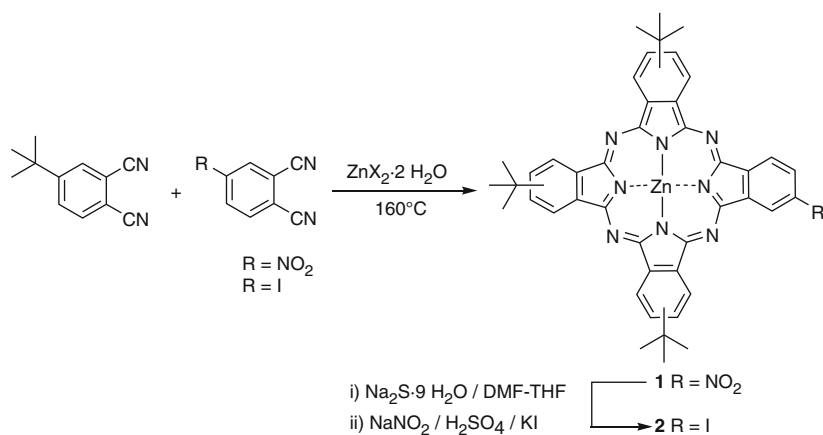


**Fig. 3** Approaches to the synthesis of monoiodo Pc 2

functionalities mirrors virtually almost all the possibilities available in organic chemistry. Among all functional groups, the preparation of Pcs that carry an iodine function is of high interest. This particular group allows, for example, the employment of metal-catalyzed reactions, thereby offering a tool or an anchor point where organic chemistry can be employed for the fabrication of conjugated structures [39, 40]. The high versatility of the functionalization via arylhalides in general is underscored by the large number of organic synthetic materials to be found in the literature. This approach permits the preparation of acetylene or vinyl-based scaffolds as well as the application of a wide range of functional group interconversions.

In this nexus, the groups of van Lier and Torres independently reported in 1997 the preparation of a highly soluble A<sub>3</sub>B-type zinc(II) Pc, where A represents substituted *tert*-butyl isoindolines, whereas B stands for an iodine-containing unit (Fig. 3). The former group started with the preparation of mononitro Pc 1 obtained through statistical condensation of 4-nitrophthalonitrile and 4-*tert*-butylphthalonitrile in the presence of zinc acetate [41]. Subsequent reduction of Pc 1 provided the amino function which was then subjected to a Sandmeyer reaction to furnish the targeted

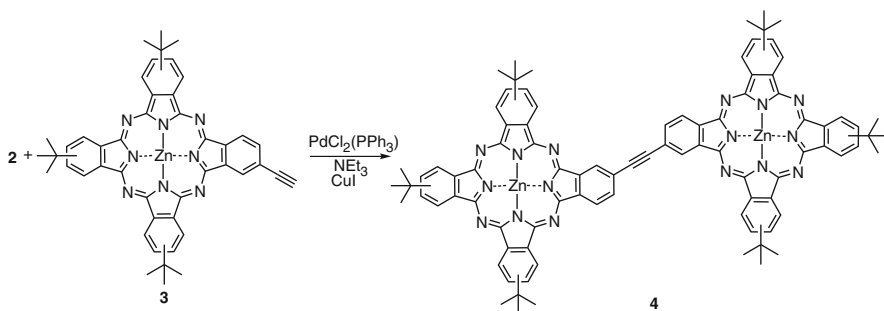


**Fig. 4** Synthesis of homodimetallic bis(phthalocyanine) **4** under the use of Sonogashira cross-coupling reactions [43]

monoiodo Pc **2**. Instead of employing a sequence of various reaction steps, the latter group applied the statistical crossover condensation of 4-*tert*-butylphthalonitrile and 4-iodophthalonitrile using zinc(II) chloride as templating metal source which led to the formation of **2** in 20% yield after purification by column chromatography [42] (Fig. 3). Optimization of the reaction conditions nowadays allows the rather facile upscale preparation of this Pc precursor with yields reaching up to 45%.

Palladium-catalyzed reactions of this halide-containing building block with appropriately chosen terminal alkynes permit the covalent linkage with other photoactive or electroactive species, thus affording rigid systems with a linear geometry. The conditions applied follow the classical Sonogashira cross-coupling, i.e., the use of a palladium-phosphane ligand complex and excess of triethylamine in the presence of a catalytic amount of copper(I) iodide. The addition of an excess of potassium iodide was found to lead to increased product yields. However, when modifying free-base Pcs or related macrocycles, the presence of copper has to be avoided as the metal would else be implemented in the free-base macrocycle. In these cases, the non-metallated species can be maintained by using a catalyst system consisting of  $[\text{Pd}_2(\text{dba})_3]$  (dba = dibenzylideneacetone) and triphenylarsine in freshly distilled and deaerated piperidine. The first specimens obtained via the cross-coupling technique were introduced in 1997, i.e., the synthesis of homo- and heterodimetallic ethynyl-bridged bis-metalloPc complexes in yields higher than 70% [42]. The Pc–Pc homodimer **4** reported in the literature that has been constructed under the use of palladium-mediated cross-coupling is depicted in Fig. 4 [43]. Accordingly, homo- and heterodimetallic bis-Pcs have been synthesized by direct coupling of the monoiodo- and the ethynyl-functionalized Pcs [44]. The zinc derivative was then subjected to a cobalt-catalyzed cyclotrimerization to provide the corresponding sterically crowded hexameric structure in which the Pc behaved like non-conjugated chromophores presumably because of the propeller-like conformational arrangement [45].

Similarly, Torres et al. also reported the preparation of perylene-Pc assemblies **5** (Fig. 5). The synthesis of these triads was thereby accomplished via palladium-catalyzed cross-coupling pursuing two different routes [46]. First preparing the perylenediimide with two bromine units in positions 1 and 7 and subsequent



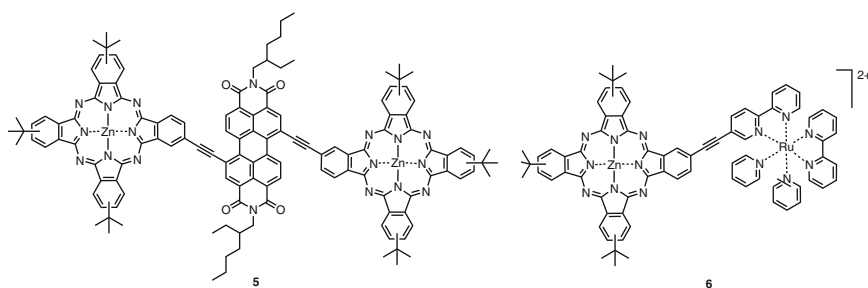


**Fig. 5** Two examples of ethynyl-bridged, phthalocyanine-based multicomponent systems (**5** [46] and **6** [47])

coupling with an ethynyl-functionalized Pc gave the target hybrid structure in 16% yield, while the other methodology by endowing the same bay positions of the perylene diimide scaffold with two terminal triple bonds followed by the conjugation with **2** furnished the triad **5** in 33% yield.

Synthetic efforts have also been devoted to implement an ethynyl bridge in between a Pc and a ruthenium(trisbpy) (bpy = bipyridine), thus giving rise to the corresponding linear, highly conjugated, two-component heteroleptic metal complex structure **6** (Fig. 5) [47]. Key to the preparation of this dyad was the palladium(0)-promoted cross-coupling of 5-bromo-2,2'-bipyridine and ethynyl-*tert*-butylphthalocyaninatozinc(II) **3** in freshly distilled and deaerated diisopropylamine as a base. Refluxing of the functionalized Pc with  $[\text{Ru}(\text{bpy})_2]\text{Cl}_2 \times 2\text{H}_2\text{O}$  then readily furnished the target dyad structure.

Similarly, the reaction of **2** with 4-ethynylbenzaldehyde furnished a benzaldehyde substituted Pc that was then subjected to a reaction with fullerene under Prato conditions [48]. The formation of well organized supramolecular nanostructures on graphitic surfaces was observed. These structures were found to be highly conductive as a result of the extremely high degree of molecular order of such dyads. A slightly shorter Pc-C<sub>60</sub> dyad, in which the Pc and C<sub>60</sub> units are separated by a triple bond has also been described [49]. Very recently, Torres et al. also described the preparation of a rather sophisticated tetrad comprising three Pc units and a fullerene sphere [50]. Tetrakis(4-iodophenyl)methane was thus monofunctionalized by means of Sonogashira cross-coupling with 4-ethynylbenzaldehyde over one of the iodophenyl moieties. The remaining three iodo-functions were then also modified via threefold Pd-assisted conjugation with a large excess of **3** to provide a formyl-containing tripod. The excess was needed because of the formation of the homo-coupling product obtained during the cross-coupling reaction. Finally, 1,3-dipolar cycloaddition with pristine fullerene gave the four-component entity **7** under formation of a fulleropyrrolidine moiety (Fig. 6). Sonogashira cross-coupling reaction conditions also proved successful for the production of further multi-component systems consisting of a Pc and subPc [51], porphyrin [52–57], ferrocene [58], or very recently with endohedral fullerenes [59]. Such highly

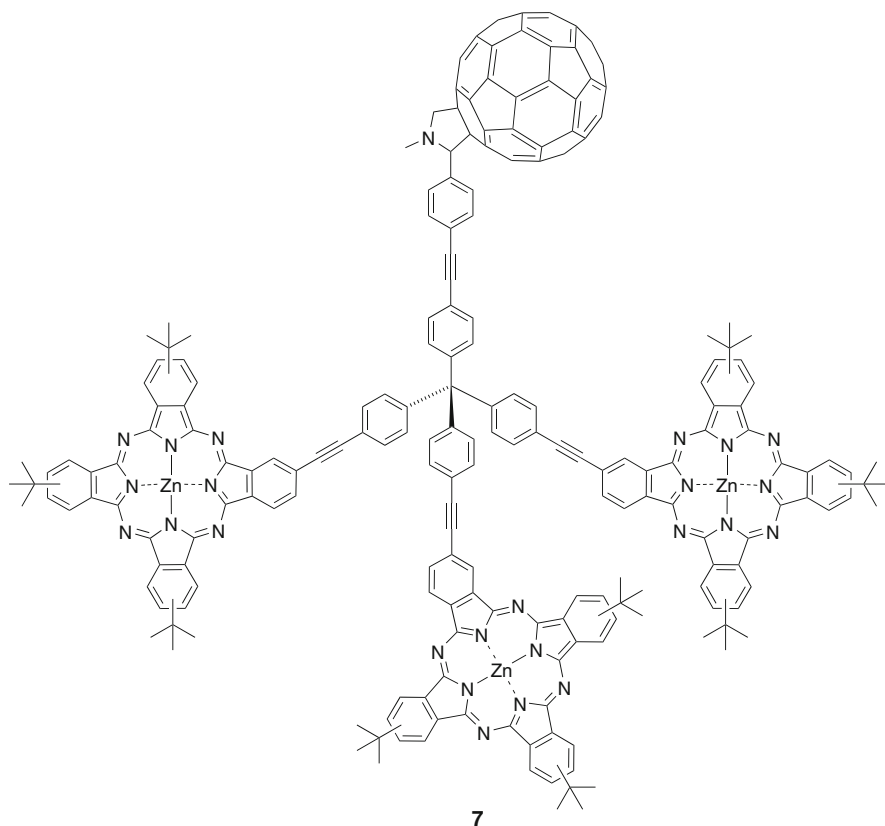


**Fig. 6** Fullerene-containing four-component system **7** [50]

conjugated systems have then been investigated on possible energy or electron transfer processes.

Compound **2** was furthermore employed in the preparation of NH-linked Porphyrin arrays [60]. The reaction between the amino-functionalized porphyrin **8** and 4-iodophthalonitrile using Buchwald-Hartwig amination conditions ( $\text{Pd}(\text{OAc})_2/\text{rac-BINAP}$  (BINAP = 2,2'-bis(diphenylphosphino)-1,1'-binaphthyl) as the catalytic system) in the presence of potassium *tert*-butoxide, delivered the entities connected either at the *meso*-phenyl group (**9** in Fig. 7) or at the  $\beta$ -pyrrolic position [61].

Apart from this direct cross-coupling of functional Pcs, also elongated systems have been described in the literature. Correspondingly, for instance conjugation of **2** with 4-trimethylsilylethynyl iodobenzene incorporated the extended bridge into the system and deliberation of the terminal triple bond allowed for the final cross-coupling with a ferrocene derivative [62]. A homo-dimetallic Pc assembly spaced by (E)-1,2-diethynylethene has been obtained by two successive Pd(0)-catalyzed cross-couplings, providing in first instance the mono-adduct which was

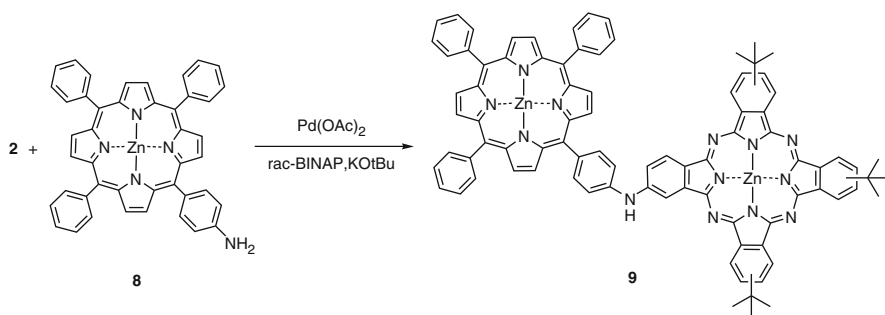


Fig. 7 Synthesis of NH-linked Pc-porphyrins **9** substituted at the *meso*-phenyl group

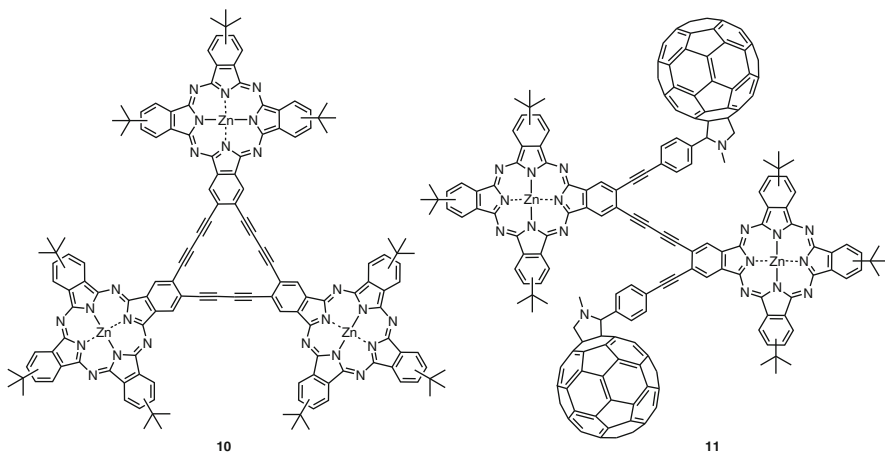
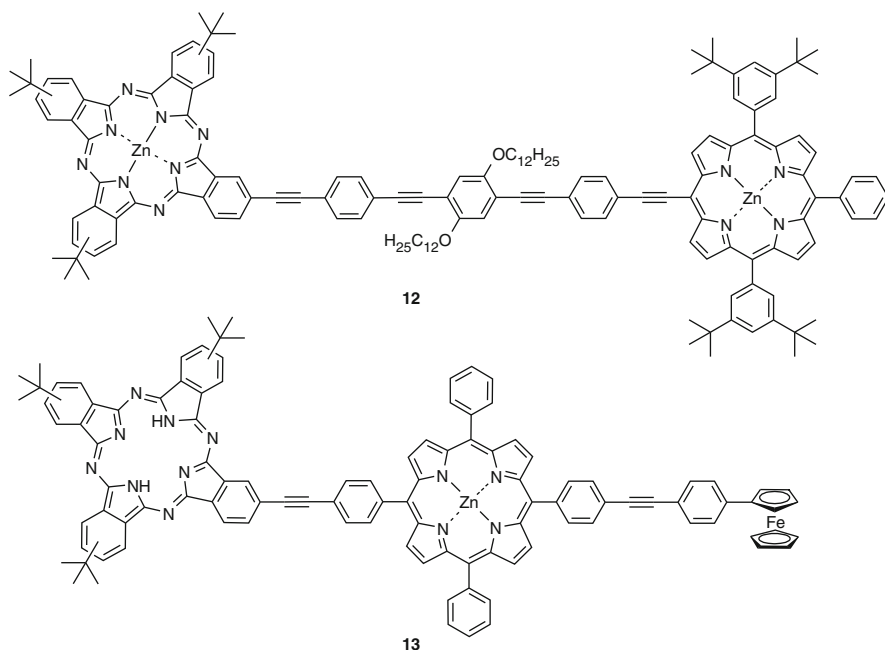


Fig. 8 Representative multicomponent systems (**10** [65] and **11** [67])

then subjected to a second cross-coupling with the other metalloPc [63]. The various entities of  $\pi$ -conjugated molecular dyads exhibited substantial electronic communication between the two metalloPcs. In connection with alkynyl-functionalized Pcs, the direct coupling of two triple bonds in the presence of copper ions and piperidine as base has also been accomplished. This oxidative homocoupling readily provided the homo-dimetallic butadiynyl-bridged bisPc complexes [43]. Similarly, Pc-fused dehydro[12]- and [18]annulenes **10** have been synthesized through copper-mediated oxidative coupling from unsymmetrical bis-alkynyl substituted Pcs (Fig. 8) [64–66]. Likewise, a more sophisticated system **11** has been introduced consisting of two Pcs and two fullerenes that are fully conjugated as the four moieties are linked by triple bonds (Fig. 8) [67].

Aiming at a Pc–porphyrin dyad **12** with an extremely long rigid linear spacer, Odobel et al. reported the ultra-fast, single step charge separation over a 3.4 nm distance [68,69]. The first step of the applied methodology consisted of the preparation of an oligo(phenyleneethynylene) spacer endowed with two terminal alkyne units



**Fig. 9** Two multicomponent systems either with an oligo(phenyleneethynylene) spacer (**12**) [68] or linked by a porphyrin bridging unit (**13**) [58]

of which one was masked with a protecting group (Fig. 9). Monoiodo Pc **2** was then coupled to the unprotected alkyne of this extended bridge under palladium-mediated conditions. Subsequent deprotection allowed then for the second Sonogashira cross-coupling with the porphyrin moiety. Also Lindsey et al. accomplished the synthesis of a three-component system based on Pc and ferrocene, which are covalently connected through a porphyrin linker (**13** in Fig. 9) [58]. Again, cross-coupling reactions proved to be key to the synthesis. Hence, to a solution containing stoichiometric amounts of the zinc(II) porphyrin with two iodo functions as well as the ferrocene and Pc building blocks modified with a terminal alkyne moiety the palladium catalyst was added. Purification of the mixture by different techniques afforded the desired triad **13** in 15% yield. Using a similar synthetic strategy, the same authors reported as well a tetrad consisting of a linear array of a perylene, two porphyrin units and a Pc [70]. The two outer photoactive functional groups, namely the perylene and the Pc, were thereby coupled under the Pd-mediated conditions to provide the target entity. This assembly exhibited efficient light-harvesting properties and rapid funneling of energy in a cascade from the perylene to the Pc unit through the bis(porphyrin).

However, such halogenated Pcs can also be the starting point for carbon-carbon bond formation by other metal-mediated reactions with terminal alkenyl-containing building blocks [39]. In terms of incorporation of alkenyl linkers for the fabrication

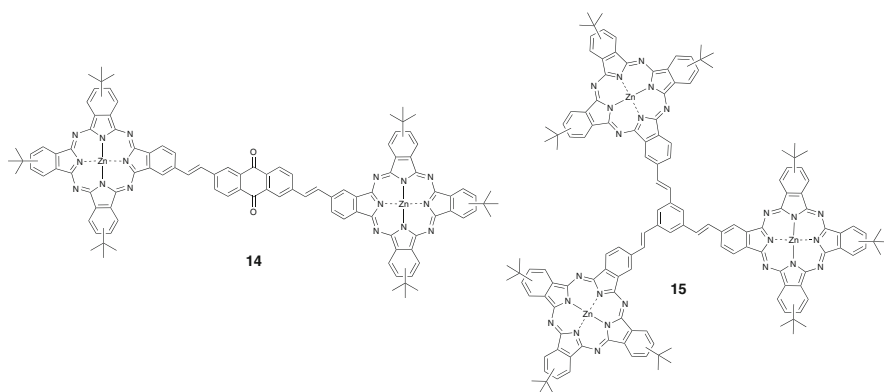


**Fig. 10** Two vinyl-bridged systems of Pcs linked to anthraquinone (**14**) [72] or a trisPc-benzene system **15** [77]

of Pc multicomponent systems, the Heck-type coupling proved successful for a vinyl-bridged anthraquinone with two covalently linked Pcs [71, 72] (**14** in Fig. 10). The reaction of monofunctionalized tri-*tert*-butylvinylphthalocyaninatozinc(II) with differently substituted diiodoanthraquinones was performed using palladium-catalyzed coupling conditions. The synthetic protocol was found to be working best when employing  $(\text{MeCN})_2\text{PdCl}_2$  as catalyst, which was applicable regardless of the substitution pattern at the anthraquinone scaffold. Similarly, another dyad has been synthesized through Heck-type coupling of *p*-vinylbenzaldehyde to **2**, thus furnishing a terminal aldehyde function that allowed for the introduction of fullerene to provide a Pc– $\text{C}_{60}$  dyad with a phenylenevinylene bridge that comprised a linear fully conjugated geometry [73,74]. Heck-type reaction played also an important role in the construction of further multiPc-containing structures. In this regard, a push–pull heterodimetallic Pc ensemble bridged by a [2.2]paracyclophane and two vinyl moieties has been prepared, in which the photo-induced charge transfer between donor and acceptor Pc units is produced through space and not through the  $\pi$ -conjugated linker [75, 76]. Likewise, the reaction of **2** with 1,3,5-trivinylbenzene furnished the corresponding multinuclearPc **15** [77].

Moreover, vinyl-bridged Pc adducts with ferrocene derivatives have been described [78, 79]. Upon reaction of 3,4-dicyanobenzylphosphonate with formylferrocene under Wittig–Horner conditions with the corresponding ferrocene-containing mono- or bisphthalonitriles have been obtained, which were then subjected to statistical cyclotetramerization with 4-*tert*-butylphthalonitrile in the presence of the appropriate metal salt. Furthermore, a double bond has also been employed as spacer between the Pc and ruthenium(trisbipyridine) [47].

In comparison with the fabrication of alkynyl- or alkenyl-linked multicomponent assemblies, there are few examples dedicated to aryl-Pcs. Such attempts are mainly based on Suzuki or Stille couplings. Hence, Odobel et al. [80] reported the construction of a Pc macrocycle carrying a trimethyltin function, thus allowing

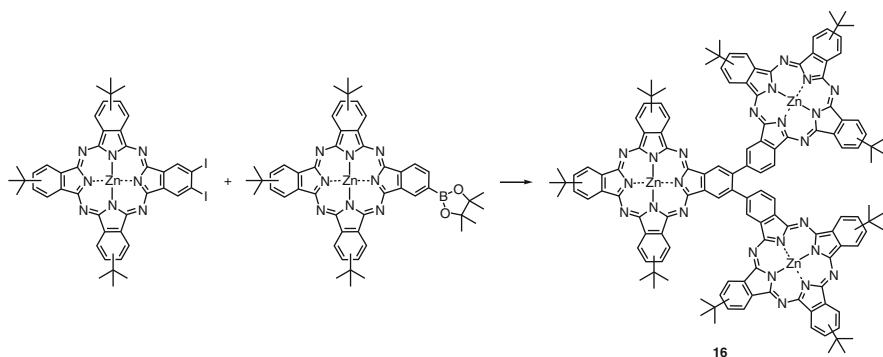


**Fig. 11** Example for the preparation of a Pc homotriad **16** under the use of Suzuki coupling conditions [81]

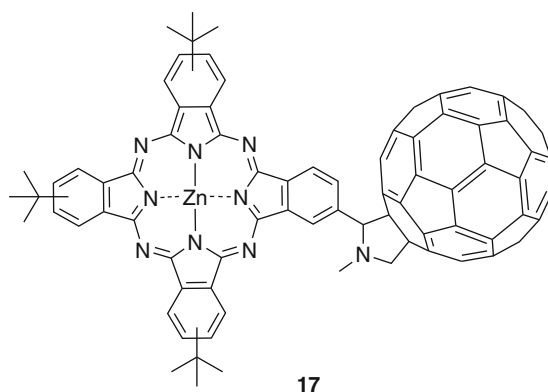


**Fig. 12** Pc-C<sub>60</sub> dyad **17** connected by a pyrrolidine group

for the palladium-mediated Stille coupling with a bromine-functionalized ruthenium complex. The best strategy appeared to be the employment of a preformed ruthenium complex with a bromine function at the terpyridine unit that permitted the Stille cross-coupling with the stannane-modified Pc in 50% yield. The Suzuki coupling was also exploited for the preparation of covalently linked Pc-Pc heterodyads, Pc-(Pc)<sub>2</sub>-homotriad **16** as well as for Pc-porphyrin hetero-dyads conjugated directly through C-C bonds [81, 82]. These compounds were prepared through the efficient one-step method that relied on a palladium-mediated Suzuki cross-coupling reaction of a Pc-boronate precursor that was coupled to the aryl-halide function(s) of either the Pc (Fig. 11) or the porphyrin moiety.

The alkenyl group can also be transformed to the aldehyde function, which can hence be used in the reaction with, e.g., fullerenes (Fig. 12) [83–89]. Correspondingly, two strategies have been pursued for the synthesis of such fullerene-containing Pcs. One of them involves the oxidative cleavage reaction of the alkenyl

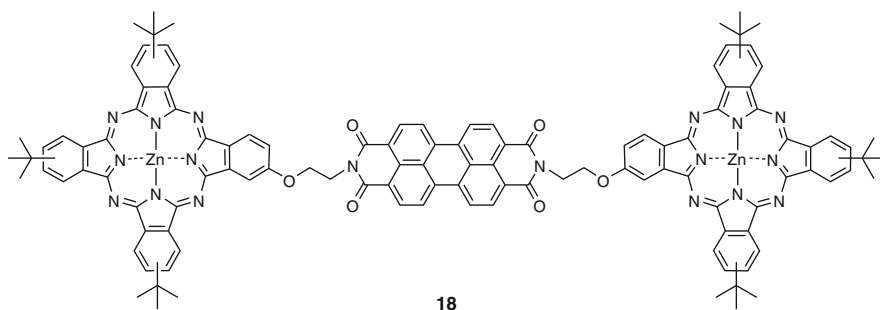


**Fig. 13** Structure of the perylene-based triad **18** [92]

Pc with osmium tetroxide and sodium periodate, and subsequent 1,3-dipolar cycloaddition of the azomethine ylide, formed in the presence of an excess of sarcosine, and C<sub>60</sub> to give the fulleropyrrolidine–Pc conjugate **17**. The second protocol relies on the fulleropyrrolidine formation prior to the statistical cyclotetramerization with 4-*tert*-butylphthalonitrile. The low yields obtained via the latter strategy are presumably a result of the steric congestion of the benzodinitrile-functionalized fullerene precursor in the statistical crossover condensation.

The amine function in Pcs was also found to be versatile as it allows for the facile incorporation of other photoactive or electroactive species. In particular such amino-functionalized Pcs can be easily reacted with perylene dianhydride to undergo formation of the corresponding diimides such as **18** (Fig. 13) [90–92]. The Pc building blocks, carrying either a spacers amino or an anilino group, respectively, were thus implemented into the perylene structure by melting of the two components in imidazole to result in the construction of the corresponding multicomponent assemblies. The pathway toward such structures can also be performed by first introduction of the phthalonitrile to the perylene followed by the formation of the macrocycle [93].

The amine function served also as the starting point for the first covalent linkage of Pcs to single-walled carbon nanotubes (SWNTs) [94]. The pipes with open-end and surface-bound acyl chloride moieties were used to prepare the Pc–SWNTs system by amide-bond formation (Fig. 14). Accordingly, statistical reaction of 4-aminophthalonitrile with 4-*tert*-butylphthalonitrile in the presence of zinc ions delivered the monoamino Pc that was then employed in the conjugation with the acid chloride modified carbon nanotubes (CNTs). Here, it should also be mentioned that other functions have been applied to the covalent modification of CNTs, i.e., amide [95], ester [96,97], or click chemistry [98].

Far more attempts have been undertaken to covalently assemble multicomponent structures with at least one Pc moiety, which will be briefly described thereafter. In particular the C<sub>60</sub> fullerene has been connected to the Pc by using different methodologies. Besides the Pc–C<sub>60</sub> dyads presented above, the Pc scaffold has also been covalently connected through employment of Diels–Alder reaction onto the

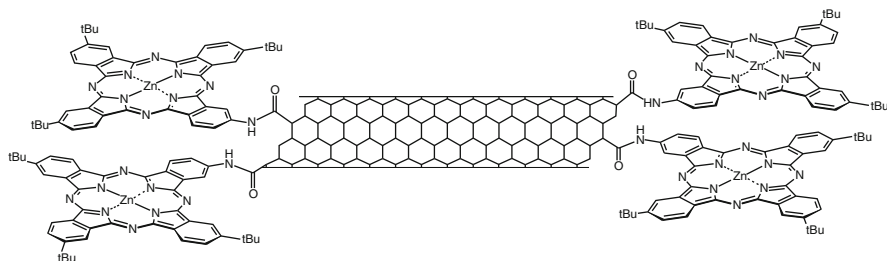


**Fig. 14** Single-walled carbon nanotubes functionalized covalently with phthalocyanines [94]

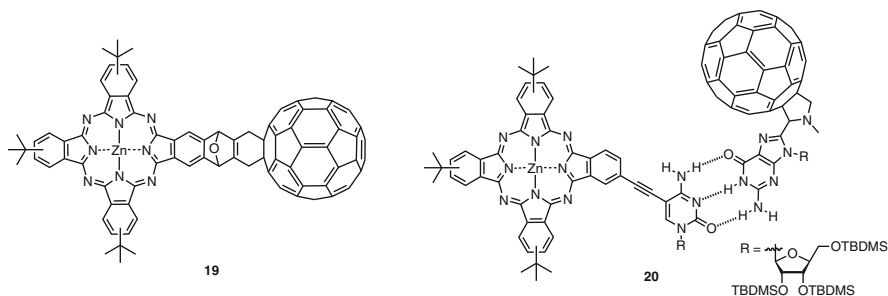


**Fig. 15** Two representative specimens for Pc–C<sub>60</sub> dyads

C<sub>60</sub> (**19** in Fig. 15) [99, 100], or via double Bingel reaction [101–104]. An elegant approach toward fullerene–Pc structures represents the modification of C<sub>60</sub> with a secondary ammonium function capable of being entrapped in a crown ether-functionalized Pc [105, 106]. Supramolecular-assisted ensembles between C<sub>60</sub> and Pc can also be obtained upon complementarily functionalizing the two units with a cytosine and a guanosine thus giving rise to the hydrogen-bonded structure **20** (Fig. 15) [107, 108]. Similarly, a system with anthraquinone has been described [109]. Very recently, photophysical characterization of a fullerene–Pc dyad in which the macrocycle was perfunctionalized with trifluoroethoxy moieties revealed no electronic communication between the two photophysically active units [110].

### 3 Supramolecular Organization of Phthalocyanines

The self-organization abilities of functional chromophores have been widely exploited to generate supramolecular architectures with improved photophysical and (opto)electronic properties as a result of excitonic interactions between the dyes. To achieve this goal, it is necessary to design programmed molecules capable of spontaneously self-organizing into highly ordered supramolecular structures with controlled dimensions and size. Commonly, noncovalent interactions such as hydrogen bonding,  $\pi$ – $\pi$  stacking, and metal–ligand coordination have been used to induce



self-organization in solution, crystals, and liquid-crystals. Self-assembly capabilities can be also transferred from solution onto solid surfaces.

The inherent  $\pi$ - $\pi$  stacking abilities of Pcs make these macrocycles easily organizable into supramolecular structures, but some structural modifications at the periphery of the Pc ring may improve their intrinsic self-organization properties. For example, by attaching long, aliphatic hydrocarbon chains a liquid crystalline behavior can be induced [111–116], owing to the formation of one-dimensional (1-D) columnar stacks of the disc-like cores surrounded by the quasi-liquid peripheral substituents. The introduction of crown ether moieties at the periphery of the Pc macrocycle [117–120] has also been classically used as a tool to obtain long cofacial aggregates in solution. Crowned Pcs exhibit two driving forces for self-assembly: typical  $\pi$ - $\pi$  interactions between aromatic cores and the cooperative complexation of alkali metal ions between peripheral crown ether moieties. Several authors have explored this approach [121–128].

A particularly interesting work by Nolte and co-workers [117–127] reports on the formation of helical, micrometer-long fibers in a chloroform solution of a Pc molecule peripherally substituted with four crown ether moieties and eight chiral, long alkyl chains (Fig. 16a). In this case, the molecules within a fiber are organized into a right-handed helix, which further self-assemble into left-handed twisted bundle as revealed by transmission electron microscopy (TEM) studies (Fig. 16b). However, the addition of alkali-metal ions, which bind in the crown ether moieties, induces the transformation of the helices into straight fibers as a consequence of the required cofacial arrangement of the crown ether moieties for cooperative binding to the metals. A modification of this derivative is a crowned Pc bearing four tetrathiafulvalene (TTF) moieties [129], which also forms a gel in solution. TEM studies showed the formation of fibers up to several micrometers in length. However, the expected columnar-type Pc fibers were not observed, thus suggesting that, in this particular case, the stacking of the molecules occurs through a combination of TTF–TTF and TTF–Pc interactions, more than through the typical Pc–Pc ones.

Pc-based helical fibers (ca. 70-nm long) have been also found in chloroform solutions of homochiral nickel(II) Pc complexes bearing four enantiopure (*p*-tolyl)ethylaminocarbonyl groups (**22**-(R) or **22**-(S)) (Fig. 17a) [130]. The intermolecular interactions responsible for the formation of the observed nanoscopic structures are hydrogen bonding,  $\pi$ - $\pi$  stacking, and homochiral interactions of the enantiopure bulky entities. These Pc supramolecules were successfully deposited on hydrophilic and hydrophobic surfaces, where higher-order, helical fibers (ca. 1  $\mu$ m) were observed. Interestingly, optically active, both left- and right-handed, supramolecular arrangements can be obtained from achiral Si(IV) octa(octyloxi)Pc dihydroxide derivatives at the air–water interface [131]. Once deposited onto solid substrates, the supramolecular chirality could be further fixed through the formation of Si–O–Si covalent bonds between adjacent molecules, thus giving rise to a helical, supramolecular polymer.

Long Pc fibers (ca. 1  $\mu$ m) are formed as well by a covalent Zn(II) tetra(perylene-diimide)Pc derivative **23** (Fig. 17b) [132], where each moiety stacks in register with the same component in an adjacent molecule. Face-to-face aggregation is

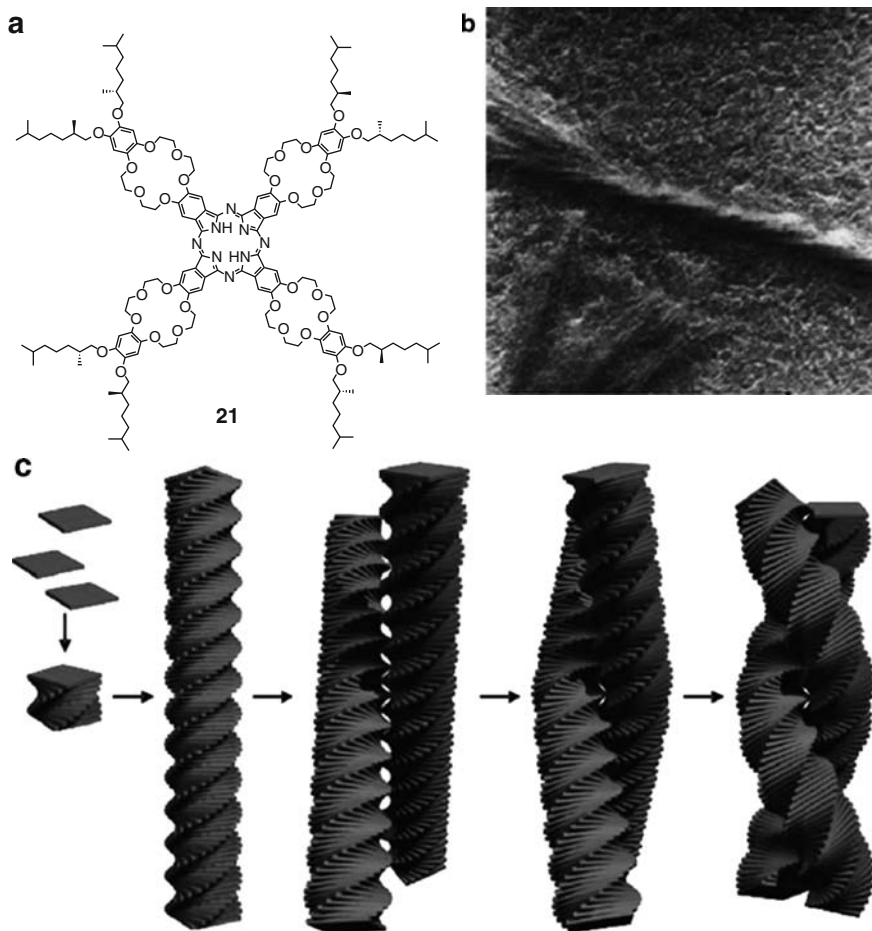


**Fig. 16** (a) Structure of the crowned metal-free phthalocyanine **21**. (b) TEM images of the fibers formed by compound **21** in chloroform solution. (c) Proposed model for the hierarchical organization of compound **21**. Reprinted with permission from [117]. Copyright 2003, American Association for the Advancement of Science

evidenced by the analysis of the absorption spectrum of this compound. In this system, ultrafast energy transfer takes place from the perylenediimide moieties to the Pc one, followed by electron migration along the Pc-column.

Ionic self-assembly may be also a powerful tool for the creation of nanostructures. Faul and co-workers have prepared a supramolecular array by using tetrasulphonate Pc (bearing four negative charges) and an ammonium-substituted perylenediimide (bearing two positive charges) as building blocks [133]. The combination of charge-transfer interactions and discotic stacking leads to the formation of irreversible, 1-D polymeric stacks, which are further stabilized through electrostatic Coulomb couplings. These 1-D stacks are formed in solution and also

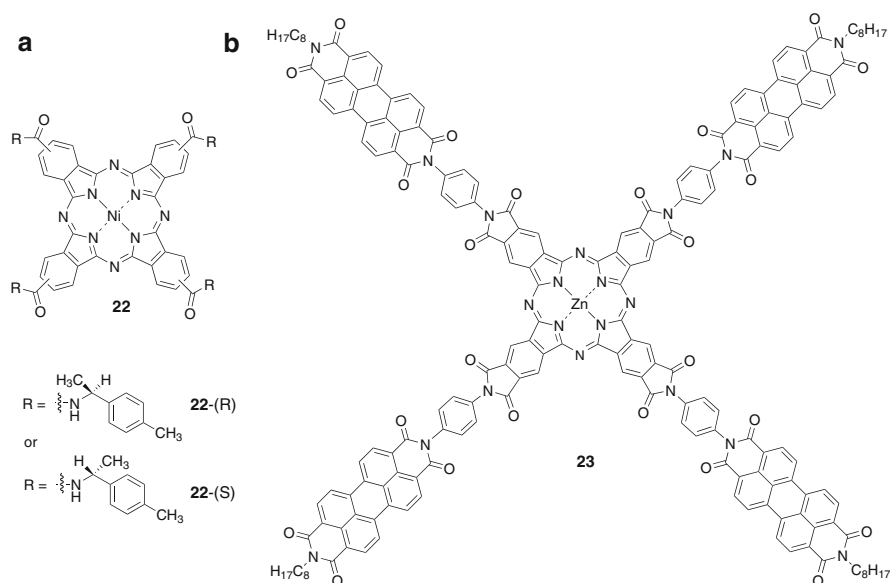


**Fig. 17** Phthalocyanine derivatives forming fibers in solution. (a) Homochiral nickel(II) phthalocyanine **22**. (b) Tetra(perylene-3,4,9,10-tetracarboxylate)zinc phthalocyanine **23**

on solid substrates. A helically twisted triple stack model is proposed on the basis of the microscopic data and spectroscopic observations.

Long, extremely well-organized nanorods are formed in aqueous solution of the amphiphilic ZnPc–C<sub>60</sub> salt **24** (Fig. 18a) [84]. TEM images showed that the nanotubules are composed of many other nanorod-like substructures (Fig. 18b). These 1-D, Pc-based micelle-like structures display remarkable photophysical properties as a result of their nanometric organization, namely, an impressive stabilization of the charge separated state (ZnPc<sup>+</sup>–C<sub>60</sub><sup>–</sup>) lifetime.

The formation of nanofibers has been induced through asymmetric functionalization of the Pc core with one polymer chain. Kobayashi and co-workers have described the synthesis of a Pc-terminated amphiphilic polymer with a narrow molecular-weight distribution, through atom-transfer radical polymerization (ATRP) of acrylate and a Pc-based initiator [134]. The resulting polymer forms a gel in methanol solution, where the Pc cores are stacked into 1-D columnar aggregates that are stabilized through  $\pi$ – $\pi$  interactions between macrocycles and van der Waals interactions between the long, polymeric alkyl chains. On the contrary, the polymerization reactions of  $\epsilon$ -caprolactone at the two axial positions of a Si(IV)Pc dihydroxide yield a Pc-containing polymer which can not give rise to columnar stacking of the Pcs but form nanoparticles through aggregation of the polymer chains [135].

Another supramolecular recognition motif for the construction of Pc wires is that based on donor–acceptor interactions. The groups of Torres and Nolte have reported the covalent Pc dimer **25** consisting of a donor ZnPc and an acceptor

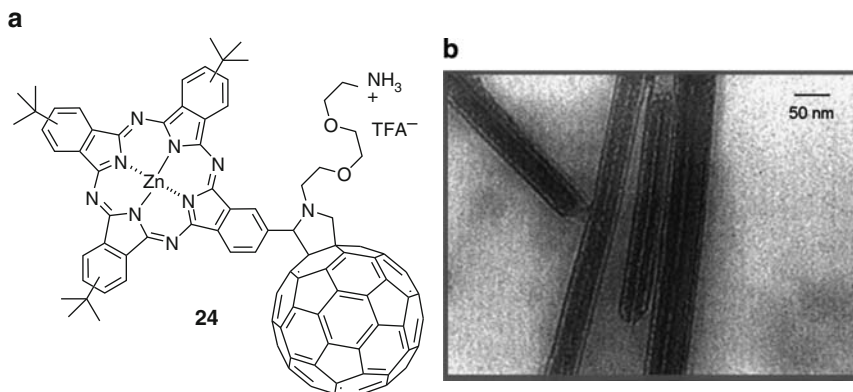


**Fig. 18** (a) Amphiphilic ZnPc-fullerene derivative **24**. (b) TEM image of the nanotubes formed by **24** in water solution deposited on a TEM grid. The image in (b) is reprinted with permission from [84]. Copyright 2005, The American Chemical Society

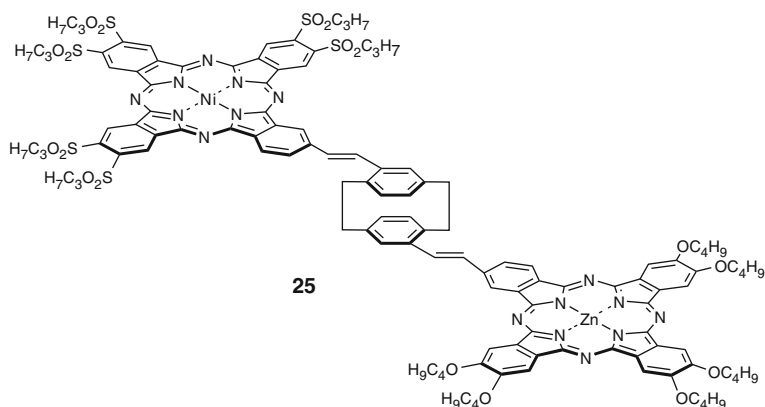


**Fig. 19** Structure of binuclear zinc(II) phthalocyanine-*p*-cyclophane-nickel(II) phthalocyanine **25**

NiPc subunits that are covalently linked to a central *p*-cyclophane (Fig. 19) [75]. In butanol solution, this molecule forms 1-D aggregates of nanometer-sized dimensions through donor–acceptor interactions between complementary Pc units. Taking advantage of this tool, Torres and Guldi have also reported a new supramolecular Pc–fullerene/Pc ensemble showing a long-lived photoinduced charge separated state. Donor–acceptor interactions between the donor ZnPc component of a covalently linked ZnPc–C<sub>60</sub> dyad and an acceptor Pd(II) phthalocyaninate account for the formation of the ensemble [73].

Metal–ligand interactions can be used to construct structurally well-defined assemblies of Pcs. In this context, a well-established method in the field of porphyrin chemistry, developed by Kobuke and coworkers, is the preparation of imidazolyl-substituted porphyrins which can coordinate through the imidazolyl group to the

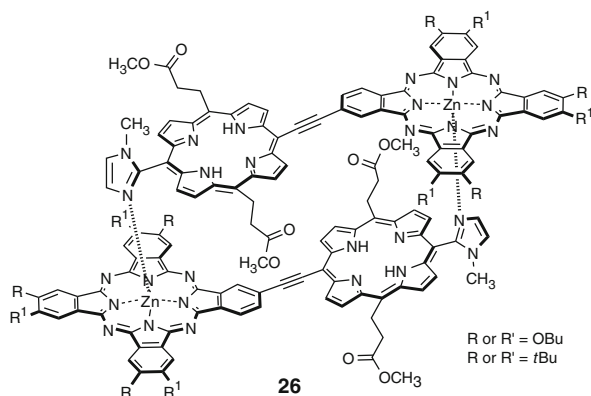


**Fig. 20** Supramolecular assembly of **26** formed via heteroassociation of an imidazolyl-substituted porphyrin-phthalocyanine covalent dimer

central zinc(II) atom of a different porphyrin unit, giving rise to linear and macrocyclic porphyrin arrays [136–138]. This approach can be applied to other macrocycles and, in fact, Kobuke has established that Pc molecules bearing one imidazolyl unit form dimers with large association constants by means of a complementary coordination between the ligand and central zinc(II) or magnesium(II) ions [139]. Covalent imidazolylporphyrin-ZnPc dimers can also form discrete heterogeneous stacks through imidazolyl-to-zinc coordination, forming highly stable, slipped cofacial tetrads **26** (Fig. 20) [140].

In this regard, Ru(II) phthalocyaninate complexes have been recently brought to light as building blocks for the preparation of supramolecular arrays [22–28]. Ruthenium Pcs have the merit of either single or double ligation, the latter allowing to attach non-identical ligands. Particularly, the coordination of the Ru(II) centers with pyridyl-type ligands has been proved to yield very stable coordination complexes. An example of the heteroleptic assembly of Pc and porphyrin molecules by means of Ru-pyridyl coordination is represented by the ensemble **27** reported by Cook and co-workers (Fig. 21) [22]. Their approach consists in the substitution at the *meso* positions of the porphyrin core with pyridyl ligands, which strongly coordinate to the Ru(II) center of the Pc macrocycles. In this regard, a supramolecular electron donor-acceptor hybrid has been assembled through axial coordination of a perylenediimide moiety, bearing two 4-pyridyl substituents at the imido positions, to the Ru(II) metal centers of two Pcs [28].

Discrete supramolecular Pc–porphyrin–Pc assemblies have also been prepared using saddle distorted components, namely a protonated dodecaphenylporphyrin and octaphenyl Zn(II) phthalocyaninate complex, using 4-pyridinecarboxylate as a supramolecular linking unit. Both metal–ligand and hydrogen bonding interactions allow the assembly of the components [27].

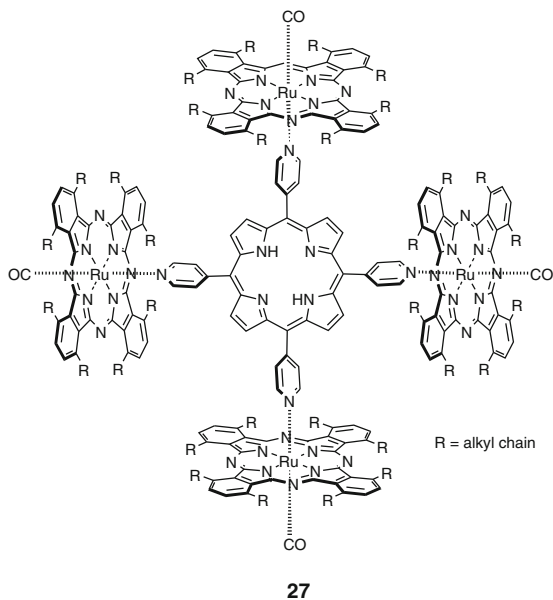


**Fig. 21** Supramolecular porphyrin-Ru(II) phthalocyanine ensemble **27**

## 4 Phthalocyanine-Based Polymers and Dendrimers

Pc-containing polymers [141–143] and dendrimers can be considered as robust and processable materials in which the relative orientation of the constituent Pc units can be controlled by strong covalent bonding. For that reason, the integration of Pcs into macromolecules is a powerful tool to obtain new materials with outstanding properties [144, 145]. Pc-containing polymers can be defined by the way in which the macrocycle is incorporated within the macromolecular structures, namely, as a side group, in the main chain, or forming a polymeric network [142]. The two latter approaches involve either polycyclotetramerization reactions of “bifunctional monomers” (namely, tetracarbonitriles) or the reaction of octa-, tetra-, or disubstituted mononuclear Pc derivatives with other bifunctional compounds [142, 146–150]. In general, these polymers are quite insoluble in organic solvents: a feature that makes difficult their processing and reduces their applicability. A particular type of Pc-based network polymer is that reported by McKeown and co-workers [151–153] who have prepared microporous materials based on Pcs linked to each other through highly rigid and nonlinear linking groups (Fig. 22). These materials are commonly prepared by reaction of octasubstituted Pcs with reactive bifunctional linking groups. The rigidity of the linkers avoids the aggregation of the macrocycles. This type of microporous polymers holds applicability in chemoselective adsorptions, separations, and heterogeneous catalysis [153].

Especially attractive is the route developed by Hanack and co-workers to obtain main-chain-type polymers based on Pcs, which relies on the connection of the

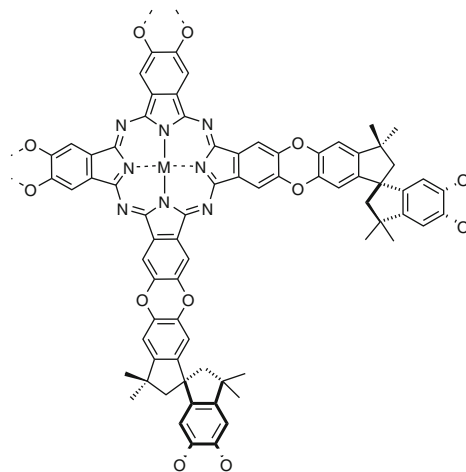


**Fig. 22** Pc-based microporous network polymer

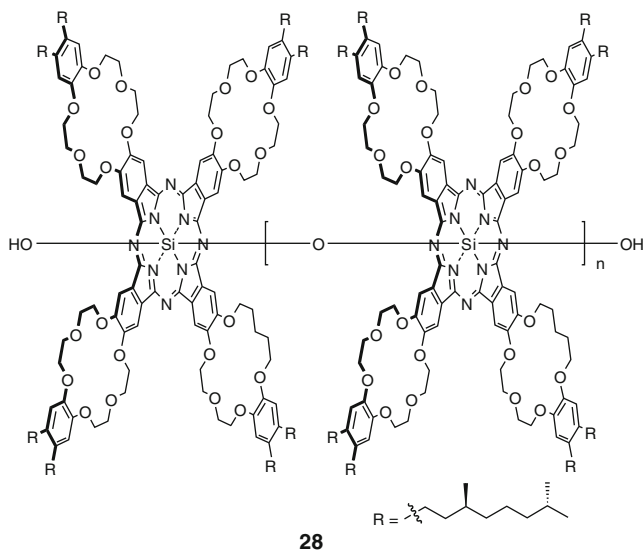


**Fig. 23** Main-chain polysiloxane Pc polymer **28**

metal ions inside the core through appropriate bivalent bridges [154, 155]. This approach sets the Pc molecules in a cofacial arrangement within the so-called “shish-kebab” polymer. The macromolecules obtained by this route can contain up to 200 macrocyclic units, and can show quite high solubility if appropriate groups are introduced at the periphery of the Pc macrocycles. A notable example of this type of rod-like polymers is the phthalocyaninato-polysiloxane **28** whose Pc units contain crown ethers linked to chiral alkyl side chains that induce helicity to the columnar architecture (Fig. 23) [156]. The polysiloxane backbone passes through

the center of the Pc rings, forcing the Pc molecules to tightly stack: the distance between the Pc rings is 0.34 nm. This feature provides the macromolecules with electrical conductivity owing to orbitals overlapping. At the solid-liquid interface and in dry films, this phthalocyaninato-polysiloxane packs head-to-tail forming long multimolecular columnar structures, which makes this polymer applicable in molecular scale electronics. Another organized phthalocyaninato-polysiloxane system has been described by Kobayashi and co-workers, who have reported the preparation of organic-inorganic composites by a sol-gel methodology, where the rod-like Pc polymers are inserted within ordered hexagonal channels [157].

Another example of a Pc-based 1-D polymer is that reported by Armstrong and co-workers [158]. They prepared a Pc with eight styrene-type polymerizable sites at the end of the peripheral substituents. This molecule forms highly ordered, rod-like aggregates at the air-water interface that can be transferred onto solid supports. Irradiation of the thin films affords polymerization between the olefin moieties of adjacent molecules by photostimulated [2 + 2] cycloaddition. The rod-like Pc macromolecules were conveniently studied by matrix-assisted laser desorption/ionization (MALDI-TOF) spectrometry and atomic force microscopy (AFM), the latter showing rods with lengths up to 290 nm.

As mentioned above, Pcs can be incorporated as side groups of a main polymeric chain. Two routes can be followed to achieve this goal. One of them involves the polymerization (or copolymerization) of unsymmetrically substituted Pcs, i.e., holding reactive sites at one of the isoindole subunits. The second one requires the preparation of a polymer with side functional groups that can react in a further step with an appropriately functionalized Pc.

Recent examples of the first route have been described by Kobayashi and co-workers, who reported the synthesis and characterization of polymeric Pcs obtained through the olefin metathesis polymerization of terminal olefin groups in the side chains of unsymmetrical Pc monomers [159]. X-ray analysis of the solid material indicates that the Pcs are ordered in stacks.

Metathesis polymerization has been also utilized as a tool for obtaining Pc-containing copolymers as pendant groups, namely with Pcs containing one norbornene polymerizable subunit and a different norbornene-based monomer [160, 161]. Particularly, C<sub>60</sub>- and Pc-containing copolymers [161] are attractive as materials for photovoltaic applications, as they permit an intimate contact between the electron-donor Pc rings and the electron-acceptor fullerene molecules for photoinduced charge separation (Fig. 24). Statistical copolymerization of fullerene- and Pc-norbornene monomers using different monomer ratios afforded a polymer **29** that shows photoinduced electron transfer from the chromophore to the fullerene units in solution. A photophysical characterization of the copolymer **29** in the solid state reveals also the occurrence of photoinduced charge transfer. However, the device showed very poor energy conversion efficiencies. On the way to find active materials for solar cell applications and to overcome the problem of phase segregation a modified poly-3-alkylthiophene bearing pendant nickel(II) phthalocyaninates has been prepared [162]. Polythiophenes are donor conjugated polymers, and the electronic character of the Pc core has been modulated (attaching electron-withdrawing groups) to achieve an electron-acceptor aromatic core, and therefore



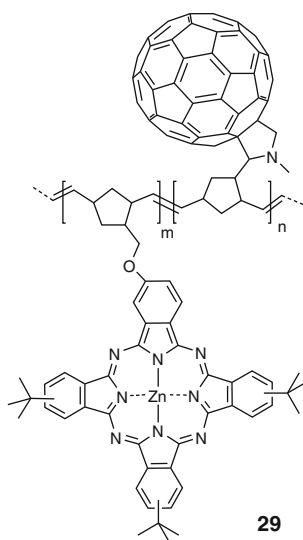


**Fig. 24** Phthalocyanine- and fullerene-containing polynorbornene **29**

to obtain a material with charge-transfer capabilities: when the Pc moieties of the material are photoexcited, a charge transfer occurs from the electron-donor polymer to the Pc units.

The incorporation of pendant Pcs to a polymeric backbone via the grafting of a suitable Pc molecule to a preformed polymer containing appropriate functional groups has been accomplished by Chen and co-workers [163]. These authors exploited the axial reactivity of some metalloPcs (namely, In(III)Pcs) to prepare an In(III)Pc-polystyrene copolymer. The most remarkable feature of this material is that cofacial association between the macrocycles is fully prevented. For some applications of the Pcs, such as optical limiting or photodynamic therapy (PDT), aggregation should be avoided because it produces the quenching of the excited-states.

Similarly, isolation of the Pc cores can be achieved by using dendrimers as substituents of the macrocycles. The steric isolation that the dendritic units afford to the macrocycle can prevent unwanted interference of the Pc functionality. Some examples of dendritic substitution have been reported, either at the periphery [164–167] or at the axial sites [36, 164, 166, 168]. An interesting example of dendritic-type architectures using Pc as central core is that reported by Majoral and co-workers, who have constructed a phosphorous dendrimer, up to generation five, from an octa-substituted metal-free Pc [169] and its copper(II) and other metal complexes [170]. UV-vis experiments show both a hyperchromic and bathochromic effects on the Q band with increasing generation, indicating that the chromophore is progressively more isolated and that the dendritic shell mimics a highly polar solvent.

On the other hand, Si(IV)Pcs with hydrophilic poly(arylether) dendrimers attached to the central silicon atom can form spherical micelles by self-assembly [171].

The spherical self-assembly in aqueous solution originates from the “mushroom” shape of the molecule. Moreover, when hydrophobic molecules are present, the micelle includes them as guest molecules, acting as a molecular capsule. As selective adsorption of Pcs to cancer cells has been used as a tool for PDT, these micelles hold potential as drug delivery systems.

In this regard, some attention has been paid to Pc-containing dendrimers as biomedical nano-devices. A dendrimer composed of a focal photosensitizing Pc unit surrounded by poly(benzylether) dendritic wedges has been examined for PDT applications [172, 173]. This dendrimer forms supramolecular micelles through the electrostatic interaction with oppositely charged block copolymers that do not show self-quenching effect of the focal photosensitizing unit because of the presence of the large dendritic wedges.

Electronic applications have been also envisaged for CuPc-based dendrimers. The electron mobility of these materials has been studied in depth [174], as well as their capability as hole injector for organic light-emitting diodes [175]. The synthesis and photophysical studies of Si(IV)Pc-cored fullerodendrimers is a representative example of the validity of Pc-containing dendrimers for applications based on electron-transfer between donor and acceptor components [36]. Dendrimers bearing up to eight axial fullerene subunits have been synthesized, showing a marked stabilization of the formed radical ion pairs through the electron migration between the C<sub>60</sub> subunits, this stabilization increasing with the dendrimer generation.

## 5 Phthalocyanine-Based Nanostructures

The construction of well-ordered supramolecular architectures in which Pcs or Pc-analogs are organized across multiple length scales is highly desirable, as it opens up the possibility of using these macrocycles for relevant technological applications such as field-effect-transistors (FETs), gas sensors, or photovoltaic cells, to mention a few.

As stated above, several supramolecular motifs such as hydrogen-bonding, donor–acceptor, or metal–ligand interactions have been used to promote the organization of Pcs in solution. Somehow different, and probably to some extent more complex, is the case when such organization is sought on solid supports, as in this latter case the interactions between the macrocycles and the surface itself should also be taken into account.

To date a great variety of highly ordered, shape-persistent Pc-based architectures have been reported and diverse spectro- and microscopic techniques have been employed in order to obtain structural and physical information from the assembled architectures [176, 177].

## 5.1 Phthalocyanine Adlayers

Since the first report on a copper(II) Pc adlayer on Cu(100) [178], several studies describing the formation of Pc adlayers in air, in ultra-high vacuum (UHV), or at the solid–liquid interface have been reported [179–183], most of them involving the use of scanning tunneling microscopy (STM), a widely used technique for studying the organization of Pc derivatives on surfaces.

Symmetrically substituted chloro-[184, 185] and phenoxy-substituted [186] Pcs have been organized on Ag(111) and Au(111) by sublimation techniques. It has been demonstrated that in the case of the alkoxy-substituted Pc, the rotational degrees of the bulky phenoxy substituents imposes a bowl-like structure to the adsorbed Pc units, which in turn enables the interaction of the macrocycle core with the metal surface.

Similarly, Au-supported adlayers of either Co(II) or Cu(II) Pcs have been prepared and the electronic and morphological features of these ensembles investigated by cyclic voltammetry and in situ STM respectively [187]. Three distinct packing arrangements could be observed for the CoPc and CuPc macrocycles depending on the surface coverage, all of them presenting the Pc units lying flat on the Au surface. In addition, it was found that the CoPc-modified Au electrode was able to enhance the electrochemical reduction of O<sub>2</sub> to H<sub>2</sub>O<sub>2</sub>.

Two-dimensional (2-D), two-component systems composed of Pcs and porphyrins self-organized by UHV techniques on Au(111) have also been reported [188–192]. It is interesting to note that, in some cases, depending on the substituent groups on the Pc and the porphyrin systems, the intermolecular interactions between these macrocycles give rise to a 2-D crystalline architecture that presents a higher stability than that of the films resulting from either parent compound [188].

The metastable, 2-D packing motif presented by some Pcs adsorbed on Ag(111) has also prompted the utilization of such ensembles as templates for the organization of complementary guest molecules such as fullerenes [193] or corannulenes [194], giving rise to the formation of two-component, 2-D architectures. More recently, a similar approach has been used to prepare a surface-supported, three-component system. In fact, the immersion of an Au substrate into a solution containing both a ZnPc and a Zn porphyrin led to the formation of a highly ordered, 2-D arrangement of both Pc and porphyrin which can act as a bimolecular “chessboard” toward the supramolecular assembly of a third component (i.e., C<sub>60</sub> fullerene) which is selectively trapped in the open spaces (Fig. 25) [195].

Complexation of metal ions by Pcs adsorbed on metal surfaces has also been reported. In fact, a CoPc adsorbed on Au(111) is able to complex two Ca(II) ions by two of its four peripherally substituted crown ether macrocycles as demonstrated by high-resolution STM studies [196]. Furthermore, it was demonstrated by using a Au(100)-(1 × 1) lattice surface that the relationship between the crown ether moieties of the CoPc and the underlying Au lattice is important in the trapping of the Ca(II) ions within the crown macrocycles [197].

During the last few years, adlayers of sandwich compounds such as bisPc double-decker complexes of Y, Ce, Pr, La, and Er have also been investigated at

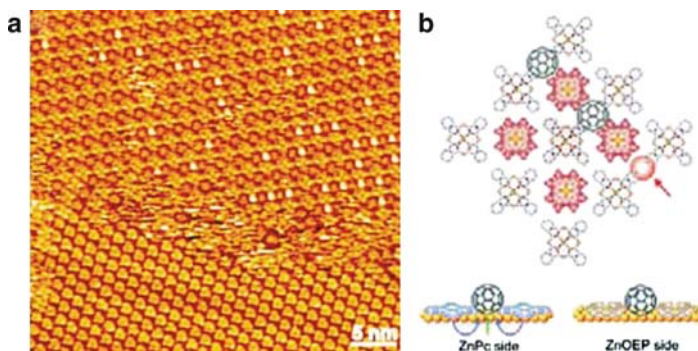


**Fig. 25** (a) STM image of a  $C_{60}$  array in the bimolecular “chessboard” consisting of ZnPc and Zn porphyrin on Au(111). (b) Proposed models for top and side views of  $C_{60}$  array in bimolecular chessboard. The STM image in (a) is reprinted with permission from [195]. Copyright 2008, The American Chemical Society

the liquid–solid interface [198–200]. In some cases, molecular rotation has been observed for these double-decker systems [201–204].

A triple-decker system consisting of two crown-ether-substituted Pc units and a tetraphenyl porphyrin macrocycle held together through the coordination of two Eu(III) ions has also been organized on surfaces [205]. The system forms adlayers on Au(111) as demonstrated by STM. High-resolution STM studies allowed to obtain some structural information of these adlayers, which revealed that the triple-decker is adsorbed onto the Au surface through the porphyrin macrocycle. Interestingly, electrochemical characterization of the triple-decker adlayer suggests the occurrence of a dynamic process in which the molecular orientation of the macrocycles in the superstructure is reversed in response to electrochemical bias.

Similarly, the precise control at the liquid–solid interface of the molecular orientation and ordering of a Pc-based triple decker, which presents dissimilar adsorption and assembling characteristics for the top and bottom moieties of the triple-decker complex, has been achieved by varying the external electric field [206]. In such a system, the interaction between the intrinsic molecular dipole of the adsorbed triple-decker molecule and the external electric field is responsible for the field-induced phase transition.

Recently, Pcs organized on surface have been used as molecular probes for the determination of quantum confined effects [207]. CoPc molecules form ordered self-assembled monolayers (SAM) on the top of Pb(111) thin films grown on a Si(111) substrate with the Pc units lying flat on the surface, as revealed by atomically resolved STM. A close analysis of the STM data revealed that the Pc molecules adsorb and self-assemble on the surface following a thickness-dependent adsorption pattern, which is ultimately related to the quantum size effects of the metal surface.

## 5.2 Self-Organization of Phthalocyanines on Surfaces by Solution-Processable Techniques

The utilization of solution-processable techniques for the fabrication of Pc-based nanoscale systems represents a relatively cheap and technologically appealing methodology, when compared to vacuum techniques, for the preparation of nanostructured architectures.

In this context, solutions of octaalkoxy substituted CuPcs drop-casted on silica surfaces give rise to the formation of highly homogeneous, 1-D (in the case of the octa(*n*-butoxy) CuPc) or 2-D (in the case of the octa(*n*-octyloxy) CuPc) aggregates [208]. Density functional computations have revealed that a combination of in-plane interactions and displaced parallel stacking for Pcs are responsible for the different self-assembled structures.

The possibility to couple the excellent self-organization ability of the Pcs with a magnetic property has also been sought through the preparation of a single-molecule magnet (SMM) alkoxy-substituted bis(phthalocyaninato)terbium(III) **30** (Fig. 26a).

The drop-casting of a solution of this complex on highly oriented pyrolytic graphite (HOPG) gives rise to the formation of 2-D domains of monodispersed molecules as observed by STM (Fig. 26b) [209]. These studies revealed that the complex **30** forms large regions of molecular arrays with domains that range from 10 up to a 100 nm in which the Pc molecules are adsorbed with their molecular plane parallel to the graphite surface. The magnetic properties of the Pc film were also investigated by magnetic force microscopy (MFM), a useful technique which

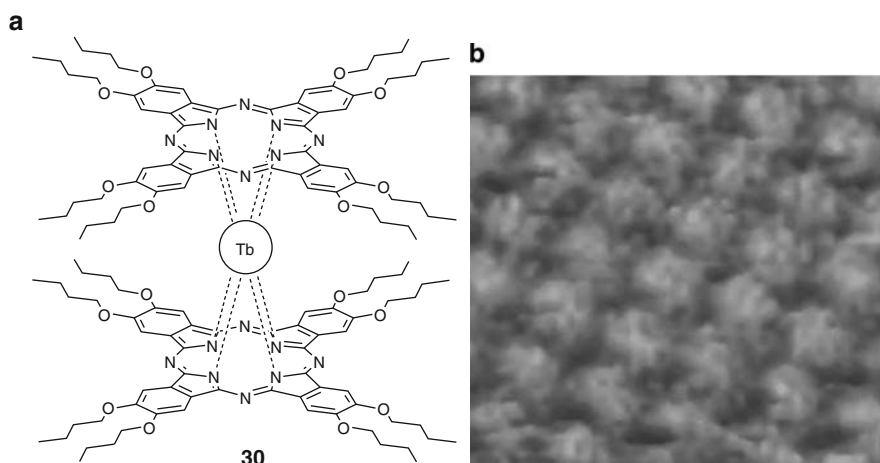


**Fig. 26** (a) Molecular structure of the bis(phthalocyaninato)terbium(III) **30**. (b) High-resolution scanning tunneling microscopy (HR-STM) image of the Pc **30** drop-casted on highly oriented pyrolytic graphite (HOPG). The Pc molecules can be clearly differentiated as bright spots. The STM image in (b) is reprinted with permission from [209]. Copyright 2006, The Royal Society of Chemistry

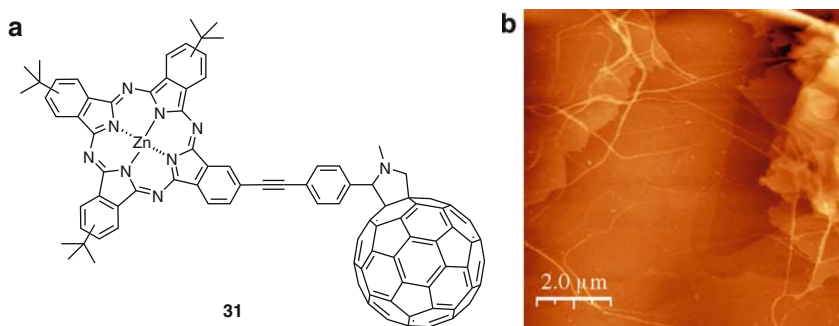


**Fig. 27** (a) Molecular structure of the Pc-C<sub>60</sub> fullerene conjugate **31**. (b) Atomic force microscopy (AFM) topographic image of the Pc-C<sub>60</sub> dyad **31** drop-casted on highly oriented pyrolytic graphite (HOPG). The AFM image in (b) is reprinted with permission from [48]. Copyright 2008, Wiley-VCH

allows probing the local magnetic field gradient of molecular aggregates on diamagnetic surfaces. In this case MFM experiments failed to reveal any magnetic contrast for the 2-D organized complex with respect to the underneath surface. This result can be probably due to the thermal instability of the self-assembled monolayer of complex **30**, which disturbs the observation of the magnetic signal, and/or most likely to the low magnetic response of the monolayer.

More recently, another example of a Pc-based system (**31**) (Fig. 27a) able to self-organize on HOPG and graphite-like surfaces by drop-casting technique was reported. AFM studies revealed that the covalently linked Pc-C<sub>60</sub> fullerene conjugate **31** is able to form nanostructured fibers and films (Fig. 27b) [48].

The electrical properties of these Pc-containing nanostructures were probed by conductive-AFM, a powerful technique used for measuring electrical properties in nanostructured architectures with nanometric resolution. High electrical conductivity values (i.e., 30  $\mu\text{A}$  for bias voltages ranging from 0.30 to 0.55 V) were measured for both the supramolecular fibers and films. Further studies pointed out that the high electrical conductivity values observed are strongly related to the molecular order of the Pc-C<sub>60</sub> conjugate within the nanostructures.

### 5.3 Phthalocyanine-Based Nanowires and Nanoparticles

Although Pcs are macrocycles that have a strong tendency to aggregate into columnar stacks by  $\pi$ - $\pi$  stacking interaction, the formation of long-range, ordered aggregates based on these systems has been seldom reported [84, 117].

In this context, a novel and interesting method for the preparation of such systems has recently been reported. The pyrolysis of a nickel naphthalocyanine (Nc), a homolog of Pc with a larger  $\pi$  system, previously organized in the nanoscale channels of a porous alumina membrane that acts as a template, leads to the formation of

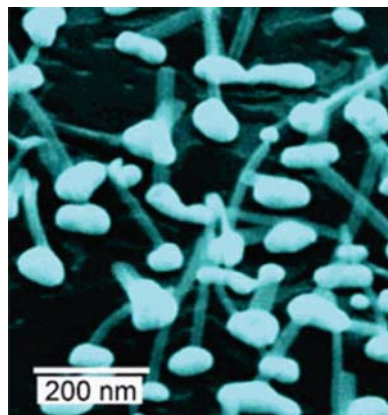


**Fig. 28** SEM image illustrating the vertical growth of CuPc wire-like nanostructures on top of the gold nanoparticles with width of 20–25 nm. The SEM image is reprinted with permission from [212]. Copyright 2006, The American Chemical Society

nanotubes which walls are constituted of intact, well-aligned Nc discs [210]. TEM and high-resolution TEM demonstrated that the tubes are hollow, with a wall thickness of about 20 nm, whereas electron diffraction shows an interplanar distance of 0.34 nm along the tube axis, which is the layer-to-layer separation of the  $\pi$ -stacked Nc units.

1-D nanoribbons and nanowires of different metal-containing Pcs have also been prepared by organic vapor-phase deposition (OVPD), a technique used to fabricate organic millimeter-sized crystals, thin films, or nanostructures [211]. Scanning electron microscopy (SEM), TEM, x-ray diffraction (XRD), and absorption measurement studies have revealed that the morphology of the nanostructures was strongly dependent on the chemical nature of the deposited macrocycle, the nature and the temperature of the substrate, and the source-to-substrate distance.

The growth of Pc-based, 1-D nanostructures on gold nanoparticles has also been achieved via vapor-phase transport, in a process in which the gold nanoparticles act as nucleation sites for the perfluorinated CuPc molecules and promote their anisotropic growth leading to very uniform, 1-D structures with high aspect ratio (Fig. 28) [212].

Pc-based nanoparticles have also been prepared employing a solution-casted method from an optically active metal-free Pc substituted with two binaphthyl units. Surprisingly, when the same process was carried out in the presence of a surfactant, the formation of hollow-sphere nanostructures was observed as revealed by TEM and SEM. Low angle XRD and electronic absorption spectroscopy revealed that these nanoscale hollow spheres are formed by stacked Pc molecules in a face-to-face configuration [213].

#### 5.4 Phthalocyanines as Precursors for the Preparation of Carbon Nanotubes

Pcs have also been used as metal-organic precursors for the preparation of nanostructured objects such as aligned 2-D [214] and (3-D) [215] CNTs. The pillar-shaped structures and patterns of 3-D CNT arrays were obtained by pyrolysis of iron(II)Pc previously deposited on a quartz glass plate in a furnace at 950°C under an Ar/H<sub>2</sub> flow. SEM and TEM analysis revealed the presence of a 2-D alignment of densely packed CNTs, in which well-distributed, pillar-shaped structures of CNTs were emerging, this resulting in the elongation of the CNT array in a third dimension. Although the growth mechanism for these CNTs patterns has not been yet completely understood, it seems plausible that the iron atoms generated by pyrolysis of the Pc together with the carbon atoms from an acetone source lead to the formation of a metal carbide, a more activating catalyst for the growth of CNTs than the metal itself.

More recently, a method for the production of bulk nitrogen-doped (2–4 atom% of pyridine-like nitrogen atoms) CNTs by hydrogen-free, solid-state pyrolysis of metal Pcs (Co or Fe) was reported, in which the morphology of the tubes could be controlled by the nature of the precursors and the pyrolysis conditions [216]. Highly curved, micrometer-long, multi-walled CNTs (MWCNTs) with a diameter of 20 to 60 nm could be obtained in the case of the CoPc, whereas straight and long CNTs were obtained in the case of the pyrolysis of FePc. In the latter case ca. 70% of the tubes were partially filled with metal as revealed by TEM analysis, thus affording unique metal core/carbon sheath nanocables (Fig. 29).

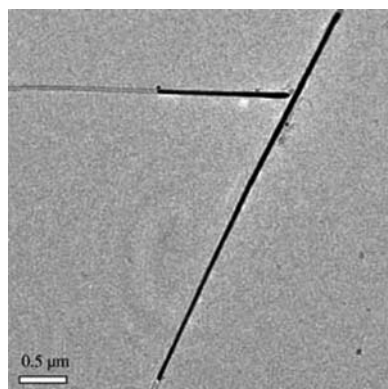


**Fig. 29** TEM image of metal core/carbon sheath nanocables with a long, iron-containing core and a spindle-like tip. The TEM image is reprinted with permission from [216]. Copyright 2005, Wiley-VCH



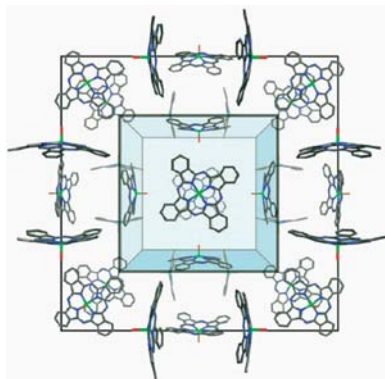


**Fig. 30** The cubic packing arrangement of the Pc bearing eight 2,6-diisopropylphenoxy substituents (the phenoxy substituents have been removed from the image for clarity). The image is reprinted with permission from [217]. Copyright 2005, Wiley-VCH

### 5.5 Nanostructuration of Phthalocyanines into Clathrates

The possibility of using Pc [217] or octaazaPc [218] macrocycles as building blocks for the assembly of crystalline, nanoporous materials has also been demonstrated. The preparation of open nanoporous structures based on these macrocycles is not a trivial task as it has to overcome the strong tendency that (aza)Pcs have to form densely packed cofacial aggregates. The strategy adopted to avoid such aggregation was to incorporate eight bulky 2,6-diisopropylphenoxy substituents at the periphery of the (aza)Pc macrocycle. Single-crystal XRD analysis of the crystals obtained by slow diffusion of acetone into a solution of the Pc in  $\text{CHCl}_3$  revealed a cubic morphology for the molecular packing arrangement. In such a structure, each of the six faces of the cube is composed of a Pc unit, with a cube edge of 2.33 nm and a cavity volume of at least  $8 \text{ nm}^3$  (Fig. 30).

XRD studies showed also that further stabilization of the cubic structure was obtained by the presence of water molecules within the cube, which appear to be associated through hydrogen-bonding interactions to the *meso* nitrogen atoms of the Pc ring. NMR solvent-exchange experiments were carried out on clathrate crystals previously submerged in deuterated acetone. These studies revealed that nearly all of the included deuterated acetone is exchanged within hours by solvents such as chloroform, methanol, or water, while the clathrate maintains its crystalline order [217].

### 5.6 Supramolecular Interactions of Phthalocyanines with Carbon Nanotubes

Supramolecular interactions between Pcs and MWCNTs have also been employed for the construction of nanostructured architectures in which the 1-D CNT scaffold acts as a platform for the assembly of the Pc macrocycles.

An erbium Pc ( $\text{ErPc}_2$ )–MWCNT ensemble has been obtained through supramolecular functionalization of the double-decker  $\text{ErPc}_2$  to the walls of the MWCNTs [219]. An increase in photoconductivity was observed for the ( $\text{ErPc}_2$ )–MWCNT composite with respect to the pristine  $\text{ErPc}_2$  molecular system which was attributed to the generation of photoinduced charge transfer from the  $\text{ErPc}_2$  donor unit to the CNT acceptor.

Using a similar approach, a water-soluble 3,4,4,4-tetrasulfonic acid tetrasodium salt Cu(II) Pc (TSCuPc) has been organized on surface-oxidized MWCNTs (*o*-MWCNTs). Upon spin coating of a solution of *o*-MWCNTs and TSCuPcs a film was formed having *o*-MWCNTs decorated with Pc units. In such ensemble the molecular plane of the macrocycle is oriented parallel to the nanotube surface as revealed by x-ray photoelectron spectroscopy (XPS), UV-vis, SEM, and AFM studies [220]. The potential application of this hybrid Pc/MWCNT system into a bulk heterojunction organic solar cell was also tested with the aim of increasing the light-harvesting capability of the device and facilitating efficient hole extraction. An enhancement in the power conversion efficiency was observed in the case of the cell fabricated with the Pc/MWCNT composite layer with respect to the one without the composite, which is rationalized in terms of the improved electronic, optical, and morphological properties provided by the Pc/MWCNT ensemble.

## 6 Phthalocyanines as Active Components of Functional Devices

### 6.1 Organic Field Effect Transistors

In the past decade, the research on organic field-effect transistors (OFETs) has experienced remarkable progress mainly because of the development of novel OFET materials, which have allowed to reach carrier mobility values good enough to compete with amorphous silicon.

Pcs are promising active materials for OFET applications, the most investigated members in this family being the CuPc and CoPc [221–223]. Thin films of vacuum deposited Pcs have shown mobilities in the range of  $10^{-5}$ – $10^{-3}$   $\text{cm}^2 \text{V}^{-1} \text{s}^{-1}$ , a value that increase to  $0.11 \text{ cm}^2 \text{V}^{-1} \text{s}^{-1}$  for vacuum deposited thin films of a sandwich-type device constructed by using two phthalocyaninato metal complexes [224]. Mobility values as high as  $1.0 \text{ cm}^2 \text{V}^{-1} \text{s}^{-1}$  have been recently reported for a single crystal CuPc-based OFET, which represent the highest value reported so far for Pc-based devices [225].

Langmuir–Blodgett (LB) technique has been also used for the preparation of Pc-based OFET, as it allows the fine control of both the structure and the thickness of the film at the molecular level [226, 227]. OFET devices based on amphiphilic tris(phthalocyaninato) rare earth, triple-decker complexes have been prepared by LB technique, showing good OFET performances [228]. More recently, ambipolar transport has also been realized in OFET devices through a combination of hole-conducting CuPc and n-conducting  $\text{C}_{60}$  fullerene, in which the asymmetry of the

electron and hole mobilities could be adjusted by varying the concentration of both materials within the mixture [229, 230].

## 6.2 *Sensors, Light-Emitting Devices and Optical Information Recording Media*

The possibility to integrate Pc-based devices into commercially viable sensors is highly desirable, in particular for the development of Pc-based electronic noses [231].

Thin films of Pcs, both metalated and metal-free, have been used as chemiresistive gas sensors, reaching gas sensitivity of the order of hundreds of ppb and satisfactory reversibility [232].

In these systems the conductivity increases in the presence of oxidant gases that generate charge carriers (holes) and decreases by electron-donating gases which trap charge carriers [233], in a process in which the formation of five- or six-coordinate species seems to occur.

Several reports on the gas sensing ability of Pc films toward nitric oxides [234–242] or H<sub>2</sub>O<sub>2</sub> [243] have appeared. Similarly, Pc-based, multimodal gas sensor systems able to respond to the presence of two gases of distinct nature such as NH<sub>3</sub>/O<sub>3</sub> [244] or NH<sub>3</sub>/NO<sub>2</sub> [245] have also been reported. On such systems, it has been proved that the film thickness and the crystal morphology exert a profound impact on the gas sensing characteristics of the device.

The increasing interest in the development of colorimetric molecular probes for sensing metal ions has attracted considerable attention in recent years as a consequence of their potential applications in the development of analytical devices [246–248].

In this context, Pcs have also been used for sensing applications because of their unique physical properties such as high photo- and thermal stability, strong absorption in the far visible region of the light spectrum, and reversible redox processes, the last one being the most interesting feature for sensing applications, as changes in the oxidation state of the Pcs are often accompanied by changes in their color [249].

Thin films of Pcs have shown to undergo reversible electrochromic changes depending upon their oxidation state [169, 250, 251]. An example of ions detection by a Pc in aqueous solution has also been recently reported. In such a system, the RuPc **32** (Fig. 31a) experiences a dramatic color change due to the Cu(II)-promoted, one-electron oxidation of the macrocycle, thus providing a useful tool for the selective and highly sensitive colorimetric detection of copper(II) ions in neat aqueous solutions (Fig. 31b) [252].

The outstanding optical properties of Pcs are also finding application in areas of technological and industrial interest such as the preparation of organic light emitting devices (OLEDs) in which Pcs have been used as active components [253–255].

On the other hand, Pcs are important components in CD and CVD technologies. Most of the information in this regard is published in the form of patents [256, 257].

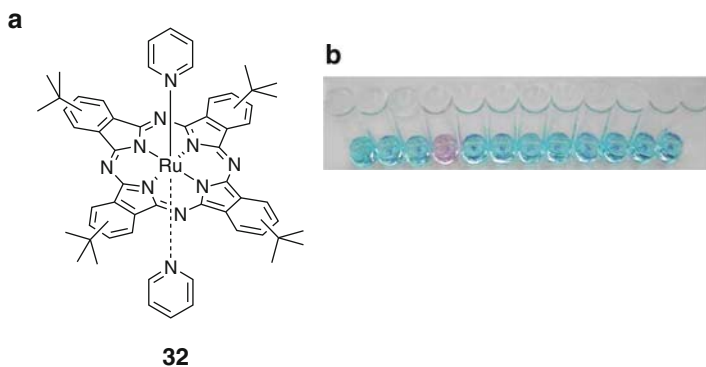


**Fig. 31** (a) Schematic molecular structure of RuPc **32**. (b) The digital picture illustrates several metal ions in a solution of **32**. From the left to the right: no ion, Hg(II), Cd(II), Cu(II), Zn(II), Pb(II), Fe(III), Ni(II), Mg(II), Ca(II), Li(I), K(I). All metal ions have been added from water solutions (total concentration 30 mM). The image in (b) is reprinted with permission from [252]. Copyright 2008, The Royal Society of Chemistry

### 6.3 Solar Cells Applications

The increasing concern related to the utilization of fossil fuels for the production of electricity in terms of both availability and environmental issues have prompted the search of new technologies for the production of “clean” energy sources. In this context, solar energy conversion represents one of the most promising and viable technologies to achieve this goal.

Within the vast field of solar cell devices, organic solar cells [258–261] are experiencing important progresses in their conversion efficiencies that will possibly make them, in the near future, a competitive alternative to silicon solar cells. Moreover, this class of solar cells presents several advantages with respect to their inorganic counterpart such as their low-cost production, easy fabrication, and lightweight, all features that could allow for the fabrication of large-area, foldable, and flexible photovoltaic devices.

Nowadays the best performing organic photovoltaic cell is represented by a bulk heterojunction (BHJ) solar cell based on the polymer poly(3-hexylthiophene) (P3HT) and the fullerene derivative [6, 6]-phenyl-C61-butyric acid methyl ester (PCBM), with reproducible efficiencies approaching 5% [262, 263]. However, a serious drawback for the preparation of efficient organic photovoltaic cells is represented by the low optical absorbance in the red/near-infrared region of the light-harvesting component(s), as well as their low extinction coefficient(s).

In this context, Pcs appear as perfect candidates for incorporation in such photovoltaic systems, as they present intense absorption in the UV/blue and the red/near IR region of the solar spectrum while still maintaining a rich redox chemistry and p-type semiconducting properties.

During the last decade, a large number of reports on the utilization of Pcs as active components in photovoltaic devices have appeared. In such devices the Pc, which acts as light-harvesting and donor unit, has been utilized in conjunction with semiconductor polymers and/or acceptor molecules such as fullerenes, either in intermolecularly mixed donor/acceptor layers [264–269] or in discrete, separate donor and acceptor layers [35, 270]. In such systems, several are the parameters that need to be adjusted in order to obtain high photoperformances, the most important ones being the electronic levels of the donor and acceptor units and their morphological arrangement within the active organic layer.

Solar cells devices based on CuPc and C<sub>60</sub> fullerene have reached power conversion efficiencies of up to 5% [266, 271], the highest efficiency for a Pc-containing solar cell being represented by a “tandem” cell in which two cells, each of them composed of a mixed donor/acceptor CuPc/C<sub>60</sub> layer sandwiched between homogeneous donor and acceptor layers, are coupled (efficiency = 5.7%) [272].

More recently, the use of supramolecular interactions for the preparation of organic solar cells has also been explored through the preparation of a C<sub>60</sub> fullerene bearing three chelating pyridyl groups capable of coordinating axially to a ZnPc macrocycle, leading to a cell which performance were slightly better than the one of a similar cell using a fullerene without specific coordination interaction with ZnPc [273, 274].

The morphological problems associated with the BHJ solar cells, such as low concentration of percolating pathways which are needed in order to bring the separated charge carriers to their corresponding electrodes, have prompted the utilization of molecules in which the donor and the acceptor moieties were covalently linked. In this connection several examples of Pc-based polymers [161, 162], Pc–C<sub>60</sub> dyads [85, 87, 88] and triads [275] have been prepared and tested for photovoltaic applications, but the efficiencies of these systems have been proved to be still low.

During the last decade, dye-sensitized solar cells (DSSCs) have gained increasing interest within the field of photovoltaics, as they allow to obtain robust, efficient, and cheap devices reaching power efficiencies close to the ones needed for commercial utilization. In such systems, the photons are collected by a dye molecule which is “anchored” through a chemical group (usually a carboxylic acid) to a wide band gap semiconducting material, the photoperformances of the cell being based upon the photoinduced electron injection from a molecular excited-state of the dye into the conduction band of the nanocrystalline metal oxide film (generally TiO<sub>2</sub>).

Similarly in the case of organic solar cells, the low optical absorbance in the red/near-infrared region of the dyes commonly used in DSSCs such as ruthenium bipyridyl [276] has prompted the incorporation of Pcs in these devices [277, 278].

Since the first report on the incorporation of a Pc in a DSSC by Grätzel and co-workers [279] several other examples of the kind have appeared.

A TiPc bearing a carboxylic acid moiety in its axial position has been used as the dye component in hybrid organic–inorganic DSSCs [280]. In such a system, the carboxylic acid-containing axial ligand is needed, as it allows to anchor the dye to the crystalline nanoparticles and to prevent the aggregation of the Pc macrocycles once anchored on the TiO<sub>2</sub> nanoparticle. Strong quenching of the Pc emission was

observed for the TiPc/TiO<sub>2</sub> films, which was assigned to electron injection from the excited state of the Pc into the conduction band of the TiO<sub>2</sub>. The occurrence of efficient electron injection was further confirmed by transient absorption studies, which revealed the spectral features of the TiPc<sup>+</sup>/TiO<sub>2</sub><sup>-</sup> species. Low energy conversion efficiency (ca. 0.2%) has been found for such systems probably because of an efficient kinetic competition between electron injection from the S<sub>2</sub> excited state of the photoexcited TiPc to the TiO<sub>2</sub> conduction band and internal conversion/vibrational relaxation of this state to the lower lying S<sub>1</sub> state of the dye.

More recently, a RuPc bearing a carboxylic moiety in its axial position was also tested for DSSC applications [281]. Transient absorption and steady-state (absorption and emission) measurements revealed that for such a system the electron injection occurs from the RuPc triplet state into the TiO<sub>2</sub> conduction band. A detailed study on the variation of the recombination rate constants for a series of metal complexes and organic dyes, including some RuPcs, has been carried out in order to identify some important parameters that should be taken into account for the implementation of DSSCs [282].

Pcs bearing the anchoring group at their peripheral position have also been reported with the aim of studying the influence of the position of the anchoring group on the DSSCs photoperformance. A power conversion efficiency of 0.54% has been obtained under standard illumination conditions by using a ZnPc bearing four tyrosine substituents at its peripheral position [283], whereas this value considerably increases when ZnPc macrocycles bearing one [284] or two [285] carboxylic acid moieties (3.05% for the monoacid and 3.52% for the diacid) have been used. In the case of the ZnPc monoacid a further increase in the power conversion efficiency up to 7.74% could be obtained by using as coadsorbant an acid-containing dye called JK2, which presents an absorption spectrum complementary to the one of the ZnPc monoacid. A study on the photoperformance of the monoacid ZnPc sensitized cell in the presence of chenodeoxycholic acid, a coadsorbent used to prevent the sensitizer aggregation by reducing its adsorption on the TiO<sub>2</sub> surface, was also carried out. These studies revealed that the open circuit voltage of the solar cell increases with increasing the concentration of the coadsorbent [286].

## 7 Conclusion

The synthesis of Pcs has been a matter of continuing scientific interest for many years. However, the preparation of adequately functionalized derivatives designed for particular purposes remains an expanding topic. The current availability of soluble Pcs has promoted a huge growth in the application of already well-established synthetic methodologies, such as transition metal-mediated carbon-carbon bond formation, thus allowing the construction of complex Pc-based structures. Non-covalent interactions play critical roles in a variety of Pc-based systems and may find applications ranging from medicine to molecular electronics. On the other

hand, the control of aggregation/organization by introduction of appropriate peripheral and axial substituents on the Pcs allows the use of these compounds in many applied fields. More recently, Pcs have emerged as attractive molecular building blocks for their arrangement into molecular materials and for fabricating materials at the nanometer scale. Thus Pcs have been successfully incorporated as active components of organic field effect transistors and solar cells, among others.

**Acknowledgements** Financial support from the Ministerio de Ciencia y Tecnología (CTQ2008–00418/BQU, Consolider-Ingenio 2010 CSD2007–00010 Nanociencia Molecular, -MEC MAT 2006–28180-E, SOHYDS), and Comunidad de Madrid (MADRISOLAR, S-0505/PPQ/0225) is gratefully acknowledged. GB and UH thank the Spanish MEC for their “Ramon y Cajal” contract.

## References

1. Leznoff CC, Lever ABP (eds) (1989, 1993, 1996) Phthalocyanines: properties and applications, vols 1–4. VCH Publishers, Cambridge
2. Kadish KM, Smith KM, Guillard R (eds) (2003) The porphyrin handbook, vols 15–20. Academic, San Diego
3. McKeown NB (1998) Phthalocyanine materials: synthesis, structure and function. Cambridge University Press, Cambridge
4. de la Torre G, Nicolau M, Torres T (2001) In: Nalwa H (ed) Supramolecular photosensitive and electroactive materials. Academic, New York, p 1
5. de la Torre G, Vazquez P, Agullo-Lopez F, Torres T (2004) Chem Rev 104:3723
6. Jiang J, Ng DKP (2009) Acc Chem Res 42:79
7. Rio Y, Rodriguez-Morgade MS, Torres T (2008) Org Biomol Chem 6:1877
8. de la Torre G, Claessens CG, Torres T (2007) Chem Commun 2000
9. Bottari G, Gonzalez-Rodriguez D (2009) J Porphyrins Phthalocyanines 13:624
10. Rodriguez-Morgade MS, de la Torre G, Torres T (2003) In: Kadish KM, Smith KM, Guillard R (eds) Porphyrin handbook, vol 15. Academic, San Diego, p 125
11. Claessens CG, Hahn U, Torres T (2008) Chem Rec 8:75
12. de la Torre G, Claessens CG, Torres T (2000) Eur J Org Chem 2821
13. Hall TW, Greenberg S, McArthur CR, Khouw B, Leznoff CC (1982) Nouv J Chim 6:653
14. Leznoff CC, Hall TW (1982) Tetrahedron Lett 23:3023
15. Wöhrle D, Krawczyk G (1986) Polym Bull 15:193
16. Leznoff CC, Snirskaya P, Khouw B, Cerny RL, Seymour P, Lever ABP (1991) J Org Chem 56:82
17. Hirth A, Sobbi AK, Wöhrle D (1997) J Porphyrins Phthalocyanines 1:275
18. Kobayashi N, Kondo R, Nakajima S, Osa T (1990) J Am Chem Soc 112:9640
19. Zhao Z, Nyokong T, Maree MD (2005) Dalton Trans 3732
20. Zhao Z, Poon C-T, Wong W-K, Wong W-Y, Tam H-L, Cheah K-W, Xie T, Wang D (2008) Eur J Inorg Chem 119
21. Xu H, Ng DKP (2008) Inorg Chem 47:7921
22. Cammidge AN, Berber G, Chambrier I, Hough PW, Cook MJ (2005) Tetrahedron 61:4067
23. Ermilov EA, Tannert S, Werncke T, Choi MTM, Ng DKP, Röder B (2006) Chem Phys 328:428
24. Leng X, Choi C-F, Lo P-C, Ng DKP (2007) Org Lett 9:231
25. Leng X, Ng DKP (2007) Eur J Inorg Chem 4615
26. Tannert S, Ermilov EA, Vogel JO, Choi MTM, Ng DKP, Röder B (2007) J Phys Chem B 111:8053
27. Kojima T, Honda T, Ohkubo K, Shiro M, Kusukawa T, Fukuda T, Kobayashi N, Fukuzumi S (2008) Angew Chem Int Ed 47:6712

28. Rodriguez-Morgade MS, Torres T, Atienza-Castellanos C, Guldi DM (2006) *J Am Chem Soc* 128:5145
29. Gao B, Li Y, Su J, Tian H (2007) *Supramol Chem* 19:207
30. El-Khouly ME, Rogers LM, Zandler ME, Gadde S, Fujitsuka M, Ito O, D'Souza F (2003) *Chem Phys Chem* 4:474
31. Kim KN, Choi CS, Kay K-Y (2005) *Tetrahedron Lett* 46:6791
32. Chen Y, El-Khouly ME, Sasaki M, Araki Y, Ito O (2005) *Org Lett* 7:1613
33. Doyle JJ, Ballesteros B, de la Torre G, McGovern DA, Kelly JM, Torres T, Blau WJ (2006) *Chem Phys Lett* 428:307
34. Ballesteros B, de la Torre G, Torres T, Hug GL, Rahman GMA, Guldi DM (2006) *Tetrahedron* 62:2097
35. Troshin PA, Koeppe R, Peregudov AS, Peregudova SM, Egginger M, Lyubovskaya RN, Sariciftci NS (2007) *Chem Mater* 19:5363
36. El-Khouly ME, Kang ES, Kay K-Y, Choi CS, Aaraki Y, Ito O (2007) *Chem Eur J* 13:2854
37. Martin-Gomis L, Ohkubo K, Fernandez-Lazaro F, Fukuzumi S, Sastre-Santos A (2007) *Org Lett* 9:3441
38. Martin-Gomis L, Ohkubo K, Fernandez-Lazaro F, Fukuzumi S, Sastre-Santos A (2008) *J Phys Chem C* 112:17694
39. Bottari G, Diaz-Diaz D, Torres T (2006) *J Porphyrins Phthalocyanines* 10:1083
40. Martinez-Diaz MV, Quintiliani M, Torres T (2008) *Synlett* 1
41. Ali H, van Lier JE (1997) *Tetrahedron Lett* 38:1157
42. Maya EM, Vazquez P, Torres T (1997) *Chem Commun* 1175
43. Maya E M, Vazquez P, Torres T (1999) *Chem Eur J* 5:2004
44. Garcia-Frutos EM, O'Flaherty SM, Maya EM, de la Torre G, Blau W, Vazquez P, Torres T (2003) *J Mater Chem* 13:749
45. Bottari G, Torres T (2004) *Chem Commun* 2668
46. Jimenez AJ, Spänig F, Rodriguez-Morgade MS, Ohkubo K, Fukuzumi S, Guldi DM, Torres T (2007) *Org Lett* 9:2481
47. Gonzalez-Cabello A, Vazquez P, Torres T, Guldi DM (2003) *J Org Chem* 68:8635
48. Bottari G, Olea D, Gomez-Navarro C, Zamora F, Gomez-Herrero, Torres T (2008) *Angew Chem Int Ed* 47:2026
49. Quintiliani M, Kahnt A, Wölflé T, Hieringer W, Vazquez P, Görling A, Guldi DM, Torres T (2008) *Chem Eur J* 14:3765
50. Quintiliani M, Kahnt A, Vazquez P, Guldi DM, Torres T (2008) *J Mater Chem* 18:1542
51. Gonzalez-Rodriguez D, Claessens CG, Torres T, Liu S, Echegoyen L, Vila N, Nonell S (2005) *Chem Eur J* 11:3881
52. Yang SI, Li J, Cho HS, Kim D, Bocian DF, Holten D, Lindsey JS (2000) *J Mater Chem* 10:283
53. Morisue M, Kobuke Y (2008) *Chem Eur J* 14:8219
54. Lo P-C, Leng X, Ng DKP (2007) *Coord Chem Rev* 251:2334
55. Kobuke Y (2006) *Eur J Inorg Chem* 2333
56. Kameyama K, Satake A, Kobuke Y (2004) *Tetrahedron Lett* 45:7617
57. Sutton JM, Boyle RW (2001) *Chem Commun* 2014
58. Ambroise A, Wagner RW, Rao PD, Riggs JA, Hascoat P, Diers JR, Seth J, Lammi RK, Bocian DF, Holten D, Lindsey JS (2001) *Chem Mater* 13:1023
59. Pinzon JR, Cardona CM, Herranz MA, Plonska-Brzezinska ME, Palkar A, Athans AJ, Martin N, Ropdriguez-Fortea A, Poblet JM, Bottari G, Torres T, Gayathri SS, Guldi DM, Echegoyen L (2009) *Chem Eur J* 15:864
60. Pereira AMVM, Soares ARM, Calvete MJF, de la Torre G (2009) *J Porphyrins Phthalocyanines* 13:419
61. Soares ARM, Martinez-Diaz MV, Bruckner A, Pereira AMVM, Toma JPC, Alonso CMA, Faustino MAF, Neves MGPMS, Toma AC, Silva AMS, Cavaleiro JAS, Torres T, Guldi DM (2007) *Org Lett* 9:1557
62. Gonzalez-Cabello A, Vazquez P, Torres T (2001) *J Organomet Chem* 637–639:751
63. Maya EM, Garcia C, Vazquez P, Torres T, Gobbi L, Diederich F, Pyo S, Echegoyen L (2000) *J Org Chem* 65:823



64. Cook MJ, Heeney MJ (2000) *Chem Eur J* 6:3958
65. Garcia-Frutos EM, Fernandez-Lazaro F, Maya EM, Vazquez P, Torres T (2000) *J Org Chem* 65:6841
66. Cook MJ, Heeney MJ (2000) *Chem Commun* 969
67. Kahnt A, Quintiliani M, Vazquez P, Guldi DM, Torres T (2008) *ChemSusChem* 1:97
68. Fortage J, Göransson E, Blart E, Becker H-C, Hammarström L, Odobel F (2007) *Chem Commun* 4629
69. Fortage J, Odobel F (2009) *C R Chimie* 12:437
70. Miller MA, Lammi RK, Prathapan S, Holten D, Lindsey JS (2000) *J Org Chem* 65:6634
71. Gouloumis A, Liu S-G, Vazquez P, Echegoyen L, Torres T (2001) *Chem Commun* 399
72. Gouloumis A, Gonzalez-Rodriguez D, Vazquez P, Torres T, Liu S, Echegoyen L, Ramey J, Hug GL, Guldi DM (2006) *J Am Chem Soc* 128:12674
73. de la Escosura A, Martinez-Diaz MV, Guldi DM, Torres T (2006) *J Am Chem Soc* 128:4112
74. de la Escosura A, Martinez-Diaz MV, Barbera J, Torres T (2008) *J Org Chem* 73:1475
75. de la Escosura A, Martinez-Diaz MV, Thordarson P, Rowan AE, Nolte RJM, Torres T (2003) *J Am Chem Soc* 125:12300
76. Kahnt A, Guldi D M, de la Escosura A, Martinez-Diaz MV, Torres T (2008) *J Mater Chem* 18:77
77. Quintiliani M, Garcia-Frutos EM, Gouloumis A, Vazquez P, Ledoux-Rak I, Zyss J, Claessens CG, Torres T (2005) *Eur J Org Chem* 3911
78. Gonzalez A, Vazquez P, Torres T (1999) *Tetrahedron Lett* 40:3263
79. Gonzalez-Cabello A, Claessens CG, Martin-Fuch G, Ledoux-Rak I, Vazquez P, Zyss J, Agullo-Lopez F, Torres T (2003) *Synth Met* 137:1487
80. Odobel F, Zabri H (2005) *Inorg Chem* 44:5600
81. Ali H, van Lier JE (2009) *Tetrahedron Lett* 50:337
82. Ali H, van Lier JE (2009) *Tetrahedron Lett* 50:1113
83. Gouloumis A, Liu S-G, Sastre A, Vazquez P, Echegoyen L, Torres T (2000) *Chem Eur J* 6:3600
84. Guldi DM, Gouloumis A, Vazquez P, Torres T, Georgakilas V, Prato M (2005) *J Am Chem Soc* 127:5811
85. Neugebauer H, Loi MA, Winder C, Sariciftci NS, Cerullo G, Gouloumis A, Vazquez P, Torres T (2004) *Sol Energy Mater Sol Cells* 83:201
86. Guldi DM, Zilbermann I, Gouloumis A, Vazquez P, Torres T (2004) *J Phys Chem B* 108:18485
87. Loi MA, Denk P, Hoppe H, Neugebauer H, Meissner D, Winder C, Brabec C, Sariciftci NS, Gouloumis A, Vazquez P, Torres T (2003) *Synth Met* 137:1491
88. Loi MA, Denk P, Hoppe H, Neugebauer H, Winder C, Meissner D, Brabec C, Sariciftci NS, Gouloumis A, Vazquez P, Torres T (2003) *J Mater Chem* 13:700
89. Guldi DM, Gouloumis A, Vazquez P, Torres T (2002) *Chem Commun* 2056
90. Fukuzumi S, Ohkubo K, Ortiz J, Gutierrez AM, Fernandez-Lazaro F, Sastre-Santos A (2005) *Chem Commun* 3814
91. Chen Y, Lin Y, El-Khouly ME, Zhuang X, Araki Y, Ito O, Zhang W (2007) *Phys Chem Lett* 111:16096
92. Fukuzumi S, Ohkubo K, Ortiz J, Gutierrez AM, Fernandez-Lazaro F, Sastre-Santos A (2008) *J Phys Chem A* 112:10744
93. Liu MO, Tai C-H, Hu AT (2004) *J Photochem Photobiol A Chem* 165:193
94. de la Torre G, Blau W, Torres T (2003) *Nanotechnol* 14:765
95. Ballesteros B, Campidelli S, de la Torre G, Ehli C, Guldi DM, Prato M, Torres T (2007) *Chem Commun* 2950
96. Ballesteros B, de la Torre G, Ehli C, Rahman GMA, Agullo-Rueda F, Guldi DM, Torres T (2007) *J Am Chem Soc* 129:5061
97. Yang Z, Pu H, Yuan J, Wan D, Liu Y (2008) *Chem Phys Lett* 465:73
98. Campidelli S, Ballesteros B, Filorama A, Diaz Diaz D, de la Torre G, Torres T, Rahman GMA, Ehli C, Kiessling D, Werner F, Sgobba V, Guldi DM, Cioffi C, Prato M, Bourgojn J-P (2008) *J Am Chem Soc* 130:11503

99. Huang W, Wang S, Liang R, Gong Q, Qiu W, Liu Y, Zhu D (2000) *Chem Phys Lett* 324:354
100. Zhu P, Wang P, Qiu W, Liu Y, Ye C, Fang G, Song Y (2001) *Appl Phys Lett* 78:1319
101. Isosomppi M, Tkachenko NV, Efimov A, Vahasalo H, Jukola J, Vainiotalo P, Lemmetyinen H (2006) *Chem Phys Lett* 430:36
102. Lehtivuori H, Kumpulainen T, Efimov A, Lemmetyinen H, Kira A, Imahori H, Tkachenko NV (2008) *J Phys Chem C* 112:9896
103. Niemi M, Tkachenko NV, Efimov A, Lehtivuori H, Ohkubo K, Fukuzumi S, Lemmetyinen H (2008) *J Phys Chem A* 112:6884
104. Lehtivuori H, Kumpulainen T, Hietala M, Efimov A, Lemmetyinen H, Kira A, Imahori H, Tkachenko NV (2009) *J Phys Chem C* 113:1984
105. Martinez-Diaz MV, Fender NS, Rodriguez-Morgade MS, Gomez-Lopez M, Diederich F, Echegoyen L, Stoddart JF, Torres T (2002) *J Mater Chem* 12:2095
106. Guldi DM, Ramey J, Martinez-Diaz MV, de la Escosura A, Torres T, Da Ros T, Prato M (2002) *Chem Commun* 2774
107. Sessler JL, Jayawickramarajah J, Gouloumis A, Pantos GD, Torres T, Guldi DM (2006) *Tetrahedron* 62:2123
108. Torres T, Gouloumis A, Sanchez-Garcia D, Jayawickramarajah J, Seitz W, Guldi DM, Sessler JL (2007) *Chem Commun* 292
109. Li X-Y, Ng DKP (2001) *Tetrahedron Lett* 42:305
110. Sukeguchi D, Yoshiyama H, Shibata N, Nakamura S, Toru T, Hayashi Y, Soga T (2009) *J Fluor Chem* 130:361
111. Piechoki C, Simon J, Skoulios A, Guillon D, Weber P (1982) *J Am Chem Soc* 104:5245
112. Simon J, Bassoul P (1996) In: Leznoff CC, Lever ABP (eds) *Phthalocyanines: properties and applications*, vol 2. VCH Publishers, Cambridge, p 223
113. Duro JA, de la Torre G, Barberá J, Serrano JL, Torres T (1996) *Chem Mat* 8:1061
114. Eichhorn H, Bruce D, Wöhrle D (1998) *Adv Mater* 10:419
115. Maeda F, Hatsusaka K, Ohta K, Kimura M (2003) *J Mater Chem* 13:243
116. Kimura M, Ueki H, Ohta K, Shirai H, Kobayashi N (2006) *Langmuir* 22:5051
117. Engelkamp H, Middlebeek S, Nolte RJM (1999) *Science* 284:785
118. Samori P, Engelkamp H, de Witte P, Rowan AE, Nolte RJM, Rabe JP (2001) *Angew Chem Int Ed* 40:2348
119. Kobayashi N (2002) *Coord Chem Rev* 219:99
120. Thordarson P, Rowan AE, Nolte RJM (2003) In: Kadish KM, Smith KM, Guillard R (eds) *The porphyrin handbook*, vol. 18. Academic, San Diego, p 281
121. Kobayashi N, Nishiyama Y (1986) *J Chem Soc Chem Commun* 1462
122. Koray AR, Ahsen V, Bekaroglu O (1986) *J Chem Soc Chem Commun* 932
123. Sielcken OE, Van de Kuil LA, Drenth W, Nolte RJM (1986) *J Chem Soc Chem Commun* 1232
124. Kobayashi N, Lever, ABP (1987) *J Am Chem Soc* 109:7433
125. Sielcken OE, van Tilborg MM, Roks MF, Hendriks R, Drenth W, Nolte RJM (1987) *J Am Chem Soc* 109:4261
126. Sielcken OE, Vandekuul LA, Drenth W, Schoonman J, Nolte RJM (1990) *J Am Chem Soc* 112:3086
127. Elemans JAAW, Rowan AE, Nolte RJM (2003) *J Mater Chem* 13:2661
128. Sheng N, Zhang Y, Xu H, Bao M, Sun X, Jiang J (2007) *Eur J Inorg Chem* 3268
129. Sly J, Kasák P, Gomar-Nadal E, Rovira C, Górriz L, Thordarson P, Amabilino DB, Rowan AE, Nolte RJM (2005) *Chem Commun* 1255
130. Rai R, Saxena A, Ohira A, Fujiki M (2005) *Langmuir* 21:3957
131. Chen P, Ma X, Liu M (2007) *Macromolecules* 40:4780
132. Li X, Links LE, Rybtchinsky B, Wasielewski MR (2004) *J Am Chem Soc* 126:10810
133. Guan Y, Yu SH, Antonietti M, Böttcher C, Faul CFJ (2005) *Chem Eur J* 11:305
134. Kimura M, Ueki H, Ohta K, Hanabusa K, Shirai H, Kobayashi N (2004) *Chem Eur J* 10:4954
135. Lee PPS, Ngai T, Huang JD, Wu C, Fong WP, Ng DKP (2003) *Macromolecules* 36:7527
136. Ogawa K, Kobuke Y (2000) *Angew Chem Int Ed* 39:4070

137. Takahashi R, Kobuke Y (2003) *J Am Chem Soc* 125:2372
138. Ozeki H, Nomoto A, Ogawa K, Kobuke Y, Murakami M, Hosoda K, Ohtani M, Nakashima S, Miyasaka H, Okada T (2004) *Chem Eur J* 10:6393
139. Kameyama K, Morisue M, Satake A, Kobuke Y (2005) *Angew Chem Int Ed* 44:4763
140. Morisue M, Kobuke Y (2008) *Chem Eur J* 14:4993
141. McKeown NB (2000) *J Mater Chem* 10:1979
142. Wöhrle D (2001) *Macromol Rapid Comm* 22:68
143. Wöhrle D, Schnurpfeil G (2003) In: Kadish KM, Smith KM, Guilard R (eds) *The porphyrin handbook*, vol 17. Academic, San Diego, p 177
144. Huang C, Zhang Q (2005) *Adv Mater* 17:1153
145. Choi, S, Hong, SH, Cho SH, Park S, Park SM, Kim O, Ree M (2008) *Adv Mater* 20:1766
146. Trombach N, Hild O, Schlettwein, Wöhrle D (2002) *J Mater Chem* 12:879
147. Biyiklioglu Z, Kantekin H (2008) *Polyhedron* 27:1650
148. Kantekin H, Dilber G, Biyiklioglu Z (2008) *J Organomet Chem* 693:1038
149. Bilgin A, Mendi A, Yildiz U (2006) *Polymer* 47:8462
150. Bilgin A, Yagci C, Mendi A, Yildiz U (2008) *J Appl Polym Sci* 110:2115
151. McKeown NB, Makhseed S, Budd PM (2002) *Chem Commun* 2780
152. McKeown NB, Budd PM, Msayib KJ, Ghanem BS, Kingston HJ, Tattershall CE, Makhseed S, Reynolds KJ, Fritsch D (2005) *Chem Eur J* 11:2610
153. Mackintosh HJ, Budd PM, McKeown NB (2008) *J Mater Chem* 18:573
154. Schultz H, Lehmann H, Rein M, Hanack M (1991) In: Buchler JW (ed) *Struct Bond* 74. Springer, Berlin, p 41
155. Hanack M, Lang M (1994) *Adv Mater* 6:819
156. Samori P, Engelkamp H, De Witte PAJ, Rowan AE, Nolte RJM, Rabe JP (2005) *Adv Mater* 17:1265
157. Kimura M, Wada K, Iwashima Y, Ohta K, Hanabusa K, Shirai H, Kobayashi N (2003) *Chem Commun* 2504
158. Drager AS, Zangmeister RAP, Armstrong NR, O'Brien DF (2001) *J Am Chem Soc* 123:3595
159. Kimura M, Wada K, Ohta K, Hanabusa K, Shirai H, Kobayashi N (2001) *Macromolecules* 34:4706
160. Kimura M, Ueki H, Ohta K, Hanabusa K, Shirai H, Kobayashi N (2002) *Langmuir* 18:7683
161. de la Escosura A, Martinez-Diaz MV, Torres T, Grubbs RH, Guldi DM, Neugebauer H, Zinder C, Drees M, Sariciftci NS (2006) *Chem Asian J* 1–2:148
162. Martinez-Diaz M, Esperanza S, de la Escosura A, Catellani M, Yunus S, Luzzati S, Torres T (2003) *Tetrahedron Lett* 44:8475
163. Chen Y, Hanack M, O'Flaherty S, Bernd G, Zeug A, Röder B, Blau WJ (2003) *Macromolecules* 36:3786
164. Brewis M, Clarkson GJ, Helliwell M, Holder AM, McKeown NB (2000) *Chem Eur J* 6:4630
165. Kernag CA, McGrath DV (2003) *Chem Commun* 1048
166. Brewis M, Helliwell M, McKeown NB (2003) *Tetrahedron* 59:3863
167. Nishida M, Momotake A, Shinohara Y, Nishimura Y, Arai T (2007) *J Porphyrins Phthalocyanines* 11:448
168. Brewis M, Clarkson GJ, Goddard V, Helliwell M, Holder AM, McKeown NB (1998) *Angew Chem Int Ed* 37:1092
169. Leclaire J, Dagiral R, Fery-Forgues S, Coppel Y, Donnadiu B, Caminade AM, Majoral JP (2005) *J Am Chem Soc* 127:15762
170. Leclaire J, Dagiral R, Pla-Quintana A, Caminade AM, Majoral JP (2007) *Eur J Inorg Chem* 2890
171. Uchiyama T, Ishii K, Nonomura T, Kobayashi N, Isoda S (2003) *Chem Eur J* 9:5757
172. Jang WD, Nakagishi Y, Nishiyama N, Kawauchi S, Morimoto Y, Kikuchi M, Kataoka K (2006) *J Control Release* 113:73
173. Jang WD, Nishiyama N, Kataoka K (2007) *Supramol Chem* 19:309
174. Guo M, Yan X, Goodson III T (2008) *Adv Mater* 20:4167
175. Lee TW, Kwon Y, Park JJ, Pu L, Hayakawa T, Kakimoto M (2007) *Macromol Rapid Comm* 28:1657

176. Yoshimoto S, Itaya K (2007) *J Porphyrins Phthalocyanines* 11:313
177. Martinez-Diaz MV, Bottari G (2009) *J Porphyrins Phthalocyanines* 13:471
178. Lippel PH, Wilson RJ, Miller MD, Woell C, Chiang S (1989) *Phys Rev Lett* 62:171
179. Lu X, Hipps KW, Wang XD, Mazur U (1996) *J Am Chem Soc* 118:7197
180. Hipps KW, Lu X, Wang XD, Mazur U (1996) *J Phys Chem* 100:11207
181. Lu X, Hipps KW (1997) *J Phys Chem B* 101:5391
182. Barlow DE, Hipps KW (2000) *J Phys Chem B* 104:5993
183. Chizhov I, Scoles G, Kahn A (2000) *Langmuir* 16:4358
184. Koudia M, Abel M, Maurel C, Bliet A, Catalin D, Mossoyan M, Mossoyan J-C, Porte L (2006) *J Phys Chem B* 110:10058
185. Abel M, Oison V, Koudia M, Maurel C, Katan C, Porte L (2006) *ChemPhysChem* 7:82
186. Samuely T, Liu S-X, Wintjes N, Haas M, Decurtins S, Jung TA, Stohr M (2008) *J Phys Chem C* 112:6139
187. Yoshimoto S, Tada A, Suto K, Itaya K (2003) *J Phys Chem B* 107:5836
188. Hipps KW, Scudiero L, Barlow DE, Cooke MP, Jr. (2002) *J Am Chem Soc* 124:2126
189. Scudiero L, Hipps KW, Barlow DE (2003) *J Phys Chem B* 107:2903
190. Suto K, Yoshimoto S, Itaya K (2003) *J Am Chem Soc* 125:14976
191. Yoshimoto S, Higa N, Itaya K (2004) *J Am Chem Soc* 126:8540
192. Suto K, Yoshimoto S, Itaya K (2006) *Langmuir* 22:10766
193. Stohr M, Wagner T, Gabriel M, Weyers B, Moller R (2001) *Adv Funct Mater* 11:175
194. Calmettes B, Nagarajan S, Gourdon A, Abel M, Porte L, Coratger R (2008) *Angew Chem Int Ed* 47:6994
195. Yoshimoto S, Honda Y, Ito O, Itaya K (2008) *J Am Chem Soc* 130:1085
196. Yoshimoto S, Suto K, Itaya K, Kobayashi N (2003) *Chem Commun* 2174
197. Yoshimoto S, Suto K, Tada A, Kobayashi N, Itaya K (2004) *J Am Chem Soc* 126:8020
198. Yang Z-Y, Gan L-H, Lei S-B, Wan L-J, Wang C, Jiang J-Z (2005) *J Phys Chem B* 109:19859
199. Klymchenko AS, Steven J, Binnemans K, De Feyter S (2006) *Langmuir* 22:723
200. Takami T, Arnold DP, Fuchs AV, Will GD, Goh R, Waclawik ER, Bell JM, Weiss PS, Sugiura K, Liu W, Jiang J (2006) *J Phys Chem B* 110:1661
201. Takeuchi M, Imada T, Shinkai S (1998) *Angew Chem Int Ed* 37:2096
202. Sugasaki A, Ikeda M, Takeuchi M, Shinkai S (2000) *Angew Chem Int Ed* 39:3839
203. Shinkai S, Ikeda M, Sugasaki A, Takeuchi M (2001) *Acc Chem Res* 34:494
204. Tashiro K, Konishi K, Aida T (2000) *J Am Chem Soc* 122:7921
205. Yoshimoto S, Sawaguchi T, Su W, Jiang J, Kobayashi N (2007) *Angew Chem Int Ed* 46:1071
206. Lei S-B, Deng K, Yang Y-L, Zeng Q-D, Wang C, Jiang J-Z (2008) *Nano Lett* 8:1836
207. Jiang P, Ma X, Ning Y, Song C, Chen X, Jia J-F, Xue Q-K (2008) *J Am Chem Soc* 130:7790
208. Wang M, Yang Y-L, Deng K, Wang C (2007) *Chem Phys Lett* 439:76
209. Gomez-Segura J, Diez-Perez I, Ishikawa N, Nakano M, Veciana J, Ruiz-Molina D (2006) *Chem Commun* 2866
210. Zhi L, Gorelik T, Wu J, Kolb U, Müllen K (2005) *J Am Chem Soc* 127:12792
211. Tong WY, Djuricic AB, Xie MH, Ng ACM, Cheung KY, Chan WK, Leung YH, Lin HW, Gwo S (2006) *J Phys Chem B* 110:17406
212. Mbenkum BN, Barrena E, Zhang X, Kelsch M, Dosch R (2006) *Nano Lett* 6:2852
213. Lv W, Zhang X, Lu J, Zhang Y, Li X, Jiang J (2008) *Eur J Inorg Chem* 2008:4255
214. Wang X, Liu Y, Zhu D (2001) *Chem Phys Lett* 340:419
215. Wang XB, Liu YQ, Zhu DB (2002) *Adv Mater* 14:165
216. Zhi L, Gorelik T, Friedlein R, Wu J, Kolb U, Salaneck WR, Müllen K (2005) *Small* 1:798
217. McKeown NB, Makhseed S, Msayib KJ, Ooi L-L, Helliwell M, Warren JE (2005) *Angew Chem Int Ed* 44:7546
218. Makhseed S, Ibrahim F, Samuel J, Helliwell M, Warren JE, Bezzu CG, McKeown NB (2008) *Chem Eur J* 14:4810
219. Cao L, Chen HZ, Zhou HB, Zhu L, Sun JZ, Zhang XB, Xu JM, Wang M (2003) *Adv Mater* 15:909
220. Hatton RA, Blanchard NP, Stolojan V, Miller AJ, Silva SRP (2007) *Langmuir* 23:6424
221. Bao Z, Lovinger AJ, Dodabalapur A (1997) *Adv Mater* 9:42

222. Eriko M, Taniguchi M, Kawai T (2005) *Appl Phys Lett* 86:143513
223. Ofuji M, Ishikawa K, Takezoe H (2005) *Appl Phys Lett* 86:062114
224. Zhang J, Wang J, Wang H, Yan D (2004) *Appl Phys Lett* 84:142
225. Zeis R, Siegrist T, Kloc C (2005) *Appl Phys Lett* 86:022103/1
226. Liu Y, Hu W, Qiu W, Xu Y, Zhou S, Zhu D (2001) *Sens Actuators B Chem* 80:202
227. Su W, Jiang J, Xiao K, Chen Y, Zhao Q, Yu G, Liu Y (2005) *Langmuir* 21:6527
228. Chen Y, Su W, Bai M, Jiang J, Li X, Liu Y, Wang L, Wang S (2005) *J Am Chem Soc* 127:15700
229. Opitz A, Bronner M, Brutting W (2007) *J Appl Phys* 101:063709/1
230. Opitz A, Bronner M, Brutting W, Himmerlich M, Schaefer JA, Krischok S (2007) *Appl Phys Lett* 90:212112/1
231. de Saja JA, Rodriguez-Mendez ML (2005) *Adv Colloid Interface Sci* 116:1
232. Snow AW, Barger WR (1989) In: Leznoff CC, Lever ABP (eds) *Phthalocyanines: properties and applications*, vol 1. Wiley, New York, p 341
233. Bohrer FI, Sharoni A, Colesniuc C, Park J, Schuller IK, Kummel AC, Trogler WC (2007) *J Am Chem Soc* 129:5640
234. Hu W, Liu Y, Liu S, Zhu D (1998) *Thin Solid Films* 324:285
235. Hsieh JC, Liu CJ, Ju YH (1998) *Thin Solid Films* 322:98
236. Li X, Shen S, Zhou Q, Xu H, Jiang D, Lu A (1998) *Thin Solid Films* 324:274
237. Nicolau M, del Rey B, Torres T, Mingotaud C, Delhaes P, Cook MJ, Thorpe SC (1999) *Synth Met* 102:1462
238. Armand F, Perez H, Fouriaux S, Araspin O, Pradeau JP, Claessens CG, Maya EM, Vazquez P, Torres T (1999) *Synth Met* 102:1476
239. Lee YL, Tsai WC, Maa JR (2001) *Appl Surf Sci* 173:352
240. Liu CJ, Shih JJ, Ju YH (2004) *Sens Actuators B Chem* 99:344
241. Generosi A, Paci B, Albertini VR, Perfetti P, Paoletti AM, Pennesi G, Rossi G, Caminiti R (2005) *Appl Phys Lett* 87:181904/1
242. Generosi A, Paci B, Rossi Albertini V, Perfetti P, Pennesi G, Paoletti AM, Rossi G, Capobianchi A, Caminiti R (2005) *Appl Phys Lett* 86:114106/1
243. Bohrer FI, Colesniuc CN, Park J, Schuller IK, Kummel AC, Trogler WC (2008) *J Am Chem Soc* 130:3712
244. Muzikante I, Parra V, Dobulans R, Fonavs E, Latvels J, Bouvet M (2007) *Sensors* 7:2984
245. Ding X, Xu H, Zhang L, Jiang D, Lu A (1999) *Mol Cryst Liq Cryst* 337:481
246. Palomares E, Vilar R, Durrant JR (2004) *Chem Commun* 362
247. Sessler JL, Melfi PJ, Seidel D, Gorden AEV, Ford DK, Palmer PD, Tait CD (2004) *Tetrahedron* 60:11089
248. Palomares E, Martinez-Diaz MV, Torres T, Coronado E (2006) *Adv Funct Mater* 16:1166
249. Mortimer RJ (1997) *Chem Soc Rev* 26:147
250. Silver J, Lukes P, Hey P, Ahmet MT (1991) *J Mater Chem* 1:881
251. Silver J, Lukes P, Hey P, Ahmet MT (1992) *J Mater Chem* 2:841
252. Rodriguez-Morgade MS, Planells M, Torres T, Ballester P, Palomares E (2008) *J Mater Chem* 18:176
253. Hohnholz D, Steinbrecher S, Hanack M (2000) *J Mol Struct* 521:231
254. Choe Y, Park SY, Park DW, Kim W (2006) *Macromol Res* 14:38
255. Yuan YY, Han S, Grozea D, Lu ZH (2006) *Appl Phys Lett* 88:093503/1
256. Zafirov A, Rakovski S, Bakardjieva-Eneva J, Prahov L, Assenova L, Marrandino F (2002) *PCT Int Appl WO* 2002080158 A1
257. Usami Y, Kakuta T, Ishida T, (2004) *Eur Pat Appl EP* 1434207 A2. Fuji Photo Film Company Ltd., Japan
258. Hoppe H, Sariciftci NS (2004) *J Mater Res* 19:1924
259. Segura JL, Martin N, Guldi DM (2005) *Chem Soc Rev* 34:31
260. Guenes S, Neugebauer H, Sariciftci NS (2007) *Chem Rev* 107:1324
261. Thompson BC, Frechet JMJ (2008) *Angew Chem Int Ed* 47:58
262. W Ma, Yang C, Gong X, Lee K, Heeger AJ (2005) *Adv Funct Mater* 15:1617
263. Li G, Shrotriya V, Huang J, Yao Y, Moriarty T, Emery K, Yang Y (2005) *Nat Mater* 4:864

264. Heutz S, Sullivan P, Sanderson BM, Schultes SM, Jones TS (2004) *Sol Energ Mater Sol Cells* 83:229
265. Sullivan P, Heutz S, Schultes SM, Jones TS (2004) *Appl Phys Lett* 84:1210
266. Uchida S, Xue J, Rand BP, Forrest SR (2004) *Appl Phys Lett* 84:4218
267. Schultes SM, Sullivan P, Heutz S, Sanderson BM, Jones TS (2005) *Mater Sci Eng C* 25:858
268. Ltaief A, Ben Chaâbane R, Bouazizi A, Davenas J (2006) *Mater Sci Eng C* 26:344
269. Janssen AGF, Riedl T, Hamwi S, Johannes HH, Kowalsky W (2007) *Appl Phys Lett* 91:073519
270. Sullivan P, Jones TS, Ferguson AJ, Heutz S (2007) *Appl Phys Lett* 91:233114/1
271. Xue J, Uchida S, Rand BP, Forrest SR (2004) *Appl Phys Lett* 84:3013
272. Xue J, Uchida S, Rand BP, Forrest SR (2004) *Appl Phys Lett* 85:5757
273. Koeppe R, Troshin PA, Fuchsbaauer A, Lyubovskaya RN, Sariciftci NS (2006) *Fullerenes, Nanotubes, Carbon Nanostruct* 14:441
274. Egginger M, Koeppe R, Meghdadi F, Troshin PA, Lyubovskaya RN, Meissner D, Sariciftci NS (2006) *Proc SPIE – Int Soc Opt Eng* 6192:61921Y/1
275. Gouloumis A, de la Escosura A, Vazquez P, Torres T, Kahnt A, Guldi DM, Neugebauer H, Winder C, Drees M, Sariciftci NS (2006) *Org Lett* 8:5187
276. Nazeeruddin MK, De Angelis F, Fantacci S, Selloni A, Viscardi G, Liska P, Ito S, Takeru B, Grätzel M (2005) *J Am Chem Soc* 127:16835
277. Robertson N (2006) *Angew Chem Int Ed* 45:2338
278. Robertson N (2008) *Angew Chem Int Ed* 47:1012
279. Nazeeruddin MK, Humphry-Baker R, Grätzel M, Murrer BA (1998) *Chem Commun* 719
280. Palomares E, Martinez-Diaz MV, Haque SA, Torres T, Durrant JR (2004) *Chem Commun* 2112
281. Morandeira A, Lopez-Duarte I, Martinez-Diaz MV, O'Regan BC, Shuttle C, Haji-Zainulabidin NA, Torres T, Palomares E, Durrant JR (2007) *J Am Chem Soc* 129:9250
282. O'Regan BC, Lopez-Duarte I, Martinez-Diaz MV, Forneli A, Albero J, Morandeira A, Palomares E, Torres T, Durrant JR (2008) *J Am Chem Soc* 130:2906
283. He J, Benko G, Korodi F, Polivka T, Lomoth R, Akermark B, Sun L, Hagfeldt A, Sundstrom V (2002) *J Am Chem Soc* 124:4922
284. Cid J-J, Yum J-H, Jang S-R, Nazeeruddin MK, Martinez-Ferrero E, Palomares E, Ko J, Grätzel M, Torres T (2007) *Angew Chem Int Ed* 46:8358
285. Reddy PY, Giribabu L, Lyness C, Snaith HJ, Vijaykumar C, Chandrasekharam M, Lakshmikantam M, Yum J-H, Kalyanasundaram K, Grätzel M, Nazeeruddin MK (2007) *Angew Chem Int Ed* 46:373
286. Yum JH, Jang SR, Humphry-Baker R, Grätzel M, Cid J-J, Torres T, Nazeeruddin MK (2008) *Langmuir* 24:5636

# Electronic Spectral and Electrochemical Behavior of Near Infrared Absorbing Metallophthalocyanines

Tebello Nyokong

**Abstract** This chapter discusses the electronic absorption spectra and electrochemistry of phthalocyanine complexes which are redshifted to  $\sim 730$  nm and beyond. These are mainly manganese phthalocyanine derivatives and phthalocyanines containing sulfur substituents. The chapter concentrates mainly on the work done during the last 10 years. There are 96 references quoted and three detailed tables on the electronic absorption spectra, redox potentials, and analytes that are electrocatalyzed using manganese and titanium phthalocyanine complexes.

**Keywords** Electrocatalysis · Electrochemistry · Electronic absorption spectra · Phthalocyanine

## Contents

1	Introduction .....	46
2	Absorption Spectral Properties .....	51
2.1	Ring Expansion .....	52
2.2	Ring Substitution .....	56
2.3	Aggregation .....	62
2.4	Effect of Central Metal .....	63
3	Electrochemical Properties .....	65
3.1	$Mn^{III}$ Pc Complexes .....	67
3.2	TiPc and VPc Complexes .....	73
4	Electrocatalytic Behavior .....	75
4.1	Self-Assembled Monolayer (SAM) .....	75
4.2	Other Forms of Electrode Modification .....	78
4.3	Electrocatalytic Detection of Selected Analytes .....	78
5	Conclusion .....	82
	References .....	82

---

T. Nyokong

Department of Chemistry, Rhodes University, P.O. Box 94, Grahamstown, South Africa  
e-mail: T.nyokong@ru.ac.za

## Abbreviations

Ac	Anthracenocyanine
BHc	Benzohelicenocyanine
<i>t</i> -butyl	<i>tert</i> -butyl
Cat	Catechol
CHM	Cyclohexylmethoxy
DCB	Dichlorobenzene
DCM	Dichloromethane
DMF	Dimethylformamide
DMSO	Dimethylsulfoxide
Hc	Helicenocyanine
Nc	Naphthalocyanine
OmePh	Methoxyphenyl
Pa	Phenanthracyanine
THF	Tetrahydrofuran
TBAP	Tetrabutyl ammonium perchlorate
TBABF <sub>4</sub>	Tetrabutylammonium tetrafluoroborate

## 1 Introduction

Phthalocyanines (Pcs) are remarkable macrocyclic compounds that possess interesting physical and chemical properties. Their bright colors, conductivity, and chemical and thermal stability have made them very desirable for many applications. Phthalocyanines continually find their usefulness in contemporary and emerging technologies such as catalysis, photodynamic therapy (PDT) nonlinear optics, gas sensors, thermal writing displays, and solar cells [1–4]. Specificity in the applications of phthalocyanines can be introduced by modification of the phthalocyanine ring or by changes in the central metal or axial ligands.

Organic materials (such as phthalocyanines) with intense absorption in the near-infrared (NIR) region ( $\sim 750$ – $1,300$  nm) are important for many applications, including thermal imaging, optical data storage, liquid crystal display devices, infrared (IR) radiation filters, and in the security industry [1–4]. Near IR absorbing materials should have excellent light, weather, and thermal resistances, and should possess high molar extinction coefficients. Naphthalocyanines (Ncs, Fig. 1) are currently in use as near IR absorbers in the 760–820 nm region. Ncs and the related benzohelicenocyanine (BHc), helicenocyanine (Hc), and phenanthracyanine (Pa) complexes (Fig. 1), as well as anthracenocyanine (Ac) are usually difficult to prepare and are highly insoluble and prone to decomposition. Phthalocyanine (Pc) complexes represent an attractive alternative as NIR absorbers, as the Pc ligand is generally more



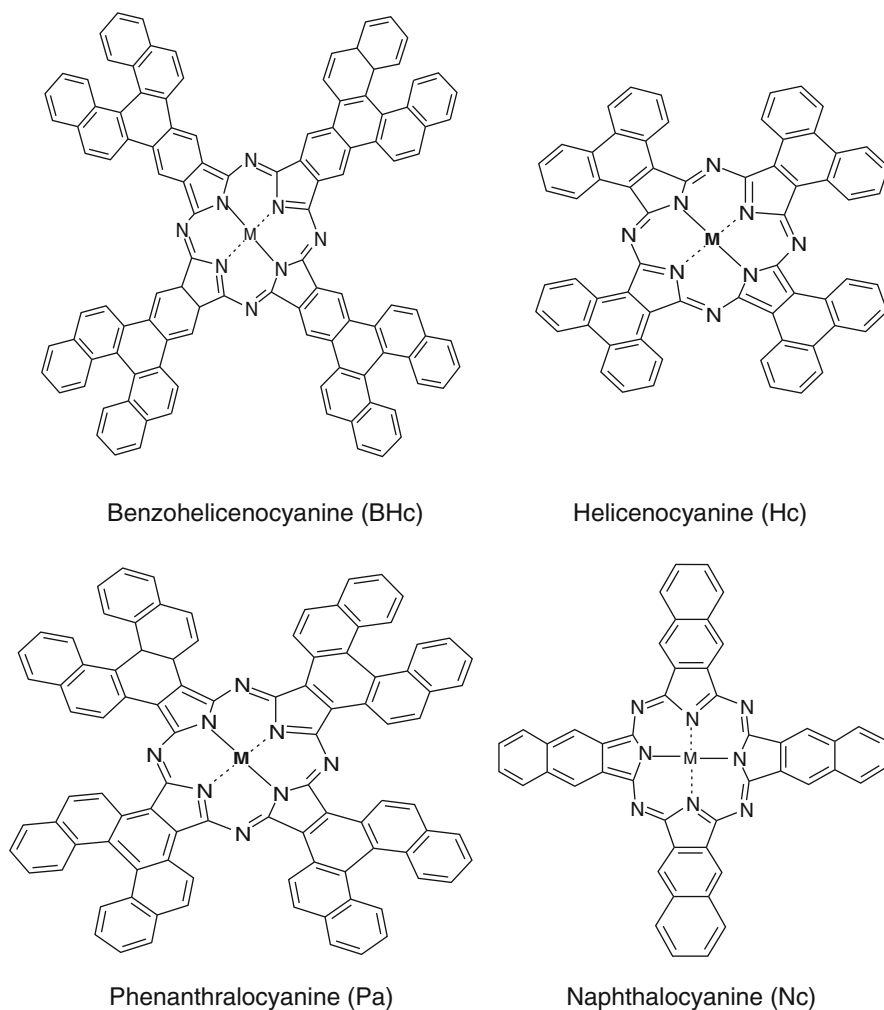


**Fig. 1** Molecular structure of conjugated phthalocyanines

stable than the Nc ligand. Thus, long wavelength absorbing phthalocyanines are interesting as materials with new electronic properties.

Phthalocyanines with sulfur or nitrogen substituents generally absorb in the NIR region [1]. Optical data storage uses sulfur-substituted Pcs which absorb near 780 nm [1]. Pcs absorbing in the NIR region to match the 780 and 830 nm semiconductor lasers are used for optical data storage (ODS), while for security applications, Pcs employed cover the 700–1,000 nm region [1–4]. NIR-absorbing Pcs have also been investigated for their nonlinear optical (NLO) applications needed for eye protection against pulsed lasers, and in photonics and photoelectronics. The use of

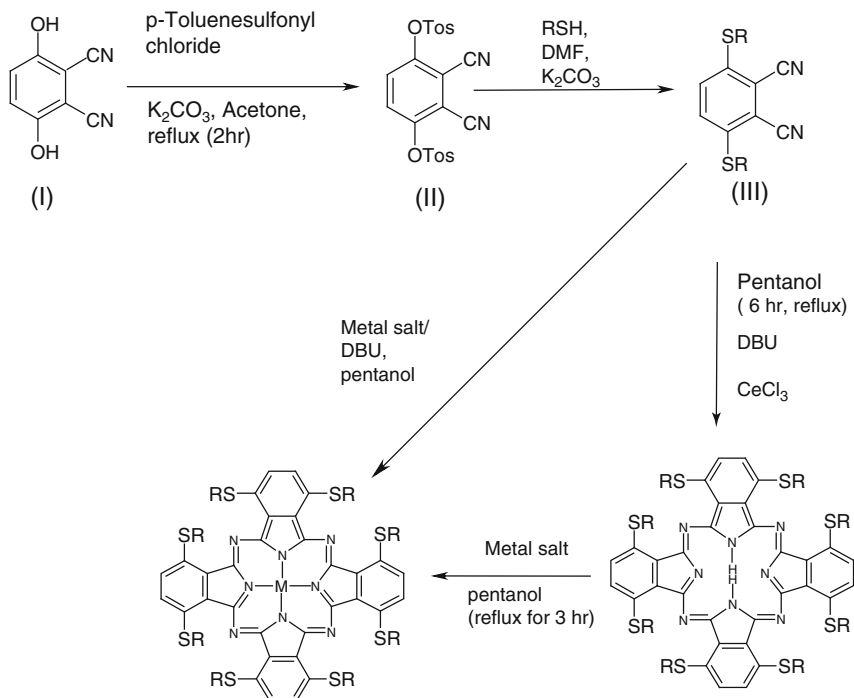
NIR fluorescence for bioanalytical applications is of importance in diagnosing disease and NIR-absorbing phthalocyanines may be used as fluorescence probes [5]. Thus, this chapter concentrates on phthalocyanine complexes absorbing from about 730 nm upwards. Even though solid state electronic absorption spectra of Pc thin films are known to be red-shifted [6–9], this work focuses on solution studies with only a few examples of the solid state studies.

Spectral properties of phthalocyanines are central to their chemical and electronic properties. The spectra of Pcs are governed by  $18\pi$  system of the inner 16-membered ring. As a result of their intense blue/green color, Pc complexes have been used extensively in dyes and pigments. The color of the phthalocyanines is mainly due to the Q band, but for highly redshifted MPc complexes which are a subject of this chapter, the Q band no longer determines the color of the complexes. Often the complexes gain intensity in the 400–500 nm region, which may contribute to the observed brown, red, or purple colors. MPc or  $H_2Pc$  complexes which are purple, red, or violet are becoming common.

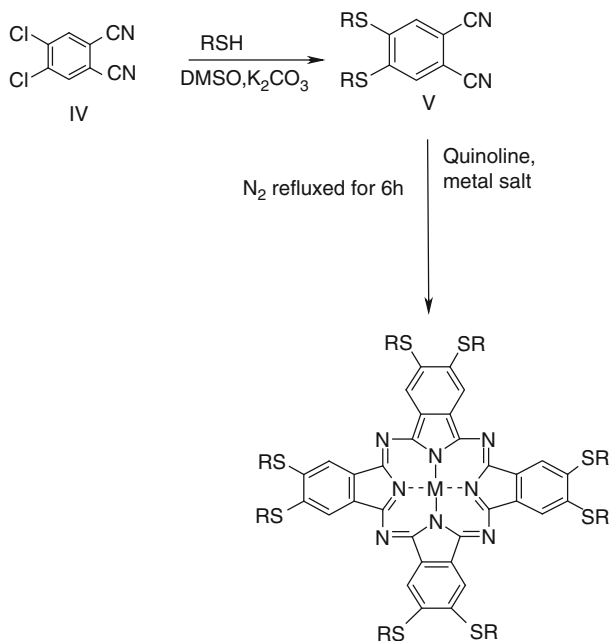
Most MPc complexes have a remarkably planar ligand structure. However, the presence of a large central metal such as lead and tin is known to distort the geometry, forming a domed conformation [10]. The essentially planar conformation of Pcs can also be significantly distorted by substituents through conformational stress [11].

A number of functions of MPc derivatives are based on electron transfer occurring in these molecules. Understanding of electrochemical behavior is required for the development of functional materials. Therefore, it is necessary to examine the electron transfer behavior of the long wavelength absorbing complexes discussed in this chapter. For main group phthalocyanine complexes, the first ring oxidation is separated from the first ring reduction by energy that is approximately equal to the HOMO (highest occupied molecular orbital) and the LUMO (lowest unoccupied molecular orbital) gap. Hence the study of the electrochemistry of main group Pc molecules may be linked to their spectra. The NIR-absorbing MPc complexes containing sulfur substituents often show complicated electrochemistry, which involves the Pc ring and the substituents on the Pc ring.

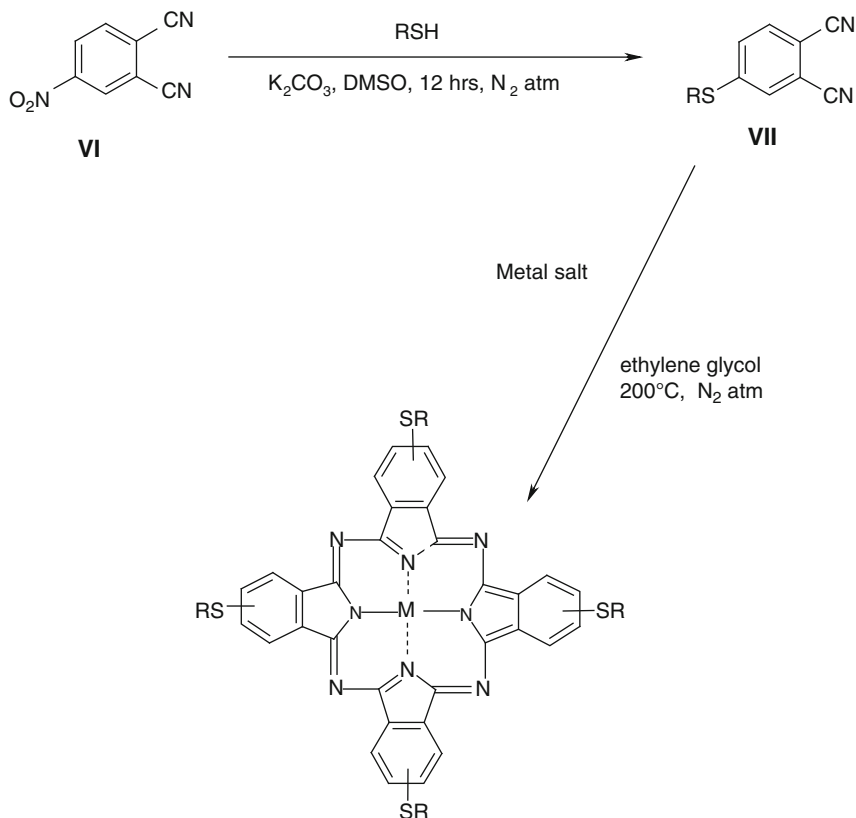
Redox activity of MPc ( $Pc^{-2}$ , phthalocyanine dianion) complexes containing central metals which are not electroactive occurs at the ring. Two successive one-electron oxidations may occur by removal of electrons from  $a_{1u}$  (HOMO) giving  $Pc^{-1}$  and  $Pc^0$  species. Reductions occur by adding electrons to  $e_g$  (LUMO) to give  $Pc^{-3}$ ,  $Pc^{-4}$ ,  $Pc^{-5}$ , and  $Pc^{-6}$  species. The spectra of main group MPc complexes provide characteristic bands for the ring reduced and ring oxidized phthalocyanine complexes. Thus, a diverse number of species can be formed following oxidation or reduction of the phthalocyanine ring. Each oxidation or reduction product has a distinct spectrum which may be used for its characterization. The presence of the electroactive central metal results in additional redox processes occurring at the central metal, with unique electronic spectral behavior. This chapter will focus on the electrochemical behavior of NIR-absorbing complexes, especially those containing sulfur substituents.



**Scheme 1** Synthesis of nonperipherally substituted derivatives. DBU = 1,8 diazabicyclo[5.4.0] undec-7-ene



**Scheme 2** Synthesis of peripherally substituted phthalocyanines. DMSO = dimethylsulfoxide



**Scheme 3** Synthesis of tetra substituted phthalocyanines

The synthesis of Pcs containing sulfur groups follow the same route as other ring substituted Pcs [12]. For example, nonperipherally octaalkylthio (or arylthio) substituted metallophthalocyanine complexes are prepared by the template reaction of alkylthio (or arylthio)-substituted phthalonitrile precursors (**III**, Scheme 1) in the presence of a metal salt and a base 1,8-diazabicyclo{5.4.0}-undec-7-ene (DBU). The alkylthio (or arylthio) substituted phthalonitriles were prepared from a readily available starting material, 2,3-dicyanohydroquinone (**I**). Complex **III** is formed via a base-catalyzed ( $\text{K}_2\text{CO}_3$ ) nucleophilic aromatic displacement reaction of the tosyl group of **II** with an alkylthio group in Scheme 1. Alternatively, an unmetallated derivative may be synthesized, followed by metal insertion using a high boiling point solvent, Scheme 1.

Peripherally octaalkylthiosubstituted derivatives may be synthesized from thio substituted phthalonitrile (**V** in Scheme 2 [13]). The latter is obtained from the commercially available 4,5-dichlorophthalonitrile (**IV**, Scheme 2). Peripherally or nonperipherally *tetra* substituted MPc complexes may be synthesized from mono-substituted thio phthalonitrile (**VII**, Scheme 3) which in turn is obtained from commercially available 4-nitrophthalonitrile (**VI**, Scheme 3) or 3-nitrophthalonitrile [14].

## 2 Absorption Spectral Properties

The spectra of MPC complexes consist of an intense absorption band in the visible region traditionally near 670 nm called the Q band and a generally weaker band near 340 nm called the Soret or B band, Fig. 2, both being  $\pi \rightarrow \pi^*$  transitions. The B band consists of two transitions, B1 and B2. At higher energies, additional  $\pi \rightarrow \pi^*$  transitions (N, L, and C, in increasing energy) may be observed [15] in UV transparent solvents. Unmetallated Pcs are of  $D_{2h}$  symmetry. Metallation which maintains the planarity of the molecule increases the symmetry to  $D_{4h}$  [16]. The introduction of a metal ion inside the cavity will generate a slight blueshift in the Q band. This occurs because the introduction of a metal ion reduces the electron density. It has been demonstrated that the more electronegative the metal ion is, the more the blueshift is.

The Q band is due to the transition from the ground state of  $A_{1g}$  symmetry to the first excited state which is of  $E_u$  symmetry, Fig. 3. The metal d orbitals for transition metals may lie between the HOMO and the LUMO of the Pc ligand. This may result in metal to ligand (MLCT) or ligand to metal (LMCT) charge transfer transitions, Fig. 3. The charge transfer absorption bands occur in general between the B and Q bands and in the near IR region. The positions of the absorption bands in phthalocyanines, (particularly the Q band) are affected to a varying degree by the central metal, axial ligation, solvents, peripheral and nonperipheral substitution, aggregation, and by extension of the conjugation. Axial ligation in general results only in a small shift in the Q band [15, 17]. Lowering of the symmetry of the phthalocyanine and other porphyrazine molecules results in splitting (or broadening) of the Q band [18]. The splitting of spectra is due to the lifting of degeneracy of the LUMO to a varying extent. Axial ligation, which results in interaction between the Pc and the axial ligands, resulted in the splitting of the Q band [19] in TiPc.

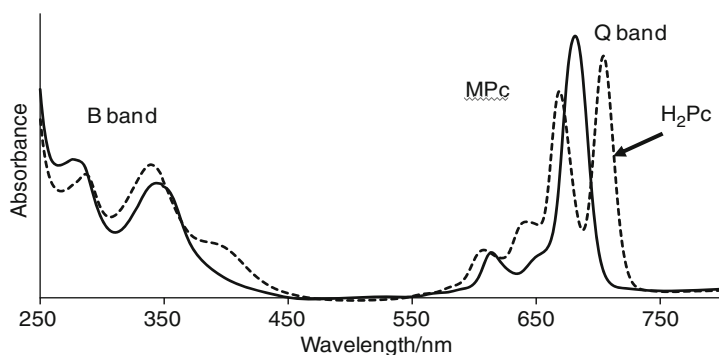


Fig. 2 Typical spectra of metal-free and metallated phthalocyanines

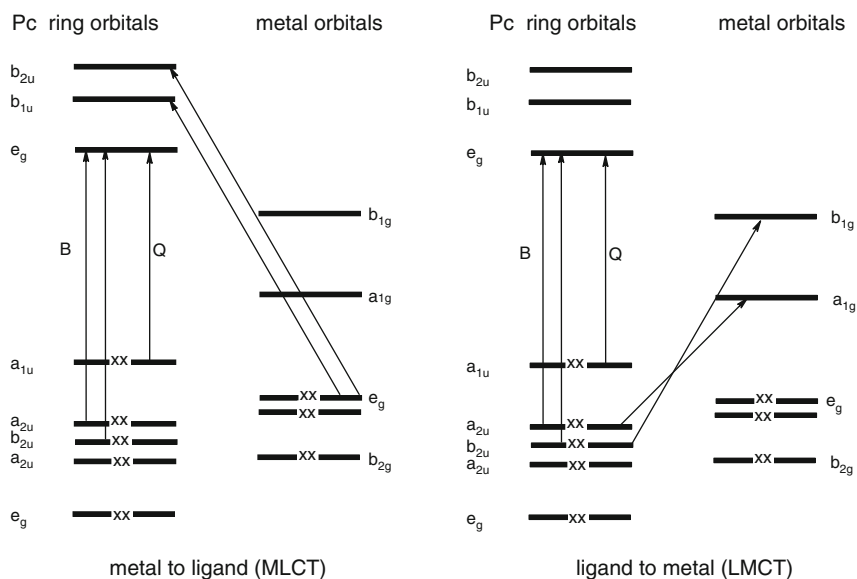


Fig. 3 Gouterman's four-orbital linear combination of atomic orbital model

## 2.1 Ring Expansion

It is well established that expansion of  $\pi$  conjugation in phthalocyanines shifts the Q band to the red [18, 20–26]. Extension of the conjugation system is accompanied by change in color from blue/green to colors including brown, red, or purple. The phthalocyanine derivatives, Nc, BHc, and Hc, Fig. 1, show Q bands that are shifted to the red (see for example  $\text{H}_2\text{BHc}^\beta(\text{OC}_{12}\text{H}_{25})_8$  [25],  $\text{H}_2\text{Nc}^\alpha(\text{OC}_4\text{H}_9)_8$  [25], CuNc [25], NiNc [25], and  $\text{PbBHc}^\beta(\text{OC}_{12}\text{H}_{25})_8$  [24] in Table 1) compared to MPc in general because of their extended macrocycle. Hc complexes show smaller shifts compared to corresponding Nc derivatives, because of an interrupted conjugation which results from the twisted naphthyl moieties. However, the stabilities of Nc, Hc, and BHc molecules are low, compared to Pcs in general. Kobayashi and coworkers have performed extensive calculations on the molecular orbitals of the Pcs and related molecules and have shown that redshifting on ring expansion is due to destabilization of the HOMO instead of stabilization of the LUMO [27].

Symmetrical expansion of the  $\pi$ -system (e.g., Pc to Nc) shifts the Q-band to the red without splitting (compare  $\text{CuPc}^\alpha(\text{OC}_5\text{H}_{11})_8$  and  $\text{CuNc}^\alpha(\text{OC}_5\text{H}_{11})_8$ , and also  $\text{NiPc}^\alpha(\text{OC}_5\text{H}_{11})_8$  and  $\text{NiNc}^\alpha(\text{OC}_5\text{H}_{11})_8$  in Table 1), whereas unsymmetrical expansion generally results in a splitting of the Q-band [18, 20–22, 28]. Annulated dinuclear and trinuclear phthalocyanines (complexes 1–3, Fig. 4) have been described by Makarov et al. [18, 20–22]. The Q band of the dimer (complex 1) is more red shifted than the corresponding monomer by 150 nm, and the complex containing three Pc units is more red shifted than the one containing two units [18],

**Table 1** Electronic absorption spectra of NIR-absorbing MPc complexes<sup>a</sup>

Complex	$\lambda$ (nm) (Log $\epsilon$ )	Solvent	Reference
<i>LMn<sup>III</sup></i> Pc complexes <sup>b</sup>			
OHMn5j	758 (4.58)	508 (3.69)	DMSO [14]
	682 (3.91)	360 (4.32)	
OHMn5k	741 (4.55)	497 (3.74)	DMSO [14]
	668 (3.98)	349 (4.3)	
		317 (4.28)	
OHMn <sup>II</sup> 5k	675		[14]
OHMn <sup>I</sup> 5k		575 (5.15)	DMSO [14]
OHMn6j	730 (5.06),	498 (4.37)	DMSO [14]
	655 (4.34)	367 (4.64)	
OHMn6k	719 (5.02),	494 (4.42)	DMSO [14]
	646 (4.38)	369 (4.56)	
		310 (4.60)	
AcMn6a	745 (5.1)	526 (4.8)	DCM [13, 34]
		452 (4.4)	
ClMn6g	723 (4.7)	500 (4.0)	DMF [35]
	667 (3.3)	368 (4.5)	
ClMn6h	720 (4.80)	497 380	DMF [34]
	649		
Mn6i	720 (4.62)	500 (3.75)	DMF [36]
	626 (4.40)	350 (4.43)	
Mn6i	720 (4.62)	500 (3.75)	DMF [36]
	626 (4.40)	350 (4.43)	
(OH)MnPc <sup><math>\alpha</math></sup> (NH <sub>2</sub> ) <sub>4</sub>	871 (4.89)	547 (4.45)	DMF [45]
	763 (3.49)	354 (4.73)	
(OH)MnPc <sup><math>\beta</math></sup> (NH <sub>2</sub> ) <sub>4</sub>	780 (4.71)	500 (4.44)	DMF [44]
		350 (4.80)	
(Ac)Mn <sup>II</sup> Pc-(OCH <sub>2</sub> C(CH <sub>3</sub> ) <sub>3</sub> ) <sub>16</sub>	744 (5.05)	546 (3.96)	THF [40]
	669 (4.67)	411 (4.19)	
(Ac)MnPc-(OCH <sub>2</sub> C(CH <sub>3</sub> ) <sub>3</sub> ) <sub>16</sub>	827 (4.8)	570 (4.15)	THF [40]
	740 (4.2)	413 (4.4)	
(Ac)Mn <sup>IV</sup> Pc-(OCH <sub>2</sub> C(CH <sub>3</sub> ) <sub>3</sub> ) <sub>16</sub>	849 (4.78)	584 (4.36)	THF [40]
	756 (4.28)		
	666 (4.06)		
[Ac]Mn <sup>II</sup> Pc(CHM) <sub>16</sub> ] <sup>-1</sup>	730 (4.97),	450 (4.76)	THF [40]
	667 (4.53)		
(Ac)MnPc(CHM) <sub>16</sub>	808		THF [40]
<i>(L)Mn<sup>III</sup></i> Pc complexes <sup>a</sup>			
(Ac)MnPc <sup><math>\alpha</math></sup> (SC <sub>5</sub> H <sub>11</sub> ) <sub>8</sub>	893 (4.8)	553 (4.0)	DCM [12]
	794 (4.3)	363 (4.5)	
		285 (5.0)	
(Ac)MnPc <sup><math>\beta</math></sup> (SC <sub>12</sub> H <sub>25</sub> ) <sub>4</sub>	749 (4.9)	528 (4.6)	DCM [13, 34]
		450 (4.3)	
(Ac)MnPc <sup><math>\alpha</math></sup> (C <sub>7</sub> H <sub>15</sub> ) <sub>4</sub>	733 685	531 358	CHCl <sub>3</sub> [48]
(Ac)MnPc <sup><math>\alpha</math></sup> (C <sub>7</sub> H <sub>15</sub> ) <sub>8</sub>	769 693	549 364	CHCl <sub>3</sub> [48]
(Ac)MnPc <sup><math>\beta</math></sup> (C <sub>7</sub> H <sub>15</sub> ) <sub>8</sub>	743 669	534 385	CHCl <sub>3</sub> [48]
[(Ac)Mn <sup>II</sup> Pc <sup><math>\alpha</math></sup> (C <sub>7</sub> H <sub>15</sub> ) <sub>8</sub> ] <sup>-</sup>	715 655	550 395 340	CHCl <sub>3</sub> [48]
[(Ac)Mn <sup>I</sup> Pc <sup><math>\alpha</math></sup> (C <sub>7</sub> H <sub>15</sub> ) <sub>8</sub> ] <sup>-</sup>	820 610	510 330	CHCl <sub>3</sub> [48]

(continued)

**Table 1** (continued)

Complex	$\lambda$ (nm) (Log $\epsilon$ )	Solvent	Reference
<i>LMn<sup>III</sup> Pc complexes<sup>a</sup></i>			
<i>ZnPc complexes</i>			
Zn1	840 (4.70)	363 (1.87)	CHCl <sub>3</sub>
	794 (0.61)		
	748 (0.93)		
	722 (1.08)		
Zn2	840 (5.67)	363 (5.27)	THF [18]
	942 (5.83)	365 (5.4)	THF [18]
	885 (4.93)		
	832 (5.06)		
	746 (5.02)		
	709 (4.79)		
	648 (4.68)		
	607 (4.68)		
Zn3	894 (5.56)	364 (4.40)	THF [18]
	787 (5.07)		
	849 (5.37)		
	715 (4.92)		
	644 (4.81)		
ZnPc <sup><math>\alpha</math></sup> (OC <sub>4</sub> H <sub>9</sub> ) <sub>8</sub>	758		Toluene [25]
ZnPc <sup><math>\alpha</math></sup> (OC <sub>5</sub> H <sub>11</sub> ) <sub>8</sub>	748		CH <sub>2</sub> Cl <sub>2</sub> [25]
ZnBHc <sup><math>\beta</math></sup> (OC <sub>12</sub> H <sub>25</sub> ) <sub>8</sub>	781, 709	430 331	Toluene [24]
Zn4m	780 (4.84)	400	Toluene [59]
Zn4l	814 (5.02)	480	Pyridine [38]
		423 (4.40)	
		3.09 (5.06)	
<i>TiPc complexes</i>			
OTi5a	745 (5.10),	342 (4.84)	DCM [23]
	675 (4.66)		
OTi5b	747 (5.36)	344 (4.94)	DCM [23]
	669 (4.68)		
OTi5c	730 (5.29)	348 (4.66)	CHCl <sub>3</sub> [31]
	653 (4.53)		
OTi5d	728 (5.41)	348 (4.88)	CHCl <sub>3</sub> [31]
	651 (4.71)		
OTi5e	730 (5.41)	346 (4.87)	CHCl <sub>3</sub> [32]
	656 (4.74)		
OTi5f	728 (5.38)	350 (4.78)	CHCl <sub>3</sub> [32]
	648 (4.67)		
OTi6a	714 (5.19)	349 (4.88)	DCM [23]
	645 (4.69)		
OTi6b	714 (5.06)	265 (4.87)	DCM [23]
	645 (3.47)		
OTi <sup><math>\beta</math></sup> Pc(NH <sub>2</sub> ) <sub>4</sub>	755 (5.24)	455 (4.02)	DMF [46]
		335 (4.91)	
OTi <sup><math>\alpha</math></sup> Pc(NH <sub>2</sub> ) <sub>4</sub>	830 (3.83)	455 (4.02)	DMF [45]
		740	

(continued)



**Table 1** (continued)

Complex	$\lambda$ (nm) (Log $\epsilon$ )	Solvent	Reference
<i>LMn<sup>III</sup> Pc complexes<sup>a</sup></i>			
OTiPc <sup><math>\alpha</math></sup> (SC <sub>5</sub> H <sub>11</sub> ) <sub>8</sub>	808 (3.9)	352 (3.5)	DCM [12]
	718 (3.3)	290 (3.9)	
OTiPc <sup><math>\beta</math></sup> (SC <sub>6</sub> H <sub>13</sub> ) <sub>4</sub>	720 (5.34)	349 (4.86)	CHCl <sub>3</sub> [33]
OTiPc <sup><math>\alpha</math></sup> (SC <sub>6</sub> H <sub>13</sub> ) <sub>8</sub>	739 (5.35)	336 (5.00)	CHCl <sub>3</sub> [33]
CatTiPc <sup><math>\beta</math></sup> (SC <sub>6</sub> H <sub>13</sub> ) <sub>4</sub>	721 (5.12)	342 (4.64)	CHCl <sub>3</sub> [33]
CatTiPc <sup><math>\beta</math></sup> (SC <sub>6</sub> H <sub>13</sub> ) <sub>8</sub>	741 (5.36)	335 (5.07)	CHCl <sub>3</sub>
<i>H<sub>2</sub>Pc complexes</i>			
H <sub>2</sub> 1	853 745	358	Toluene [20, 21]
	944 887	362	Toluene [21]
H <sub>2</sub> 2	833		
	760		
	907 (5.46)	420 (4.92)	THF [18]
H <sub>2</sub> 3	810 (5.07)	357 (5.37)	
	773 (5.01)		
	860 (5.32)		
	729 (5.03)		
	688 (4.82)		
H <sub>2</sub> Pc <sup><math>\alpha</math></sup> (OMePh) <sub>8</sub>	826 (5.09)	496 402	Pyridine [38]
	728	308 (5.09)	
H <sub>2</sub> Pc <sup><math>\alpha</math></sup> (OC <sub>4</sub> H <sub>9</sub> ) <sub>8</sub>	761, 739		Toluene [25]
H <sub>2</sub> Pc <sup><math>\alpha</math></sup> (OC <sub>5</sub> H <sub>11</sub> ) <sub>8</sub>	762, 738		Toluene [25]
H <sub>2</sub> Pc <sup><math>\alpha</math></sup> (OC <sub>8</sub> H <sub>17</sub> ) <sub>8</sub>	762, 740		Toluene [25]
H <sub>2</sub> BHc <sup><math>\beta</math></sup> (OC <sub>12</sub> H <sub>25</sub> ) <sub>8</sub>	793 708	439 332	Toluene [25]
H <sub>2</sub> Nc <sup><math>\alpha</math></sup> (OC <sub>4</sub> H <sub>9</sub> ) <sub>8</sub>	863 (2.05)		Toluene [25]
H <sub>2</sub> Nc <sup><math>\alpha</math></sup> (OC <sub>5</sub> H <sub>11</sub> ) <sub>8</sub>	862		Toluene [25]
H <sub>2</sub> Nc <sup><math>\alpha</math></sup> (OC <sub>8</sub> H <sub>17</sub> ) <sub>8</sub>	862		Toluene [25]
H <sub>2</sub> Nc	765		Toluene [25]
H <sub>2</sub> 4m	790 (4.90)	393 (4.60)	Toluene [59]
H <sub>2</sub> Pc <sup><math>\alpha</math></sup> (SC <sub>12</sub> H <sub>25</sub> ) <sub>8</sub>	815		[47]
H <sub>2</sub> Pc <sup><math>\alpha</math></sup> (SC <sub>12</sub> H <sub>25</sub> ) <sub>4</sub>	709, 738		[47]
<i>Other MPc complexes</i>			
CrPc <sup><math>\beta</math></sup> (NH <sub>2</sub> ) <sub>4</sub>	735 (4.8), 665	502, 450, 363	DMF [58]
CuPc <sup><math>\alpha</math></sup> (OC <sub>5</sub> H <sub>11</sub> ) <sub>8</sub>	752		CH <sub>2</sub> Cl <sub>2</sub> [25]
CuNc	776		Not provided [25]
CuNc <sup><math>\alpha</math></sup> (OC <sub>5</sub> H <sub>11</sub> ) <sub>8</sub>	849		Toluene [25]
NiPc <sup><math>\alpha</math></sup> (OC <sub>5</sub> H <sub>11</sub> ) <sub>8</sub>	734		Toluene [25]
NiPc(OCH <sub>2</sub> C(CH <sub>3</sub> ) <sub>3</sub> ) <sub>16</sub>	758		THF [41]
NiNc	768		Not provided [25]
NiNc <sup><math>\alpha</math></sup> (OC <sub>5</sub> H <sub>11</sub> ) <sub>8</sub>	766		Toluene [25]
Ni4m	758 (5.00)		Toluene [59]
Pb4m	861 831 (4.78)	455	Toluene [59]
PbBHc <sup><math>\beta</math></sup> (OC <sub>12</sub> H <sub>25</sub> ) <sub>8</sub>	831 731	428 337	Toluene [24]
Sn4m	837, 796 (5.00)	485 352	Toluene [59]
(Cl) <sub>2</sub> SnPc <sup><math>\alpha</math></sup> (C <sub>6</sub> H <sub>13</sub> ) <sub>8</sub>	735 (5.34),	364 (4.89)	THF [43]
	699 (4.65)		
	660 (4.73)		

(continued)

**Table 1** (continued)

Complex	$\lambda$ (nm) (Log $\epsilon$ )	Solvent	Reference
<i>LMn<sup>III</sup></i> Pc complexes <sup>a</sup>			
(Cl) <sub>2</sub> SnPc <sup><math>\alpha</math></sup> (C <sub>10</sub> H <sub>21</sub> ) <sub>8</sub>	735 (5.34),	429 (4.46)	THF [43]
	701 (4.64)	365 (4.80)	
	661 (4.68)	324 (4.78)	
(Cl) <sub>2</sub> SnPc <sup><math>\alpha</math></sup> (SC <sub>12</sub> H <sub>25</sub> ) <sub>8</sub>	918 (5.00),	355 (4.56)	CHCl <sub>3</sub> [47]
	805 (4.62)		
	635 (4.02)		
(Cl) <sub>2</sub> SnPc <sup><math>\alpha</math></sup> (SC <sub>12</sub> H <sub>25</sub> ) <sub>4</sub>	769 (6.06),	506 (5.37)	CHCl <sub>3</sub> [47]
	687 (5.58)	355 (6.00)	
[SbPc( <i>t</i> -butyl) <sub>4</sub> ] <sup>+</sup>	762 (5.15)		CH <sub>2</sub> Cl <sub>2</sub> [39]
[SbPc( <i>t</i> -butyl) <sub>4</sub> Cl <sub>2</sub> ] <sup>+</sup>	739 (5.25)		CH <sub>2</sub> Cl <sub>2</sub> [39]
OVPc <sup><math>\alpha</math></sup> (SC <sub>5</sub> H <sub>11</sub> ) <sub>8</sub>	850 (4.24),	344 (3.96)	DCM [30]
	754 (3.46)		

<sup>a</sup> OmePh = methoxyphenyl, DMF = dimethylformamide, DMSO = dimethylsulfoxide, THF = tetrahydrofuran, DCM = dichloromethane, Nc = naphthalocyanine, Cat = catechol, *t*-butyl = *tert*-butyl, CHM = cyclohexylmethoxy, Hc = helicenocyanine, BHc = benzohelicenocyanine

<sup>b</sup> Oxidation state indicated for Mn<sup>IV</sup>Pc, Mn<sup>III</sup>Pc and Mn<sup>I</sup>Pc complexes.

(compare **H<sub>2</sub>2** and **H<sub>2</sub>1** or **Zn1** and **Zn2** in Table 1, Fig. 4). This has been explained in terms of the splitting of the energy levels resulting in the decrease in energy separation. Also the destabilization of the HOMO increases with addition of Pc units in a linear fashion [18]. The rectangular annulations of the third Pc ring in complex **3** compared to linear arrangement in complex **2**, Fig. 4, results in the splitting of the Q band because of lowering of symmetry; compare **H<sub>2</sub>2** and **H<sub>2</sub>3**, or **Zn2** and **Zn3** in Table 1. The Q band of **3** also shifts to higher energy compared to complex **2** (Table 1). Complexes **1**, **2**, and **3** (Fig. 4) showed good stability compared to Ncs, Hcs, and BHcs.

Unmetallated Pc complexes show a split in the Q band because of the lifting of the degeneracy of the LUMO ( $e_g$ ) level. However, the Q band splitting of H<sub>2</sub>Pcs becomes smaller at longer wavelength [29], resulting in red shifted H<sub>2</sub>Pc complexes not showing the typical split Q band, Fig. 5. The single Q band for unmetallated phthalocyanines is usually accounted for as coincidental degeneracy of the molecular orbitals [25].

## 2.2 Ring Substitution

### 2.2.1 Nature of Substituent

The location of the Q band in Pc complexes can be adjusted by attaching suitable substituents onto the peripheral and nonperipheral positions of the ring and by the change in the nature, size, and number of substituents. Addition of electron donating

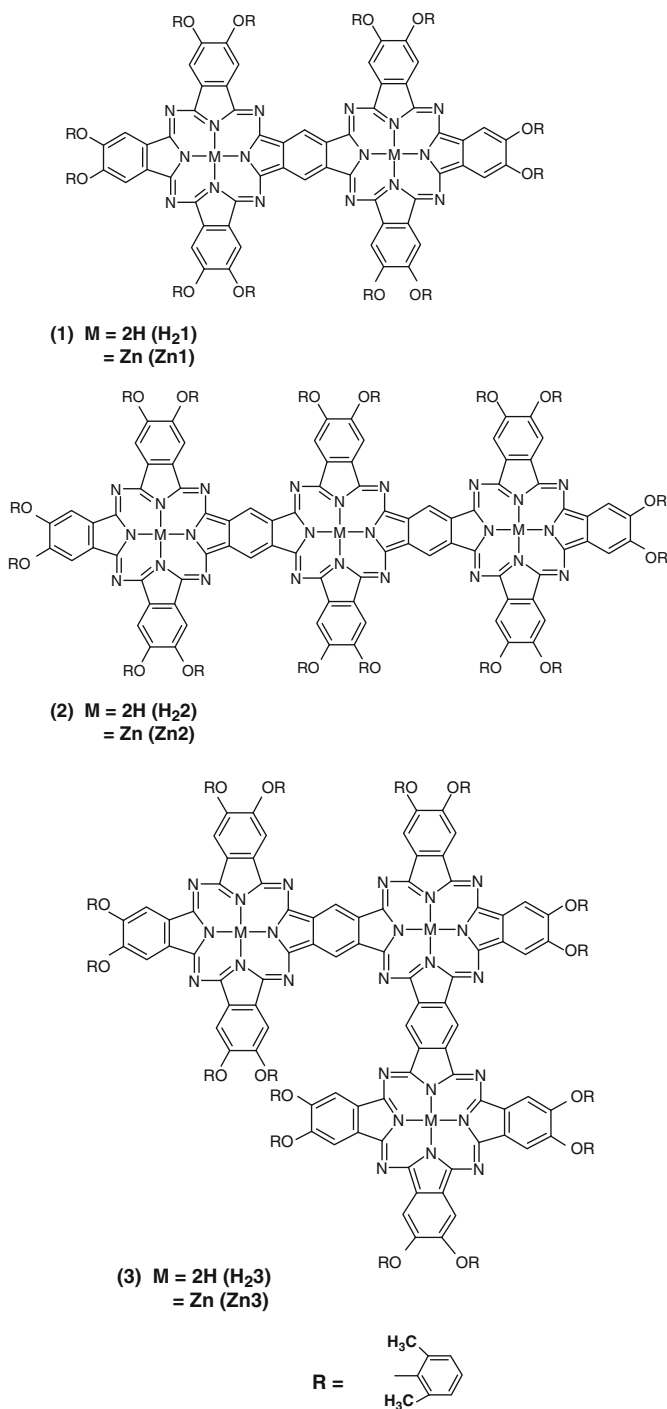


Fig. 4 Molecular structure of phthalocyanine dimers and trimers [20–22]

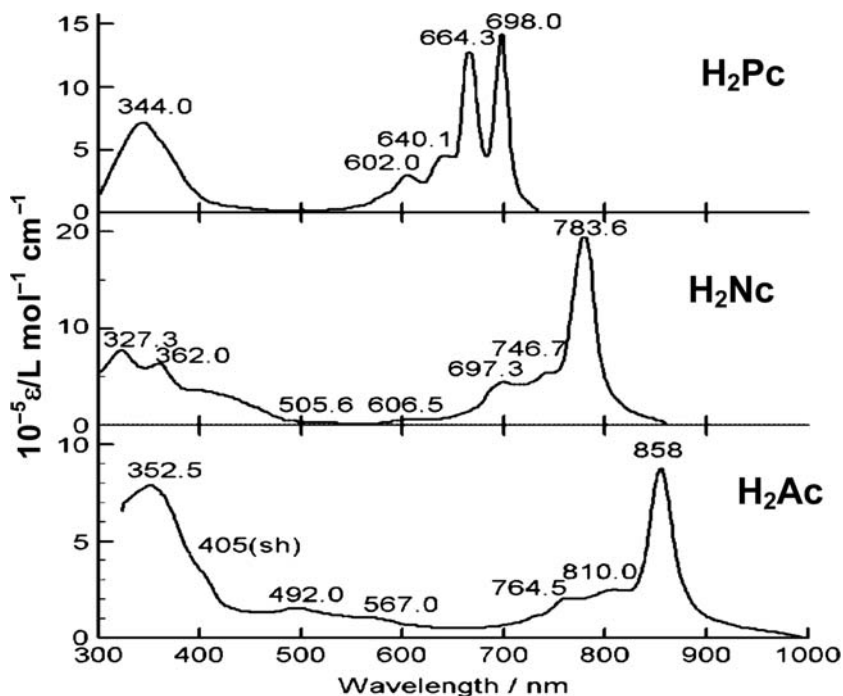
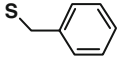
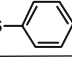
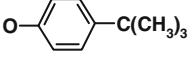
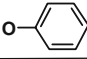
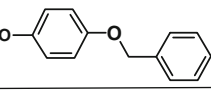
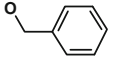
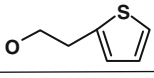
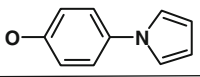
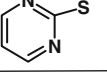
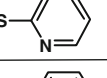
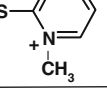
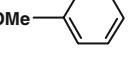
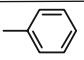
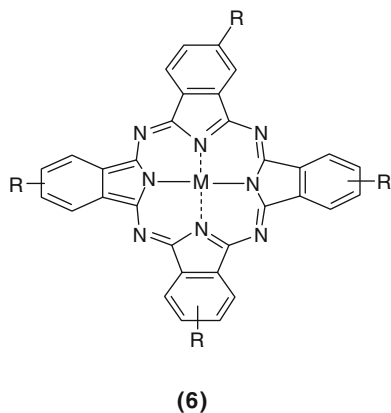
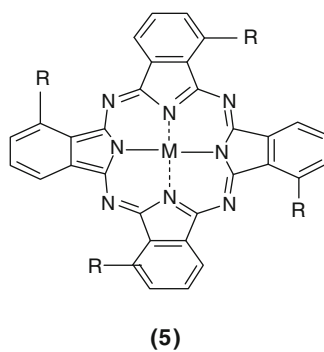
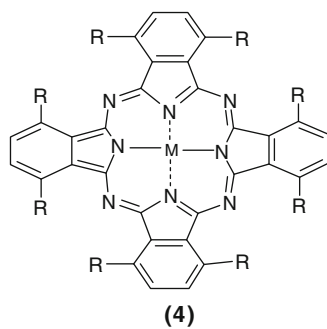


Fig. 5 Absorption spectra observed on expansion of the ring in porphyrin-type complexes. Reproduced with permission from [29]

groups such as  $-NH_2$ , OR, and SR (Table 1) at the nonperipheral (1,4,8,11,15,18, 22,25) or peripheral (2,3,9,10,16,17,23,24) positions of the Pc ring results in a redshift to the NIR region. As stated above, substitution of the ring with sulfur containing groups results in a large redshift of the Q band, because of the large electron-donating ability of these groups. Thus, the Q band of the vanadium complex,  $OVPc^\alpha(SC_5H_{11})_8$  at 850 nm (Table 1) is highly redshifted (by 160 nm) [30] compared to that of unsubstituted OVPc. Alkylthio or arylthio substituted Pcs are more redshifted compared to the corresponding oxo derivatives because of the electron donating ability of sulfur; compare **OTi5b** [23] and **OTi5d** [31], as well as **OTi5a** and **OTi5f** [23, 32] in Table 1. The structures of complexes are shown in Fig. 6. TiPc derivatives, **OTi5a** ( $\lambda_{Q\text{ band}} = 745\text{ nm}$ ) and **OTi5b** ( $\lambda_{Q\text{ band}} = 747\text{ nm}$ ), Table 1 [23], tetra substituted with benzyl thio and phenyl thio substituents at the nonperipheral positions (see Fig. 6 for structures) were not as highly redshifted as the octa substituted  $OTiPc^\alpha(SC_5H_{11})_8$  [12] complex ( $\lambda_{Q\text{ band}} = 808\text{ nm}$ ) probably because of the nature and plurality of the substituents. Changing axial ligands from oxygen to catechol for  $OTiPc^\beta(SC_6H_{13})_4$  [33] did not result in any significant shift in the Q band. Amino substituted MnPc complexes are redshifted compared to unsubstituted complexes, because of the electron donating nature of the amino group.  $TiPc^\beta(NH_2)_4$ , showing a Q band at 755 nm is redshifted compared to 714 nm

Complex number	R
<b>a</b>	
<b>b</b>	
<b>c</b>	
<b>d</b>	
<b>e</b>	
<b>f</b>	
<b>g</b>	
<b>h</b>	
<b>i</b>	
<b>j</b>	
<b>k</b>	
<b>l</b>	
<b>m</b>	



**Fig. 6** Molecular structures of complexes 4–6. Complexes represented as axial ligand (e.g., O): central metal (e.g., Ti); complex (e.g., 6) and substituent (e.g., a) – **OTi6a**

observed for **OTi6a** and **OTi6b** which are peripherally tetra substituted with arylthio substituents (Table 1).

Quaternization results in the blueshift of the Q band (compare **OHMn5j** and **OHMn5k**, and also **OHMn6j** and **OHMn6k** in Table 1) [14]. There is very little variation in Q band maxima with changes in the R substituent for MPc(OR) complexes: compare **CIMn6g** and **CIMn6h** [34, 35], or **OTi5c**, **OTi5d**, and **OTi5e** [31, 32], Table 1. There was also no difference in Q band wavelength when comparing benzylthio (**OTi6a**) and phenylthio (**OTi6b**) complexes [23], Table 1. **Mn6i** containing sulfur substituents was not redshifted compared to **Mn6h** [36].

The Pc complex containing phosphorous in the centre ( $[(C_4H_7O)_8(Pc(P)(OCH_3)_2)^+OH^-]$ ) is highly redshifted absorbing at 889 nm in methanol [37]. Kobayashi's group [38] synthesized a NIR-absorbing ZnPc derivatives which showed a redshift because of deformation of the ligand and the electron donating properties of the methoxyphenyl substituents (complex **Zn4I**). In this ZnPc derivative, the HOMO–LUMO gap was narrowed because of destabilization of the HOMO caused by increased electrostatic repulsion between carbon atoms at the nonperipheral positions and the electron-rich methoxy substituents [38]. Cationic  $[SbPc(t\text{-butyl})_4]^+$  is redshifted compared to an analogous complex containing chloride axial ligands ( $[SbPc(t\text{-butyl})_4Cl_2]^+$ ) [39], Table 1, reflecting the electron withdrawing nature of the chloride ligands.

### 2.2.2 Point of Substitution

Substitution at the nonperipheral position shows more redshift than at the peripheral position. A large redshift is obtained for benzene rings substituted at the 1,4 positions with substituent groups that allow conjugation with the  $18\pi$  system. Hexadecaalkoxy-substituted NiPc complex  $NiPc(OCH_2C(CH_3)_3)_{16}$ , in which both peripheral and nonperipheral positions are occupied by electron donating groups, showed a large redshift [40–42], Table 1 ( $\lambda_{Q\text{ band}} = 758\text{ nm}$  [41]) compared to unsubstituted NiPc, Table 1. It was suggested that substituents at the peripheral positions bolster the substituents at the nonperipheral position, making nonperipheral substituents bulkier [42]. Thus,  $NiPc(OCH_2C(CH_3)_3)_{16}$  showed a large redshift to 758 nm [41] because of the electronic interaction of the substituents with the Pc ring. Less red shift is observed for the corresponding  $Mn^{II}Pc(OCH_2C(CH_3)_3)_{16}$  ( $\lambda_{Q\text{ band}} = 744$ ) and  $(Ac)Mn^{II}Pc(CHM)_{16}]^{-1}$  [40], Table 1.

Octahexyltetrabenzo-5,10,15-triazaporphyrinato dichlorotin(IV) containing a CH group in place of one of the aza nitrogen atoms of the phthalocyanine core was less redshifted compared to octahexylphthalocyaninato dichlorotin(IV) ( $(Cl)_2SnPc^\alpha(C_6H_{13})_8$ , Table 1) because of the interruption of the conjugation [43].  $Mn^{III}Pc$  in DMSO (or DMF) absorbs at 758 nm, whereas peripherally substituted manganese tetraamino phthalocyanine ( $\beta\text{-}Mn^{III}Pc(NH_2)_4$ ) absorbs at 780 nm [44] and nonperipherally substituted  $MnPc^\alpha(NH_2)_4$  at 871 nm [45], Table 1. Nonperipherally substituted  $TiPc^\alpha(NH_2)_4$  showed a Q band at 830 nm [46] compared to that at 755 nm observed for  $TiPc^\beta(NH_2)_4$  [45], Table 1.

### 2.2.3 Length of Alkyl Chain

Increasing the length of the alkyl substituent in unmetallated Pc complexes did not change the wavelength of the Q band significantly comparing  $\text{H}_2\text{Nc}^\alpha(\text{OC}_4\text{H}_9)_8$ ,  $\text{H}_2\text{Nc}^\alpha(\text{OC}_5\text{H}_{11})_8$  and  $\text{H}_2\text{Nc}^\alpha(\text{OC}_8\text{H}_{17})_8$  [25], Table 1, with Q band ranging between 862 and 863 nm. Compare also the corresponding Pc derivatives,  $\text{H}_2\text{Pc}^\alpha(\text{OC}_4\text{H}_9)_8$ ,  $\text{H}_2\text{Pc}^\alpha(\text{OC}_5\text{H}_{11})_8$ , and  $\text{H}_2\text{Pc}^\alpha(\text{OC}_8\text{H}_{17})_8$  [25] (with Q band ranging between 761 and 762 nm) and the SnPc derivatives,  $(\text{Cl})_2\text{SnPc}^\alpha(\text{C}_6\text{H}_{13})_8$  and  $(\text{Cl})_2\text{SnPc}^\alpha(\text{C}_{10}\text{H}_{21})_8$  [43], Table 1 (with Q band at 735 nm for both), thus showing that the length of the alkyl chain does not affect the Q band.

### 2.2.4 Number of Substituents

The number of thio substituents results in a large redshift of the Q band. Alkylthio substituted TiPc complexes showed a larger redshift on increasing the number of substituents from 4 to 8; compare  $\text{CatTiPc}^\beta(\text{SC}_6\text{H}_{13})_4$  ( $\lambda = 721$  nm) and  $\text{CatTiPc}^\beta(\text{SC}_6\text{H}_{13})_8$  ( $\lambda = 741$  nm) [33]; also  $(\text{Cl})_2\text{SnPc}^\alpha(\text{SC}_{12}\text{H}_{25})_4$  and  $(\text{Cl})_2\text{SnPc}^\alpha(\text{SC}_{12}\text{H}_{25})_8$ ;  $\text{H}_2\text{Pc}^\alpha(\text{SC}_{12}\text{H}_{25})_8$  and  $\text{H}_2\text{Pc}^\alpha(\text{SC}_{12}\text{H}_{25})_4$  [47]; and  $(\text{Ac})\text{MnPc}^\alpha(\text{C}_7\text{H}_{15})_8$  and  $(\text{Ac})\text{MnPc}^\alpha(\text{C}_7\text{H}_{15})_4$  [48], Table 1.

A large shift to NIR region was in particular observed for SnPc complexes containing alkylthio substituents, Table 1, Fig. 7. The nonperipherally substituted

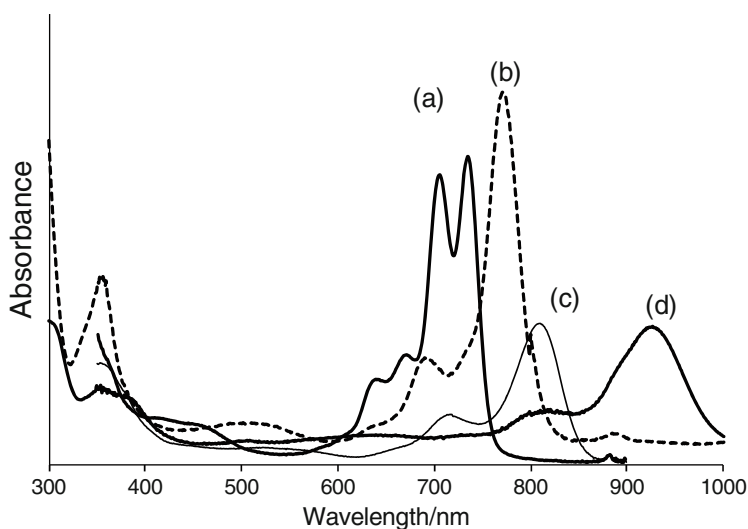


**Fig. 7** Electronic absorption spectra of (a)  $\text{H}_2\text{Pc}^\alpha(\text{SC}_{12}\text{H}_{25})_4$ , (b)  $(\text{Cl})_2\text{SnPc}^\alpha(\text{SC}_{12}\text{H}_{25})_4$ , (c)  $\text{H}_2\text{Pc}^\alpha(\text{SC}_{12}\text{H}_{25})_8$ , and (d)  $(\text{Cl})_2\text{SnPc}^\alpha(\text{SC}_{12}\text{H}_{25})_8$  in chloroform (concentration  $\sim 1 \times 10^{-6}$  M). Reproduced with permission from [47]

(Cl)<sub>2</sub>SnPc<sup>α</sup>(SC<sub>12</sub>H<sub>25</sub>)<sub>8</sub>, showed a Q band at 918 nm in chloroform [47]. The spectrum of the nonperipherally octa substituted unmetallated derivative (H<sub>2</sub>Pc<sup>α</sup>(SC<sub>12</sub>H<sub>25</sub>)<sub>8</sub>) does not show the typical split Q band [47]. As stated above, the splitting of the Q band decreases with increasing wavelength [29], hence for these complexes, a large redshift resulted in an unsplit Q band. A split Q band is observed for the less redshifted H<sub>2</sub>Pc<sup>α</sup>(SC<sub>12</sub>H<sub>25</sub>)<sub>4</sub> complex, Table 1.

### 2.3 Aggregation

Aggregation of dye molecules plays an important role in energy and electron transfer, and in light harvesting systems. The propensity of phthalocyanines to form aggregates because of the strong interactions between planar macrocycles in solution is well-known [2]. The relative geometry of the macrocycles determines the spectroscopic behavior of aggregates. According to Kasha's molecular exciton theory [49], the absorption band of aggregates will be blueshifted, Fig. 8, with respect to the monomer band when the angle between the polarization axes of monomer and the line of molecular center of the aggregate is larger than 54.7°. If the angle is 90°, the molecules are in a face-to-face fashion (the so called H-type aggregate). On the other hand, when the angle is smaller than the critical angle of 54.7°, the aggregate peak is redshifted (the so called J-type aggregate). The cofacial arrangement (common in most Pc aggregates) generally yields the blueshifted H-aggregates, whereas an edge-to-edge arrangement of the J-aggregates is less common. A SbPc complex containing *tert*-butyl substituents gave an unusually redshifted Q band upon aggregation in nonaqueous media [39]. This is unusual as redshifted (J aggregates) have been limited to water-soluble derivatives rather than nonaqueous media.

The peripheral coordination of metals on MPc complexes results in aggregation and blueshifting of the spectra [50]. Coordination of palladium to (2,3,9,10,16,17,23,24-octakis-benzyl thiophthalocyaninato) magnesium(II) [MgPc(SBz)<sub>8</sub>] and (2,3,9,10,16,17,23,24-octakis-benzhydryl thiophthalocyaninato) magnesium(II),

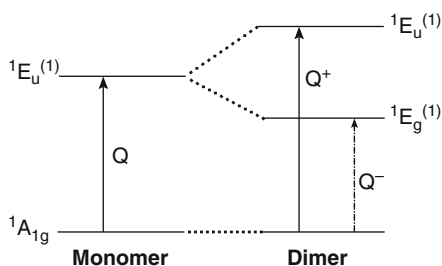


Fig. 8 Energy levels showing the transitions in aggregated MPc complexes



[MgPc(SBh)<sub>8</sub>] resulted in the formation of J aggregates [51]. It was suggested that the presence of the bulky substituents prevents the formation of the more common H aggregates. Nonperipheral substitution by bulky groups results in steric hindrance with substituents at the other 1,4-positions of the adjacent benzene ring.

## 2.4 Effect of Central Metal

### 2.4.1 Nature of Central Metal

Another method of obtaining redshifted MPc spectra is by choice of the central metal. However, the effect of the central metal in MPc complexes is usually small except for a few metals such as Mn, Sb, Bi, and V [30, 39, 44, 52].

Alkyl- or arylthio MPc, containing transition metals such as Fe and Co, do not show the NIR absorption and they remain blue or green in color [53–55], regardless of whether they are substituted at the peripheral or nonperipheral positions. However, alkyl- or arylthio substituted Mn<sup>III</sup>Pc and Ti<sup>IV</sup>Pc complexes show redshifting [12, 13]. Mn<sup>III</sup>Pc and Ti<sup>IV</sup>Pc complexes octa substituted with pentylthio groups gave Q band maxima at 893 and 808 nm [12], respectively in dichloromethane, Table 1.

It has also been observed that considering the same substituents, in (SC<sub>5</sub>H<sub>11</sub>)<sub>8</sub> there is a redshift in the Q band on going from Ti<sup>IV</sup> (808 nm) [12] to V<sup>IV</sup> (850 nm) [30] and Mn<sup>III</sup> (893 nm) [12], as the covalent radii decreases in the first transition series. This shows the strong redshifting ability of the Mn<sup>III</sup> ion with the order of redshifting decreasing as follows: Mn<sup>III</sup> > V<sup>IV</sup> > Ti<sup>IV</sup>.

Comparison of ZnPc(*t*-butyl)<sub>4</sub> with SbPc counterparts shows a redshift for the latter [39]. (Ac)Mn6a (*Q* = 745 nm) containing benzyl mercapto substituents (Table 1) has the Q band at the same position as (Ac)MnPc<sup>β</sup>(SC<sub>12</sub>H<sub>25</sub>)<sub>4</sub> (*Q* = 745 nm) [13, 34], Table 1, showing that the nature of the substituent (aryl vs. alkyl) does not affect the Q band as much as the nature of the central metal. The Mn<sup>III</sup>Pc derivatives (Cl)Mn6g and (Cl)Mn6h [35, 56, 57] did not show much effect of the substituent on the Q band. The central Mn<sup>III</sup> metal had the largest redshifting effect compared to corresponding Fe and Co derivatives [56].

OTi5c, OTi5d, OTi5e and OTi5f, Fig. 6, [31, 32] did not show much shift in the Q band with change in ring substituents. Comparison of OTi6a (714 nm [23]) with AcMn6a (745 nm [13, 34]) shows the strong effect of the central metal and also, the displacement of the central metal from the ring (as is the case with Ti in TiPc) does not necessarily result in the redshift of the Q band. CrPc<sup>β</sup>(NH<sub>2</sub>)<sub>4</sub> [58], TiPc<sup>β</sup>(NH<sub>2</sub>)<sub>4</sub> [46], and MnPc<sup>β</sup>(NH<sub>2</sub>)<sub>4</sub> [44] in DMF show Q band maxima at 735, 755, and 780 nm, Table 1, respectively, thereby showing the influence of the central metal.

The spectra of octa phenyl phthalocyanines: Pb4m, Ni4m, Zn4m, Sn4m, and H<sub>2</sub>4m [59] were studied in toluene. Ni and Zn complexes showed only slight color

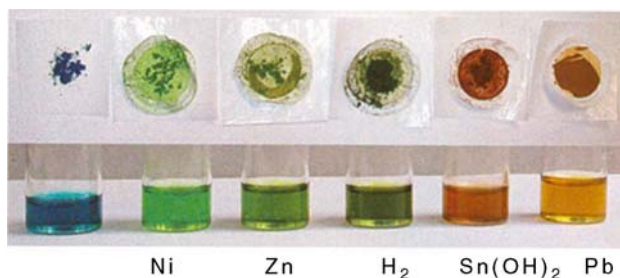


**Fig. 9** Color dependence on the central metal for complexes *4m*. Reproduced with permission from [59]

changes, but the Sn and Pb complexes showed drastically different colors, red and ochre, respectively, Fig. 9 [59], shown in Fig. 9 as different shades of grey. The changes in absorption spectra were related to the planarity of the molecules as unsubstituted SnPc and PbPc show Q band at wavelengths lower than 700 nm, showing that both Pb and Sn do not result in redshifting. The large redshift was attributed to highly deformed Pc skeleton due to the central metals not fitting into the cavity of the Pc molecule. The deformed Pc ligand then interacts with the protruding central metal, hence the observed redshift of the spectra. As discussed earlier, deformation of the Pc ligand and the electron donating nature of the substituents result in the redshifting of the Q band.

#### 2.4.2 Oxidation State of the Central Metal

Mn<sup>III</sup>Pc complex shows a redshifted Q band (with a brown solution) even in the absence of substituents, while Mn<sup>II</sup>Pc does not show redshifting and is blue or green in color depending on substituents. On electrochemical reduction of Mn<sup>III</sup>Pc or Ti<sup>IV</sup>Pc derivatives, a blueshift of the Q band is observed [12, 13], with a change of color to green or blue, Fig. 10. It thus suggests that NIR absorption is favored for MPc complexes containing central metals in a high oxidation state. The redshift is a result of the lowering of the HOMO–LUMO gap, by either destabilizing the HOMO or stabilizing the LUMO by the central metal. The Q band absorption of unsubstituted Mn<sup>III</sup>Pc is redshifted from unsubstituted Mn<sup>II</sup>Pc by 107 nm in DMF.

The Mn<sup>II</sup>Pc(OCH<sub>2</sub>C(CH<sub>3</sub>)<sub>3</sub>)<sub>16</sub> was blueshifted (to 744 nm) compared to Ni<sup>II</sup>Pc(OCH<sub>2</sub>C(CH<sub>3</sub>)<sub>3</sub>)<sub>16</sub> (at 758 nm, Table 1) containing the same substituents. Even though the Mn<sup>III</sup>Pc complexes are redshifted compared to corresponding Ni<sup>II</sup>Pc derivatives, the Mn<sup>II</sup>Pc complexes are blue shifted. The corresponding (Ac)Mn<sup>III</sup>Pc(OCH<sub>2</sub>C(CH<sub>3</sub>)<sub>3</sub>)<sub>16</sub> was highly redshifted (to 827 nm, Table 1). Thus it seems it is the Mn<sup>III</sup>Pc (not Mn<sup>II</sup>Pc) derivatives which cause a red shifting. Comparison of Mn<sup>II</sup>Pc(OCH<sub>2</sub>C(CH<sub>3</sub>)<sub>3</sub>)<sub>16</sub>, ( $\lambda = 744$  nm), (Ac)Mn<sup>III</sup>Pc(OCH<sub>2</sub>C(CH<sub>3</sub>)<sub>3</sub>)<sub>16</sub> ( $\lambda = 827$  nm), and (Ac)Mn<sup>IV</sup>Pc(OCH<sub>2</sub>C(CH<sub>3</sub>)<sub>3</sub>)<sub>16</sub> ( $\lambda = 849$  nm) clearly shows

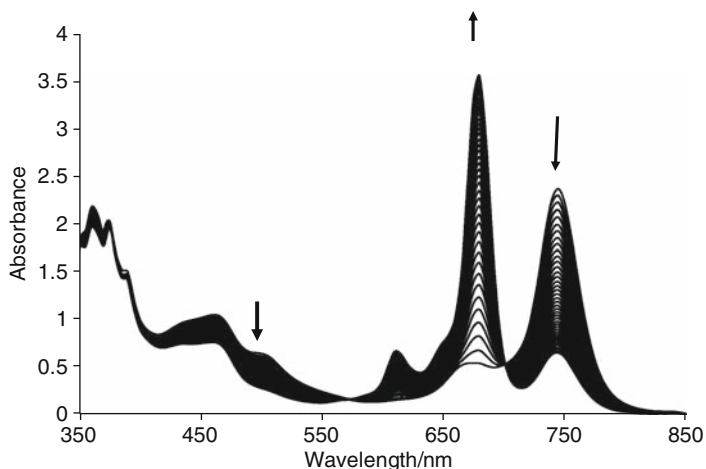


**Fig. 10** Reduction of  $\text{Mn}^{\text{III}}\text{Pc}$  solution in DMSO. Reproduced with permission from [34]

that an increase in the oxidation state shifts the Q band to the red. The redshift in the Q band  $\text{MPC}(\text{OCH}_2\text{C}(\text{CH}_3)_3)_{16}$  was explained to be either due to electronic interaction of the 16 neopentoxy groups with the Pc ring or due to steric effects of the groups leading to buckling. An INDO analysis led to the conclusion that the ring is not buckled, and that the electronic effects of the substituents were responsible for the redshift [41].

$\text{MnPc}$  derivative  $(\text{Ac})\text{Mn}^{\text{III}}\text{Pc}^\alpha(\text{C}_7\text{H}_{15})_8$  gave a Q band at 769 nm, which upon reduction to  $(\text{Ac})\text{Mn}^{\text{II}}\text{Pc}^\alpha(\text{C}_7\text{H}_{15})_8$  was blueshifted to 715 nm and further reduction resulted in the formation of the  $(\text{Ac})\text{Mn}^{\text{I}}\text{Pc}^\alpha(\text{C}_7\text{H}_{15})_8$  species, with a typical band at 610 nm [48], Table 1. As stated above, the Q band of  $\text{MnPc}$  complexes shifts to the red as the oxidation state of the Mn ion increases. Thus  $\text{Mn}^{\text{IV}}\text{Pc}$  complexes are more redshifted than  $\text{Mn}^{\text{III}}$  complexes, which in turn are more red shifted than  $\text{Mn}^{\text{II}}$  complexes [12]. This was also observed for the tetra-(2-mercaptopyridine) substituted complexes  $\text{OHMn}^{\text{III}}\mathbf{5k}$  (741 nm) and  $\text{OHMn}^{\text{II}}\mathbf{5k}$  (675 nm) [14], Table 1.

### 3 Electrochemical Properties

As Table 1 shows, the most highly redshifted  $\text{MPc}$  complexes are the ones containing Mn, V, or Ti as central metal and/or thio substituents, and those containing nonperipheral substituents. Therefore, this section deals with the electrochemical behavior of these complexes. It is well known that the position of the Q band can be related to the potential difference between the first ring oxidation and the first ring reduction, for  $\text{MPc}$ s containing nonredox active central metals.

The Pc exists as a dianion, i.e.,  $\text{Pc}^{2-}$ , which may be oxidized or reduced in successive steps. The Pc ring redox activity is directly related to the frontier orbitals in

the molecule in which oxidation is the removal of electron(s) from the HOMO ( $a_{1u}$ ) while reduction is the addition of electron(s) to the LUMO ( $e_g$ ). As stated above, up to four electrons can be successively added to the doubly degenerate  $e_g$  orbitals of the LUMO to form  $Pc^{-3}$ ,  $Pc^{-4}$ ,  $Pc^{-5}$ , and  $Pc^{-6}$ , and two electrons can be removed from the HOMO to form  $Pc^{-1}$  and  $Pc^0$ . Oxidation or reduction of MPCs with redox active metals (i.e., those with vacant or partially occupied orbitals) may occur both at the metal and at the ring depending on the relative energies and proximity of metal d and Pc ring  $\pi$  orbitals.

The nature of the central metal, axial ligands, and solvents as well as that of substituents on the ring periphery determines the redox properties of a given complex. Electron-donating substituents such as alkylthio groups, increase the electron density of the ring and the central metal atom, thereby making it easier to oxidize and harder to reduce MPC complexes. MPC redox processes may take place at the central metal atom or at the ring, and cyclic voltammetry alone cannot give information on the nature of these redox processes. Redox processes for MPC complexes occurring at the central metal or ring often result in color changes, with ring redox processes showing more drastic color changes. New peaks are formed on oxidation or reduction of the Pc ring because of transitions shown in Fig. 11.

The electrochemistry of alkyl- or arylthio substituted MPC complexes (which result in redshifted spectra, depending on the central metal) is often different from that of other substituted MPC complexes. For example irreversible ring reductions for the thio Pcs have been reported [60] often coupled with chemical reactions and adsorption of the reduction products. Overlaps of reduction couples to form

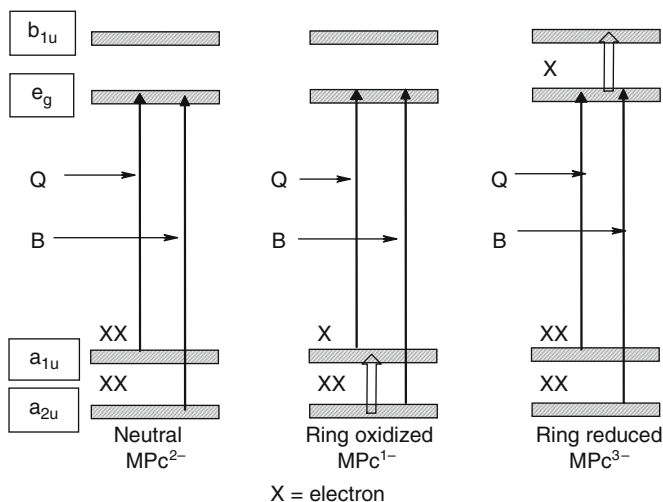


**Fig. 11** Energy level diagrams of neutral, one-electron ring oxidized, and one-electron ring reduced MPC complex

one peak, and single step (irreversible) multielectron oxidation accompanied by decomposition have also been reported [61].

### 3.1 $Mn^{III}Pc$ Complexes

By far the most studied electrochemistry of NIR complexes is that of  $Mn^{III}Pc$  derivatives. Manganese phthalocyanine complexes have very interesting electrochemistry because of the fact that the manganese metal exhibits variable oxidation states ranging from  $Mn^I$  to  $Mn^{IV}$  [8, 35, 44, 48, 58]. This makes manganese phthalocyanine complexes potential electrocatalysts for many reactions. Substituted manganese phthalocyanine complexes are still relatively few, and their electrochemistry is not fully understood. For example the first reduction in  $Mn^II Pc^{-2}$  complexes has been a subject of some controversy, with some reports proposing ring reduction to the  $Mn^II Pc^{-3}$  species and others suggesting metal reduction to the  $Mn^I Pc^{-2}$  species [14]. The spectra of  $Mn^II Pc$  and  $Mn^{III} Pc$  complexes are now well known. However, the spectra of  $Mn^{IV} Pc$  complexes are virtually unknown, except for a few studies [12, 40]. The formation of  $Mn^II Pc$  by reduction of  $Mn^{III} Pc$  derivatives occurs readily in the presence of mild reducing agents Fig. 10 (for complex **Mn6a** [34]). The change in color in going from  $Mn^{III} Pc$  to  $Mn^II Pc$  is dramatic (red to green) as was discussed in Section 2.

In  $MnPc$  complexes, the spectrum may consist of three absorption bands corresponding to three different species in solution, Fig. 12, thus complicating the electrochemistry. This is typical of  $MnPc$  species in equilibrium in the presence of oxygen [62]. The presence of the  $Mn^II$ ,  $Mn^{III}$ , and  $\mu$ -oxo  $MnPc$  species was reported [36] for **Mn6i** in DMF. In the presence of  $O_2$ ,  $Mn^II Pc$  is known to form

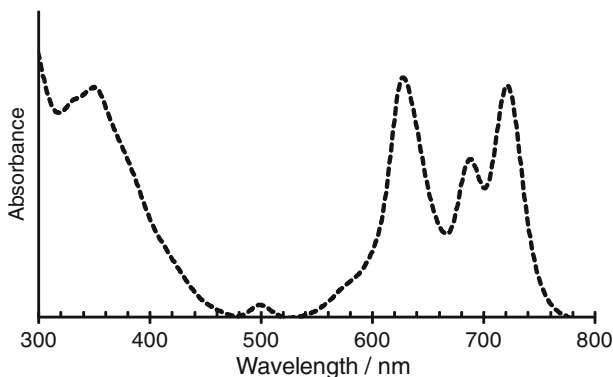
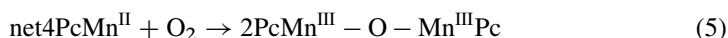
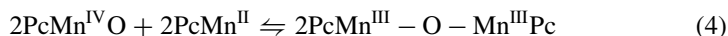
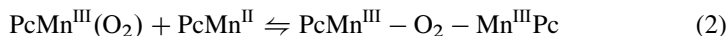
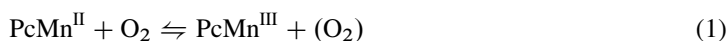


**Fig. 12** Electronic absorption spectra of **Mn6i** in DMF. Concentrations:  $5 \times 10^{-6}$  mol dm $^{-3}$ . Reproduced with permission from [36]

an oxygen adduct (1), which has been described as a  $(O_2^-)Mn^{III}Pc$  species [14, 62], with subsequent formation of the species shown by (2)–(4), and the net result shown by (5).



In Fig. 12 the absorption band at 719 nm was assigned to the  $Mn^{III}$  in complex **Mn6i** [36]. The peak at 626 nm was assigned to  $\mu$ -oxo  $MnPc$  species and the peak at 686 nm to  $Mn^{II}Pc$  [36]. When the solution was deaerated with dry  $N_2$ , the peaks due to  $Mn^{III}$  at 719 nm decreased in intensity accompanied by an increase in the intensity of the peak characteristic of  $Mn^{II}Pc$  species at 686 nm, and  $\mu$ -oxo  $MnPc$  species peak at 626 nm decreased in intensity with time on bubbling nitrogen. This shows that solution of  $MnPc$  derivatives should be thoroughly deaerated before spectra are recorded.

The shape and reversible behavior of cyclic voltammograms for  $MnPc$  derivatives are highly dependent on the substituents. The **Mn6i** complex gave a cyclic voltammogram shown in Fig. 13a. The voltammogram was recorded in solutions, in which only the  $Mn^{III}Pc$  species was present. Couples **III** ( $E_{1/2} = -0.73$  V) and **II** ( $E_{1/2} = -0.11$  V) were assigned to  $Mn^{II}Pc^{-2}/Mn^{I}Pc^{-2}$  and  $Mn^{III}Pc^{-2}/Mn^{II}Pc^{-2}$ , respectively [36], using spectroelectrochemistry. The redox processes in the region of **I** were assigned to ring-based oxidations in **Mn6i** and to the mercaptopyrimidine substituent, and **IV** and **V** to ring based reductions.

For  $(Ac)MnPc^{\beta}(SC_{12}H_{25})_4$  derivative that was tetra substituted with long-chain alkylthio substituents, the voltammograms showed broad peaks [13], Fig. 13b. For  $(Ac)MnPc^{\alpha}(SC_5H_{11})_8$  octa substituted at the nonperipheral position with relatively short alkyl chain thio substituents, clearly defined voltammograms were observed, Fig. 13c [12]. This complex exhibited four main processes labeled **I** ( $E_{1/2} = +0.71$  V), **II** ( $E_{1/2} = +0.43$  V), **III** ( $E_{1/2} = -0.51$  V), and **IV** ( $E_{1/2} = -1.29$  V) vs.  $Ag|AgCl$ , Table 2, whose cathodic to anodic peak separations suggested slow electron transfer. Processes **II** and **I** were assigned (using spectroelectrochemistry) to  $Mn^{IV}Pc^{-2}/Mn^{III}Pc^{-2}$  and  $Mn^{IV}Pc^{-1}/Mn^{IV}Pc^{-2}$ , respectively, and **III** and **IV** to  $Mn^{III}Pc^{-2}/Mn^{II}Pc^{-2}$  and  $Mn^{II}Pc^{-2}/Mn^{II}Pc^{-3}$ , respectively, Table 2.

$MnPc$  complexes, tetra substituted with 2-mercaptopyridine at the  $\alpha$  (**Mn5j**) and  $\beta$  (**Mn6j**) positions and then quaternized to give **Mn5k** and **Mn6k** respectively, showed similar cyclic voltammograms (except for difference in redox potentials), Fig. 13d. Complexes **Mn5j** and **Mn6j** and their quaternized derivatives, **Mn5k** and **Mn6k**, showed three well-resolved reduction processes labeled **I**, **II**, and **III**, Table 2

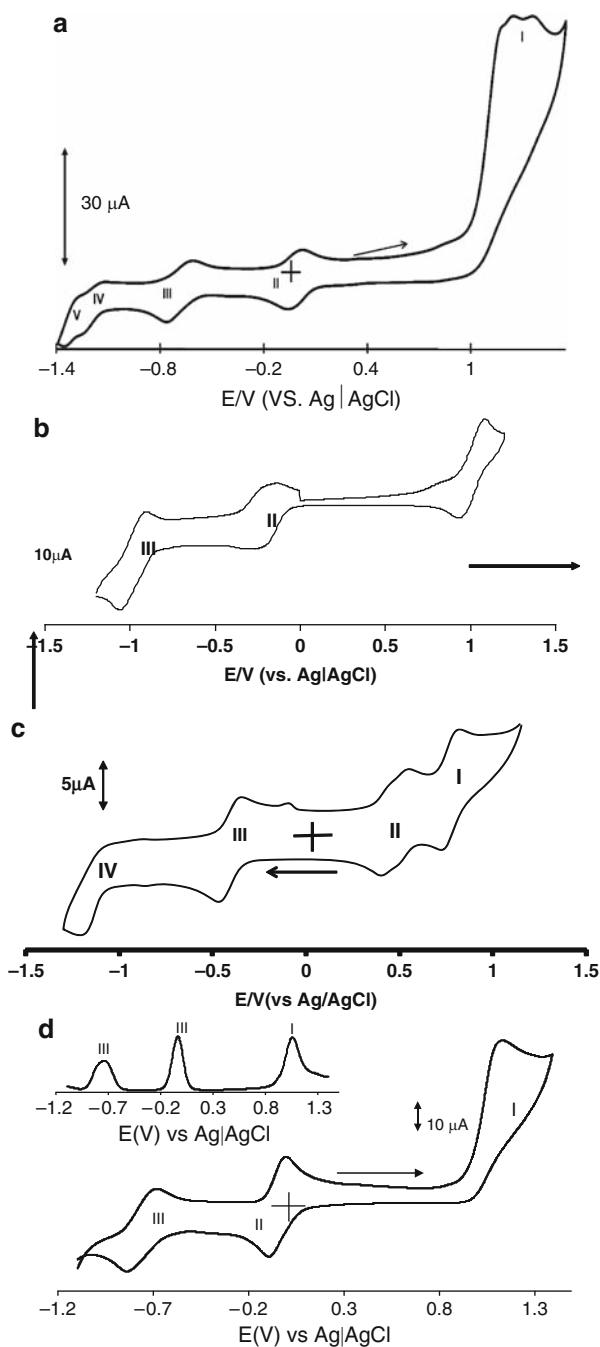


**Fig. 13** Cyclic voltammograms of **Mn6i** (a) [36],  $\text{MnPc}^\beta(\text{C}_{12}\text{H}_{25})_4$  (b) [13],  $\text{MnPc}^\alpha(\text{SC}_5\text{H}_{11})_8$  (c) [12] and **Mn5j** [14] (d) in DMF containing TBABF<sub>4</sub>. Scan rate = 100 mV s<sup>-1</sup>. Reproduced with permission from [12–14, 36]. The starting points were: -1.4 V (a); 0 V (b), +1.5 V (c) and -1.1 V (d)

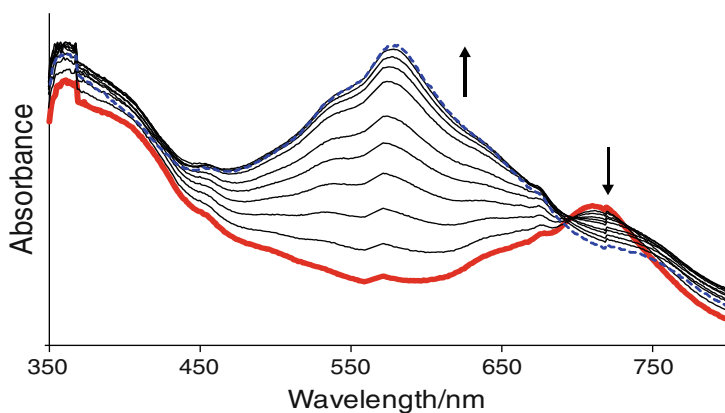


**Fig. 14** UV-Vis spectral changes for **Mn5j** observed using controlled potential electrolysis at potential of process **III** ( $-700$  mV). Electrolyte = DMF containing  $0.1$  M TBABF<sub>4</sub>. Electrolysis time was 30 min for each redox process. Reproduced with permission from [14]

[14]. Chronocoulometry showed that the ratios of currents for processes **II** and **III** were equal, and were one-third of that of process **I**. The latter is most probably due to the combination of Pc ring oxidation and the oxidation of thio substituents. Compared to corresponding peripherally alkylthio substituted derivatives (**Mn6j** and **Mn6k**), nonperipherally substituted complexes **Mn5j** and **Mn5k** are more difficult to reduce, Table 2, considering the second reductions.

As stated already, the first reduction in  $\text{Mn}^{\text{II}}\text{Pc}^{-2}$  complexes has been a subject of some controversy, with some reports proposing ring reduction to the  $\text{Mn}^{\text{II}}\text{Pc}^{-3}$  species and others suggesting metal reduction to the  $\text{Mn}^{\text{I}}\text{Pc}^{-2}$  species. Table 2 also shows that both  $\text{Mn}^{\text{I}}\text{Pc}^{-2}$  and  $\text{Mn}^{\text{II}}\text{Pc}^{-3}$  are obtained under different conditions. For the 2-mercaptopyridine tetra substituted complexes **Mn5j** and **Mn6j** and their quaternized derivatives, **Mn5k** and **Mn6k**, spectroelectrochemistry showed that the reduction of  $\text{Mn}^{\text{II}}\text{Pc}$  to  $\text{Mn}^{\text{I}}\text{Pc}$  occurs only when the complexes are in their quaternized form (**Mn5k** and **Mn6k**). The reduction (to  $\text{Mn}^{\text{I}}\text{Pc}^{-2}$ ) of the quaternized form occurs at a lower potential than that of the unquaternized form (to  $\text{Mn}^{\text{II}}\text{Pc}^{-3}$ ), showing that metal reduction (to  $\text{Mn}^{\text{I}}\text{Pc}^{-2}$ ) vs. ligand reduction (to  $\text{Mn}^{\text{II}}\text{Pc}^{-3}$ ) in  $\text{Mn}^{\text{II}}\text{Pc}$  complexes depends on the nature of the ring substituents. The reduction to  $\text{Mn}^{\text{I}}\text{Pc}^{-2}$  species has a distinct broad absorption at 575 nm (Fig. 14), typical of  $\text{Mn}^{\text{I}}\text{Pc}$  species [14].

Comparison of the peripherally and nonperipherally substituted tetra amino phthalocyanine complexes of  $\text{Mn}((\text{OH})\text{Mn}\text{Pc}^{\beta}(\text{NH}_2)_4)$  with  $(\text{OH})\text{Mn}\text{Pc}^{\alpha}(\text{NH}_2)_4$ , shows that the nonperipherally substituted derivatives are slightly more difficult to reduce (considering second reductions), Table 2 [44, 45]. Substitution at the nonperipheral position, using electron donating substituents, results in greater enhancement of electron density compared to peripheral substitution, and hence should result in ease of oxidation, and more difficult reduction as shown in some cases Table 2.



**Table 2** Electrochemical data of MnPc complexes<sup>a</sup>

Complex	$\text{Mn}^{\text{II}}\text{Pc}^{-2} / \text{Mn}^{\text{III}}\text{Pc}^{-2}$		$\text{Mn}^{\text{III}}\text{Pc}^{-2} / \text{Mn}^{\text{IV}}\text{Pc}^{-2}$		Ring oxidation processes	Solvent/Electrolyte <sup>b</sup>	References
	$\text{Mn}^{\text{II}}\text{Pc}^{-2} / \text{Mn}^{\text{III}}\text{Pc}^{-3}$	$\text{Mn}^{\text{III}}\text{Pc}^{-2} / \text{Mn}^{\text{IV}}\text{Pc}^{-2}$	$\text{Mn}^{\text{III}}\text{Pc}^{-2} / \text{Mn}^{\text{IV}}\text{Pc}^{-2}$	$\text{Mn}^{\text{IV}}\text{Pc}^{-2} / \text{Mn}^{\text{III}}\text{Pc}^{-2}$			
(Ac)MnPc <sup>α</sup> (SC <sub>3</sub> H <sub>11</sub> ) <sub>8</sub>	-1.29	-0.51	0.43	0.71	0.71	DCM/TBAPF <sub>4</sub>	[12]
(AcO)Mn6a	-0.89	-0.13	~0.3	0.83	0.83	DMF/TBAPF <sub>4</sub>	[13]
(Ac)MnPc <sup>β</sup> (SC <sub>12</sub> H <sub>25</sub> ) <sub>4</sub>	-1.03	-0.31	~0.3	0.79, 1.02	0.79, 1.02	DMF/TBAPF <sub>4</sub>	[13]
(Cl)Mn6g	-1.00	-0.28		0.71, 1.12	0.71, 1.12	DMF/TBAPF <sub>4</sub>	[35]
Mn6i		-0.11				DMF/TBAPF <sub>4</sub>	[36]
(OH)MnPc <sup>β</sup> (NH <sub>2</sub> ) <sub>4</sub>	-1.03	-0.35	0.54	0.71	0.71	DMF/TBAPF <sub>4</sub>	[44]
(OH)MnPc <sup>α</sup> (NH <sub>2</sub> ) <sub>4</sub>	-1.11	-0.35		0.52, 0.75, 1.01 (NH <sub>2</sub> )	0.52, 0.75, 1.01 (NH <sub>2</sub> )	DMF/TBAPF <sub>4</sub>	[45]
(OH)Mn5j	-0.81	-0.096		1.14	1.14	DMF/TBAPF <sub>4</sub>	[14]
(OH)Mn5k		-0.10		1.06	1.06	DMF/TBAPF <sub>4</sub>	[14]
(OH)Mn6j	-0.76	-0.10		1.30	1.30	DMF/TBAPF <sub>4</sub>	[14]
(OH)Mn6k		-0.11	1.09			DMF/TBAPF <sub>4</sub>	[14]
ClMn6h	-0.70	0.11				DMF/TEAP	[56]
(Ac)MnPc-(OCH <sub>2</sub> C(CH <sub>3</sub> ) <sub>3</sub> ) <sub>16</sub>		-0.41	0.72	1.04	1.04	THF/TBAP	[40]
(Ac)MnPc-(cyclohexylmethoxy) <sub>16</sub>	-0.89	-0.60				THF/TBAP	[40]
(Ac) <sup>α</sup> MnPc(C <sub>7</sub> H <sub>15</sub> ) <sub>8</sub>		-0.21		1.0, 1.63	1.0, 1.63	DCM/TBAPF <sub>6</sub>	[48]
(Ac) <sup>β</sup> MnPc(C <sub>7</sub> H <sub>15</sub> ) <sub>8</sub>		-1.17		0.79, 1.31	0.79, 1.31	DCM/TBAPF <sub>6</sub>	[48]

(continued)

Table 2 (continued)

(B) <i>TiPc complexes</i>						
Complex	$Ti^{III}Pc^{-2}/Ti^{II}Pc^{-2}$	$Ti^{IV}Pc^{-2}/Ti^{III}Pc^{-2}$	Ring oxidation processes	Solvent/electrolyte <sup>a</sup>	References	
$OTiPc^e(SC_5H_{11})_8$	-1.14	-0.78	0.59, 0.39, 1.0		[12]	
$OTi6a$	-0.37	-0.07	-	DMF/TBABF <sub>4</sub>	[23]	
$OTi6b$	-0.42	-0.09	-	DMF/TBABF <sub>4</sub>	[23]	
$OTi5a$	-0.40	-0.09	-	DMF/TBABF <sub>4</sub>	[23]	
$OTi5b$	-0.46	-0.07	-	DMF/TBABF <sub>4</sub>	[23]	
$OTiPc^b(NH_2)_4$	-0.85	-0.47	0.71, 0.94	DMF/TBABF <sub>4</sub>	[46]	
$OTiPc^e(NH_2)_4$	-0.89	-0.49	0.71, 0.87, 1.24	DMF/TBABF <sub>4</sub>	[45]	
(C) <i>Redox inactive metals</i>						
Complex	Ring reductions	Ring oxidations	Solvent/electrolyte	References		
H <sub>2</sub> 4m	-0.90	0.39	o-DCB/TBAP	[59]		
Ni4m	-0.97	0.64	o-DCB/TBAP	[59]		
Zn4m	-1.32	0.27	o-DCB/TBAP	[59]		
(OH) <sub>2</sub> Sn4m	-0.46	0.98	o-DCB/TBAP	[59]		
Pb4m	-0.94	0.27	o-DCB/TBAP	[59]		
$OVPC^e(SC_5H_{11})_8$	-0.54, -0.89, -1.14	0.68, 1.02	DCM/TBABF <sub>4</sub>	[30]		
$OVPC(OC_6H_5(t\text{-butyl}))_2,4$	-0.62, -1.12, -2.07	0.76, 1.21	DMF/TBAP	[64]		
$OVPC(C_8H_{17})_4$	-0.51, -0.97, -1.94	0.94, 1.34	DMF/TBAP	[64]		

<sup>a</sup>Half-wave potential ( $E_{1/2}$ ) vs. saturated calomel electrode (SCE). Values vs. Ag/AgCl or Fc<sup>+</sup>/Fc have been converted to vs. SCE using a conversion factor of 0.045 V or 0.49, respectively [96]. <sup>b</sup>DMF = dimethylformamide, DMSO = dimethylsulfoxide, DCM = dichloromethane, DCEB = dichlorobenzene, THF = tetrahydrofuran, TBAP = tetrabutyl ammonium perchlorate, TBABF<sub>4</sub> = tetrabutylammonium tetrafluoroborate, *t*-butyl = *tert*-butyl

Comparison of  $(\text{Ac})^\alpha\text{MnPc}(\text{C}_7\text{H}_{15})_8$  and  $(\text{Ac})^\beta\text{MnPc}(\text{C}_7\text{H}_{15})_8$  showed the latter to be more difficult to reduce than the former, Table 2 [48], contradicting the observation above.  $(\text{Ac})\text{MnPc}(\text{cyclohexylmethoxy})_{16}$  is more difficult to reduce compared to  $(\text{Ac})\text{MnPc}(\text{OCH}_2\text{C}(\text{CH}_3)_3)_{16}$  [40].

### 3.2 TiPc and VPc Complexes

Like MnPc derivatives, titanium phthalocyanine (TiPc) complexes also exhibit variable oxidation states. For TiPc octa substituted at nonperipheral positions with pentythio substituents,  $(\text{OTiPc}^\alpha(\text{SC}_5\text{H}_{11})_8)$ , four main redox processes (**I–IV**) are observed in Fig. 15. Couples **III** ( $-0.78$  V vs. SCE) and **IV** ( $-1.14$  V vs. SCE) are well defined and reversible, and are both due to metal based processes. Couples **III** and **IV** shifted to more positive potentials with scan number (Fig. 15) probably because of polymerization effects discussed in the following section. The oxidation processes for  $\text{OTiPc}^\alpha(\text{SC}_5\text{H}_{11})_8$  showed a peculiar behavior in that the anodic process **II** had a broad prepeak followed by a sharp peak typical of adsorption [12, 63]. During the first scan, Fig. 15, a broad peak preceding a sharp peak around 0.5 V was observed. The cathodic (return) scan of process **II**, Fig. 15, showed a sharp peak corresponding to the peak observed in the forward direction. It was observed that the cyclic voltammograms obtained for second and subsequent scans showed additional weak peaks (at  $\sim 0, 0.14$  and  $0.75$  V), most likely because of the polymer formed on cycling the monomer in solution. Electropolymerisation of the complex onto the electrode may be facilitated through radical polymerization from sulfur groups, as is the case with amino groups in MPc complexes [44].

The redox potentials for  $\alpha\text{-OTiPc}(\text{NH}_2)_4$  and  $\beta\text{-OTiPc}(\text{NH}_2)_4$  complexes are similar, though the former is slightly more difficult to reduce as was observed

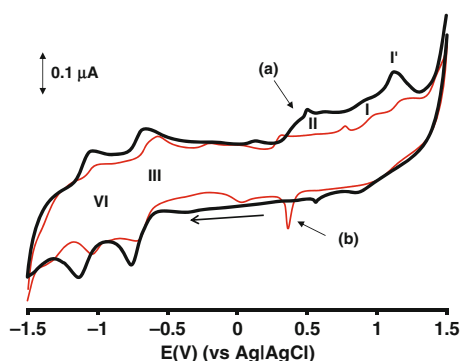
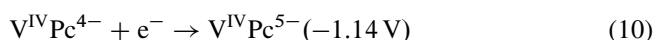
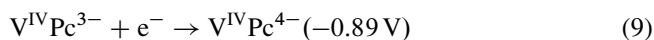
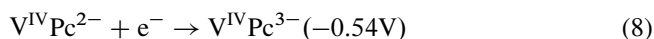
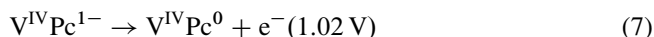
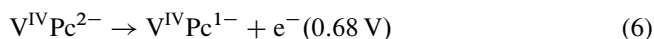


**Fig. 15** Cyclic voltammogram of  $\text{OTiPc}^\alpha(\text{SC}_5\text{H}_{11})_8$  in DCM containing 0.1 M TBABF<sub>4</sub>. (a) first scan and (b) 20th Scan. Scan rate =  $100 \text{ mV s}^{-1}$ . Reproduced with permission from [12]

for the corresponding MnPc complexes [45, 46]. Similarly for peripherally substituted **OTi6a** and the corresponding nonperipherally substituted **OTi5a**, the latter is slightly more difficult to reduce compared to the former, Table 2.

For  $\text{OVPC}^\alpha(\text{SC}_5\text{H}_{11})_8$ , the redox processes were observed at  $E_{1/2} = 1.02, 0.68, -0.54, -0.89,$  and  $-1.14$  V, vs.  $\text{Ag}|\text{AgCl}$ , Table 2. All are ring based processes [30]. On the basis of the electrochemical and spectroelectrochemical data these processes were assigned as follows:



The VPc complexes are reduced at approximately the same potential, Table 2 [30, 64, 65]. The UV-Vis spectral changes observed for the reduction of the  $\text{OVPC}^\alpha(\text{SC}_5\text{H}_{11})_8$  complex did not show the typical [15] spectra for ring reduction, Fig. 16. Complexes **Zn4m** and **H24m** are readily oxidized because of the deformed nature of the ring [59, 66], Table 2.

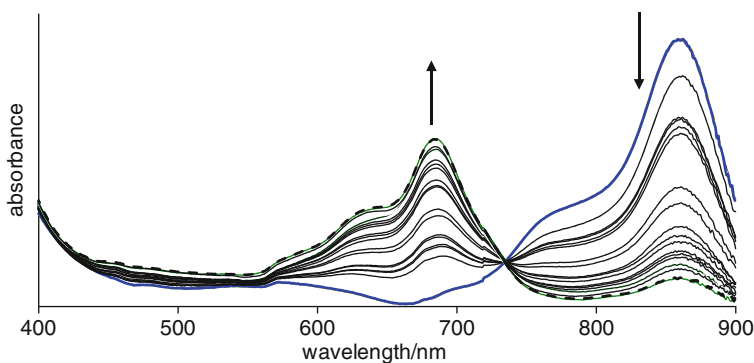


**Fig. 16** UV-Vis spectral changes for  $(\text{OVPC}^\alpha(\text{SC}_5\text{H}_{11})_8)$ , observed using controlled potential electrolysis at potentials for the first reduction. Electrolyte = DCM containing 0.1 M TBABF<sub>4</sub>. Electrolysis time was 30 min. Reproduced with permission from [30]

## 4 Electrocatalytic Behavior

The use of MPc complexes as electrocatalysts for the detection of analytes relies on the formation of modified electrodes. Thiol, alkylthio, or arylthio substituted MPc complexes readily form self-assembled monolayers (SAMs) on gold. Amino substituted MPc complexes can easily be electropolymerized onto electrodes. Direct adsorption of the monomer onto electrodes (especially carbon electrodes) also occurs. The modified electrodes are then employed for detection of analytes ranging from neurotransmitters, thiols, phenols, and other biologically and environmentally important molecules.

### 4.1 Self-Assembled Monolayer (SAM)

A SAM is a self-organized array of molecules chemically bound onto a solid substrate, forming reproducible stable films. Such a single layer of highly oriented molecules on a substrate is formed spontaneously on immersing a solid substrate into a solution containing the desired species with an appropriate functional group. Vacuum deposition has also been reported for SAM formation [67, 68]. SAMs have been formed on electrodes (surfaces) such as gold, silver, platinum, mercury [69], InSb [70], and graphite [67], but the most common ones are those formed by reactions of thiols at gold surfaces. Careful placement of thio groups can constrain the Pc molecule to a particular packing preference on the surface.

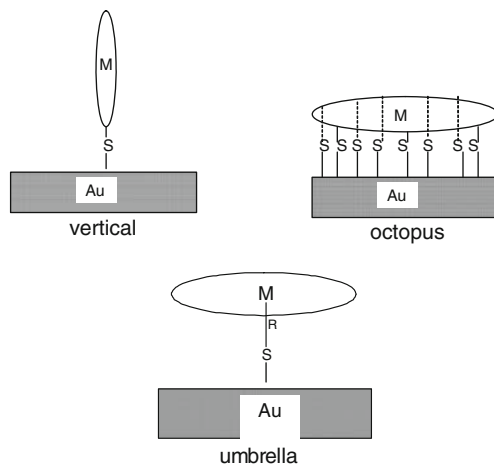


Fig. 17 Representations of octopus, vertical, and umbrella orientations of MPC-SAM

### 4.1.1 Ring Substituted MPc Complexes

The orientation of SAMs on gold (Fig. 17) is affected by factors such as the number and nature of substituents on the phthalocyanine ring, and axial, as opposed to ring, substitution. The electrocatalytic behavior of MPc SAM is strongly influenced by its orientation on the gold surface [71, 72]. Several techniques have been employed for the analyses of SAMs. X-ray photoelectron spectroscopy (XPS) was used to confirm the attachment and orientation of MPc complexes onto the gold surface [73]. Transmission Fourier transform infrared (FTIR) spectroscopy and reflection absorption infrared spectroscopy (RAIRS) have also been employed in confirming the formation of SAMs and showing the effects of ring substituents on SAM formation [74, 75]. Electrochemical methods have also been used to confirm SAM formation, using the blocking of well established Faradaic processes such as gold surface oxidation, solution redox chemistry of  $[\text{Fe}(\text{H}_2\text{O})_6^{3+}]/[\text{Fe}(\text{H}_2\text{O})_6^{2+}]$ , and underpotential deposition (UPD) of copper on formation of SAMs. The blocking of the gold electrode is evidenced by a drastic decrease in currents in the presence of SAM, showing that the gold electrode is no longer available to the electrolyte because of the presence of SAMs.

Another method employed for characterizing SAMs is the scanning electrochemical microscopy (SECM), Fig. 18 [76]. Clear dissimilarities in surface topography can be observed between the unmodified gold surface and **AcMn5b**-SAM modified surface in Fig. 18. The differences in topography and surface conductivity proved that the **AcMn5b** did attach to the gold surface forming a dense SAM. Also, the relatively high currents indicate that the unmodified gold electrode surface is, as expected, highly conductive.

Cook and coworkers have synthesized disulfide MPcs and a number of thiol substituted MPc complexes containing single tethers at nonperipheral positions [74, 75, 77, 78]. This resulted in SAMs which were tilted at various angles to the gold surface which depended on the length of the tether chain length [78], represented as vertical in Fig. 17. In order to control the orientation of the thiol MPc-SAMs, Li et al [73] synthesized octa substituted MPc complexes containing terminal SH groups. The orientation of the octa-substituted thiol MPc onto the gold surface was described as octopus (Fig. 17). However, it was found that not all of the eight thiol linkers on the periphery of the ring bound to the gold surface at the same time [73]. 2,9,16-Tri(*tert*-butyl)-23-(10-mercaptodecyloxy) phthalocyanine and its disulfide were employed as SAMs on Au [79], and triple decker porphyrin (Por)/phthalocyanines (Pc) of the form PcEuPcEuPor, di- or mono-substituted with acetyl thio groups have been used to form SAMs on Au [80]. SAMs of NIR MnPcs have been formed using alkyl- or arylthio ring substituted MnPc complexes [34]. SAMs of redshifted MPc complexes such as alkylthio MPc have generally been the tetra substituted derivatives [13]. SAMs of **AcMn6a** and (Ac)MnPc <sup>$\beta$</sup> (SC<sub>12</sub>H<sub>25</sub>)<sub>4</sub> showed the Mn<sup>IV</sup>/Mn<sup>III</sup> couple at  $\sim 0.3$  V [13].

SAMs of the substituted MPc complexes containing terminal R groups were found to form without cleavage of the C–S bonds [81, 82]. Also, when the terminal R group contained an OH function, octopus (horizontal) orientation was not obtained;

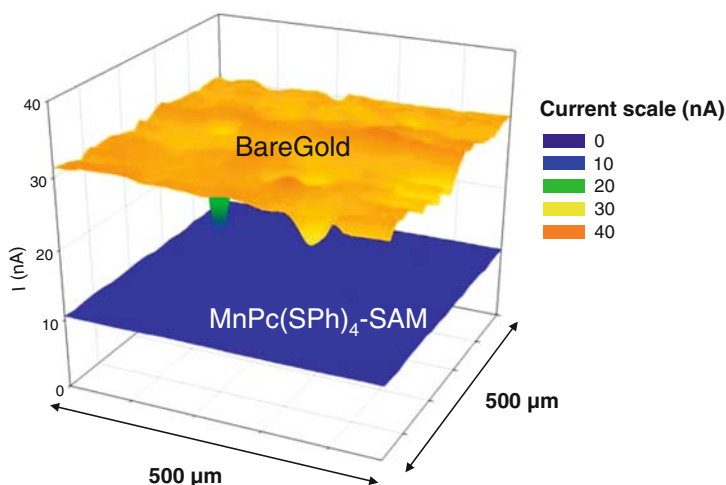


**Fig. 18** Scanning electrochemical microscope (SECM) surface images of bare gold electrode (*top*) and **AcMn5b** modified gold electrode (*bottom*) containing 5 mM ferrocyanide as redox mediator in phosphate buffer. Reproduced with permission from [76]

the molecules were oriented in a vertical position (Fig. 17), and this was explained in terms of electrostatic repulsion in the presence of OH groups [81]. MPC complexes containing axial thiol groups form SAMs which are described as umbrella shaped [73, 83] Fig. 17. The SiPc containing a short tether in the axial position was reported to form an ordered (umbrella) monolayer on gold. However, not much work has been done on these types of SAMs.

#### 4.1.2 MPcs Coordinated to Preformed SAMs

MPC complexes may coordinate to SAMs formed from simple thiols such as 2-mercaptoethanol (2-ME), referred to as preformed SAMs (in this case 2-ME-SAM) [84–87]. The attachment of MPC to preformed SAM occurs through formation of a bond between the exposed functional group of the preformed SAM (such as the OH of 2-ME) and axial or ring substituent on the MPC, forming for example MPC-2-ME-SAM. In the first case (coordination via axial substituents), there is no need for the time consuming synthesis of ring substituted MPC complexes. Unsubstituted MPC complexes have been bound to gold surface through preformed SAMs containing N-donor ligands such as 4-mercaptopyridine (4-MPy) [84–86] in an umbrella form as shown in Fig. 17. In the second case umbrella type SAMs may also be formed by first synthesizing MPC complexes axially coordinated with groups which can self-assemble on a metal surface. For example RuPc, bearing pyridine-4-carboxaldehyde as an axial ligand, formed a SAM through linking of the exposed

carboxaldehyde ligand with the chemically modified surface [88]. The use of simple (often commercially available) ring substituted MPc complexes and coordinating them to preformed SAMs via the ring substituents is also known [87].

## 4.2 Other Forms of Electrode Modification

As stated above, amino substituted MPc complexes can easily be electropolymerized onto electrodes [45,46,89–93]. Polymerization is effected by scanning the electrode in the solution of the monomer within a well-defined potential range. Growth of the polymeric films or more precisely, control of the amount of deposited materials (or the polymer film thickness) can be easily achieved by monitoring the total charge passed during the electrooxidative polymerization process. Figure 19a shows a series of CVs (30 scans) during electropolymerisation of (OH)MnPc(NH<sub>2</sub>)<sub>4</sub> cycled in the potential range of  $-0.6$  to  $1.0$  V vs. Ag|AgCl. Similarly for OTiPc(NH<sub>2</sub>)<sub>4</sub>, electropolymerisation was achieved through repetitive cycling of the monomer, Fig. 19b. Electropolymerization is evidenced by the first voltammetric scan being different from the second and subsequent scans, Fig. 19. The shifts and formation of new peaks confirm the formation of an electroactive polymer on the electrode surface.

The success of the polymerization depends on the solvent used for the process. Most studies of electropolymerized MPc have concentrated on the electrochemical polymerization of MPc(NH<sub>2</sub>)<sub>4</sub> complexes [89–93]. The polymerization process of these complexes involves the oxidation of the amino group forming radicals which attack phenyl rings of neighboring molecules [93]. The formation of the polymers of (OH)MnPc(NH<sub>2</sub>)<sub>4</sub> and OTiPc(NH<sub>2</sub>)<sub>4</sub> on glassy carbon electrode (GCE) was successfully achieved via electropolymerisation of these complexes in DMF by repetitive scanning at a constant scan rate of  $0.1$  Vs<sup>-1</sup>. Simple adsorption of the monomer onto carbon electrodes (using MnPc derivatives) has been reported [94].

## 4.3 Electrocatalytic Detection of Selected Analytes

The detection of many analytes on unmodified electrodes occurs at high potentials, hence the need for modified electrodes. Even though different types of SAMs have been reported, only a few of them have been employed as catalysts for electrochemical reactions. Most work has concentrated on the characterization of SAMs, with limited studies devoted to detection. Table 3 summarizes the analytes which have been detected by employing NIR-absorbing MPcs (such as MnPc and TiPc) containing amino or alkylthio substituents. In Table 3, the electrodes are modified by SAMs, polymers, electrodeposition, and adsorption.



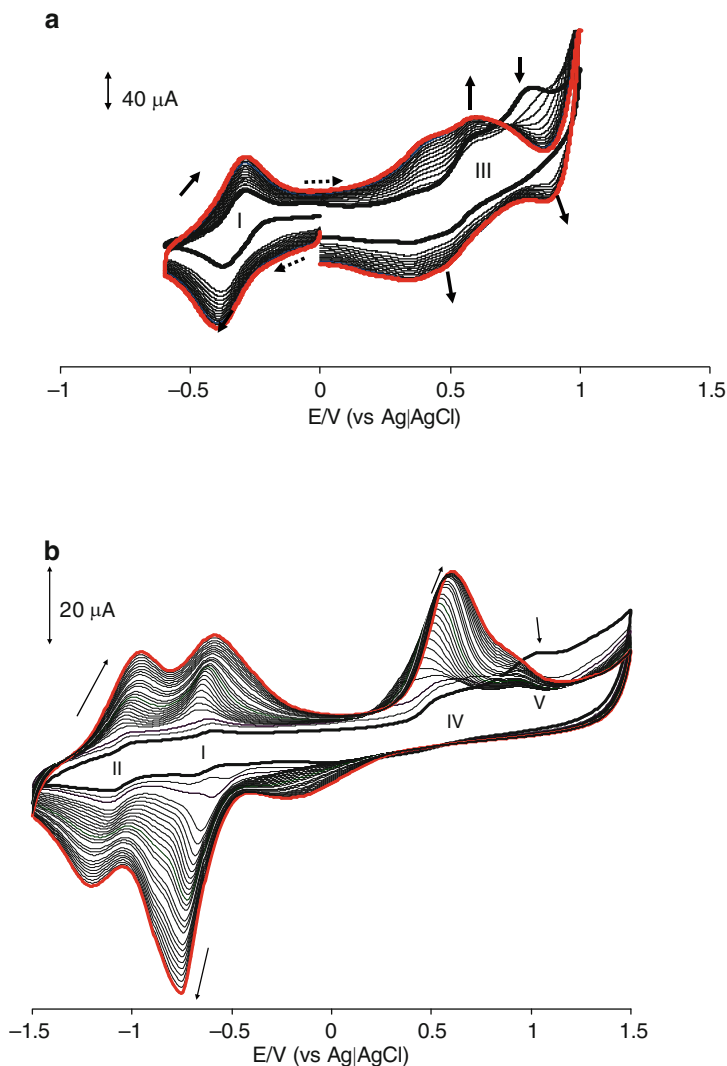


**Fig. 19** Evolution of cyclic voltammograms on GCE in DMF containing 0.1 M TBABF<sub>4</sub> during repeated successive scans showing the formation of (a)  $\text{poly}-(\text{OH})\text{MnPc}^\alpha(\text{NH}_2)_4$  and (b)  $\text{poly-OTiPc}^\alpha(\text{NH}_2)_4$ . Scan rate = 100  $\text{mVs}^{-1}$ . Reproduced with permission from [45]

### 4.3.1 Nitrite

The modified electrodes were investigated for catalysis of nitrite electrooxidation in pH 7.4 phosphate buffer solution. Nitrite disproportionation to nitric oxide (NO) is insignificant at this pH and thus the catalysis monitored is that of nitrite oxidation. Nitrite oxidation occurred at 0.71 V on the SAM of **Mn5b** [76], at 0.63 V on polymerized  $\text{OTiPc}^\alpha(\text{NH}_2)_4$  [45], and at 0.65 V on polymerized  $\text{MnPc}^\alpha(\text{NH}_2)_4$

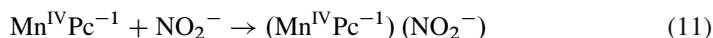
**Table 3** Selected analytes electrocatalysed by MnPc and TiPc derivatives

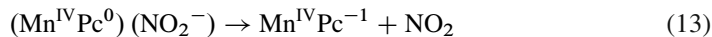
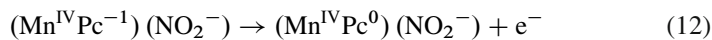
Complex	Electrode and mode of modification	Analyte	$E_p/V$ (SCE)	Medium	References
MnPc <sup><math>\beta</math></sup> (NH <sub>2</sub> ) <sub>4</sub>	GCE, polymer	Glycine	-0.67 (R)	pH 7.4	44
MnPc	Au, preformed SAM	Cysteine	0.20 (O)	pH 4	86
MnPc	Au, preformed SAM	Thiocyanate	0.50 (O)	pH 4	86
MnPc	GCE, adsorption	Oxygen	-0.51 (R)	pH 12	94
MnPc <sup><math>\beta</math></sup> (NH <sub>2</sub> ) <sub>4</sub>	GCE, adsorption	Oxygen	-0.55 (R)	pH 12	94
Mn6h	GCE, adsorption	Oxygen	-0.69 (R)	pH 12	94
Mn6i	GCE, adsorption	Oxygen	-0.61 (R)	pH 12	94
Mn6g	GCE, adsorption	Oxygen	-0.67 (R)	pH 12	94
MnPc <sup><math>\alpha</math></sup> (NH <sub>2</sub> ) <sub>4</sub>	GCE, polymer	Nitrite	0.65(O)	pH 7.4	45
Mn5b	Au, SAM	Nitrite	0.71 (O)	pH 7	76
Mn6a	Au, electrodeposition	Nitrite	0.72 (O)	pH 7.4	34
Mn(CH <sub>2</sub> (CH <sub>2</sub> ) <sub>10</sub> CH <sub>2</sub> S) <sub>4</sub>	Au, electrodeposition	Nitrite	0.75(O)	pH 7.4	34
TiPc <sup><math>\alpha</math></sup> (NH <sub>2</sub> ) <sub>4</sub>	GCE, polymer	Nitrite	0.63(O)	pH 7.4	45
TiPc <sup><math>\beta</math></sup> (NH <sub>2</sub> ) <sub>4</sub>	GCE, polymer	Nitrite	0.65 (O)	pH 7.4	46
Ti5a	GCE, polymer	Nitrite	0.60 (O)	pH 7.4	95
Ti6b	GCE, polymer	Nitrite	0.65 (O)	pH 7.4	95
Ti6a	GCE, polymer	Nitrite	0.63 (O)	pH 7.4	95
Ti6b	GCE, polymer	Nitrite	0.55 (O)	pH 7.4	95
Ti5c	GCE-adsorption	Nitrite	0.71 (O)	pH 7.4	46
Ti5d	GCE-adsorption	Nitrite	0.73(O)	pH 7.4	46
Ti5e	GCE-adsorption	Nitrite	0.66 (O)	pH 7.4	46
Ti5f	GCE-adsorption	Nitrite	0.70(O)	pH 7.4	46
Ti6c	GCE-adsorption	Nitrite	0.73 (O)	pH 7.4	46
Ti6d	GCE-adsorption	Nitrite	0.73(O)	pH 7.4	46
Ti6e	GCE-adsorption	Nitrite	0.62(O)	pH 7.4	46
Ti6f	GCE-adsorption	Nitrite	0.64(O)	pH 7.4	46

Values vs. Ag|AgCl or Fc<sup>+</sup>/Fc have been converted to vs. SCE using a conversion factor of 0.045 V or 0.49, respectively [96]. GCE = glassy carbon electrode, O = oxidation, R = reduction

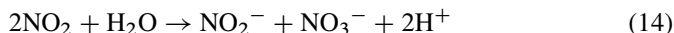
[45]. Thus the overpotential was lowered from 0.92 V at the bare electrode to 0.65 and 0.63 V at the polymerized MnPc <sup>$\alpha$</sup> (NH<sub>2</sub>)<sub>4</sub> and OTiPc <sup>$\alpha$</sup> (NH<sub>2</sub>)<sub>4</sub> modified electrodes, respectively. Hence the central Mn and Ti metals did not differ much in terms of lowering the nitrite oxidation potential. Also there was no significant influence on the point of substitution (OTiPc <sup>$\beta$</sup> (NH<sub>2</sub>)<sub>4</sub> vs. OTiPc <sup>$\alpha$</sup> (NH<sub>2</sub>)<sub>4</sub>) on the oxidation potential of nitrite, Table 3. Oxidation of nitrite occurred at potentials ranging from 0.55 to 0.75 V on TiPc and MnPc derivatives, Table 3 [34, 45, 46, 95].

The proposed mechanism for the electrocatalytic oxidation of nitrite on **Mn5b**-SAM is as given by (11)–(14) [76]:

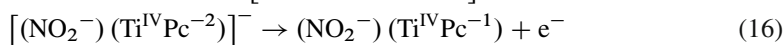




And the  $\text{NO}_2$  species may then disproportionate to give nitrite and nitrate as follows:



For TiPc derivatives in which only ring-based oxidation processes are possible, the following mechanism was proposed [46], (15)–(17):



### 4.3.2 Cysteine

The oxidation of L-cysteine on MPc ( $M = \text{Fe}, \text{Mn}, \text{and Co}$ ) linked to 4-mercaptopyridine preformed SAMs (MPc-4-MPy-SAM) occurred at  $\sim 0.2 \text{ V}$ , Table 3, with FePc-4-MPy-SAM showing better catalytic activity as judged by higher peak current when compared to CoPc-4-MPy-SAM and MnPc-4-MPy-SAM [86]. Long term stability (over a 2-week period) of MPc-4-MPy-SAM ( $M = \text{Fe}, \text{Co}, \text{Mn}$ ) towards the oxidation of L-cysteine decreased as follows: FePc > MnPc > CoPc. Thus, the oxidation of cysteine is less stable on CoPc modified electrode and this complex is less catalytic compared to corresponding MnPc and FePc derivatives.

### 4.3.3 Thiocyanate

MnPc-SAMs have been employed for the detection of thiocyanate [86] on SAMs formed by coordination of MPc complexes to preformed SAMs. On MnPc-4-MPy-SAM the oxidation of  $\text{SCN}^{-}$  occurred at  $0.50 \text{ V}$  (Table 3). The stability of the electrode was less on MnPc compared to CoPc preformed SAM. Analysis of  $\text{SCN}^{-}$  in the presence of possible interfering species (uric acid, oxalic acid, and ascorbic acid) in biological samples revealed insignificant effects from these compounds [86]. Thus,  $\text{SCN}^{-}$  can be analyzed in the presence of ascorbic acid. An analysis of the urine of smokers and nonsmokers showed clearly that the SAM electrode could be used to differentiate between the two groups.

### 4.3.4 Other Analytes

Adsorbed **Mn6g** and **Mn6i** were employed for the detection of oxygen [94]. Rotating disk electrode voltammetry revealed two electron reduction in acidic and slightly

alkaline media because of the formation of hydrogen peroxide. In highly basic media, water is the major product formed via four electron transfer. Polymerized  $\text{MnPc}^{\beta}(\text{NH}_2)_4$  was employed for the detection of glycine [44], which occurred at  $-0.67\text{ V}$  vs. SCE. The catalytic efficiency for reduction of glycine decreased with increasing pH suggesting that the protonated form of glycine is the most active. Also the redox potential shifted to more negative values with increasing pH, i.e., by  $80\text{ mV}$  per pH unit, consistent with a one-electron, one proton process. The electrode was found to be stable for the detection of glycine, as there was no significant decrease in currents with scan number.

## 5 Conclusion

This work summarizes the electronic absorption spectra and electrochemical behavior of near infrared absorbing phthalocyanine complexes. The complexes which exhibit this redshift include those containing electron donating ring substituents such as alkyl- or arylthio and amino groups. Ring expansion also leads to the redshifting of the phthalocyanine complexes. The central metal plays a significant role in the redshifting behavior of phthalocyanines, with manganese complexes showing the largest redshift compared to the others. Only a few metals are known to cause a redshift of the Q band. These include Mn, Sb, Bi, Pb, Ti, and V. Mn and Ti phthalocyanine complexes also show interesting electrochemistry, with the central metal showing oxidation states varying from I to IV and II to IV, respectively. The catalytic behavior of the Mn and Ti phthalocyanine towards some analytes is also discussed. These complexes lower the oxidation of nitrite to much lower potentials when compared to the more commonly employed Co phthalocyanine derivatives.

**Acknowledgements** This work was supported by the Department of Science and Technology (DST) and National Research Foundation (NRF), South Africa through DST/NRF South African Research Chairs Initiative for Professor of Medicinal Chemistry and Nanotechnology and Rhodes.

## References

1. Gregory P (2000) Industrial applications of phthalocyanines. *J Porphyrins Phthalocyanines* 4(4):432–437
2. Snow AW (2003) Phthalocyanine aggregation. In: Kadish KM, Smith KM, Guillard R (eds) *Porphyrin handbook, phthalocyanine properties and materials*, vol 17, Chap 109. Academic Press, New York
3. Dini D, Hanack M (2003) Physical properties of phthalocyanine-based materials In: Kadish KM, Smith KM, Guillard R (eds) *Porphyrin handbook, phthalocyanine properties and materials*, vol 17, Chap. 107. Academic Press, New York
4. Ben-Hur E, Chan WS (2003) Phthalocyanines in photobiology and their medical applications In: Kadish KM, Smith KM, Guillard R (eds) *Porphyrin handbook, phthalocyanine properties and materials*, vol 19, Chap. 117. Academic Press, New York

- Verdree VT, Su G, Pakhamov S, Nesterova I, Hammer RP, Soper SA (2006) Synthesis and photophysical characterization of near-IR metallo-phthalocyanines and other biopolymer conjugates, Abstract 2nd Southwest Regional Meeting of Am Chem Soc Oct. 19–22
- Auger, A, Burnham P M, Chambrier I, Cook M J, Hughes D L (2005) X-ray crystallographic studies of three substituted indium(III) phthalocyanines: effect of ring substitution and the axial ligand on molecular geometry and packing. *J Mater Chem* 15(1):168–176
- Nakai K, Ishii K, Kobayashi N, Yonehara H, Pac C (2003) Theoretical calculations of the electronic absorption spectra of oxotitanium(IV) phthalocyanine in the solid State. *J Phys Chem B* 107(36):9749–9755
- Zhu J, Shen Y, Gu F, Tao J, Zhang J (2007) Preparation and photovoltaic properties of near-infrared absorbing manganese(II) phthalocyanine polymer films. *Mater Lett* 61(6):1296–1298
- Endo A, Matsumoto S, Mizuguchi J (1999) Interpretation of the near-infrared absorption of magnesium phthalocyanine complexes in terms of exciton coupling effects. *J Phys Chem A* 103(41):8193–8199
- Bian Y, Li L, Dou J, Cheng DYY, Li R, Ma, Ng DKP, Kobayashi N, Jiang J (2004) Synthesis, structure, spectroscopic properties, and electrochemistry of (1,8,15,22-tetra substituted phthalocyaninato)lead complexes. *Inorg Chem* 43(23):7539–7544
- Chambrier I, Cook M J, Wood P T (2000) Conformationally stressed phthalocyanines: the non-planarity of the 1,4,8,11,15,18,22,25-octaisopentyl derivative. *Chem Commun* 21:2133–2134
- Mbambisa G, Tau P, Antunes E, Nyokong T (2007) Synthesis and electrochemical properties of purple manganese(III) and red titanium(IV) phthalocyanine complexes octa-substituted at non-peripheral positions with pentyl thio groups. *Polyhedron* 26(18):5355–5364
- Agboola B, Ozoemena KI, Westbroek P, Nyokong T (2007) Synthesis and electrochemical properties of benzylmercapto and dodecylmercapto tetra substituted manganese phthalocyanine complexes. *Electrochim Acta* 52(7):2520–2526
- Sehlotho N, Durmus M, Ahsen V, Nyokong T (2008) The synthesis and electrochemical behaviour of water soluble manganese phthalocyanines: Anion radical versus  $Mn^I$  species. *Inorg Chem Commun* 11(5):479–483
- Mark J, Stillman MJ (2003) Optical spectra and electronic structure of metallophthalocyanines and metalloporphyrins. In: Kadish KM, Smith KM, Guillard R (eds) *Porphyrin handbook, phthalocyanine properties and materials*, vol 16, Chap 103. Academic Press, New York
- Mack J, Stillman MJ (2001) Assignment of the optical spectra of metal phthalocyanines through spectral band deconvolution analysis and ZINDO calculations. *Coord Chem Rev* 219–221:993–1032
- Muranaka A, Okuda M, Kobayashi N, Somers K, Ceulemans A (2004) Recognition of chiral catechols using oxo-titanium phthalocyanine. *J Am Chem Soc* 126(14):4596–4604
- Makarov SG, Suvorova ON, Litwinski C, Ermilov EA, Roeder B, Tsaryova O, Woehrle D, Woehrle D (2007) Linear and rectangular trinuclear phthalocyanines. *Eur J Inorg Chem* (4):546–552
- Kobayashi N, Muranaka A, Ishii K (2000) Symmetry-lowering of the phthalocyanine chromophore by a C2 type axial ligand. *Inorg Chem* 39(11):2256–2257
- Makarov SG, Piskunov AV, Suvorova ON, Schnurpfeil G, Domrachev GA, Woehrle D (2007) Near-infrared absorbing ligand-oxidized dinuclear phthalocyanines. *Chem Eur J* 13(11):3227–3233
- Makarov SG, Litwinski C, Ermilov EA, Suvorova O, Roeder B, Woehrle D (2006) Synthesis and photophysical properties of annulated dinuclear and trinuclear phthalocyanines. *Chem Eur J* 12(5):1468–1474
- Makarov SG, Maksimova KN, Baranov EV, Fukin GK, Suvorova ON, Woehrle D, Domrachev GA (2006) Synthesis and electronic spectra of dimeric phthalocyanines. *Russ Chem Bull* 55(10):1748–1754
- Tau P, Nyokong T (2006) Synthesis, electrochemical and photophysical properties of phthalocyaninato oxotitanium(IV) complexes tetra substituted at the  $\alpha$  and  $\beta$  positions with aryl thio groups. *Dalton Trans* (37):4482–4490
- Sooksimuang T, Mandal BK (2003) [5]Helicene-fused phthalocyanine derivatives. New members of the phthalocyanine family. *J Org Chem* 68(2):652–655

25. Jin S, Cheng G, Chen GZ, Ji Z (2005) Tuning the maximum absorption wavelengths of phthalocyanine derivatives. *J Porphyrins Phthalocyanines* 9(1):32–39
26. Chen Y, Hanack M, Blau WJ, Dini D, Liu Y, Lin Y, Bai J (2006) Soluble axially substituted phthalocyanines: synthesis and nonlinear optical response. *J Mater Sci* 41(8):2169–2185
27. Kobayashi N, Konami H (1999) Molecular orbitals and electronic spectra of phthalocyanine analogues. In: Leznoff CC, Lever ABP (eds) *Phthalocyanines: properties and applications*, vol 4, Chap 9. VCH, New York
28. Nyokong T, Isago H (2004) The renaissance in optical spectroscopy of phthalocyanines and other tetraazaporphyrins. *J Porphyrins Phthalocyanines* 8(9):1083–1090
29. Kobayashi N, Ogata H, Nonaka N, Luk'yanets EA (2003) Effect of peripheral substitution on the electronic absorption and fluorescence spectra of metal-free and zinc phthalocyanines. *Chem Eur J* 9(20):5123–5134
30. Mbambisa G, Nyokong T (2008) Synthesis and electrochemical characterization of a near infrared absorbing oxo vanadium(IV) octa pentyl thio-phthalocyanine. *Polyhedron* 27(13):2799–2804
31. Tau P, Nyokong T (2006) Synthesis and electrochemical characterization of  $\alpha$ - and  $\beta$ -tetra-substituted oxo(phthalocyaninato) titanium(IV) complexes. *Polyhedron* 25(8):1802–1810
32. Tau P, Nyokong T (2007) Electrochemical characterisation of tetra- and octa-substituted oxo(phthalocyaninato)titanium(IV) complexes. *Electrochim Acta* 52(11):3641–3650
33. Arslanoglu Y, Mert-Sevim A, Hamuryudan E, Guel A (2005) Near-IR absorbing phthalocyanines. *Dyes Pigment* 68(2–3):129–132
34. Agboola B, Nyokong T (2007) Comparative electrooxidation of nitrite by electrodeposited  $\text{Co}^{\text{II}}$ ,  $\text{Fe}^{\text{II}}$  and  $\text{Mn}^{\text{III}}$  tetrakis(benzylmercapto) and tetrakis(dodecylmercapto) phthalocyanines on gold electrodes. *Anal Chim Acta* 587(1):116–123
35. Obirai J, Nyokong T (2005) Synthesis, electrochemical and electrocatalytic behaviour of thiophene-appended cobalt, manganese and zinc phthalocyanine complexes. *Electrochim Acta* 50(27):5427–5434
36. Obirai J, Nyokong T (2005) Synthesis, spectral and electrochemical characterization of mercaptopyrimidine-substituted cobalt, manganese and  $\text{Zn}^{\text{II}}$  phthalocyanine complexes. *Electrochim Acta* 50(16–17):3296–3304
37. Fox J P, Goldberg DP (2003) Octa alkoxy-substituted phosphorus(V) triazetetrabenzcorroles via ring contraction of phthalocyanine precursors. *Inorg Chem* 42(25):8181–8191
38. Fukuda T, Ishiguro T, Kobayashi N (2005) Non-planar phthalocyanines with Q-bands beyond 800 nm. *Tetrahedron Lett* 46(16):2907–2909
39. Isago H (2003) Spectral properties of a novel antimony(III)-phthalocyanine complex that behaves like J-aggregates in non-aqueous media. *Chem Commun* 15:1864–1865
40. Leznoff CC, Black LS, Hiebert A, Causey PW, Christendat D, Lever ABP (2006) Red manganese phthalocyanines from highly hindered hexadecaalkoxyphthalocyanines *Inorg Chim Acta* 359(9):2690–2699
41. Bhardwaj N, Andraos J, Leznoff CC (2002) The syntheses and NMR studies of hexadeca- and octaneopentoxypthalocyanines. *Can J Chem* 80(2):141–147
42. Eberhardt W, Hanack M (1997) Synthesis of hexadecaalkoxy-substituted nickel and iron phthalocyanines. *Synthesis* 1:95–100
43. Khene S, Cammidge AN, Cook MJ, Nyokong T (2007) Electrochemical and photophysical characterization of non-peripherally-octa alkyl substituted dichlorotin(IV) phthalocyanine and tetrabenzotriazaporphyrin compounds. *J Porphyrins Phthalocyanines* 11(10):761–770
44. Obirai J, Nyokong T (2004) Electrochemical studies of manganese tetraamminophthalocyanine monomer and polymer. *Electrochim Acta* 49(9–10):1417–1428
45. Nombona N, Tau P, Sehlotho N, Nyokong T (2008) Electrochemical and electrocatalytic properties of  $\alpha$ -substituted manganese and titanium phthalocyanines. *Electrochim Acta* 53(7):3139–3148
46. Tau P, Nyokong T (2007) Electrocatalytic oxidation of nitrite by tetra substituted oxotitanium(IV) phthalocyanines adsorbed or polymerized on glassy carbon electrode. *J Electroanal Chem* 611(1–2):10–18

47. Khene S, Geraldo DA, Togo CA, Limson J, Nyokong T (2008) Synthesis, electrochemical characterization of tetra- and octa-substituted dodecyl-mercapto tin phthalocyanines in solution and as self-assembled monolayers. *Electrochim Acta* 54:183–191
48. Knecht S, Durr K, Schmid G, Subramanian LR, Hanack M (1999) Synthesis and properties of soluble phthalocyaninatomanganese(III) complexes. *J Porphyrins Phthalocyanines* 3(4):292–298
49. Kasha M, Rawls HR, El-Bayoumi MA (1965) Exciton model in molecular spectroscopy. *Pure Appl Chem* 11(3–4):371–392
50. Yarasir MN, Kandaz M, Koca A, Salih B (2006) Functional alcohol-soluble double-decker phthalocyanines: synthesis, characterization, electrochemistry and peripheral metal ion binding. *J Porphyrins Phthalocyanines* 10(8):1022–1033
51. Adachi K, Watarai H (2005) Interfacial aggregation of thioether-substituted phthalocyaninatomagnesium(II)-palladium(II) complexes in the toluene/water system. *J Mater Chem* 15(44):4701–4710
52. Engelkamp H, Nolte RJM (2000) Molecular materials based on crown ether functionalized phthalocyanines. *J Porphyrins Phthalocyanines* 4(5):454–459
53. Matemadombo F, Maree MD, Ozoemena K I, Westbroek P, Nyokong T (2005) Synthesis, electrochemical and spectroelectrochemical studies of octa phenyl thio-substituted phthalocyanines. *J Porphyrins Phthalocyanines* 9(7):484–490
54. Agboola BO, Ozoemena KI, Nyokong T (2006) Electrochemical properties of benzylmercapto and dodecylmercapto tetra substituted nickel phthalocyanine complexes: electrocatalytic oxidation of nitrite. *Electrochim Acta* 51(28):6470–6478
55. Agboola B, Ozoemena KI, Nyokong T (2006) Synthesis and electrochemical characterisation of benzylmercapto and dodecylmercapto tetra substituted cobalt, iron, and zinc phthalocyanines complexes. *Electrochim Acta* 51(21):4379–4387
56. Obirai J, Rodrigues Pereira N, Bedioui F, Nyokong T (2003) Synthesis, spectral and electrochemical properties of a new family of pyrrole substituted cobalt, iron, manganese, nickel and zinc phthalocyanine complexes. *J Porphyrins Phthalocyanines* 7(7):508–520
57. Rodrigues Pereira N, Obirai J, Nyokong T, Bedioui F (2005) Electropolymerized pyrrole-substituted manganese phthalocyanine films for the electroassisted biomimetic catalytic reduction of molecular oxygen. *Electroanalysis* 17(2):186–190
58. Obirai J, Nyokong T (2004) Electrochemical and catalytic properties of chromium tetra aminophthalocyanine. *J Electroanal Chem* 573:77–85
59. A Fukuda T, Ono K, Homma S, Kobayashi N (2003) Phthalocyanine producing green, ochre, and red colors depending on the central metals. *Chem Lett* 32(8):736–737
60. Ozkaya AR, Gurek AG, Gul A, Bekaroglu O (1997) Electrochemical and spectral properties of octakis(hexyl thio)-substituted phthalocyanines. *Polyhedron* 16(11):1877–1883
61. Takahashi K, Kawashima M, Tomita Y, Itoh M (1995) Synthesis and spectral and electrochemical properties of 2,3,9,10,16,17,23,24-octa butyl thiophthalocyaninatozinc(II). *Inorg Chim Acta* 232(1–2):69–73
62. Janczak J, Kubiak R, Śledź M, Borrmann H, Grin Y (2003) Synthesis, structural investigations and magnetic properties of dipyrrodated manganese phthalocyanine,  $MnPc(py)_2$ . *Polyhedron* 22:2689–2697
63. Bard AJ, Faulkner, LR (2000) *Electrochemical methods, fundamentals and applications*, 2nd edn. Wiley, New York
64. Jiang Z, Ou Z, Chen N, Wang J, Huang J, Shao J, Kadish KM (2005) Synthesis, spectral and electrochemical characterization of non-aggregating  $\alpha$ -substituted vanadium(IV)-oxo phthalocyanines *J Porphyrins Phthalocyanines* 9(5):352–360
65. L'Her, M, Pondaven A (2003) Redox properties and electrochemistry of phthalocyanines In: Kadish KM, Smith KM, Guillard R (eds) *Porphyrin handbook, phthalocyanine properties and materials*, vol 16, Chap 104. Academic Press, New York
66. Fukuda F, Homma S, Kobayashi N (2005) Deformed phthalocyanines: synthesis and characterization of zinc phthalocyanines bearing phenyl substituents at the 1,4,8,11,15,18,22, and/or 25-positions. *Chem Euro J* 11(18):5205–5216

67. Lackinger M, Mueller T, Gopakumar TG, Mueller F, Hietschold M, Flynn G W (2004) Tunneling voltage polarity-dependent submolecular contrast of naphthalocyanine on graphite. An STM study of close-packed monolayers under ultrahigh-vacuum conditions. *J Phys Chem B* 108(7):2279–2284
68. Yonehara H, Ogawa K, Etori H, Pac C (2002) Vapor deposition of oxotitanium(IV) phthalocyanine on surface-modified substrates: Effects of organic surfaces on molecular alignment. *Langmuir* 18(20):7557–7563
69. Finklea HO (2000) Self-assembled monolayers on electrodes. In: Meyers RA (ed) *Encyclopedia of analytical chemistry*, Chap 11. Wiley, New York
70. Salomon E, Angot T, Papageorgiou N, Layet J-M (2005) Self-assembled monolayer of tin-phthalocyanine on InSb(001)-(4 × 2)/c(8 × 2). *Surf Sci* 596(1–3):74–81
71. Somashekarappa MP, Keshavayya J, Sampath S (2002) Self-assembled molecular films of tetra amino metal (Co, Cu, Fe) phthalocyanines on gold and silver. *Electrochemical and spectroscopic characterization*. *Pure Appl Chem* 74(9):1609–1620
72. Somashekarappa MP, Sampath S (2002) Orientation dependent electrocatalysis using self-assembled molecular films. *Chem Commun* 12:1262–1263
73. Li, Z, Lieberman M, Hill W (2001) XPS and SERS study of silicon phthalocyanine monolayers: Umbrella vs octopus design strategies for formation of oriented SAMs. *Langmuir* 17(16):4887–4894
74. Revell DJ, Chambrier I, Cook MJ, Russell D A (2000) Formation and spectroscopic characterization of self-assembled phthalocyanine monolayers. *J Mater Chem* 10(1):31–37
75. Cook MJ, Chambrier I (2003) Phthalocyanine thin films and structural studies In: Kadish KM, Smith KM, Guillard R (eds) *Porphyrin handbook, phthalocyanine properties and materials*, vol 17, Chap 108. Academic Press, New York
76. Matemadombo F, Griveau S, Bedioui F, Nyokong T (2008) Electrochemical characterization of self-assembled monolayer of a novel manganese tetra benzyl thio-substituted phthalocyanine and its use in nitrite oxidation. *Electroanalysis* 20(17):1863–1872
77. Hone DC, Walker PI, Evans-Gowing R, FitzGerald S, Beeby A, Chambrier I, Cook MJ, Russell DA (2002) Generation of cytotoxic singlet oxygen via phthalocyanine-stabilized gold nanoparticles: A potential delivery vehicle for photodynamic therapy. *Langmuir* 18(8):2985–2987
78. Cook MJ (1999) Phthalocyanine thin films. *Pure Appl Chem* 71(11):2145–2151
79. Huang X, Liu Y, Wang S, Zhou S, Zhu D (2002) Synthesis and self-assembly of 2,9,16-Tri(*tert*-butyl)-23-(10-mercaptodecyloxy)phthalocyanine and the application of its self-assembled monolayers in organic light-emitting diodes. *Chem Eur J* 8(18):4179–4184
80. Schweikart K, Malinovskii VL, Yasserli AA, Li J, Lysenko AB, Bocian DF, Lindsey JS (2003) Synthesis and characterization of bis(S-acetyl thio)-derivatized europium triple-decker monomers and oligomers. *Inorg Chem* 42(23):7431–7446
81. Ozoemena K I, Nyokong T; Westbroek P (2003) Self-assembled monolayers of cobalt and iron phthalocyanine complexes on gold electrodes: Comparative surface electrochemistry and electrocatalytic interaction with thiols and thiocyanate. *Electroanalysis* 15(22):1762–1770
82. Ozoemena K, Nyokong T (2002) Voltammetric characterization of the self-assembled monolayer (SAM) of octa butyl thiophthalocyaninatoiron(II): a potential electrochemical sensor. *Electrochim Acta* 47(25):4035–4043
83. Li Z, Lieberman M (2001) Axial reactivity of soluble silicon(IV) phthalocyanines. *Inorg Chem* 40(5):932–939
84. Ozoemena KI, Nyokong T (2005) Electrocatalytic oxidation and detection of hydrazine at gold electrode modified with iron phthalocyanine complex linked to mercaptopyrindine self-assembled monolayer. *Talanta* 67(1):162–168
85. Ozoemena KI, Nyokong T (2005) Surface electrochemistry of iron phthalocyanine axially ligated to 4-mercaptopyridine self-assembled monolayers at gold electrode: Applications to electrocatalytic oxidation and detection of thiocyanate. *J Electroanal Chem* 579(2):283–289
86. Ozoemena KI, Nyokong T (2006) Comparative electrochemistry and electrocatalytic activities of cobalt, iron and manganese phthalocyanine complexes axially co-ordinated to mercaptopyrindine self-assembled monolayer at gold electrodes. *Electrochim Acta* 51(13):2669–2677



87. Mashazi PN, Ozoemena K I, Maree DM, Nyokong T (2006) Self-assembled monolayers (SAMs) of cobalt tetra carboxylic acid chloride phthalocyanine covalently attached onto a preformed mercaptoethanol SAM: A novel method. *Electrochim Acta* 51(17):3489–3494
88. Huc V, Saveyroux M, Bourgoin JP, Valin F, Zalcer G, Albouy PA, Palacin S (2000) Grafting ruthenium phthalocyanine on gold and silica: Using apical ligands as linkers. *Langmuir* 16(4):1770–1776
89. Brown KL, Shaw J, Ambrose M, Mottola HA (2002) Voltammetric, chronocoulometric and spectroelectrochemical studies of electropolymerized films based on  $\text{Co}^{\text{II/III}}$ - and  $\text{Zn}^{\text{II}}$ -4,9,16,23-tetra aminophthalocyanine: effect of high pH. *Microchem J* 72(3):285–298
90. Trollund E, Ardiles P, Aguirre M J, Biaggio SR, Rocha-Filho RC (2000) Spectroelectrochemical and electrical characterization of poly(cobalt-tetra aminophthalocyanine)-modified electrodes: electrocatalytic oxidation of hydrazine. *Polyhedron* 19(22–23):2303–2312
91. Zhang S, Sun W-l, Xian Y-z, Zhang W, Jin L, Yamamoto K, Tao S, Jin, J (1999) Multichannel amperometric detection system for liquid chromatography to assay the thiols in human whole blood using the platinum microelectrodes chemically modified by copper tetra aminophthalocyanine. *Anal Chim Acta* 399(3):213–221
92. Alpatova NM, Ovsyannikova EV, Tomilova LG, Korenchenko OV, Kondrashov YV (2001) Anodic doping of electropolymerized copper 2,9,16,23-tetra aminophthalocyanine. *Russ J Electrochem* 37(10):1012–1016
93. Goux A, Bedioui F, Robbiola L, Pontie M (2003) Nickel tetra aminophthalocyanine based films for the electrocatalytic activation of dopamine. *Electroanalysis* 15(11):969–974
94. Sehlotho N, Nyokong T (2006) Effects of ring substituents on electrocatalytic activity of manganese phthalocyanines towards the reduction of molecular oxygen. *J Electroanal Chem* 595(2):161–167
95. Tau P, Nyokong T (2007) Electrocatalytic activity of aryl thio tetra substituted oxotitanium(IV) phthalocyanines towards the oxidation of nitrite. *Electrochim Acta* 52(13):4547–4553
96. Lever ABP, Milaeva, ER, Speier, G (1993) The redox chemistry of metallophthalocyanines in solution In: Leznoff CC, Lever ABP (eds) *Phthalocyanines: properties and a  $\text{H}_2\text{Pc}$*  vol 3, Chap 1. VCH, New York

# Photochromic Dithienylethene–Phthalocyanines and Their Analogs

Qianfu Luo, Yi Liu, and He Tian

**Abstract** Photochromic dithienylethenes have been extensively investigated because of their striking features and potential uses in molecular devices, optoelectronic equipment, memory media, etc. Many photochromic dithienylethenes and their derivatives have been so far synthesized and their excellent performances have been examined. Dithienylethene, incorporating phthalocyanine hybrids and their analogs, is one of the most important types among these photochromic compounds. In this review, the molecular design and the general methods of preparation of photochromic dithienylethene–phthalocyanine hybrids and their analogs are highlighted. Their versatile performances are described.

**Keywords** Dithienylethene · Functional materials · Photochromism · Phthalocyanines and analogs

## Contents

1	Introduction .....	89
2	Dithienylethene-Bridged Porphyrins and Their Analogs .....	90
3	Porphyrim-Bridged Dithienylethenes and Their Analogs .....	94
4	Photochromic Dithiophenes-Fused Phthalocyanines and Their Analogs .....	97
5	Conclusion .....	102
	References .....	102

## 1 Introduction

Photochromism is defined as the reversible photo-induced transformation of a substance into its two isomers that differ in absorption spectra and other physicochemical parameters [1–4]. Over the past decade, the molecular design and synthesis

---

Q. Luo, Y. Liu, and H. Tian (✉)  
Key Lab for Advanced Materials and Institute of Fine Chemicals,  
East China University of Science and Technology, Shanghai 200237, China  
e-mail: tianhe@ecust.edu.cn

of photochromic materials have been well-studied because of their potential applicability in many technological fields, such as information storage, imaging devices, signal transmission system, and molecular switches [5–9]. Among various types of reported photochromic systems, dithienylethenes have been attracting more and more attention. Their favorable properties, such as thermal and optical stability of the ring-open and ring-closed isomers, high fatigue resistance, high sensitivity, and the rapid response, make them promising candidates for photochromic functional materials. Therefore, they can serve as memory media, optical switches, logic circuits, liquid crystal displays, and magnetic materials, particularly for optical inputs and memory media [10–23].

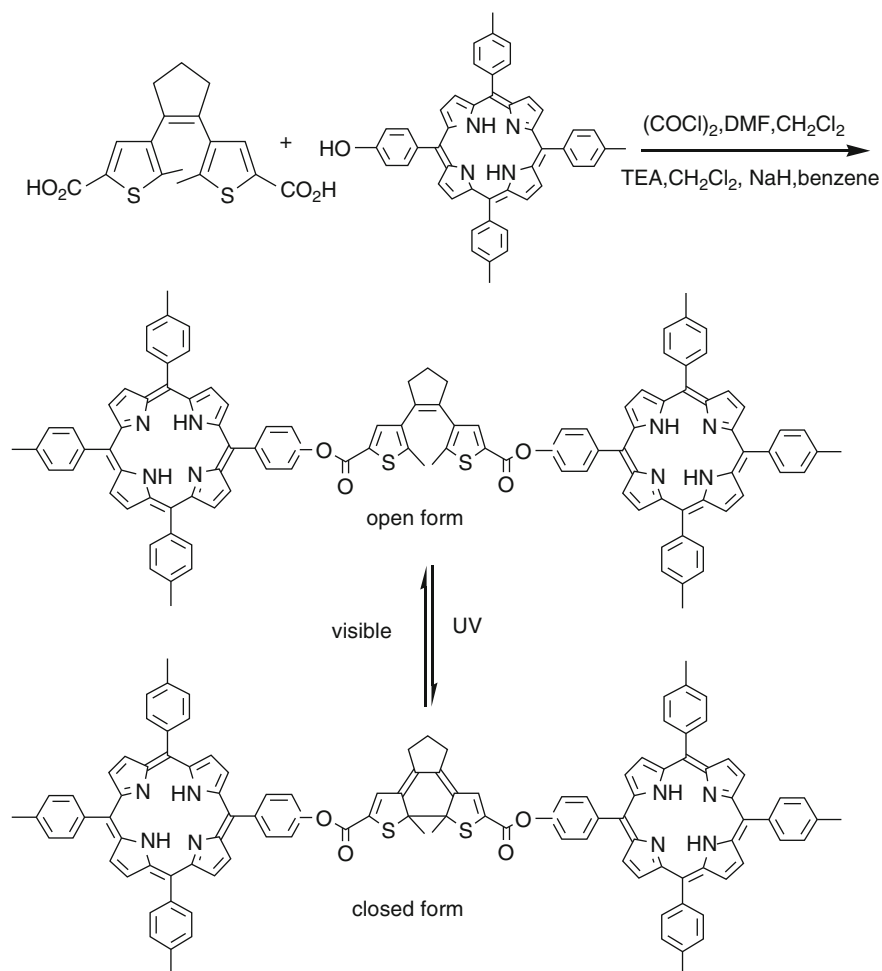
As the photochromic dithienylethenes have a series of useful performances and applications, various dithienylethenes have been so far prepared and their excellent properties have been studied. Dithienylethene, in combination with phthalocyanines and their analogs, is one of the most important types among these photochromic compounds.

It is well-known that phthalocyanines and their analogs, including their hybrids, porphyrins, and tetraaza-porphyrines, are a robust and versatile class of compounds. They have been investigated extensively and used in many fields, including chemical sensors, photodynamic therapy, electrochromism, optical computer read/write disc, etc. [24–28]. Combination of photochromic dithienylethenes with phthalocyanines and phthalocyanine analogs has derived many novel photochromic functional materials. They mainly involve three types: one is dithienylethene-bridged porphyrins and their analogs, the second is porphyrin-bridged dithienylethenes, and the third is that photochromic dithienylethenes fused directly to the pyrrole units of phthalocyanines and their analogs. In the following, we will briefly review their preparations, fundamental properties, and potential applications.

## 2 Dithienylethene-Bridged Porphyrins and Their Analogs

Photochromic dithienylethenes have been considered as extremely promising systems to store information. The success of optical information processing requires the facile detection method which can read the stored information in a non-invasive manner. It is to say that the non-destructive readout capability is indispensable. On the basis of the ability to fine-tune the excitation wavelengths of porphyrins and the fact that they exhibit strong luminescence and attractive coordination properties, Branda covalently attached two porphyrins to the dithienylethene backbone, and synthesized a hybrid for non-destructive information processing [29], as shown in Scheme 1. It was the first example of photochromic porphyrinic dithienylethene.

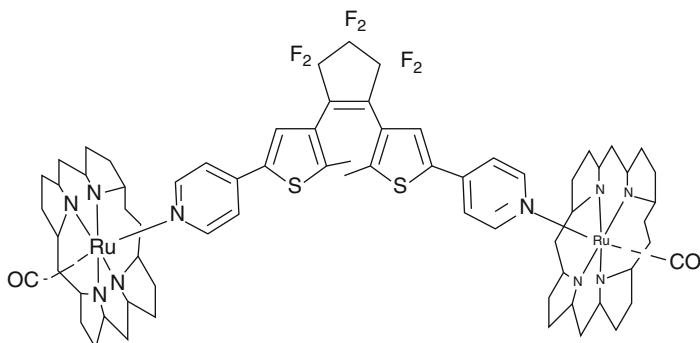
In this compound, 1,2-bis(3-thienyl)cyclopentene was designed as molecular backbone and two brandishing porphyrin macrocycles were chosen as substituents. It was prepared by the esterification of 5,10,15-tris(tolyl)-20-(4-hydroxyphenyl)-porphyrin and 1,2-bis(5-carboxy-2-methyl-3-thienyl) cyclopentene in the presence of pyridine and triethylamine.



Scheme 1

Illuminated alternately with UV and visible light, the porphyrinic dithienylethene underwent a reversible photoisomerization reaction (Scheme 1). Meanwhile, the fluorescence intensity of the porphyrin macrocycles could be regulated by alternate irradiation with UV (313 nm) and visible light (longer than 480 nm). Moreover, the selective excitation band of the fluorophore was beyond the spectral band which could induce the photoisomerization reaction. Therefore, the authors asserted that this compound could act as a system for reversible data processing using fluorescence as the non-destructive detection method.

However, although the selective excitation band was a photochemically non-active absorbance band, the emission wavelength slightly overlapped with absorption band associated with the ring-opening reaction. This phenomenon might also result in photochemical interconversion of the porphyrinic photochrome and limit its



Scheme 2

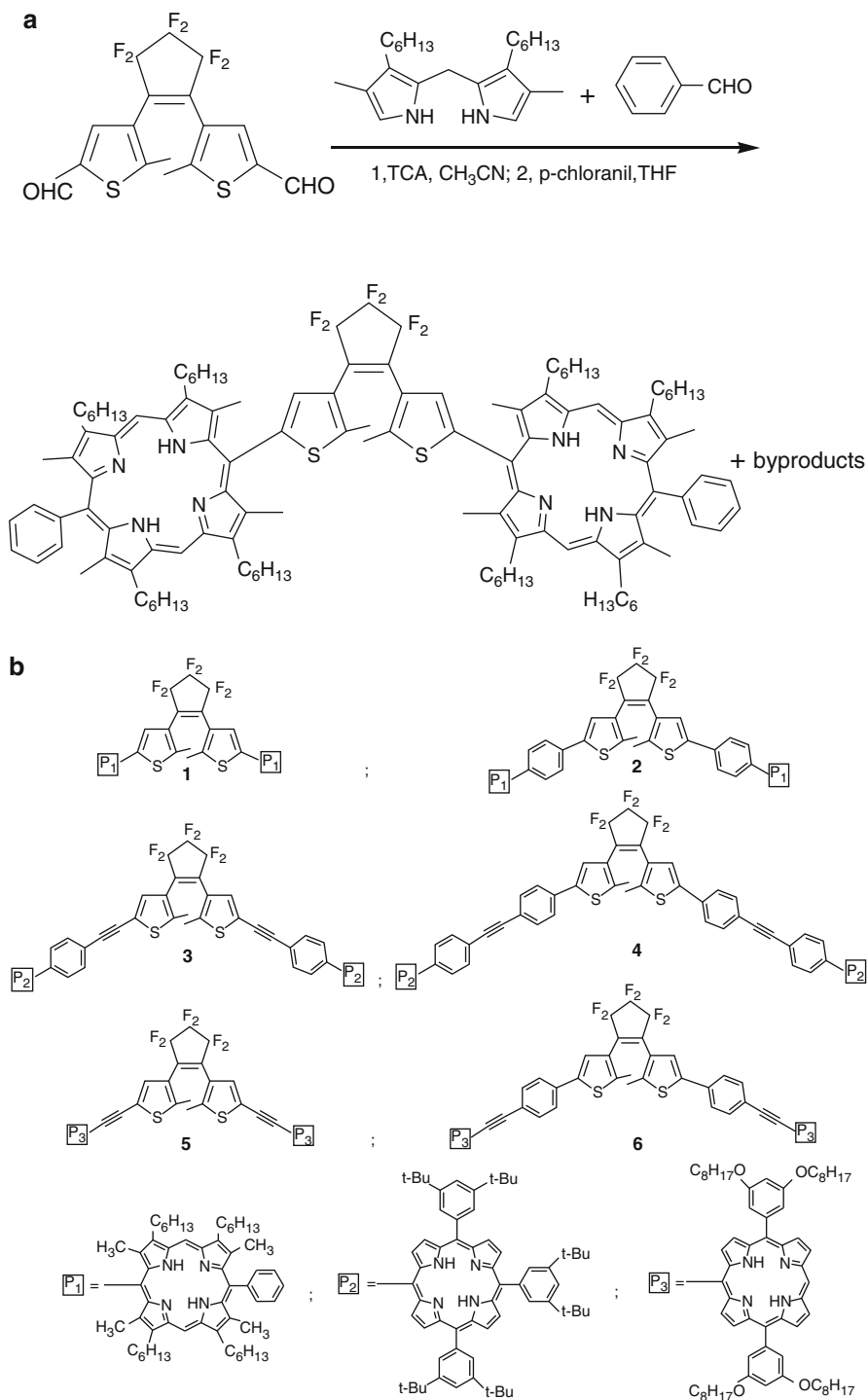
application. Due to some metalloporphyrins phosphoresced at wavelengths remote from the spectral regions which might be used to induce the photochromism, an axially coordinated ruthenium porphyrin to the pyridyl-derivatized dithienylethene compound was designed sequentially by Branda and his co-workers [30], as illustrated in Scheme 2.

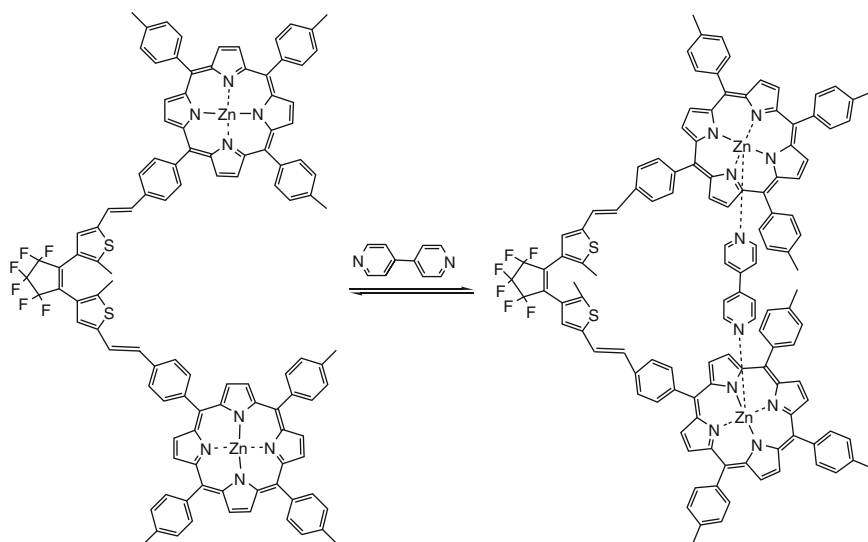
This complex phosphoresced at infrared region when excited with the UV-vis light. The excitation wavelengths that yielded the highest emission intensity existed in a narrow region of the visible spectrum. The absorption spectra, for both open-form and closed-form of the substituted dithienylethene, were far from this region and avoided their interconversion when irradiated with the light in this region. Therefore, it could tackle the problem that the excitation resulted in photochemical interconversion of the porphyrinic dithienylethene reported above. Moreover, it exhibited excellent photochromic properties and provided an alternative to fluorescence as a means to detect information in a non-invasive manner.

Almost at the same time, Irie and his coworkers synthesized a series of dithienylethene-bridged diporphyrins as photochemical switching materials (Scheme 3) [31]. Changing the connecting spaces between the porphyrin and thienylethene by inserting 1,4-phenylene, 4-ethynylphenylene, di-4-phenylethynylene, and *meso*-ethynylene, six dithienylethene-bridged diporphyrins were produced.

Scheme 3a gives a representation of the main synthetic procedure for these compounds. It started with the condensation of diformyl-substituted dithienylethene and benzaldehyde with dipyrrolemethane, followed by oxidation with *p*-chloranil. The dithienylethene-bridged diporphyrin was given in 19% yield. The other products were synthesized by analogous approaches.

However, not all the six prepared compounds (Scheme 3b) underwent photochemical isomerization; the photoisomerization reactivity of these dithienylethene-bridged diporphyrins strongly depended on the distance between the porphyrin and dithienylethene. The three compounds, in which porphyrin and dithienylethene were directly linked (**1**), linked through a 1,4-phenylene (**2**), and linked through *meso*-ethynylene (**5**), did not exhibit any photochromism. The authors attributed it to the efficient quenching of the excited dithienylethene by the attached porphyrin moiety through intramolecular energy transfer.





Scheme 4

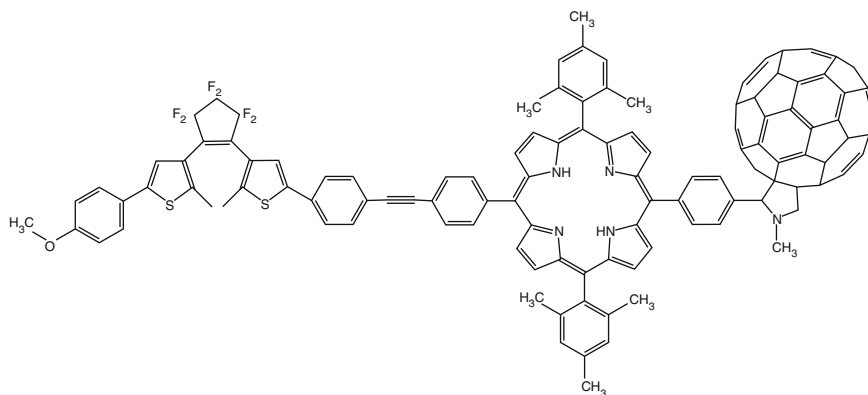
In addition, the absorption spectra and fluorescence intensity of some porphyrins changed along with the photochromic reaction of the dithienylethene functional group, which was possible for constructing some optical chemical switching systems with emission signal.

In 2007, a photoresponsive molecular tweezer, zinc porphyrin–dithienylethene–zinc porphyrin (ZnP–DTE–ZnP) triad was reported by Park and Shin (Scheme 4) [32]. The main synthesis procedure was the Wittig reaction between 5-(4-bromomethylphenyl)-10,15,20-tris (4-methylphenyl)-porphyrin and 1,2-di(2-methyl-4-formyl-3-thiophenyl) perfluorocyclopentene.

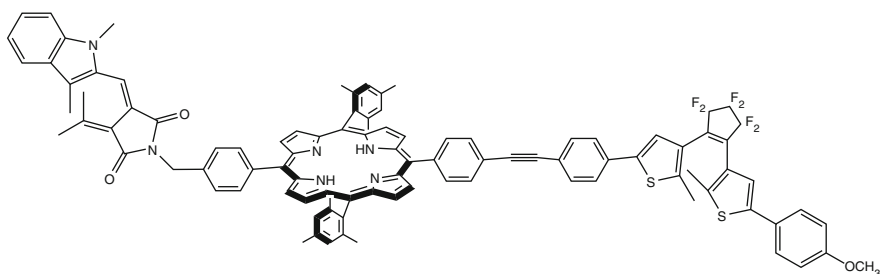
The open-isomer of DTE having two zinc porphyrin moieties could form coordination complex with 4,4-bipyridyl like a tweezer (see Scheme 4), but the closed isomer could not bind cooperatively because of its structural rigidity. The different binding behavior of ZnP–DTE–ZnP with 4,4-bipyridyl was though to make the photo-control of affinity to guest molecules possible.

### 3 Porphyrin-Bridged Dithienylethenes and Their Analogs

In 2002, a triad molecule including dithienylethene (DTE), porphyrin (P), and fullerene (DTE-P-C60) was first designed and synthesized as a photoinduced electron transfer (PET) switch by D. Gust et al. [33], as shown in Scheme 5. This molecule was synthesized by modified procedures reported literature: Porphyrin chromophore was covalently linked to substituted dithienylethene by Sonogashira coupling reaction. Fullerene was introduced by the cycloaddition reaction of dyad aldehyde (dithienylethene–porphyrin aldehyde) with the fullerene and the N-methylglycine.



Scheme 5



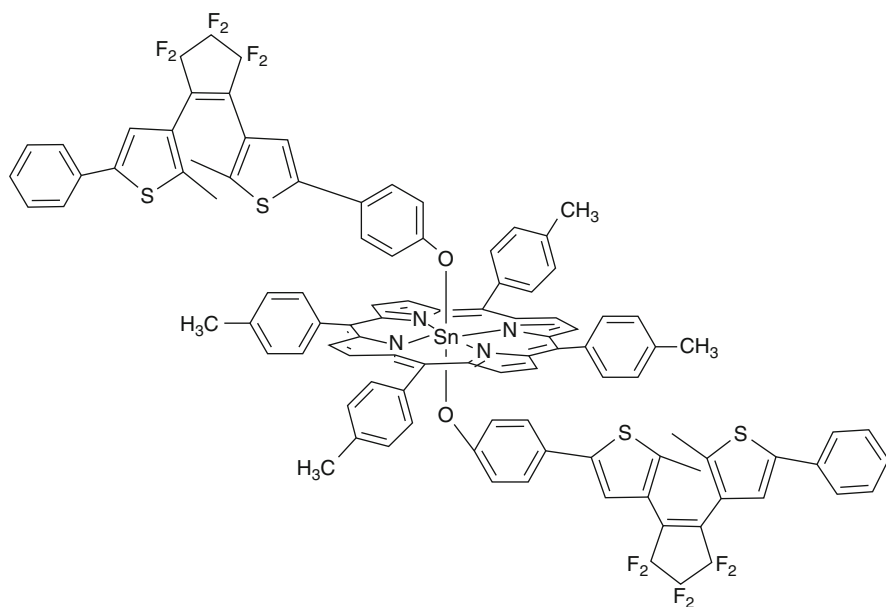
Scheme 6

Illuminating the open-ring state of the triad with visible light, the porphyrin's excited state proceeded photoinduced-electron transfer and donated an electron to fullerene to form open-ring isomer:  $\text{DTE-P}^+ - \text{C}_{60}^-$ . Upon irradiation with UV, the open form of the dithienylethene exhibited photo-cyclization reaction and produced its closed form. In the closed-ring form, the porphyrin excited state was quenched by energy transfer (not electron transfer) to the closed isomer of DTE. The ring-opening photoreaction took place on irradiation of the closed-ring state with visible light. These distinctive characteristics were due to the elaborative molecular design. The authors believed that this system could be applied in the construction of molecular-scale optoelectronic devices for digital logic and memory applications and for even more complex molecular systems.

Five years later, Gust's group [34] developed another triad incorporating a porphyrin (P) linked to a dithienylethene (DTE) and a fulgimide (FG) (Scheme 6). The main synthetic approach was still the Sonogashira coupling of dithienylethene and fulgimide-appended zinc porphyrin (FG-PZn-DTE). Trifluoroacetic acid-induced demetalation of FG-PZn-DTE produced FG-P-DTE in 57% yield.

This molecule consisted of two photochromes: a fulgimide and a dithienylethene. Both of them could isomerize with UV light from the open form to the closed form. And each photo-unit was thermally stable in either isomeric state. Moreover, the photoisomerization of fulgimide could efficiently transfer singlet excitation energy





Scheme 7

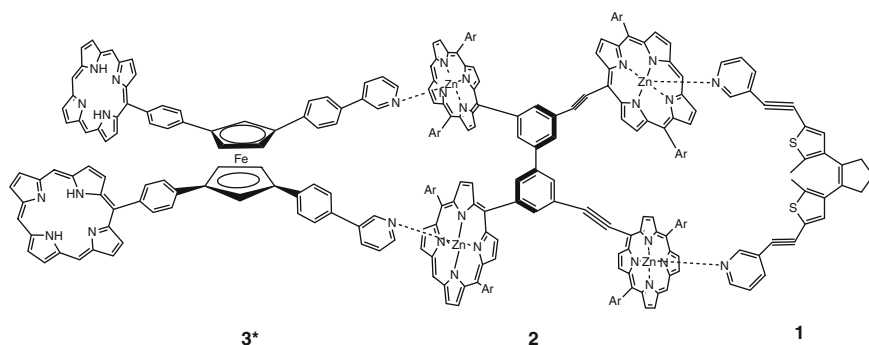
to the porphyrin, and the photocyclization of dithienylethene was able to rapidly quench the first singlet excited state of porphyrin. Thus, the molecular triad had four unique isomeric states and each isomer had different light absorption and singlet energy-transfer performances. Therefore, these isomers were considered to play an important role in outputs of logic gates and all-photonic switching.

Furthermore, they demonstrated that monitoring porphyrin emission with 470 nm excitation could perform either NOT-OR (NOR) or exclusive OR (XOR) logic functions. Of course, the performances of the triad were investigated in liquid solution, which will pose major challenges for the technological application.

In 2008, Kim H-J et al. reported a photochromic fluorescence switching of porphyrin-bridged dithienylethenes, in which two dithienylethene derivatives were axially coordinated to the two sides of porphyrinato tin complex [35]. As depicted in Scheme 7, this photochromic fluorophore ( $\text{Sn}(\text{TTP})(\text{DTE})_2$ ) was synthesized by the inter-molecular etherification of trans-dihydroxo (5,10,15,20-tetratolylporphyrinato) tin and two phenolic derivatives of 1,2-dithienylethene.

The reversible photoisomerization of this compound was investigated by spectroscopic methods in solution. On irradiation of the solution with the UV light, the absorbance in the Q band was obviously increased because of the appearance of the closed form of 1,2-dithienylethene moiety in  $\text{Sn}(\text{TTP})(\text{DTE})_2$ . The backward reaction was generated by irradiation of the closed isomer with visible light at wavelengths greater than 500 nm.

By alternate irradiations with the UV and the visible light, the fluorescence intensity of the tin porphyrin macrocycle was also obviously regulated by photochromic



Scheme 8

switching between the open form and closed form of  $\text{Sn}(\text{TTP})(\text{DTE})_2$ . This performance was promising for the potential application in ultrahigh-density reversible optical data processing using fluorescence as the detection method.

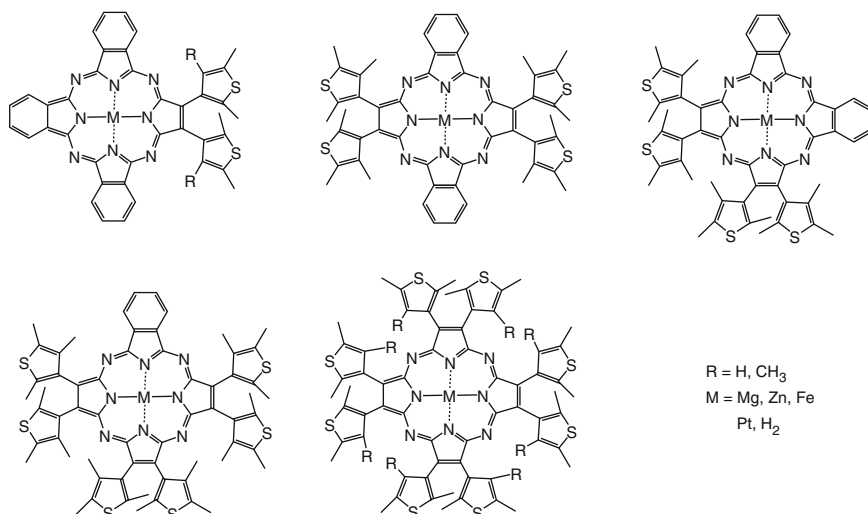
Recently, a ternary complex for a signal transmission system has been constructed by Aida and his co-workers [36]. It involved three movable components: a biaryl derivative bearing four zinc porphyrins (**2**), a pyridine-appended dithienylethene derivative (**1**), and a chiral tetrasubstituted ferrocene (**3\***), as illustrated by its structure (Scheme 8). The three components were interconnected with bidentate coordination bonds. Component **2** was the bridge between **1** and **3\***. The well-designed triad was built up by multi-step reactions through routine methods.

Upon irradiations with UV or visible light, the configurational change (closing/opening motion) of photochromic “signaling” unit (**1**) could transmit a scissoring motion to the chiral “scissoring” unit (**3\***) through an angular rotary motion of the “bridging” unit (**2**). This property might be used for remote manipulation of molecular events or long-distance mechanical communication.

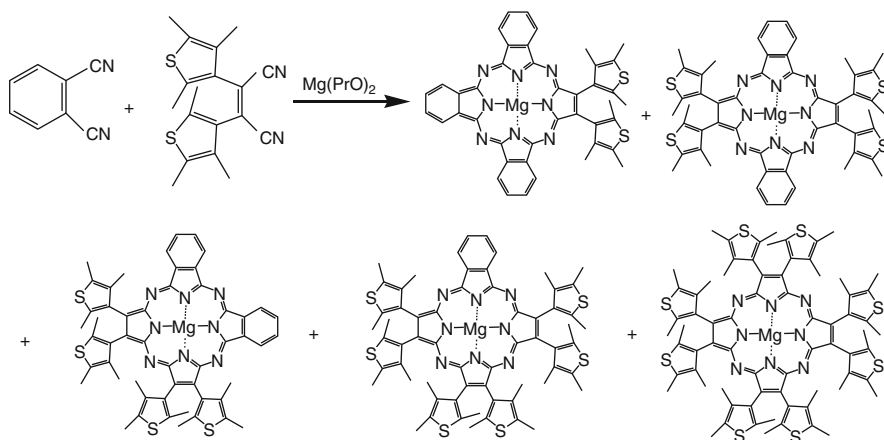
## 4 Photochromic Dithiophenes-Fused Phthalocyanines and Their Analogs

Over the past few years, in terms of atom economy and extension the conjugated system of dithienylethene, we fused photochromic dithienylethene directly to the  $\beta^-$  position of the pyrrole units of porphyrazines (tetra-azaporphyrines) or phthalocyanines, and developed a class of unsymmetrical and symmetrical phthalocyanine and porphyrazine hybrids containing 2, 4, 6, and 8 thiophenyl groups (BTE–TAPs), as illustrated in Scheme 9 [37–39].

The synthetic strategy of unsymmetrical BTE–TAPs involved the co-cyclization of bis(3-thiophenyl)maleonitrile and 1,2-dicyanobenzene in different molar ratios under nitrogen atmosphere in the dark, as was described in Scheme 10. Magnesium was a template to gain the unsymmetrical macrocycles. The preparation of the symmetrical phthalocyanine hybrids began with the reaction of magnesium powder



Scheme 9



Scheme 10

with dry n-propanol under an inert atmosphere; after the formation of Mg (PrO)<sub>2</sub>, 1,2-dicyano-bis (3-thiophenyl) ethane was added to yield the symmetrical product.

Their absorption spectra were typical for macrocycles of this type (Fig. 1). They all displayed an intense split Q band and an intense single peak in the Soret region. The peripheral functionalization affected the electronic structure of the tetraazaporphyrin  $\pi$ -system and resulted in perturbations of the Q bands. Their maximum extinction coefficients were much higher than those of ordinary diarylethenes.

All of the dithienylethene-based tetraazaporphyrin and phthalocyanine hybrids exhibited obvious photochromism by alternate irradiation with UV and visible light. Their photochromism in solution depended on the solvents to some degree. Scheme 11 gives a representation of the most typical photochromic reaction of these

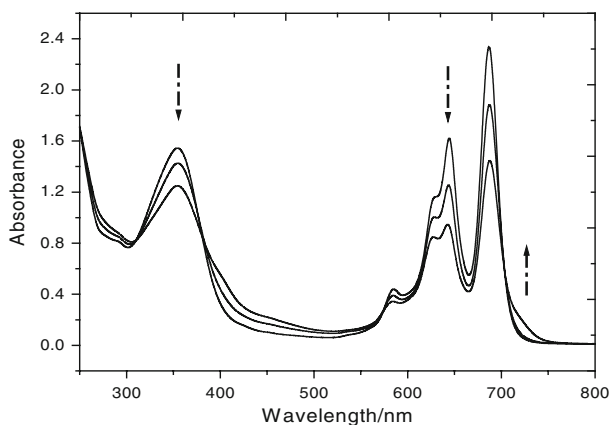
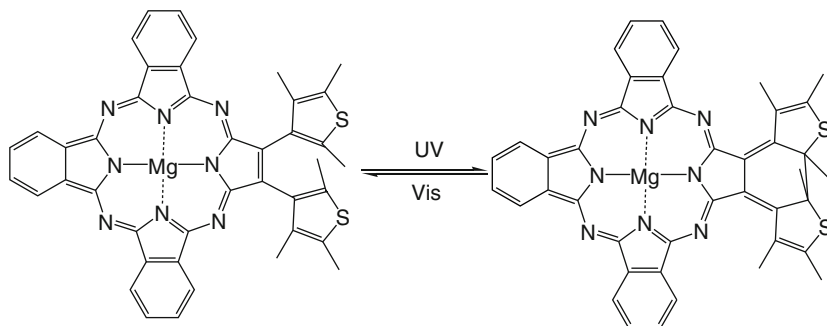


**Fig. 1** Typical absorption spectra of BTE-TAPs in solution and the changes in absorption spectra of the compound under different irradiation times by UV light

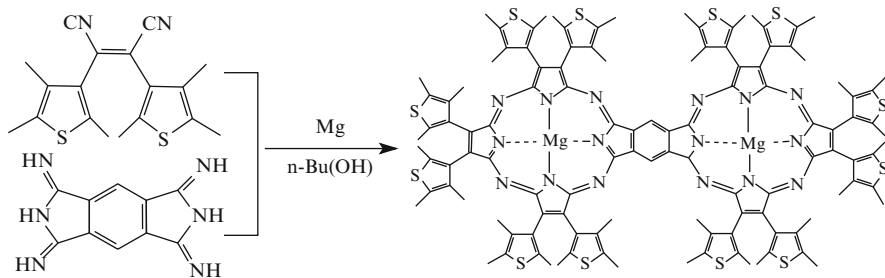


**Scheme 11**

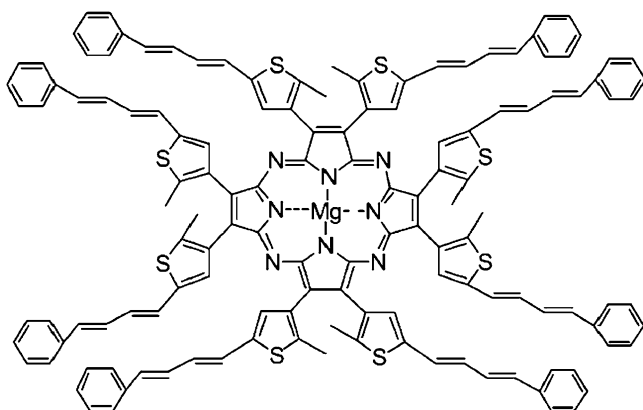
photochromes. Both the open and closed forms were thermally stable at room temperature. Some of the photochromic processes were also observed in solid films. But their performances of photochromism in solution were better than that in solid films. In addition, the cyclization quantum yields in solution at room temperature were relatively higher than the ring-opening quantum yields.

Their emission bands that excited at the region away from the photochromically active absorption bands could be conveniently regulated in a reversible manner by the photoisomerization of the dithienylethene moieties. This characteristic was useful for the application in fluorescence probes and non-destructive readout for erasable memory media.

With the purpose of further increasing the number of adjustable photochromic parameters of the subunit, a binuclear metal complex of porphyrazine bearing six bis(trimethylthiophenyl) functionalities at the periphery was synthesized in our laboratory [40] (Scheme 12). The structure of binuclear porphyrazine was rigidly constrained in a coplanar arrangement with extended  $\pi$ -conjugated subunits.



Scheme 12



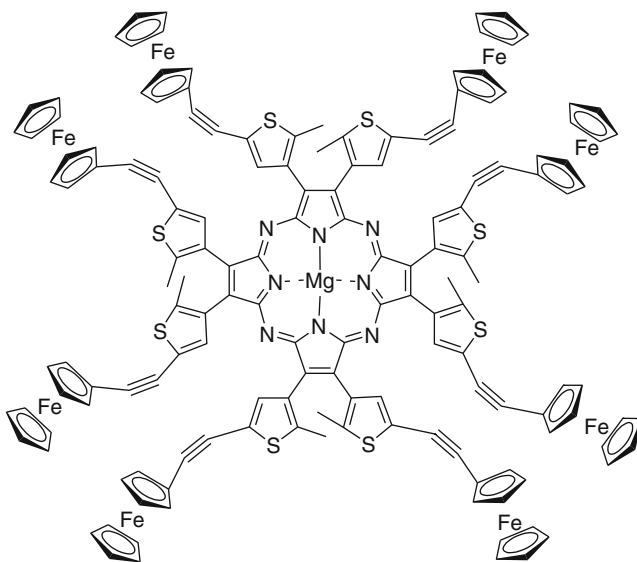
Scheme 13

The synthetic approach was the cyclization of the benzobis(1,3-diimino pyrroline) and 1,2-dicyano-bis(trimethyl-3-thiophenyl) ethane under nitrogen atmosphere under reflux for 2 days. Although this method was concise and convenient, the yield was low and less than 10%.

In comparison with the mononuclear porphyrazine bearing bis(trimethyl-thiophenyl) functionalities, its UV-vis absorption spectra were broader and even extended into the near-IR regions. This region was further remote from the bands inducing photochromic reaction. It showed open-to-closed ring or closed-to-open ring photoisomerizations in different quantum yields by irradiation with UV or visible light. Likewise, the near-IR luminescence changes of the binuclear tetraazaporphyrin could be regulated in a reversible manner by alternate irradiation with UV and visible light.

In order to functionalize the dithienylethene backbone, we designed and synthesized successfully phthalocyanines and their analog-based dithienylethenes containing octakis(4-phenyl-but-1,3-dienyl) substituents (TAP) and eight ferrocene units (TPF) [41, 42], as shown in Scheme 13 and Scheme 14.

The synthesis of  $\pi$ -conjugated photochromic Mg(II) tetraazaporphyrin appended with octakis(4-phenyl-but-1,3-dienyl) hybrid (Scheme 13) began with the reaction of the magnesium powder with dry *n*-propanol under Ar. After the formation of

**Scheme 14**

Mg(PrO)<sub>2</sub>, 1,2-dicyano-ethane or different ratios of phthalonitrile and 1,2-dicyano-bis(3-thiophenyl) ethane were added to obtain a mixture of different phthalocyanines and their analogous macrocycles.

This octa-substituted hybrid (TAP) exhibited high molar absorption coefficient and the long-wavelength absorption band of the closed-ring isomers. These characteristics were viable to application in optical memory. The spectroscopic properties including fluorescence and UV-vis absorption spectra of the compound were all similar to those of the multi-dithienylethene ring-fused photochromic hybrids reported before.

Because the eight ferrocene moieties linking to tetraazaporphyrin magnesium moiety by ethynyl could extend the conjugation of the whole molecule system, both the B band and the Q band of TPF (Scheme 14) were redshifted in comparison with those of tetraazaporphyrin magnesium (II) with dithienylethene moieties aforementioned.

Although all of the former multi-dithienylethene ring-fused photochromic hybrids emitted strong luminescence with varying intensity when excited by UV light, no fluorescence emission was observed for the TPF accompanying its photoisomerization by irradiation with UV light. It might be a result of the efficient quenching via intramolecular electron transfer from the ferrocene to tetraazaporphyrin magnesium (II) moiety.

More interestingly, a reversible photo-induced transformation of the cyclic voltammograms between the open-ring form and closed-ring form of the TPF was observed. This property could be used as the detecting signal for application in electrochemical switches.

## 5 Conclusion

It is evident that photochromic dithienylethenes, as a whole, exhibit the unique photochromic properties. However, for a single molecule it is difficult to possess excellent performances in every aspect, for example, quantum yield, fatigue resistance, thermal stability, etc. As a result of the introduction of versatile phthalocyanines or their analogs, it is no doubt that these kinds of compounds are highly promising in photonic, photoelectric, and photo-chemical switches, digital logic and logic gates, and non-destructive readout capability. Although the quantum yield of cycloreversion often decreases with the extending of the  $\pi$ -conjugated length, the incorporation of bulky substituents or fusing of large-rings enhances their stability and increases the quantum yield of cyclization reaction.

As for the preparation method, further functionalizing of dithienylethene and assembling of multiple components into a single system often result in multi-step reactions and then decrease the overall yields greatly. Therefore, exploration of convenient and industrially available methods to synthesize these functional materials is required.

In addition, most photochromic reactions are performed in solution. Generally, the practical uses require them to undergo photochromism in solid films or even at the level of single molecules. Therefore, it is desirable to develop new photochromic dithienylethene-phthalocyanines and their analog systems such as single crystals and polymers.

**Acknowledgements** This work was financially supported by NSFC/China (No. 20702014).

## References

1. Irie M (2000) *Chem Rev* 100:1685
2. Feringa BL (2001) *Molecular switches*. Wiley-VCH, Weinheim
3. Tian H, Yang SJ (2004) *Chem Soc Rev* 32(2):85
4. Krayushkin MM (2001) *Chem Heterocycl Comp* 37(1):15
5. Tian H, Wang S (2007) *Chem Commun* 7(8):781
6. Kawata S, Kawata Y (2000) *Chem Rev* 100:1777
7. Kobatake S, Irie M (2003) *Annu Rep Prog Chem C* 99:277
8. Wigglesorth TJ, Myles AJ, Branda NR (2005) *Eur J Org Chem* 7:1233
9. Fukaminato T, Umemoto T, Iwata Y, Yokojima S, Yoneyama M, Nakamura S, Irie M (2007) *J Am Chem Soc* 129:5932
10. Okuyama T, Tani Y, Miyake K, Yokoyama Y (2007) *J Org Chem* 72:1634
11. Lee PHM, Ko CC, Zhu NY, Yam VWW (2007) *J Am Chem Soc* 129:6058
12. Raymo FM, Tomasulo M (2006) *Chem Eur J* 12:3186
13. Li L, Sun X, Jiang JZ (2008) *Aust J Chem* 61:640
14. Katsonis N, Kudernac T, Walko M, Molen SJ, Wees BJ, Feringa BL (2006) *Adv Mater* 18:1397
15. Lemieux V, Gauthier S, Branda NR (2006) *Angew Chem Int Ed* 45:6820
16. Ko CC, Kwok WM, Yam VWW, Phillips DL (2006) *Chem Eur J* 12:5840
17. Frigoli M, Welch C, Mehl GH (2004) *J Am Chem Soc* 126:15382
18. Choi H, Lee H, Kang Y, Kim E, Kang SO, Ko JJ (2005) *J Org Chem* 70:8291

19. Lucas LN, Jong JJD, Esch JH, Kellogg RM, Feringa BL (2003) *Eur J Org Chem* 1:155
20. Luo QF, Sheng SH, Cheng SH, Tian H (2005) *Aust J Chem* 58:321
21. Frigoli M, Mehl GH (2005) *Angew Chem Int Ed* 44:5048
22. Chen Y, Zeng DX, Fan MG (2003) *Org Lett* 5:1435
23. Pu SZ, Liu G, Shen L, Xu JK (2007) *Org Lett* 9:2139
24. Torre G, Vázquez P, Agulló-López F, Torres T (2004) *Chem Rev* 104:3723
25. Bellec N, Montalban AG, Williams DBG, Cook AS, Anderson ME, Feng X, Barrett AGM, Hoffman BM (2000) *J Org Chem* 65:1774
26. Fukuda T, Makarova EA, Lukyantes EA, Kobayashi N (2004) *Chem Eur J* 10:117
27. Kobayashi N, Lam H, Nevin WA (1994) *J Am Chem Soc* 116:879
28. Pandey, RK (2000) *J Porphyr Phthalocyanines* 4:368
29. Norsten TB, Branda NR (2001) *J Am Chem Soc* 123: 1784
30. Norsten TB, Branda NR (2001) *Adv Mater* 13: 347
31. Osuka A, Fujikane D, Shinmori H, Kobatake S, Irie M (2001) *J Org Chem* 66:3913
32. Park JE, Shin EJ (2007) *Spectrochim Acta A* 68:554
33. Liddell PA, Kodis G, Moore AL, Moore TA, Gust D (2002) *J Am Chem Soc* 124:7668
34. Straight SD, Liddell PA, Terazono Y, Moore TA, Moore AL, Gust D (2007) *Adv Funct Mater* 17:777
35. Kim HJ, Jang JH, Choi H, Lee T, Ko J, Yoon M, Kim H-J (2008) *Inorg Chem* 47(7):2411
36. Kai H, Nara S, Kinbara K, Aida T (2008) *J Am Chem Soc* 130(21):6725
37. Tian H, Chen BZ, Tu HY, Müllen K (2002) *Adv Mater* 14:918
38. Chen BZ, Wang MZ, Wu YQ, Tian H (2002) *Chem Commun* 2(10):1060
39. Luo QF, Chen BZ, Wang MZ, Tian H (2003) *Adv Funct Mater* 13:233
40. Luo QF, Cheng SH, Tian H (2004) *Tetrahedron Lett* 45:7737
41. Sun L, Wang S, Tian H (2007) *Chem Lett* 36(2):250
42. Wang S, Li XC, Cheng SH, Feng YL, Tian H (2005) *Mol Cryst Liq Cryst* 431:69



# Ball-Type Phthalocyanines: Synthesis and Properties

Özer Bekaroğlu

**Abstract** Phthalocyanines (Pcs) are unique synthetic macrocycles with a long history of 100 years from their first publications and of growing interest in many fields of technology. Nevertheless, ball-type Pcs, as a new class of compounds, were first published only recently and are rather rare in the literature. But they promise applications in several fields of technology. In present review, the methods applied for the synthesis and characterization of the structures of ball-type Pcs, as well as also some of their measurement techniques, are considered. In addition, the results of the investigations into the electrochemical, nonlinear optical, electrical, and gas-sensing properties of these new class of Pcs are also given.

**Keywords** Ball-type phthalocyanines · Chemo-sensor · Cyclic voltammetry · Mass spectroscopy · Nonlinear optical · Synthesis

## Contents

1	Introduction .....	106
2	Synthesis .....	107
3	Separation and Purification .....	115
4	UV-Visible Spectra of Ball-Type Pcs .....	116
5	Electrochemistry of Ball-Type Pcs .....	120
6	MALDI-TOF-MS of Ball-Type Pcs .....	123
7	Nonlinear Optical (NLO) Properties of Ball-Type Pcs .....	126
8	Electrical and Gas-Sensing Properties of Ball-Type Pcs .....	130
9	Conclusion and Outlook.....	133
	References .....	134

## Abbreviations

ac	Alternating current
ACCA	$\alpha$ -Cyano-4-hydroxycinnamic acid

CBH	Correlated barrier hopping
CPC	Controlled potential coulometry
CV	Cyclic voltammetry
DBU	1,8-Diazabicyclo[5.4.0]undec-7-ene
dc	Direct current
DCM	Dichloromethane
DMF	Dimethyl formamide
DMSO	Dimethyl sulfoxide
GW	Gigawatt
h	hour(s)
HOMO	Highest occupied molecular orbital
$\text{Im}\{\chi^{(3)}\}$	Imaginary part of third order nonlinear susceptibility
LUMO	Lowest occupied molecular orbital
min	Minute(s)
NLA	Nonlinear absorption
NLO	Nonlinear optical
NLR	Nonlinear refraction
ns	Nanosecond
OL	Optical limiting
Pc	Phthalocyanine
POSS	4,5-Bis[1-(3-mercapto)propyl-3,5,7,9,11,13,15-isobutylpentacyclo]octasiloxane
RSA	Reverse saturable absorption
rt	Room temperature
TBAP	Tetrabutylammonium perchlorate
TEGDT	Tetraethyleneglicol ditocylate
THF	Tetrahydrofuran

## 1 Introduction

Phthalocynines (Pcs) are synthetic macrocyclic compounds which were first reported in 1907 [1]. The characterization of their structures was first published in 1934 [2–5], and X-ray diffraction analyses were performed by Robertson in order to clear their structures [6–8]. By adding various substituents to the nonperipheral ( $\alpha$ ) and peripheral ( $\beta$ ) positions of the benzene rings, numerous Pcs have been prepared with almost all metal ions in the periodic table. Pcs are very stable blue or green pigments and are an important class of chemicals for commercial use in inks, dyestuff for textiles, and colorant for metals and plastics. Now, they are being used in many areas of technology as sensitizers for photodynamic therapy of cancer and for other medical applications, and they have been receiving much attention in a variety of new fields such as chemo-sensors and electrochromic displays [9, 10]. Other applications comprise computer read–write disc and related information storage systems. Because of their diverse application in fields such as photovoltaic cells, liquid crystals, catalysts for oxidizing saturated hydrocarbons, hydrogenation of olefins [11, 12], increasing

the octane rate of gasoline [13], nonlinear optics, and optical limiting materials [14], they continue to be the subject of the increasing research activity. These suggest that their potential use in many fields of technology is likely to increase significantly.

For these applications, the solubility of Pcs plays a significant role. The Pc core without the substituent is insoluble, which stems from the stacked oligomerization. To increase the solubility of Pcs for desired applications, two approaches are possible: one to incorporate a solubilizing substituent to the molecule, and the other to have the molecule in such a manner that its stacking ability is reduced [15].

Besides the network and one-dimensional polymeric Pcs, binuclear, binuclear double decker [16–22], binuclear clamshell and double decker clamshell [9, 23–26], trinuclear [27–31], tetranuclear [9, 32], pentanuclear [33], and octanuclear Pcs [34] have been reported.

Ball-type Pcs are a new class of Pcs, the first of which was reported by Tomilova's group in 2002 [35, 36]. This new type of Pcs has four bridged substituents on the peripheral positions of the each benzene rings of the two Pc monomers which are arranged cofacially. The distance between the two Pc rings and chemical and physical properties depend on the constituents of those linkers and differ significantly from the parent monomers. A strong interaction between the two face-to-face-arranged Pc rings or the two metal centers in this type of compounds has been detected with spectroscopic and electrochemical measurements.

Research reporting on the synthesis and properties of ball-type Pcs with the number of different cross links is rather rare in the literature.

## 2 Synthesis

Currently, two methods have been followed for the synthesis of ball-type Pcs: synthesis in solvent and in the solid phase.

The first published ball-type Pc was obtained by the reaction of 1,2-bis(3,4-dicyanophenoxy)methyl)-benzene with zinc acetate and DBU as base in boiling dichlorobenzene under argon atmosphere for 14 h. The yield of this reaction was rather low (1.84%) [35]. In the next study, the same ball-type ZnPc was prepared by the solid-phase method increasing the amount of zinc acetate by a factor of 10 and heating the reaction mixture in the absence of catalysts at 250°C for 5 min. This time, the yield was 33% [36].

Because of expected electrical, electrochemical, optical, chemo-sensor, and other properties of the ball-type Pcs, several metallo and metal-free ball-type Pcs with different linkers have been reported. Metallo and metal free ball-type Pcs containing four calyx[4]arene units as linkers have been synthesized, Fig. 1 [37]. The structures of compounds **1–3** were confirmed by UV-vis, IR, <sup>1</sup>H-NMR, matrix-assisted laser desorption/ionization time-of-flight mass spectrometry (MALDI-TOF-MS), and elemental analysis. Because of their unique structure and versatile complexation properties [38], calixarenes were found to be one type of interesting compounds to be incorporated into Pc. The cone conformation of the *t*-butylcalix[4]arene direct

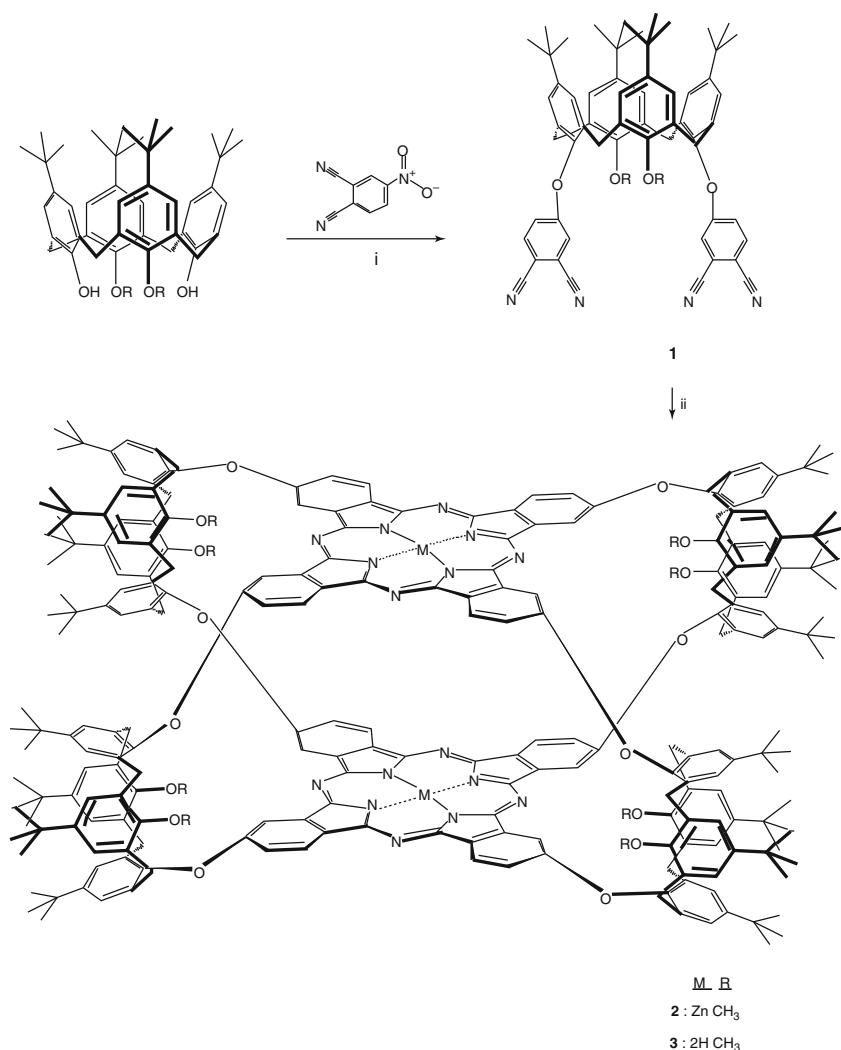


**Fig. 1** Schematic illustration of the synthesis of four *t*-butylcalix[4]arene bridged ball-type Zn-Pc **2** and metal-free Pc **3**. Reagents and conditions: for **1** (i)  $\text{K}_2\text{CO}_3$ , DMSO,  $85^\circ\text{C}$ , 76 h, (ii) for **2**: DMF,  $\text{Zn}(\text{OAc})_2$ ,  $2\text{H}_2\text{O}$ ,  $190^\circ\text{C}$ , 24 h in sealed tube. Yield 17%; (iii) for **3**: lithium metal, 1-pentanol in sealed tube  $176^\circ\text{C}$ , 18 h. Yield 55% [37]

the tetramerization of the two phthalonitriles at the lower rim to form Pcs with ball-type structures.

Several works have been reported for selective substitution of nitro groups at the upper rim of the calix[4]arene [39, 40]. The selectively *ipso*-nitrated *p*-*tert*-butylcalix[4]arene was used as starting material for the preparation of bisphthalonitrile **5**. Nitro groups at the upper rims of **6** were coupled with nitro groups of four unsymmetrical Pcs **7** in order to obtain the hexanuclear zinc Pc **8**, Fig. 2 [41].

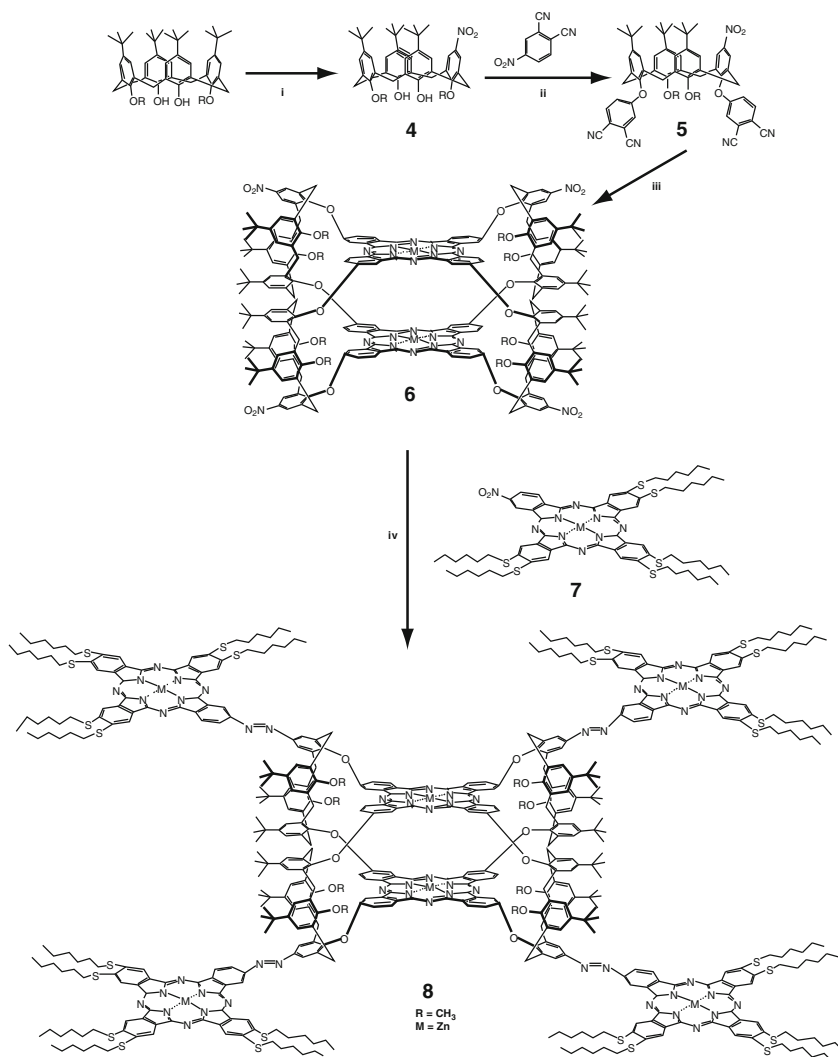


**Fig. 2** Synthetic pathway for compounds **4–6** and **8**. (i)  $\text{HNO}_3$ ,  $\text{CH}_2\text{Cl}_2$ ,  $\text{CH}_3\text{COOH}$ ; (ii),  $\text{K}_2\text{CO}_3$ ,  $\text{DMSO}$ ,  $80^\circ\text{C}$ , 70 h; (iii)  $\text{Zn}(\text{OAc})_2 \cdot 2\text{H}_2\text{O}$ , DBU, 1-pentanol reflux; (iv)  $\text{NaOH}$  solution, powdered Zn,  $\text{MeOH}/\text{THF}$ , reflux 18 h [41]

The key starting compound is the mono nitro derivative of calix[4]arene **4**, which was obtained via a single-step reaction with 10 equivalents of 63%  $\text{HNO}_3$  in a mixture of dichloromethane and glacial acetic acid in less than 5 min in 94% yield according to the literature method. Compound **4** converted to bisphthalonitrile derivative **5** by the given method in 59% yield. Ball-type ZnPc **6** was prepared from **5** and zinc acetate in 1-pentanol in the presence of DBU. Hexanuclear ball-type ZnPc **8** was obtained by the reaction of **6** with **7** in a mixture of  $\text{NaOH}$ ,  $\text{MeOH}$ ,  $\text{THF}$ , and activated zinc powder with a yield of 55%.

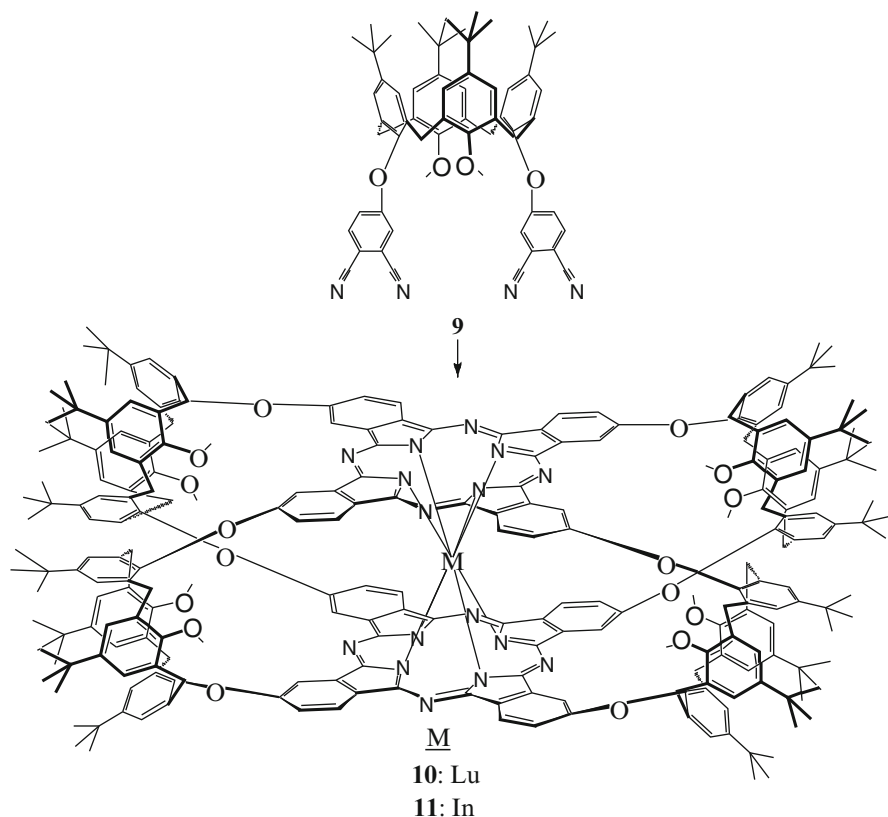


**Fig. 3** Synthesis of compound **10** and **11** [42]

Rare-earth bisphthalocyaninates, especially  $\text{LuPc}_2$ , are one of the important objects of intense investigation because of their electrochemical (electrochromic effect), electrical, and optical properties. The ball-type four *t*-butyl-calix[4]arene bridged double decker lutetium(III) and indium(III) Pcs have also been prepared, Fig. 3 [42].

Novel ball-type four *t*-butyl-calix[4]arene bridged double deckers lutetium(III) phthalocyanine  $[\text{LuPc}_2(\text{tbca})_4]$  **10** and indium(III) phthalocyanine  $[\text{InPc}_2(\text{tbca})_4]$  **11** were prepared by the reaction of 1,3-bis(3,4-dicyanophenoxy)-4-*tert*-butylcalix arene **9** and the corresponding metal salts ( $\text{Lu}(\text{OAc})_3 \cdot 3\text{H}_2\text{O}$  and  $\text{InCl}_3$ ) in the presence of lithium metal in 1-pentanol under  $\text{N}_2$  in a sealed tube for 15 h, Fig. 3. Yields of **10** and **11** were 18 and 55%, respectively.

Starting with 1,1'-methylene-di(2-naphthol) **13** and 5-nitro-phthalonitrile **12**, bis-phthalonitrile **14** was prepared. To obtain metal-free ball-type Pc **15**, a suspension of **14** in dry amyl alcohol and lithium metal was heated in a sealed tube at  $170^\circ\text{C}$  for 8 h, Fig. 4. The metallo Pcs with zinc **16** and cobalt **17** were synthesized by heating a

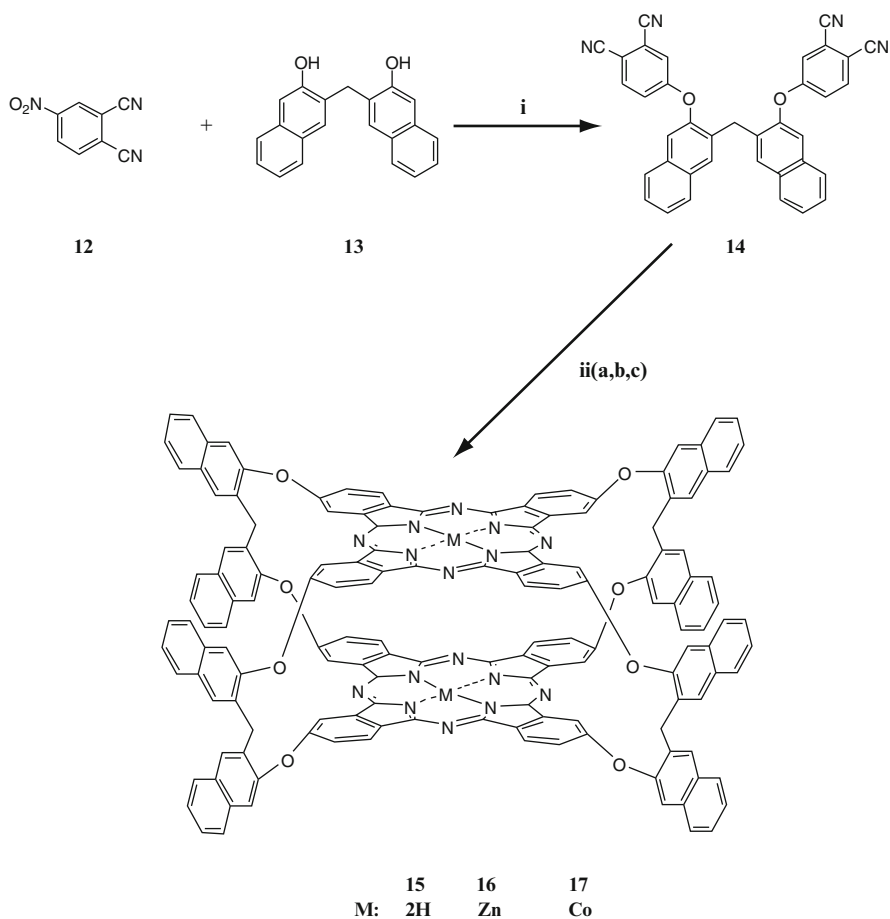


**Fig. 4** Synthesis of **14–17**. (i)  $\text{K}_2\text{CO}_3$ , DMSO; (ii) a: Li, 1-pentanol,  $\text{N}_2$ ,  $170^\circ\text{C}$ , b:  $\text{Zn}(\text{CH}_3\text{COO})_2 \cdot 2\text{H}_2\text{O}$ ,  $280^\circ\text{C}$ , c:  $\text{Co}(\text{CH}_3\text{OO})_2 \cdot 4\text{H}_2\text{O}$ ,  $280^\circ\text{C}$  [24]

powdered mixture of **14** and the corresponding metal salts in a sealed tube at  $280^\circ\text{C}$  for 3 min, Fig. 4 [24].

But, the reaction of **14** with the cobalt salt in a solid phase at  $320^\circ\text{C}$  for 10 min and washing the reaction mixture with hot methanol and acetic acid gave a mixture of several Pcs. MALDI-TOF measurements with the matrix of 2,5-dihydroxybenzoic acid showed that not only ball-type Pc **17** but also four more Pcs **18**, **19**, **20**, and **21** were present in the product, Figs. 5 and 6 [43]. Two of these five Pcs, namely **17** and **18** in Fig. 5, could be separated with silica gel column, but three other Pcs, namely **19**, **20**, and **21**, could not be isolated.

1a,8b-Dihydronaphto[b]naphthofuro-[3,2-d]furan-7,10-diyl **22** being converted into **23** was heated with zinc or cobalt salts in a sealed tube at  $300^\circ\text{C}$  for 5 min

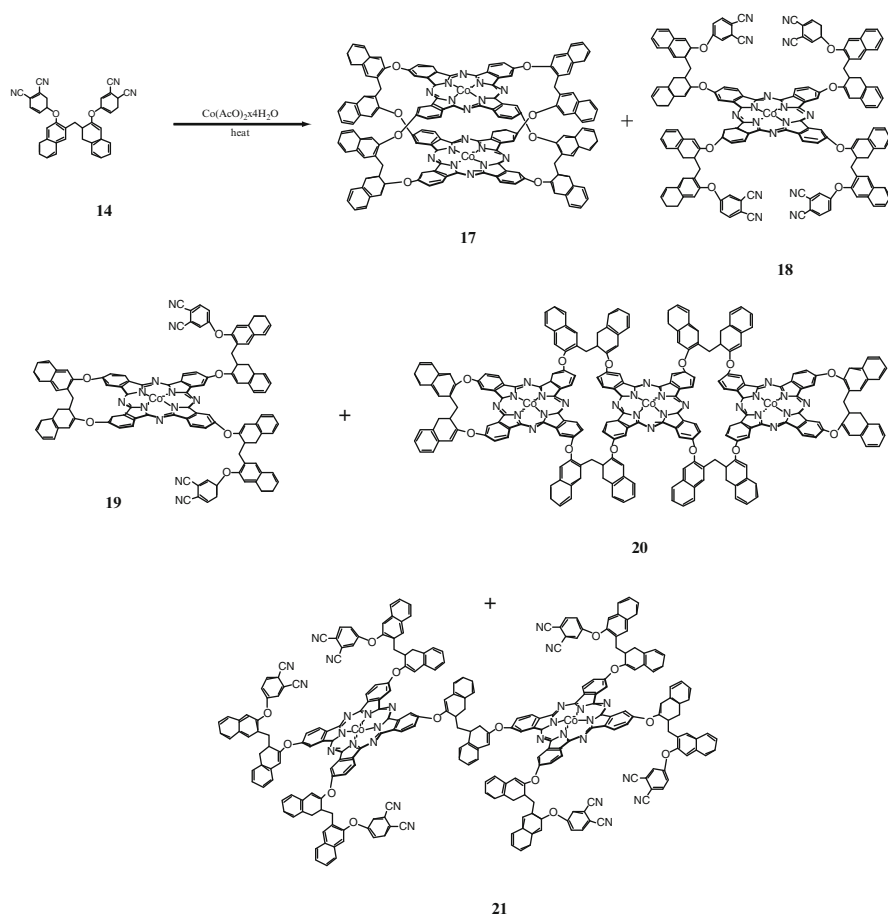
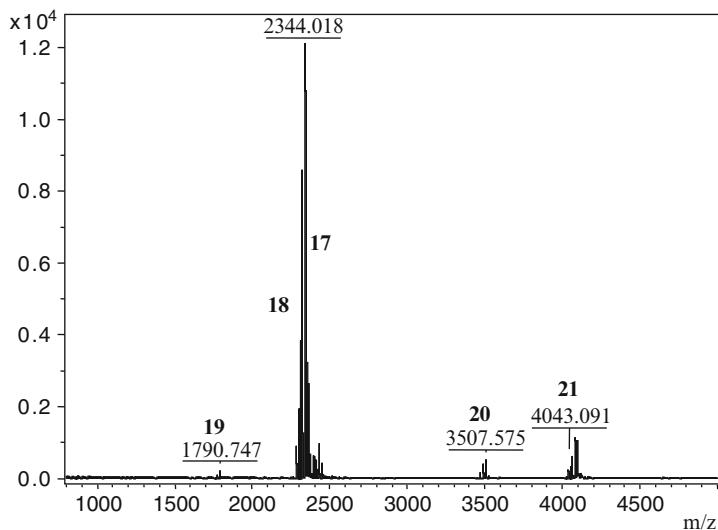


**Fig. 5** Synthesis of **17–21** [43]

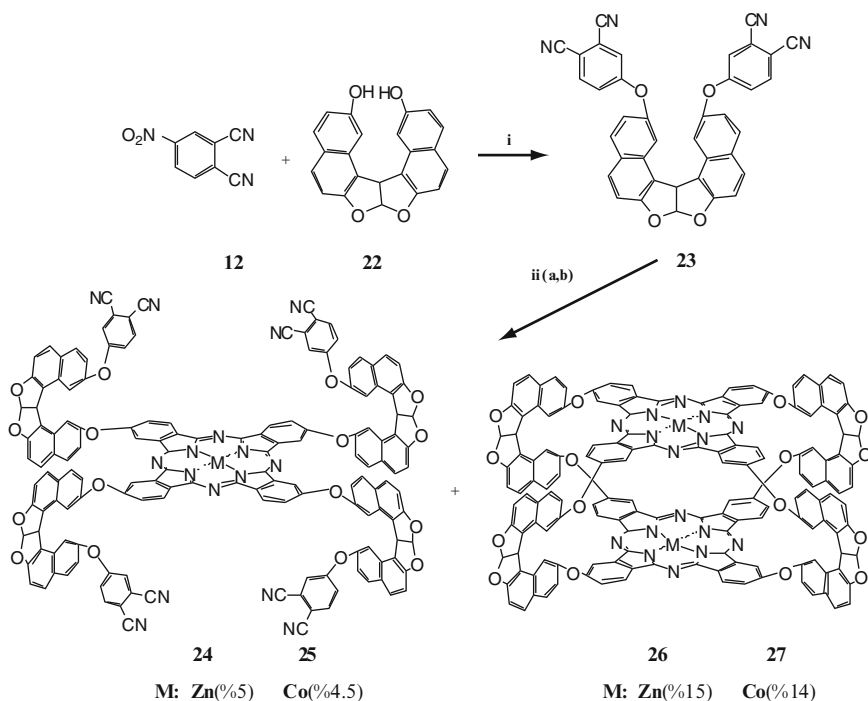
without solvent, resulting two types of Pcs: one was mono zinc Pc **24** or cobalt Pc **25** and the other was the ball-type zinc Pc **26** or cobalt Pc **27** with the yields of 5 and 4.5% for mono and 15 and 14% for ball-type Pcs, respectively, Fig. 7 [44]. When the compound **23** was heated with lithium metal in hexanol at  $170^\circ\text{C}$  for 8 h, only metal-free mono Pc **28** was obtained. However, when compound **23** was heated with magnesium acetate without the solvent in a sealed tube at  $300^\circ\text{C}$  for 5 min, both metal-free mono **29** and metal-free ball-type **30** Pcs were formed, Fig. 8 [45].

Pentaerythritol with four OH functionalities has also been employed for the preparation of ball-type Pcs, Fig. 9 [46]. In order to obtain the starting compound bisphthalonitrile **32**, two of the four hydroxy groups of pentaerythritol were protected with benzaldehyde as mono acetal **31**. Heating the powdered mixture of bisphthalonitrile **32** and metal salts in a sealed tube at  $300^\circ\text{C}$  for 10 min gave the zinc and cobalt ball-type Pcs **33** and **34** with yields of 23 and 18%, respectively,

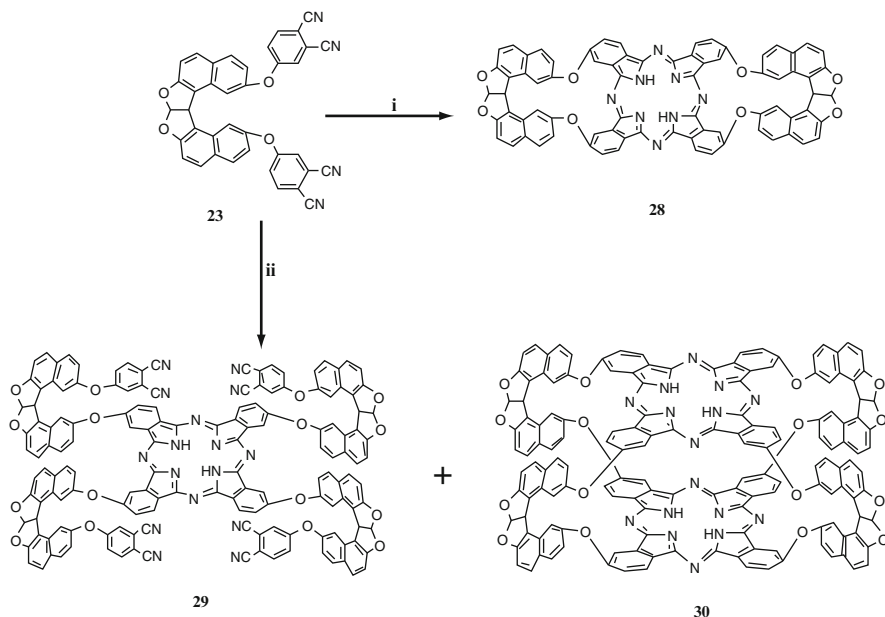




**Fig. 6** The MALDI-TOF spectra of the mixture of compounds **17–21** in Fig. 5 [43]



**Fig. 7** Synthesis of **23–27**. (i)  $K_2CO_3$ , DMSO; (ii) a:  $Zn(CH_3COO)_2 \cdot 2H_2O$ ,  $300^\circ C$ , b:  $Co(CH_3COO)_2 \cdot 4H_2O$ ,  $280^\circ C$  [44]



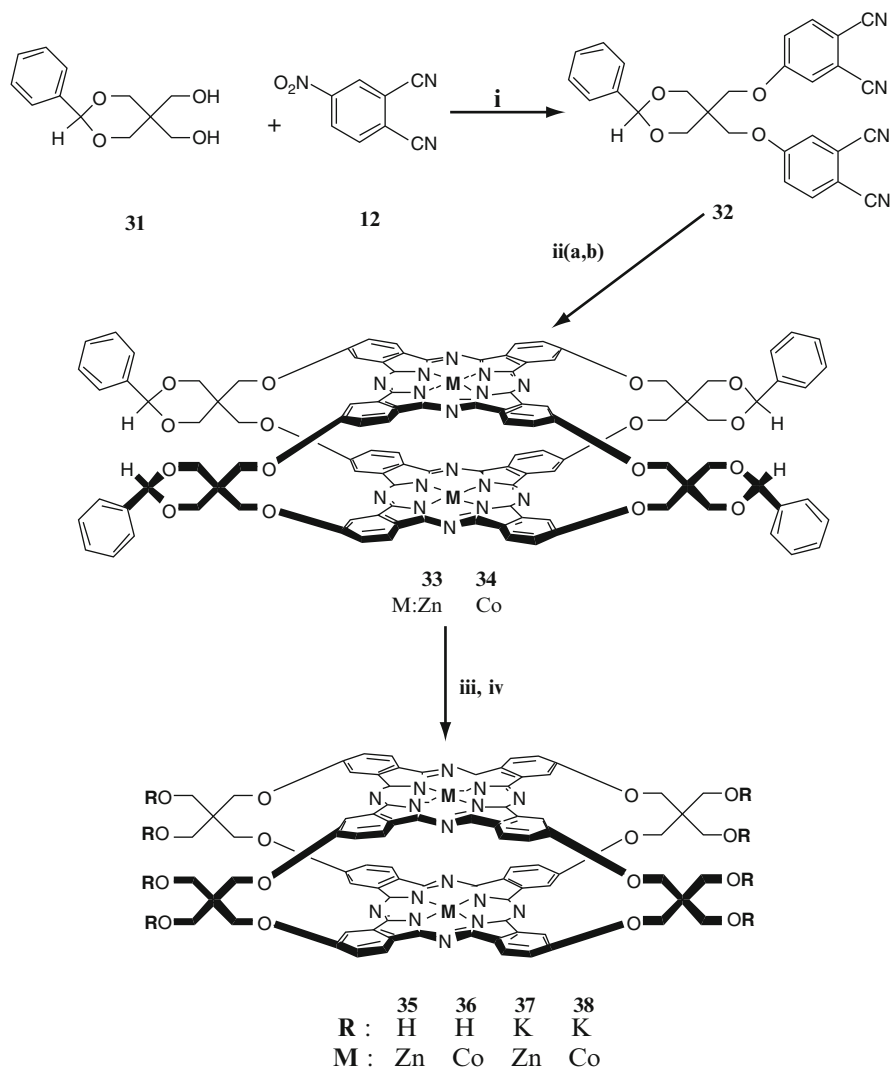
**Fig. 8** Synthesis of **28–30**. (i) Li, *n*-hexanol, N<sub>2</sub>, 170° C; (ii) Mg(CH<sub>3</sub>COO)<sub>2</sub>·4H<sub>2</sub>O, N<sub>2</sub>, 300° C [45]

Fig. 9. After removing the mono acetal groups of **33** and **34** by hydrogenation, ball-type Pcs with free hydroxy groups **35** and **36** or water-soluble alkali metal salts of ball-type Pcs **37** and **38** were obtained.

Those free eight hydroxy groups of the ball-type Pcs give the possibility to make further reactions to obtain novel ball-type Pcs with various properties. For example, the eight hydroxy groups can be converted to four crown-ethers **39**, **40**, **39a**, and **40a** (Fig. 10) [47] or to eight perfluorodecyl units **42** and **43** (Fig. 11) [48].

4, 4'-Isopropylidendiiodoxydiphenyl was used as a bridged compound in order to obtain ball-type Pc. Mixing the bisphthalonitril derivative **44** with zinc or cobalt salt in the solid phase and heating the mixtures in a sealed tube at 250° C for 10 min gave the Pcs **45** and **46** with the yields of 9.39 and 8.27%, respectively, Fig. 12 [49].

Not all reactions in the solid phase convert bisphthalonitrile derivatives into ball-type Pcs. One example of such reactions is the conversion of the bisphthalonitrile derivative of phenolphthalein into ball-type Pc [50]. As can be seen in Fig. 13, when a solid mixture of bisphthalonitrile **48** and metal salt was heated in a sealed tube at 320° C for 5 min, only mono Pcs **49** and **50** were formed. Further reaction of **49** or **50** with an excess of the corresponding metal salt in a refluxing solvent for 24 h resulted in the formation of ball-type Pcs **51** or **52**.



**Fig. 9** Synthesis of **32–38** (i)  $\text{K}_2\text{CO}_3$ , DMF, (ii) a:  $\text{Zn}(\text{CH}_3\text{COO})_2 \cdot 2\text{H}_2\text{O}$ , b:  $\text{Co}(\text{CH}_3\text{COO})_2 \cdot 4\text{H}_2\text{O}$ , (iii)  $\text{H}_2$ , Pd/C(10%), KOH (20%) [46]

### 3 Separation and Purification

Separation and purification of the ball-type Pcs are in some cases easy depending on the bridged substituents but generally difficult and sometimes tedious like in other Pcs. The general purification methods of the Pcs are described elsewhere [9]. The ball-type Pcs are usually soluble in common organic solvents depending on the bridged substituents and metal ions. Purification by sublimation or using

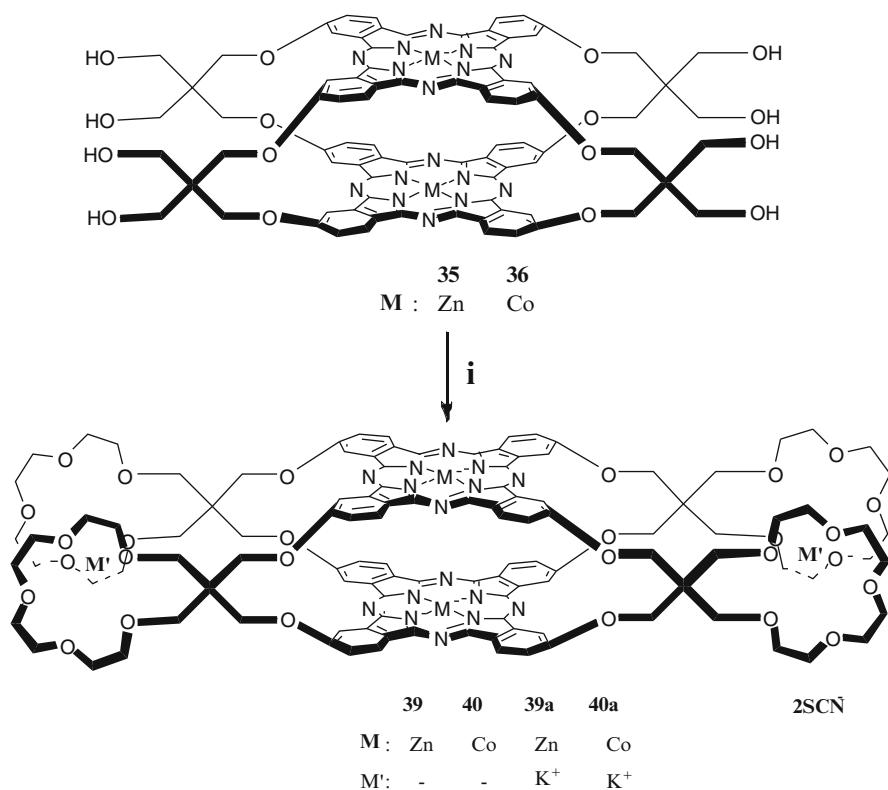


**Fig. 10** Synthesis of **39** and **40** (i) TEGDT, NaH, THF [47]

concentrated sulfuric acid followed by precipitation in ice water has not been used until now.

The solubility difference between the starting materials and the end products in various solvents should be considered first. Column chromatography on silica gel or other column materials is usually used for the purification of the Pcs. In the case of more than one main end product, such as given in Fig. 5, preparative gel permeation chromatography will be efficient.

#### 4 UV-Visible Spectra of Ball-Type Pcs

The UV-vis spectral properties of Pcs have been of intrinsic interest since the beginning of their history. These deep blue-green dyes show some intense band(s) located at 600–700 nm (Q band) and around 300–400 nm (soret or B band) depending on the substituents at the benzene rings, the metal complexed, and axial coordination ligands. In the case of metal-free Pcs, all states are nondegenerate and the Q band splits

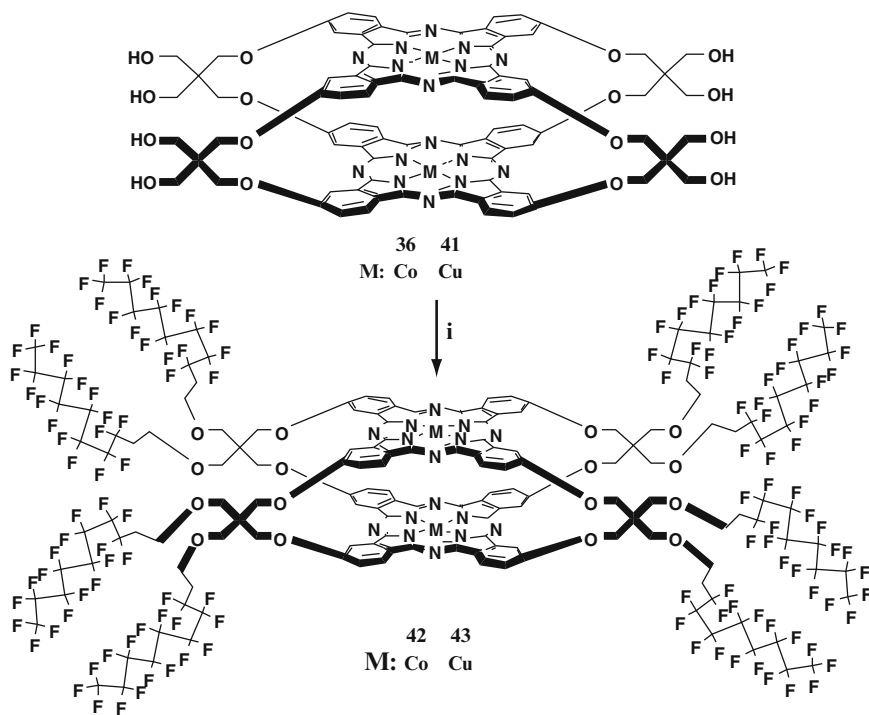


Fig. 11 Synthesis of **42** and **43** (i) NaH and HDFID in DMF at 120° C [48]

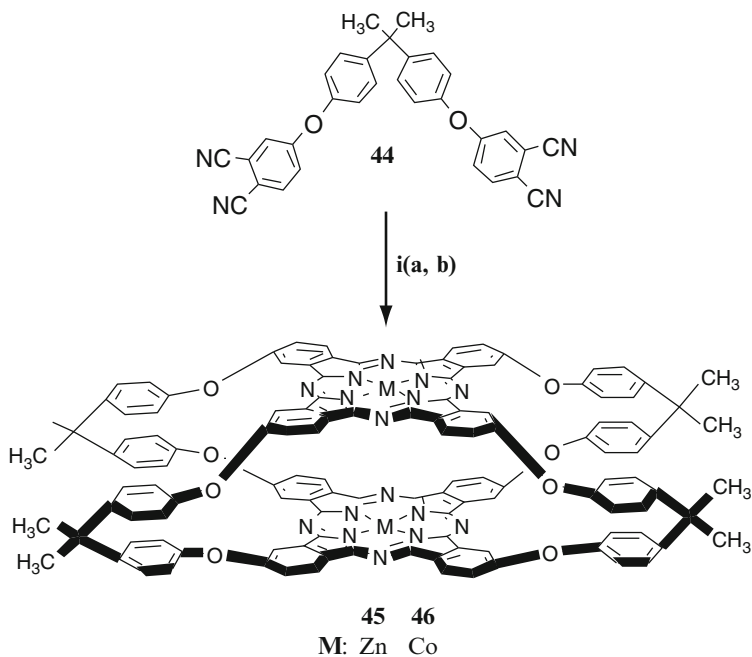
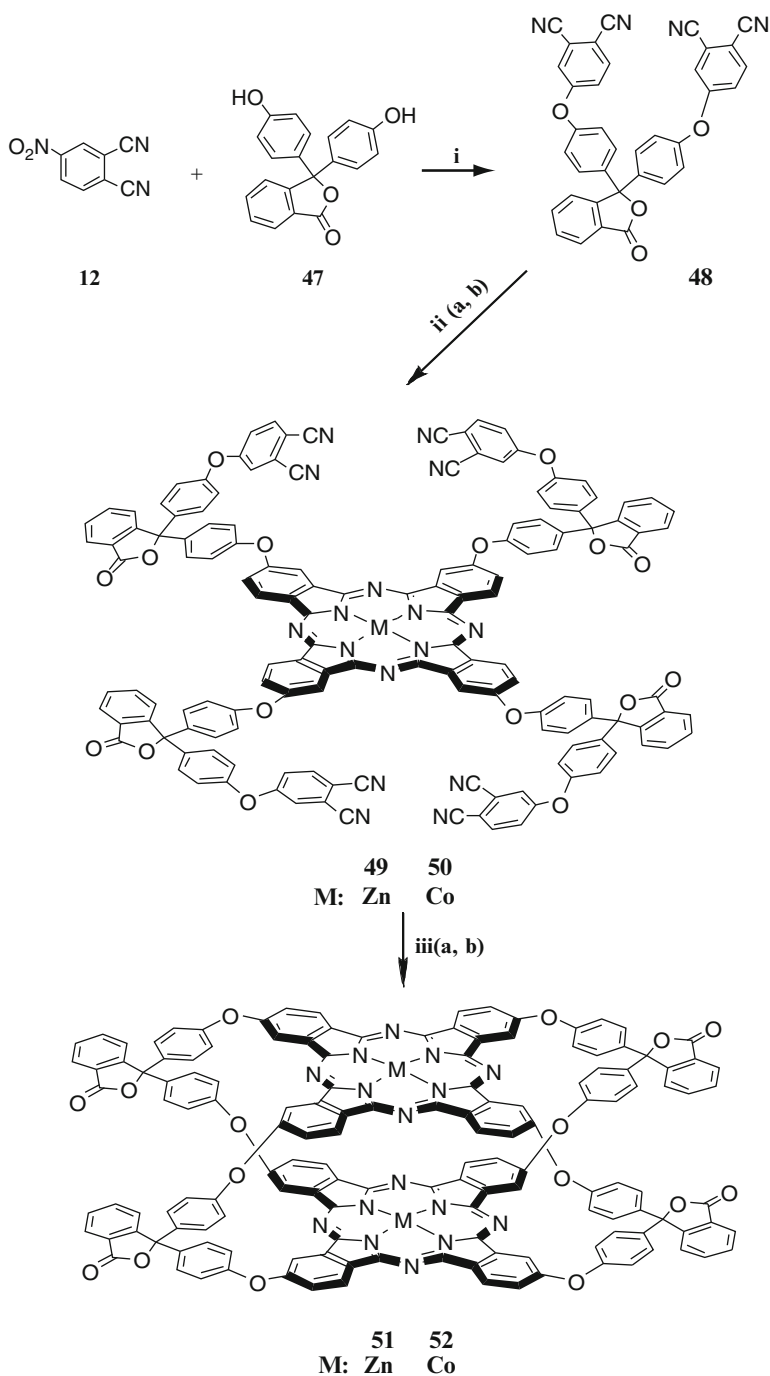


Fig. 12 Synthesis of **45** and **46**. (i)  $K_2CO_3$ , DMF; (ii) a:  $Zn(CH_3COO)_2 \cdot 2H_2O$ , b:  $Co(CH_3COO)_2 \cdot 4H_2O$  [49]



**Fig. 13** Synthesis of **48-52**. (i)  $K_2CO_3$ ,  $N_2$ , DMSO, rt 24 h; (ii)  $Zn(CH_3COO)_2 \cdot 2H_2O$  or  $Co(CH_3COO)_2 \cdot 4H_2O$ ,  $320^\circ C$ , 5 min; (iii)  $Zn((CH_3COO)_2 \cdot 2H_2O$  or  $Co(CH_3COO)_2 \cdot 4H_2O$ ,  $N_2$ , DMF, reflux temperature, 24 h [50]

into two components due to the reduced  $D_{2h}$  molecular symmetry. UV-vis spectra of the Pcs have been studied in detail, comparing them with porphyrins and related compounds [51].

The UV-vis spectra of the ball-type Pcs resemble those of the other Pcs with some differences. Depending on the bridged compounds, metals, and solvent, the electronic and other properties of ball-type Pcs change dramatically. Also, due to the bridged substituents, the distance between two Pc molecules of the ball-type Pcs changes considerably, affecting their degree of interaction.

UV-vis spectra of the four calix[4]arene bridged ball-type metallo and metal-free Pcs are illustrated in Fig. 14 [25]. In the spectrum of **2** in chloroform at room temperature, an intense Q band was observed at 688 nm, which is attributable to  $\pi \rightarrow \pi^*$  transition from HOMO to LUMO, and another band in the UV region at 350 nm (B band) arising from the deeper  $\pi$  level to LUMO transition. An additional weak vibrational satellite band at ca. 68 nm blue-shifted from the normal Q band was observed as a result of exciton coupling between the Pc units [25]. Although the Q band of **2** is not split, a well-defined absorption at 620 nm of **2** can be interpreted in terms of intramolecular interactions between two Pc rings. The energies and relative intensities, as well as the broadening of the bands observed, are in accordance with the pattern that would be anticipated on the basis of the excitation coupling theory. In the case of the electronic spectrum of **3** in methanol at room temperature, the Q band is split as expected, and there are two strong bands at 710 and 670 nm. The splitting of the Q band is characteristic for metal-free Pcs indicating a  $D_{2h}$  symmetry of the molecule. Such split Q band absorptions are due to  $\pi \rightarrow \pi^*$  transitions of the fully conjugated 18  $\pi$  electron systems. In addition, a band at 626 nm to the blue side of the double Q band is indicative of strong intramolecular interactions between the Pc rings, perhaps due to the ball-type cofacial structure [25].

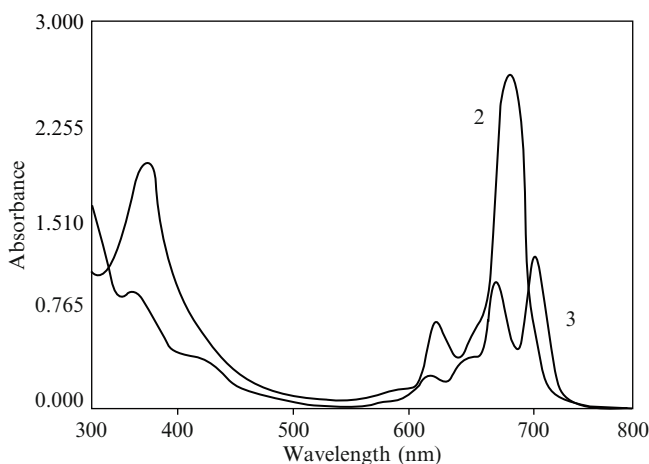


**Fig. 14** UV-vis spectra for Zn(II) **2** in  $\text{CHCl}_3$  and metal-free **3** in methanol [25]

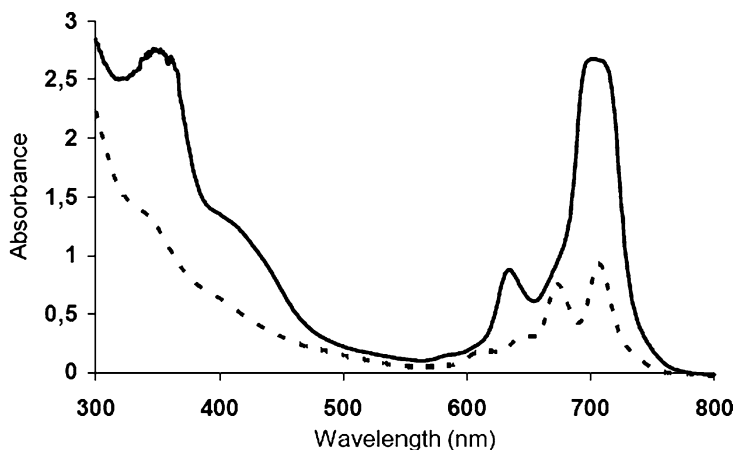


**Fig. 15** UV-vis spectra for compounds Lu(III) **10** (dashed line) and for In(III) **11** (solid line) in acetic acid [42]

The electronic spectra of Lu(III) **10** and In(III) **11** complexes of calix[4]arene ball-type Pcs in Fig. 3 are worthy of being cited, Fig. 15. It can be seen from the electronic absorption spectrum of **10** that Q band splits into two, with maxima 708 and 673 nm, as a result of exciton coupling between two Pc units. Compound **11** exhibits a broadened Q band indicating additional amount of aggregation of that compound, and a weak band around 630 nm due to exciton coupling [42, 52–57].

The electronic spectra of the other published ball-type Pcs resemble more or less to each other with respect to the current factors of the theory [24, 41, 44, 46, 49, 50].

A comparison of the UV-vis spectra of the ball-type, its precursor, and mono Pc **28**, **29**, and **30** in (Fig. 8) in THF shows characteristic absorptions between 610 and 710 nm in the Q band region for metal-free Pcs. Because of the lower symmetry of the metal-free Pcs, the Q band splits into two intense bands in that region. An additional third band at 636 nm and a fourth band/shoulder at 610 nm are exciton coupling and charge transfer bands, respectively. The intensity of the third band of the compound **30** clearly indicates the presence of strong intramolecular interactions between two Pc macrocycles [45].

## 5 Electrochemistry of Ball-Type Pcs

The electrochemical and spectroelectrochemical properties of some ball-type Pcs have been investigated and compared with those of the monomer or clamshell dimeric Pcs which contain the same substituents at the periphery as bridged groups. The striking feature of cyclic voltammetric (CV) measurements of the ball-type Pcs is the shift of potential due to HOMO–HOMO interactions between the cofacial Pc rings [38]. For example, the voltammetric measurements of the four



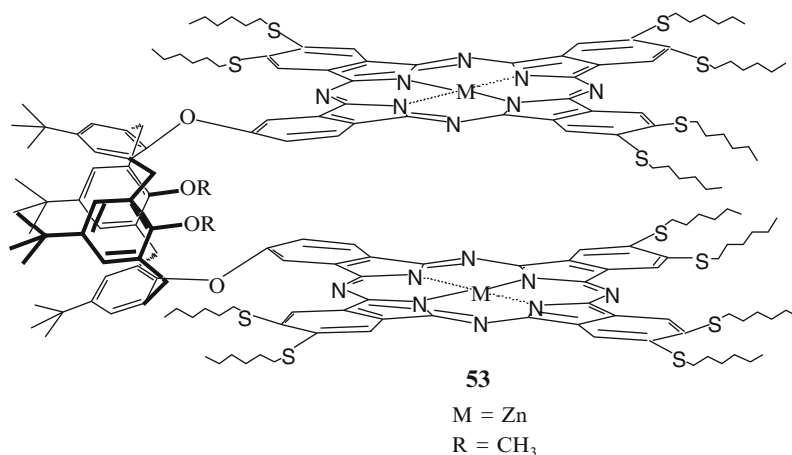


**Fig. 16** Zn(II) clamshell Pc **53** [25]

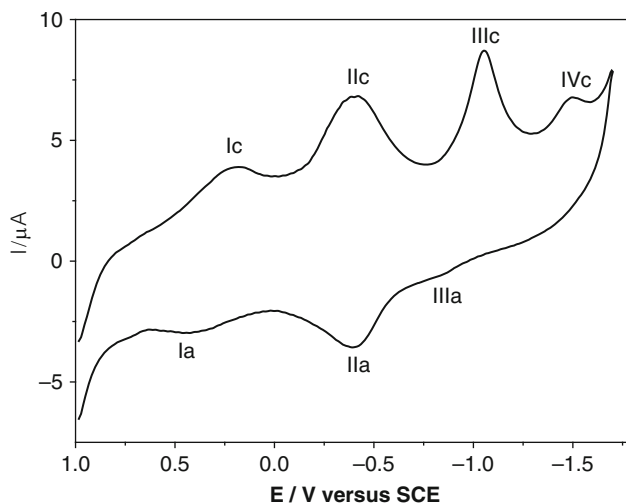


**Fig. 17** CV of **2** ( $1.5 \times 10^{-4}$  M) at  $0.100 \text{ V s}^{-1}$  on Pt in DMSO/TBAP [25]

*t*-butylcalix[4]arene bridged ball-type ZnPc **2** and metal-free Pc **3** in Fig. 1 and comparison with those of clamshell type of ZnPc **53** in Fig. 16 clearly indicated the interaction between two Pc rings.

CV measurements of ball-type Pcs **2** and **3** [25] show four one-electron redox processes. The transfer of one electron in each step indicates that the splitting of molecular orbital occurs as a consequence of the strong interaction between the two Pc rings of **2** and **3**. The strong interaction between the molecular orbitals of two Pcs results in remarkable change in the redox potentials, compared with the corresponding mono Pcs and noninteracting planar dimers, Figs. 17–19.

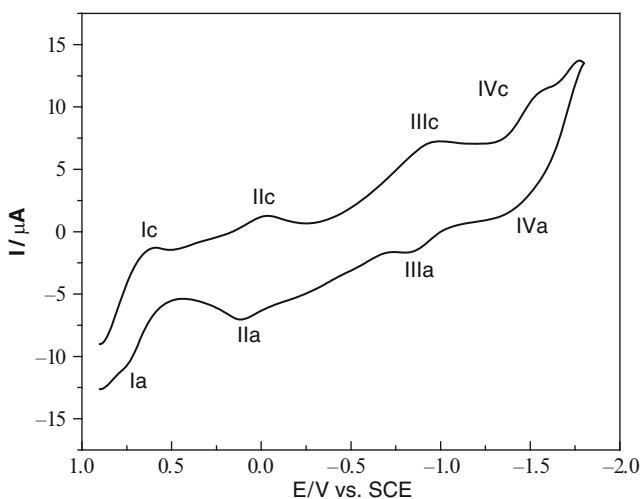


**Fig. 18** CV of **3** ( $1.5 \times 10^{-4}$  M) at  $0.100 \text{ V s}^{-1}$  on Pt in DMSO/TBAP [25]

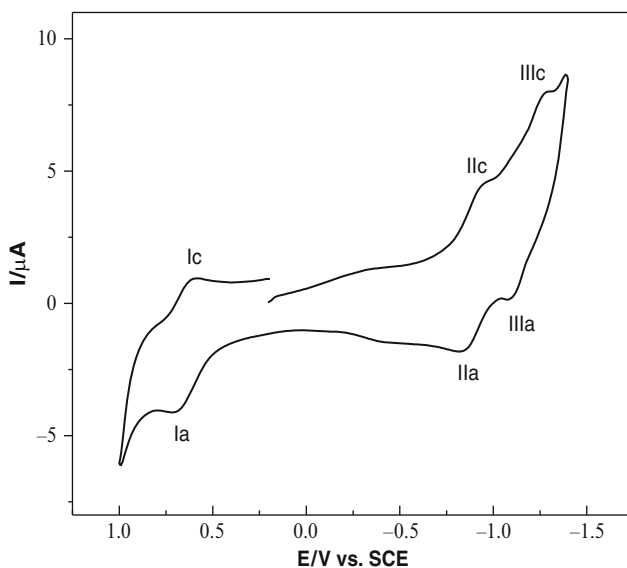
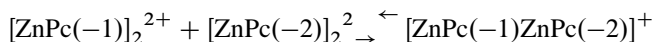


**Fig. 19** CV of **53** ( $1.5 \times 10^{-4}$  M) at  $0.100 \text{ V s}^{-1}$  on Pt in DMSO/TBAP [25]

Generally, the oxidation potentials shift to less positive potentials, while the reduction potentials shift to less negative potentials, with the shift in oxidation potentials being more remarkable. The comparison of voltammetric behaviors of **2** and **3** with that of **53** [25] showed that one-electron redox processes I and II of each dimer **2** and **3** should correspond to the oxidation of two Pcs rings of each dimer, and the processes III and IV to their reduction.

A high splitting of the redox processes was detected with mixed-valence splitting,  $\Delta E_s$  values of 0.44 V for the first reduction, Pc(-2)/Pc(-3), and 0.69 V for the first oxidation, Pc(-1)/Pc(-2) for **2**, and 0.55 V for the first reduction and 0.62 V for the first oxidation for **3**. The splitting of the redox process, i.e., Pc(-1)/Pc(-2) for **2**, due to the formation of a stable mixed-valence intermediate  $[\text{ZnPc}(-1)\text{ZnPc}(-2)]^+$ , is a measure of the equilibrium (comproportionation) constant  $K_c$  for a reaction such as [53]:



where the mixed-valence splitting  $\Delta E_s$  is related to  $K_c$  via:

$$\Delta E_s = (RT/nF) \ln(K_c).$$

The high mixed-valence splitting values give evidence of the delocalization of charge among the cofacial Pc rings in each ball-type Pc **2** and **3**, and thus the formation of electrochemically stable oxidized and reduced mixed-valence species. A large  $K_c$  value of  $86 \times 10^9$  for mixed-valence ring reduction was obtained for **3**. But it could not be determined for **2** since the equation is not appropriate because of the irreversibility of couple IV in Fig. 17. However, the large mixed-valence splitting energy of **2** (0.44 V), taking the difference between the cathodic peak potentials of the relevant redox processes into consideration, reflects strong interactions between the Pc rings. In case of **53** in Fig. 19, there is no considerable interaction between the two Pc rings [25].

The electrochemical measurements of one *t*-butylcalix[4]arene bridged Lu clamshell and Lu double decker clamshell Pcs were investigated in solution [23] and with cast film on indium tin oxide (ITO) glass electrode also by means of spectroelectrochemistry in detail [26].

The electrochemistry and spectroelectrochemistry of other ball-type Pcs have also been investigated in detail [24, 41, 44, 46, 49, 50].

## 6 MALDI-TOF-MS of Ball-Type Pcs

MALDI-TOF mass measurement of the ball-type Pcs is the most powerful technique in order to determine their molecular weight and to characterize their structures. In this technique, it is important to find the appropriate matrix in order to obtain highly resolved spectra, thereby obtaining good mass resolution. If we take into account the MALDI-TOF-MS of the ball-type Pcs **33**, **34**, **35**, and **36** in Fig. 9 [46] and **39** and **40** in Fig. 10 [47] as examples, the protonated molecular ion peaks of **33** and **34** were observed at low intensity, but the sodium adduct peaks of Pcs **33** and **34** were found to be dominant, intense peaks in the linear-mode MALDI-TOF-MS by using

3-indoleacrylic acid as matrix. On the other hand, protonated molecular ion peaks of Pcs **35** and **36** were observed at 1,685 and 1,672 DA respectively, which exactly overlap with the mass of the protonated molecules calculated from the elemental composition of the compounds. Following the protonated molecular ion peak of **35**, a peak at 88 DA mass lower than that of the protonated ion peak was observed at 1,596 DA. This peak is due to the elimination of  $C_4H_8O_2$  side group from the protonated ion peak of zinc Pc. Also, the second  $C_4H_8O_2$  side group elimination was observed at low intensity. However, no fragmentation was observed for **36**.

When the MALDI-TOF-MS of **35** and **36** were evaluated at the low mass range between 100 and 500 DA, no meaningful intensity peak was observed representing impurities, but mainly matrix species peaks were followed. This means that either **35** or **36** Pc was very pure. Several different compounds were tested as matrix to obtain highly resolved spectra, but only  $\alpha$ -cyano-4-hydroxycinnamic acid (ACCA) was found to be the best matrix for **35** and **36**. Because of the short life time of the protonated Pcs **35** and **36** in MALDI-TOF-MS, highly resolved spectra could not be obtained in the reflectron mode. Beyond the protonated and two fragment ion peaks of **35** and the only protonated ion peak of **36**, MALDI-TOF-MS spectra of the Pcs showed very clear and low fragmentations, Figs. 20 and 21 [46].

MALDI-TOF-MS of the same ball-type Pc substituted with four 6-crown-5-ether units **39** and **40** in Fig. 10 [47] showed that not only the right mass but also the pure compounds were present, Figs. 22, 23.

For the ZnPc **38**, a linear-mode positive-ion mass spectrum could be obtained only in ACCA matrix even though other MALDI matrices were tested. The protonated molecular ion peak of **39** was observed at 2,315 DA, which coincided with the theoretical value. Besides the protonated molecular ion peak, no other peak was

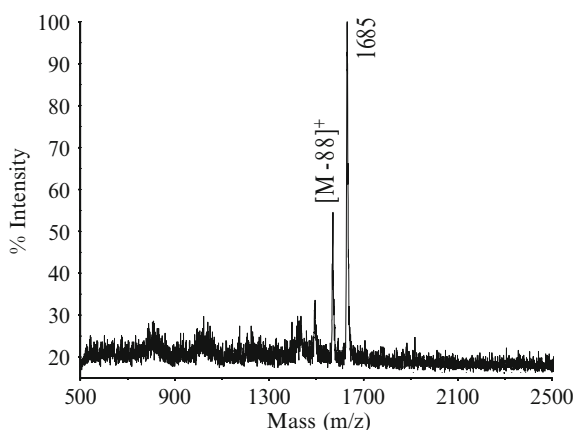


**Fig. 20** Positive-ion mode MALDI-TOF-MS spectrum of **35** with ACCA as matrix [46]

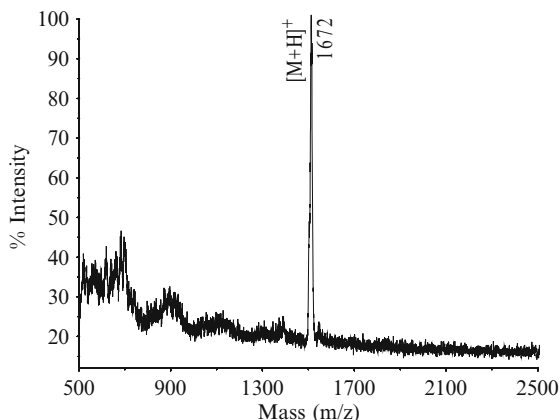


**Fig. 21** Positive ion mode MALDI-MS spectrum of **36** in ACCA MALDI matrix using nitrogen laser accumulating 20 shots [46]

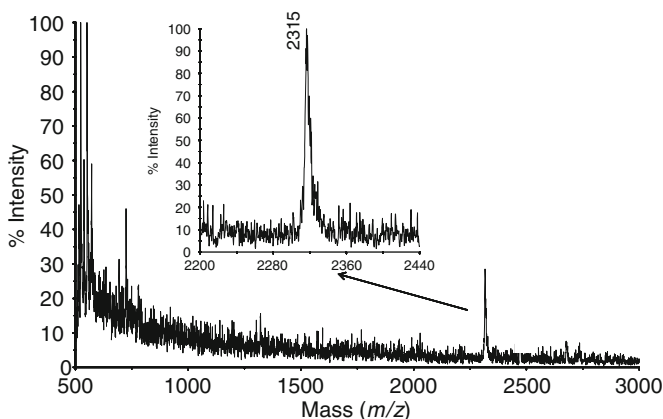


**Fig. 22** The positive ion and linear mode MALDI-MS spectrum of **39** in ACCA (15 mg/mL 1:1 water–acetonitrile) MALDI matrix using nitrogen laser accumulating 50 shots. Inset spectrum shows expanded mass region of **39** [47]

observed in the spectrum, and this shows that no impurity was present in the sample. Compound **39** is reasonably stable under MALDI-TOF-MS conditions.

Positive-ion and reflectron-mode MALDI spectra of the CoPc **40** could be obtained in ACCA matrix. The isotopic peak distribution of the protonated molecular ion peak was due to the carbon and cobalt isotopes, and the experimental isotopic peak distribution (shown as inset) in Fig. 23 corresponded to the theoretical calculations. For the other ball-type Pcs, MALDI-TOF-MS and their details can be found in the following references or in the Supplementary Materials sections [24, 25, 41, 42, 44, 45, 49].

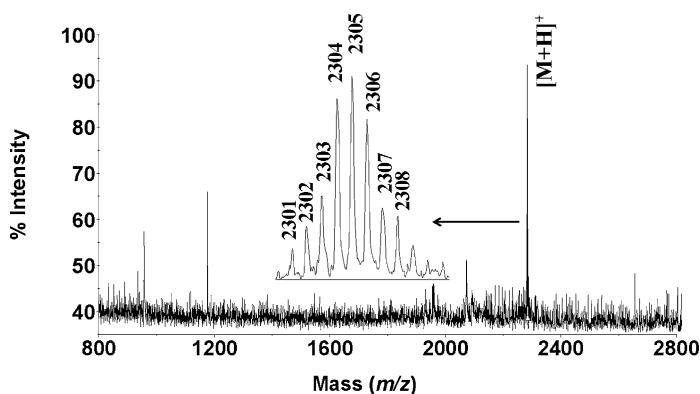


**Fig. 23** The positive ion and reflectron mode MALDI-MS spectrum of **40** in ACCA (15 mg/mL 1:1 water–acetonitrile) MALDI matrix using nitrogen laser accumulated 50 laser shots. The inset spectrum shows the expanded molecular mass of **40** [47]

## 7 Nonlinear Optical (NLO) Properties of Ball-Type Pcs

The NLO property is important for the applications in some fields of electronics. Since the past two decades, aromatic materials have been created for NLO applications, which were found to offer more advantages than inorganic compounds because of their  $\pi$ -electron systems and structural modification.

Pcs are one class of such compounds with their delocalized two-dimensional 18  $\pi$ -electron systems and exceptional stabilities, which make them suitable candidates for NLO applications. From this point of view, Pcs, subphthalocyanines, and related compounds have been investigated extensively in recent years [14]. Besides the excellent 18  $\pi$ -electron systems, the substituents at the benzene rings, coordinative metal, and axial coordination ligands of the Pcs affect the degree of the NLO properties significantly. However, correlation between these factors has not been fully established yet.

There is a close relation between NLO and optical limiting (OL) properties. The main mechanisms to achieve OL are nonlinear absorption (NLA) and nonlinear refraction (NLR), but other effects such as nonlinear scattering can also contribute to OL. Materials with a positive NLA coefficient exhibit reverse saturable absorption (RSA), causing a decrease in transmittance at high intensity levels, and so operate as optical limiters [14].

We deal here with an interesting metallo Pc and ball-type metallo Pcs as the only examples in the literature for NLO and OL. [Octakis(mercaptopropylisobutyl)-POSS]phthalocyaninato]Co(II), Cu(II), and Zn(II) complexes were investigated and compared with respect to NLO and OL properties [58]. These compounds showed that the change of the central metal ion in Pc leads to the variation of the relevant NLO and OL properties. All metallo Pcs with Co(II), Cu(II), and Zn(II) reveal NL absorption. CuPc exhibits the largest NL absorption, while CoPc and ZnPc

show a very low NL absorption [58]. The NL absorption decreases in the order of  $\text{Zn} < \text{Co} < \text{Cu}$ . Therefore, only CuPc was studied for OL property. No single parameters can be used to describe the efficiency of OL. There are several NLO parameters used to characterize the OL properties of Pcs such as the ratio of the excited state to ground state absorption cross sections  $\kappa$ , the effective NL absorption coefficient  $\beta_{\text{eff}}$ , the linear absorption coefficient  $\alpha_o$ , the effective third-order susceptibility  $\text{Im}\{\chi^{(3)}\}$ , and the saturation density  $F_{\text{sat}}$  [59]. For a good optical limiter, the values of  $\kappa$  and  $\beta_{\text{eff}}$  must be high and the values of  $F_{\text{sat}}$  and  $\alpha_o$  must be low.

The investigated CuPc in solution showed a good combination of a relatively high absorption cross section  $\kappa$ , a relatively high effective NL absorption coefficient  $\beta_{\text{eff}}$ , a very low energy-dependent saturation  $F_{\text{sat}}$ , and a low linear absorption coefficient  $\alpha_o$ . The excellent combination of these values makes CuPc a very good candidate as an OL material [58].

In case of ball-type Pcs, there are only two studies reported on the NLO and OL properties of metallo and double-decker Lu(III) and In(III) Pcs in the literature [42, 60]. The NL refraction and absorption dependence on thermal effect for 4-ns pulse duration in ball-type with four *t*-butylcalix[4]arene bridged ZnPc **2** in Fig. 1 in solution have been studied [60]. *z*-Scan experiments were performed on **2** in chloroform solution with a 10-cm-focal length lens. The results are shown in Fig. 24a.

Open-aperture *z*-scan experiments with 7 and 20  $\mu\text{m}$  beam radii are given in Fig. 25. The sample **2** in Fig. 24a with 68% transmittance with 7  $\mu\text{m}$  beam waist radius shows very low NL absorption. The sample has no NL absorption, while the transmittance is 82%. On the other hand, open-aperture *z*-scan experiments with 20  $\mu\text{m}$  beam waist radius have high NL absorption for both transmittances, Fig. 25.

Any thermal effect due to heat accumulation was not observed in these experiments. The NL absorption coefficients obtained from 7  $\mu\text{m}$  beam waist radius were

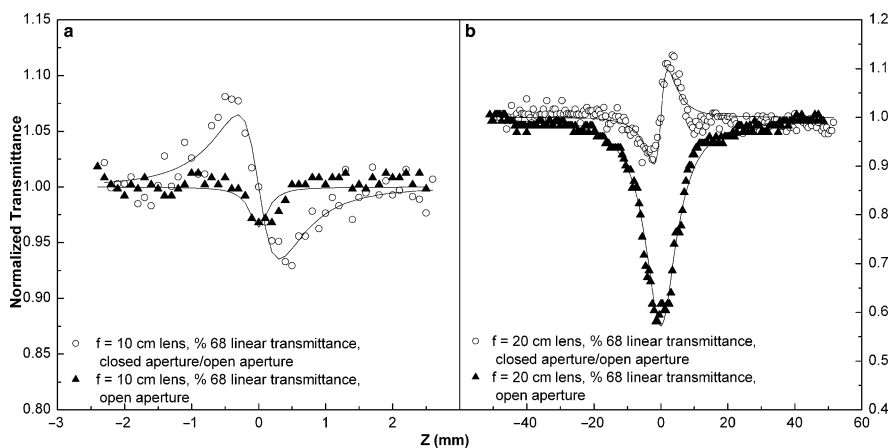


**Fig. 24** Typical *z*-scan spectra of **2** for 4-ns pulse train with about 0.06 mW input power for (a)  $w_0 = 7 \mu\text{m}$  beam radius and  $3 \text{ GW}/\text{cm}^2$  on-focus intensity and (b)  $w_0 = 20 \mu\text{m}$  beam radius and  $0.06 \text{ GW}/\text{cm}^2$  on-focus intensity (solid curves represent theoretical fit) [60]

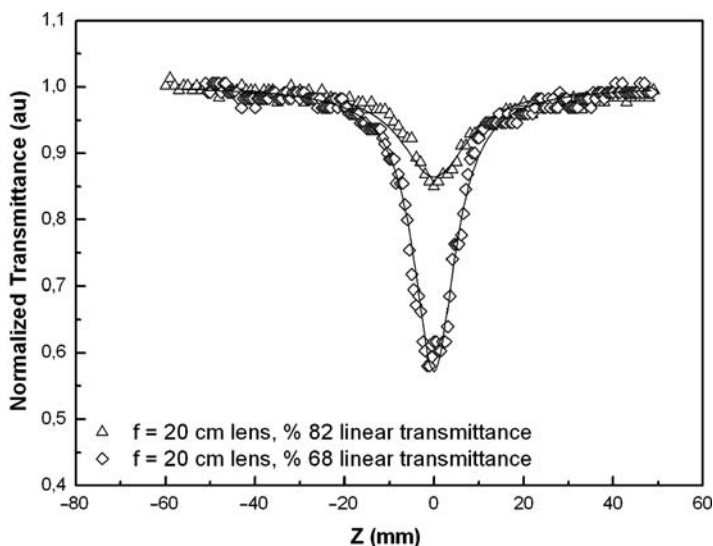


**Fig. 25** Typical open-aperture  $z$ -scan spectra of **2** with normalized transmittance plotted as a function of sample position  $z$  for two different linear transmittance of  $w_0 = 20 \mu\text{m}$  beam radius at the same input power (0.06 mW) [60]

about 200 times smaller in comparison with  $20 \mu\text{m}$  beam waist radius. Thermal effects should be taken into account for both NLO refraction and absorption investigations with nanosecond pulses. Changing the beam waist radius is a simple way to reduce the thermal effect on the NLO parameters [60].

*t*-Butylcalix[4]arene bridged double-decker Lu(III) and In(III) Pcs were also investigated for OL properties [42]. Because the NLO response of compound **11** is negligible, only NLO properties of **10** in Fig. 3 were investigated.  $z$ -Scan experiment with a frequency-doubled (532 nm), Q-switched, mode-locked Nd:YAG laser at about 4 ns pulse duration was measured at far field with a 2-mm-diameter aperture (close aperture) and without aperture (open aperture). Since this compound showed a considerably large NL absorption, open aperture  $z$ -scan experiments and OL experiment were performed in mixed acetic acid and DMSO (1:1) solution which yielded 82% linear transmittance. The absorption coefficient is  $0.9 \text{ cm}^{-1}$  at 532 nm [42].

All open-aperture  $z$ -scan data were fitted using an NL regression method with an equation in which the normalized transmittance is given as a function of position  $z$ :

$$T_{\text{norm}}(z) = \log_e [1 + (q_{000}/1 + (z/z_0)^2)/q_{000}/1 + (z/z_0)^2].$$

In this equation,  $z_0$  is the diffraction length of the beam and  $q_{000} = \beta_{\text{eff}} I_0 L_{\text{eff}}$ , where  $L_{\text{eff}} = 1 - e^{-(\alpha L)}/\alpha$  and  $\beta_{\text{eff}}$  is the effective intensity-dependent NL absorption coefficient and  $I_0$  is the intensity of the light at focus.  $L_{\text{eff}}$  is known as the effective length of the sample,  $\alpha$  is the absorption coefficient, and  $L$  is the sample thickness.



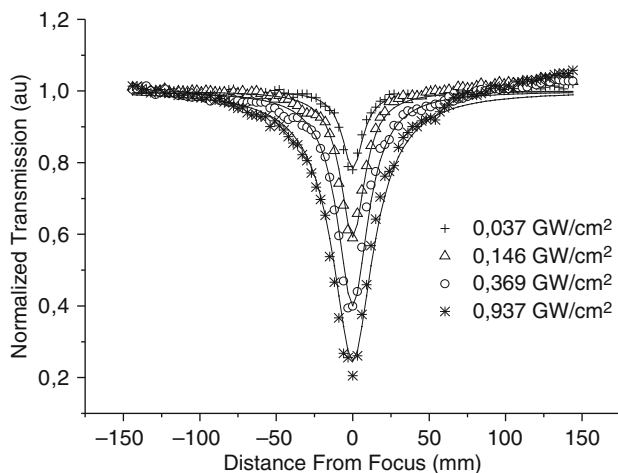


**Fig. 26** Typical open aperture  $z$ -scan spectra of **10** with normalized transmission plotted as a function of sample position  $z$ ; concentration =  $2.9 \times 10^{-3}$  M [42]

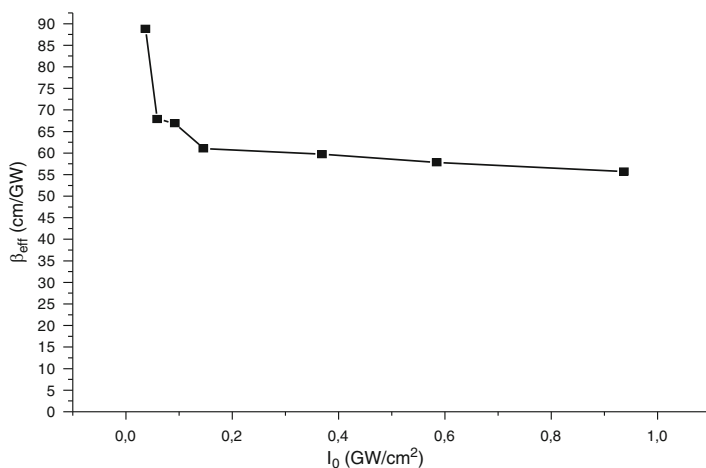


**Fig. 27** Plot effective NL absorption coefficient  $\beta_{\text{eff}}$  against the on-focus beam intensity  $I_0$  for **10** [42]

In the above equation, the normalized transmittance is given as a function of position  $z$  [61, 62].

The beam radius  $w_0$ , which was found to be almost constant for various input intensities  $I_0$ , and the NL absorption coefficient  $\beta_{\text{eff}}$  were used as free parameters in Fig. 26 [42].

The effective NL absorption coefficient  $\beta_{\text{eff}}$  vs. on-focus intensities are plotted in Fig. 26. The effective NL coefficient  $\beta_{\text{eff}}$  decreases slightly with increasing beam intensity in Pcs [59, 63]. In this case, although there is a sharp decrease of  $\beta_{\text{eff}}$  at lower intensities, it becomes almost stable at higher intensities, Fig. 27 [42].

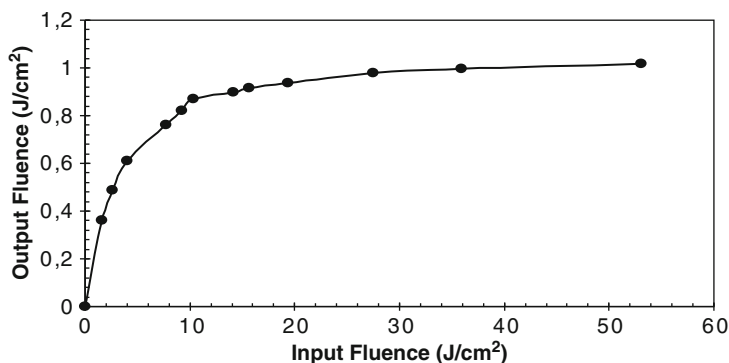


Fig. 28 OL response of **10** at 532 nm, concentration =  $2.9 \times 10^{-3}$  M [42]

Due to the high NLA of **10**, the sample was placed at the focus where beam radius was  $34.2 \mu\text{m}$ . Input fluences vs. output fluences are plotted in Fig. 28. Compound **10** shows good OL behavior, since input fluences increase up to  $60 \text{ J/cm}^2$ , and output fluences remain almost constant at about  $1 \text{ J/cm}^2$ .

## 8 Electrical and Gas-Sensing Properties of Ball-Type Pcs

Generally, Pcs are semiconductor materials. For the electrical characterization and conductivity and impedance measurements, ten-finger interdigital gold electrodes with  $50 \mu\text{m}$  gap were deposited photolithographically on precleaned Corning glass substrates. Thin films were obtained by spin-coating in appropriate solutions of the products over the electrode arrays to obtain devices suitable for conductivity and impedance measurements, which were carried out in dark and under vacuum. Introducing electron donor and acceptor groups into Pc rings also strongly affect the electrical properties of the compound. From the point of view of organic semiconductors, it is known that substitution of electron donor and acceptor groups leads to p-type and n-type characteristics of the Pc ring, respectively [64, 65]. The electrical dc and ac characterizations of the Pc film are crucial in order to study relevant mechanism and to realize its future applications. Measurement of dc and ac conductivity is also a reliable method to study the localized states near the band edges below the conduction and above the valence bands produced by the substitutional disorders which control many of the opto-electronic properties. Hence, a study of the dc and ac conductivity in these materials will throw light on the nature of these levels. Dc electrical properties of many metallo Pcs have been studied in some detail by researchers in the form of both single crystals and thin films [66, 67]. However, only very little previous work has been performed on ac conduction, most of this being confined to metallo Pcs [68–70]. Unlike some other Pcs, the electronic properties and dependence of conductivity on temperature of lutetium-Pc have not been widely studied [71, 72].

Because of their electrical, optical, and redox properties as well as the thermal and chemical stability, the Pcs also have been tried in the detection of volatile organic compounds and poisonous gases, which is very important for environment and human health. In the past decades, the possible applications of Pc thin film as sensor for atmospheric gaseous pollutants have been extensively studied [73, 74]. Langmuir–Blodgett films of some multinuclear and multidouble-decker lutetium Pcs have also been used for those measurements [75, 76]. More details about conductivity and sensing properties of Pcs can be found elsewhere [77, 78].

As mentioned earlier, the ball-type Pcs are a new class of compounds and rather rare in the literature. For the first time, dc and detailed impedance spectroscopy technique have been used to investigate the charge transport mechanism and gas-sensing properties of spin-coated film of *t*-butylcalix[4]arene bridged ball-type ZnPc **2**, shown in Fig. 1 [37], as a function of temperature and gas concentration. Usually, Pcs are characterized by an Arrhenius-type of dependence for their electrical conductivity. But in the case of **2**, a strong deviation from Arrhenius law was observed, Fig. 29, for this film, as it does in fast ion conducting glasses, which is the basis of electrochemical energy-based devices. The ac conductivity  $\sigma_{ac}(\omega)$  varied as  $\omega^s$ , where the exponent  $s$  is found to be a temperature-dependent variable and always less than unity. The measurements on ac conductivity data can be explained by the correlated barrier-hopping model. The response characteristics of the film to toluene vapor were also investigated. Very high sensitivity was obtained for 50 ppm toluene vapor at room temperature, Fig. 29 [37].

Dc conductivity  $\sigma_{dc}$  as a function of reciprocal temperature for the spin-coated film of compound **8** in Fig. 2 was found to be  $2.60 \times 10^{-12}$  and  $1.80 \times 10^{-8}$  S/cm at room temperature and 425 K, respectively. It was seen from the Arrhenius plot that there is more than one slope in the conductivity, which indicates the presence of different levels in the film for the conduction mechanism [41]. The activation energies obtained for the low and high temperature regions were found to be 0.36 and 1.02 eV,

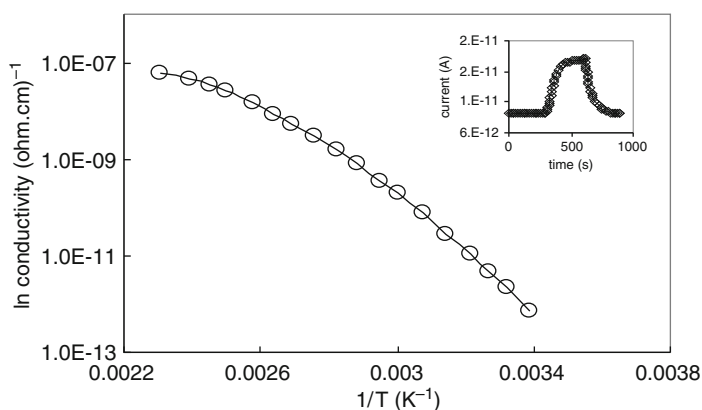


**Fig. 29** Arrhenius plot of dc conductivity for the film **2** and its response characteristic to 50 ppm toluene vapor at room temperature (inset) [37]

respectively. Dc conductivity can be related to the temperature  $T$ , according to the relation:  $\sigma_{dc} = \sigma_o \exp(-E_A/kT)$ , where  $\sigma_o$  is the pre-exponential factor,  $E_A$  is the thermal activation energy, and  $k$  is the Boltzmann constant. The same type of temperature dependence of dc conductivity was observed for multinuclear ZnPc [32]. The two different activation energy values can be interpreted as a transition from extrinsic to intrinsic conductivity. The activation energy corresponding to intrinsic generation is associated with resonance energy involved in a short-lived excited state, and that corresponding to impurity scattering is attributed to a short-lived charge transfer between impurity and the complex [73].

Ac conductivity  $\sigma_{ac}$  as a function of frequency of **8** was measured at 305, 380, and 420 K. Two linear regions of ac conductivity were distinguished: one at lower frequency, in which ac conductivity is nearly frequency-independent; another at higher frequency  $\sigma_{ac}$ , which obeys the power-law relation:  $\sigma_{ac} \sim \omega^n$ , where  $\omega$  is the angular frequency, and the frequency exponent  $n$  is a material-dependent constant [41]. The measured ac conductivity should be frequency-independent and drop at sufficiently high frequency. The values of the frequency exponent were derived from the straight-line fits in the frequency-dependent region. The index  $n$  in this study was found to vary with temperature, and it was observed that the value is very close to unity (0.97) at low temperatures and decreases at higher temperatures (0.23). The values found and the temperature dependence of the frequency exponent allow explaining the conduction mechanism for compound **8** by the correlated barrier hopping (CBH) model [41].

Detailed dc, ac, and impedance measurements of the compounds **15**, **16**, and **17** in Fig. 4 showed that hopping conduction process [79] is applicable for all three compounds [24]. A comparison of the experimentally determined  $s$  values with the prediction of the CBH model suggests that dependence of the exponent  $s$  on temperature is in agreement with the prediction of the CBH model for those compounds [24].

Comparative conductivity measurements of the compounds **24–27** in Fig. 7 showed that the order of dc conductivities observed for these compounds are **26** > **25** > **24** > **27** for all temperatures investigated. All measurements and calculations of those compounds were in agreement with the prediction of the CBH model [44]. The measurements of the same but metal-free mono and ball-type compounds **29** and **30** also indicated the same CBH model [45].

Dc, ac, impedance, and thermoelectric power of the compounds **33–38** in Fig. 9 have been investigated in detail. The measured temperature dependence of the thermoelectric power of **33–38** in thin film varied approximately exponentially with temperature. Compared to **38**, the absolute value of the thermopower for the film of **34** is larger by nearly a factor of 3. The positive sign of Seebeck coefficient confirms that thin films of the compounds behave as a p-type semiconductor [46].

The conductivity measurements of the films of **39**, **40**, **39a**, and **40a** in Fig. 10, which were carried out in the temperature range 290–476 K, suggested the presence of only one conduction mechanism. The conduction behavior of **39** and **40** could be interpreted as the usual Arrhenius type. It was observed that the insertion of alkali metals increased the dc conductivity. The order of conductivities observed for these

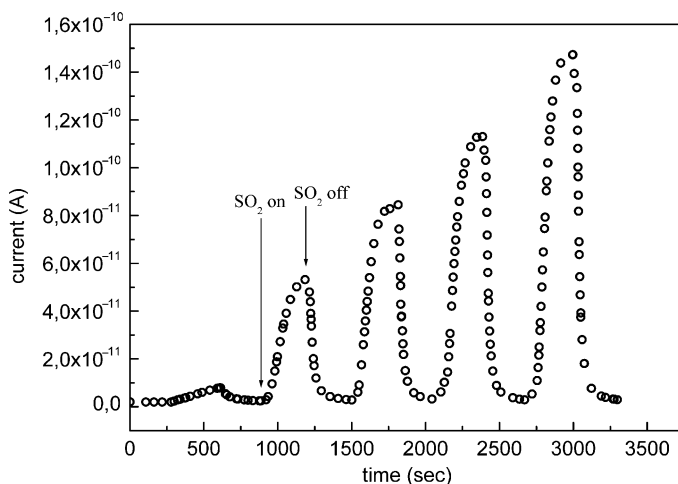


**Fig. 30** Response characteristic of **42**-coated sensor to 50, 100, 150, 200 and 250 ppm of  $\text{SO}_2$  gas at room temperature [48]

compounds was **40a** > **39a** > **40** > **39** for all temperatures investigated [47]. The detailed electrical measurements and activation energies of compounds **45** and **46** in Fig. 12 and related compounds have been studied [49].

Gas-sensing properties of some newly synthesized ball-type Pcs have also been investigated. The response and recovery characteristics of a spin-coated film of **52** in Fig. 13 [50] at room temperature under  $\text{CO}_2$  atmosphere (10,000 ppm) suggested that the conductivity of the sensor increased during the initial doping stage for a few minutes and then the rate of increase slowed down. This could be explained in terms of the formation of acceptor states which lie below the Fermi level during the initial stage of adsorption [29]. From impedance measurements, semicircular-shaped curves, the diameter of which decreased with increased  $\text{CO}_2$  concentration, were obtained. These results indicate the presence of charge transfer interaction between the Pc rings and the target molecules [50].

The effect of the various concentrations of  $\text{SO}_2$ ,  $\text{CO}_2$ , CO, and volatile organic chemical vapors on the conductivity of compounds **42** and **43** in Fig. 30 was tested at different temperatures. The results showed that compound **42** is not sensitive for the gases investigated, with the exception of  $\text{SO}_2$  for which very high sensitivity was obtained. The response characteristics of **42** to the various concentrations (50–250 ppm) of  $\text{SO}_2$  at room temperature are shown in Fig. 30 [48].

## 9 Conclusion and Outlook

We summarized in this chapter ball-type Pcs, which are a new class of Pcs first published 6 years ago [35]. Since that time, several papers appeared in the literature, which were published only by our group as far as we know. Therefore, comparison

with other works is not possible. The first ball-type Pc was prepared in a solvent and also assisted by microwave [35,36]. Later, it was observed that the synthesis of such Pcs mostly depended on the four bridged units between two Pc macrocycles and to a lesser extent on metals. In other words, in some cases heating in a solvent gives only ball-type [37, 42]; without a solvent in solid mixture at high temperatures for a short time gives the mixture of mono and ball-type Pcs [24, 45]. In some cases, heating a mixture of solid compounds results in only mono Pc, which on further reaction in a solvent produces ball-type Pc [50]. In all these reactions, the steric effects of the bridged compounds should play a significant role. The electrochemical, electrical, NLO, and gas-sensor properties of all synthesized ball-type Pcs have not been measured yet. However, the compounds measured showed good results for these properties and are promising candidates for application in many fields of technology. The functional groups of the bridged compounds of ball-type Pcs are also of intrinsic advantage in designing versatile new compounds that will show new properties for applications in several fields in the near future [41, 48].

**Acknowledgements** The author expresses his appreciation to his competent coworkers who during the past years have carried out the synthesis as well as electrical, gas-sensing, electrochemical, and NLO characterization of new classes of ball-type Pcs very successfully. Their names appear in the references. The author is very grateful to Dr. Zafer Odabaş; for his skillful and fruitful collaboration for drawing to all figures, to Associate Prof. Dr. Tanju Ceyhan for his collaboration during all this period, and to Pinar Ergün for her endless patience during the typing of the manuscript. The author is also thankful to the Turkish Academy of Sciences (TUBA) for partially supporting this work.

## References

1. Braun A, Tscherniac J (1907) *J Ber Dscht Chem Ges* 40:2709
2. Byrne GT, Linstead RP, Lowe AR (1934) *J Chem Soc* 1017
3. Linstead RP, Lowe AR (1934) *J Chem Soc* 1022
4. Dent CE, Linstead RP (1934) *J Chem Soc* 1027
5. Dent CE, Linstead RP, Lowe AR (1934) *J Chem Soc* 1033
6. Robertson JM (1935) *J Chem Soc* 615
7. Robertson JM (1936) *J Chem Soc* 1195
8. Robertson JM, Woodward I (1937) *J Chem Soc* 219
9. Leznoff CC, Lever ABP (eds) (1989) *Phthalocyanines properties and applications 1*. VCH, New York
10. Gregory P (1991) *High-technology applications of organic colorant*. Plenum Press, New York
11. Özer M, Yılmaz F, Erer H, Kani I, Bekaroğlu Ö (2009) *Appl Organomet Chem* 23:55
12. Yılmaz F, Özer M, Kani I, Bekaroğlu Ö (2009) *Catal Lett*, DOI:10.1007/s10562-009-9959-1
13. Shabanov AL, Hamidov AF, Hasanova UA, Musluoğlu E, Bekaroğlu Ö, unpublished work
14. De la Torre G, Vázquez P, Lopez FA, Torres T (2004) *Chem Rev* 104:3723
15. Chen MJ, Rathke JW, Sinclair S, Slocum DW (1990) *J Macromol Sci-Chem A* 27(9-11):1415
16. Gürek AG, Bekaroğlu Ö (1997) *J Porphyrins Phthalocyanines* 1:67
17. Gürek AG, Bekaroğlu Ö (1997) *J Porphyrins Phthalocyanines* 1:227
18. Abdurrahmanoğlu Ş, Özkaya AR, Bulut M, Bekaroğlu Ö (2004) *Chem Commun* 2096
19. Abdurrahmanoğlu Ş, Özkaya AR, Bulut M, Bekaroğlu Ö (2004) *Dalton Trans* 4022
20. Salan Ü, Altındal A, Bulut M, Bekaroğlu Ö (2005) *Tetrahedron Lett* 46:6057

21. Altındal A, Abdurrahmanoğlu Ş, Bulut M, Bekaroğlu Ö (2005) *Synth Met* 150:181
22. Yazıcı A, Ateş D, Bekaroğlu Ö, Kobayashi N (2006) *J Porphyrins Phthalocyanines* 10:1140
23. Ceyhan T, Altındal A, Özkaya AR, Erbil MK, Bekaroğlu Ö (2007) *Polyhedron* 26:73
24. Odabaş Z, Altındal A, Özkaya AR, Bulut M, Salih B, Bekaroğlu Ö (2007) *Polyhedron* 26:695
25. Ceyhan T, Altındal A, Özkaya AR, Çelikbaş Ö, Salih B, Erbil MK, Bekaroğlu Ö (2007) *Polyhedron* 26:4239
26. Koca H, Ceyhan T, Erbil MK, Özkaya AR, Bekaroğlu Ö (2007) *Chem Physics* 340:283
27. Ozan N, Bekaroğlu Ö (2003) *Polyhedron* 22:819
28. Ceyhan T, Korkmaz M, Erbil MK, Bekaroğlu Ö (2005) *J Porphyrins Phthalocyanines* 9:423
29. Sütlü M, Altındal A, Bekaroğlu Ö (2005) *Synth Metal* 155:211
30. Özer M, Altındal A, Özkaya AR, Bulut M, Bekaroğlu Ö (2005) *Synth Met* 155:222
31. Açıkbaş Y, Evyapan M, Ceyhan T, Çapan R, Bekaroğlu Ö (2007) *Sens Actuators B* 123:1017
32. Ceyhan T, Altındal A, Erbil MK, Bekaroğlu Ö (2006) *Polyhedron* 25:737
33. Kobayashi N (2002) *Coord Chem Rev* 227:129
34. Abdurrahmanoğlu S, Altındal A, Bulut M, Bekaroğlu Ö (2006) *Polyhedron* 25:3636
35. Tolbin AY, Ivanov AV, Tomilova LG, Zefirov NS (2002) *Mendeleev Commun* 96
36. Tolbin AY, Ivanov AV, Tomilova LG, Zefirov NS (2003) *J Porphyrins Phthalocyanines* 7:162
37. Ceyhan T, Altındal A, Özkaya AR, Erbil MK, Salih B, Bekaroğlu Ö (2006) *Chem Commun* 320
38. Böhmer V (1995) *Angew Chem Int Ed Ing* 34:713
39. Van Loon JD, Ardium A, Coppil L, Verboom W, Pochini A, Ungaro R, Herkama S, Reinhoudt DN (1990) *J Org Chem* 55:5639
40. Mogh L, Bohmer B, Ferguson G, Vought W (1996) *J Chem Soc Perkin Trans* 1711
41. Ceyhan T, Altındal A, Özkaya AR, Salih B, Erbil MK, Bekaroğlu Ö (2007) *J Porphyrins Phthalocyanines* 11:625
42. Ceyhan T, Yağlıoğlu G, Ünver H, Salih B, Erbil MK, Elmali A, Bekaroğlu Ö (2008) *Macroheterocycles* 1: 44
43. Odabaş Z, Bekaroğlu Ö, unpublished work
44. Odabaş Z, Altındal A, Özkaya AR, Bulut M, Salih B, Bekaroğlu Ö (2007) *Polyhedron* 26:3505
45. Odabaş Z, Altındal A, Salih B, Bulut M, Bekaroğlu Ö (2007) *Tetrahedron Lett* 48:6326
46. Özer M, Altındal A, Özkaya AR, Salih B, Bulut M, Bekaroğlu Ö (2007) *Eur J Ing Chem* 3519
47. Özer M, Altındal A, Salih B, Bulut M, Bekaroğlu Ö (2008) *Tetrahedron Lett* 49:896
48. Özer M, Altındal A, Özkaya AR, Bekaroğlu Ö (2009) *Dalton Trans* 3175
49. Canlica M, Altındal A, Özkaya AR, Salih B, Bekaroğlu Ö (2008) *Polyhedron* 27:1883
50. Altun S, Altındal A, Özkaya AR, Bulut M, Bekaroğlu Ö (2008) *Tetrahedron Lett* 49:4483
51. Stillman MJ, Nyokong T (1989) In: Leznoff CC, Lever ABP (eds) *Phthalocyanines properties and applications* 1. VCH, New York
52. Nevin WA, Liu W, Hempstead MR, Marcuccio SM, Melnik M, Leznoff CC, Lever ABP (1987) *Inorg Chem* 26:891
53. Lever ABP, Milaeva ER, Speier G (1993) In: Leznoff CC, Lever ABP (eds) *Phthalocyanines properties and applications* 3. VCH, New York
54. Manivannan V, Nevin WA, Leznoff CC, Lever ABP (1998) *J Coor Chem* 19:139
55. Darwent JR, McCubbin I, Porter G (1982) *J Chem Soc Faraday Trans* 78:903
56. Ishicawa N, Ohno O, Kaizu Y, Kobayashi H (1992) *J Phys Chem* 96:8832
57. Whörle D, Went A, Weitemeyer A, Stark J, Spiller W, Schneider G, Müller S, Michelsen U, Kliesch H, Hevermann A, Ardeshirpur A (1994) *Russ Chem Bull* 43:1953
58. Ceyhan T, Yüksel M, Yağlıoğlu HG, Salih B, Erbil MK, Elmali A, Bekaroğlu Ö (2008) *Dalton Trans* 2407
59. O'Flaherty SM, Hold SV, Cook M, Torres T, Chen Y, Hanack M, Blau W (2003) *Adv Mat* 15:19
60. Yüksek M, Ceyhan T, Bağcı F, Yağlıoğlu HG, Elmali A, Bekaroğlu Ö (2008) *Optic Commun* 281:3897
61. Coulter DR, Miskowski VM, Perry JW, Weit H, Van Stryland EW, Hagan DJ (1989) *SPIE Proc* 1105:42

62. Sheik-bahane M, Said AA, Wei TH, David DH, Van Stryland EW (1990) *IEEE J Quantum Electron* 26:760
63. Slodek A, Wöhrle D, Doyle JJ, Blau W (2006) *Macromol Symp* 235:9
64. Yanagi H, Tamura N, Taira S, Furuto H, Douko S, Schnurpfeil G, Wöhrle D (1995) *Mol Cryst Liq Cryst* 264:435
65. Manaka T, Iwamoto M (2003) *Thin Solid Films* 438–439:157
66. Öztürk ZZ, Altındal A, Gürek A, Bekaroğlu Ö (1992) *Synth Met* 52:291
67. Shafai TS, Anthopoulos TD (2001) *Thin Solid Films* 398–399:361
68. Narayanan Unni KN, Menon CS (2000) *Mater Lett* 45:326
69. Saleh AM, Abu-Hilal AO, Gould RD (2003) *Curr Appl Phys* 3:345
70. Pakhomov GL, Shashkin VI, Pozdnyaev DE, Müller C, Ribo JM (2002) *Org Electron* 3:93
71. Jones R, Krier A, Davidson K (1997) *Thin Solid Films* 298:228
72. Belarbi Z, Sirlin C, Simon J, Andrea JJ (1989) *J Phys Chem* 93:8105
73. Abdel-Malik TG, Cox GA (1997) *J Phys C Solid State Phys* 10:63
74. Pedrosa JM, Dooling CM, Richardson TH, Hyde RK, Hunter CA, Martin MT, Camacho L (2002) *J Mat Chem* 12:2659
75. Spadavecchia J, Ciccarella G, Buccolieri A, Vasapollo G, Rella R (2003) *J Porphyrins Phthalocyanines* 7:572
76. Açıkbaş Y, Evyapan M, Ceyhan T, Çapan R, Bekaroğlu Ö (2007) *Sens Actuators B Chem* 123:1017
77. Açıkbaş Y, Evyapan M, Ceyhan T, Çapan R, Bekaroğlu Ö (2009) *Sens Actuators B Chem* 135:426
78. Moser FH, Thomas AL (1983) *The phthalocyanines 1 properties* CRC Press, Boca Raton, FL
79. Eliot SR (1987) *Adv Phys* 36:135



# Supramolecular Nanostructures of Phthalocyanines and Porphyrins at Surfaces Based on the “Bottom-Up Assembly”

Soichiro Yoshimoto and Nagao Kobayashi

**Abstract** The “bottom-up” strategy is an attractive and promising approach for the construction of nanoarchitectures. Supramolecular assemblies based on noncovalent interactions have been explored in an attempt to control the surface properties. In this chapter, we focus on advances made in the past 5 years in the field of scanning tunneling microscopy (STM) on supramolecularly nanostructured phthalocyanines and porphyrins on single-crystal surfaces. The design of supramolecular nanoarchitectures consisting of phthalocyanines and porphyrins, supramolecular traps of C<sub>60</sub> and coannulene, direct metallation on phthalocyanines and porphyrins adlayers, direct synthesis of porphyrin oligomers at surfaces, axial coordination of phthalocyanines and porphyrins, and nanoapplications induced by tip manipulation at surfaces were clearly visualized by STM.

**Keywords** Metal single-crystal surface · Phthalocyanines · Porphyrins · Scanning tunneling microscopy (STM) · Supramolecular assembly

## Contents

1	Introduction .....	138
2	Two-Dimensional Molecular Assembly .....	139
2.1	Single-Component Adlayers in UHV .....	139
2.2	Single-Component Adlayers at Electrochemical Interface .....	143
2.3	Hydrogen-Bonding Architectures .....	145
3	Controlled Bimolecular Arrays .....	147
3.1	Phthalocyanine and Porphyrin Mixed Adlayers .....	147
3.2	Porphyrin and Fullerene Supramolecular Assembly .....	149

---

S. Yoshimoto (✉)

Priority Organization for Innovation and Excellence, Kumamoto University,  
2–39–1 Kurokami, Kumamoto 860–8555, Japan  
e-mail: so-yoshi@kumamoto-u.ac.jp

N. Kobayashi

Department of Chemistry, Graduate School of Science, Tohoku University, Sendai  
980–8578, Japan  
e-mail: nagaok@mail.tains.tohoku.ac.jp

4	Direct Formation of Nanostructures on Surface .....	152
4.1	Direct Metallation on Surface .....	152
4.2	Direct Connection on Surface .....	154
5	Self-Assembly of Porphyrins by Axial Ligand Coordination .....	156
5.1	Monomeric Complexes .....	156
5.2	Double- and Triple-Decker Complexes .....	159
6	Nanoapplications .....	160
7	Conclusions and Perspectives .....	161
	References .....	163

## 1 Introduction

Construction of characteristic nanoarchitectures and fabrication by the self-assembly of organic molecules are a subject of significant interest [1]. Many functional architectures in nature are formed as a result of the self-assembly and self-organization of smaller building blocks. Since establishing the concept of supramolecular chemistry, the self-assembly of organic molecules has recently gained considerable attention as a key technique for the “bottom-up” fabrication of nanoscale functional structures [2–5]. On the basis of supramolecular chemistry, it is possible to create desired supramolecular crystals or complexes from the solution phase. For example, self-assembled porphyrin trimers and graphitic nanotubes are attractive materials for surface patterning [6] and molecular electronics [7]. This type of self-organization is mainly controlled by noncovalent bonds such as hydrogen bonds, van der Waals interactions, and  $\pi$ -stacking. However, it is not easy to directly apply the knowledge of supramolecular chemistry to surfaces. Since functional groups in a building-block molecule might chemically react with the substrate through a strong interaction, appropriate modification for concepts of solution-based supramolecular chemistry is needed to extend the supramolecular assembly technique onto substrates, as described by Barth et al. [8]. Therefore, it is very important to fully understand not only the interactions between a substrate and adsorbates, but also the influence of the electronic properties of adsorbed ligands on noncovalent bonds.

Scanning tunneling microscopy (STM) has been widely accepted as one of the most powerful tools for understanding the structure of adsorbed layers of molecules on metal surfaces at the atomic level in totally different environments from ultrahigh vacuum (UHV) [8–10] to solution [11–19]. Since its invention by Binnig and Rohrer in 1982 [20], STM has proved to be a powerful surface analysis technique with atomic resolution in UHV. On the other hand, Sonnenfeld and Hansma demonstrated for the first time in 1986 that STM can be used even in an electrolyte solution [21]. In 1988, Itaya and other groups proposed a new approach for in situ STM imaging with a four-electrode configuration, in which the electrode potentials of the substrate and the tip are independently controlled with respect to a reference electrode [22]. Under potentiostatic conditions, in situ STM makes it possible to monitor, under reaction conditions, a wide variety of electrode processes such as the adsorption of inorganic and organic species, the reconstruction of electrode surfaces, and the dissolution and deposition of metals and semiconductors. High-resolution STM has made it possible to directly determine the packing arrangements and even the internal structures of organic molecules adsorbed at solid–liquid interfaces. Nowadays, STM studies

on solid–liquid interfaces have been extended to not only the electrochemical interface but also to nonconductive solvent interfaces. For example, the supramolecular assembly of many compounds has also been investigated in organic solvents such as 1-phenyloctane [17, 23], heptanoic acid [24, 25], and dichlorobenzene [26], because these kinds of solvents have low vapor pressure and are electrochemically inert. The examination of organic adlayers is usually carried out directly in organic solvent containing molecules at the liquid–solid interface under no potential control. Although the choice of solvent can be tuned as a function of the particular solute and/or substrate, the molecular assembly is significantly influenced by the kind of organic solvent.

In this chapter, we focus on molecular assemblies of functionalized molecules consisting of phthalocyanines (Pcs) and porphyrins noncovalently bounded on metal surfaces, in order to explore their potential as building blocks for the construction of nanostructures, by using scanning probe microscopy (SPM) including STM and atomic force microscopy (AFM).

## 2 Two-Dimensional Molecular Assembly

### 2.1 *Single-Component Adlayers in UHV*

Adlayer structures of Pc and porphyrin derivatives have been previously studied, mainly under UHV using STM on various metal surfaces [27–37]. Lippel et al. reported the first STM images of a copper(II) phthalocyanine (CuPc) adlayer on Cu(100) [27]. Gimzewski and coworkers investigated copper(II) 5,10,15,20-tetrakis (3,5-di-*t*-butylphenyl)porphyrin (CuTBPP) on Cu(100), Au(110), and Ag(110) under UHV [28, 29], and found that the packing arrangement of CuTBPP depends on the metal substrate used. Hipps and coworkers reported various MPcs (M: Cu [30, 31], Co [30, 31], Ni [32], Fe [32], VO [33]) and metallotetraphenylporphyrins (MTPP) [34, 35] on reconstructed Au(111), and found that the brightness of the center spot of Pc or TPP is dependent on the active center metal. The difference in contrast between the metal ions in STM images was explained in terms of the occupation of the  $d_{z^2}$  orbital. As listed above, STM imaging of hydrophobic MPc or MTPP molecules was successful in UHV.

After the middle of 2000, the surface science of adlayers of Pc and porphyrin derivatives has been extended to the understanding surface-supported templates and to more complicated surfaces such as higher index planes of Au and InSb(001). For example, details of the epitaxial growth of FePc on Au(111) were reported by Gao's group [36, 37]. FePc preferentially adsorbs along the herring bone structure of a reconstructed Au(111) surface (see Fig. 1a) [37]. In particular, a cyclic hexamer consisting of six FePc molecules was found at elbow of the reconstructed rows of Au(111), as shown in Fig. 1b, 1c. Such characteristic nanoarchitectures are often found at a lower coverage of Pc and/or porphyrin adlayer. A CoPc adlayer on a vicinal Au(788) surface was reported by Kröger's group [38]. CoPc molecules preferentially adsorbed at step edges, with the molecular plane tilted so as to bridge adjacent terraces on Au(788) at a submonolayer coverage (Fig. 1d).

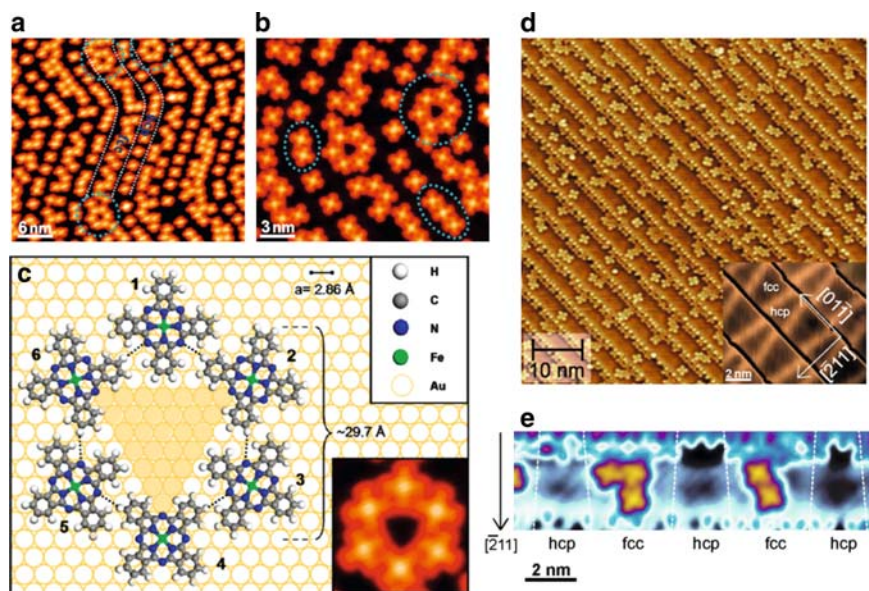


**Fig. 1** (a) and (b) STM images of FePc submonolayer ( $\sim 0.6$  ML) on a Au(111) surface: (a)  $40 \times 40$  nm<sup>2</sup>; (b)  $20 \times 20$  nm<sup>2</sup>. Broken white lines indicate domain walls of the Au(111) herringbone reconstruction. (c) Proposed model of FePc molecules forming hexamer with the underlying Au(111) substrate. The directional electrostatic interactions between the neighboring molecules are indicated by the dashed lines. Each molecule positioned at no. 2, 4, and 6 connects with its neighboring molecules (no. 1, 3, and 5) by its two phenyl groups fitting into the hollow sites of its neighboring molecules, where the nitrogen atoms reside close to hydrogen atoms of neighboring molecules. Reprinted with permission from [37], Copyright (2007) American Chemical Society. (d): Large-scale STM image of CoPc covered Au(788) at 8 K; (inset) STM image of clean Au(788) showing five adjacent terraces. (e): High-resolution STM image of CoPc molecules adsorbed on a Au(788) terrace. Dashed lines serve as a guide to the eye. Reprinted with permission from [38], Copyright (2007) Elsevier Science

Figure 1e reveals that molecules that adsorb on terraces leave the surface reconstruction of Au(788) unchanged and exhibit the propensity to occupy face-centered cubic stacking domains. In other cases, there are several reports on fullerene C<sub>60</sub> arrays on Au(788) [39] and Au(11 12 12) [40], and bimolecular one-dimensional arrays consisting of naphthalene tetracarboxylic diimide (NTCDI) and benzodiguanamine (BDG) on Au(455) [41]. On the other hand, InSb(001) was used as a substrate for molecular growth of FePc [42]. Because the InSb(001) shows a characteristic reconstructed row, the so-called  $c(8 \times 2)$  structure, the reconstructed rows act as a template for FePc. The growth pattern depends closely on the substrate phase domains, i.e., the molecular diffusion of FePc is controlled by the main surface dopattern. Thus, precise control of the substrate can be applicable to nanotemplates for Pc and porphyrin derivatives.

Other recent topics are the supramolecular organization of nonplanar Pc derivatives. In particular, several interesting nanostructures of Pc derivatives were found

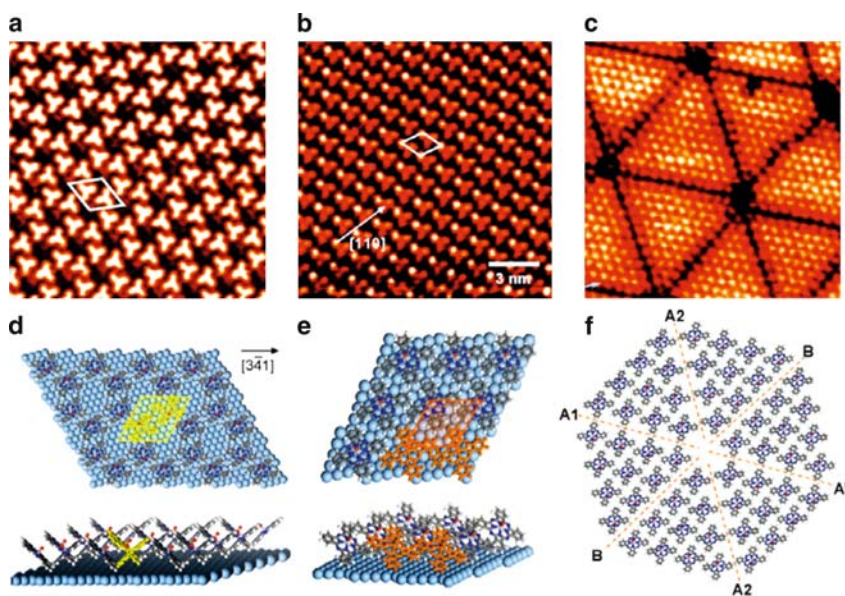


**Fig. 2** STM images of: (a) honeycomb phase, (b) hexagonal phase, and (c) the misfit dislocation triangular network of TiOPc on Ag(111) in UHV, and (d)–(f): the corresponding proposed models, respectively. Reprinted with permission from [43], Copyright (2008) American Chemical Society

on Ag(111). Reutt-Robey's group reported the molecular architecture of titanyl phthalocyanine (TiOPc) monolayer films [43]. They described how local electrostatic intermolecular interactions stabilize kinetically accessible structures, driving phase selection. As shown in Fig. 2, three phases of TiOPc depending on the coverage were found on Ag(111) in UHV: i.e., a well-ordered  $(2\sqrt{13} \times 2\sqrt{13})R13.9^\circ$  honeycomb phase comprising interlocked molecular pairs; a meta-stable  $(\sqrt{21} \times \sqrt{21})R10.9^\circ$  hexagonal phase of uniformly tilted TiOPc; and a misfit dislocation triangular network appeared at lower ( $< 0.1$  ML/min), intermediate (0.2 ML/min), and higher (0.4 ML/min) fluxes, respectively. In particular, Fig. 2c shows the formation of a characteristic triangular network. It is noteworthy that a similar triangular structure was found in the electrochemically induced sulfur adlayer on Cu(111) in 0.1 M KOH containing 0.5 mM  $\text{Na}_2\text{S}$ ,  $(19 \times 19)$  structure which is composed of S atoms forming  $(\sqrt{3} \times \sqrt{3})R30^\circ$  [44]. It is very interesting to form such an attractive nanostructure using Pc molecules. For tin-Pc (SnPc), which is also a non-planar Pc, Kröger et al. reported a characteristic growth mode of SnPc thin films and the electronic properties of individual SnPc molecules on Ag(111) [45]. Jung and coworkers demonstrated that symmetrically substituted Pcs with eight peripheral di-(*tert*-butyl)phenoxy (DTPO) groups (Fig. 3a) self-organize on both Ag(111) and Au(111) substrates into various assembly structures [46]. Several characteristic phases, depending on the surface coverage, were found on both Au(111) and Ag(111) surfaces. Figure 3b shows the Pc core and 10 *tert*-butyl groups positioned in close proximity to the Ag(111) surface. Four of the lobes correspond to two DTPO

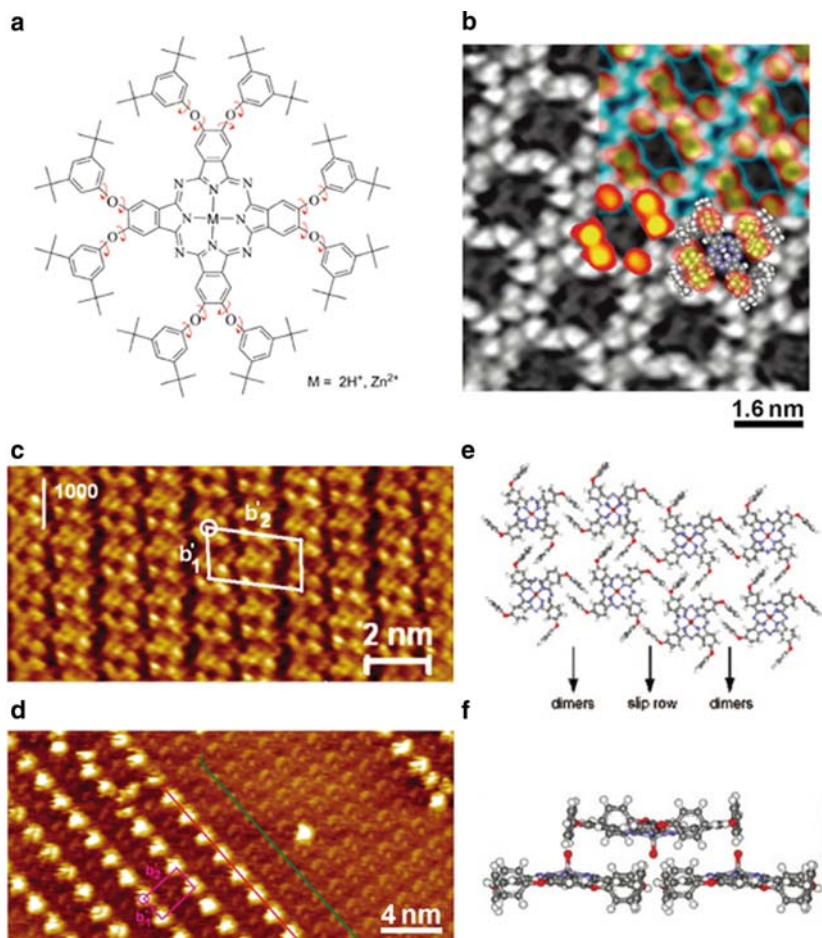


**Fig. 3** (a) Molecular structure of the phthalocyanine derivative symmetrically octasubstituted with di-*tert*-butylphenoxy (DTPO) groups; (b) High-resolution STM image ( $8 \times 8 \text{ nm}^2$ ) featuring an alternative view of Pc-DTPOs on Ag(111) in UHV. Reprinted with permission from [46], Copyright (2008) American Chemical Society. High-resolution STM images of VOPcPhO adlayer for (c) monolayer and (d) bilayer observed in 1-phenyloctane on HOPG. The unit cells are superimposed on both the monolayer and the bilayer. Schematic illustrations of the packing arrangement for the adlayer are shown in (e) and (f), respectively. Reprinted with permission from [47], Copyright (2008) American Chemical Society

substituents oriented almost coplanar with the Pc core, as the model structure is superimposed on the STM image. The adlayers of PcDTPO functionalized with *tert*-buthyl groups on Ag(111) were dependent on the coverage.

Mazur et al. described the organization of vanadyl oxide 2,9,16,23-tetraphenoxy-29*H*, 31*H*-phthalocyanine ( $\text{VO}^{2+}\text{PcPhO}$ ) on highly oriented pyrolytic graphite (HOPG) [47]. They focused on the fact that the adsorption geometry of nonplanar Pc complexes of titanyl and vanadyl (TiOPc and VOPc) is not well understood

and has not yet been definitely assigned. The  $\text{VO}^{2+}\text{PcPhO}$  adlayer formed three different stable architectures at HOPG-*n*-alkyl benzene interfaces. One of stable  $\text{VO}^{2+}\text{PcPhO}$  adlayers obtained in 1-phenyloctane is shown in Fig. 3c. The first adlayer of  $\text{VO}^{2+}\text{PcPhO}$  lies flat on the surface of the substrate with the oxygen atoms turned upward. The second layer of  $\text{VO}^{2+}\text{PcPhO}$  was also formed on the same adlayer. Individual  $\text{VO}^{2+}\text{PcPhO}$  molecules are stacked with the  $\text{VO}^{2+}$  group pointing down, to give rise to the head-to-head geometry (see Fig. 3f).

## 2.2 Single-Component Adlayers at Electrochemical Interface

On the other hand, STM has also been utilized in understanding the structures of adlayers of water-soluble porphyrin molecules in aqueous solutions [48–54]. In particular, in the field of electrochemistry, Pc and porphyrins have been extensively investigated as models for the catalysis of fuel cell and bio-related materials. However, little attention had been paid so far to these types of adlayer structure. In the mid-1990s, a highly ordered array of free-base 5,10,15,20-tetrakis(*N*-methylpyridinium-4-yl)porphyrin ( $\text{H}_2\text{TMPyP}$ ) molecules on iodine (I) modified Au(111) was first reported by Kunitake and Itaya's group [48–50].  $\text{H}_2\text{TMPyP}$  ordered arrays were also formed on the I-Ag(111) [51], I-Pt(100) [52], I-Cu(111) [53], and S-modified Au(111) [54] electrodes in 0.1 M  $\text{HClO}_4$ . The surface diffusion of the molecules adsorbed on bare Au was found to be very slow. Relatively weak van der Waals interaction between hydrophobic iodine adlayers and the organic molecules could be the key factor promoting self-ordering processes on the I-Au(111) substrate. Thus, the iodine adlayer plays an important role in the control of the interactions between the molecule and the substrate [48–56]. Another appealing application of iodine adlayers was demonstrated by Sakaguchi et al. They succeeded in the electrochemical epitaxial growth of polythiophene in dichloromethane containing iodine [57]. High-density arrays of single conjugated polymer wires were found to grow from nuclei adsorbed on the iodine-covered Au(111) surface. Another interesting aspect is the understanding of redox chemistry and charge transfer reaction at the electrode-porphyrin interface [58, 59]. The ordering of a free-base porphyrin array directly attached to a bare Au(111) surface at the electrochemical interface was subsequently reported by Borguet group [59–61]. Potential manipulation plays a significant role in controlling the surface mobility of tetrakis(4-pyridyl)porphyrin ( $\text{H}_2\text{TPyP}$ ) molecules [60]. The authors also reported the kinetics during the electrochemical oxidation of  $\text{H}_2\text{TPyP}$  molecules [59]. Tao et al. also investigated adlayers of three water-soluble molecules, iron(III) protoporphyrin, zinc(II) protoporphyrin, and protoporphyrin(IX), on graphite basal planes in aqueous solution with both STM [62, 63] and AFM [62]. Similar adlayer structures were formed using these three molecules, although the internal structures obtained by in situ STM were significantly different [62]. The formation of a highly ordered array of  $\text{TMPyP}$  on a sulfate/bisulfate adlayer on Cu(111) was also reported [64]. Recently, Yoshimoto and Sawaguchi reported that an electrochemically produced

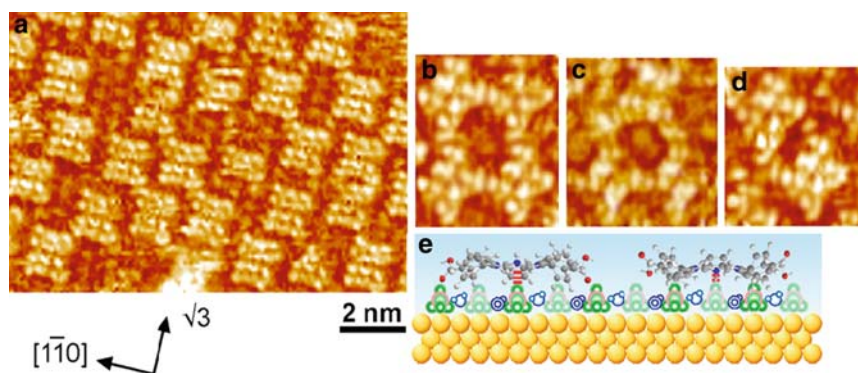


**Fig. 4** High-resolution STM images of (a) both  $cis$ -H<sub>4</sub>DCPP<sup>2+</sup> array and sulfate/bisulfate rows and (b)–(d) nanostructured  $cis$ -H<sub>4</sub>DCPP<sup>2+</sup> array; (b) tetramer, (c) trimer, (d) dimer forms. (e) schematic illustration of the interaction between  $cis$ -H<sub>4</sub>DCPP<sup>2+</sup> and sulfate/bisulfate adlayer. Reprinted with permission from [65], Copyright (2008) American Chemical Society

sulfate/bisulfate adlayer on Au(111) serves as a template for a cationic tetraphenyl porphyrin with two carboxyphenyl moieties in the  $cis$ -positions ( $cis$ -H<sub>4</sub>DCPP<sup>2+</sup>) [65]. In this system, the formation of supramolecularly organized nanostructures of  $cis$ -H<sub>4</sub>DCPP<sup>2+</sup> such as dimers, trimers, and tetramers on the ( $\sqrt{3} \times \sqrt{7}$ ) sulfate/bisulfate (SO<sub>4</sub><sup>2-</sup>/HSO<sub>4</sub><sup>-</sup>) adlayer is seen, suggesting the importance of both electrostatic interactions between the cationic porphyrin core and the SO<sub>4</sub><sup>2-</sup>/HSO<sub>4</sub><sup>-</sup> adlayer and hydrogen-bond formation between the carboxyl groups of the nearest neighbor cationic porphyrins (see Fig. 4). In contrast, when 0.1 M HClO<sub>4</sub> was used as an electrolyte solution, only a disordered array was observed.

Several water-insoluble porphyrin adlayers, such as cobalt(II) porphine (CoP) [66], cobalt(II) octaethylporphyrin (CoOEP) [66], cobalt(II) tetraphenylporphyrin (CoTPP) [67], cobalt(II) coordinated “picket-fence” porphyrin (CoT<sub>piv</sub>PP) [68] (these molecules are abbreviated as CoPor), and cobalt(II) phthalocyanine (CoPc) [69] were subsequently investigated by Yoshimoto and Itaya’s group. They were successful in spontaneously forming highly ordered molecular arrays of these molecules on Au(111) surfaces by immersing Au(111) in benzene solutions containing the molecules. In particular, the authors focused on the relationship between adlayer structure and the electrocatalytic activity of dioxygen (O<sub>2</sub>) reduction. The enhancement of the reductive current for O<sub>2</sub> reduction at these modified Au(111) electrodes compared to bare Au(111) electrodes clearly shows that CoPor and CoPc adlayers catalyze the reduction of O<sub>2</sub>. By using rotating CoPor- or CoPc-modified Au(111) disc electrodes, it was indicated that a two-electron reduction process of O<sub>2</sub> to H<sub>2</sub>O<sub>2</sub> proceeded on the CoP-, CoTPP-, CoOEP-, and CoPc-modified Au(111) surfaces [18, 66–69]. The adlayer structures of CoOEP and CoTPP formed in benzene solutions were identical to those obtained in UHV [35, 70]. The CoOEP and CoTPP adlayers formed an incommensurate structure with respect to the reconstructed Au(111) surface. For CoT<sub>piv</sub>PP, individual CoT<sub>piv</sub>PP molecules were recognized to be square-shaped with four bright spots at the corners



in the characteristic nanobelt array, whereas the adlattice was almost identical to that of CoTPP. The state of O<sub>2</sub> trapped in the cavity of CoT<sub>piv</sub>PP was distinctly observed in STM images as a bright spot in the nanobelt array formed on the reconstructed Au(100)-(hex) surface, but not on the Au(111) surface, indicating that the formation of nanobelt arrays consisting of O<sub>2</sub>-adducted CoT<sub>piv</sub>PP molecules depended on the crystallographic orientation of Au[68]. In the case of CoPc, the packing arrangement of CoPc on the reconstructed Au(111) surface was also consistent with that obtained in UHV by Lu et al. [30, 31]. However, the preparation from the solution phase also provided different adlayer structures [69]. CoPc molecules formed three packing arrangements on the Au(111) surface: one rectangular arrangement on reconstructed Au(111) and two hexagonal arrangements on Au(111)-(1 × 1), depending on the surface coverage [69]. The method of immersion into benzene solution was further extended to larger molecules such as 15-crown-5-ether-substituted cobalt(II) phthalocyanine (CoCRPc) [71]. The adlattice of the CoCRPc array on Au(111) was determined to be  $p(8 \times 4\sqrt{3}R - 30^\circ)$ . In the absence of Ca<sup>2+</sup>, four additional spots were observed at the corners, whereas in the presence of Ca<sup>2+</sup>, only two additional bright spots were seen at diagonal positions with respect to the Pc ligand, as a result of encapsulation of two Ca<sup>2+</sup> ions by crown ether rings [71]. Furthermore, it was demonstrated by using an Au(100)-(1 × 1) lattice that the relationship between the crown moieties of CRPc and the underlying Au lattice is important in the trapping of Ca<sup>2+</sup> ions in crown rings [72].

In contrast, adlayers containing other central metal ions, e.g., CuTPP, NiTPP, ZnTPP, CuOEP, NiOEP, ZnOEP, CuPc, and ZnPc, were observed as dark spots in the center both in UHV [30–35] and in solution [67, 69, 73–75]. Molecular resolution STM revealed either a propeller shaped admolecule or a circle shape one with eight additional spots at the corners with its center imaged as a protrusion for Co<sup>II</sup> and a depression for other metal ions. The CoPc or CoTPP molecules were easily identified by the strong tunneling current resulting from orbital-mediated tunneling through the half-filled d<sub>z<sup>2</sup></sub> orbital of the Co<sup>II</sup> ion (d<sup>7</sup>): a bright spot appeared at the center of each molecule, whereas Ni<sup>II</sup>(d<sup>8</sup>), Cu<sup>II</sup>(d<sup>9</sup>), and Zn<sup>II</sup>(d<sup>10</sup>) ions have a fully filled d<sub>z<sup>2</sup></sub> orbital [30–35, 73–75]. The remarkable contrast in tunneling current afforded by the difference in electronic configuration of transition-metal ions allows one to clearly distinguish between species for chemical identification at the molecular level. In the case of the Zn<sup>II</sup> ion, we discovered the possibility of epitaxial growth of a ZnPc layer from the solution phase. ZnPc molecules can be epitaxially assembled because of the attractive interaction between the electron donating pair in the Pc scaffold and the zinc ion. The formation of epitaxial layers of ZnPc molecules from benzene solution was controllable by changing the immersion time [73].

### 2.3 Hydrogen-Bonding Architectures

Hydrogen bonding is a very attractive and effective method for forming two-dimensional networks or arrays of porphyrins at surfaces. For example, Lei et al. reported that highly ordered arrays of 5,10,15,20-tetrakis(4-carboxyphenyl)

porphyrin ( $H_2TCPP$ ) and copper(II) 2,3,9,10,16,17,23,24-octakis(carboxyl)phthalocyanine ( $CuPc8C$ ) were formed on HOPG by the coadsorption of stearic acid and 1-iodooctadecane, respectively, under ambient conditions [76]. Because 2D hydrogen bonds of Pc and porphyrin were stabilized by the presence of these alkane derivatives, the alkane derivatives contribute to the minimization of the surface free energy in a 2D system. Furthermore, 5,10-bis(4-carboxyphenyl)-15,20-bis(4-octadecyloxyphenyl)porphyrin was found to form dimeric rows at the dichlorobenzene–HOPG interface by Otsuki et al., suggesting that the adlayer structure is determined by directional hydrogen-bonding interactions between nearest neighbor molecules [77]. Hill and coworkers reported on self-assembled structures of the 5,10,15,20-tetrakis(3,5-dimethyl-4-hydroxyphenyl)porphyrin on  $Cu(111)$  [78]. The molecules are held in a hatch-like structure with linear arrays of the molecules arranged approximately orthogonally under the strong influence of hydrogen-bonding interactions involving phenolic protons and porphyrin imino nitrogen atoms.

Supramolecular assembly using porphyrin derivatives has also been investigated to potentially fabricate precisely controlled molecular wires. Yokoyama and coworkers showed that selective aggregation of porphyrin derivatives can be controlled rationally by tuning the dipole–dipole interactions between the molecules [79]. This report can be considered a breakthrough paper on noncovalently assembled porphyrins based on the supramolecular assembly concept on a surface. The authors found that CN-substituted (3,5-di-*t*-butylphenyl)porphyrin derivative (TBPP) molecules could produce supramolecular aggregates such as trimers, tetramers, and one-dimensionally extended wire-like structures on  $Au(111)$  at low temperatures (63 K) in UHV. Dipole–dipole interactions between CN moieties are a key factor for the molecular assembly of TBPP. A similar selective assembly was also formed by carboxyphenyl porphyrins [80]. A remarkable difference between the CN and COOH moieties in TBPP derivatives is a variation of the intermolecular interactions between the porphyrin derivatives. For example, one-carboxyphenyl-substituted TBPP molecules form a dimeric structure through hydrogen bonding between two molecules (see Fig. 5a), whereas one-CN-substituted TBPP molecules arrange in clusters of trimers. The supramolecular selective assembly of 5,15-bis

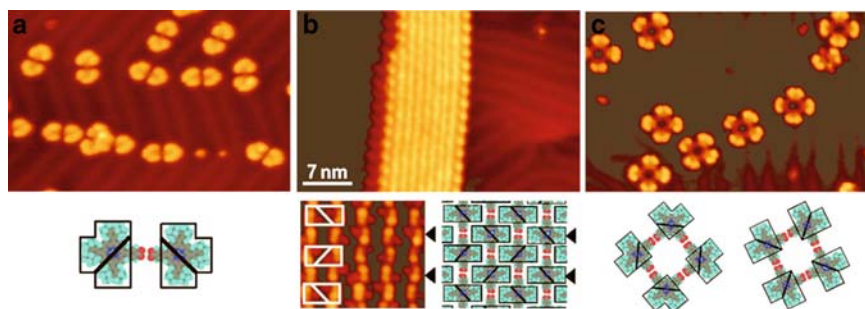


**Fig. 5** STM images ( $25 \times 40 \text{ nm}^2$ ) and the corresponding structural models of supramolecularly assembled (a)  $CaTBPP$ , (b) *trans*- $BCaTBPP$ , and (c) *cis*- $BCaTBPP$  on  $Au(111)$  at 63 K obtained in UHV. Reprinted with permission from [80], Copyright (2004) American Institute of Physics

(4-carboxyphenyl)-10,20-bis(3,5-di-*t*-butylphenyl)porphyrin (*trans*-BCaTBPP) with a long, straight wire was observed on an Au(111) surface by sequential hydrogen bonding between carboxyphenyl groups (see Fig. 5b), while isolated supramolecular wires were formed by cyanophenyl-substituted TBPP molecules [80]. The supramolecular nanostructures on the surfaces can be precisely controlled by the conformation-selective assembly. Furthermore, the organization and hydrogen-bonding network formation of carboxyphenyl porphyrin derivatives was also investigated at electrochemical interfaces by our group [81]. The results demonstrated that the ordered arrays of monocarboxy- or tetracarboxy-substituted porphyrin derivatives formed on Au(111) depend on the number of peripheral substituents. Electrochemical control of the self-assembly of porphyrin complexes is an effective method for constructing novel surface architectures.

### 3 Controlled Bimolecular Arrays

#### 3.1 Phthalocyanine and Porphyrin Mixed Adlayers

Hipps and coworkers found the formation of well-ordered regions having an entirely new structure of a 1:1 composition of cobalt(II) hexadecafluoro-phthalocyanine ( $F_{16}CoPc$ ) and NiTPP on Au(111) by vapor-phase deposition in UHV [82].  $F_{16}CoPc$  and NiTPP molecules were distinguished from each other by the difference in brightness of the central metal ions between the  $F_{16}CoPc$  and NiTPP molecules. The remarkable contrast in tunneling current afforded by the difference in electronic configuration of transition-metal ions allows one to clearly discriminate between species for chemical identification at the molecular level. When CoPc and NiTPP molecules were deposited on Au(111), a densely packed, well-ordered structure was also found on the terrace. However, a binary adlayer consisting of CoPc and NiTPP prepared in UHV revealed a densely packed, apparently well-defined structure, which was compositionally disordered [83]. It was concluded that the ability of the two types of molecule to interlace was due to an attractive energy of up to 4 kJ/mol for each closely approaching fluorine–hydrogen intermolecular interaction, together with reduced repulsive interaction between the  $F_{16}CoPc$  and NiTPP molecules [82, 83]. CoPc and CoTPP mixed system was also investigated on Au(111) by the same authors [84].

Another system, a bimolecular array consisting of CoPc and CuTPP, was examined on both Au(111) and Au(100) surfaces by immersing the surfaces into benzene solution [85, 86]. Yoshimoto and Itaya's group found that an alternate mixed layer consisting of CoPc and CuTPP was formed on reconstructed Au(100)-(hex) but not on reconstructed Au(111), suggesting that the supramolecular assembly comprising two chemical components also depends on the crystallographic orientation of Au [85]. In this case, the terrace of Au(111) was completely covered with two different phases: a disordered region and a highly ordered region consisting of CuTPP,

whereas stripes composed of alternate bright and dark lines were observed on Au(100)-(hex). Subsequently, we found that a similar two-component supramolecular adlayer consisting of CoPc and CuTPP was formed on Au(111) following different modification conditions [86]. It is likely that the adsorbate–substrate interaction is much weaker on Au(111) than on Au(100)-(hex). The formation of the striped structure was independent of the crystallographic orientation, while the corrugation periodicity of reconstruction for the underlying substrate is quite different compared to Au(111) and Au(100). A bimolecular system consisting of CuOEP and CoPc on Au(111) was also examined by the same group at the electrochemical interface [87]. In the case of the bimolecular array consisting of CuOEP and CoPc, it was found that the structure  $p(9 \times 3\sqrt{7}R - 19.1^\circ)$  and its mirror structure  $p(9 \times 3\sqrt{7}R - 40.9^\circ)$  were alternately formed on the Au(111) terrace. Furthermore, potential manipulation in the negative direction in HClO<sub>4</sub> demonstrated that one-dimensional (1D) molecular chains of CuOEP were clearly observed as dark gaps between bright rows consisting of two or three CoPc molecular rows [87]. The surface mobility and molecular reorganization of CuOEP and CoPc were accelerated by varying the electrode potential. This kind of precise and unique control of electrochemical interfaces is of great interest for exploring further applications of Pc and phthalocyanine molecular assemblies. Wakayama et al. investigated F<sub>16</sub>CuPc and di-indenoperylene (DIP) mixed arrays on both Au(111) and Cu(111) in UHV [88]. The occurrence of C–F⋯H–C interactions produced an extraordinary structural ordering, pointing to a promising avenue toward the controlled design of bicomponent adlayers. Another mixed system comprising supramolecular structures constructed from fullerene (C<sub>60</sub>) and chloro-[subphthalocyaninato]boron(III) (SubPc) was found on Ag(111) in UHV by de Wild and coworkers [89]. Here, an interesting bimolecular 2D adlayer was formed with alternate arrangements of C<sub>60</sub> and SubPc.

Very recently, Calmettes et al. reported bicomponent supramolecular packing arrays comprising 2,3,9,10,16,17,23,24-octachloro ZnPc (ZnPcCl<sub>8</sub>) and 1,3,5,7,9-penta-tert-butylcorannulene (PTBC) on Ag(111) [90]. In this system, since ZnPcCl<sub>8</sub> molecules can form weakly bonded networks, the ZnPcCl<sub>8</sub> adlayer on Ag(111) can be used as a deformable flexible template for the controlled insertion of a guest molecule. The authors also described the fabrication of the bicomponent adlayer using the STM tip, as illustrated in Fig. 6, where “holes” in the packing have been created. They reported that a PTBC molecule could be removed by vertical manipulation when the STM tip was positioned over it, and this process was found to be reproducible.

For HOPG, there are several reports on interesting nanoarchitectures. Kong et al. examined a VOPc array incorporated into a host architecture comprising 1,3,5-tris(10-carboxydecyloxy) benzene (TCDB) through hydrogen bonding on HOPG [91]. In this case, thermal annealing is one of the most important factors for controlling the VOPc and TCDB complex architecture. The TiOPc case was also reported by the same authors [92]. Similar mixed systems were also reported by a Chinese group [93, 94].

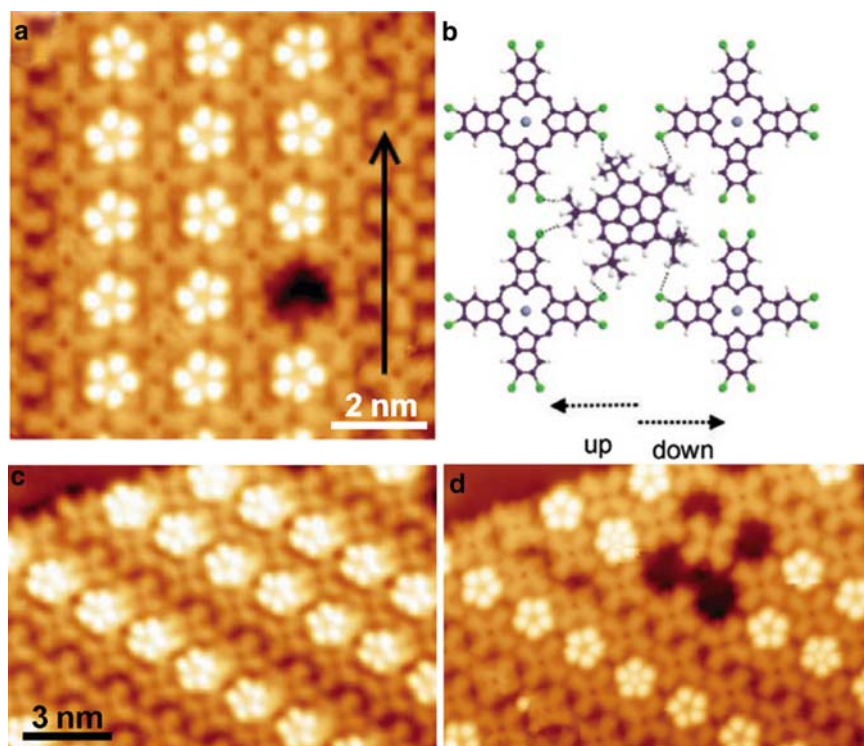


**Fig. 6** (a) High-resolution STM image of PTBC molecules in a  $\text{ZnPcCl}_8$  network on  $\text{Ag}(111)$  obtained in UHV at  $T = 4.6\text{ K}$ . (b) Schematic representation of PTBC inserted into the Pc network stabilized by H-bonding. Panel (d) was obtained after the repetitive vertical manipulation at same positions in panel (c). Holes in the packing have been created, and isolation of a Pc molecule was found in panel (d). Reprinted with permission from [90], Copyright (2008) Wiley-VCH

### 3.2 Porphyrin and Fullerene Supramolecular Assembly

It is known that porphyrins and fullerenes spontaneously attach to each other [95]. For example, MOEP and  $\text{C}_{60}$  form a supramolecular assembly through  $\pi$ - $\pi$  interactions in cocrystallites with a ratio of 2:1 [96]. To control these supramolecular assemblies between porphyrins and fullerenes during three-dimensional construction, layer-by-layer growth on metal surfaces must be used as a first step. This kind of supramolecular assembly produced through  $\pi$ - $\pi$  or donor-acceptor interactions would be useful for the design and organization of functional organic molecules on electrode surfaces. For example, individual  $\text{CuPc}$  molecules were observed on a highly ordered  $\text{C}_{60}$  array formed on  $\text{Au}(111)$  in UHV [97]. Subsequently, Yoshimoto and Itaya's group first reported a supramolecularly assembled array of  $\text{C}_{60}$  molecules on a  $\text{ZnOEP}$  adlayer on  $\text{Au}(111)$  formed through a wet process, by successive immersion into a benzene solution containing  $\text{ZnOEP}$  and

C<sub>60</sub> molecules. The adlayers were observed under the electrochemical environment [74]. As reported in several papers [74, 75, 98–100], they succeeded in forming a 1:1 supramolecular assembly consisting of fullerenes such as C<sub>60</sub> [74], open-cage C<sub>60</sub> derivative [98, 99], and ferrocene-linked C<sub>60</sub> [100], as well as metalloporphyrins such as ZnOEP and NiOEP on both Au(111) and Au(100) surfaces. This kind of supramolecular assembly produced through donor–acceptor interactions improves the electrochemical performance by controlling the molecular orientation of the fullerenes [9, 100]. In addition, it was demonstrated that the stability of the first adlayer is an important factor in the surface design of host–guest selectivity of fullerenes on electrode surfaces [75]. The identical structures of C<sub>60</sub> and C<sub>70</sub> were also observed on an NiOEP array formed on Au(111) [75], whereas the replacement reaction of the first adlayer of NiTPP occurred upon adsorption of fullerene molecules as the second layer. The result suggests that supramolecular assemblies of C<sub>60</sub> and C<sub>70</sub> are strongly influenced by the underlying layer of porphyrin. The authors also reported that a supramolecularly organized “chessboard” structure was formed for a bimolecular array of ZnPc and ZnOEP on Au(111) [101], as shown in Fig. 7a. A “bottom-up” hybrid assembly of fullerene molecules was formed successfully on an alternate array of bimolecular ZnPc and ZnOEP molecules. The bimolecular “chessboard” served as a template to form a supramolecular assembly of C<sub>60</sub> by selective trapping in the open spaces (see Fig. 7b–e). They also found that supramolecularly assembled layers of C<sub>60</sub> were formed on both coronene- and perylene-modified Au(111) surfaces [102]. As reported in their previous papers, coronene formed a highly ordered array having a (4 × 4) symmetry on Au(111) [102, 103]. The adlayer structure of the C<sub>60</sub> was found to be strongly influenced by the underlying organic layers, suggesting that the latter underlying organic adlayers play an important role in the process of formation of the C<sub>60</sub> molecular adlayer. Epitaxial molecular assemblies for other fullerenes, such as C<sub>70</sub>, C<sub>60</sub>–C<sub>60</sub> dumbbell-dimer (C<sub>120</sub>), and C<sub>60</sub>–C<sub>70</sub> cross-dimer (C<sub>130</sub>), were also observed on the coronene-modified Au(111) surface [103].

In addition, it was reported by the same group that linear C<sub>60</sub> arrays were formed on supramolecular assembled *trans*-BCaTBPP wires on Au(111) [104]. High-resolution STM images revealed that each C<sub>60</sub> molecule was located in the open nanopores, not at the center of each *trans*-BCaTBPP molecule, suggesting that the opening of the nanopores results from a subtle balancing of substrate–molecule and molecule–molecule interactions. Bonifazi et al. synthesized Zn<sup>II</sup> porphyrin derivatives and investigated supramolecular assemblies of C<sub>60</sub> on those arrays formed on Ag single-crystal surfaces in a UHV environment [105]. An unprecedented molecular assembly of C<sub>60</sub> was caused by thermal annealing (453 K). The C<sub>60</sub> molecules were arranged in vertically aligned pairs (intrapair C<sub>60</sub>–C<sub>60</sub> distance of 2.3 nm) with an intermolecular distance of about 6.0 nm, whereas the paired line pattern was repeated every 7.3 nm in the horizontal direction. The supramolecular assembly of C<sub>60</sub> also depends on the crystallographic orientation of the metal substrate [105]. These kinds of bimolecular construction are one of the effective methods for patterning fullerenes at heterogeneous molecular interface.

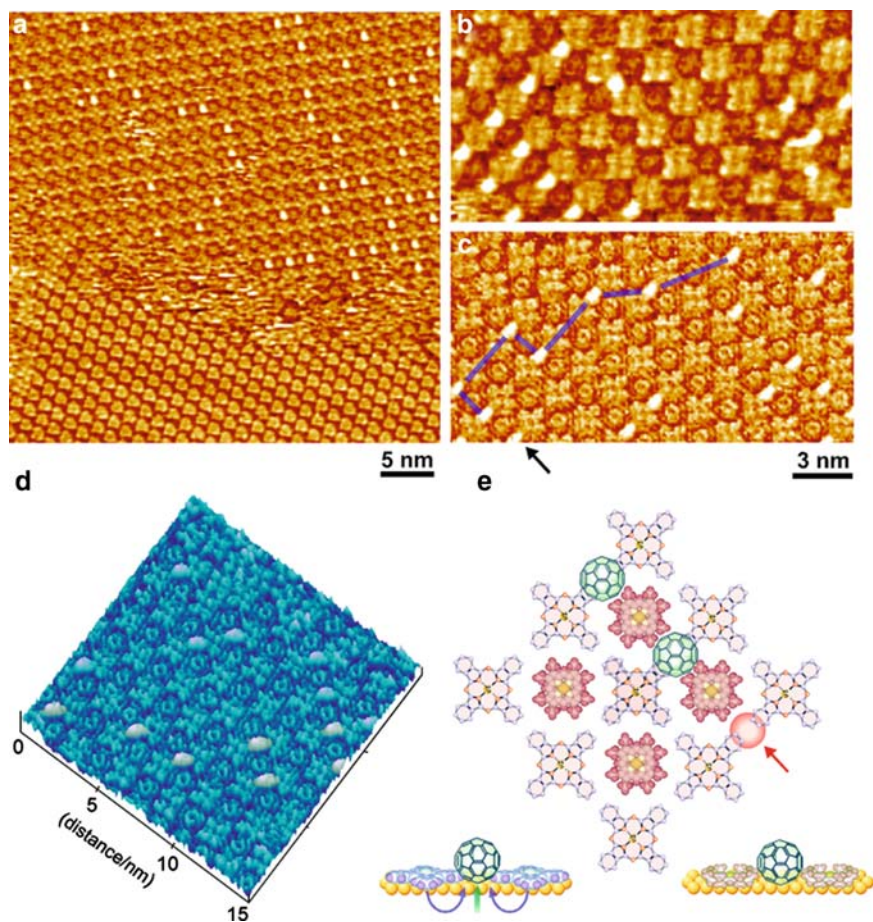


**Fig. 7** (a) Large-scale ( $40 \times 40 \text{ nm}^2$ ) and (b) and (c) high-resolution ( $10 \times 20 \text{ nm}^2$ ) STM images of  $\text{C}_{60}$  array in the bimolecular chessboard consisting of ZnPc and ZnOEP on Au(111) in  $0.1 \text{ M HClO}_4$ . (d) Height-shaded view of (c). (e) Proposed models for top and side views of  $\text{C}_{60}$  array in bimolecular chessboard. Reprinted with permission from [101], Copyright (2008) American Chemical Society

Other interesting observations are dendritic supramolecular assembly of porphyrins and  $\text{C}_{60}$ . Dendritic molecules appended with multiple zinc porphyrin units ( $\text{DP}_m$   $m$ : number of  $\text{Zn}^{\text{II}}$  porphyrin moiety) and bipyridine compounds carrying multiple fullerene units ( $\text{Py}_2\text{F}_n$ )  $n$ : number of  $\text{C}_{60}$  units) were synthesized by Aida and coworkers [106]. These types of segregated arrays of multiple donor and acceptor units using a dendritic scaffold indicate a photoinduced charge separation. Some of the coordination complexes between  $\text{DP}_m$  and  $\text{Py}_2\text{F}_n$  were imaged by STM under UHV conditions [106]. Bottari et al. reported that one  $\text{C}_{60}$  covalently linked ZnPc conjugate is able to self-organize on graphite and graphite-like surfaces, which give rise to supramolecular fibers and films [107]. The obtained nanostructures were

electrically characterized by conductive atomic force microscopy (C-AFM) and showed outstanding nanoscale electrical conductivity. This is one of the reports on the appearance of the characteristic property for supramolecularly assembled thin film, which has excellent donor and acceptor units. SPM technique is useful not only to observe surface morphology but also to measure various physical properties at the surface.

One of applications of porphyrin–fullerene supramolecular assembly is to use honeycomb network array. Hydrogen bond-based network structures provide a potential pathway to the design of host–guest interfaces, because the cavity size can be controlled through careful selection of the component molecules. For example, the formation of a self-assembled bimolecular network through hydrogen bonds by coadsorption of perylene tetra-carboxylic di-imide (PTCDI) and 1,3,5-triazine-2,4,6-triamine (melamine; ML) on Ag/Si(111)-( $\sqrt{3} \times \sqrt{3}$ )R30° in UHV was reported by Theobald et al. [108]. The substrate, Ag deposited on Si(111), is one of the most suitable surfaces for the adsorption of organic molecules such as fullerenes, phthalocyanine, and naphthalene tetracarboxylic di-imide (NTCDI) in a UHV environment, as these molecules diffuse freely across the deposited surface and form islands in which the order is predominantly governed by intermolecular interactions. The framework provides a regular array of identical nanoscale traps in which further deposited molecules nucleate cluster growth. A similar host–guest function was also found on Au(111) [109, 110]. Supramolecular traps of C<sub>60</sub> molecules occurred at the template of a bimolecular network comprising ML and PTCDI. The honeycomb array can be prepared from solution phase [111]. Thiols are trapped in the cavities, indicating that this kind of hydrogen-bond formation through three points is much stronger. The binding energy of ML-PTCDI honeycomb array was estimated to be 200 kJ mol<sup>-1</sup>, which is higher than 160 kJ mol<sup>-1</sup> of an Au–S bond [111].

Stöhr and Jung's group reported a hierarchical supramolecular rotor–stator system consisting of ZnOEP and 4,9-diaminoperylenequinone-3,10-diimine (DPDI) molecules on Cu(111) [112]. Figure 8 contains the STM images and model structures for the ZnOEP molecules trapped inside the dehydro–DPDI network. The molecular orientation of the ZnOEP molecule trapped inside the dehydro–DPDI honeycomb network change when the temperature is varied. Both the structure of the substrate lattice and the size and symmetry of the organic network play an important role in determining the preferred orientations of the ZnOEP molecule.

## 4 Direct Formation of Nanostructures on Surface

### 4.1 Direct Metallation on Surface

Direct synthesis of metalloporphyrins at Ag(111) was reported by Gottfried et al. [113, 114]. This group prepared a free-base H<sub>2</sub>TPP adlayer on Ag(111) in UHV, and further deposited Co at the adlayer. X-ray photoelectron spectroscopy (XPS) results



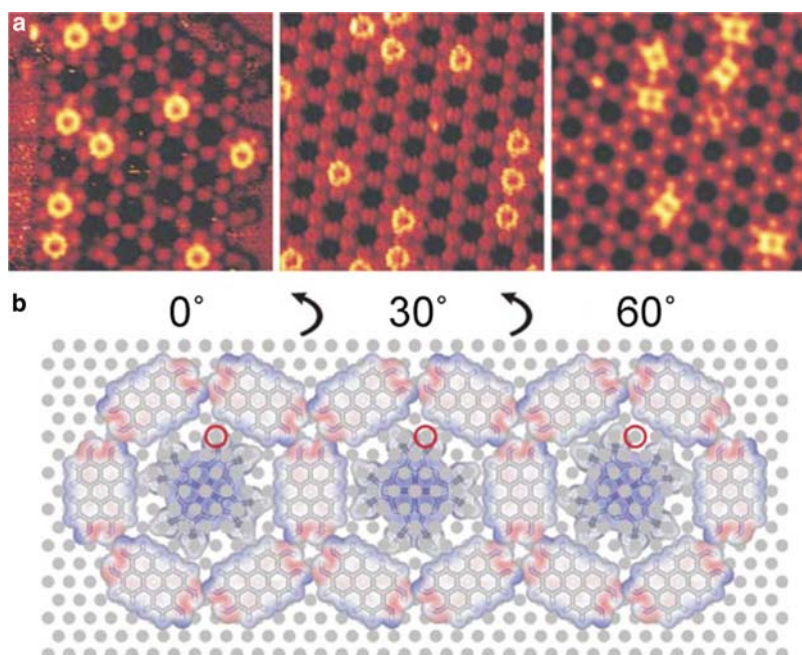


**Fig. 8** (a) ZnOEP molecules trapped in the dehydro-DPDI honeycomb network. STM images were recorded at room temperature (*left*), 77 K (*middle*), and 5 K (*right*), respectively. (b) model structures of the arrangement of the ZnOEP molecule inside the honeycomb dehydro-DPDI network on Cu(111). Reprinted with permission from [112], Copyright (2007) The Royal Society of Chemistry

indicated that a Co ion can be coordinated to a porphyrin ring [113]. The direct synthesis method was also effective for Zn metallation onto H<sub>2</sub>TPP adlayers by Zn deposition [114]. Direct observation of iron metallation into a free-base porphyrin array was independently reported by two groups [115, 116]. Auwärter and coworkers succeeded in directly observing Fe metallation at an H<sub>2</sub>TPyP array on Ag(111) in UHV [115]. Buchner et al. also demonstrated Fe metallation of an H<sub>2</sub>TPP array formed on Ag(111) by using UHV-STM [116] and XPS [117]. In both cases, each H<sub>2</sub>TPyP or H<sub>2</sub>TPP molecule appeared as brighter spots in the high-resolution STM image after the deposition of iron onto the adlayers, suggesting that the metallation of the Fe atom occurred at the H<sub>2</sub>TPyP and H<sub>2</sub>TPP adlayers on Ag(111). The characteristics of Co deposition onto a highly ordered H<sub>2</sub>TPP array on Ag(111) were also investigated by UHV-STM, STS, and ultraviolet photoelectron spectroscopy (UPS) by the same group [118, 119]. In addition, Ce metallation onto an H<sub>2</sub>TPP array formed on Ag(111) was recently reported by Auwärter and Barth group [120]. In the case of the direct metallation of an H<sub>2</sub>TPP array by Ce, a difference in the electronic structure between CoTPP and CeTPP was found in the high-resolution STM image and scanning tunneling spectroscopy (STS). The geometric and electronic structure of the novel species was additionally assessed by systematic density

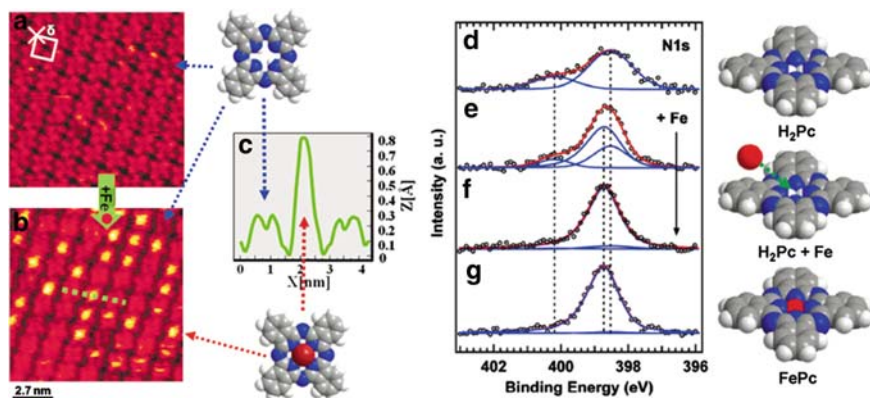


**Fig. 9** *Left*: Constant-current STM image (a) of a complete monolayer of H<sub>2</sub>Pc and (b) after the deposition of iron ( $\theta_{\text{Fe}} = 0.012$ ) onto the H<sub>2</sub>Pc monolayer. In part (b) some molecules exhibit a central bright spot, suggesting the formation of FePc. (c) Cross-sectional profile extracted along the green line in (b). Space-filling models of H<sub>2</sub>Pc and FePc are shown above and below the height profile, respectively. The *arrows* indicate the positions of the molecules in the images and the profile. *Right*: N1s XP spectra of a monolayer of H<sub>2</sub>Pc. (d) a monolayer of H<sub>2</sub>Pc after the deposition of increasing amounts of iron,  $\theta_{\text{Fe}} = 0.027$  (e) and  $\theta_{\text{Fe}} = 0.044$  (f), and a monolayer of directly deposited commercially available FePc as a reference (g). The fit neglects the small binding energy difference of 0.4 eV between the iminic nitrogen atoms in the peripheral *meso*-positions and in the center, for both H<sub>2</sub>Pc with six and FePc with eight iminic nitrogen atoms. Reprinted with permission from [122], Copyright (2008) American Chemical Society

functional theory (DFT) calculations, suggesting that the “bottom-up” approach can be applied to directly construct novel rare-earth Pcs and porphyrins on surfaces, as scaffolds to design multidecker superstructures. Fe coordination was also observed on a *meso*-tetramesitylporphyrin (TMP) adlayer formed on Cu(100) in UHV [121].

Subsequently, Marbach and Gottfried’s group reported that the direct metallation of Fe atoms onto a free-base phthalocyanine (H<sub>2</sub>Pc) adlayer was observed on Ag(111) by using UHV-STM [122]. As shown in Fig. 9, after the deposition of iron atoms the STM image of the H<sub>2</sub>Pc array was clearly changed, with bright spots appearing in the central part of each H<sub>2</sub>Pc molecule. The STM image was similar to that obtained at an FePc adlayer on Au(111), as previously reported by Hipps’ group [32]. In addition, XPS results indicated the coordination of Fe to N atoms in the Pc ligand, depending on the deposition of increasing amounts of Fe (see Fig. 9).

## 4.2 Direct Connection on Surface

The connection technique of molecules is important for the preparation of covalently bonded 2D arrays. As described in the previous section, the direct synthesis of metallophthalocyanine and metalloporphyrin can be achieved by the deposition

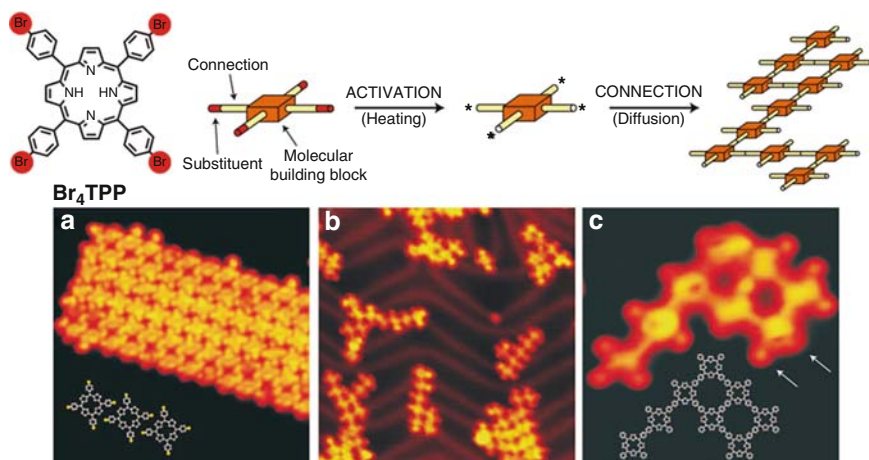


**Fig. 10** Upper: chemical structure of the Br<sub>4</sub>TPP molecule (substituent Br atoms are highlighted in red) and conceptual illustration of the formation of covalently bound networks by connecting activated molecular building blocks. (a) STM images (20 × 20 nm<sup>2</sup>) of a molecular island of Br<sub>4</sub>TPP monomer on Au(111) after deposition at low evaporator temperatures of 550 K prior to being activated. (b) large-scale STM image (41 × 41 nm<sup>2</sup>) for deposition at an elevated evaporator temperature of 610 K, causing the activation and connection of the molecules to form networks. (c) high-resolution STM image (8.5 × 8.5 nm<sup>2</sup>) of a network of eight molecular building blocks. The white arrows indicate molecular legs with and without Br atoms, respectively. Reprinted with permission from [123], Copyright (2007) Nature Publishing Group

of metals onto a free-base Pc or porphyrin array. Here, direct formation of 2D covalently bonded array is described.

Grill's group reported the connection of molecular building blocks by covalent assembly [123]. As schematically illustrated in Fig. 10, they first prepared an adlayer of tetra-(4-bromophenyl) porphyrin (Br<sub>4</sub>TPP) on Au(111). Next, the Br<sub>4</sub>TPP molecules were activated by heating the substrate and directly connected with each other on the Au(111) surface. By changing the substituted positions of the bromophenyl moieties, covalently bonded nanoarchitectures such as dimers and 1D molecular wires can be directly prepared on Au(111). A similar concept using thermally induced activation was also reported by Raval's group [124]. They showed connection of tetra(mesityl)porphyrin on Cu(110) in UHV, suggesting that a reaction with the copper reduces a methyl group on the mesityl functionality generating a CH<sub>2</sub><sup>•</sup> radical group.

Another interesting surface reaction on surfaces is the direct synthesis of a metal-coordinated porphyrin array. As reported by Barth's group, it is well known that highly ordered 2D arrays of metal–organic coordination are directly formed on a metal surface as a result of the codeposition of organic molecules functionalized with –COOH moieties and metals such as Fe, Co, and Cu [8, 125–127]. They have reported various 2D molecular patterns such as rectangular and honeycomb cavities on Au, Ag, and Cu single-crystal surfaces [127]. The symmetry of the evolving coordination networks is independent of the difference in metal substrate and

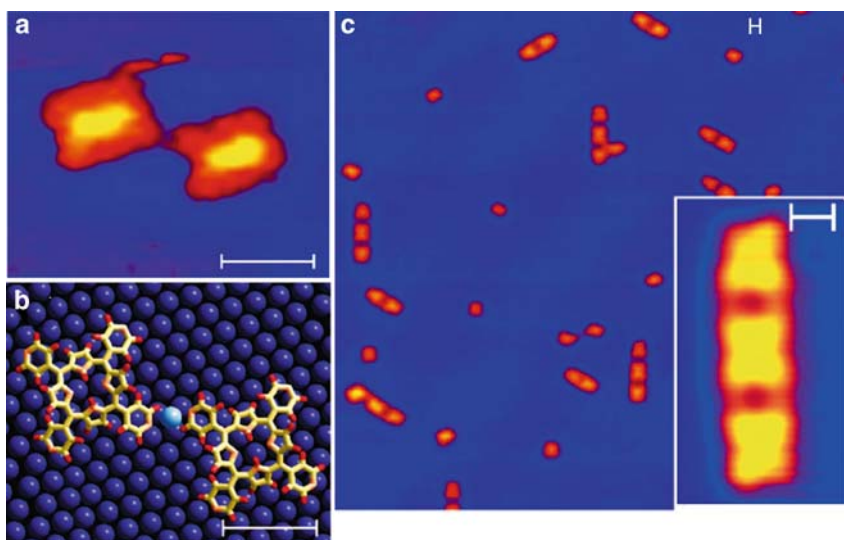


**Fig. 11** (a) High-resolution STM image of a TPyP dimer and (b) corresponding coordination model of a Cu adatom with the pyridyl ligands. (c) Upon annealing to  $\sim 414$  K for  $\sim 30$  min, supramolecular strings evolve in a conformation-dependent metal-directed assembly where two pyridyl endgroups are linked (imaged at 300 K). Scale bars 1 nm each. Reprinted with permission from [129], Copyright (2008) American Chemical Society

in crystallographic orientation, which indicates that the metal–ligand coordination predominates over the substrate. Recently, the authors demonstrated coordination between Cu adatoms and  $H_2TPyP$  molecules on Cu(111) by controlling the surface mobility as a function of temperature [128]. Figure 11 shows that  $H_2TPyP$  molecules are supramolecularly and directly bridged on Cu(111) by elevating the temperature. Dimer and trimer forms coordinated with Cu atoms are created on the terrace, as shown in Fig. 11c. They explained that a functionalization by pyridyl groups opens up pathways to control the anchoring of large organic molecules on metal surfaces and tune their conformational state. Furthermore, they demonstrated that the affinity of the terminal groups for metal centers permits the selective capture of individual iron atoms at low temperature [129]. Thus, selection of coordination metal makes it possible to precisely control this kind of nanostructure.

## 5 Self-Assembly of Porphyrins by Axial Ligand Coordination

### 5.1 Monomeric Complexes

Self-assembly of complementary subunits via noncovalent interactions such as hydrogen bonding or metal–ligand interactions is an attractive approach for the

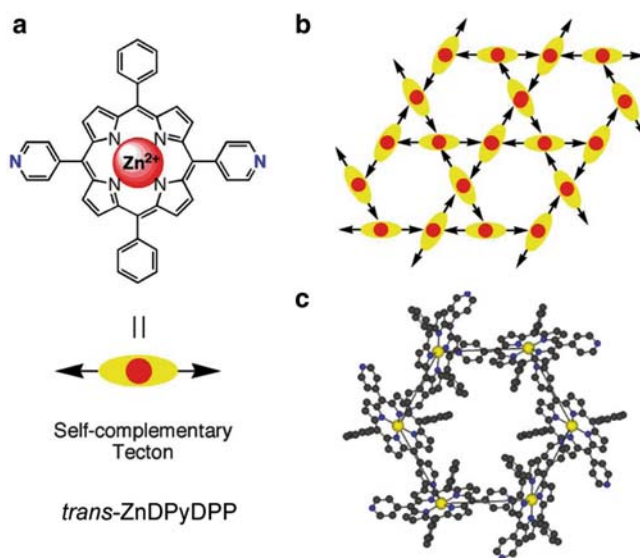


**Fig. 12** (a) Chemical structure of *trans*-dipyridyldiphenylporphyrinate zinc(II), **1**, (b) a schematic illustration of the 3D network formed by the self-complementary tecton of **1** and (c) a portion of the X-ray structure showing the empty hexagonal channel generated. Reprinted with permission from [137], Copyright (2005) The Royal Society of Chemistry

controlled oligomerization of monomers to form large supramolecular architectures. Porphyrin assembly based on metal–ligand coordination was reported in 1990 by Sanders' group [130–132]. The key to coordination-based self-assembly is the ability to manipulate the process of molecular recognition and to generate an enormous variety of rigid framework assemblies featuring well-defined nanoscale cavities [133, 134]. It is considered a promising approach for the recognition/binding phase of small-molecule sensing [135, 136]. Recent reports on a 3D coordination network of zinc porphyrins by Hosseini's group have encouraged us to investigate further the formation of this kind of high-class molecular architecture on surfaces [137–139], for example, as shown in Fig. 12. Indeed, a covalent porphyrin box consisting of cyclic tetramers was found on HOPG, and the tetramers were indicated to self-assemble into highly ordered arrays on the surface [140]. In this section, we briefly describe recent STM studies on molecular assemblies of porphyrins based on coordination.

The group of Rowan and Nolte synthesized giant porphyrin molecules such as porphyrin hexamers [141, 142] and dodecamers [143] from the viewpoint of photosynthetic systems and functional components in nanodevices. For example, the self-assembly behavior of a disc-like porphyrin dodecamer, in which 12 porphyrins are arranged in a circular fashion around a rigid central core, was investigated on HOPG in 1-phenyloctane containing the porphyrin dodecamer [143]. By adding a bidentate ligand diaza[2.2.2]bicyclooctane (DABCO) to a HOPG–solution interface, a highly ordered lamellae array was observed through the formation of a

supramolecular complex, suggesting that the coordination of DABCO to Zn ions causes the instantaneous formation of a large domain, and that DABCO acts as a “glue” to connect the porphyrin dodecamers to each other. Highly ordered domains of “edge-on” and “face-on” oriented Zn porphyrin hexamer and dodecamer assemblies were controlled on HOPG by the addition of coordinating axial ligands such as DABCO and BPy, which control the supramolecular architecture formed. Regarding to the control of “edge-on” and “face-on” orientation of porphyrin array on HOPG, another type was reported by Bhosale et al. [144]. According to their paper, they synthesized *meso*-tetraarylporphyrins bearing 2-etoxyethanol side chains as “sticky ends” which are capable of displaying directive hydrogen-bonding motifs. In this case, “edge-on” orientation was formed for free-base type, whereas the “face-on” orientation of zinc-coordinated porphyrin derivative was controlled by the axial coordination of pyridine. Thus, metallation and subsequent axial coordination is key factor in controlling the topology of the adlayer.

The coordination of DABCO to a central zinc ion was directly observed for a zinc porphyrin derivative (ZnTBPP)-adsorbed onto an Ag(100) surface in UHV [145]. The central dark part of each ZnTBPP was capped by the coordination of a DABCO molecule, resulting in a bright spot in the center.

An interesting ferrocene-bridged zinc porphyrin macrocycle was synthesized by Shoji et al. [146]. This group succeeded in visualizing a single molecule of a supramolecular coordination assembly on Au(111) in UHV [147]. The discrete

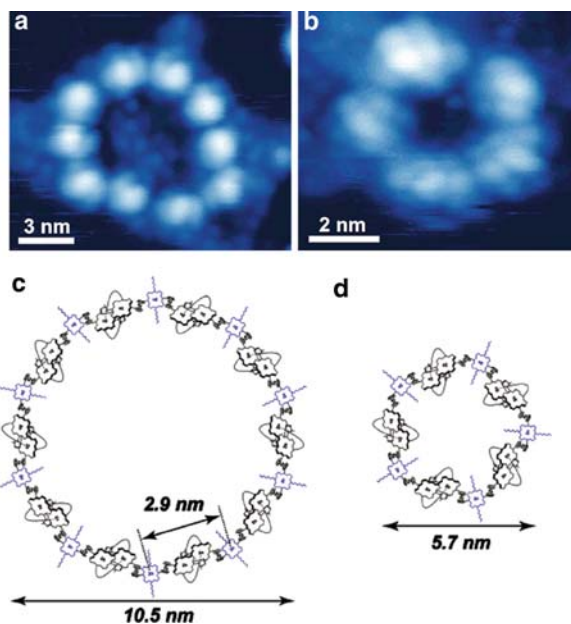


**Fig. 13** (a) and (b) STM images and (c) and (d) the corresponding schematic representation of the rings of ferrocene-bridged trisporphyrin on a Au(111) surface at liquid nitrogen temperature in UHV. (a) 10-mer and (b) 5-mer. Reprinted with permission from [147], Copyright (2005) American Chemical Society

system consisting of coordination of imidazol moieties to central zinc ion in each porphyrin is clearly seen in Fig. 13. Pyridine coordination to alkyl chain substituted rhodium porphyrin chloride ( $\text{Rh}(\text{C}_{18}\text{OPP})\text{Cl}(\text{Py})$  and  $\text{Rh}(\text{C}_{30}\text{OPP})\text{Cl}(\text{Py})$ ) self-organized on a graphite surface was also observed at a dichlorobenzene–graphite interface [148]. Ikeda et al. reported that a highly ordered adlayer of  $\text{Rh}(\text{C}_{18}\text{OPP})\text{Cl}(\text{Py})$  molecules was not formed on the graphite surface, whereas a highly ordered array of  $\text{Rh}(\text{C}_{30}\text{OPP})\text{Cl}(\text{Py})$  was clearly observed.  $\text{Rh}(\text{C}_{18}\text{OPP})\text{Cl}(\text{Py})$  molecules could form a highly ordered array by a mixture of metal-free  $\text{C}_{18}\text{OPP}$  (molecular ratio of  $\text{C}_{18}\text{OPP}/\text{Rh}(\text{C}_{18}\text{OPP})\text{Cl}(\text{Py})$  1:9), and the coordination of pyridine to the  $\text{Rh}(\text{C}_{18}\text{OPP})\text{Cl}(\text{Py})$  molecule was discriminated as a bright spot by high-resolution STM imaging in the mixed system.

## 5.2 Double- and Triple-Decker Complexes

In recent years, adlayers of several sandwich compounds, such as the bisphthalocyanine double-decker complexes of Y, Ce, Pr La, and Er, have been investigated at the liquid–solid interface. This kind of investigation is mainly performed on HOPG in 1-phenyloctance [149–154]. Possible future applications for these rare-earth complexes include their use as organic field-effect transistors, liquid crystals, chemical sensors [155], and, particularly, molecular memories of surfaces, as has been proposed by Lindsey and coworkers [156]. In the case of double-decker heterodimers, several groups have reported a unique molecular rotation characteristic [157–160]. This rotation can be controlled by coordination to specific functional groups within the molecule [157–159] or through the redox properties of the central rare-earth metal [160]. Thus, it is very important to understand the formation of double- or triple-decker adlayers by rotation control and electrochemical properties. We firstly reported the adlayer of a 15-crown-5-ether-substituted Pc and tetraphenyl porphyrin (TPP) triple-decker complex coordinated by  $\text{Eu}^{\text{III}}$ , TPP/CRPc/CRPc on an Au(111) surface, to create a three-dimensional functional molecular architecture [161]. A unique molecular assembly and new surface properties of TPP/CRPc/CRPc were observed as a result of adsorption orientation and electrochemical potential variation on the Au(111) surface. As can be seen in Fig. 14a, b, a characteristic well-ordered domain of a 2:1 sandwich complex consisting of Pcs and tetraphenylporphyrin was found on a Au(111) surface in 0.05 M  $\text{HClO}_4$  by in situ STM, indicating that a highly ordered array was formed by alternately arranging two different molecular orientations, as shown in Fig. 14. Electrochemical potential variation caused phase transition from square to hexagonal arrangements in the **1** adlayer. This finding is applicable to “bottom-up” nano-fabrication of the surface by controlling the molecular orientation and the rotation of the ligands. Vitali et al. reported the electronic structure of isolated bis(phthalocyaninato) terbium(III) molecules, a novel single-molecular magnet (SMM), supported on the Cu(111) surface by density functional theory and (STS) [162]. They showed that the interaction with the metal surface

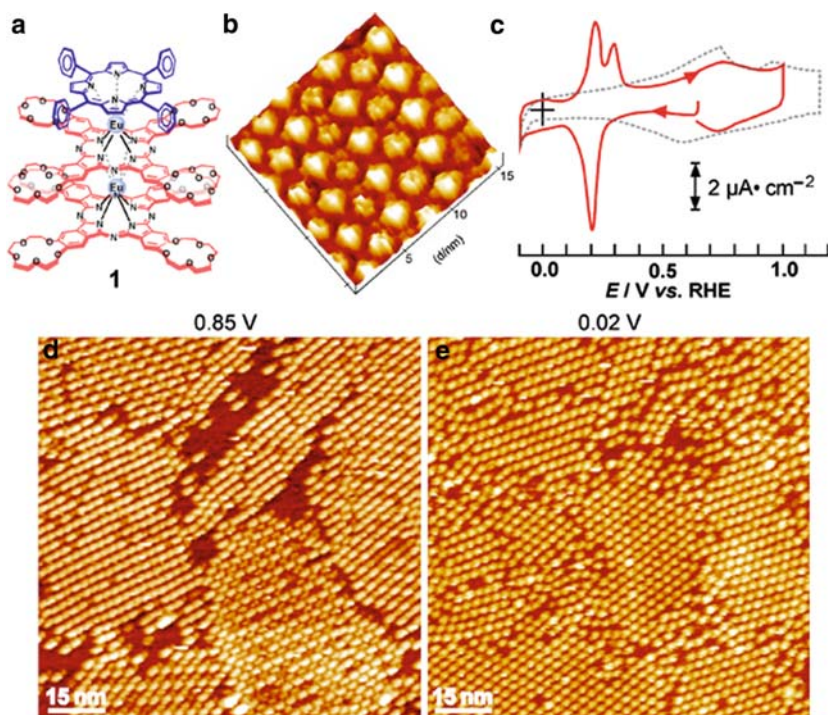


**Fig. 14** (a) Chemical structure of triple-decker **1**, (b) a height-shaded image of **1** adlayer on Au(111). (c) cyclic voltammogram of **1**-modified Au(111) electrode in 0.05 M HClO<sub>4</sub>. (d) and (e) potential-dependent STM images of **1** adlayer on Au(111) in 0.05 M HClO<sub>4</sub>, obtained at 0.85 V for panel (d) and 0.02 V for panel (e), respectively. Reprinted with permission from [161], Copyright (2007) Wiley-VCH

preserves both the molecular structure and the large spin magnetic moment of the metal center.

## 6 Nanoapplications

Phthalocyanines and porphyrins are often used as model compounds for the manipulation (guest molecule) of surface-supported supramolecular two-dimensional arrays both in UHV and in solution. Spillmann et al. reported that zinc(II) 5,15-bis(3-cyanophenyl)-10,20-bis[3,5-di(*tert*-butyl)phenyl] porphyrin, **2**, molecules predominantly formed a hexagonal pattern by trimer formation, when 0.5–0.7 MLs of **2** was deposited on Ag(111); especially, **2** forms a characteristic nanostructure on Ag(111) at low coverage [163]. As reported by Yokoyama et al., it is suggested that the molecular assembly is driven by both van der Waals and dipole–dipole interactions involving the polar 3-cyanophenyl residues [79]. After further deposition of C<sub>60</sub>



molecules, these molecules were trapped on the porphyrin network. Furthermore, driven by thermal fluctuations, single  $C_{60}$  ad molecules migrate to neighboring pores as time proceeds. The same group subsequently reported a difference in mobility of single fullerene molecules between  $C_{60}$  and  $C_{70}$  [164]. The hopping rate of  $C_{60}$  was  $1 \times 10^{-3} \text{ s}^{-1}$  at a coverage of 0.06, whereas the rate of  $C_{70}$  was  $9 \times 10^{-2} \text{ s}^{-1}$  at a coverage of 0.01. The hopping rate also depends on the coverage of fullerene on the porphyrin network [164]. The same authors also proposed the concept of a supramolecular rotary switch by using molecule **2**. Self-assembly of **2** on Cu(111) also leads to the formation of a porous network that features chiral cavities similar to Ag(111) [165]. In this case, the porous network structure consisting of **2** also serve as hosts for **2**. By applying short pulse by using the STM tip, rotation of **2** can be induced in each cavity. A supramolecular rotary device, reminiscent of a mechanical rotary switch, was engineered by a bottom-up approach.

Such an approach was also tried at solid–liquid interface. Ziener’s group reported a self-assembled host–guest network consisting of the oligopyridine derivative 3, 3'-BTP to manipulate CuPc at the solid–liquid interface [166]. They proposed that the slow movement of the CuPc guest molecules and the competition between oligopyridine and CuPc guest molecules make it possible to manipulate individual guest molecules in analogy to “writing” and “erasing” [166].

In contrast, Kröger’s group recently demonstrated that push and pull motions can be observed for the central Sn ions of SnPc molecules on a Ag(111) surface under UHV [167]. The up and down motions of the central Sn ion of second layer SnPc molecule can be controlled in a reversible manner by changing the bias voltage. The motions are irreversible in the context of a single SnPc layer attached directly to the Ag(111) surface, however, due to the stronger interaction between the SnPc molecules and the Ag(111) substrate. The bright spots observed for SnPc molecules in Fig. 15 change to darker spots as the Sn ion is pushed further below the Pc plane. The authors concluded that the reversibility of the up and down motions of the central Sn ion depended on the difference in the energy barriers of the single- and second-layer SnPc molecules. They concluded that reversible motion is achieved when either a resonant electron or a hole is created in the molecular orbitals. Applications in molecular switch device are envisaged, Fig. 15e–k.

## 7 Conclusions and Perspectives

This chapter primarily described the results of studies into the self-organization and supramolecular assembly of phthalocyanines and porphyrins at surfaces. The understanding of both intermolecular and molecule–substrate interactions in two-dimensionally self-organized films at the molecular level in UHV as well as in solution has been advanced considerably by the use of STM techniques. The construction of surface-supported supramolecular assemblies have provided the knowledge necessary for new surface design and patterning using characteristic molecular

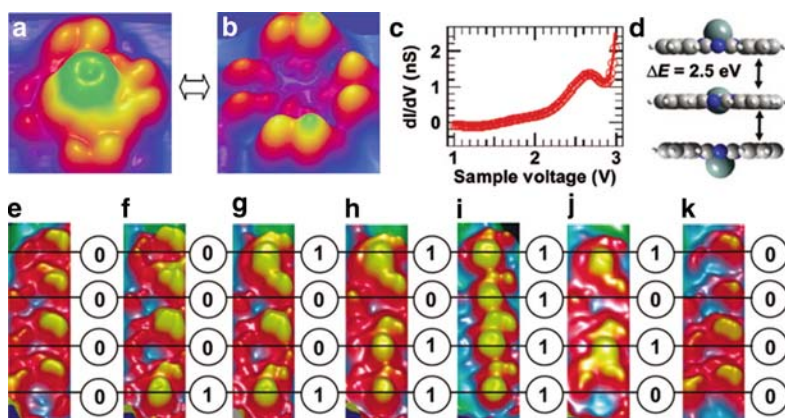


**Fig. 15** High-resolution STM images ( $2.0 \times 2.0 \text{ nm}^2$ ) of (a) Sn-up (+0.9 V, 0.2 nA) and (b) Sn-down (−1.8 V, 0.2 nA) molecules adsorbed on a single SnPc layer. (c)  $dI/dV$  spectrum of unoccupied states obtained on a single Sn-up molecule residing on the first SnPc adlayer on Ag(111). The peak at 2.6 V is due to the LUMO + 1. (d) schematic illustration of the reversible transformation of a neutral or negatively charged Sn-up molecule via a planar molecule geometry to a Sn-down molecule. Sequence of STM images ( $2.5 \times 7.5 \text{ nm}^2$ ) of SnPc molecules switching from the Sn-down conformation (e) one by one to the Sn-up conformation (i) and back to the Sn-down conformation (k) by applying 4 V at the center of the individually addressed molecules (3.0 V, 0.03 nA). The numbers added to the STM images as binary digits where 0 and 1 corresponds to Sn-down and Sn-up, respectively. Reprinted with permissions from [167], Copyrights (2009) American Chemical Society

assemblies through noncovalent intermolecular interactions, such as dipole–dipole interactions, hydrogen bonding, electrostatic interactions, metal–ligand coordination, and  $\pi$ – $\pi$  interactions. To produce new functional materials and molecular devices based on the above knowledge, it is necessary to continue to further explore nanostructures at surfaces and pursue the design of attractive molecules by organic synthesis in the future. As the next step, it is important to demonstrate a special function such as catalytic activity, photo-induced electron transfer, and conductivity due to the formation of these nanostructures. A demonstration of special functions by the formation of characteristic nanostructures would provide a “breakthrough” to the next stage of the “bottom up” strategy.

**Acknowledgements** This work was supported in part by the JST program “Special Coordination Funds for Promoting Science and Technology” (S.Y.) and by a Grant-in-Aid for Scientific Research on Innovative Areas (No. 20108007, “ $\pi$ -Space”) from the Ministry of Education, Culture, Sports, Science and Technology of Japan.

## References

1. Li G, Fudickar W, Skupin M, Klyszcz A, Draeger C, Lauer M, Fuhrhop JH (2002) *Angew Chem Int Ed* 41:1828
2. Lehn JM (1995) *Supramolecular chemistry*. Wiley-VCH, Weinheim
3. Choi IS, Bowden N, Whitesides GM (1999) *Angew Chem Int Ed* 38:3078
4. Ruben M, Rojo J, Romero-Salguero FJ, Uppadine LH, Lehn JM (2004) *Angew Chem Int Ed* 43:3644
5. Lehn JM (2007) *Chem Soc Rev* 36:151
6. van Hameren R, Schön P, van Bul AM, Hoogboom J, Lazarenko SV, Gerritsen JW, Engelkamp H, Christianen PCM, Heus HA, Maan JC, Rasing T, Speller S, Rowan AE, Elemans JAAW, Nolte RJM (2006) *Science* 314:1433
7. Hill JP, Jin W, Kosaka A, Fukushima T, Ichihara H, Shimomura T, Ito K, Hashizume T, Ishii N, Aida T (2004) *Science* 304:1481
8. Barth JV, Costantini G, Kern K (2005) *Nature* 437:671–679
9. Yoshimoto S, Itaya K (2007) *J Porphyrins Phthalocyanines* 11:313
10. De Feyter S, De Schryver FC (2003) *Chem Soc Rev* 32:139
11. Gewirth AA, Niece BK (1997) *Chem Rev* 97:1129
12. Itaya K (1998) *Prog Surf Sci* 58:121
13. Itaya K (2006) *Electrochemistry* 74:19
14. Wieckowski A (1999) *Interfacial Electrochemistry*. Marcel Dekker, New York
15. Kolb DM (2001) *Angew Chem Int Ed* 40:1162
16. Magnussen OM (2002) *Chem Rev* 102:672
17. De Feyter S, De Schryver FC (2005) *J Phys Chem B* 109:4290
18. Yoshimoto S (2006) *Bull Chem Soc Jpn* 79:1167
19. Wang D, Wan LJ (2007) *J Phys Chem C* 111:16109
20. Binnig G, Rohrer H, Gerber Ch, Weibel E (1982) *Phys Rev Lett* 49:57
21. Sonnenfeld R, Hansma PK (1986) *Science* 232:211
22. Itaya K, Tomita E (1988) *Surf Sci* 201:L507
23. Mamdouh W, Ujii H, Dulcey AE, Percec V, De Feyter S, De Schryver FC (2004) *Langmuir* 20:7678
24. Lackinger M, Griessl S, Heckl WM, Hietschold M, Flynn GW (2005) *Langmuir* 21:4984
25. Gyarfas BJ, Wiggins B, Zosel M, Hipps KW (2005) *Langmuir* 21:919
26. Ikeda T, Asakawa M, Miyake K, Shimizu T (2004) *Chem Lett* 33:1418
27. Lippel PH, Wilson RJ, Miller MD, Wöll C, Chiang S (1989) *Phys Rev Lett* 62:171
28. Jung TA, Schlittler RR, Gimzewski JK, Tang H, Joachim C (1996) *Science* 271:181
29. Jung TA, Schlittler RR, Gimzewski JK (1997) *Nature* 386:696
30. Lu X, Hipps KW, Wang XD, Mazur U (1996) *J Am Chem Soc* 118:7197
31. Hipps KW, Lu X, Wang XD, Mazur U (1996) *J Phys Chem* 100:11207
32. Lu X, Hipps KW (1997) *J Phys Chem B* 101:5391
33. Barlow DE, Hipps KW (2000) *J Phys Chem B* 104:5993
34. Scudiero L, Barlow DE, Hipps KW (2000) *J Phys Chem B* 104:11899
35. Scudiero L, Barlow DE, Mazur U, Hipps KW (2001) *J Am Chem Soc* 123:4073
36. Cheng ZH, Gao L, Deng ZT, Liu Q, Jiang N, Lin X, He XB, Du SX, Gao HJ (2007) *J Phys Chem C* 111:2656
37. Cheng ZH, Gao L, Deng ZT, Jiang N, Liu Q, Shi DX, Du SX, Guo HM, Gao HJ (2007) *J Phys Chem C* 111:9240
38. Kröger J, Jensen H, Néel N, Berndt R (2007) *Surf Sci* 601:4180
39. Néel N, Kröger J, Berndt R (2006) *Adv Mater* 18:174
40. Canas-Ventura ME, Xiao W, Wasserfallen D, Müllen K, Brune H, Barth JV, Fasel R (2007) *Angew Chem Int Ed* 46:1814
41. Ruiz-Osés M, González-Lakunza N, Silanes I, Gourdon A, Arnau A, Ortega JE (2006) *J Phys Chem B* 110:25573

42. Nilson K, Palmgren P, Åhlund J, Schiessling J, Göthelid E, Mårtensson N, Puglia C, Göthelid M (2008) *Surf Sci* 602:452
43. Wei Y, Robey SW, Reutt-Robey JE (2008) *J Phys Chem C* 112:18537
44. Sugimasa M, Inukai J, Itaya K (2003) *J Electrochem Soc* 150:E110
45. Wang YF, Kröger J, Berndt R, Hofer W (2009) *Angew Chem Int Ed* 48:1261
46. Samuely T, Liu SX, Wintjes N, Haas M, Decurtins S, Jung TA, Stöhr M (2008) *J Phys Chem C* 112:6139
47. Mazur U, Hipps KW, Riechers SL (2008) *J Phys Chem C* 112:20347
48. Kunitake M, Batina N, Itaya K (1995) *Langmuir* 11:2337
49. Batina N, Kunitake M, Itaya K (1996) *J Electroanal Chem* 405:245
50. Kunitake M, Akiba U, Batina N, Itaya K (1997) *Langmuir* 13:1607
51. Ogaki K, Batina N, Kunitake M, Itaya K (1996) *J Phys Chem* 100:7185
52. Sashikata K, Sugata T, Sugimasa M, Itaya K (1998) *Langmuir* 14:2896
53. Hai NTM, Gasparovic B, Wandelt K, Broekmann P (2007) *Surf Sci* 601:2597
54. Wan LJ, Shundo S, Inukai J, Itaya K (2000) *Langmuir* 16:2164
55. Safarowsky C, Wandelt K, Broekmann P (2004) *Langmuir* 20:8261
56. Safarowsky C, Merz L, Rang A, Broekmann P, Hermann BA, Schalley CA (2004) *Angew Chem Int Ed* 43:1291
57. Sakaguchi H, Matsumura H, Gong H (2004) *Nat Mater* 3:551
58. Han WH, Durantini EN, Moore TA, Moore AL, Gust D, Rez P, Leatherman G, Seely GR, Tao N-J, Lindsay SM (1997) *J Phys Chem B* 101:10719
59. He Y, Borguet E (2007) *Angew Chem Int Ed* 46:6098
60. He Y, Ye T, Borguet E (2002) *J Am Chem Soc* 124:11964
61. Ye T, He Y, Borguet E (2006) *J Phys Chem B* 110:6141
62. Tao NJ, Cardenas G, Cunha F, Shi Z (1995) *Langmuir* 11:4445
63. Tao NJ (1996) *Phys Rev Lett* 76:4066
64. Hai NTM, Wandelt K, Broekmann P (2008) *J Phys Chem C* 112:10176
65. Yoshimoto S, Sawaguchi T (2008) *J Am Chem Soc* 130:15944
66. Yoshimoto S, Inukai J, Tada A, Abe T, Morimoto T, Osuka A, Furuta H, Itaya K (2004) *J Phys Chem B* 108:1948
67. Yoshimoto S, Tada A, Suto K, Narita R, Itaya K (2003) *Langmuir* 19:672
68. Yoshimoto S, Sato K, Sugawara S, Chen Y, Ito O, Sawaguchi T, Niwa O, Itaya K (2007) *Langmuir* 23:809
69. Yoshimoto S, Tada A, Suto K, Itaya K (2003) *J Phys Chem B* 107:5836
70. Scudiero L, Barlow DE, Hipps KW (2002) *J Phys Chem B* 106:996
71. Yoshimoto S, Suto K, Itaya K, Kobayashi N (2003) *Chem Commun*:2174
72. Yoshimoto S, Suto K, Tada A, Kobayashi N, Itaya K (2004) *J Am Chem Soc* 126:8020
73. Yoshimoto S, Tsutsumi E, Suto K, Honda Y, Itaya K (2005) *Chem Phys* 319:147
74. Yoshimoto S, Tsutsumi E, Honda Y, Ito O, Itaya K (2004) *Chem Lett* 33:914
75. Yoshimoto S, Sugawara S, Itaya K (2006) *Electrochemistry* 74:17578
76. Lei SB, Wang C, Yin SX, Wang HN, Wi F, Liu HW, Xu B, Wan LJ, Bai CL (2001) *J Phys Chem B* 105:10838
77. Otsuki J, Nagamine E, Kondo T, Iwasaki K, Asakawa M, Miyake K (2005) *J Am Chem Soc* 127:10400
78. Hill JP, Wakayama Y, Akada M, Ariga K (2007) *J Phys Chem C* 111:16174
79. Yokoyama T, Yokoyama S, Kamikado T, Okuno Y, Mashiko S (2001) *Nature* 413:619
80. Yokoyama T, Kamikado T, Yokoyama S, Mashiko S (2004) *J Chem Phys* 121:11993
81. Yoshimoto S, Yokoo N, Fukuda T, Kobayashi N, Itaya K (2006) *Chem Commun*:500
82. Hipps KW, Scudiero L, Barlow DE, Cooke Jr MP (2002) *J Am Chem Soc* 124:2126
83. Scudiero L, Hipps KW, Barlow DE (2003) *J Phys Chem B* 107:2903
84. Barlow DE, Scudiero L, Hipps KW (2004) *Langmuir* 20:4413
85. Suto K, Yoshimoto S, Itaya K (2003) *J Am Chem Soc* 125:14976
86. Suto K, Yoshimoto S, Itaya K (2006) *Langmuir* 22:10766
87. Yoshimoto S, Higa N, Itaya K (2004) *J Am Chem Soc* 126:8540
88. Barrena E, de Oteyza DG, Dosch H, Wakayama Y (2007) *ChemPhysChem* 8:1915

89. de Wild M, Berner S, Suzuki H, Yanagi H, Schlettwein D, Ivan S, Baratoff A, Güntherodt HJ, Jung TA (2002) *ChemPhysChem* 3:881
90. Calmettes B, Nagarajan S, Gourdon A, Abel M, Porte L, Coratger R (2008) *Angew Chem Int Ed* 47:6994
91. Kong XH, Deng K, Yang YL, Zeng QD, Wang C (2007) *J Phys Chem C* 111:9235
92. Kong XH, Yang YL, Lei SB, Wang C (2008) *Surf Sci* 602:684
93. Yang ZY, Lei SB, Gan LH, Wan LJ, Wang C, Bai CL (2005) *ChemPhysChem* 6:65
94. Lu J, Lei SB, Zeng QD, Kang SZ, Wang C, Wan LJ, Bai CL (2004) *J Phys Chem B* 108:5161
95. Ishii T, Aizawa N, Kanehama R, Yamashita M, Sugiura Ki, Miyasaka H (2002) *Coord Chem Rev* 226:113
96. Boyd PDW, Reed CA (2005) *Acc Chem Res* 38:235
97. Stöhr M, Wagner T, Gabriel M, Weyers B, Möller R (2001) *Adv Funct Mater* 11:175
98. Yoshimoto S, Tsutsumi E, Honda Y, Murata Y, Murata M, Komatsu K, Ito O, Itaya K (2004) *Angew Chem Int Ed* 43:3044
99. Yoshimoto S, Honda Y, Murata Y, Murata M, Komatsu K, Ito O, Itaya K (2005) *J Phys Chem B* 109:8547
100. Yoshimoto S, Saito A, Tsutsumi E, D'Souza F, Ito O, Itaya K (2004) *Langmuir* 20:11046
101. Yoshimoto S, Honda Y, Ito O, Itaya K (2008) *J Am Chem Soc* 130:1085
102. Yoshimoto S, Tsutsumi E, Fujii O, Narita R, Itaya K (2005) *Chem Commun*:1188
103. Yoshimoto S, Tsutsumi E, Narita R, Fujiwara K, Murata M, Murata Y, Komatsu K, Ito O, Itaya K (2007) *J Am Chem Soc* 129:4366
104. Nishiyama F, Yokoyama T, Kamikado T, Yokoyama S, Mashiko S, Sakaguchi K, Kikuchi K (2007) *Adv Mater* 19:117
105. Bonifazi D, Spillmann H, Kiebele A, de Wild M, Seiler P, Cheng F, Jung T, Diederich F (2004) *Angew Chem Int Ed* 43:4759
106. Li WS, Kim KS, Jiang DL, Tanaka H, Kawai T, Kwon JH, Kim D, Aida T (2006) *J Am Chem Soc* 128:10527
107. Bottari G, Olea D, Gómez-Navarro C, Zamora F, Gómez-Herrero J, Torres T (2008) *Angew Chem Int Ed* 47:2026
108. Theobald JA, Oxtoby NS, Phillips MA, Champness NR, Beton PH (2003) *Nature* 424:1029
109. Perdigão LMA, Perkins EW, Ma J, Staniec PA, Rogers BL, Champness NR, Beton PH (2006) *J Phys Chem B* 110:12539
110. Saywell A, Magnano G, Satterley CJ, Perdigão LMA, Champness NR, Beton PH, O'Shea JN (2008) *J Phys Chem C* 112:7706
111. Madueno R, Räsänen MT, Silien C, Buck M (2008) *Nature* 454:618
112. Wahl M, Stöhr M, Spillmann H, Jung TA, Gade LH (2007) *Chem Commun*:1349
113. Gottfried JM, Flechtner K, Kretschmann A, Lukaszczuk T, Steinrück HP (2006) *J Am Chem Soc* 128:5644
114. Kretschmann A, Walz MM, Flechtner K, Steinrück HP, Gottfried JM (2007) *Chem Commun*:568
115. Auwärter W, Weber-Bargioni A, Brink S, Riemann A, Schiffrin A, Ruben M, Barth JV (2007) *ChemPhysChem* 8:250
116. Buchner F, Schwald V, Comanici K, Steinrück HP, Marbach H (2007) *ChemPhysChem* 8:241
117. Buchner F, Flechtner K, Bai Y, Zillne, E, Kellner I, Steinrück HP, Marbach H, Gottfried JM (2008) *J Phys Chem C* 112:15458
118. Lukaszczuk T, Flechtner K, Merte LR, Jux N, Maier F, Gottfried JM, Steinrück HP (2007) *J Phys Chem C* 111:3090
119. Comanici K, Buchner F, Flechtner K, Lukaszczuk T, Gottfried JM, Steinrück HP, Marbach H (2008) *Langmuir* 24:1897
120. Weber-Bargioni A, Reichert J, Seitsonen AP, Auwärter W, Schiffrin A, Barth JV (2008) *J Phys Chem C* 112:3453
121. Écija D, Trelka M, Urban C, Mendoza P, Mateo-Martí E, Rogero C, Martín-Gago JA, Echavarren AM, Otero R, Gallego JM, Miranda R (2008) *J Phys Chem C* 112:8988
122. Bai Y, Buchner F, Wendahl MT, Kellner I, Bayer A, Steinrück HP, Marbach H, Gottfried JM (2008) *J Phys Chem C* 112:6087

123. Grill L, Dyer M, Lafferentz L, Persson M, Peters MV, Hecht S (2007) *Nature Nanotechnol* 2:687
124. In't Veld M, Iavicoli P, Haq S, Amabilino DB, Raval R (2008) *Chem Commun*:1536
125. Spillmann H, Dmitriev A, Lin N, Messina P, Barth JV, Kern K (2003) *J Am Chem Soc* 125:10725
126. Stepanow S, Lingenfelder M, Dmitriev A, Spillmann H, Delvigne E, Lin N, Deng X, Cai C, Barth JV, Kern K (2004) *Nature Mater* 3:229
127. Stepanow S, Lin N, Barth JV (2008) *J Phys:Condens Matter* 20:184002
128. Eichberger M, Marschall M, Reichert J, Weber-Bargioni A, Auwärter W, Wang RLC, Kreuzer HJ, Pennec Y, Schiffrin A, Barth JV (2008) *Nano Lett* 8:4608
129. Auwärter W, Klappenberger F, Weber-Bargioni A, Schiffrin A, Strunskus T, Wöll C, Pennec Y, Riemann A, Barth JV (2007) *J Am Chem Soc* 129:11279
130. Hunter CA, Sanders JKM (1990) *J Am Chem Soc* 112:5525
131. Hunter CA, Mesh MN, Sanders JKM (1990) *J Am Chem Soc* 112:5773
132. Anderson HL, Hunter CA, Mesh MN, Sanders JKM (1990) *J Am Chem Soc* 112:5780
133. Fujita M, Tominaga M, Hori A, Therrien B (2005) *Acc Chem Res* 38:371
134. Claessens CG, Vicente-Aranab MJ, Torres T (2008) *Chem Commun*:6378
135. Kitagawa S, Noro S, Nakamura T (2006) *Chem Commun*:701
136. Bar AK, Chakrabarty R, Mostafa G, Mukherjee PS (2008) *Angew Chem Int Ed* 47:8455
137. Hosseini MW (2005) *Chem Commun*:5825
138. Deiters E, Bulach V, Hosseini MW (2005) *Chem Commun*:3906
139. Kühn E, Bulach V, Hosseini MW (2008) *Chem Commun*:5104
140. van Gerven PCM, Elemans JAAW, Gerritsen JW, Speller S, Nolte RJM, Rowan AE (2005) *Chem Commun*:3535
141. Elemans JAAW, Lensen MC, Gerritsen JW, Kerpen H, Speller S, Nolte RJM, Rowan AE (2003) *Adv Mater* 15:2070
142. Lensen MC, Takazawa K, Elemans JAAW, Jeukens CRLPN, Christianen PCM, Maan JC, Rowan AE, Nolte RJM (2004) *Chem Eur J* 10:831
143. Lensen MC, van Dingenen SJT, Elemans JAAW, Dijkstra HP, van Klink GPM, van Koten G, Gerritsen JW, Speller S, Nolte RJM, Rowan AE (2004) *Chem Commun*:762
144. Bhosale SV, Bissett MA, Forsyth C, Langford SJ, Neville SM, Shapter JG, Weeks L, Woodward CP (2008) *Org Lett* 10:2943
145. Williams FJ, Vaughan OPH, Knox KJ, Bampos N, Lambert RM (2004) *Chem Commun*:1688
146. Shoji O, Okada S, Satake A, Kobuke Y (2005) *J Am Chem Soc* 127:2201
147. Shoji O, Tanaka H, Kawai T, Kobuke Y (2005) *J Am Chem Soc* 127:8598
148. Ikeda T, Asakawa M, Goto M, Miyake K, Ishida T, Shimizu T (2004) *Langmuir* 20:5454
149. Yang ZY, Gan LH, Lei SB, Wan LJ, Wang C, Jiang JZ (2005) *J Phys Chem B* 109:19859
150. Klymchenko AS, Slevin J, Binnemans K, De Feyter S (2006) *Langmuir* 22:723
151. Takami T, Arnold DP, Fuchs AV, Will GD, Goh R, Waclawik ER, Bell JM, Weiss PS, Sugiura Ki, Liu W, Jiang JZ (2006) *J Phys Chem B* 110:1661
152. Ye T, Takami T, Wang R, Jiang JZ, Weiss PS (2006) *J Am Chem Soc* 128:10984
153. Takami T, Ye T, Arnold DP, Sugiura Ki, Wang R, Jiang JZ, Weiss PS (2007) *J Phys Chem C* 111:2077
154. Otsuki J, Kawaguchi S, Yamakawa T, Asakawa M, Miyake K (2006) *Langmuir* 22:5708
155. Kottas GS, Clarke LI, Horinek D, Michl J (2005) *Chem Rev* 105:1281
156. Liu Z, Yasserli AA, Lindsey JS, Bocian DF (2003) *Science* 302:1543
157. Takeuchi M, Imada T, Shinkai S (1998) *Angew Chem Int Ed* 37:2096
158. Sugasaki A, Ikeda M, Takeuchi M, Shinkai S (2000) *Angew Chem Int Ed* 39:3839
159. Shinkai S, Ikeda M, Sugasaki A, Takeuchi M (2001) *Acc Chem Res* 34:494
160. Tashiro K, Konishi K, Aida T (2000) *J Am Chem Soc* 122:7921
161. Yoshimoto S, Sawaguchi T, Su W, Jiang JZ, Kobayashi N (2007) *Angew Chem Int Ed* 46:1071
162. Vitali L, Fabris S, Conte AM, Brink S, Ruben M, Baroni S, Kern K (2008) *Nano Lett* 8:3364
163. Spillmann H, Kiebele A, Stöhr M, Jung TA, Bonifazi D, Cheng FY, Diederich F (2006) *Adv Mater* 18:275

164. Kiebele A, Bonifazi D, Cheng F, Stöhr M, Diederich F, Jung T, Spillmann H (2006) *ChemPhysChem* 7:1462
165. Wintjes N, Bonifazi D, Cheng F, Kiebele A, Stöhr M, Jung T, Spillmann H, Diederich F (2007) *Angew Chem Int Ed* 46:4089
166. Meier C, Landfester K, Künzel D, Markert T, Groß A, Ziener U (2008) *Angew Chem Int Ed* 47:3821
167. Wang Y, Kröger J, Berndt R, Hofer WA (2009) *J Am Chem Soc* 131:3639

# Phthalocyanine-Containing Supramolecular Arrays

Jian-Yong Liu, Pui-Chi Lo, and Dennis K.P. Ng

**Abstract** Phthalocyanines represent a versatile class of functional dyes which have found applications in various disciplines ranging from materials science, catalysis, nanotechnology to medicine. The intrinsic properties of the macrocycles as well as their molecular arrangements, both in solution and in the condensed phase, can be altered through rational chemical modification. Conjugation of other functional units to phthalocyanines can also complement the characteristics of the macrocycles. All these approaches can improve the performance of these macrocyclic compounds as advanced functional materials. The purpose of this article is to provide an up-to-date review of the current research status of phthalocyanine-containing supramolecular systems. The formation, structures, and properties of self-assembled phthalocyanines as well as the non-covalent hetero-arrays containing phthalocyanines and other functional units are reviewed herein.

**Keywords** Axial coordination · Host–guest complexes · Phthalocyanines · Self-assembly · Supramolecular chemistry

## Contents

1	Introduction .....	170
2	Supramolecular Arrays Held by Axial Coordination .....	171
2.1	Phthalocyanine–Porphyrin Hetero-Arrays .....	171
2.2	Phthalocyanine–Subphthalocyanine Hetero-Arrays .....	177
2.3	Phthalocyanine–Fullerene Hetero-Arrays .....	177
2.4	Phthalocyanine–Perylenediimide Hetero-Arrays .....	182
2.5	Phthalocyanine–Polypyridyl Ruthenium(II) Hetero-Arrays .....	184
2.6	Phthalocyanine–Oligothiophene Hetero-Arrays .....	184

---

J.-Y. Liu, P.-C. Lo, and D.K.P. Ng (✉)  
Department of Chemistry and Center of Novel Functional Molecules,  
The Chinese University of Hong Kong, Shatin, N.T., Hong Kong, China  
e-mail: dkpn@cuhk.edu.hk



2.7	A Phthalocyanine-Squaraine Hetero-Array .....	185
2.8	Self-Coordinated Phthalocyanine Dimers .....	186
3	Supramolecular Arrays Held by Hydrogen Bonding .....	190
3.1	Hydrogen-Bonded Phthalocyanine–Fullerene Hetero-Arrays .....	190
3.2	Hydrogen-Bonded Phthalocyanine Aggregates .....	193
4	Supramolecular Arrays Held by Electrostatic Interactions .....	198
5	Supramolecular Arrays Held by Donor–Acceptor Interactions .....	200
6	Supramolecular Arrays Held by Host–Guest Interactions .....	203
7	Concluding Remarks .....	207
	References .....	207

## 1 Introduction

Phthalocyanines are macrocyclic compounds containing four *N*-fused isoindole units. Since these compounds have a large  $\pi$ -conjugated system, they absorb strongly in the red visible region (at ca. 670 nm), giving a characteristic blue-green color. This property together with their extraordinary stability renders them to be used as industrial pigments for several decades [1]. In addition to this traditional application, these compounds have been extensively studied as advanced materials in various disciplines as a result of their intriguing and tunable characteristics [2, 3]. Some recent focuses have been put on their applications as optical recording materials [4], semiconductors for organic field effect transistors [5, 6], catalysts for oxidative degradation of pollutants [7, 8], and sensitizers for photovoltaics [9–11] and photodynamic therapy [12, 13]. These macrocyclic compounds are therefore versatile functional dyes receiving much current attention.

To enhance the functionalities of these compounds which can improve their performance as advanced materials, a vast number of functional units have been conjugated to the macrocycles. Photo- and redox-active groups such as porphyrins, fullerenes, and carotenoids are of particular interest because the resulting conjugates are potentially useful in light-harvesting devices, photovoltaics, and molecular photonics [14–16]. In most of these conjugates, individual components are linked up together in a covalent manner, while supramolecular hetero-arrays remain relatively rare despite the fact that this facile self-assembly strategy can be used to construct sophisticated systems readily. This review aims to provide an overview of the current research status of phthalocyanine-containing supramolecular arrays. We include herein the systems held by axial coordination, hydrogen bonding, electrostatic forces, donor–acceptor interactions, and host–guest interactions that have been reported over the past decades. Heteroleptic phthalocyaninato and porphyrinato sandwich-type complexes have been reviewed comprehensively [17–19] and are not covered in this article. There are also a number of  $\mu$ -nitrido and  $\mu$ -oxo bi- and tri-metallic complexes with mixed phthalocyaninato and porphyrinato ligands [20, 21], the chemistry of which is also excluded herein. Recently, we have published a review article on hetero-arrays of porphyrins and phthalocyanines [22]. Some of

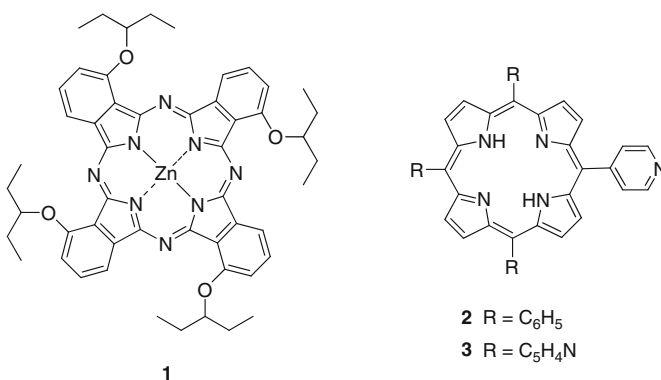
the recent examples described in this article will also be included in this review for the sake of completeness. During the preparation of this review, a feature article has appeared in which D'Souza and Ito summarize their work in supramolecular donor-acceptor hybrids of porphyrins/phthalocyanines with fullerenes/carbon nanotubes [23]. Another micro-review highlighting the contribution of several Spain's research groups has also been published [24].

## 2 Supramolecular Arrays Held by Axial Coordination

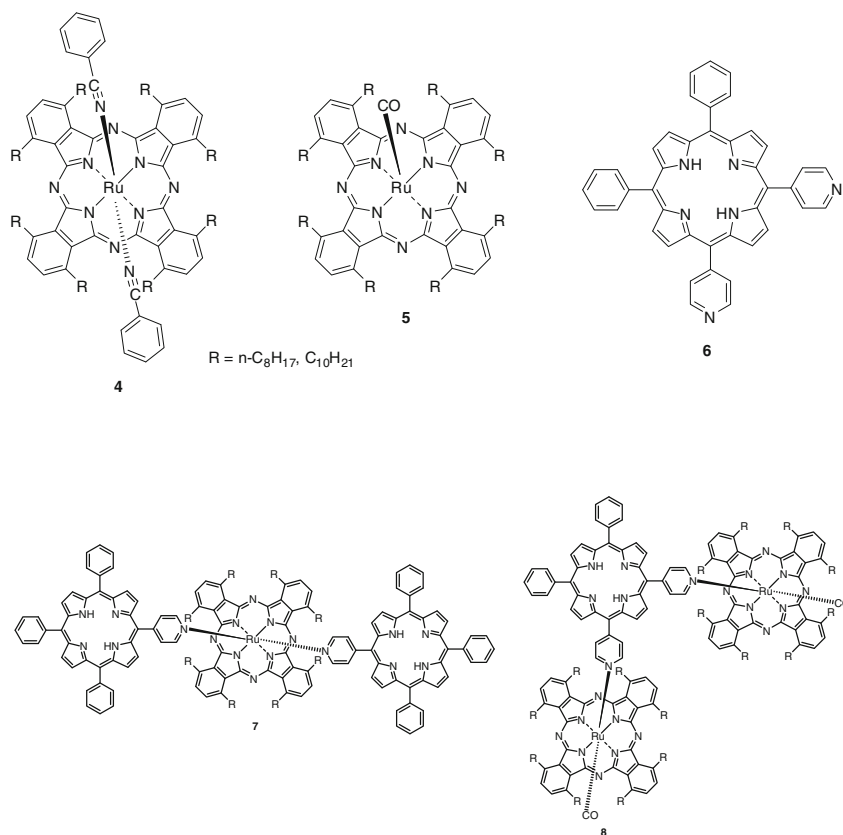
Axial coordination of metallo-phthalocyanines has been relatively little studied compared with that of the porphyrin analogs. Nevertheless, this approach has been employed to construct various phthalocyanine-based hetero-arrays as described below.

### 2.1 Phthalocyanine-Porphyrin Hetero-Arrays

Ng et al. first reported the axial ligation of zinc(II) 1,8,15,22-tetrakis(3-pentyloxy) phthalocyanine (**1**) with meso-pyridyl porphyrins **2** and **3** in chloroform, which form the corresponding edge-to-face dyad and pentad, respectively [25]. As shown by UV-Vis spectroscopy, the ground-state  $\pi$ - $\pi$  interactions between the perpendicularly disposed macrocycles in these arrays are insignificant. Upon mixing of phthalocyanine **1**, zinc(II) meso-tetra(*p*-tolyl)porphyrin, and 4,4'-bipyridine in chloroform, the formation of a face-to-face hetero-dyad was also inferred by fluorescence quenching experiments.



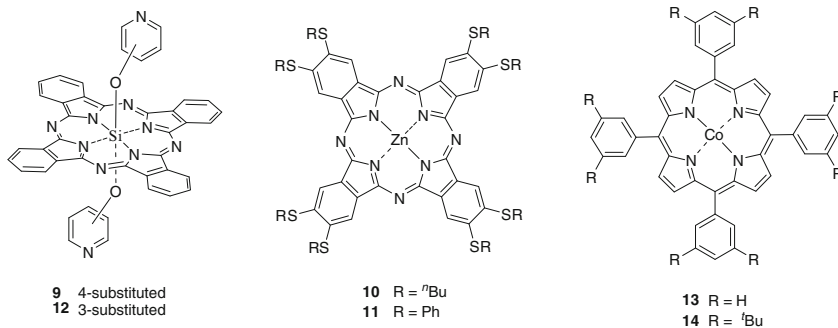
Cook et al. further explored the complexation of meso-pyridyl porphyrins with ruthenium(II) phthalocyanines [26, 27]. Compounds **4** and **5** ( $R = n\text{-C}_8\text{H}_{17}$ ,  $n\text{-C}_{10}\text{H}_{21}$ ), which can be prepared by controlled metallation of the corresponding metal-free phthalocyanines with  $\text{Ru}_3(\text{CO})_{12}$  in refluxing benzonitrile, bind to various pyridyl ligands. Treatment of these compounds ( $R = n\text{-C}_8\text{H}_{17}$ ) with pyridyl porphyrins **2** and **3**, as well as the dipyrindyl analog **6** leads to the formation of a series of mixed phthalocyanine–porphyrin arrays, which can be isolated by flash chromatography followed by reprecipitation. For example, reaction of **4** ( $R = n\text{-C}_8\text{H}_{17}$ ) with 2 equiv. of monopyridyl porphyrin **2** gives the triad **7**, while complexation of **5** ( $R = n\text{-C}_8\text{H}_{17}$ ) with half equiv. of dipyrindyl porphyrin **6** affords the triad **8**, both in ca. 70% yield. The individual chromophores in these arrays were also found to have little ground-state interaction.



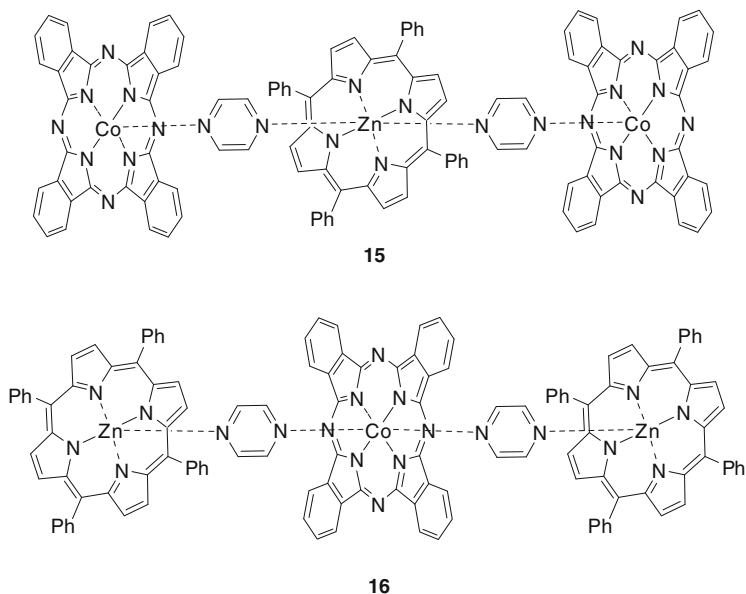
Similar arrays can also be assembled using pyridyl phthalocyanines as building blocks. Compound **9**, having two 4-pyridinolato axial ligands, binds to zinc(II)

meso-tetraphenylporphyrin (ZnTPP) forming the 1:2 hetero-triad  $\mathbf{9} \cdot [\text{ZnTPP}]_2$ , of which the molecular structure was determined by X-ray diffraction analysis [28]. By contrast, complexation of  $\mathbf{9}$  with zinc(II) octathiobutoxy or octathiophenoxy phthalocyanine ( $\mathbf{10}$  or  $\mathbf{11}$ ) proceeds in a 1:1 manner. It is likely that an alternating polymeric structure is formed in which each zinc center binds to two pyridyl groups from two molecules of  $\mathbf{9}$ . As determined by NMR spectroscopy, the binding constants ( $390 \text{ M}^{-1}$  (for  $\mathbf{10}$ ) and  $270 \text{ M}^{-1}$  (for  $\mathbf{11}$ )) are about one order of magnitude smaller than the typical values for axial coordination of zinc(II) porphyrins with pyridine.

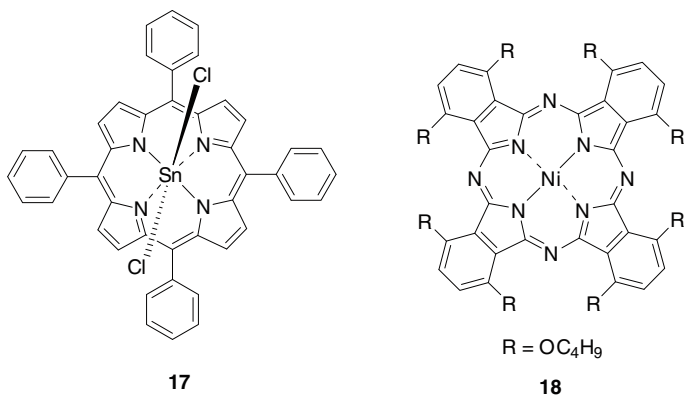
Similarly, phthalocyanine  $\mathbf{9}$  as well as the 3-pyridyl analog  $\mathbf{12}$  also axially complexes with cobalt(II) meso-tetraphenylporphyrin (CoTPP) ( $\mathbf{13}$ ) and meso-tetrakis(3,5-di-*tert*-butylphenyl)porphyrin (CoTBPP) ( $\mathbf{14}$ ) [29]. The 1:2 binding stoichiometry was confirmed by UV-Vis spectroscopic Job's plot analysis. The binding constants  $K_1$  between the 4-pyridyl phthalocyanine  $\mathbf{9}$  and the cobalt(II) porphyrins in chloroform ( $(1.1\text{--}1.2) \times 10^4 \text{ M}^{-1}$ ) are about threefold higher than those for the 3-pyridyl analog  $\mathbf{12}$ , mainly due to an electronic factor. As the hetero-triads  $\mathbf{9} \cdot [\text{CoTPP}]_2$  and  $\mathbf{9} \cdot [\text{CoTBPP}]_2$  have relatively strong binding interactions, they were isolated by silica-gel column chromatography and characterized by mass and UV-Vis spectroscopic methods.

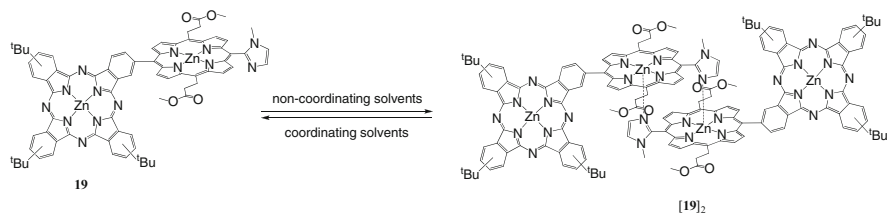


Recently, two pyrazine (pz)-linked hetero-triads of cobalt phthalocyanine (CoPc) and ZnTPP, namely (CoPc)-pz-(ZnTPP)-pz-(CoPc) ( $\mathbf{15}$ ) and (ZnTPP)-pz-(CoPc)-pz-(ZnTPP) ( $\mathbf{16}$ ), have been prepared [30]. The thermal properties of these triads and related macrocyclic components have been studied by thermal gravimetric analysis and differential scanning calorimetry. It has been found that the thermal stability of axial coordination increases in the order:  $\text{ZnPc}(\text{pz})_2 < \text{ZnTPP}(\text{pz})_2 \approx \text{CoPc}(\text{pz})_2$ , and the thermal decomposition of the triads  $\mathbf{15}$  and  $\mathbf{16}$  proceeds firstly via the degradation of the spacer ligand.



A related alternating phthalocyanine–porphyrin aggregate has also been prepared by mixing tin(IV) porphyrin dichloride **17** and nickel(II) phthalocyanine **18** in dichloromethane [31]. The UV–Vis spectrum shows a red-shifted Q band at 844 nm, which may be associated with charge-transfer interactions through metal–halide bonding rather than  $\pi$ – $\pi$  cofacial interactions. This suggests that the macrocycles are linked through a bridging chloro ligand. The formation of alternating structure is also supported by Ni K-edge X-ray absorption near edge structure study, which shows that the nickel center changes from a square planar environment to an octahedral structure upon addition of **17**. There is also a higher-energy shift (0.2 eV) of the pre-edge peak, indicating that the nickel center is partially oxidized by charge transfer in the array.

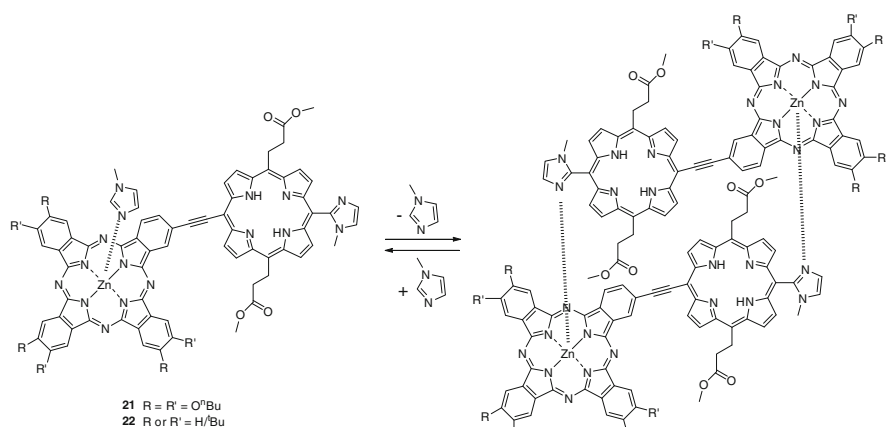




**Scheme 1** Monomer–dimer equilibrium of **19**

Kobuke et al. have previously reported a methodology for supramolecular self-organization of porphyrins [32–34]. For imidazolyl-substituted porphyrins, complementary coordination of the imidazolyl group of one porphyrin molecule with the zinc center of another porphyrin molecule forms a slipped cofacial dimer with an extremely large stability constant (ca.  $10^{11} \text{ M}^{-1}$ ). This methodology has been extended to prepare dimeric phthalocyanine–porphyrin hetero-dyad [**19**]<sub>2</sub> (Scheme 1) [35, 36]. The two macrocyclic components in the dyad **19** are essentially orthogonal to each other so that their intermolecular  $\pi$ – $\pi$  stacking can be avoided. The binding between the meso-imidazolyl substituent and the zinc center of the porphyrin ring affords a stable coordination dimeric hetero-dyad in non-coordinating solvents such as chloroform, dichloromethane, and toluene. The steady-state absorption spectrum of the dyad **19** in dichloromethane in the presence of 0.1 M 1-methylimidazole shows broadened phthalocyanine Q band and porphyrin Soret band, suggesting that the two components are electronically coupled in the ground state. In the absence of 1-methylimidazole, under which the dimer [**19**]<sub>2</sub> is formed, the broadened Soret band splits into two bands at 413 and 437 nm, which can be explained by the exciton splitting theory. For both **19** and [**19**]<sub>2</sub>, selective excitation at the porphyrin's absorption gives exclusively a strong fluorescence due to the phthalocyanine part, indicating that an efficient energy transfer process occurs from the excited porphyrin to the phthalocyanine moiety. The fluorescence quantum yield decreases with increasing the solvent dielectric constant. The values are much smaller than the corresponding values of zinc(II) tetra-*tert*-butylphthalocyanine [ $\text{ZnPc}(\text{tBu})_4$ ] (**20**) used as a reference. The results suggest that an electron transfer reaction has also taken place.

The photoinduced energy and electron transfer processes in these systems have also been studied by picosecond and femtosecond transient absorption spectroscopies [36]. For the dimeric hetero-dyad [**19**]<sub>2</sub>, the energy transfer occurs in a subpicosecond time scale, which is followed by photoinduced charge separation and charge recombination with time constants of 47 and 510 ps, respectively. By contrast, the charge-separated state has not been observed for the monomer **19**. The results suggest that the slipped cofacial arrangement of porphyrin rings facilitates the formation of the charge-separated state. It is believed that this is the result of a decrease in reorganization energy upon dimerization and the strong electronic interaction in the donor–acceptor pair.



**Scheme 2** Monomer–dimer equilibrium of **21** and **22**

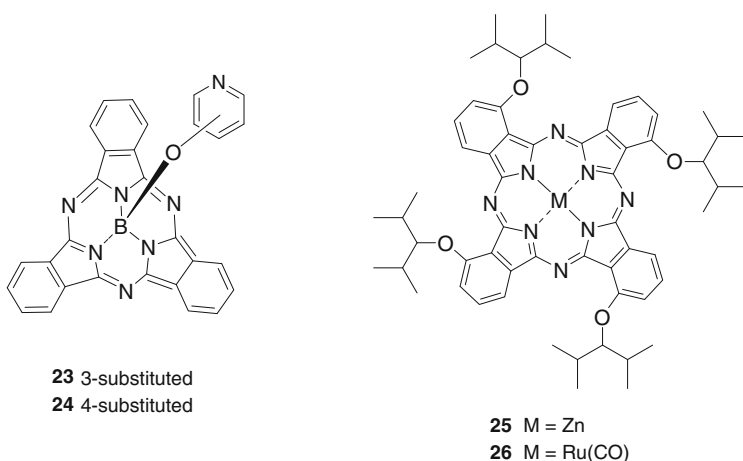
Two closely related hetero-dyads (**21** and **22**) have also been synthesized in which the porphyrin and phthalocyanine moieties are connected via an ethynyl unit [37]. With a coplanar configuration, these dyads have an extended  $\pi$  system. In the absence of coordinating ligands, they form cofacial stacks through an imidazolyl-to-zinc complementary coordination protocol (Scheme 2) as shown by size-exclusion chromatography, UV–Vis spectral titration, and NMR spectroscopy. The association constants, in the order of  $10^{14} \text{ M}^{-1}$  in toluene, are even higher than those of imidazolyl zinc(II) porphyrins [32–34]. It is believed that the coordination is assisted by the large  $\pi$ -electron framework and strong charge-transfer interactions. Upon addition of trifluoroacetic acid or 1-methylimidazole, the dimeric structure is disrupted giving monomeric hetero-dyad.

The interplanar distance within these stacks is assumed to be as close as 3.23 Å. The slipped-cofacial arrangement of porphyrin and phthalocyanine rings ensures a strong  $\pi$ -electron overlap as reflected by the large bathochromic shifts for both the phthalocyanine Q band and the porphyrin Soret band. In addition, the dimerization restricts the free rotation around the ethynyl bond, thereby enhancing the electronic communication between the coplanar porphyrin and phthalocyanine subunits. The dimeric stacks exhibit strong exciton coupling and charge-transfer properties between the two macrocyclic components, which can be modulated by the peripheral substituents of the phthalocyanine subunit and by the solvent.

A related imidazole-appended zinc(II) porphyrin linked via an ethynylphenyl unit to a magnesium(II) phthalocyanine has recently been reported [38]. The imidazole group binds to the magnesium center to form a stacked dimer in non-coordinating solvents such as chloroform even at submicromolar concentration ( $<10^{-6} \text{ M}$ ). Upon addition of dimethyl sulfoxide, the stacked dimer transforms to an extended dimer in which the imidazole group binds to the zinc center on the basis of the hard and soft acid and base principle. The extended dimer exhibits a much stronger fluorescence (by a factor of 28) compared with the stacked dimer, and this coordination-induced sliding motion has been found to be reversible.

## 2.2 Phthalocyanine–Subphthalocyanine Hetero-Arrays

Treatment of boron(III) subphthalocyanine chloride with 3- or 4-hydroxypyridine gives the corresponding pyridyl subphthalocyanine **23** or **24**. As these two compounds have a pyridyl group, they can axially complex with zinc(II) and ruthenium(II) phthalocyanines **25** and **26**, respectively, to form the corresponding phthalocyanine–subphthalocyanine hetero-dyads [39]. The complexation processes have been studied by  $^1\text{H}$  NMR and fluorescence spectroscopic methods, and the formation of all of these hetero-dyads has also been confirmed by electrospray ionization (ESI) mass spectrometry. Upon addition of the pyridyl subphthalocyanines, the Q bands of phthalocyanines **25** and **26** are virtually unchanged, suggesting that the ground-state interactions between the two chromophores in these dyads are not significant. The binding stoichiometry has been determined to be 1:1 in all cases. The association constants are generally higher for the ruthenium(II) phthalocyanine  $((2.5\text{--}4.7) \times 10^4 \text{ M}^{-1})$  than that for the zinc(II) counterpart  $((3.1\text{--}6.1) \times 10^3 \text{ M}^{-1})$ .

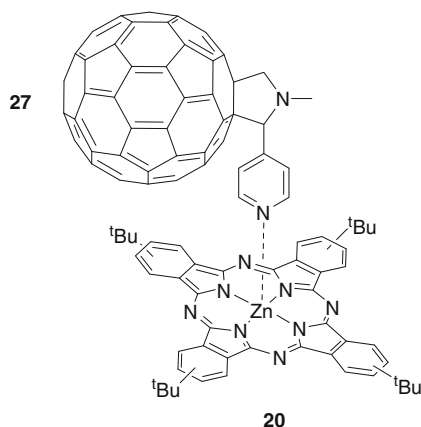


## 2.3 Phthalocyanine–Fullerene Hetero-Arrays

Guldi et al. have described the coordination of pyridine-linked fulleropyrrolidine **27** ( $\text{C}_{60}\text{Py}$ ) with  $\text{ZnPc}(\text{tBu})_4$  (**20**) [40]. The binding is through the N(pyridine) instead of N(pyrrolidine) to the zinc center with an association constant of  $4.8 \times 10^3 \text{ M}^{-1}$ . Upon photoexcitation, the radical pair  $\text{ZnPc}(\text{tBu})_4^+ \text{--} \text{C}_{60}\text{Py}^-$  is generated through an efficient intracomplex electron transfer pathway. The weak coordination between the  $\text{C}_{60}$  and phthalocyanine units facilitates the dissociation of the radical pair into the free radical ions  $\text{ZnPc}(\text{tBu})_4^+$  and  $\text{C}_{60}\text{Py}^-$ . The lifetime of the latter species is



governed by a nearly diffusion-controlled intermolecular back electron transfer of about  $10^9 \text{ M}^{-1} \text{ s}^{-1}$ .



Ito et al. have also investigated the self-assembly of zinc(II) tetra-*tert*-butyl-2,3-naphthalocyanine  $[\text{ZnNc}(\text{tBu})_4]$  (**28**) and fulleropyrrolidine **29** ( $\text{C}_{60}\text{Im}$ ), which has an imidazole coordinating ligand [41]. By using electronic absorption spectroscopy and *ab initio* B3LYP/3–21G(\*) computational method, it has been found that they form a supramolecular 1:1 dyad through axial coordination. The association constant of the dyad has been determined by the Scatchard method using the absorption spectral data. The value ( $6.2 \times 10^4 \text{ M}^{-1}$  in toluene) is an order of magnitude higher than that for the dyad  $[\text{ZnTPP}] \cdot [\text{C}_{60}\text{Im}]$  [42], suggesting that  $\text{ZnNc}(\text{tBu})_4$  has a better donor ability than ZnTPP. In the optimized structure, the HOMO is entirely located on the  $\text{ZnNc}(\text{tBu})_4$  entity, while the LUMO is entirely on the fullerene entity (Fig. 1). These results are in good agreement with those obtained from the cyclic voltammetric studies of the dyad and individual components in *o*-dichlorobenzene.

The photoinduced electron-transfer process of this dyad has been studied by both steady-state and transient absorption spectroscopy [41]. The fluorescence spectrum of  $\text{ZnNc}(\text{tBu})_4$  (**28**) in toluene shows an emission at 781 nm with a shoulder at 812 nm. Upon addition of  $\text{C}_{60}\text{Im}$  (**29**), the fluorescence of **28** is quenched significantly. The bimolecular quenching constant, calculated from the linear segment of the Stern-Volmer plot, is about four orders of magnitude higher than that expected for a diffusion-controlled process. The results suggest that a static instead of dynamic quenching process has taken place in which the self-assembled dyad  $[\text{ZnNc}(\text{tBu})_4] \cdot [\text{C}_{60}\text{Im}]$  is formed. Picosecond transient absorption spectroscopic studies reveal the formation of the radical pair  $\text{ZnNc}(\text{tBu})_4^{\cdot+} - \text{C}_{60}\text{Im}^{\cdot-}$ . The measured rates of charge-separation ( $k_{\text{cs}}$ ) and quantum yields ( $\Phi_{\text{cs}}$ ) ( $1.4 \times 10^{10} \text{ s}^{-1}$  and 0.97 in toluene and  $8.9 \times 10^9 \text{ s}^{-1}$  and 0.96 in *o*-dichlorobenzene, respectively) indicate that this is a very efficient process, as in the cases of covalent and self-assembled porphyrin counterparts [42].

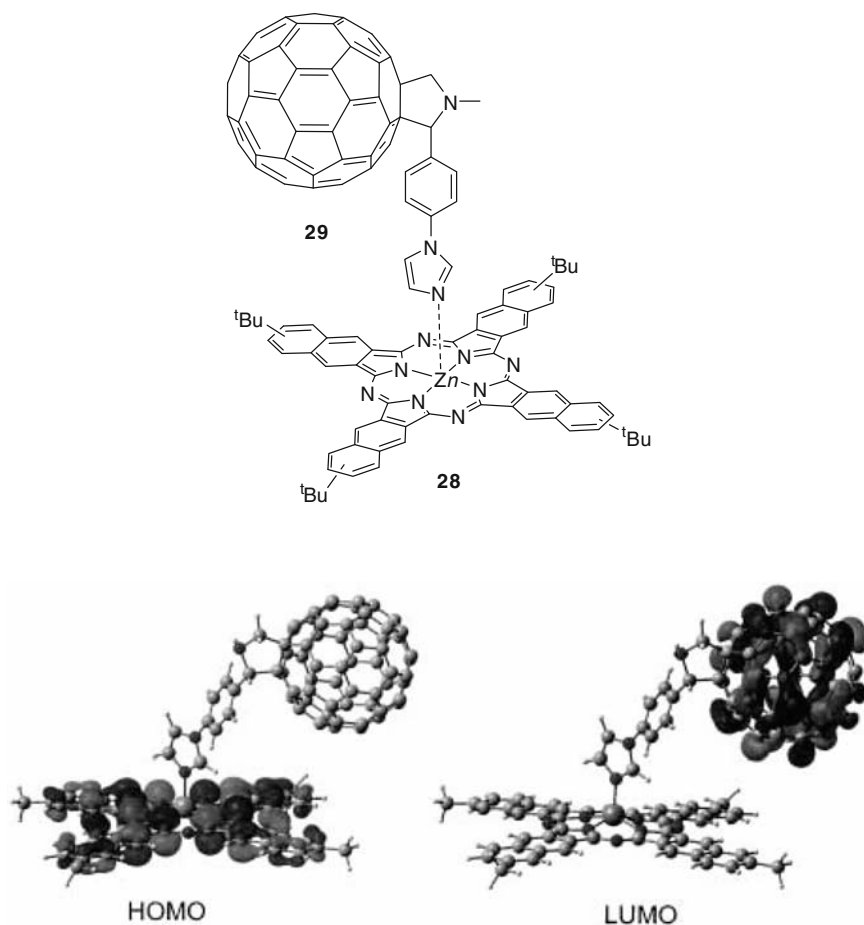


**Fig. 1** Ab initio B3LYP/3–21G(\*) calculated frontier HOMO and LUMO orbitals of the dyad  $[\text{ZnNc}(\text{tBu})_4] \cdot [\text{C}_{60}\text{Im}]$ . The *tert*-butyl groups of the naphthalocyanine are replaced by methyl groups and the *N*-methyl group of  $\text{C}_{60}\text{Im}$  is replaced by an H atom (reproduced with permission from [41]). Copyright Wiley-VCH verlag GmbH & Co. KGaA

Similarly, the pyridyl fullerenes **30** and **31** also axially bind to  $\text{ZnNc}(\text{tBu})_4$  (**28**) to form supramolecular triads in which the zinc(II) naphthalocyanine acts as an electron donor, the pyridyl fullerenes act as primary electron acceptors, and either the ferrocene (Fc) or *N,N*-dimethylaminophenyl (DMA) moiety serves as a second electron donor [43]. Fig. 2 shows the optimized structures of the resulting triads calculated by density functional theory (DFT), showing that the three components are arranged in a linear fashion. The binding constants of these systems ( $7.4 \times 10^4 \text{ M}^{-1}$  for  $[\text{ZnNc}(\text{tBu})_4] \cdot \mathbf{30}$  and  $10.2 \times 10^4 \text{ M}^{-1}$  for  $[\text{ZnNc}(\text{tBu})_4] \cdot \mathbf{31}$  in *o*-dichlorobenzene) determined by UV–Vis spectroscopy are comparable with

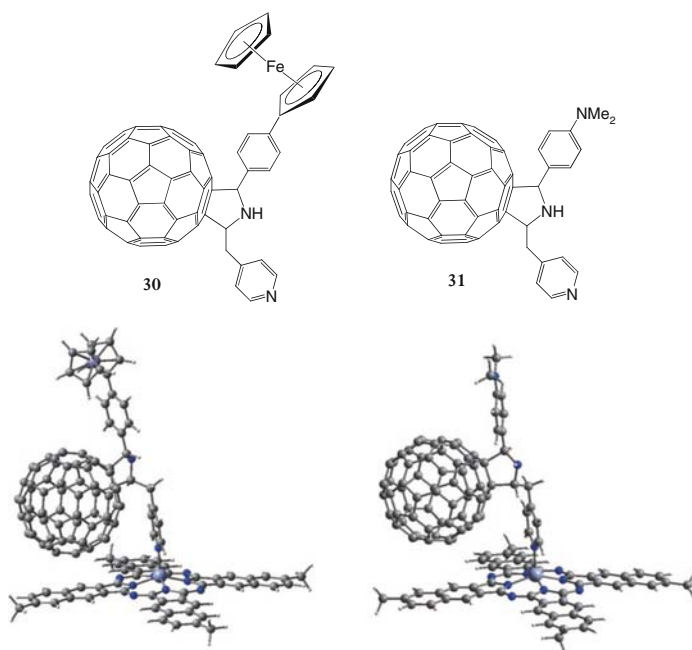
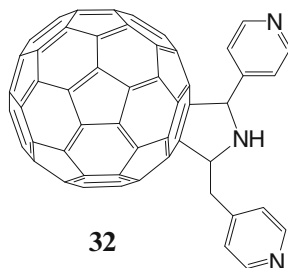


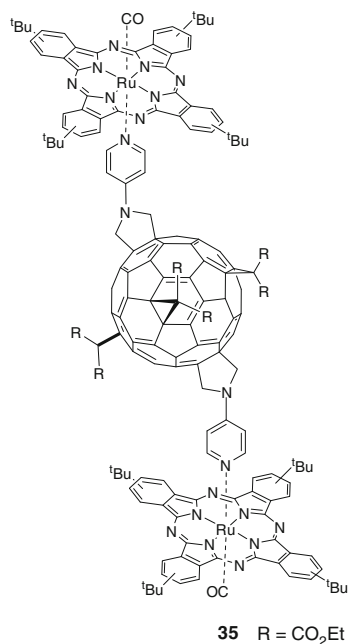
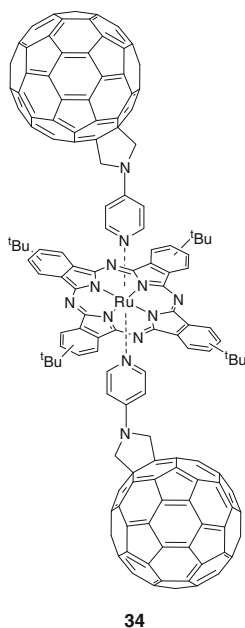
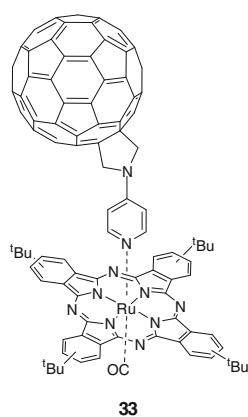
**Fig. 2** Optimized structures of  $[\text{ZnNc}(\text{tBu})_4] \cdot \mathbf{30}$  (left) and  $[\text{ZnNc}(\text{tBu})_4] \cdot \mathbf{31}$  (right) calculated by DFT at the B3LYP/3-21G(\*) level (reproduced with permission from [43]). Copyright society of porphyrins & phthalocyanines

that of  $[\text{ZnNc}(\text{tBu})_4] \cdot [\text{C}_{60}\text{Im}] (6.2 \times 10^4 \text{ M}^{-1}$  in toluene) [41]. On the basis that imidazole is much more basic than pyrrolidine, the comparable binding constants suggest that the incorporation of a second electron donor on the pyrrolidine ring increases the basicity of the pyridyl group, which in turn facilitates the axial coordination. As revealed by electrochemical studies, the donor ability follows the order  $\text{ZnNc}(\text{tBu})_4 < \text{Fc} < \text{DMA}$ . Photoexcitation of  $\text{ZnNc}(\text{tBu})_4$  (**28**) in these triads leads to an efficient electron transfer to the fullerenes [ $k_{\text{CS}} = (2.0\text{--}2.4) \times 10^9 \text{ s}^{-1}$ ,  $\Phi_{\text{CS}} = 0.80\text{--}0.83$  in *o*-dichlorobenzene]. The presence of the second electron donor can prolong the lifetime of the resulting radical ion pairs (to 10–15 ns).

By using a fulleropyrrolidine bearing two pyridine moieties (compound **32**), the same research group has also constructed the supramolecular naphthalocyanine– $\text{C}_{60}$  triad  $[\text{ZnNc}(\text{tBu})_4]_2 \cdot \mathbf{32}$  in toluene [44]. The high-measured charge-separation rate ( $k_{\text{CS}} = 5.7 \times 10^9 \text{ s}^{-1}$ ) and quantum yield ( $\Phi_{\text{CS}} = 0.93$ ) suggest that the photo-induced electron transfer (from the singlet excited  $\text{ZnNc}(\text{tBu})_4$  to the fulleropyrrolidine) is an efficient process within the supramolecular triad. The resulting radical ion pair has a lifetime of 30 ns. Similarly, changing the solvent from the non-coordinating toluene to the coordinating tetrahydrofuran or benzonitrile destroys the supramolecular structure.

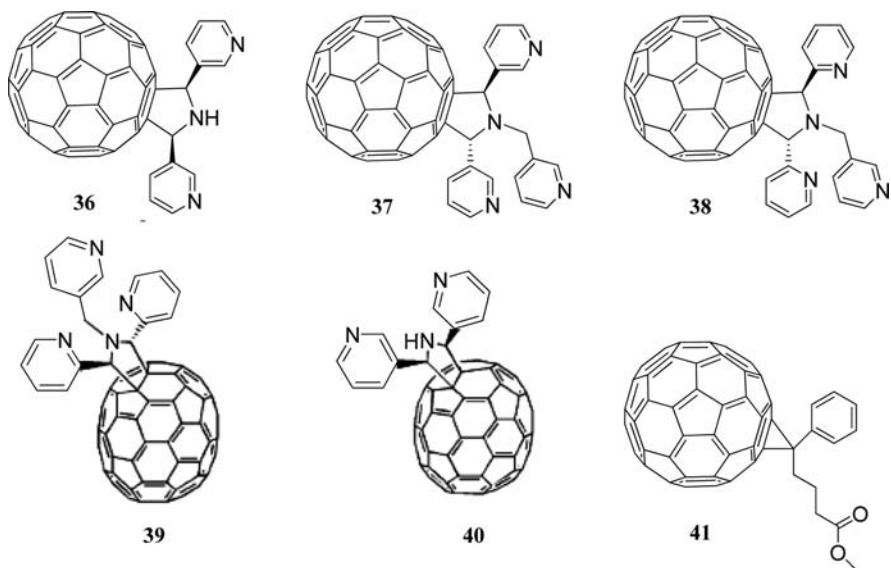


Apart from zinc(II) (na)phthalocyanines, the ruthenium(II) analogs have also been used to complex with pyridyl fullerenes. Arrays **33–35** show electronic coupling between the two electroactive components in the ground state as shown by UV–Vis spectroscopy and electrochemical measurements [45]. The use of ruthenium(II) instead of zinc(II) phthalocyanines reduces the undesired charge recombination, increasing the lifetime of the radical ion pair state (on the order of hundreds of nanoseconds).



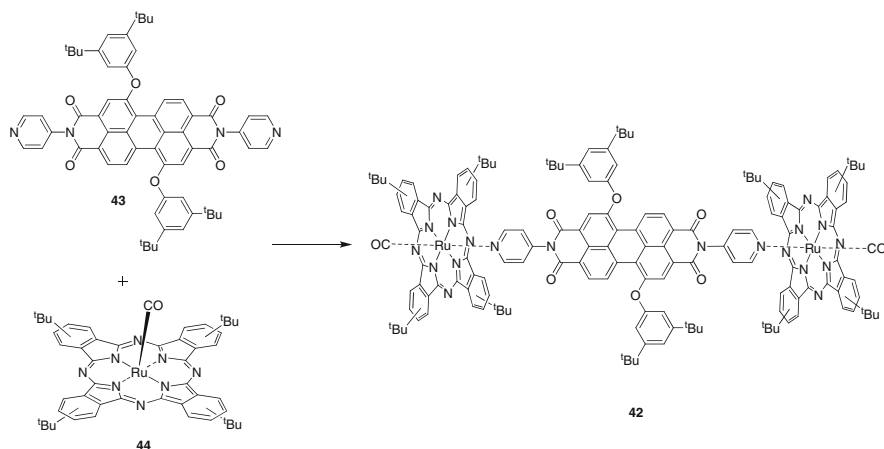
In addition to the complexation in solutions, pyridine-appended fulleropyrrolidines can also form coordination complexes with zinc(II) phthalocyanines in solid-state thin films. Troshin et al. have investigated the photovoltaic behavior of bilayer solar cells fabricated by deposition of solution-processed fulleropyrrolidines **36–40**, which contain chelating pyridyl groups, on vacuum-evaporated films of unsubstituted zinc(II) phthalocyanine (ZnPc) [46]. The UV–Vis spectra of these films resemble the spectrum of ZnPc recorded in pyridine, showing a sharp

phthalocyanine Q band at 690–694 nm. They are, however, remarkably different from that measured in solid film, which displays two maxima at about 630 nm and 712 nm. The results suggest that coordination complexes are formed at the interface between these donor and acceptor components. The bilayer fulleropyrrolidine–ZnPc solar cells exhibit high power conversion efficiencies of up to 1.5%, which are almost three times higher than those of the reference cells (0.4%–0.6%) based on the nonchelating fullerene derivative [6,6]-phenyl-C<sub>61</sub> butyric acid methyl ester (**41**) as the acceptor component. The efficiencies of these reference cells can also be significantly improved by mixing **41** with a small amount (4% w/w) of these pyridine-containing fulleropyrrolidines in the acceptor layer. The improved performance of these photovoltaic devices can be attributed to the association of fulleropyrrolidines and ZnPc, which can significantly lower the activation energy barrier, thereby facilitating the photoinduced charge separation.



## 2.4 Phthalocyanine–Perylenediimide Hetero-Arrays

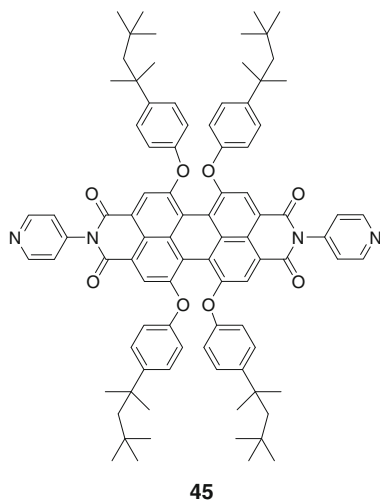
Perylenediimides represent another class of photoactive dyes which are characterized by their strong fluorescence emission and facile electrochemical reduction. Recently, a supramolecular bis(phthalocyanine)–perylene diimide hetero-triad (compound **42**) has been assembled through axial coordination [47]. Treatment of perylenediimide **43**, which has two 4-pyridyl substituents at the imido positions, with 2.5 equiv. of ruthenium(II) phthalocyanine **44** in chloroform affords **42** in 68% yield (Scheme 3). This array shows remarkable stability in solution due to the robustness of the ruthenium–pyridyl bond. Its electronic absorption spectrum is essentially the sum of the spectra of its molecular components **43** and **44** in

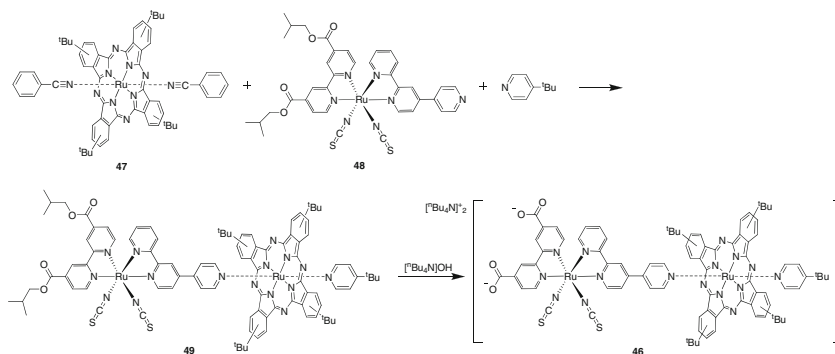


**Scheme 3** Synthesis of bis(phthalocyanine)-perylene diimide triad **42**

1:2 ratio, suggesting that the subunits are not electronically coupled in the ground state. The photophysical properties of this array have also been studied by ultrafast and fast time-resolved techniques. Photoexcitation of either chromophore leads to a rapid intraensemble charge separation generating a long-lived radical ion pair [ $44^{\cdot+}$ - $43^{\cdot-}$ - $44$ ], which has a lifetime of  $115 \pm 5$  ns.

Similarly, the dipyriddy perylene diimide **45** also axially binds to zinc(II) 1,8,15,22-tetrakis(2,4-dimethyl-3-pentoxy)phthalocyanine (**25**) to form the corresponding 1:1 and 1:2 supramolecular complexes [48]. The coordination of these two compounds has been monitored by UV-Vis, fluorescence, and  $^1\text{H}$  NMR spectroscopic methods. It has been found that the ligation of pyridyl ligand to zinc phthalocyanine is relatively weak and labile with a binding constant of  $2,080 \text{ M}^{-1}$  in  $\text{CDCl}_3$ . The two components can mutually quench the fluorescence of their partner through an electron transfer process.





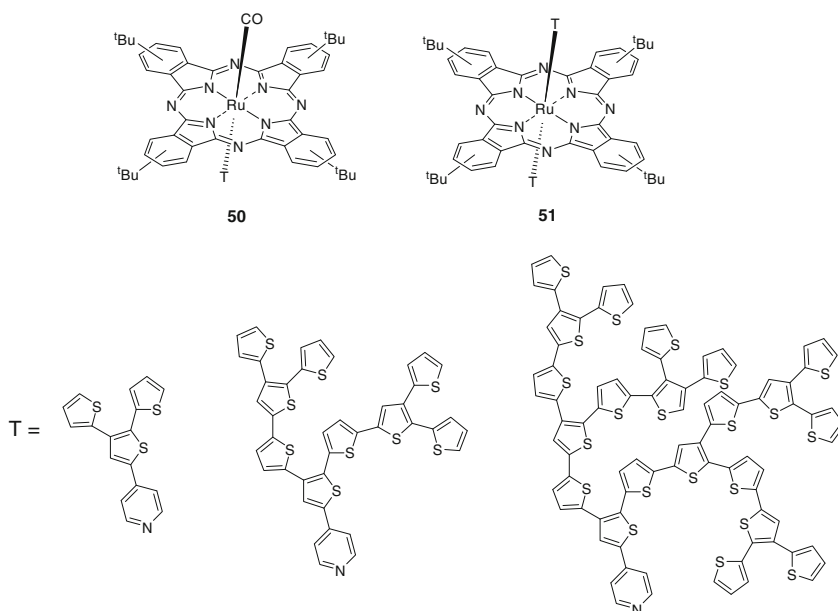
**Scheme 4** Synthesis of phthalocyanine–poly(pyridyl) ruthenium(II) dyad **46**

## 2.5 Phthalocyanine–Polypyridyl Ruthenium(II) Hetero-Arrays

McDonagh et al. have recently prepared two isomeric ruthenium(II) phthalocyanine–bipyridyl hetero-dyads and examined their efficiency as sensitizers for dye-sensitized solar cells (DSCs) [49]. The complementary absorptions of these chromophores cover most of the solar spectrum which facilitate the photocurrent generation. Scheme 4 shows the preparation of one of these hetero-dyads **46**. Treatment of ruthenium(II) phthalocyanine **47** with poly(pyridyl) **48** and 4-*tert*-butylpyridine gives the unsymmetrically substituted complex **49**. Upon treatment with tetra-*n*-butylammonium hydroxide, it undergoes de-esterification giving **46**. With two carboxyl functional groups, these hetero-dyads can anchor to TiO<sub>2</sub> electrode surfaces forming DSCs. The efficiencies of these solar cells are lower than that of the cell fabricated with the commercial DSC dye N719. However, on a per molecule basis, these dyads are more efficient photocurrent generators.

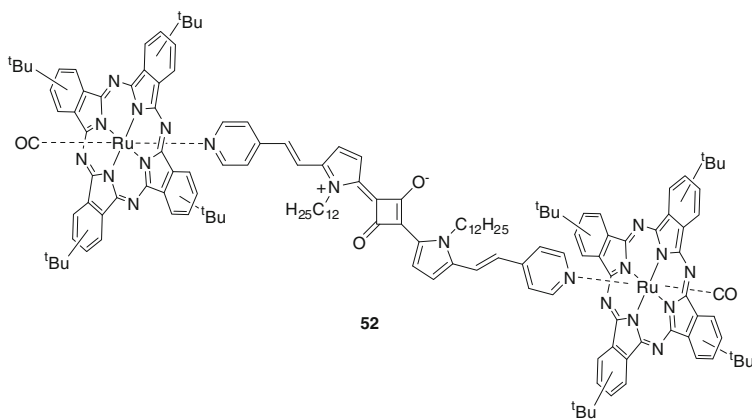
## 2.6 Phthalocyanine–Oligothiophene Hetero-Arrays

A series of ruthenium(II) phthalocyanines with one or two pyridyl dendritic oligothiophene axial substituent(s) have also been reported (compounds **50** and **51**) [50]. The dendritic ligands absorb in the region from 380 to 550 nm, which complements the absorptions of the phthalocyanine core. This combination results in better light harvesting property and enhancement in efficiency of the corresponding solar cells. The solution-processed photovoltaic devices made with these compounds and fullerene acceptor give efficiencies of up to 1.6%. These represent the most efficient phthalocyanine-based bulk heterojunction solar cells reported so far.



## 2.7 A Phthalocyanine-Squaraine Hetero-Array

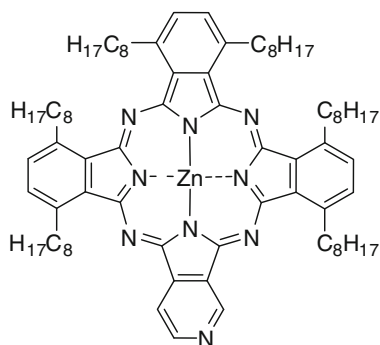
Both phthalocyanines and squaraines are good candidates for bulk heterojunction solar cells. Recently, a supramolecular hetero-array of these functional dyes Pc–Sq–Pc (compound **52**) has been reported for the first time, which exhibits a large coverage of the solar spectrum from 250 to 850 nm [51]. This axially held assembly serves as a robust panchromatic sensitizer. Upon excitation, it forms the radical ion pair  $\text{Pc}^{\cdot+}\text{-Sq}^{\cdot-}\text{-Pc}$  with a long lifetime of  $24 \pm 2 \mu\text{s}$ . The use of this assembly as a donor material in solution processable bulk heterojunction solar cells has also been briefly studied.





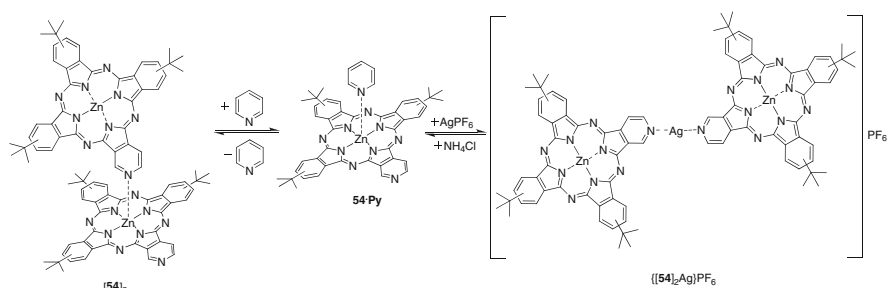
## 2.8 Self-Coordinated Phthalocyanine Dimers

Cook et al. reported the self-aggregation behavior of zinc(II) hexaocetylpyridino-[3,4]tribenzoporphyrazine (**53**), in which one of the benzenoid rings of the phthalocyanine core is replaced by a pyridinoid ring [52]. In non-coordinating solvents such as cyclohexane, toluene, and dichloromethane, this compound forms an edge-to-face complex through intermolecular axial ligation of the pyridyl nitrogen atom of one molecule with the zinc center of another molecule. The self-assembly process was studied by UV-Vis, fluorescence, and  $^1\text{H}$  NMR spectroscopic methods. By contrast, the metal-free and nickel analogs form conventional face-to-face aggregates in solution and exhibit columnar liquid crystal behavior in condensed phase.



**53**

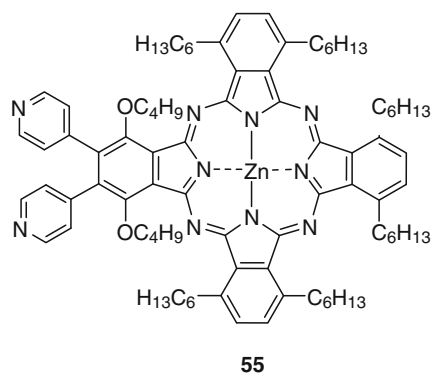
Similarly, the analog **54** also forms a self-assembled dimer [**54**]<sub>2</sub> in non-polar solvents. In the presence of pyridine, the dimer dissociates into the monomeric species **54** · Py [53, 54]. Further addition of AgPF<sub>6</sub> leads to the formation of a novel Ag-linked phthalocyanine dimer {[**54**]<sub>2</sub>Ag}PF<sub>6</sub> (Scheme 5) [55]. On the basis of its electronic absorption and magnetic circular dichroism properties, it has been suggested that this dimer adopts a planar and *trans*-conformation. Addition of NH<sub>4</sub>Cl, which can remove the silver ions as AgCl, regenerates the monomeric **54** · Py.



**Scheme 5** Self-assembly processes of **54**

The photophysical properties of the self-assembled dimer **[54]<sub>2</sub>** have been studied in detail with various spectroscopic and computational methods [53,54]. In the lowest excited singlet ( $S_1$ ) state, the excitation delocalizes over the two macrocycles, and the non-radiative decay is enhanced by dimerization. By contrast, the exciton interaction is very weak in the lowest excited triplet ( $T_1$ ) state. In the excited-state absorption spectrum recorded in 1-decane, two sharp bands at 658 and 694 nm are observed, which can be attributed to the Q bands of the  $T_1$  self-assembled phthalocyanine dimer.

Zinc(II) phthalocyanine **55** bearing two pyridyl substituents is also capable of forming a self-assembled array [56]. This compound forms intermolecular zinc–nitrogen coordinated species in solution and self-assembles to form a coordination polymer in the solid state. As shown in the crystal structure revealed by single-crystal X-ray diffraction analysis, the compound self-assembles in an edge-to-face manner forming a zig-zag polymer in the solid state (Fig. 3).



In addition to the zinc–imidazolyl coordinated dimeric phthalocyanine–porphyrin hetero-dyads described in Sect. 2.1, Kobuke et al. have also reported three related phthalocyanine dimers as shown in Scheme 6 [57]. The self-association behavior of phthalocyanines **56–58** has been studied by UV–Vis,  $^1\text{H}$  NMR, and MALDI-TOF mass spectroscopic methods. Generally, these phthalocyanines exist in a dimeric form in toluene even at a very low concentration of about  $1.0 \times 10^{-9}$  M. A large excess of *N*-methylimidazole (ca.  $1.3 \times 10^4$  equiv.) can induce the conversion of dimer to monomer with axial coordination of the ligand. The formation of stable self-assembled dimers has also been observed in other non-coordinating solvents such as chloroform and dichloromethane. The extremely large association constants ( $1.1 \times 10^{12} \text{ M}^{-1}$  (for **56**),  $1.7 \times 10^{11} \text{ M}^{-1}$  (for **57**), and  $1.4 \times 10^{11} \text{ M}^{-1}$  (for **58**) in toluene) are believed to originate from the complementary nature of the coordination.  $^1\text{H}$  NMR spectra of these compounds in  $\text{CDCl}_3$  reveal the formation of *J*-type phthalocyanine dimers. All these dimers emit a strong fluorescence in toluene. The quantum yields are comparable with those of the corresponding dissociated monomers.

Two related zinc(II) and magnesium(II) azaphthalocyanines substituted with eight diethylamino groups (compounds **59** and **60**) have recently been reported

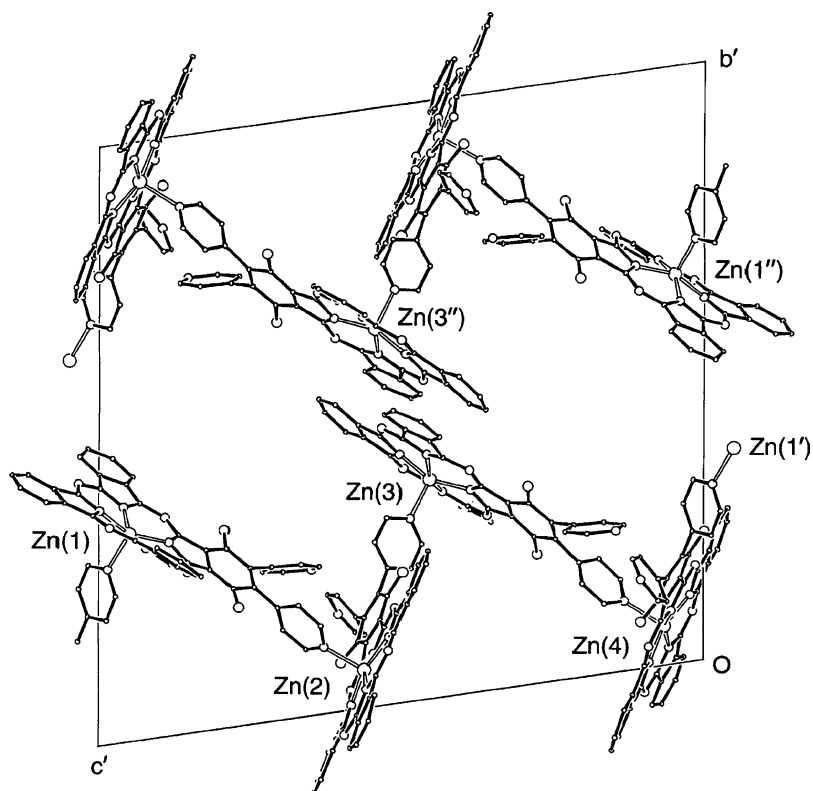
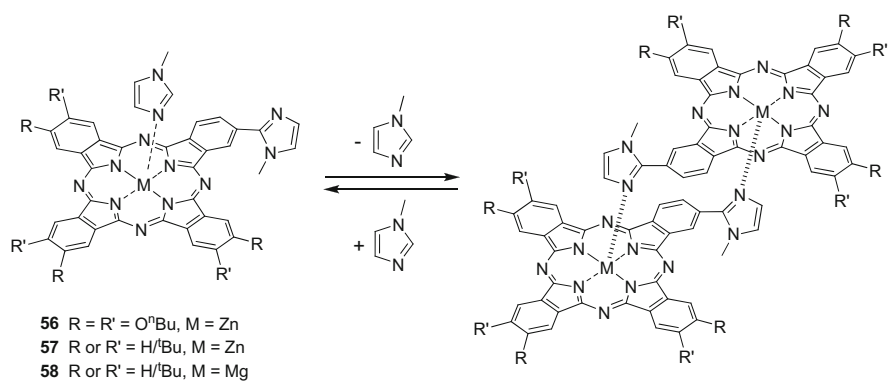
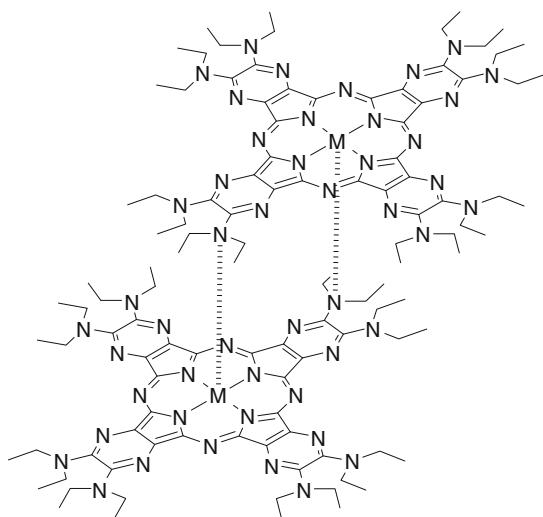


**Fig. 3** Crystal structure of **55** (reproduced from [56] with permission from the Royal Society of Chemistry)



**Scheme 6** Monomer–dimer equilibrium of **56–58**

[58]. They also form self-assembled *J*-dimers in non-coordinating solvents probably through coordination of one of the diethylamino nitrogen atoms with the central metal of adjacent molecule. Upon addition of pyridine, they are converted back to the monomeric species. The fluorescence is significantly quenched and the efficiency of singlet oxygen formation is also reduced as a result of intramolecular photoinduced electron transfer, which is inhibited in the dimers.



[59]<sub>2</sub> M = Zn  
[60]<sub>2</sub> M = Mg

The self-assembly behavior of several zinc(II) tetra-aryloxy or alkoxy phthalocyanines in non-coordinating solvents has also been investigated [59–62]. The absorption spectra of these compounds in chloroform show red-shifted and split Q bands even at very low concentrations, suggesting the formation of *J*-aggregates induced by Zn–O coordination (Fig. 4). The self-association constant of zinc(II) 1,8,15,22-tetraphenoxyphthalocyanine in chloroform has been determined to be about  $1.1 \times 10^7 \text{ M}^{-1}$ . It is three orders of magnitude higher than that of  $\text{ZnPc}(\text{}^t\text{Bu})_4$  (**20**), which undergoes  $\pi$ – $\pi$  stacking dimerization. The MALDI-TOF mass spectra of these dyes in chloroform give signals due to the presence of monomer and aggregates. The transmission electron microscopy images of these samples display an infinite two-dimensional network structure. The aggregates dissociate into the monomer when a coordinating solvent is added to the solution.

Zeng et al. have examined the coordination of  $\text{ZnPc}$  with three bipyridines, namely 1,2-bis(4-pyridyl)ethane (**61**), *trans*-1,2-bis(4-pyridyl)ethene (**62**), and 1,3-bis(4-pyridyl)propane (**63**) [63]. The former two bipyridines are linear molecules favoring the formation of H-shaped supramolecular complexes  $\text{ZnPc} \cdot \mathbf{61} \cdot \text{ZnPc}$  and  $\text{ZnPc} \cdot \mathbf{62} \cdot \text{ZnPc}$ , while the last bipyridine adopts a V-shaped conformation leading to the formation of a T-shaped 1:1 complex ( $\text{ZnPc} \cdot \mathbf{63}$ ). The molecular structures of all these complexes have been determined by X-ray diffraction analyses. The

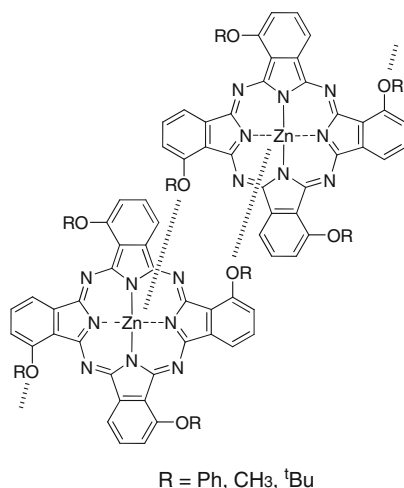


**Fig. 4** Proposed mode of self-aggregation of zinc(II) tetra-aryloxy or alkoxy phthalocyanines

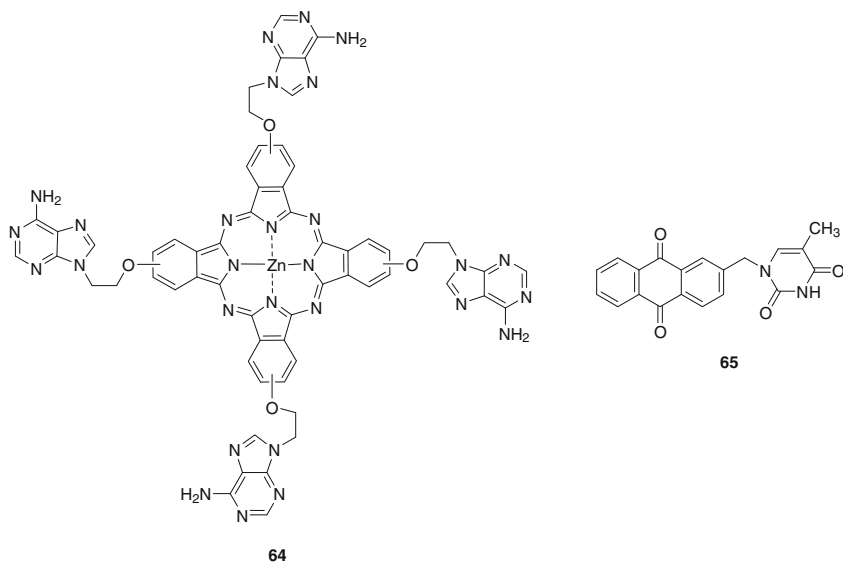
study shows that the conformation of the bipyridines plays an important role in the assembly processes.

### 3 Supramolecular Arrays Held by Hydrogen Bonding

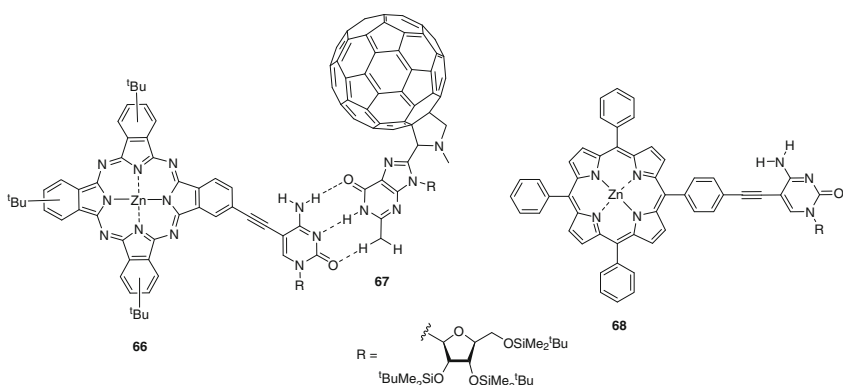
In addition to axial coordination, hydrogen bonding is another important approach to construct various supramolecular systems. This strategy, however, has not been widely used to assemble phthalocyanines and other functional units. To our knowledge, examples are so far confined to several phthalocyanine–fullerene arrays and self-assembled phthalocyanine aggregates, which are described in this section.

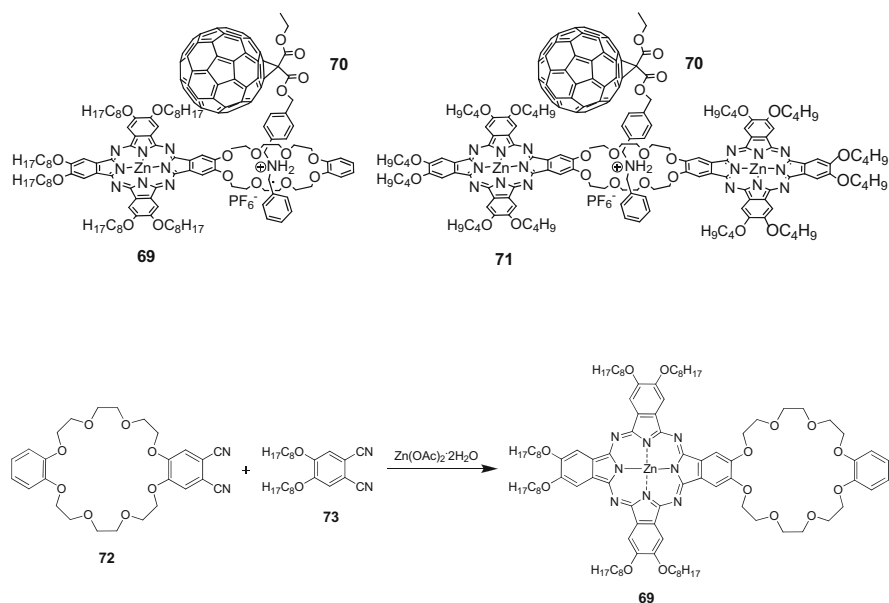
#### 3.1 Hydrogen-Bonded Phthalocyanine–Fullerene Hetero-Arrays

Nucleobases and nucleosides are common motifs for hydrogen-bonded supramolecular arrays. Ng et al. first reported a series of phthalocyanine–nucleobase conjugates [64]. The tetra-adenine phthalocyanine **64** was prepared by standard *O*-alkylation of zinc(II) tetrahydroxyphthalocyanine with 9-(2-bromoethyl)adenine in the presence of K<sub>2</sub>CO<sub>3</sub>. The fluorescence of **64** is quenched substantially upon addition of thymine-substituted 9,10-anthraquinone **65**, and the rate is much faster compared with that for the situation when the unsubstituted 9,10-anthraquinone is used as the quencher. These results suggest that **64** forms a supramolecular complex with **65** through the Watson–Crick base-pairing interactions.



Torres et al. employed this supramolecular approach to assemble the phthalocyanine- $C_{60}$  array **66** · **67**, which is linked by the cytosine-guanosine hydrogen bonding interactions [65, 66]. UV-Vis spectroscopic studies indicate that the cytosine-appended phthalocyanine (ZnPc-C) **66** self-assembles to form aggregates in organic media. Addition of guanosine-linked  $C_{60}$  (G- $C_{60}$ ) **67** leads to deaggregation of **66** and the formation of ZnPc-C:G- $C_{60}$  **66** · **67**, which is accompanied by a substantial fluorescence quenching of the phthalocyanine core. The lifetime of the charge-separated state (3.0 ns in toluene) is much shorter than that of the porphyrin analog ZnTPP-C:G- $C_{60}$  **68** · **67** (2.0  $\mu$ s in dichloromethane) [67]. It may be due to the pronounced electronic interactions between the zinc(II) phthalocyanine and  $C_{60}$  subunits, which in fact is supported by the broadened electronic absorption signals in the spectrum of **66** · **67**. The formation constant of **66** · **67** ( $2.6 \times 10^6 \text{ M}^{-1}$ ) is much higher than that of the porphyrin analog **68** · **67** ( $5.1 \times 10^4 \text{ M}^{-1}$ ). It is likely that in addition to the base-pairing interactions, **66** and **67** are held by  $\pi$ - $\pi$  interactions and/or charge-transfer interactions.

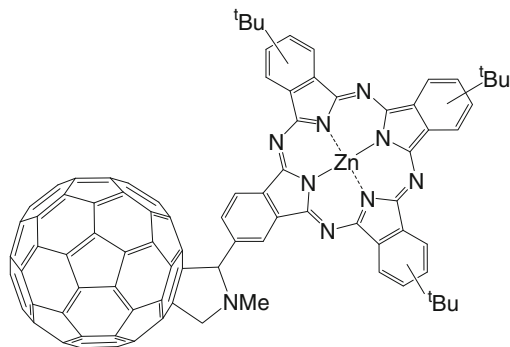




**Scheme 7** Preparation of phthalocyanine **69**

Two phthalocyanine–C<sub>60</sub> donor–acceptor supramolecular systems (dyads **69 · 70** and **71 · 70**) have also been constructed through the interactions between a dibenzo-24-crown-8 ring and a secondary dibenzylammonium cation [40, 68]. The unsymmetrically substituted phthalocyanine **69** can be prepared in 30% yield by statistical condensation of dicyano-dibenzo-24-crown-8 **72** with 4,5-dioctoxyphthalonitrile (**73**) in the presence of Zn(OAc)<sub>2</sub> · 2H<sub>2</sub>O (Scheme 7). Using tetracyano-dibenzo-24-crown-8 instead of the dicyano derivative **72** and 4,5-dibutoxyphthalonitrile leads to the formation of bis(phthalocyanine) **71** in 10% yield. By using <sup>1</sup>H NMR and MALDI-TOF mass spectroscopy, it has been shown that the C<sub>60</sub>-containing dibenzylammonium cation **70** threads through the crown ether void of these two phthalocyanines forming stable pseudorotaxane-like complexes in chloroform. The association constants ( $1.4 \times 10^4 \text{ M}^{-1}$  (for **69 · 70**) and  $1.9 \times 10^4 \text{ M}^{-1}$  (for **71 · 70**)) are comparable with those of related pseudorotaxane systems. Addition of base results in deprotonation of the dibenzylammonium cation and destruction of the ensembles. Hence, two reversible states can be switched by controlling the pH.

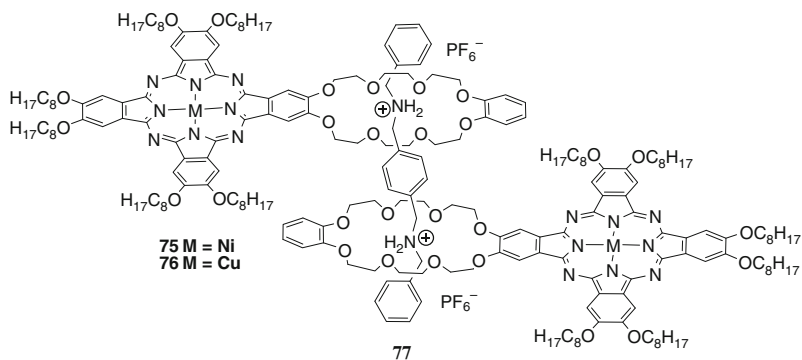
As shown by electrochemical and UV–Vis studies, the electronic interactions between the phthalocyanine and the C<sub>60</sub> subunits in these ensembles are negligible in the ground state. Their photophysical behavior has also been investigated by time-resolved fluorescence and transient absorption measurements. Upon photoexcitation of the phthalocyanine subunit, a rapid intracomplex electron transfer occurs from phthalocyanine to C<sub>60</sub>, leading to the formation of the radical ion pairs **69**<sup>•+</sup> · **70**<sup>•-</sup> and **71**<sup>•+</sup> · **70**<sup>•-</sup> with an efficiency of about 0.9. The lifetimes (1.5 μs for **69 · 70** and 1.3 μs for **71 · 70**) are substantially longer than those of the covalently-linked analog **74** (ca. 3 ns) [69].



74

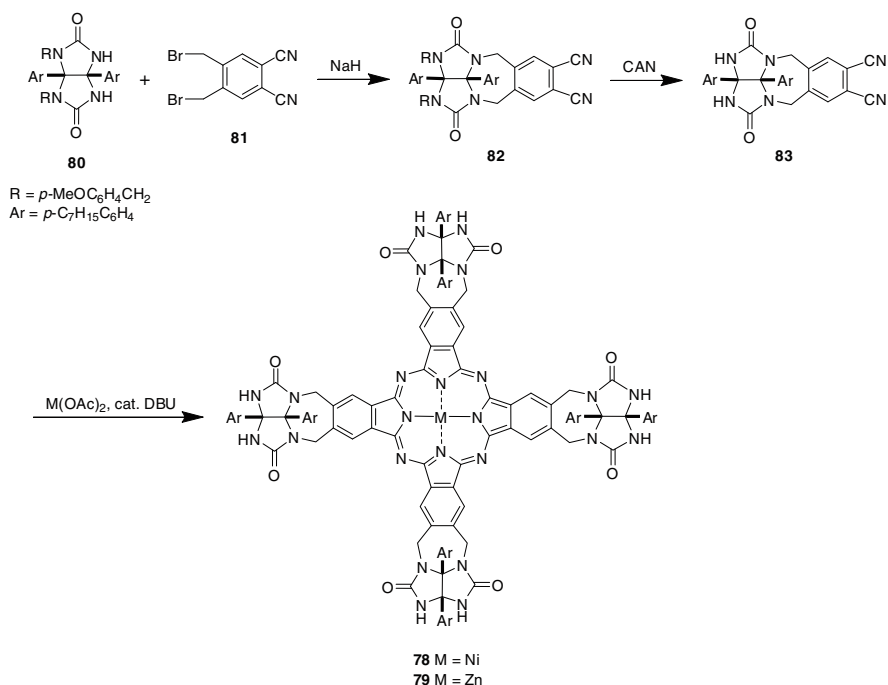
### 3.2 Hydrogen-Bonded Phthalocyanine Aggregates

By using the same approach, Torres et al. have also assembled the hydrogen-bonded phthalocyanine dimers  $[75]_2 \cdot 77$  and  $[76]_2 \cdot 77$  in solution [70]. The formation of these arrays has been inferred by  $^1\text{H}$  NMR spectroscopy. Upon addition of a large excess of **77** in acetonitrile, the UV–Vis spectrum of **75** in chloroform remains essentially unchanged. This observation indicates that in the supramolecular dimer, the phthalocyanine rings are not electronically coupled with each other. EPR study of the dimer  $[76]_2 \cdot 77$  also reveals that the Cu centers in adjacent phthalocyanine rings do not have significant interactions. In fact, the distance between the two  $\text{NH}_2^+$  centers of **77** (7.2 Å calculated from CPK molecular models) is far too large to expect any intracomplex  $\pi$ – $\pi$  stacking between the phthalocyanine rings in the supramolecular dimer.



77





**Scheme 8** Preparation of phthalocyanines **78** and **79**

Rebek et al. have synthesized phthalocyanines **78** and **79** appended with four glycoluril modules according to Scheme 8 [71]. Reaction of *p*-methoxybenzyl-protected glycoluril **80** with NaH and 4,5-di(bromomethyl)phthalonitrile (**81**) gives the substituted product **82**. Upon treatment with ceric ammonium nitrate (CAN), it undergoes deprotection to afford **83**. Cyclization of this compound in the presence of Ni(OAc)<sub>2</sub> or Zn(OAc)<sub>2</sub> and a catalytic amount of 1,8-diazabicyclo[5.4.0]undec-7-ene (DBU) gives **78** or **79** (as the  $\alpha\alpha\alpha$  isomer), which can be separated from the other three stereoisomers ( $\alpha\alpha\alpha\beta$ ,  $\alpha\alpha\beta\beta$ , and  $\alpha\beta\alpha\beta$ ). Interestingly, both **78** and **79** self-assemble by means of hydrogen bonding to form discrete dimeric capsules in aromatic solvents with a calculated internal volume of about 275 Å<sup>3</sup> (Fig. 5). In the assembled state, both compounds expose 16 solubilizing alkyl groups to the solvent while shielding two of their four aromatic surfaces. As a result, these two compounds are more soluble than the other stereoisomers in *p*-xylene, which facilitates their purification.

Phthalocyanines **84** and **85** substituted with six optically active alkyl chains and one chiral diol have been synthesized by mixed cyclization of the two corresponding phthalonitriles [72]. The self-organizing properties of these compounds in chloroform solution and thin film have been studied by a range of spectroscopic and physical methods. Both compounds show split Q-band absorptions at 678 and 694 nm in chloroform, and the emission (at 696 nm) is red-shifted compared with that of a non-diol-containing analog. Upon addition of 0.5% methanol, the absorption at 694 nm

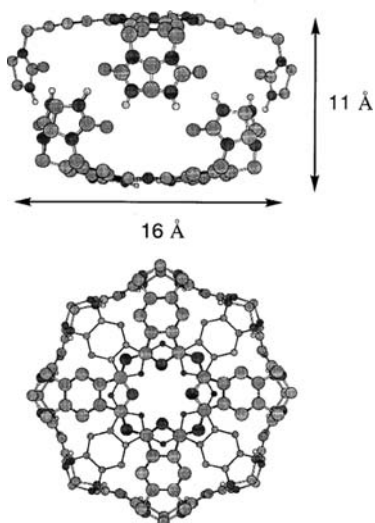
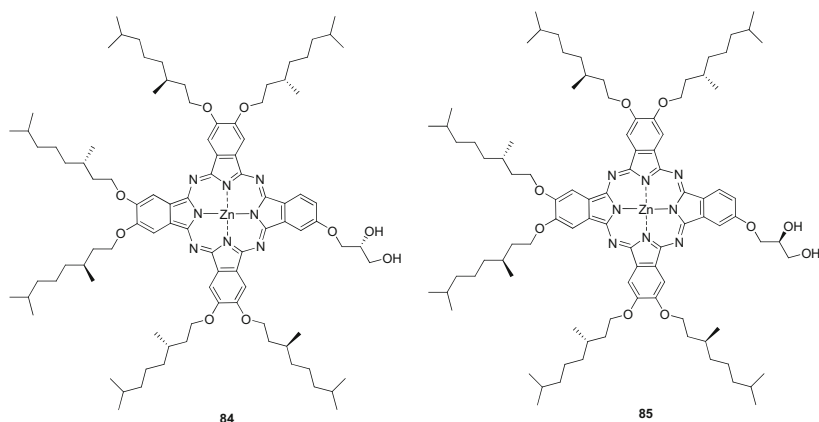


**Fig. 5** Side view and top view of the energy-minimized dimeric assembly of the metal-free analog of **78** and **79**. The CH hydrogens and  $C_7H_{15}$  chains are omitted for clarity (reproduced from [71] with permission from Elsevier)

disappears. These observations suggest the formation of edge-to-edge dimers held by hydrogen bonding as shown in Fig. 6, which is also supported by the presence of broad IR band at  $3,484\text{ cm}^{-1}$  assignable to the hydrogen-bonded OH stretching vibration. Vapor pressure osmometric measurements of **84** at a concentration range from 0.1 to 5.0 mM in chloroform have also revealed a molecular weight of 3,250, which is about two-fold of the molecular weight of **84**.



As shown by differential scanning calorimetry, temperature-controlled FT-IR spectroscopy, UV-Vis spectroscopy, powder X-ray diffraction, and circular

dichroism measurements, phthalocyanines **84** and **85** in thin films organized into two different structures depending on the temperature. At room temperature, the hydrogen bonds among the diol groups link up the phthalocyanine molecules forming a lamellar sheet. However, at above 130°C, the hydrogen-bonded network is cleaved causing the structure to change to a hexagonal columnar phase, in which the phthalocyanine molecules are arranged in a left-handed helix.

Kojima et al. have recently constructed an interesting discrete supramolecular conglomerate composed of two molecules of saddle-distorted zinc(II) 1,4,8,11,15,18,22,25-octaphenylphthalocyanine (**86**) and one molecule of diprotonated dodecaphenylporphyrin (**87**) held by two molecules of 4-pyridinecarboxylate (**88**) through axial coordination (with the pyridine nitrogen to the zinc center of **86**) and hydrogen bonding (with the carboxylate group forming two-point intermolecular hydrogen bonding with the two pyrrole protons of **87**) [73, 74]. Both interactions are strengthened by the saddle distortion of the porphyrin and phthalocyanine components. This supramolecular array has been prepared by treating  $\mathbf{87} \cdot \mathbf{88}$  with **86** in toluene and the structure has been established by X-ray diffraction analysis (Fig. 7).  $^1\text{H}$  Diffusion ordered spectroscopy ( $^1\text{H}$  DOSY) has also confirmed that this supramolecular structure is preserved even in solution.

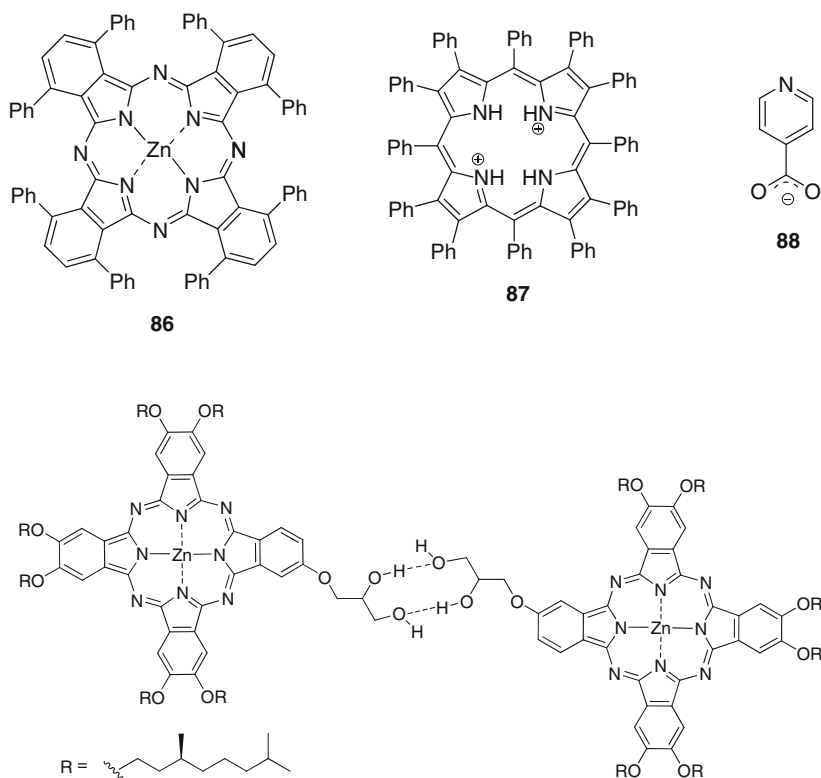


Fig. 6 Proposed mode of dimerization of **84** and **85** in chloroform

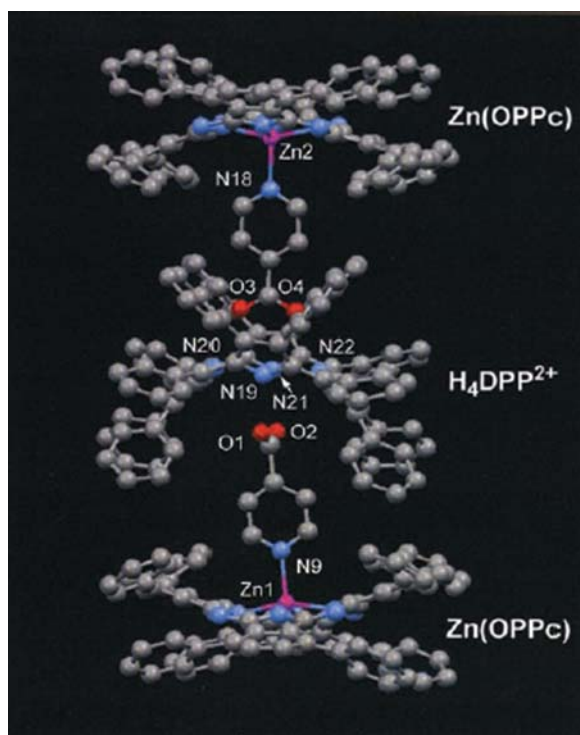
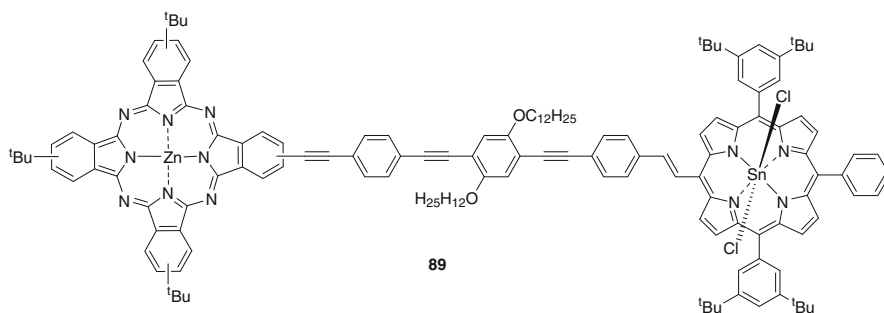


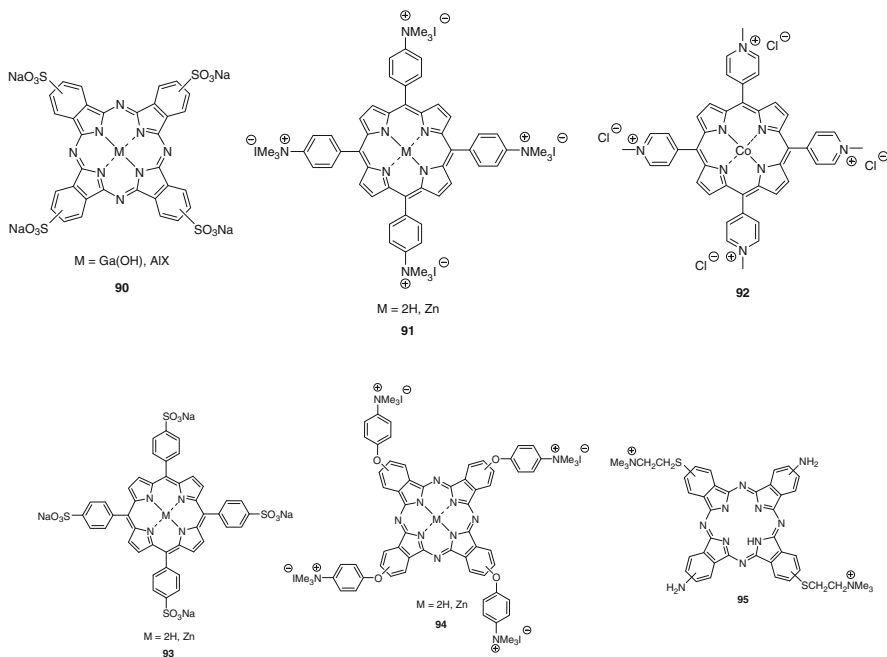
Fig. 7 Molecular structure of the supramolecular array **86** · **88** · **87** · **88** · **86** (reproduced with permission from [73]). Copyright Wiley-VCH verlag GmbH & Co. KGaA

Photoexcitation of the assembly at 410 nm generates a charge-separated state involving the one-electron-reduced diprotonated porphyrin **87**<sup>-</sup> and the one-electron-oxidized phthalocyanine **86**<sup>+</sup> through intraensemble electron transfer. This represents the first detection of charge-separated state of supramolecular phthalocyanine–porphyrin conglomerates. The lifetime of the charge-separated state of this assembly (667 ps) is much longer than that observed for the covalently linked phthalocyanine–porphyrin dyad **89** (85 ps) [75].



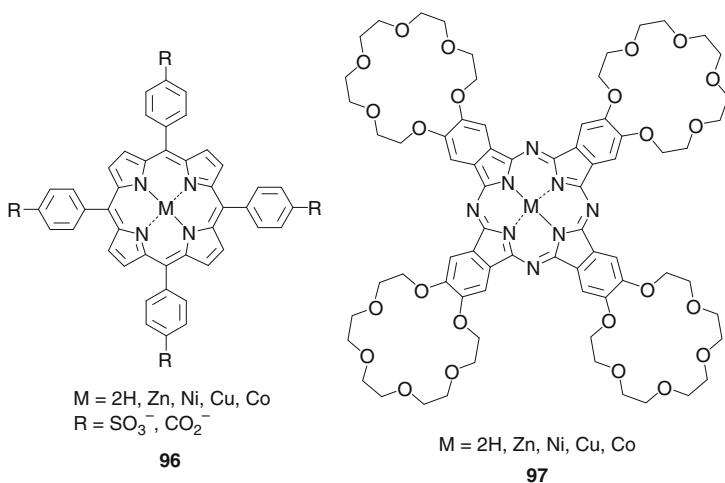
## 4 Supramolecular Arrays Held by Electrostatic Interactions

Another way of building phthalocyanine-containing supramolecular arrays is through ion pair interactions between oppositely charged components. In these cases, the electrostatic attractions between the charged substituents and the hydrophobic interactions of the aromatic macrocycles work in a synergistic manner holding the individual components together. The planar geometry of the macrocycles results in the formation of face-to-face aggregates in which the components have a close contact and extensive orbital overlap. Face-to-face phthalocyanine–porphyrin aggregates are the most common examples which have been reviewed previously [22, 76]. Some examples include the complexes of tetrasulfonated phthalocyanine **90** ( $M = \text{Ga}(\text{OH}), \text{AlX}$ ) with tetra(ammonium) porphyrins **91** [77], tetrasulfonated phthalocyanine **90** ( $M = \text{AlX}$ ) with tetra(pyridinium) porphyrin **92** [78], and tetrasulfonated porphyrins **93** with tetra- and di(ammonium) phthalocyanines **94** and **95** [79,80]. They form 1:1 or 1:2 complexes in water or polar solvents depending on the affinity of the metal center of these macrocycles for axially bound coordinating solvent molecules. The binding between the components is usually very strong with binding constants in the order of  $10^6$ – $10^8 \text{ M}^{-1}$ . In most of these cases, the chromophoric components have ground-state interactions and exhibit mutual quenching of the fluorescence through electron transfer.



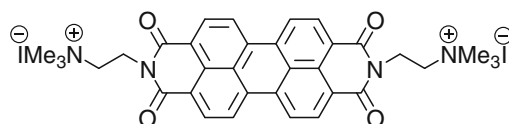
The self-assembly of these oppositely charged macrocycles can be extended to form multilayer and Langmuir-Blodgett (LB) films [81–83]. As shown by absorption spectroscopy, the chromophores are aggregated within the layer. Upon excitation of the porphyrin subunit, long-lived radical ions are formed in the layers as a result of the high polarity experienced by the complexes in this medium.

Rodgers et al. have also reported the complexation of a series of tetra-sulfonated and carboxylated porphyrins (compounds **96**) with phthalocyanines fused with four 18-crown-6 moieties (compounds **97**) in the presence of a potassium salt in dimethyl sulfoxide or ethanol [84, 85]. The potassium ions, being trapped inside the crown ether voids, bind to the anionic groups of porphyrins by electrostatic interactions to form 1:1 or 1:2 face-to-face hetero-arrays. The UV–Vis spectra are changed remarkably, showing that the macrocyclic components have strong electronic interactions in the ground state. As shown by spectroelectrochemical studies, the complexes possess a significant charge transfer character in the ground state in which the phthalocyanine serves as an electron donor. Upon excitation at 400 nm, a charge-transfer state is populated, which deactivates to form the metal-centered (d,d) state within 2 ps. Then it repopulates the ground state with a lifetime of 7–200 ps depending on the metal center of the macrocycles. A related hetero-dyad of a mono-carboxylated porphyrin and a mono-18-crown-6-substituted phthalocyanine has also been assembled in solution and fabricated into highly ordered LB films [86].



The ionic self-assembly of copper(II) tetrasulfonated phthalocyanine **90** ( $M = Cu$ ) and the dicationic perylenediimide **98** in water has also been investigated [87]. By using UV–Vis and fluorescence spectroscopy, it has been found that the two components bind in a 1:1 manner and exhibit electronic coupling or charge-transfer interactions in the ground state. Upon mixing the two components at high concentrations, high molecular-weight polymers are formed. The viscosity of the

polymer solution increases dramatically as the concentration increases, which is a typical property of supramolecular polymers. These polymers have a large association constant ( $2.4 \times 10^7 \text{ M}^{-1}$ ) as a result of the combination of electrostatic and charge-transfer interactions as well as discotic stacking between the dyes. By using a range of direct and indirect imaging techniques, it has been found that the polymers exhibit an extended rod-like helical structure with a width of 2.4 nm and a high mechanical stability.



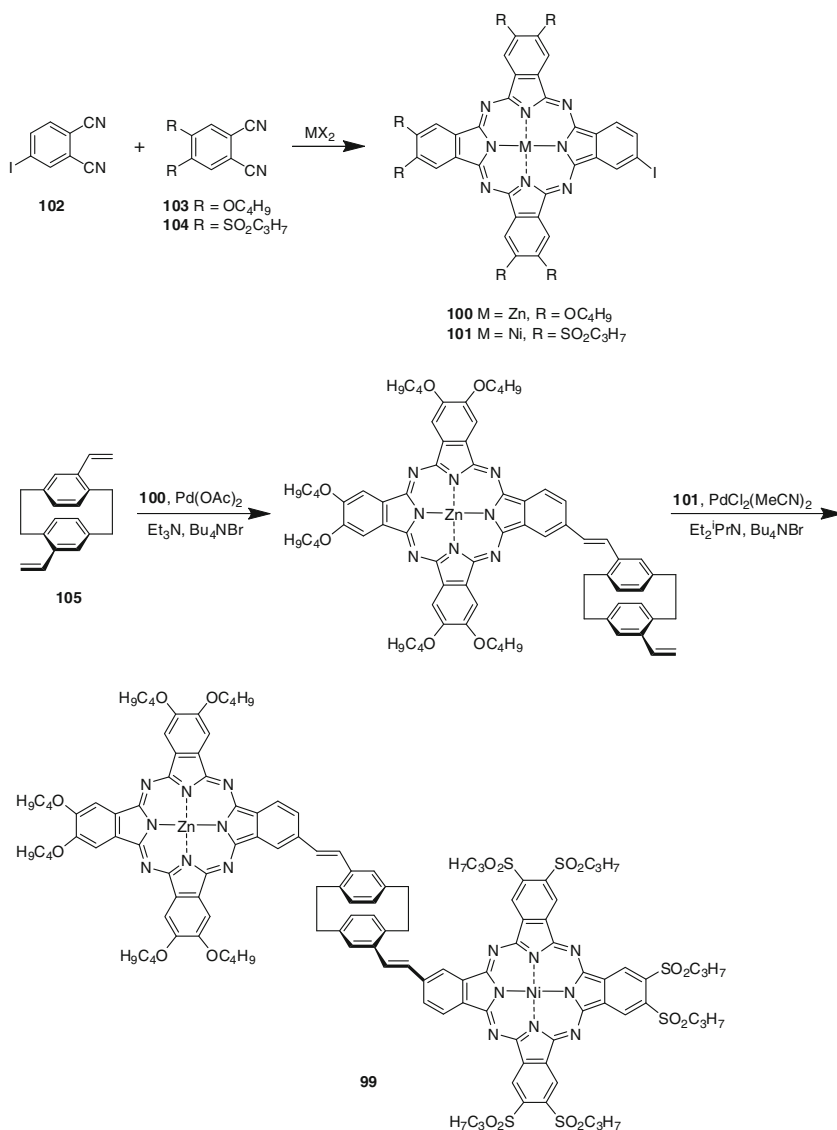
98

## 5 Supramolecular Arrays Held by Donor–Acceptor Interactions

Donor–acceptor interactions have also been employed to construct phthalocyanine-containing supramolecular arrays. Torres et al. described the self-assembly of a novel donor–acceptor bis(phthalocyanine) (compound **99**), in which an electron-rich hexabutoxyphthalocyanine ring is linked to an electron-deficient hexa(propylsulfonyl)phthalocyanine ring via a divinyl[2.2]paracyclophane unit [88]. This compound was prepared by a convergent approach as shown in Scheme 9. The iodophthalocyanines **100** and **101** were first prepared by mixed cyclization of 4-iodophthalonitrile (**102**) with **103** and **104**, respectively. These compounds then underwent two successive Heck reactions with divinyl[2.2]paracyclophane **105** to give **99**. For comparison, two monophthalocyanines **106** and **107** were also prepared by coupling the monovinyl analog of **105** with **100** and **101**, respectively.

The monophthalocyanines **106** and **107** show a weak aggregation tendency in chloroform. The latter has a self-dimerization constant of  $1,175 \text{ M}^{-1}$ . By contrast, the donor–acceptor bis(phthalocyanine) **99** exhibits a much stronger aggregation tendency with a dimerization constant of  $1.1 \times 10^6 \text{ M}^{-1}$  in chloroform. It is believed that in addition to the hydrophobic effect, the two phthalocyanine halves of compound **99** may be considered as donor and acceptor subunits that interact with each other. As revealed by electron microscopy, **99** forms one-dimensional nanoaggregates through intermolecular interactions between its complementary donor and acceptor phthalocyanine units as shown in Fig. 8. The dimerization constant of **99** is about one order of magnitude lower than that observed for the hetero-dimerization of **106** and **107**, which may be due to the cyclophane step that hinders the formation of columnar aggregates of double phthalocyanine dimer.

The same research group also reported the hetero-association of phthalocyanines **108** with **109** as well as **108** with **110**, both of which are stabilized by donor–acceptor interactions [89]. Compounds **108** and **109** were prepared by standard



**Scheme 9** Preparation of donor–acceptor bis(phthalocyanine) **99**

cyclization of the corresponding phthalonitriles in the presence of an appropriate metal salt. The synthesis of ZnPc–C<sub>60</sub> dyad **110** involved a Heck reaction of **100** with 4-vinylbenzaldehyde, followed by a Prato reaction with C<sub>60</sub> and sarcosine. These donor–acceptor counterparts form 1:1 supramolecular complexes in chloroform with a stability constant of about 10<sup>5</sup> M<sup>-1</sup>. Photoexcitation of the zinc(II) phthalocyanine **109** in toluene gives a strong fluorescence emission at 704 nm, which is quenched upon addition of the palladium(II) phthalocyanine **108** in an



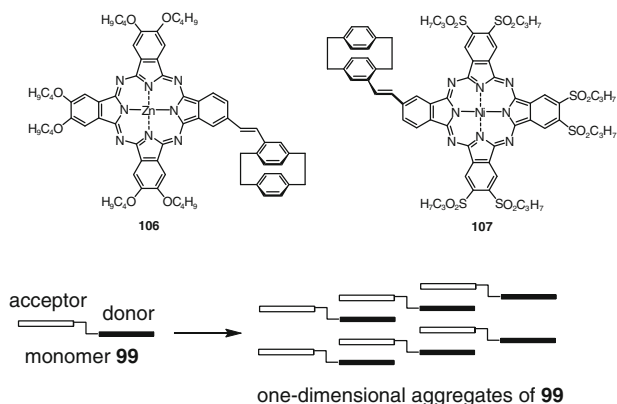
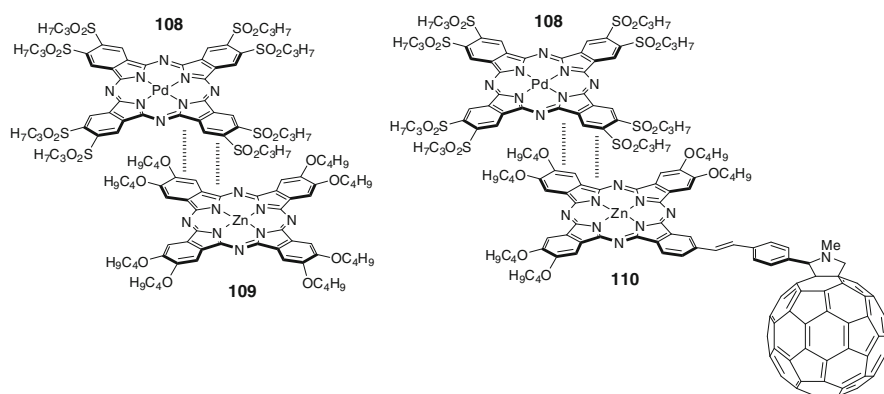


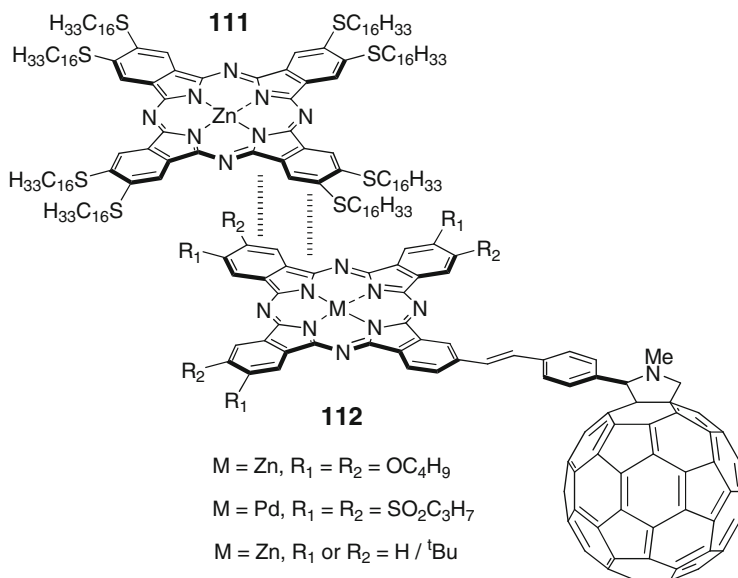
**Fig. 8** Schematic diagram showing the formation of one-dimensional aggregates of **99**

exponential manner. This is mainly due to photoinduced electron transfer within the donor–acceptor complex. Two lifetimes were revealed by time-resolved fluorescence measurements. The one due to the ensemble **108**–**109** (0.19 ns) is much shorter than that for **109** (2.5 ns).

The ZnPc–C<sub>60</sub> dyad **110** has a low fluorescence quantum yield ( $\Phi_f = 0.01$ ) in toluene due to the intramolecular electron-transfer deactivation. Addition of **108** leads to a further reduction in the fluorescence intensity ( $\Phi_f = 0.002$ ) and a slight blue shift of the emission maximum, suggesting the formation of the ensemble **108**–**110**, in which the two components have strong excitonic coupling. The addition of **108** (i.e. the hetero-association) also stabilizes the radical ion pair ZnPc<sup>+</sup>–C<sub>60</sub><sup>–</sup>, increasing the lifetime from 130 ns (for **110**) to 475 ns (for **108**–**110**) (measured in tetrahydrofuran).

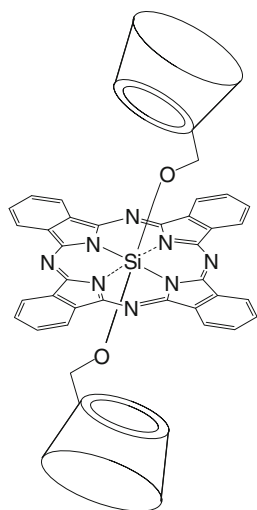
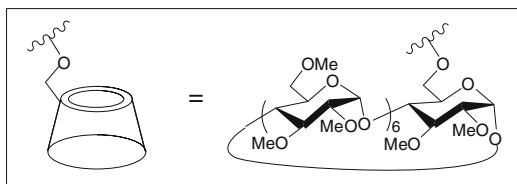


As an extension of these works, Torres et al. also studied the self-organization of the liquid crystalline zinc(II) phthalocyanine **111** and the non-mesogenic metallophthalocyanine- $C_{60}$  dyads **112** [90]. As shown by polarizing optical microscopy, differential scanning calorimetry, and X-ray diffraction, the former induces mesomorphism in the latter upon blending. This represents a new strategy to organize phthalocyanine- $C_{60}$  dyads into a mesogenic form. For all the blends of **111** and **112**, they exhibit a hexagonal columnar mesophase regardless the peripheral substituents of **112**.



## 6 Supramolecular Arrays Held by Host–Guest Interactions

Assembling through host–guest interactions is a powerful way to construct supramolecular arrays. However, this method, to our knowledge, has been rarely employed to assemble phthalocyanine-containing supramolecular systems. Ng et al. have recently prepared a silicon(IV) phthalocyanine with two axial permethylated  $\beta$ -cyclodextrin units (compound **113**), which binds strongly with tetrasulfonated porphyrin **93** ( $M = 2H$ ) in a 1:1 manner in water with a stability constant of  $2.1 \times 10^8 M^{-1}$  [91]. The complexation has been studied in detail with various spectroscopic methods including UV–Vis, fluorescence, 2D NMR, and ESI mass spectroscopy.

**113**

When the porphyrin component in the host–guest complex is excited at 510 nm, a strong fluorescence at 683 nm, assignable to the phthalocyanine core, is observed along with a weak residual porphyrin emission at 639 nm. This observation clearly indicates the presence of an efficient singlet–singlet energy transfer process. By comparing the normalized absorption and excitation spectra at the porphyrin’s Soret band region, the energy transfer quantum yield has been estimated to be 47%.

In addition to the light-harvesting property, this host–guest complex also exhibits a high photocytotoxicity. Its IC<sub>50</sub> value, defined as the dye concentration required to kill 50% of the cells, for HT29 human colon adenocarcinoma cells is only 0.09 μM, which is comparable with that of **113** itself formulated with Cremophor EL (0.15 μM). The complexation with **93** ( $M = 2H$ ) enhances the water solubility of **113** and therefore can prevent the use of Cremophor EL, which may cause serious hypersensitivity reactions.

The unsubstituted metal-free and zinc(II) phthalocyanines (H<sub>2</sub>Pc and ZnPc) also form host–guest complexes with C<sub>60</sub> and C<sub>70</sub> in toluene [92]. Well-defined charge-transfer bands have been observed in the UV–Vis spectra, suggesting that the components have ground-state charge-transfer (2%–4%) electronic interactions. The binding constants for the 1:1 phthalocyanine–fullerene complexes have been determined by fluorescence quenching experiments and found to be in the order of 10<sup>4</sup> M<sup>-1</sup>. The values are not significantly different for C<sub>60</sub> and C<sub>70</sub>, showing that these phthalocyanines are not good discriminators for these fullerenes. According to the theoretical and <sup>13</sup>C NMR spectroscopic studies, the orientation of C<sub>70</sub> toward phthalocyanine is favored in end-on orientation (Fig. 9). The result suggests that the interactions between these phthalocyanines and fullerenes are mainly electrostatic rather than π–π interactions in nature.

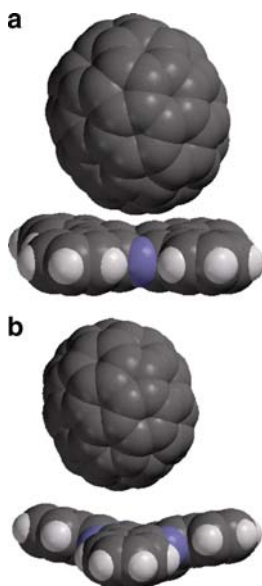


**Fig. 9** Calculated space filling models of the C<sub>70</sub> complexes of (a) H<sub>2</sub>Pc and (b) ZnPc in end-on orientation of C<sub>70</sub> (reproduced from [92] with permission from the American chemical society)

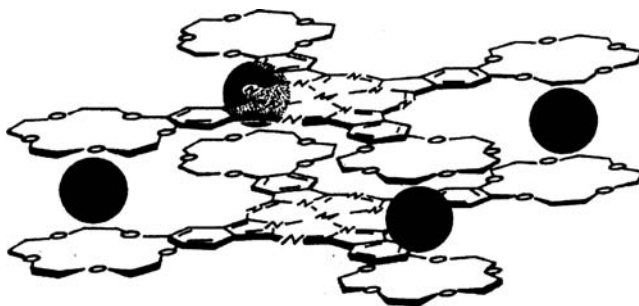
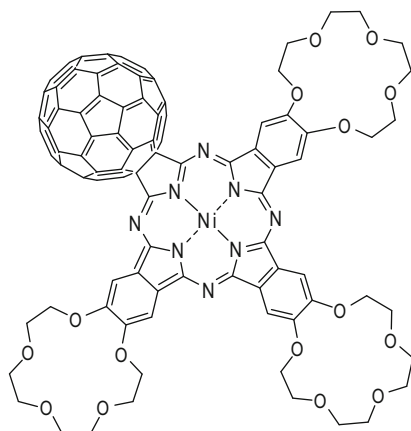


**Fig. 10** Proposed structure for the cation-induced dimer of crown ether substituted metallophthalocyanines. Solid circles indicate cations such as K<sup>+</sup> and Ca<sup>2+</sup> (reproduced from Kobayashi N, Lever ABP (1987) J Am Chem Soc 109:7433 with permission from the American Chemical Society)

Cation-induced supramolecular formation of crown ether substituted phthalocyanines can also be regarded as due to host-guest interactions. Fig. 10 shows the proposed structure for the K<sup>+</sup>- and Ca<sup>2+</sup>-induced dimer of metallophthalocyanines fused with four 15-crown-5 units, which serves as a typical example. The formation of these cofacial dimers has been found to go through a two-step three-stage process. The earlier works have been briefly reviewed [93, 94]. Recently, Jiang et al. have prepared a series of copper(II) phthalocyanines fused with one to four 15-crown-5 unit(s) [CuPc(15-C-5)<sub>n</sub>] (*n* = 1–4) by heating a solution of the double-decker complexes Eu(Pc)[Pc(15-C-5)<sub>n</sub>] (*n* = 1–4) with Cu(OAc)<sub>2</sub> in

*N,N*-dimethylformamide at 100° C [95]. The  $K^+$ -induced dimerization of these interesting macrocycles has also been studied by UV–Vis spectroscopy.

A novel tribenzotetraazachlorin fused with a  $C_{60}$  unit and three 15-crown-5 moieties (compound **114**) has recently been prepared by Kobayashi et al. [96]. As expected, the  $C_{60}$  unit and the macrocyclic core show strong electronic interactions. As shown by UV–Vis, magnetic circular dichroism, and mass spectroscopic methods, this compound undergoes edge-to-edge dimerization in the presence of  $K^+$  ions, while for  $Na^+$  ions, they are simply trapped inside the crown ether voids of **114**.



**114**

This self-assembly strategy has recently been extended to construct an interesting biomimetic model for the bacterial photosynthetic reaction center complex [97]. In this system, a cofacial zinc(II) phthalocyanine dimer is formed via the interactions between  $K^+$  ions and the four 15-crown-5 units fused to the phthalocyanine ring.

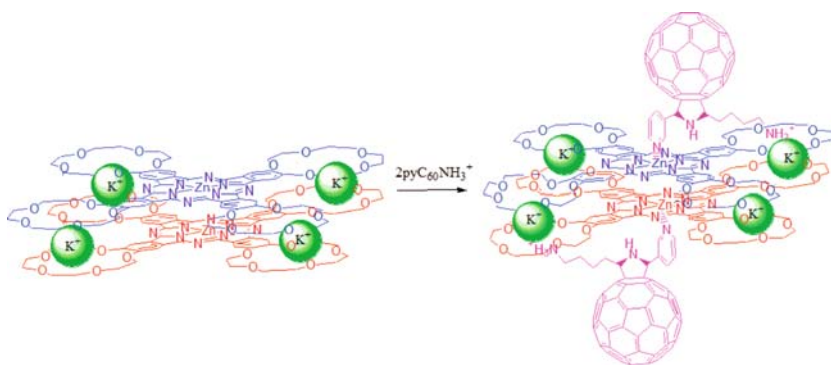


**Fig. 11** Supramolecular structure of a cofacial phthalocyanine dimer –  $C_{60}$  conjugate (reproduced from [97] with permission from the American Chemical Society)

The dimer is subsequently coordinated with a pyridyl-ammonium C<sub>60</sub> in a two-point binding manner (Fig. 11). The pyridyl group axially binds to the zinc center, while the ammonium ion is held by hydrogen bonding inside the crown ether void. This supramolecular donor–acceptor pair shows superior electron-transfer properties, including the formation of a long-lived charge-separated state (6.7 μs). The slow charge-recombination process has been attributed to the small reorganization energy of the relatively rigid cofacial phthalocyanine dimer.

## 7 Concluding Remarks

While supramolecular chemistry of porphyrins has been extensively studied over the last few decades, related study of phthalocyanines is still in its infancy. Despite the great potential of phthalocyanine-based supramolecular arrays in various applications as mentioned earlier, only a handful systems have been reported so far. Self-assembled systems held by hydrogen bonding, donor–acceptor interactions, and host–guest interactions are still very rare. There is certainly much room for further investigation in the chemistry of this important class of compounds, particularly on their structural and functional aspects. We hope this article can provide the grounding for further studies.

**Acknowledgements** We thank the Chinese University of Hong Kong for support through a strategic investments scheme and for a postdoctoral fellowship to J.-Y. Liu.

## References

1. Erk P, Hengelsberg H (2003) Phthalocyanine dyes and pigments. In: Kadish KM, Smith KM, Guillard R (eds) *The porphyrin handbook*, vol 19. Academic Press, San Diego, p 105
2. de la Torre G, Claessens CG, Torres T (2007) *Chem Commun* 2000
3. Claessens CG, Hahn U, Torres T (2008) *Chem Rec* 8:75
4. Mustroph H, Stollenwerk M, Bressau V (2006) *Angew Chem Int Ed* 45:2016
5. Li L, Tang Q, Li H, Hu W, Yang X, Shuai Z, Liu Y, Zhu D (2008) *Pure Appl Chem* 80:2231
6. Tang ML, Oh JH, Reichardt AD, Bao Z (2009) *J Am Chem Soc* 131:3733
7. Meunier B, Sorokin A (1997) *Acc Chem Res* 30:470
8. Tao X, Ma W, Zhang T, Zhao J (2002) *Chem Eur J* 8:1321
9. Cid JJ, Yum JH, Jang SR, Nazeeruddin MK, Martínez-Ferrero E, Palomares E, Ko J, Grätzel M, Torres T (2007) *Angew Chem Int Ed* 46:8358
10. O'Regan BC, López-Duarte I, Martínez-Díaz MV, Forneli A, Albero J, Morandeira A, Palomares E, Torres T, Durrant JR (2008) *J Am Chem Soc* 130:2906
11. Cid JJ, García-Iglesias M, Yum JH, Forneli A, Albero J, Martínez-Ferrero E, Vázquez P, Grätzel M, Nazeeruddin MK, Palomares E, Torres T (2009) *Chem Eur J* 15:5130
12. Ali H, van Lier JE (1999) *Chem Rev* 99:2379
13. Liu JY, Lo PC, Jiang XJ, Fong WP, Ng DKP (2009) *Dalton Trans* 4129 and references cited therein
14. Berera R, Herrero C, van Stokkum IHM, Vengris M, Kodis G, Palacios RE, van Amerongen H, van Grondelle R, Gust D, Moore TA, Moore AL, Kennis JTM (2006) *Proc Natl Acad Sci USA* 103:5343

15. Tannert S, Ermilov EA, Vogel JO, Choi MTM, Ng DKP, Röder B (2007) *J Phys Chem B* 111:8053
16. Bottari G, Olea D, Gómez-Navarro C, Zamora F, Gómez-Herrero J, Torres T (2008) *Angew Chem Int Ed* 47:2026
17. Ng DKP, Jiang J (1997) *Chem Soc Rev* 26:433
18. Buchler JW, Ng DKP (2000) Metal tetrapyrrole double- and triple-deckers with special emphasis on porphyrin systems. In: Kadish KM, Smith KM, Guillard R (eds) *The porphyrin handbook*, vol 3. Academic Press, San Diego, p 245
19. Jiang J, Ng DKP (2009) *Acc Chem Res* 42:79
20. Floris B, Donzello MP, Ercolani C (2003) Single-atom bridged dinuclear metal complexes with emphasis on phthalocyanine systems. In: Kadish KM, Smith KM, Guillard R (eds) *The porphyrin handbook*, vol 18. Academic Press, San Diego, p 1
21. Donzello MP, Bartolino L, Ercolani C, Rizzoli C (2006) *Inorg Chem* 45:6988
22. Lo PC, Leng X, Ng DKP (2007) *Coord Chem Rev* 251:2334
23. D'Souza F, Ito O (2009) *Chem Commun* 4913
24. Martínez-Díaz MV, Bottari G (2009) *J Porphyrins Phthalocyanines* 13:471
25. Li XY, Ng DKP (2000) *Eur J Inorg Chem* 1845
26. Berber G, Cammidge AN, Chambrier I, Cook MJ, Hough PW (2003) *Tetrahedron Lett* 44:5527
27. Cammidge AN, Berber G, Chambrier I, Hough PW, Cook MJ (2005) *Tetrahedron* 61:4067
28. Choi MTM, Choi CF, Ng DKP (2004) *Tetrahedron* 60:6889
29. Leng X, Ng DKP (2007) *Eur J Inorg Chem* 4615
30. Cordeiro MR, Moreira WC (2009) *Thermochim Acta* 486:52
31. Kwag G, Park E, Kim S (2004) *Bull Korean Chem Soc* 25:298
32. Kobuke Y, Miyaji H (1994) *J Am Chem Soc* 116:4111
33. Kobuke Y (2006) *Struct Bond* 121:49
34. Satake A, Kobuke Y (2007) *Org Biomol Chem* 5:1679
35. Kameyama K, Satake A, Kobuke Y (2004) *Tetrahedron Lett* 45:7617
36. Ito F, Ishibashi Y, Khan SR, Miyasaka H, Kameyama K, Morisue M, Satake A, Ogawa K, Kobuke Y (2006) *J Phys Chem A* 110:12734
37. Morisue M, Kobuke Y (2008) *Chem Eur J* 14:4993
38. Satake A, Sugimura T, Kobuke Y (2009) *J Porphyrins Phthalocyanines* 13:326
39. Xu H, Ng DKP (2008) *Inorg Chem* 47:7921
40. Guldi DM, Ramey J, Martínez-Díaz MV, de la Escosura A, Torres T, Da Ros T, Prato M (2002) *Chem Commun* 2774
41. El-Khouly ME, Rogers LM, Zandler ME, Suresh G, Fujitsuka M, Ito O, D'Souza F (2003) *ChemPhysChem* 4:474
42. D'Souza F, Deviprasad GR, Zandler ME, Hoang VT, Klykov A, VanStipdonk M, Perera A, El-Khouly ME, Fujitsuka M, Ito O (2002) *J Phys Chem A* 106:3243 and references cited therein
43. El-Khouly ME, Araki Y, Ito O, Gadde S, Zandler ME, D'Souza F (2006) *J Porphyrins Phthalocyanines* 10:1156
44. D'Souza F, Gadde S, El-Khouly ME, Zandler ME, Araki Y, Ito O (2005) *J Porphyrins Phthalocyanines* 9:698
45. Rodríguez-Morgade MS, Plonska-Brzezinska ME, Athans AJ, Carbonell E, de Miguel G, Guldi DM, Echegoyen L, Torres T (2009) *J Am Chem Soc* 131:10484
46. Troshin PA, Koeppe R, Peregudov AS, Peregudova SM, Egginger M, Lyubovskaya RN, Sariciftci NS (2007) *Chem Mater* 19:5363
47. Rodríguez-Morgade MS, Torres T, Atienza-Castellanos C, Guldi DM (2006) *J Am Chem Soc* 128:15145
48. Gao B, Li Y, Su J, Tian H (2007) *Supramol Chem* 19:207
49. Rawling T, Austin C, Buchholz F, Colbran SB, McDonagh AM (2009) *Inorg Chem* 48:3215
50. Fischer MKR, López-Duarte I, Wienk MM, Martínez-Díaz MV, Janssen RAJ, Bäuerle P, Torres T (2009) *J Am Chem Soc* 131:8669
51. Silvestri F, López-Duarte I, Seitz W, Beverina L, Martínez-Díaz MV, Marks TJ, Guldi DM, Pagani GA, Torres T (2009) *Chem Commun* 4500

52. Cook MJ, Jafari-Fini A (1997) *J Mater Chem* 7:2327
53. Ishii K, Abiko S, Fujitsuka M, Ito O, Kobayashi N (2002) *J Chem Soc Dalton Trans* 1735
54. Ishii K, Iwasaki M, Kobayashi N (2007) *Chem Phys Lett* 436:94
55. Ishii K, Watanabe Y, Abiko S, Kobayashi N (2002) *Chem Lett* 450
56. Al-Raqa SY, Cook MJ, Hughes DL (2003) *Chem Commun* 62
57. Kameyama K, Morisue M, Satake A, Kobuke Y (2005) *Angew Chem Int Ed* 44:4763
58. Novakova V, Zimcik P, Kopecky K, Miletin M, Kuneš J, Lang K (2008) *Eur J Org Chem* 3260
59. Huang X, Zhao F, Li Z, Huang L, Tang Y, Zhang F, Tung CH (2007) *Chem Lett* 36:108
60. Huang X, Zhao F, Li Z, Tang Y, Zhang F, Tung CH (2007) *Langmuir* 23:5167
61. Huang X, Zhao FQ, Li ZY, Zhao P, Tang YW, Zhang FS (2007) *Chem J Chin Univ* 28:487
62. Niu LH, Zhong C, Chen ZH, Zhang Z, Li ZY, Zhang FS, Tang YW (2009) *Chin Sci Bull* 54:1169
63. Zeng Q, Wu D, Wang C, Lu J, Ma B, Shu C, Ma H, Li Y, Bai C (2005) *CrystEngComm* 7:243
64. Li XY, Ng DKP (2001) *Tetrahedron Lett* 42:305
65. Sessler JL, Jayawickramarajah J, Gouloumis A, Pantos GD, Torres T, Guldi DM (2006) *Tetrahedron* 62:2123
66. Torres T, Gouloumis A, Sanchez-Garcia D, Jayawickramarajah J, Seitz W, Guldi DM, Sessler JL (2007) *Chem Commun* 292
67. Sessler JL, Jayawickramarajah J, Gouloumis A, Torres T, Guldi DM, Maldonado S, Stevenson KJ (2005) *Chem Commun* 1892
68. Martínez-Díaz MV, Fender NS, Rodríguez-Morgade MS, Gómez-López M, Diederich F, Echegoyen L, Stoddart JF, Torres T (2002) *J Mater Chem* 12:2095
69. Guldi DM, Gouloumis A, Vázquez P, Torres T (2002) *Chem Commun* 2056
70. Martínez-Díaz MV, Rodríguez-Morgade MS, Feiters MC, van Kan PJM, Nolte RJM, Stoddart JF, Torres T (2000) *Org Lett* 2:1057
71. Lützen A, Starnes SD, Rudkevich DM, Rebek Jr J (2000) *Tetrahedron Lett* 41:3777
72. Kimura M, Kuroda T, Ohta K, Hanabusa K, Shirai H, Kobayashi N (2003) *Langmuir* 19:4825
73. Kojima T, Honda T, Ohkubo K, Shiro M, Kusakawa T, Fukuda T, Kobayashi N, Fukuzumi S (2008) *Angew Chem Int Ed* 47:6712
74. Kojima T, Nakanishi T, Honda T, Fukuzumi S (2009) *J Porphyrins Phthalocyanines* 13:14
75. Fortage J, Göransson E, Blart E, Becker HC, Hammarström L, Odobel F (2007) *Chem Commun* 4629
76. Tran-Thi TH (1997) *Coord Chem Rev* 160:53
77. Mao HF, Tian HJ, Xu, HJ (1995) *Chin J Chem* 13:223
78. Fournier T, Liu Z, Tran-Thi TH, Houde D, Brasseur N, La Madeleine C, Langlois R, van Lier JE, Lexa D (1999) *J Phys Chem A* 103:1179
79. Tian H, Zhou Q, Shen S, Xu H (1996) *Acta Phys Chim Sin* 12:44
80. Agirtas S, Ion RM, Bekaroglu O (2000) *Mater Sci Eng C: Biomim Supramol Syst* 7:105
81. Tran-Thi TH, Lipskier JF, Simoes M, Palacin S (1992) *Thin Solid Films* 210–211:150
82. Liu J, Xu L, Shen S, Zhou Q, Li T, Xu H (1993) *J Photochem Photobiol A: Chem* 71:275
83. Sun Y, Zhang X, Sun C, Wang Z, Shen J, Wang D, Li T (1996) *Chem Commun* 2379
84. Gusev AV, Rodgers MAJ (2002) *J Phys Chem A* 106:1985
85. Gusev AV, Danilov EO, Rodgers MAJ (2002) *J Phys Chem A* 106:1993
86. Li XY, Chen YL, Xu HJ (1999) *Chin Chem Lett* 10:167
87. Guan Y, Yu SH, Antonietti M, Böttcher C, Faul CFJ (2005) *Chem Eur J* 11:1305
88. de la Escosura A, Martínez-Díaz MV, Thordarson P, Rowan AE, Nolte RJM, Torres T (2003) *J Am Chem Soc* 125:12300
89. de la Escosura A, Martínez-Díaz MV, Guldi DM, Torres T (2006) *J Am Chem Soc* 128:4112
90. de la Escosura A, Martínez-Díaz MV, Barberá J (2008) *J Org Chem* 73:1475
91. Leng X, Choi CF, Lo PC, Ng DKP (2007) *Org Lett* 9:231
92. Ray A, Goswami D, Chattopadhyay S, Bhattacharya S (2008) *J Phys Chem A* 112:11627
93. Kobayashi N (2002) *Coord Chem Rev* 227:129
94. Gorbunova YG, Lapkina LA, Tsivadze AY (2003) *J Coord Chem* 56:1223
95. Sheng N, Zhang Y, Xu H, Bao M, Sun X, Jiang J (2007) *Eur J Inorg Chem* 3268
96. Fukada T, Sugita I, Kobayashi N (2009) *Chem Commun* 3449
97. D'Souza F, Maligaspe E, Ohkubo K, Zandler ME, Subbaiyan NK, Fukuzumi S (2009) *J Am Chem Soc* 131:8787



# Phthalocyanine-Based Magnets

Naoto Ishikawa

**Abstract** Magnetism and electronic structure of two types of phthalocyanine-based magnets, “ferromagnets” and “single-molecule magnets,” both of which exhibit spontaneous magnetization but by different mechanism, are reviewed.

**Keywords** Electronic structure · Ferromagnet · Phthalocyanine · Single molecule magnet

## Contents

1	Introduction .....	212
2	Magnetism of <i>d</i> -Metal Phthalocyanines .....	212
2.1	Manganese(II) Phthalocyanine .....	213
2.2	Iron(II) Phthalocyanine .....	214
2.3	Chromium(II) Phthalocyanine .....	215
2.4	Cobalt(II) Phthalocyanine .....	216
2.5	Nickel(II) Phthalocyanine .....	216
2.6	Copper(II) Phthalocyanine .....	216
2.7	Oxo-Vanadium(IV) Phthalocyanine .....	216
3	Magnetism of $\pi$ -Radical Phthalocyanines .....	216
3.1	Lithium Phthalocyanine $\pi$ -Radical .....	216
3.2	$\pi$ -Radical Double-Decker Phthalocyanine Complexes .....	217
4	Magnetism of <i>4f</i> Metal Phthalocyanines .....	217
4.1	Bis(phthalocyaninato)terbium Anion and Bis(phthalocyaninato)dysprosium Anion .....	218
4.2	Electronic Structure of Bis(phthalocyaninato)lanthanide Anions .....	219
4.3	Quantum Tunneling of Magnetization in Bis(phthalocyaninato)lanthanide Anions [42, 43] .....	221
4.4	Electronic Structure and SMM Behavior of Tris(phthalocyaninato)bislanthanide ..	224
	References .....	227

---

N. Ishikawa  
Department of Applied Chemistry, Chuo University, 1–13–27 Kasuga, Bunkyo-ku,  
Tokyo 112–8551, Japan  
e-mail: ishikawa@chem.chuo-u.ac.jp

## 1 Introduction

Metallophthalocyanines with one or more unpaired electrons in many cases essentially behave as simple paramagnetic substances. Some complexes, however, can act as “magnet” that exhibit spontaneous magnetization. There are two types of such complexes that have been known. The first one is “ferromagnet” and the other is “single-molecule magnet.”

Phthalocyanine (Pc) and divalent transition metal ion can form planar molecules with no axial ligand, which in crystals take various stacking columnar structures with different tilting angles and interplanar distances. In such a circumstance, complexes can be coupled by exchange interaction, which in some instances takes a large positive value that leads to a ferromagnetic magnetic ordering below a transition temperature and spontaneous magnetization in the absence of an applied magnetic field. Substances in such a state are generally called ferromagnets.

Single-molecule magnet (SMM) on the other hand is a relatively new class of magnetic substances that also exhibit spontaneous magnetization, but without any collective magnetic order. The first SMM was a polynuclear manganese complex  $[\text{Mn}_{12}\text{O}_{12}(\text{O}_2\text{CMe})_{16}(\text{H}_2\text{O})_4]$  with  $S = 10$  spin state and negative zero field splitting constant  $D = -0.50 \text{ cm}^{-1}$ . Since then, various type of  $3d$  metal cluster-based SMMs have been reported. SMM containing a lanthanide ion was first reported for the Pc–lanthanide “double-decker” complexes. Despite there being only one magnetic ion in the complex, unlike in the typical  $3d$  metal SMMs composed of multiple metal ions, the Pc complexes show SMM behavior with a significantly higher temperature range than any other SMM systems known at present.

In what follows, the first section is devoted to describing transition-metal Pc complex-based ferromagnets and also other related complexes exhibiting no ferromagnetic order. The second section describes the magnetic interaction of  $\pi$ -radical phthalocyanines in crystals. In the last section, we present Pc-based SMMs and a general discussion on magnetism and electronic structure of lanthanide Pc complexes.

## 2 Magnetism of $d$ -Metal Phthalocyanines

Understanding of magnetism of  $d$ -metal phthalocyanine complexes requires consideration on both intrinsic molecular properties, which depend on the  $d$ -electronic configuration, and intermolecular magnetic interactions depending on the crystal structure. In the typical  $d$ -metal phthalocyanines, the  $d$  orbitals exhibit typical ligand-field splitting of the square-planar ligand field of  $D_{4h}$  point group (Fig. 1). To date only few Pc complexes are known to become ferromagnetic, in which the complexes exhibit ferromagnetic ordering below a certain transition temperature. In this section, general aspects of magnetism of the  $d$ -metal phthalocyanines, including those ferromagnets and non-ferromagnets are reviewed.

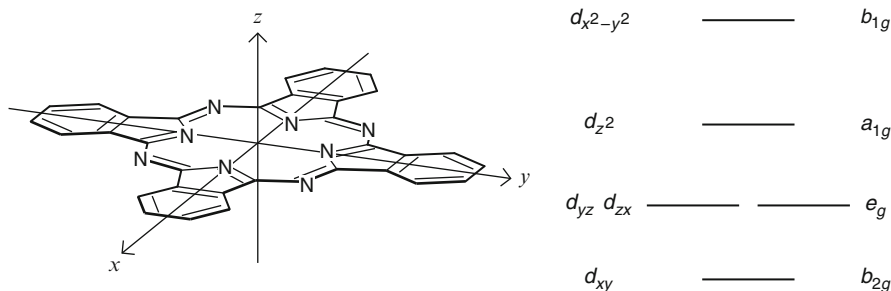
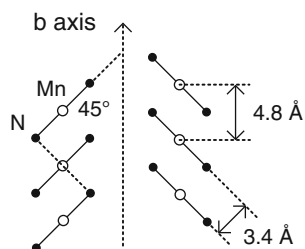


**Fig. 1** Schematic energy levels of the  $d$  orbitals in square-planar coordination of  $3d$  metal phthalocyanine complexes. The ordering of the energy levels can be changed except for the highest orbital. The labels on the right are the irreducible representation in the  $D_{4h}$  point group

**Fig. 2** Schematic stacking arrangement of MnPc in  $\beta$ -polymorph along the crystallographic  $b$  axis



## 2.1 Manganese(II) Phthalocyanine

The first and most investigated Pc-based ferromagnet is  $\beta$ -polymorphic manganese (II) phthalocyanine ( $\beta$ -MnPc). In this polymorph, the two pyrrole nitrogen atoms of Pc lie exactly above or below the Mn belonging to nearest neighbors (Fig. 2). The distance between these axially located nitrogen atoms and Mn atom is  $3.4 \text{ \AA}$ , which, is sufficiently short to provide a possible pathway for magnetic exchange interaction. The angle between the  $b$  axis and the MnPc plane is  $45^\circ$ .

Magnetic susceptibility at high temperature region obeys Curie–Weiss law,  $\chi = C/(T-\theta)$  with positive Weiss constant  $\theta$  [1]. The reported values for  $\theta$  are somehow dependent on the experimental data to be used:  $6$  [1],  $18.4$  [2], or  $23 \text{ K}$  [3]. At temperatures below about  $20 \text{ K}$ , the susceptibility deviates from the Curie–Weiss law and reaches a constant maximum value below  $7 \text{ K}$  [2]. The Curie temperature  $T_c$ , at which ferromagnetic transition occurs, has been determined to be  $8.6 \text{ K}$ , from broad-line NMR studies [3], and  $8.3 \text{ K}$ , with susceptibility measurement for single crystals [4]. The ground state of MnPc is in  $S = 3/2$  state (quartet) [1, 4] and its  $d$ -electronic configuration has been determined to be  $(b_{2g})^2(e_g)^2(a_{1g})^1$ , i.e.  $(d_{xy})^2(d_{yz} d_{zx})^2(d_{z^2})^1$  [5]. In a model calculation with  $S = 3/2$  linear chain the exchange energy was deduced to be  $J = +7.7 \text{ cm}^{-1}$  [6]. The ferromagnetic behavior is understood qualitatively in terms of the electronic configuration and the  $90^\circ$  superexchange interaction between nearest-neighbor Mn atoms via nitrogen atoms in Pc rings, resulting in the ordering of  $\text{Mn}^{2+}$  with  $S = 3/2$  state [5]. It has

been shown that the overlap of  $e_g$  and  $a_{1g}$   $d$ -orbitals with Pc orbital of  $a_{2u}$ ,  $e_g$ ,  $b_{2u}$ , and  $b_{1u}$  symmetry can lead to ferromagnetism [4]. The spins in MnPc are appreciably canted, arising from the substantially large zero-splitting of the  $^4A_2$  ground state of the  $Mn^{2+}$  ion [5].

Awaga et al. reported the increase in  $T_c$  under high pressure [7]. The enhancement of ferromagnetic interaction is interpreted by the pressure dependence of the distance between Mn and N atoms.

Magnetic measurements on  $\alpha$ -polymorphic MnPc was reported for epitaxial thin film grown on hydrogen-terminated Si(111) surface [8]. In the  $\alpha$ -polymorph the stacking angle was  $65^\circ$ . The susceptibility was highly anisotropic and easy axis was perpendicular to the film surface. The susceptibility along the easy axis obeyed the Curie–Weiss law even below 10 K, and  $\theta$  was estimated to be  $-3$  K indicating the existence of antiferromagnetic interaction between MnPc molecules.

Regarding the ground state electronic configuration of MnPc, another assignment has been reported based on magnetic circular dichroism (MCD) and absorption spectra of MnPc isolated in an Ar matrix [9]. They concluded that the ground state is in an orbitally degenerate  $(b_{2g})^1(e_g)^3(a_{1g})^1$  state. A DFT study by Liao et al., which was performed on the Amsterdam density functional package with VWN-B-P exchange-correlation functional and a Slater-type orbital basis set, supported this assignment [10]. On the other hand, Wu et al. obtained  $(b_{2g})^2(e_g)^2(a_{1g})^1$  configuration as the ground state by a DFT calculation with B3LYP exchange-correlation functional and 6–31G basis set on the GAUSSIAN 98 [11], which is consistent with the magnetic measurement for the  $\beta$ -MnPc and also with an early extended Hückel calculation [12].

## 2.2 Iron(II) Phthalocyanine

Second Pc-based ferromagnet, FePc in a meta-stable  $\alpha$ -polymorph (Fig. 3), was reported in 2002 by Evangelisti et al. [13]. They showed that in the  $\alpha$ -FePc Fe(II) moments are strongly coupled into ferromagnetic chains, with the weak interchain coupling leading to a canted, soft molecular ferromagnet below 10 K. Magnetic susceptibility data from 50 to 300 K were fitted to the Curie–Weiss law  $\chi = C/(T-\theta)$  with an effective spin  $S = 1$ ,  $g = 2.54$  and  $\theta = (40 \pm 2)$ K, from which

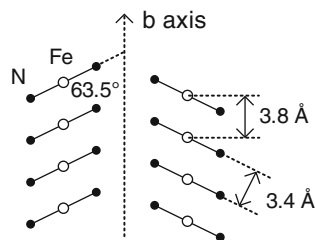


**Fig. 3** Schematic stacking arrangement of FePc in  $\alpha$ -polymorph along the crystallographic  $b$  axis

$J/k_B = +15 \text{ K}$  was estimated for the ferromagnetic interaction along the chains. For ac susceptibility data, they obtained best fit to the experimental data with  $J = +25.7 \text{ K}(18 \text{ cm}^{-1})$ ,  $g = 2.54$  and  $D = 53.2 \text{ K}(37 \text{ cm}^{-1})$ , where positive  $D$  indicates that  $S_z = \pm 1$  doublet lies above  $S_z = 0$  singlet. In spite of the nonmagnetic ground singlet state,  $S = 1$  spins in the  $\alpha$ -FePc remain ferromagnetically coupled in magnetic chains down to lowest temperatures because the ferromagnetic interaction  $2zJ$  ( $z$  is the number of nearest neighbors) is larger than  $D$ , as the criterion described by Moriya for magnetic ordering in  $S = 1$  triplets [14].

In contrast to the metastable  $\alpha$ -polymorph, FePc in stable  $\beta$ -polymorph has been intensively investigated in a pioneering work by Klemm et al. reported in 1935 [15].  $\beta$ -FePc shows no magnetic order unlike the  $\alpha$ -FePc mentioned above. Generally accepted assignment has been based on the study by Dale et al., in which they deduced  $(b_{2g})^2(e_g)^3(a_{1g})^1$  configuration and  $S = 1$  ground state from magnetic susceptibility measurement in the temperature range 1.25–300 K [16]. The data in high temperature region (100–300 K) obeyed Curie–Weiss law with  $\theta = 3 \text{ K}$ . From the behavior in the low temperature region, the triplet was shown to be split to  $S_z = \pm 1$  and 0 states by second-order spin–orbital interaction. The  $S_z = 0$  state lies below  $S_z = \pm 1$ . The zero field splitting  $D$  and  $g$  values were estimated at  $70 \text{ cm}^{-1}$ ,  $g_{//} = 1.93$  and  $g_{\perp} = 2.86$ . Because of the  $S_z = 0$  ground state and small exchange coupling, no magnetic order was observed.

Assignment for the electronic configuration seems to be still in debate. For FePc molecule in solution, Stillman et al. reported MCD spectrum and assigned electronic configuration to be  $(b_{2g})^2(e_g)^2(a_{1g})^2$  [17]. Labarta et al. proposed  $(b_{2g})^1(e_g)^3(a_{1g})^2$  configuration on the basis of Mössbauer and magnetic susceptibility measurements [18]. Coppens et al. assigned to  $(b_{2g})^2(e_g)^3(a_{1g})^1$  for  $\beta$ -form FePc from X-ray diffraction [19]. Evangelisti et al. suggested that  $\alpha$ -form and  $\beta$ -form have the same electronic configuration but with different  $D$  values, and the last configuration  $(b_{2g})^2(e_g)^3(a_{1g})^1$  best support the large direct Fe–Fe exchange interaction in the  $\alpha$ -form, which may be enhanced with the shorter Fe–Fe distance in the  $\alpha$ -form than that in the  $\beta$ -form [13].

### 2.3 Chromium(II) Phthalocyanine

The ground state of Cr(II)Pc was assigned to a  $S = 2$  spin state [20], most probably corresponding to  $(b_{2g})^1(e_g)^2(a_{1g})^1$  configuration. In crystals, distance between chromium ions is  $3.4 \text{ \AA}$ , which is shorter than that in the  $\beta$ -form that is a generally stable form in other metal Pc cases. A strong antiferromagnetic interaction is present between the Cr ions. From analysis of temperature dependence of magnetic susceptibility data, exchange coupling constant was estimated to be  $J = -38.2 \text{ K}(26.5 \text{ cm}^{-1})$ , indicating Cr(II)Pc exists as a one-dimensional chain of  $S = 2$  spins coupling antiferromagnetically [20].

## 2.4 Cobalt(II) Phthalocyanine

The generally accepted assignment for the electronic configuration for Co(II)Pc is  $(b_{2g})^2(e_g)^4(a_{1g})^1$  configuration with  $S = 1/2$  spin state [1]. Miyoshi showed that the magnetic susceptibility obeys the Curie–Weiss law above 5 K with  $\theta = -3$  K, indicating the presence of a weak antiferromagnetic interaction among molecules [3]. The magnetic susceptibility in the low temperature region was reproduced by the one-dimensional Ising model of  $S = 1/2$  spins with  $J = -2.3$  K ( $1.6$  cm<sup>-1</sup>) and  $g = 2.66$  [3].

## 2.5 Nickel(II) Phthalocyanine

Ni(II)Pc is diamagnetic, having  $(b_{2g})^2(e_g)^4(a_{1g})^2$  configuration. Magnetic susceptibility at room temperature is reported to be  $-288 \times 10^{-6}$  cm<sup>3</sup> mol<sup>-1</sup> [21]. Anisotropy of the diamagnetic susceptibility is reported by Barraclough et al. [4].

## 2.6 Copper(II) Phthalocyanine

Effective magnetic moment of Cu(II)Pc is 1.75 BM [22], which corresponds to that of a free  $S = 1/2$  spin. The complex has  $(b_{2g})^2(e_g)^4(a_{1g})^2(b_{1g})^1$  configuration, with one unpaired electron in the  $d_{x^2-y^2}$  orbital. The magnetic susceptibility shows typical paramagnetic behavior down to 1.8 K with no indication of magnetic ordering [3]. It was suggested that the  $d_{x^2-y^2}$  unpaired orbital, which has a  $\sigma$  character and spreads into the molecular plane, leads to a very small overlap between adjacent molecules, and hence a very small exchange coupling [3].

## 2.7 Oxo-Vanadium(IV) Phthalocyanine

The VOPc contains metal–oxygen double bond and has a five-coordinate square pyramidal structure. Effective magnetic moment at room temperature was reported to be 1.71 BM, which corresponds to that of free  $S = 1/2$  spin indicating no orbital contribution [1].

# 3 Magnetism of $\pi$ -Radical Phthalocyanines

## 3.1 Lithium Phthalocyanine $\pi$ -Radical

Oxidation of dilithium phthalocyanine Li<sub>2</sub>Pc affords a mono-lithium Pc  $\pi$ -radical, LiPc, in which one unpaired electron resided in HOMO  $a_{1u}$   $\pi$ -orbital [23–25]. ESR spectrum in chloronaphthalene solution was reported by Simon et al. [26]. LiPc

crystallizes in different crystal structures, including  $\alpha$ -form,  $\beta$ -form and  $\gamma$ -form, depending on the synthetic route [27]. The crystal grown by electrochemical oxidation in acetonitrile takes  $\alpha$ -form, in which LiPc molecules form a columnar structure with each molecule's  $C_4$  axis coincides with the direction of the stacking of molecules. Interplanar distance is 3.25 Å, which is substantially shorter than the van der Waals distance (3.40 Å). Because of this and large overlap among adjacent  $\pi$ -orbitals, ESR line-width is extremely narrowed (hwhm = 2.0  $\mu$ T, at 300 K in single crystal). Temperature dependence of the magnetic susceptibility comprises two components: including the one that obeys Curie–Weiss law and the one that is thermally activated. Below about 100 K, the former is dominant. Weiss constant  $\theta$  was found to be  $-2$  K for powder sample and 4 K for a single crystal. In  $\alpha$ -form and  $\beta$ -form, LiPc molecules are inclined from the perpendicular direction of the stacking axis and the interplanar distance is larger than the  $\alpha$ -form. Because of this, the ESR linewidth becomes much wider than that of  $\alpha$ -form (hwhm = 130  $\mu$ T for  $\alpha$ -form and 130–160  $\mu$ T for  $\beta$ -form at 300 K in single crystal) [27]. The magnetic susceptibility obeys Curie–Weiss law with  $\theta = 4.5$  K for  $\alpha$ -form,  $\theta = -60$  K for single crystal of  $\beta$ -form and  $\theta = -37$  K for powder of  $\beta$ -form [27].

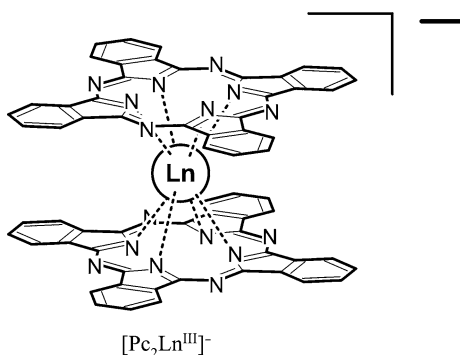
### 3.2 $\pi$ -Radical Double-Decker Phthalocyanine Complexes

Electrically neutral species of bis(phthalocyaninato)lanthanides with double-decker structure  $\text{Ln(III)(Pc)}_2$ , where Ln(III) is trivalent lanthanide or Yttrium, has an unpaired electron in  $\pi$ -orbital delocalized over two Pc ligands. The magnetic interaction among the  $\pi$ -radical complexes in the solid states has been investigated for the two types of crystals of  $\text{Y(Pc)}_2$  with diamagnetic  $\text{Y}^{\text{III}}$  ion [28]. In a crystal of a composition  $\text{Y(Pc)}_2 \cdot \text{CH}_2\text{Cl}_2$ ,  $C_4$  axis of each molecule is inclined by  $35^\circ$  from the direction of stacking. The temperature dependence of magnetic susceptibility data was fit under a Heisenberg model of a one-dimensional chain of  $S = 1/2$  spins with  $J = 1.76$  K and  $g = 1.997$ , indicating the presence of weak ferromagnetic interaction. On the other hand, in a crystal containing no solvent molecule,  $\text{Y(Pc)}_2$  forms a columnar structure with each molecule's  $C_4$  axis coinciding with the direction of the stacking of molecules. In this case, the magnetic susceptibility data was fit under the same model with  $J = -4.78$  K and  $g = 1.91$ , showing that the interaction is antiferromagnetic.

## 4 Magnetism of 4f Metal Phthalocyanines

To date there has been no report of observation of magnetic order of 4f metal phthalocyanines in solid state. However, in 2003, it was revealed that some of lanthanide phthalocyanine complexes exhibit an intriguing property as “SMM,” a relatively new class of magnetic compounds [29, 30]. The SMMs are the paramagnetic

**Fig. 4** Structure of  $[\text{Pc}_2\text{Ln}^{\text{III}}]^-$  (Pc = dianion of phthalocyanine,  $\text{Ln}^{\text{III}}$  = trivalent lanthanide ion)



molecules, usually  $3d$  metal polynuclear complexes, with extremely slow spin reversal rate so that the electronic magnetic moment of the system is fixed to a certain direction without magnetic ordering due to intermolecular interaction [31–39]. The possibility of constructing SMM using a single lanthanide ion was first demonstrated experimentally on phthalocyaninato–lanthanide complexes having a double-decker structure (Fig. 4).

The lanthanide complexes showing SMM behaviors have significantly large axial magnetic anisotropy, which is given to the complexes by essentially different mechanisms than those of the well-established  $3d$  metal-cluster SMMs. In the  $3d$  cluster SMM cases, the easy-axis-type magnetic anisotropy, which is represented by the negative zero-field-splitting constant  $D$ , is caused by the magnetic interactions among high-spin  $3d$  metal ions in a molecule. In the lanthanide single-ionic SMM cases, on the other hand, such anisotropy is given by the ligand field (LF) in which the lanthanide ion is placed.

#### 4.1 *Bis(phthalocyaninato)terbium Anion and Bis(phthalocyaninato)dysprosium Anion*

Figure 5 shows ac magnetic susceptibilities as a function of temperature of polycrystalline powder sample of  $[\text{Pc}_2\text{Tb}]^- \cdot \text{TBA}^+$  ( $\text{TBA}^+ = (\text{C}_4\text{H}_9)_4\text{N}^+$ ). The undiluted sample of the Tb complex with a  $(4f)^8$  electronic configuration showed  $\chi_M''/\chi_M$  maximum, where  $\chi_M$  and  $\chi_M''$  are dc and out-of-phase ac susceptibilities, at 15, 32 and 40 K with ac frequency of 10, 100 and 997 Hz, respectively (Fig. 5, *open marks*). At these temperatures, each corresponding  $\chi_M'T$  value, where  $\chi_M'$  is in-phase ac susceptibility, decreases with lowering temperature. The measurement for a diluted sample in diamagnetic iso-structural yttrium complex  $[\text{Pc}_2\text{Y}]^- \cdot \text{TBA}^+$  (Fig. 5, *filled marks*) showed that the  $\chi_M''/\chi_M$  peaks and the  $\chi_M'T$  drops not only remained but shifted to higher temperatures by dilution. This clearly proves that the slow magnetization relaxation is the single molecular property of  $[\text{Pc}_2\text{Tb}]^-$ , rather than resulting from intermolecular interactions and magnetic order.



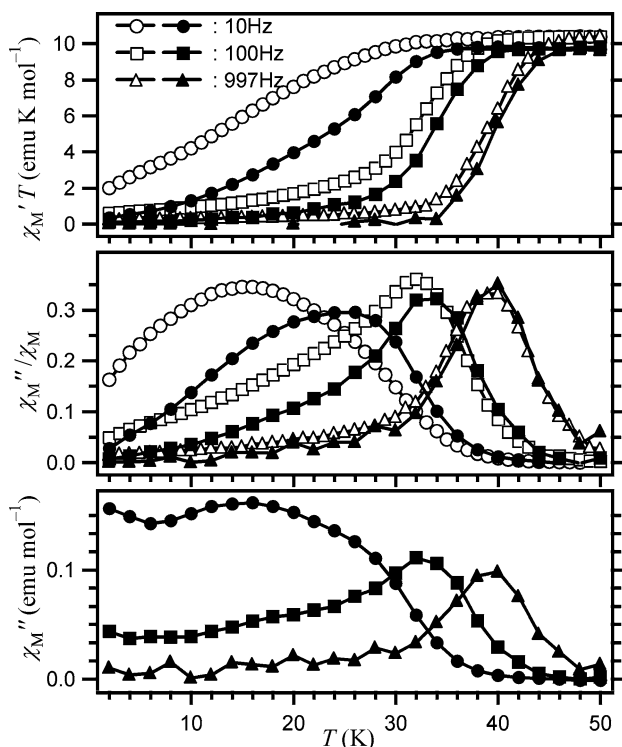


**Fig. 5** Plots of (top)  $\chi_M' T$ , (center)  $\chi_M''/\chi_M$  and (bottom)  $\chi_M''$  against temperature  $T$ , where  $\chi_M'$ ,  $\chi_M''$  and  $\chi_M$  are in-phase-ac, out-of-phase-ac and dc molar magnetic susceptibilities, respectively, for a powder sample of  $[\text{Pc}_2\text{Tb}]^- \cdot \text{TBA}^+$  (open marks) and that diluted in  $[\text{Pc}_2\text{Y}]^- \cdot \text{TBA}^+$  with the molar ratio  $[\text{Pc}_2\text{Tb}]^-/[\text{Pc}_2\text{Y}]^- = 1/4$  (filled marks) measured in 3.5 G ac magnetic field oscillating at indicated frequencies

Similar temperature dependence of ac susceptibility was also observed for  $[\text{Pc}_2\text{Dy}]^- \cdot \text{TBA}^+$ , which has a  $(4f)^9$  electronic configuration. The peaks of  $\chi_M''/\chi_M$  plot were at 4.5, 7 and 11.5 K, with ac frequency of 10, 100 and 997 Hz, respectively.

The temperature ranges in which the magnetization relaxations are observed in  $[\text{Pc}_2\text{Tb}]^- \cdot \text{TBA}^+$  and  $[\text{Pc}_2\text{Dy}]^- \cdot \text{TBA}^+$ , are significantly higher than any of the 3d metal-cluster SMMs. The SMM behavior was not observed for the Pc double-decker complexes with other heavy-lanthanide (Ho, Er, Tm and Yb).

## 4.2 Electronic Structure of Bis(phthalocyaninato)lanthanide Anions

Magnetic properties of the lanthanide complexes such as the SMM behavior and temperature dependence of the magnetic susceptibility can only be understood with

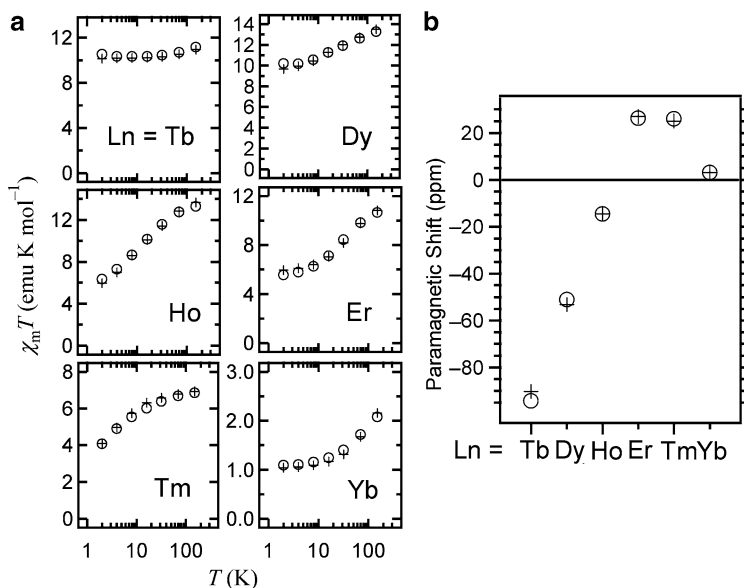


**Fig. 6** Theoretical values (*crosses*) and the experimental data (*circles*) of (a) temperature dependence of the  $\chi_M T$  of  $[\text{Pc}_2\text{Ln}]\text{TBA}$  and (b) paramagnetic shifts of the  $^1\text{H-NMR}$  signal of the  $\alpha$ -proton on the Pc ligands

a detailed information of the multiplet sub-structures of the ground multiplet of the complexes. The author's group determined the electronic structure of  $[\text{Pc}_2\text{Ln}]^-$ , using a simultaneous fitting of the experimental data of the six heavy lanthanide complexes. Under a restriction that each LF parameter was approximated as a linear function of the atomic number [40], the set of LF parameters was determined so that it reproduces both  $^1\text{H-NMR}$  paramagnetic shifts ( $\Delta\delta$ ) and magnetic susceptibility ( $\chi_M$ ) data of iso-structural complexes with  $(4f)^8$ – $(4f)^{13}$  electronic configurations.

Figure 6 shows the theoretical values of  $\chi_M T$  and  $\Delta\delta$  obtained with the LF parameters determined thus. The sub-structures of the ground multiplets of the six complexes are determined as shown in Fig. 7 [41].

In the Tb complex, the lowest substates are assigned to  $J_z = \pm 6$ , which are the maximum and minimum values and correspond to the “spin-up” and “spin-down” states in the  $J = 6$  ground multiplet. In the Dy complex, the lowest substates are characterized as  $J_z = \pm 13/2$ , the second largest in the  $J = 15/2$  ground state. This means the two complexes have strong axial magnetic anisotropy, which is a requirement for an SMM. In Er and Tm case, the  $|J_z|$  values of the lowest substates are the smallest within the multiplet, indicating their strong planar magnetic anisotropy. In the Ho and Yb case,  $|J_z|$  of the lowest substates takes an intermediate value within each multiplet.

Arrhenius analysis showed two-phonon Orbach process was dominant in the temperature range 25–40 K in the Tb complex, and 3–12 K in the Dy complex.

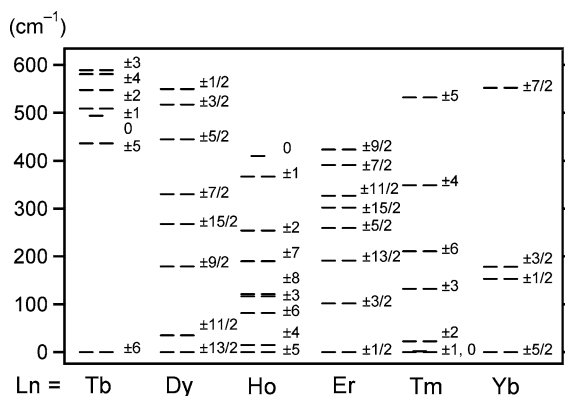


Fig. 7 Energy diagram for the ground multiplets of  $[\text{Pc}_2\text{Ln}]^-$  ( $\text{Ln} = \text{Tb}, \text{Dy}, \text{Ho}, \text{Er}, \text{Tm}, \text{or Yb}$ )

The energy barrier through which the Orbach process occurs was estimated to be  $2.6 \times 10^2 \text{ cm}^{-1}$  and  $3.1 \times 10^1 \text{ cm}^{-1}$  for the Tb and Dy complexes, respectively. These values are close to the energy differences between the lowest and the second lowest sublevels (Fig. 7), supporting the dominance of the Orbach process.

### 4.3 Quantum Tunneling of Magnetization in Bis(phthalocyaninato)lanthanide Anions [42, 43]

Observation of staircase-like magnetization hysteresis loops in the 3d metal-cluster SMMs has generated much attention to the quantum nature of these compounds. At each step relaxation of magnetization of an SMM occurs through a quantum tunneling of magnetization (QTM) [44, 45]. This discovery has led to the idea of using of SMMs for quantum computing [46]. The QTM process is also observed in the lanthanide-Pc SMMs. Figure 8 shows magnetization versus field plots obtained for the diluted  $[\text{Pc}_2\text{Tb}]^-$  sample at 0.04 K with several field scan rates. In these hysteresis loops clear staircase-like steps are observed, indicating the occurrence of QTM.

In the 3d metal-cluster SMM cases, where energy separations between substates with different  $|S_z|$  values are of the order of  $1\text{--}10 \text{ cm}^{-1}$ , QTM occurs when energy levels of two substates coincide under an appropriate magnetic field and the two states are brought to resonance. In the  $[\text{Pc}_2\text{Tb}]^-$  case, such level coincidence cannot occur with magnetic fields below several tesla, because the lowest substates are separated from the rest of the substates by a few hundred per centimeter. The steps observed for  $[\text{Pc}_2\text{Tb}]^-$  must therefore be caused by a different mechanism.

Tb nucleus has a spin of  $I = 3/2$  with a natural abundance of 100%. There is disregarable interaction between this spin and the  $(4f)^8$  system. Figure 9 shows the Zeeman diagram obtained by numerical diagonalization of a  $[(2J + 1)(2I + 1) \times$

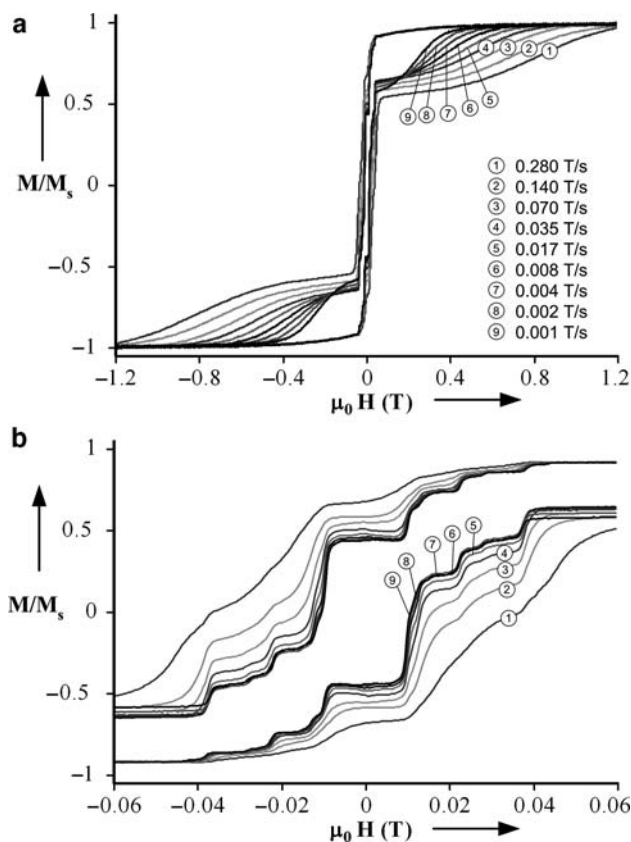
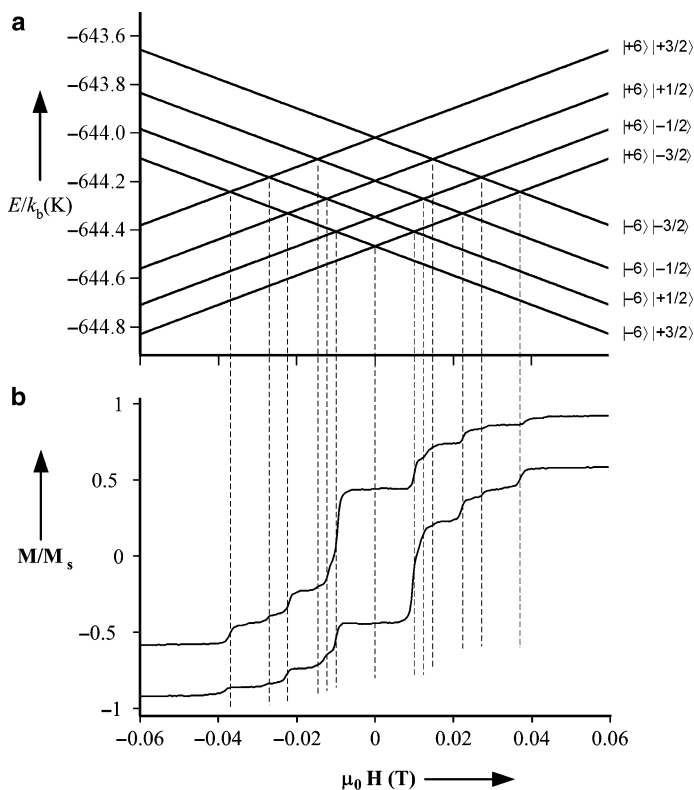


**Fig. 8** (a) Hysteresis loops at 0.04 K for a single crystal of  $[(Pc)_2Tb_{0.02}Y_{0.98}]^- \cdot TBA^+$  measured at several field scan rates. (b) Enlargement of the hysteresis loops in (a)

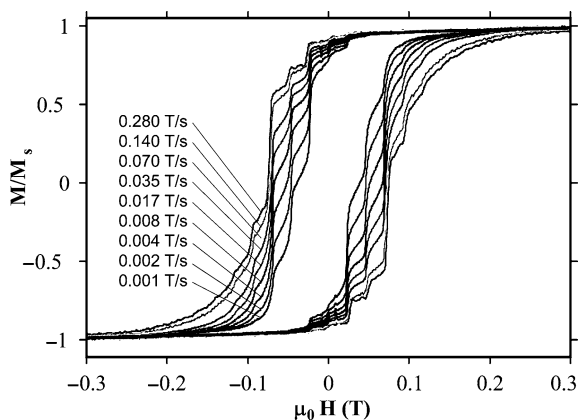
$(2J + 1)(2I + 1)$ ] matrix for the states generated from  $J = 6$  electronic multiplet and  $I = 3/2$  nuclear multiplet, including the LF term, the hyperfine interaction term  $A_{\text{hf}}\mathbf{J} \cdot \mathbf{I}$ , and the nuclear quadrupole interaction term  $P\{I_z^2 - 1/3I(I + 1)\}$ . The figure shows the lowest eight  $|J_z\rangle|I_z\rangle$  states. Using  $A_{\text{hf}} = 0.0173 \text{ cm}^{-1}$  and  $P = 0.010 \text{ cm}^{-1}$ , all positions of the steps are reproduced. It should be noted that the inclusion of the nuclear quadrupole term is mandatory to explain the seemingly irregularly arranged staircase structures in the hysteresis loops of  $[Pc_2Tb]^-$ .

Figure 10 shows magnetization vs. field measurements for a single crystal of  $[(Pc)_2Ho_{0.02}Y_{0.98}]^- \cdot TBA^+$  with the ratio of  $[Ho]/[Y] = 1/49$ . Hysteresis was observed below 0.5 K. The hysteresis loops at 0.04 K showed a clear staircase-like structure indicating the occurrence of QTM. The steps are positioned equidistantly along the magnetic field axis at  $\mu_0 H_n = n \times 23.5 \text{ mT}$  ( $n = 0, 1, 2, 3, \dots$ ).

Holmium has a nucleus with  $I = 7/2$  spin in a natural abundance of 100%. Each sublevel of the  $J = 8$  ground multiplet is split into an octet by the hyperfine interaction between the  $(4f)^{10}$  system and the nucleus. All observed step positions are



**Fig. 9** (a) Zeeman diagrams calculated with  $A_{\text{hf}} = 0.0173 \text{ cm}^{-1}$  for the hyperfine interaction term  $A_{\text{hf}} \mathbf{J} \cdot \mathbf{I}$  and  $P = 0.010 \text{ cm}^{-1}$  for the nuclear quadrupole interaction term  $P \{I_z^2 - 1/3 I(I + 1)\}$ . (b) Hysteresis loop at 0.04 K for a single crystal of  $[(\text{Pc})_2\text{Tb}_{0.02}\text{Y}_{0.98}]^- \cdot \text{TBA}^+$  measured at  $0.001 \text{ T s}^{-1}$



**Fig. 10** Hysteresis loops for a single crystal of  $[(\text{Pc})_2\text{Ho}_{0.02}\text{Y}_{0.98}]^- \cdot \text{TBA}^+$  at 0.04 K measured at several field scan rates

reproduced with numerical diagonalization of a  $[(2J+1)(2I+1) \times (2J+1)(2I+1)]$  matrix including the hyperfine interaction  $A_{\text{hf}}\mathbf{J} \cdot \mathbf{I}$  ( $A_{\text{hf}} = 0.0276 \text{ cm}^{-1}$ ) and the LF term as in the preceding section. In this  $[(\text{Pc})_2\text{Ho}]^-$  case, the nuclear quadrupole term was negligibly small, which corresponds to the equidistantly positioned steps. This shows a sharp contrast to the non-equidistant separations in the  $[(\text{Pc})_2\text{Tb}]^-$  case, where nuclear quadrupole term has a large contribution.

#### 4.4 Electronic Structure and SMM Behavior of Tris(phthalocyaninato)bislanthanide

Another type of Pc sandwich complexes  $[\text{Ln}_2(\text{Pc})_3]$ , often referred to as “triple-deckers,” possess two lanthanide ions placed along the fourfold symmetry axis with a separation of about  $3.6 \text{ \AA}$ . If  $\text{Tb}^{\text{III}}$  ions are placed at these sites, the complex can be viewed as a very intriguing system in which two  $(4f)^8$  systems, each behaving as an SMM, are coupled by some type of interaction.

The nature of the interaction between the lanthanide ions in the triple-deckers was investigated using hetero-dinuclear complexes composed of a diamagnetic  $\text{Y}^{\text{III}}$  and a paramagnetic trivalent lanthanide ion (Fig. 11),  $\text{PcYPcLnPc}^*$  and  $\text{PcLnPcYPc}^*$  (abbreviated as  $[\text{Y}, \text{Ln}]$  and  $[\text{Ln}, \text{Y}]$ ,  $\text{Pc}^* =$  dianion of 2,3,9,10,16,17,23,24-octabutoxyphthalocyanine) [47–50].

The LF parameters of individual lanthanide sites in the dinuclear complexes were determined [29]. The nature of the  $f-f$  interaction was determined by comparison of the temperature dependence of  $\chi_M T$  values of homo-nuclear  $[\text{Ln}, \text{Ln}]$  and theoretical predictions made with the LF parameters [30].

In Fig. 12, the deviation of the  $\chi_M T$  values of  $[\text{Ln}, \text{Ln}]$  from the sum of those of  $[\text{Ln}, \text{Y}]$  and  $[\text{Y}, \text{Ln}]$  are plotted. The figure shows that the two lanthanide ions interact “ferromagnetically” in  $[\text{Tb}, \text{Tb}]$ ,  $[\text{Dy}, \text{Dy}]$  and  $[\text{Ho}, \text{Ho}]$ , and “antiferromagnetically” in  $[\text{Er}, \text{Er}]$  and  $[\text{Tm}, \text{Tm}]$ , whereas the interaction is very small in  $[\text{Yb}, \text{Yb}]$ . These observations are reproduced quantitatively, as shown by the solid lines in Fig. 12, by considering magnetic-dipolar interaction between the ions while omitting exchange interaction term. The theoretical values are obtained using the LF parameters determined for  $[\text{Ln}, \text{Y}]$  and  $[\text{Y}, \text{Ln}]$ . Thus the  $f-f$  interaction in the triple-decker complexes was determined to be essentially of magnetic-dipolar nature, and contribution from exchange term was negligibly small.

Temperature dependence of ac susceptibilities of the three complexes was investigated for  $[\text{Tb}, \text{Tb}]$ ,  $[\text{Tb}, \text{Y}]$  and  $[\text{Y}, \text{Tb}]$  (Fig. 13). The  $\chi_M''/\chi_M$  peaks for the 997 Hz field are observed at 7 and 18 K for  $[\text{Y}, \text{Tb}]$  and  $[\text{Tb}, \text{Y}]$ , respectively. The difference in the temperature ranges where the relaxation phenomena are observed reflects the difference of the ligand field potential between the two lanthanide sites.

Tb complex  $[\text{Tb}, \text{Tb}]$  shows the relaxation phenomenon at higher temperature ranges than the mono-Tb complexes (Fig. 13, *bottom*). This means that the  $f-f$  interaction has an effect to increase the magnetization relaxation time of  $[\text{Tb}, \text{Tb}]$  at a given temperature. Even more interestingly, the  $\chi_M''/\chi_M$  plot for the 997 Hz field

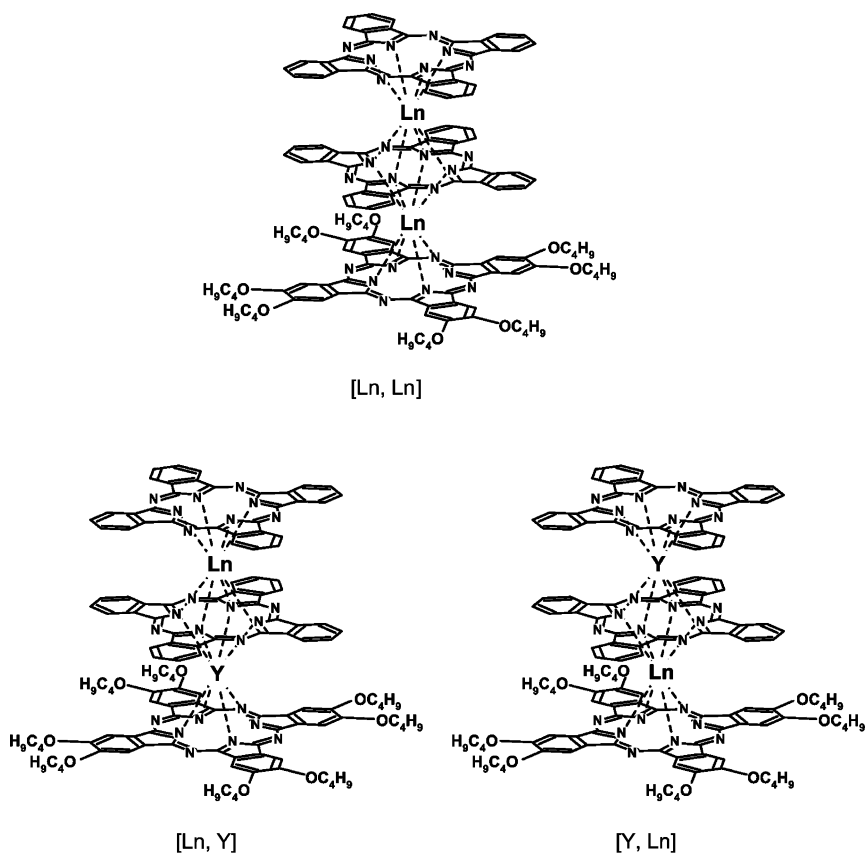


Fig. 11 Three types of dinuclear complexes to be prepared for study of  $f-f$  interaction

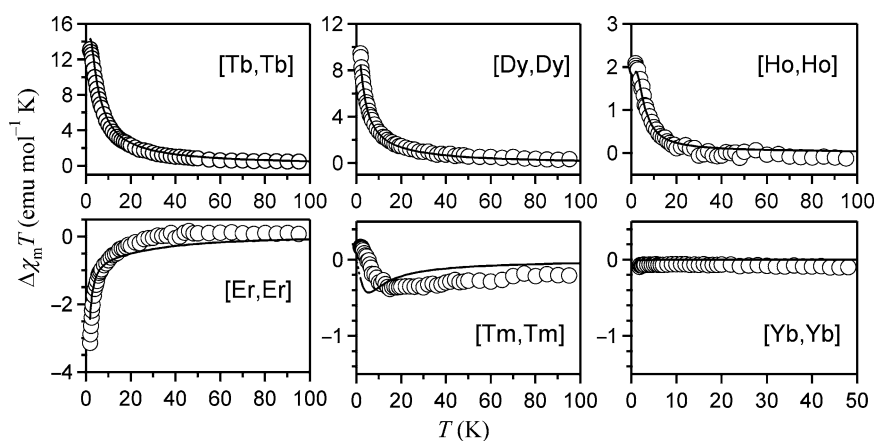
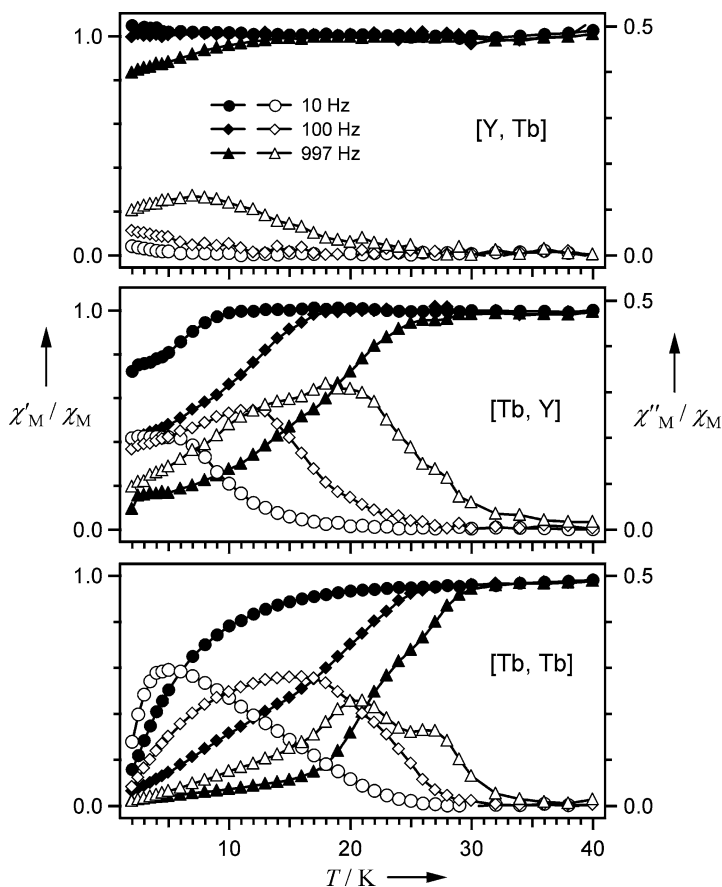


Fig. 12 The experimental and theoretical  $\Delta\chi_M T$  values of the six lanthanide cases. The experimental data and theoretical values are shown by circles and solid lines, respectively



**Fig. 13** Plots of  $\chi'_M/\chi_M$  (closed markers) and  $\chi''_M/\chi_M$  (open markers) against temperature  $T$ , where  $\chi'_M$ ,  $\chi''_M$  and  $\chi_M$  are in-phase-ac, out-of-phase-ac and DC molar magnetic susceptibilities, respectively, for a powder sample of [Y, Tb] (top), [Tb, Y] (center) and [Tb, Tb] diluted in a diamagnetic [Y, Y] matrix with a concentration of 5%

contains two peaks at 27 and 20 K. It appears as if the  $\chi''_M/\chi_M$  peaks of mono-Tb complexes are shifted to higher temperatures in the bis-Tb complex. This is, in fact, experimentally proved to be the case as follows.

Figure 14 shows the ac susceptibility data taken under non-zero dc magnetic field. As the dc field is increased, the  $\chi''_M/\chi_M$  peaks of the [Y, Tb] and [Tb, Y] complexes are shifted to higher temperatures. The shift reaches its maximum at a dc field of about 2,000 Oe. On the contrary, [Tb, Tb] does not change the positions of the two  $\chi''_M/\chi_M$  peaks. The positions of the shifted peaks of mono-Tb complexes almost coincide with the two peak of the bis-Tb complex. This clearly indicates that the two peaks of [Tb, Tb] at 27 and 20 K actually correspond to the  $\text{Tb}^{\text{III}}$  ions at the two different sites.



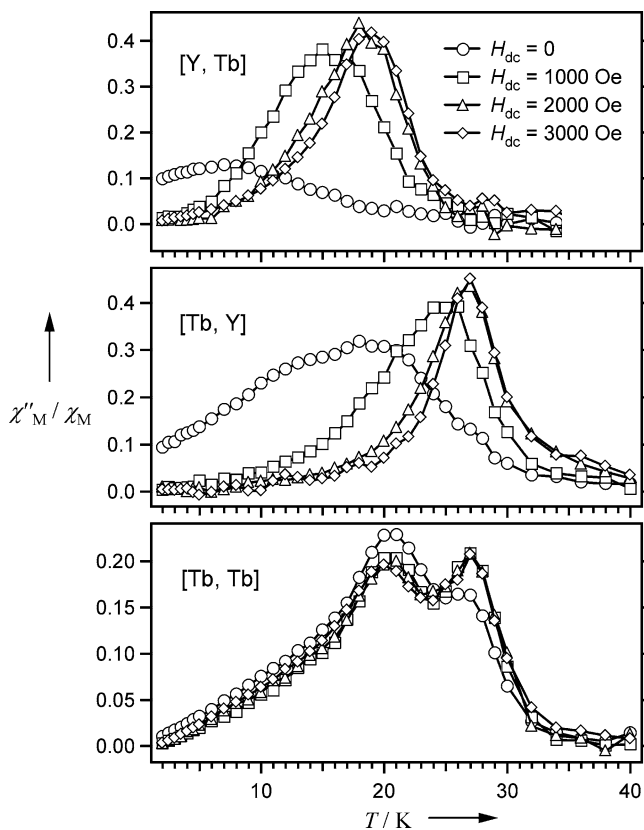


**Fig. 14** Plots of  $\chi''_M / \chi'_M$  against temperature  $T$  of [Y, Tb], [Tb, Y] and [Tb, Tb] measured in 5G ac magnetic field of 997 Hz with dc field  $H_{dc}$  of indicated magnitudes

The upward-temperature shift of the  $\chi''_M$  peaks in [Tb, Tb], as well as the small dc-field dependence of the ac susceptibility, is explained by the effect of the dipolar interaction, which prevents admixing of  $|+6\rangle$  and  $|-6\rangle$  states. In contrast, in the [Tb, Y] and [Y, Tb] case,  $|+6\rangle$  and  $|-6\rangle$  states can be mixed at zero magnetic field through off-diagonal LF terms. In other words, the effect of the “quantum tunneling of magnetization,” which governs the relaxation process of the mono-Tb complex in near zero magnetic fields, is removed in the [Tb, Tb] by the presence of  $f-f$  interaction.

## References

1. Lever ABP (1965) J Chem Soc 1821
2. Miyoshi H, Ohya-Mishiguchi H, Deguchi Y (1973) Bull Chem Soc Jpn 46:2724
3. Miyoshi H (1974) Bull Chem Soc Jpn 47:561

4. Barraclough CG, Martin RL, Mitra S, Sherwood RC (1970) *J Chem Phys* 53:1638
5. Mitra S, Gregson AK, Hatfield W, Weller R (1983) *Inorg Chem* 22:1729
6. Barraclough CG, Gregson AK, Mitra S (1974) *J Chem Phys* 60:962
7. Awaga K, Maruyama Y (1991) *Phys Rev B* 44: 2589
8. Yamada H, Shimada T, Koma A. (1998) *J Chem Phys* 108:10256
9. Williamson BE, VanCott TC, Boyle, ME, Christian Misener G, Stillman MJ, Schatz PN (1992) *J Am Chem Soc* 114:2412
10. Liao MS, Watts JD, Huang MJ (2005) *Inorg Chem* 44:1941
11. Wu W, Kerridge A, Harker AH, Fisher A (2008) *J Phys Rev B* 77:184403
12. Zerner M, Gouterman M (1960) *Theor Chim Acta* 4:44
13. Evangelisti M, Bartolome J, de Jongh LJ, Filoti G (2002) *Phys Rev B* 66:144410
14. Moriya T (1960) *Phys Rev* 177:635
15. Klemm L, Klemm W (1935) *J Prakt Chem* 143:82
16. Dale BW, Williams RJP, Johnson C E, Thorp TL (1968) *J Chem Phys* 49:3441
17. Stillman M, Thomson A (1974) *J Chem Soc, Faraday Trans* 70:790
18. Labarta A, Molins E, Viñas X, Tejada J, Caubet A, Alvarez S (1984) *J Chem Phys* 80:444
19. Coppens P, Li L, Zhu NJ (1983) *J Am Chem Soc* 105:6174
20. Lever ABP (1965) *J Chem Soc* 1821
21. Senff H, Klemm W (1939) *J Prakt Chem* 154:73
22. Mader HH (1962) *Z Phys Chem (Leipzig)* 218:71
23. Homborg H, Kalz W (1978) *Z Naturforsch* 33b:1067
24. Sugimono H, Higashi T, Mori M (1983) *J Chem Soc Chem Commun* 62;
25. Sugimoto H, Mori M, Masuda H, Taga T (1986) *J Chem Soc Chem Commun* 962
26. Turek P, Andre JJ, Giraudeau A, Simon J (1987) *Chem Phys Lett* 134:471
27. Brinkmann M, Chaumont C, Wachtel H, Andre J (1996) *Thin Solid Films* 283:97
28. Paillaud JL, Drillon M, DeCian A, Fiscer J, Weiss R, Poinot R, Herr A (1991) *Physica B* 175:337
29. Ishikawa N, Sugita M, Ishikawa T, Koshihara S, Kaizu Y (2003) *J Am Chem Soc* 125:8694
30. Ishikawa N, Sugita M, Ishikawa T, Koshihara S, Kaizu Y (2004) *J Phys Chem B* 108:11265
31. Sessoli R, Tsai HL, Schake AR, Wang S, Vincent JB, Folting K, Gatteschi D, Christou G, Hendrickson DN (1993) *J Am Chem Soc* 115:1804
32. Sessoli R, Gatteschi D, Caneschi A, Novak MA (1993) *Nature* 365:141
33. Thomas L, Lioni F, Ballou R, Gatteschi, D, Sessoli R, Barbara B (1996) *Nature* 383:145
34. Friedman JR, Sarachik MP (1996) *Phys Rev Lett* 76:3830
35. Eppley HJ, Tsai HL, de Vries N, Folting K, Christou G, Hendrickson DN (1995) *J Am Chem Soc* 117:301
36. Aubin SMJ, Spagna S, Eppley HJ, Sager R E, Christou G, Hendrickson DN (1998) *Chem Commun* 803
37. Aubin SMJ, Sun Z, Pardi L, Krzystek J, Folting K, Brunel LC, Rheingold AL, Christou G, Hendrickson DN (1999) *Inorg. Chem* 38:5329
38. Soler M, Chandra S K, Ruiz D, Davidson E R, Hendrickson DN, Christou G (2000) *Chem Commun* 2417
39. Boskovic C, Pink M, Huffman JC, Hendrickson DN, Christou G (2001) *J Am Chem Soc* 123:9914
40. Ishikawa N (2003) *J Phys Chem A* 107:5831
41. Ishikawa N, Sugita M, Okubo T, Tanaka N, Iino T, Kaizu Y (2003) *Inorg Chem* 42:2440
42. Ishikawa N, Sugita M, Wernsdorfer W (2005) *J Am Chem Soc* 127:3650
43. Ishikawa N, Sugita M, Wernsdorfer W (2005) *Angew Chem Int Ed* 44:2931
44. Friedman JR, Sarachik MP (1996) *Phys Rev Lett* 76:3830
45. Thomas L, Lioni F, Ballou R, Gatteschi D, Sessoli R, Barbara B (1996) *Nature* 383:145
46. Leuenberger MN, Loss D (2001) *Nature* 410:789
47. Ishikawa N, Iino T, Kaizu Y (2002) *J Phys Chem A* 106:9543
48. Ishikawa N, Sugita M, Iino T, Kaizu Y (2002) *J Am Chem Soc* 124:11440
49. Ishikawa N, Iino T, Kaizu Y (2002) *J Phys Chem A* 107:7879
50. Ishikawa N, Otsuka S, Kaizu Y (2005) *Angew Chem Int Ed* 44:731

# Phthalocyanines and Their Analogs Applied in Dye-Sensitized Solar Cell

Xiyou Li, Haixia Wang, and Haixia Wu

**Abstract** In this chapter, recent progress in the application of phthalocyanines and related tetrapyrrole metal complexes in dye-sensitized solar cell (DSSC) is summarized and analyzed. Three categories of phthalocyanines defined by the connecting positions of anchoring groups, namely symmetrically substituted phthalocyanines, asymmetrically substituted phthalocyanines and axially substituted phthalocyanines, are discussed separately. The effects of the distance of the dye molecule from the surface of the semiconductor nanoparticles, the redox potentials and the directionality of the anchoring groups on the performance of the dyes were reviewed. Porphyrins are good sensitizers to wide band semiconductors too. The performance of these sensitizers is predominantly affected by the nature, the connection position of the anchoring groups and the central metal ions. Modifications on the molecular structure of porphyrin by introducing different groups at different positions aimed at extending the absorption spectra, tuning the electronic configuration of the excited states, and inhibiting the aggregation are reviewed. The application of natural porphyrins as sensitizers in DSSCs is also discussed at the end of this chapter.

**Keywords** Photocurrent · Phthalocyanine · Porphyrin · Sensitizer · Solar cell

## Contents

1	Introduction .....	230
2	Phthalocyanine Sensitizers .....	231
2.1	Phthalocyanines with Anchoring Groups at Peripheral Positions.....	231
2.2	Phthalocyanines with Anchoring Groups at Axial Direction .....	240
2.3	Phthalocyanines Without Specific Anchoring Groups.....	244
3	Porphyrin Sensitizers .....	245
3.1	Porphyrin Monomers.....	246
3.2	Porphyrin Arrays .....	259
4	Natural Porphyrin Sensitizers .....	265

5 Conclusion .....	269
References .....	271

## Abbreviations

AAS	Atomic absorption spectrometry
BMI	Butylmethylimidazolium iodide
CNHs	Carbon nanohorns
DSSC	Dye-sensitized solar cell
H <sub>2</sub> Pc	Metal-free phthalocyanine
HOMO	Highest occupied molecular orbital
IPCE	Incident-photon-to-current-conversion efficiency
LUMO	Lowest unoccupied molecular orbital
MPc	Metal phthalocyanine
M-UP	Metallo-uroporphyrins
Q-CdSe	CdSe nano particle
RRS	Resonance Raman spectroscopy
tBu	<i>tert</i> -butyl
TCPP	Tetra( <i>p</i> -carboxylic acid)phenyl porphyrin
TsPP	Tetra( <i>p</i> -sulphonic acid) phenyl porphyrin
UPS	Ultraviolet photoemission spectroscopy
XPS	X-ray photoemission spectroscopy
ZnCyt-c	Zinc-substituted cytochrome c

## 1 Introduction

Energy is the most important issue for mankind in the twenty-first century because of the accelerating decrease in the reserves of fossil fuels and the more and more serious environmental problems (water pollution, green house effect etc.) caused by the excessive consumption of fossil fuels [1]. Looking for alternative renewable energy source for the sustainable development of our civilization is currently an inevitable and emergent assignment for scientists. Solar energy, which is an inexhaustible power flow from the sun carried by electromagnetic radiation, has already sustained the development of our civilization for several thousands of years in the form of fossil fuels [2]. How we can take full advantage of the extraordinary amount of energy that the sun supplies us with, by changing it into a directly usable and environmental friendly form is the main focus of the scientific research in this field [2–4].

Efforts that have been made so far to change the solar energy into a directly usable energy form for our daily life include the construction of artificial photosynthesis systems [5–8], building solar cell to convert light energy directly into electricity [9–13], and synthesis of molecular machine to convert light energy into mechanical energy at the molecular level [14–17]. It is worth noting that the research on artificial photosynthesis and molecular machine has led only to hopes, not fruits

so far, while the solar cell has already powered more than two million households around the world in areas where we do not have access to the central power networks [2]. The commercialized solar cells so far have been built from crystalline or amorphous silicon. There is an increasing awareness, however, that devices based on mesoscopic inorganic or organic semiconductors might show improved properties because of the interconnected three-dimensional structure. A device based on this interpenetrating network junctions has been developed by Grätzel and co-workers in the early 1990s, which demonstrated laboratory conversion efficiencies of up to 10.4% and represented a promising method for the large-scale conversion of solar energy into electricity. The key component of this device is a nanocrystalline wide-band-gap semiconductor electrode, which is associated with a sensitizer as a light-absorbing material. This device is called dye-sensitized solar cell (DSSC) or Grätzel cell [18–21].

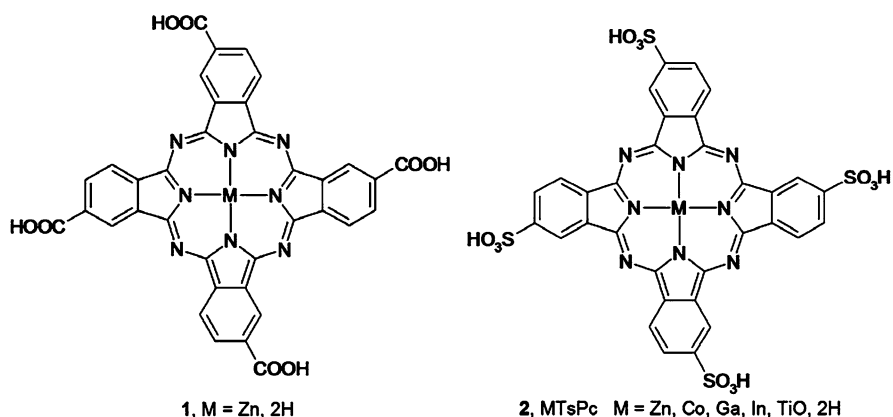
To achieve high power conversion efficiency, the sensitizer in the DSSC should be a dye, which absorbs across the entire visible spectrum, binds strongly to the surface of the semiconductor nanoparticles, has high redox potential for regeneration after excitation, and most importantly is stable enough to exposure to sunlight for many years. The ruthenium polypyridyl complexes utilized by Grätzel come close to fulfilling these requirements, although sensitization at longer wavelength could be improved because of the low optical absorbance in the red/near IR region [22, 23]. As several chlorophyll molecules with different structure are involved in the light collection in light-harvesting arrays of photosynthesis, it is likely that better photosensitization in DSSCs could be achieved by co-sensitization of several different dyes. In addition, the ruthenium complexes are expensive because of the increasing demand in industry. Therefore, a wide variety of dyes with different structures have been developed and tested as sensitizers in the DSSCs. Among these dyes, phthalocyanine and porphyrin compounds are particularly attractive because of their similar molecular structures and photophysical properties to chlorophylls [24–26]. In the present review, we discuss on the light-harvesting and the electron-injection properties of some phthalocyanine and porphyrin compounds, which have been tested as sensitizers in DSSCs.

## 2 Phthalocyanine Sensitizers

### 2.1 *Phthalocyanines with Anchoring Groups at Peripheral Positions*

Phthalocyanines are well known for their high stabilities toward heat and light, large extinction co-efficient in the near IR region, the controllable redox potentials, and most importantly, the semiconducting properties [27, 28]. They were employed in the study of photo-to-electron conversion long before. For example, the research conducted by Armstrong on the photovoltaic properties of metal free, copper, cobalt, titanyl, and vanadyl phthalocyanines in the 1980s has revealed that the packing structure affects the photoelectrochemical performance of the phthalocyanine

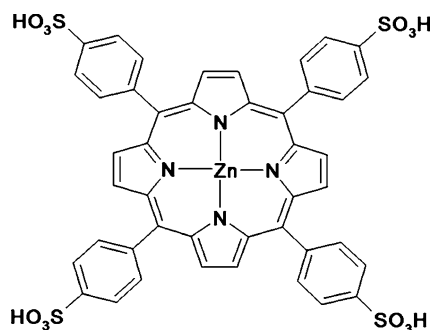
films [29–32]. Bard and co-workers had demonstrated that the behavior of the sensitized photocurrent by metal-free phthalocyanine ( $H_2Pc$ ) thin films on several single-crystal n-type semiconductors correlated well with the relative positions of the energy levels of the semiconductors,  $H_2Pc$ , and the redox couples in solution. The sensitization of different metal phthalocyanines (MgPc, ZnPc, AlClPc, TiOPc, CoPc, FePc,  $H_2Pc$ ) to  $TiO_2$  and  $WO_3$  was tested in a sandwich type cell. The efficiencies of the sensitized photooxidation of several redox couples are strongly dependent on the oxidation potential of MPC [33, 34]. All these researches revealed that phthalocyanines are promising sensitizers for semiconductor electrode in solar cell with different structures.



### 2.1.1 Symmetrically Substituted Phthalocyanines

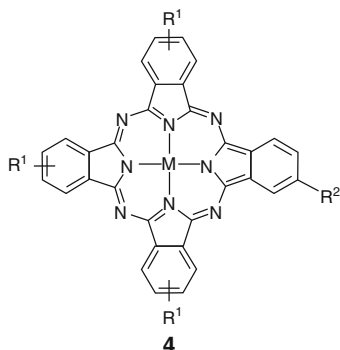
After the invention of Grätzel cell in 1991, the importance of the binding of sensitizer on the surface of the nano-crystalline semiconductor electrode was realized and therefore phthalocyanines with anchoring groups were prepared and employed in the sensitization of nano-crystalline semiconductor electrode. The first report on the sensitization of titanium dioxide nanoparticles by phthalocyanine functionalized with carboxylic acid groups appeared in 1995 [35]. Shen and Xu prepared a zinc phthalocyanine (ZnPc) substituted with four carboxylic groups at the peripheral positions (**1**). After the adsorption of this phthalocyanine onto the surface of electrode, the absorbance of the titanium dioxide electrode was extended successfully to the visible region. At the maximum absorption band of phthalocyanine (690 nm), the incident-photon-to-current-conversion efficiency (IPCE) is about 4%, one of the highest ever reported for phthalocyanine-based photovoltaic devices. The improvement on IPCE is attributed to the fact that almost all the ZnPc molecules are in direct contact with the  $TiO_2$  surface because of the extra large surface area of the nano-crystalline electrode. Later, the same research group modified the structure of the electrode further by introducing a layer of CdSe nano particle (Q-CdSe) onto the titanium dioxide electrode before phthalocyanine **1** was deposited. Since the optical absorption spectra of Q-CdSe particles and phthalocyanine molecules

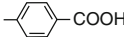
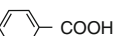
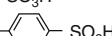
are different, a better spectral match to solar spectrum was achieved for ZnTCPc–CdSe/TiO<sub>2</sub> electrode. The IPCE was therefore increased to ca. 10% at the point of the maximum absorption peak at 690 nm [36, 37].



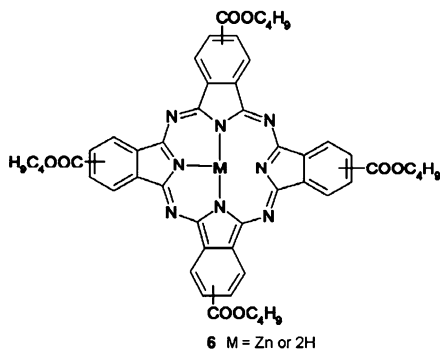
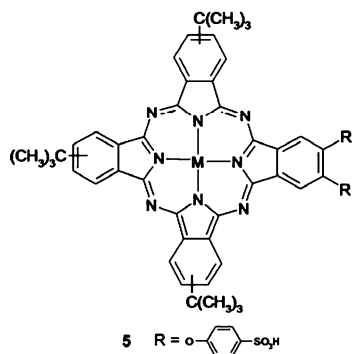
**3, TsPP**

Sensitization of nano-crystalline electrode by sulphonated phthalocyanine (**2**) with different central metals was also tested. Absorption spectroscopy of tetrasulphonated Zn, Co, Ga, In, TiO and metal-free phthalocyanine on a transparent titanium dioxide film electrode, which is made up of interconnected particles and pores has revealed the formation of aggregates of phthalocyanines at the surface of the electrode. Comparison of the photocurrent action spectra with the absorption spectra of the electrode reveal that the photocurrent generated only from the absorption of monomeric phthalocyanines. The aggregated phthalocyanine molecules do not contribute to the photocurrent generation. The rapid internal conversion in the molecular aggregates of phthalocyanines, which causes rapid deactivation of the excited states, hindered the electron injection from the excited phthalocyanine molecules to TiO<sub>2</sub> [38, 39]. In order to reduce the aggregation of phthalocyanines at the surface of the electrode, the same group introduced a doping process for the solid films of **2** (GaTsPc) with tetrasulphonated Zn porphyrin **3** (ZnTsPP). The doping has successfully extended the absorption of GaTsPc-sensitized TiO<sub>2</sub> electrode and thus enhanced the light-harvesting efficiency probably because of the spectral complementarities of GaTsPc and ZnTsPP. More importantly, the photocurrent response at the Q band of GaTsPc is remarkably enhanced with 20- or 60-fold improvement, while the photocurrent response at the Soret band of ZnTsPP is markedly decreased eight-fold. This photoelectric behavior is attributed to the possible formation of phthalocyanine/porphyrin heteroaggregates during the cosensitization of the TiO<sub>2</sub> electrode, which prevents the formation of GaTsPc aggregates on the one hand and leads to a low-lying charge separated state between porphyrin and phthalocyanine on the other hand. The latter quenches the photogenerated charge carriers of the Soret band of ZnTsPP [40, 41].



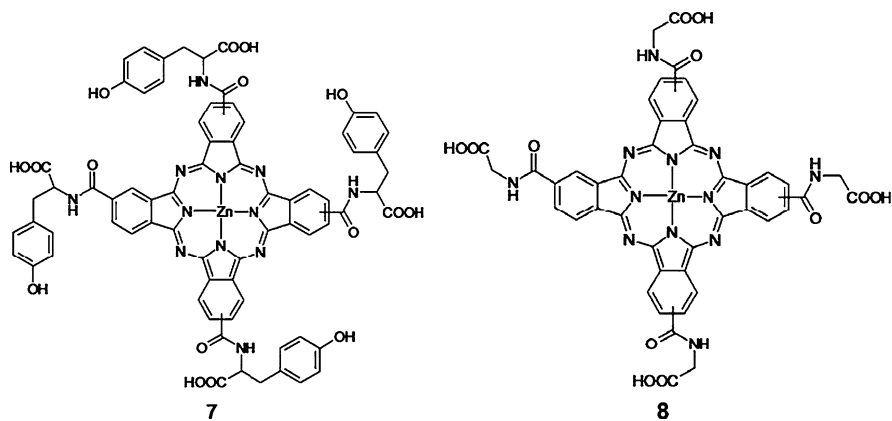
- a.  $M = \text{Zn(II)}$ ,  $R^1, R^2 = \text{COOH}$   
 b.  $M = \text{Al(III)OH}$ ,  $R^1, R^2 = \text{COOH}$   
 c.  $M = \text{Zn(II)}$ ,  $R^1, R^2 = \text{O}$    
 d.  $M = \text{Zn(II)}$ ,  $R^1, R^2 = \text{O}$    
 e.  $M = \text{Zn(II)}$ ,  $R^1 = \text{C(CH}_3)_3$ ,  $R^2 = \text{O}$    
 f.  $M = \text{Zn(II)}$ ,  $R^1 = \text{C(CH}_3)_3$ ,  $R^2 = \text{O}$    
 g.  $M = \text{Zn(II)}$ ,  $R^1, R^2 = \text{SO}_3\text{H}$   
 h.  $M = \text{Al(III)OH}$ ,  $R^1, R^2 = \text{SO}_3\text{H}$   
 i.  $M = \text{Zn(II)}$ ,  $R^1, R^2 = \text{O}$    
 j.  $M = \text{Zn(II)}$ ,  $R^1 = \text{C(CH}_3)_3$ ,  $R^2 = \text{O}$  

An extensive study on the sensitizing properties of phthalocyanines to  $\text{TiO}_2$  nano-crystalline electrode was reported by Grätzel and co-workers in 1998. They connected carboxylic groups to the zinc(II) or aluminum(III) phthalocyanine ring with different linkages and prepared a series of phthalocyanine compounds which can anchor to the surface of  $\text{TiO}_2$  nanoparticles (**4** and **5**). To get an efficient electron injection from phthalocyanines to the electrode, the anchoring groups should be connected to the phthalocyanine ring as close as possible. Both sulphonyl and carboxylic acid groups could achieve a stable binding to the surface of  $\text{TiO}_2$ , which did not present significant influence on the electron injection. The  $\text{ZnPc}$  presented peak IPCE as high as 45%, whereas aluminum phthalocyanine under identical conditions gave only 15% IPCE. This result suggested that the central metal of phthalocyanine played an important role in the sensitizing process. By introducing small organic molecules, which can coordinate to the central metal ions of phthalocyanine along the axial direction, the aggregation of phthalocyanines can be harnessed efficiently. Similarly, the aggregation of phthalocyanines on the surface of  $\text{TiO}_2$  nanoparticles can also be reduced efficiently by introducing *tert*-butyl groups at the peripheral positions. This provides a facile way to improve the sensitizing efficiency of phthalocyanines. The most notable finding of this research is that phthalocyanines are strikingly stable on the surface of  $\text{TiO}_2$  under continuous light exposure. It is expected that phthalocyanines could be applied in the solar cells which can transmit some visible light but absorb strongly in the near IR region [42].





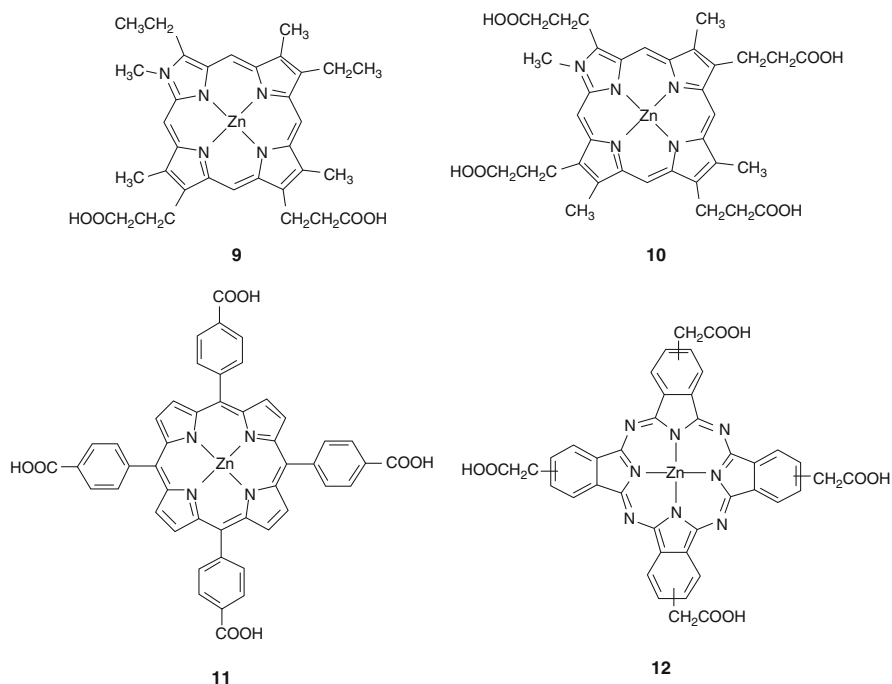
Anchoring groups in the ruthenium (II) polypyridyl complexes are proven to be essential for the sensitization [20, 43]. The carboxylate groups establish good electronic coupling with the Ti (3d) conduction band orbital manifold. However, phthalocyanines with carboxylic acid groups have poor solubility in organic solvents and are difficult to be purified. Therefore, He and co-workers have developed an alternative anchoring method for phthalocyanines. This new method includes a deprotonation step of the surface of TiO<sub>2</sub> with (CH<sub>3</sub>)<sub>3</sub>COLi and then followed with a reaction of ester groups of phthalocyanine with the deprotonated surface of TiO<sub>2</sub>. With this method, He and co-workers had successfully deposited free-base and zinc 2,9,16,23-tetra(*n*-butoxycarbonyl)phthalocyanines (**6**) onto the TiO<sub>2</sub> nano-crystalline electrode. The IPCEs measured for the metal free and ZnPc were 0.30% and 4.3% respectively, indicating that ZnPc is a better sensitizer for TiO<sub>2</sub> than metal free phthalocyanine [44]. Later, He and co-workers connected tyrosine (**7**) and glycine (**8**) groups to the peripheral positions of phthalocyanine and successfully prepared a Grätzel type cell with high IPCE (24%). Incorporation of tyrosine groups makes the dye ethanol-soluble and decreases considerably surface aggregation of the sensitizer due to the steric effects and as a result improves the solar cell performance. The transient absorption spectra revealed that the electron injection from phthalocyanine to the conduction band of TiO<sub>2</sub> occurred in ~ 500 fs while the charge recombination happened in ~ 300 ps. Comparing with those of bipyridyl ruthenium complexes, the faster charge recombination is the dominating factor, which encumbers a better sensitization [45].



In order to clarify the electron injection and recombination process, the alignment of the energy levels at the interface between phthalocyanine **8** and TiO<sub>2</sub> were studied by the combination of X-ray photoemission spectroscopy (XPS) and ultraviolet photoemission spectroscopy (UPS) measurements. The results indicate that energy of the LUMO of **8** (0.1 eV above that of the conduction band of TiO<sub>2</sub>) fits well with the energy requirements for efficient electron injection into the conduction band of TiO<sub>2</sub> from the excited state of the molecule. However, the fast charge recombination caused the low conversion efficiency. Tuning the redox potential matching between the dye and the redox couple in the electrolyte or adding electron donating groups

around phthalocyanine to suppress the charge recombination process are expected to be efficient ways to improve the conversion efficiency of the solar cell [46].

With the help of transient absorption spectra, Durrant and coworkers had systematically examined the dependence of the charge recombination kinetics upon the dye oxidation potential and spatial separation of the dye HOMO orbital from the metal oxide surface. The dyes they used include a series of ruthenium bipyridyl dyes in addition to porphyrin and phthalocyanine dyes (**9–12**). A strong correlation is observed between the recombination dynamics and the spatial separation, which is found to be in agreement with electron tunneling theory. However, the recombination dynamics were not insensitive to the variations in redox potential of dyes because the free energy changes of the recombination reaction lying near the peak of the Marcus free energy curve. This research has pointed out for the first time that to get a better conversion efficiency, the distance between the dye and the nanoparticle surface is crucial and the shorter distance between the dye and the surface of the nanoparticle will not definitely lead to higher conversion efficiency [47].

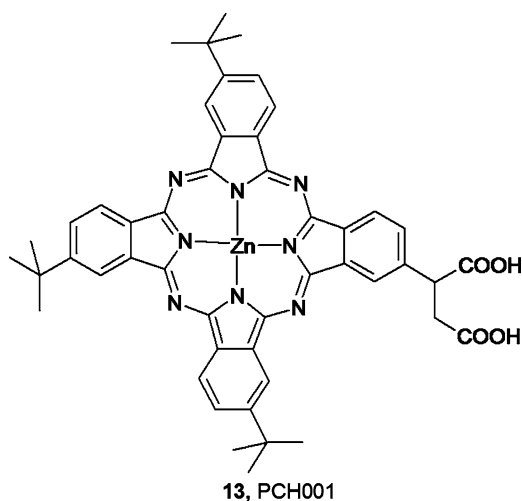


### 2.1.2 Asymmetrically Substituted Phthalocyanines

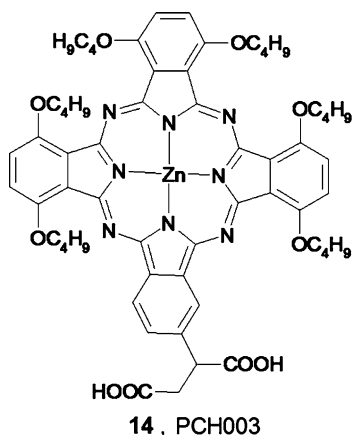
In order to achieve efficient sensitization of a nano-crystalline TiO<sub>2</sub> electrode, the sensitizer requires not only proper energy levels but also directionality for their excited states. The directionality should be arranged to provide an efficient electron transfer from the excited dye to the TiO<sub>2</sub> conduction band by good electronic

coupling between the lowest unoccupied molecular orbital (LUMO) of the dye and the Ti(3d) orbital. The energy levels of LUMO of phthalocyanines can be tuned by incorporation of electron donating or withdrawing groups at bay or peripheral positions. The directionality of LUMO can be varied by changing the relative orientation of phthalocyanine ring toward the surface of TiO<sub>2</sub> nanoparticle. Therefore, the substituents around the phthalocyanine ring are endowed with two different functionalities, tuning the energy level of LUMO and the orientation of the phthalocyanine aromatic plane at the same time. This requirement leads to the development of phthalocyanine sensitizers with asymmetrically distributed substituents.

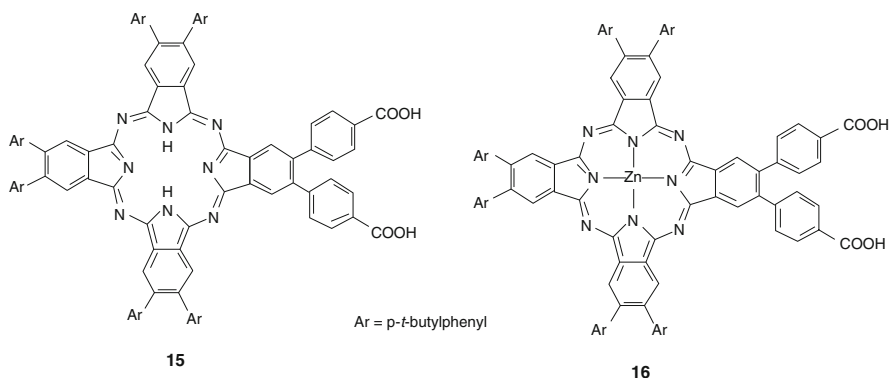
In 1999, Nazeeruddin and co-workers reported the first example of the application of asymmetrical phthalocyanine in DSSC. They have tested several asymmetrically substituted phthalocyanines (see **4** and **5** for the structures) with both alkyl groups and -COOH or SO<sub>3</sub>H anchoring groups and zinc or aluminum central metals. But the results revealed that these compounds do not show any advantages over the corresponding symmetrically substituted compounds under identical conditions [42]. However, the continued efforts on the research of asymmetrical phthalocyanines have seen a large progress recently. Nazeeruddin designed a novel asymmetrical phthalocyanine (**13**) with three *tert*-butyl groups and one carboxylic acid anchoring group attached at the peripheral positions. The *tert*-butyl groups together with the carboxylic acid groups act as “push-pull” groups, which tune the energy levels of LUMO. The carboxylic acid groups graft the dye molecules onto the surface of TiO<sub>2</sub> to provide intimate electronic coupling between its excited-states and the conduction-band manifold of the semiconductor. The bulky *tert*-butyl groups can also minimize the aggregation due to the large steric hindrance. The IPCE of the standard Grätzel solar cell based on **13** is as high as 75% at 680 nm and an overall power conversion efficiency of 3.05% is achieved. The most impressive is that this compound presents high IPCEs in solid state cell as well. This research has successfully demonstrated the importance of creating directionality of the excited states in the design of new phthalocyanine sensitizers [48].



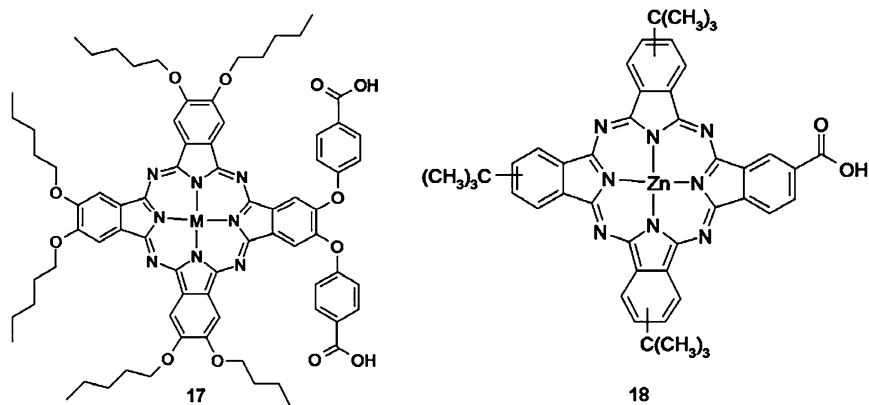
On the basis of the same “push–pull” strategy, Giribabu and co-workers designed a series of phthalocyanine compounds (**14**) with electron donating groups connected at the bay positions of phthalocyanine and the same anchoring groups with that of compound **13** at peripheral positions. But the IPCE of the solar cell made from **14** is significantly smaller than that made from compound **13**. The low IPCE can be certainly attributed to a low electron-injection yield, because a residual fluorescence emission was detected upon adsorption of the dye on TiO<sub>2</sub>. This suggests that the radioactive process competes with the electron injection, thus decreasing the branching ratio between these two deactivation channels [49].



The “push–pull” strategy has also been employed in the design of a series of asymmetrical metal free (**15**) or ZnPc (**16**) with large steric hindrance. In this series of phthalocyanines, the aryl groups (phenyls) were connected directly to the peripheral positions. Since the two neighboring peripheral positions are occupied by the same functional groups, these compounds can be isolated free of regioisomers. The large steric hindrance of the phenyl groups at the peripheral positions are expected to reduce the tendency of aggregation remarkably. The carboxylic acid groups could guarantee stable immobilization of the dye molecule on the surface of TiO<sub>2</sub> nanocrystalline. The Grätzel cell based on **15** does not show any photocurrent response because of the low laid first excited state. However, the ZnPc **16** presents 0.57% power conversion efficiency and 4.9% peak IPCE. Introduction of axial coordination compound (chenodeoxycholic acid) do not show noticeable difference on the cell performance, indicating the aggregation of **16** has been suppressed by the large steric hindrance effectively. The performance of the cell based on **16** is not as good as that based on **13**. This could be attributed to the small driving force for the electron injection from the dye molecule to TiO<sub>2</sub> as well as the poor electronic coupling between the LUMO of phthalocyanine and the conduction band of TiO<sub>2</sub> due to the larger distance between the surface of TiO<sub>2</sub> nanoparticle and sensitizer molecule [50].



A ruthenium phthalocyanine complex with peripheral linked carboxylic groups and axial coordination (**17**) has been tested as sensitizer for TiO<sub>2</sub> nanocrystalline electrode. The phthalocyanine molecules were anchored onto the surface of TiO<sub>2</sub> with the macrocyclic plane assumed to be perpendicular to the semiconductor surface while the 4-methylpyridine axial ligand served to prevent aggregation. An IPCE of 23% at the absorption peak and overall conversion efficiency of 0.40% were recorded for the testing DSSCs. However, the Zn analog, without the axial picoline ligands, exhibited poorer efficiency and was attributed to the aggregation. This finding has revealed the high efficiency of the axial coordinated groups on reducing the aggregation of phthalocyanines and provided a promising way to improve the sensitization performance of phthalocyanines [51].



For the purpose of reducing the aggregation of phthalocyanines on the surface of TiO<sub>2</sub>, co-deposition of asymmetrical substituted phthalocyanine with chenodeoxycholic acid has also been employed. The co-deposition of chenodeoxycholic acid with phthalocyanine **18** is expected to reduce the aggregation further and thus could

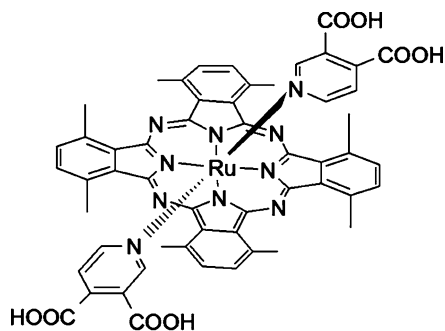
improve the performance of the solar cell. The absorption spectra of the solid electrode revealed that the presence of chenodeoxycholic acid indeed suppresses the aggregation of phthalocyanine, but reduced the phthalocyanine sensitizer's load too, as observed from the absorption and IPCE data. The decrease in the load of sensitizers induced a significant drop on the IPCEs [52].

Co-adsorption strategy has also been extended to two dye systems with the desire of expanding the responding spectra of the electrode and improving the overall conversion efficiency. A successful example was presented by Nazeeruddin and co-workers in 2007 [53]. They co-adsorbed phthalocyanine **18** and a triaryl amino dye (JK2) onto the surface of TiO<sub>2</sub>. An astounding increase on IPCE was observed for the solar cell based on this co-sensitized electrode. The IPCE at 690 nm was recorded as high as 80% with an overall energy conversion efficiency of 3.52% under standard illumination conditions. The time resolved emission spectra revealed efficient electron injection from the excited states of the sensitizer to the conduction band of TiO<sub>2</sub> with very fast kinetics. The laser transient-absorption spectroscopy measurement indicates a charge recombination lifetime of 3.2 ms, which is of the same order of magnitude as that of the standard ruthenium dye used for efficient DSSC devices. Improving the conversion efficiency by co-sensitization with two or more dyes with compensated absorption spectra has been highlighted by Robertson in 2008 [54]. The co-sensitization strategy may take the overall energy transfer efficiency beyond the high of 10–11% in the near future [53,55].

## 2.2 *Phthalocyanines with Anchoring Groups at Axial Direction*

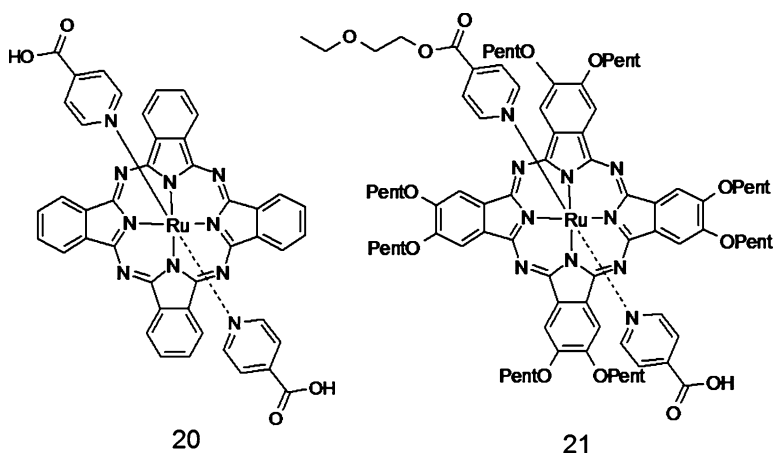
Aggregation of phthalocyanines on the surface of TiO<sub>2</sub> nanoparticles always induces significant drop on the overall energy conversion efficiency because of the rapid non-radioactive deactivation of the dye excited states in aggregates. Axial coordination has been proved to hinder the aggregation of phthalocyanine efficiently. Therefore the axial ligand functionalized with carboxylic acid groups are expected not only to hinder the aggregation, but also to graft the phthalocyanines to TiO<sub>2</sub> in a “face-on” configuration.

Ruthenium phthalocyanine complexes have spectral, electronic, photoelectrochemical and redox properties that satisfy the requirement of a good sensitizer for DSSC and have therefore been targeted for investigation. Nazeeruddin has reported the first use of a ruthenium phthalocyanine (**19**) as a sensitizer in a DSSC in 1998. In this compound, eight methyl groups were connected at the bay positions while 3,4-dicarboxypyridine was connected at the axial direction by coordination. The carboxylic acid groups help anchoring the dye molecule on the surface of TiO<sub>2</sub>. The resulting DSSC had an IPCE of over 60% in the near IR region (660 nm). This research established an efficient new pathway for adsorption of phthalocyanines onto the surface of TiO<sub>2</sub> [56].



19

Yanagisawa had compared the sensitization properties of an axially anchoring phthalocyanine (**20**) with that of a peripherally substituted phthalocyanine (**21**) in the identical conditions. Phthalocyanine **20** with axially connected carboxylic acid groups can sensitize the  $\text{TiO}_2$  electrode efficiently with an IPCE of 21% at 640 nm and an overall conversion efficiency of 0.61% was found for the standard testing DSSC. When pentyloxy groups were introduced at the peripheral positions and extra axial coordination groups introduced to prevent the aggregation, phthalocyanine **21** showed a less efficient sensitization to the  $\text{TiO}_2$  electrode relative to phthalocyanine **20** with the IPCE decreased to 6.6% at 640 nm and an overall energy conversion efficiency reduced to 0.58%. The reduced sensitization performance of **21** was attributed to the pentyloxy groups at peripheral position, which may reduce the stability of the adsorption of phthalocyanine **21** on the surface of  $\text{TiO}_2$  [57].



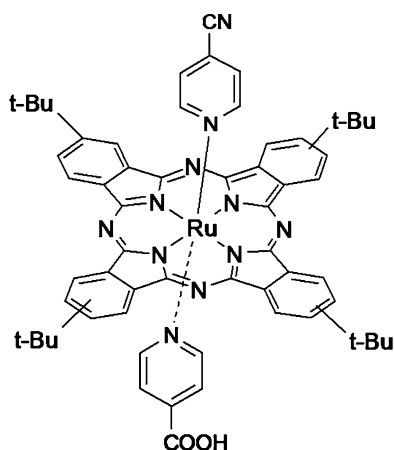
20

21

The X-ray and UV-photoemission spectroscopy study has revealed that ruthenium (II) phthalocyanine **20** has similar HOMO and LUMO energy with that of *cis*-bis(4,4-dicarboxy-2,2-bipyridine)-bis-(isothiocyanato)-ruthenium(II),  $[\text{Ru}(\text{dcbpy})_2(\text{NCS})_2]$ , the most efficient sensitizer so far. The oxidation potentials for both

ground and excited states are also similar for these two complexes. The energy difference between the LUMO of phthalocyanine **20** and the  $\text{TiO}_2$  conduction band was favorable for an efficient electron injection from phthalocyanine to  $\text{TiO}_2$ . This result suggests that ruthenium phthalocyanines, like **20**, are principally very promising sensitizers for DSSC [58].

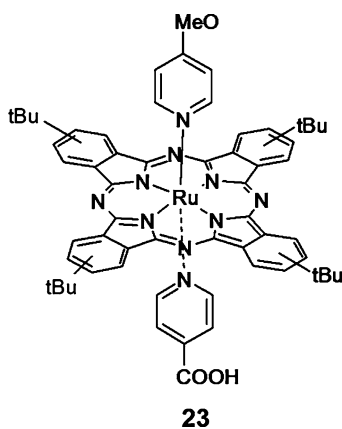
The electron injection from ruthenium phthalocyanine with axially connected anchoring group to  $\text{TiO}_2$  was further investigated by Durrant and co-workers with transient absorption experiments. They employed a ruthenium phthalocyanine with two axially coordinated pyridine groups (**22**). One of the axially connected pyridine bears a carboxylic acid group, which serve as a binding site, while the other one is substituted with a CN. The research reveals surprisingly that the electron injection is from the triplet states of ruthenium phthalocyanine. The long lifetime of the triplet states leads to efficient electron injection occurred in hundreds of nanoseconds and an IPCE magnitude of 45%. This finding suggests clearly that the ultrafast electron injection from the singlet states is not a prerequisite for high IPCEs. Optimizing the kinetics of the triplet states of ruthenium phthalocyanines might be a key factor to achieve a high IPCE for the ruthenium phthalocyanine-sensitized solar cell [59].



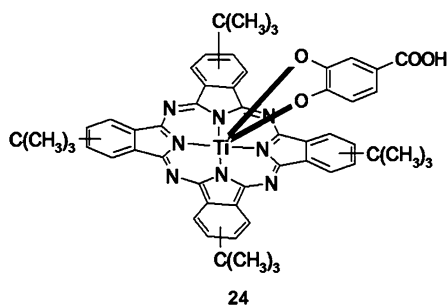
Compared with the ruthenium polypyridyl complexes (N719), most of phthalocyanine dyes used for the sensitization of  $\text{TiO}_2$  gave significantly lower output voltages. For a deep understanding of this output voltage reducing, O'Regan and co-workers has investigated the electron injection and recombination process of a ruthenium phthalocyanine (**23**) with different axial coordinated groups at the interface of  $\text{TiO}_2$  or  $\text{SnO}_2$ . Compared with the polypyridyl ruthenium complexes, the charge recombination processes are accelerated by the ruthenium phthalocyanine probably because of the binding of phthalocyanine with  $\text{I}_2$  which causes significant



increase on the local concentration of  $I_2$  close to the surface of the  $TiO_2$ . This accelerated charge recombination process induces the drop of output voltage of DSSC. The problem with these ruthenium phthalocyanines is inherent in the structure and is shared with other organic dyes with large aromatic rings, including porphyrins, coumarins, perylenes, cyanines, merocyanines, and azulene. Uncovering the mystery between the structure and charge recombination rate is a key step to improve the sensitization of organic dyes to the  $TiO_2$  nano particle further [60].

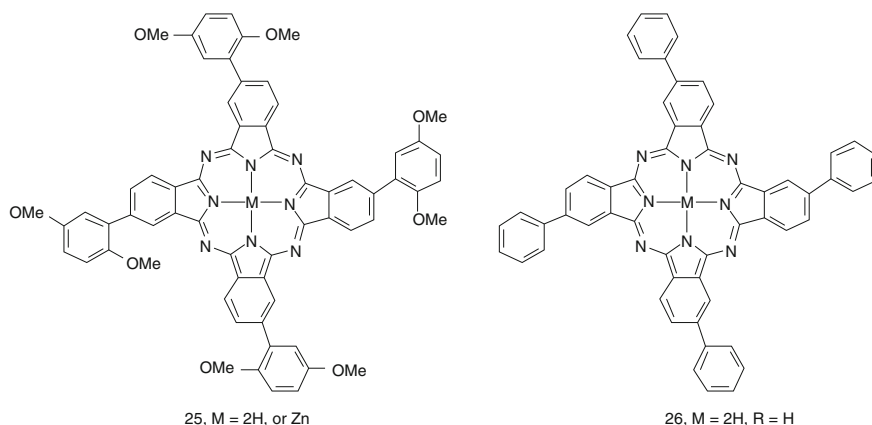


Durrant and co-workers has also prepared a novel titanium phthalocyanine (**24**) with the anchoring groups attached at the axial direction. The choice of Ti as a central metal allows axial ligation to the metal center, which is expected to reduce the aggregation efficiently. The carboxylic acid group on the axial ligand can anchor the dye to the nanocrystalline particles with the plane of the phthalocyanine ring parallel to the surface of the nanoparticle. The bulky peripheral *tert*-butyl groups help to solubilize the dye in conventional organic solvents as well as to avoid dye aggregation. Moreover, the distance between the HOMO orbital of the chromophore and the  $TiO_2$  surface can be controlled by the axial ligation. The absorption spectra of the electrode revealed a large dye molecule loading and the absence of aggregation for the dye molecules adsorbed. The quick electron injection from phthalocyanine to  $TiO_2$  is suggested by the strong quenching of the fluorescence of phthalocyanine and it is further confirmed by the transient absorption studies. However, the electron injection is wavelength dependent. The efficient electron injection happened after Soret band excitation, but only negligible electron injection occurred after the Q-band excitation. The observation has shown for the first time the potential of titanium phthalocyanine for the sensitization of nanocrystalline  $TiO_2$  films. The combination of catechol axial attachment to the  $TiO_2$  surface and *tert*-butyl peripheral groups allows efficient sensitization with no dye aggregation. These titanium phthalocyanines represent an attractive route to the development of efficient, red absorbing sensitizer dyes for DSSC [61].

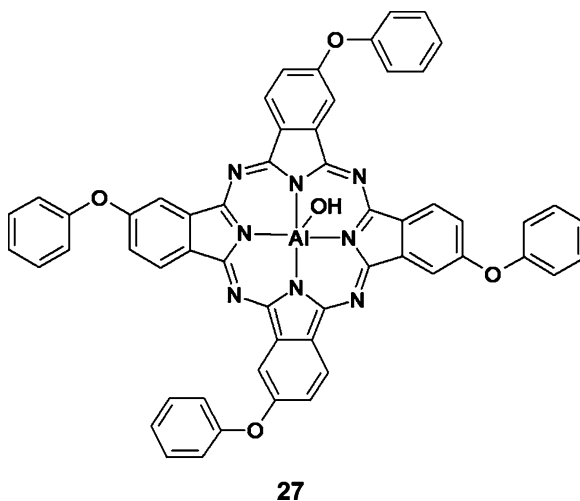


### 2.3 Phthalocyanines Without Specific Anchoring Groups

Although plenty of researches revealed that anchoring groups on phthalocyanine are essential for the sensitization, several phthalocyanines without anchoring groups can indeed sensitize the TiO<sub>2</sub> electrode with reasonable efficiency. Aranyos and co-workers have reported that a series of metal free phthalocyanines (**25**, **26**) with aryl groups connected at the peripheral positions show surprising sensitization to TiO<sub>2</sub> nano-crystalline electrode. Despite the absence of conventional anchoring groups in compound **25** and **26**, such as -COOH or SO<sub>3</sub>H, the DSSC based on these compounds show reasonable IPCEs in the range of 5–9%. It is the aryl groups connected at the peripheral positions that are designated to facilitate the absorption of dyes at the surface of the nanoparticles. More interestingly, these compounds show sensitization even in aggregated states. Although without further discussion on how the aggregated phthalocyanines inject electrons to TiO<sub>2</sub>, one should suspect a quicker electron injection from these aryl substituted phthalocyanines than that from phthalocyanines with -COOH or SO<sub>3</sub>H. The results also indicate that not only the directly adsorbed monolayer of dye injects electrons into the oxide, but also the molecules aggregated on top of this layer contribute to the photocurrent [62].

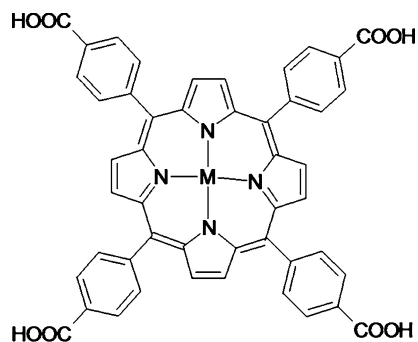


In 2003, another phthalocyanine (**27**) with aluminum in the center but without  $-\text{COOH}$  or  $\text{SO}_3\text{H}$  as anchoring groups attached has been successfully applied in the Grätzel type cell. To prevent the aggregation of the phthalocyanine molecules on the surface of the electrode, an alkyl carboxylic acid with long alkyl chain (myristic acid) has been deposited to the surface of the electrode simultaneously. The peak IPCE of the electrode sensitized by **27** and myristic acid has been promoted for 1.7 times relative to that sensitized by pure **27**. The results indicate that the addition of myristic acid can suppress the aggregation of phthalocyanine significantly and thus improve the performance of the solar cell [63]. The successful sensitization of  $\text{TiO}_2$  nano-crystalline electrode by phthalocyanine **25–27** strongly suggests that the aryl groups connected at the peripheral positions might be efficient anchoring groups too. Careful design on the connection position and the functionality on the aryl groups might lead to unpredictable results. More attention should be paid to these non-carboxylic acid anchoring phthalocyanines in the near future.



### 3 Porphyrin Sensitizers

The use of porphyrins as sensitizers for the nano-crystalline electrode in DSSC is particularly attractive given their important role in photosynthesis and the relative ease modification on molecular structure. Not only the porphyrin monomers, but also the large porphyrin arrays have been tested extensively as sensitizers of wide-band-gap semiconductors like  $\text{NiO}$ ,  $\text{ZnO}$  and  $\text{TiO}_2$  in the past several decades. The focus of this section is the various molecular structure modification of porphyrins for the purpose of applying as sensitizer in DSSCs.

**28** M=2H, Zn

### 3.1 Porphyrin Monomers

#### 3.1.1 Porphyrins with Anchoring Groups Connected at *Meso*-Phenyls

The most commonly used porphyrins in DSSC are free-base and zinc derivatives of the *meso*-benzoic acid substituted porphyrin **TCPP** (**28**). Grätzel and co-workers had investigated the sensitization of **28** to TiO<sub>2</sub> in 1987. The energy levels of LUMOs reside right above the conduction band of the TiO<sub>2</sub>, which ensure an efficient electron injection from the excited states to the conduction band as revealed by the steady state fluorescence and transient absorption spectra. The electron injection process was found to be very sensitive to the pH of the solution. No sensitization was observed in alkaline solution because of lack of adsorption of the anionic dye on the negatively charged surfaces of TiO<sub>2</sub>. The electron injection can occur only from the adsorbed porphyrin molecules [64]. The efficient electron injection was further proved by the work of Fox and co-workers in 1988 [65]. In a DSSC with **28** as sensitizer, Goossens and co-workers found that the electron traps at the interface of dye/TiO<sub>2</sub> affected the energy conversion efficiency significantly. The electronic traps can be filled by a negative potential applied at the interface and therefore enlarge the active region where charge separation takes place, which finally leads to an enhanced collection efficiency [66].

The sensitization behavior of porphyrin with or without carboxylic acid groups was compared by Waclawik and co-workers. Their results indicate that the presence of carboxylic acid groups indeed generated higher IPCE values compared to that without carboxylic groups. The difference is ascribed to poor electronic coupling of the sensitizer without carboxylic acid groups to the titania conduction band [67].

Wamser and co-workers have investigated the nature of the binding of **28** onto the TiO<sub>2</sub> electrodes by using X-ray photoelectron spectroscopy (XPS) and Resonance Raman Spectroscopy (RRS). The XPS spectra of TiO<sub>2</sub> revealed the changes of the binding energy of both O (1s) and Ti (2p<sub>3/2</sub>) upon adsorption of **28**.

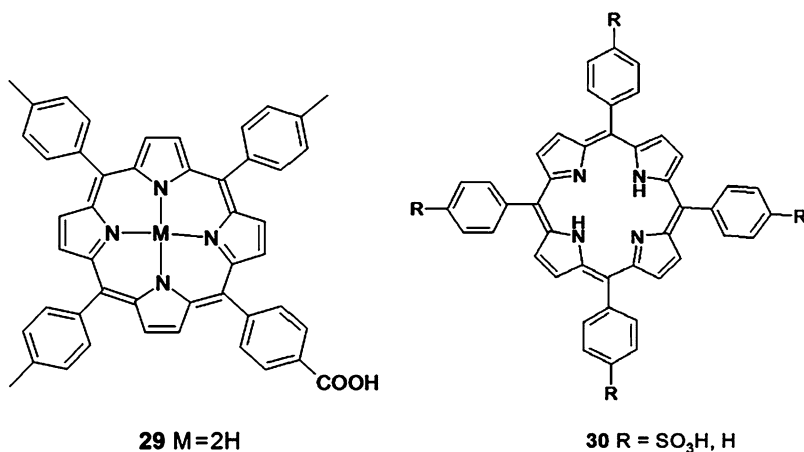
Similarly, the peaks of O (1 s) and N (1 s) of **28** were also shifted to a higher binding energy. All these changes suggest the efficient binding of **28** on the surface of TiO<sub>2</sub>. The RRS results indicated that for cases in which **28** was adsorbed onto TiO<sub>2</sub> films from a much diluted solution, the porphyrin molecules interact mainly with the TiO<sub>2</sub> surface. Contrarily, if porphyrin were adsorbed onto the TiO<sub>2</sub> films from a concentrated solution, the RRS spectra were similar to that of TCPP powder, indicating the dominance of porphyrin–porphyrin interactions in this film. The optimized Grätzel cells with **28**-sensitized TiO<sub>2</sub> and deoxycholic acid as co-adsorbent gave good solar-energy conversion efficiencies. The IPCE was 55% at the Soret peak and 25–45% at the Q-band peaks and an overall energy conversion efficiency of about 3% [68]. The chemical adsorption of TCPP on the surface of TiO<sub>2</sub> nanoparticle was also confirmed by XPS, atomic absorption spectrometry (AAS), Fourier transform infrared spectroscopy (FT-IR) and UV-vis spectroscopy, etc. [69].

Durrant and co-workers have compared the electron injection and recombination processes of **28** or Zn-**28** with that of N3 (a famous ruthenium polypyridyl complex with very high IPCE). Their experiments revealed that the electron injection and recombination kinetic for these three dyes on the surface of TiO<sub>2</sub> are almost identical. The high IPCE for N3 dye probably originates from the electron transfer from the iodide redox couple to the dye cations. It is also possible that the lower efficiency of porphyrin sensitizers was caused by the annihilation of the excited states between the neighboring porphyrin molecules because of the closed proximity [70].

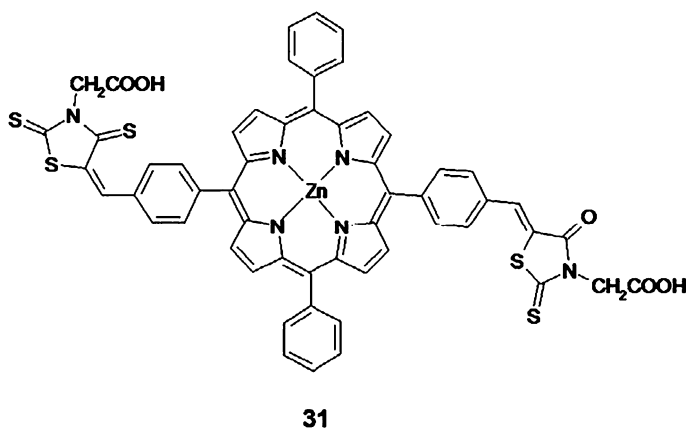
For the purpose of determining the ion potentials of both TiO<sub>2</sub> and dyes adsorbed under working conditions, Inoue measured the UV photoemission yield under an atmospheric condition by using a surface analysis apparatus. The results suggested that the adsorption of dyes on the surface of TiO<sub>2</sub> caused significant shift on the LUMO energy levels. This finding suggests that the energy level alignment at the interface, which is estimated from the vacuum levels or oxidation and redox potential that are independently measured, is inappropriate and these shifts must be taken into account in the discussion on the energy levels of DSSC [71]. The overall energy conversion efficiency of the DSSC sensitized by monocarboxylic acid substituted porphyrin can be improved further by doping of TiO<sub>2</sub> nanoparticle with Nb, Ge, or Zr. The improvement is attributed to the negative shift on the conduction band of TiO<sub>2</sub> electrode. The Ge-doping of TiO<sub>2</sub> electrode sensitized by porphyrin could promote the over all energy conversion efficiency to as high as 3.5% [72].

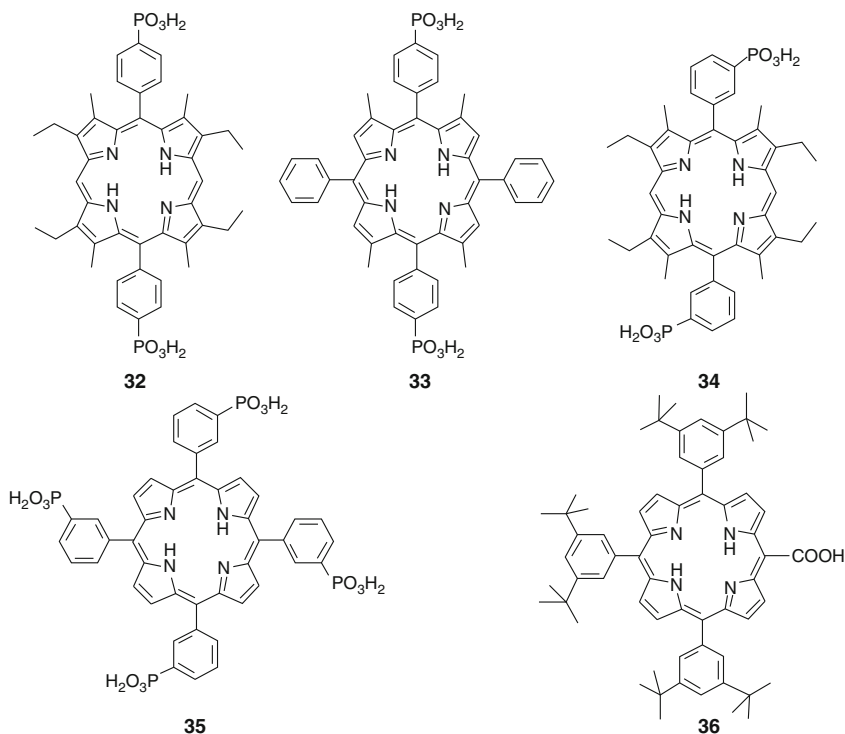
As the anchoring groups in the dye molecules have been proved to play a key factor on the sensitization performance, different anchoring groups with different numbers have been investigated for the porphyrin sensitizers. Ma and co-workers have compared the sensitization properties of porphyrin with only one carboxylic group (**29**) to that of the porphyrin with four carboxylic groups (**28**). Their research revealed that the number of carboxylic acid groups does not vary the binding behavior dramatically, but it indeed influences the fluorescence spectra of the adsorbed porphyrin. The IPCE and the overall energy conversion efficiency for **28** are higher than that of **29** probably because of the more stabilized adsorption on the surface of TiO<sub>2</sub> nanoparticles by the four carboxylic acid groups [73]. A comparison on the binding ability between carboxylic acid and sulphonic acid group has been made by

the same group. Ma and co-workers have prepared a series of metal free porphyrins connected with carboxylic acid groups (**28**), sulphonic acid groups (**30**) or hydrogen respectively. The binding strength of the porphyrin on the surface of TiO<sub>2</sub> was found to drop following the order of -COOH > SO<sub>3</sub>H > H while the ICPE and the overall energy conversion efficiency decreased following the same order [74].



Giribaru has prepared a novel porphyrin sensitizer (**31**) by connecting two rhodanine acetic acid groups at *para* position of *meso*-phenyl groups. The IPCE of the solar cell fabricated from this dye is 45% at Soret band and 20% at Q band; both of them are higher than that of the porphyrin with only one rhodanine acetic acid group. This may be due to the more stable binding of **31** on the surface of TiO<sub>2</sub> nanoparticle, which induces more efficient electron injection to the conduction band of TiO<sub>2</sub> [75].

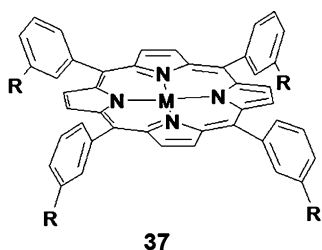




Odobel's research on the application of a series of new free base porphyrins (**32–36**) as photo-sensitizers in DSSC indicates that the anchoring groups seem to have no effect on the sensitization performance. However, the substituted position of anchoring group has great influence on the overall performance of the DSSC. This can be interpreted as due to differences in the orientation and distance of the dye molecules with respect to the  $\text{TiO}_2$  surface imposed by the directionality of the anchoring groups, which lead to significant difference on the electronic coupling between porphyrin and  $\text{TiO}_2$ . Compared with porphyrin **32** and **33**, compound **34** presents a significant higher IPCE (21% vs.  $\sim 10\%$ ) due to the face-on configuration of porphyrin ring on the surface of  $\text{TiO}_2$ . Although porphyrin **36** and **28** exhibit quite similar excited state, oxidation potentials and similar absorption and emission characteristics, they lead to very different IPCE values in identical standard DSSCs. Porphyrin **36** bears the  $-\text{COOH}$  anchoring group directly on the aromatic core, which allows stronger electronic coupling with  $\text{TiO}_2$  [76].

The effects of the connecting position of anchoring groups on the sensitization behavior of porphyrin compounds were further examined by Galoppini in 2007. They tested the sensitizing properties of a series of porphyrin with carboxylic acid or ammonium salt groups attached at different positions with linkages of different length. Both  $-\text{COOH}$  and  $\text{COOEt}_3\text{N}^+\text{H}$  derivatives were employed for the binding studies as well as solution studies. When anchoring groups were connected at *meta* positions on the *meso*-phenyl rings (**37**), the porphyrin molecules preferred a planar binding mode to the metal oxide surfaces with no obvious aggregation.

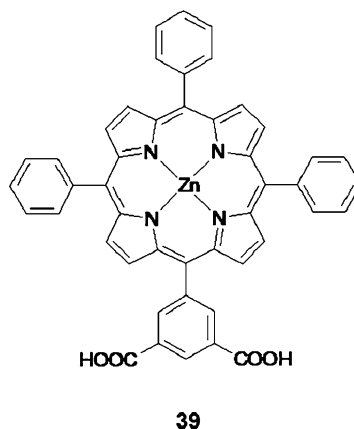
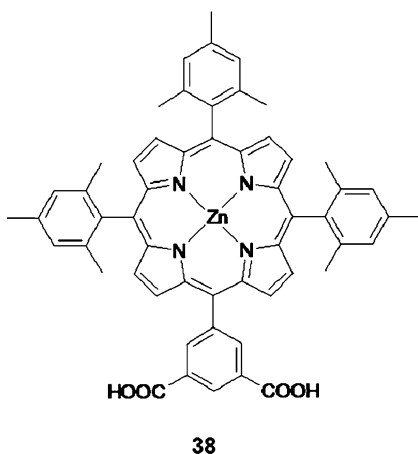
But the porphyrin with carboxylic groups connected at *para* position on the *meso*-phenyl rings presented aggregation, suggesting close packing of the dye molecules on the semiconductor surface. Greater sensitizing efficiencies were found for the *meta*-substituted porphyrins and were explained in terms of a more efficient charge injection into the TiO<sub>2</sub> conduction band from rings that lie flat, and closer to the surface. The length of the bridge between the carboxylic acid groups and the porphyrin ring was found to affect the sensing efficiency significantly because it determined the distance between the porphyrin and TiO<sub>2</sub> nanoparticle surface. Porphyrin with two phenyl ring as bridge (**37b**) presented the highest IPCE. The longer or shorter bridge led to significant drop on the IPCEs. Ammonium salt groups were revealed for the first time to be good anchoring groups with similar binding abilities to that of carboxylic acid groups [77].



**a:** R = COOH, CO<sub>2</sub>(Et)<sub>3</sub>NH

**b:** R = COOH, CO<sub>2</sub>(Et)<sub>3</sub>NH

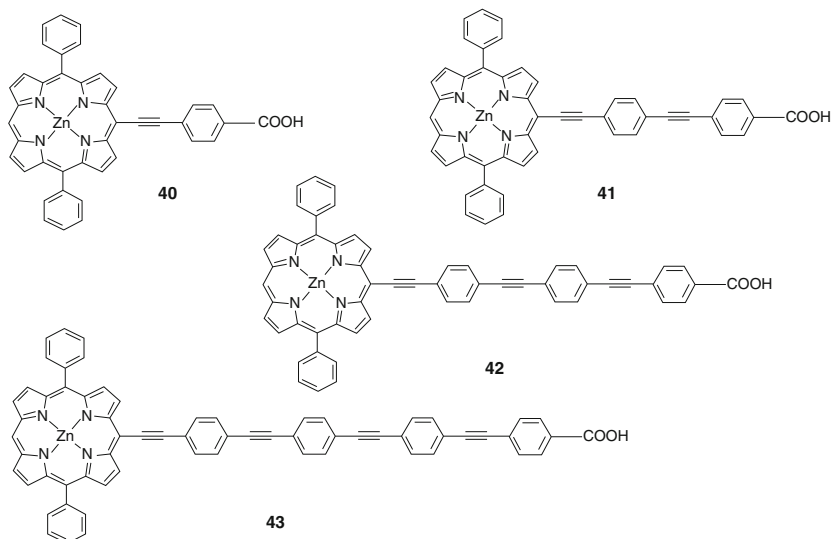
**c:** R = COOH, CO<sub>2</sub>(Et)<sub>3</sub>NH



Porphyrin **37a** and **37b** have also been employed as sensitizer for a TiO<sub>2</sub> nanotube electrode. For comparison purpose, asymmetrical porphyrin sensitizer with two carboxylic acid groups (**38**, **39**) and **28** have also been tested under identical conditions. The DSSC fabricated from these sensitized TiO<sub>2</sub> nanotube presents enhanced charge-collection efficiency respect to the nanoporous TiO<sub>2</sub> film built from TiO<sub>2</sub> nanoparticles. All the tested five porphyrin sensitizers exhibited efficient sensitization to TiO<sub>2</sub> nanotube as revealed by the photocurrent action spectra.

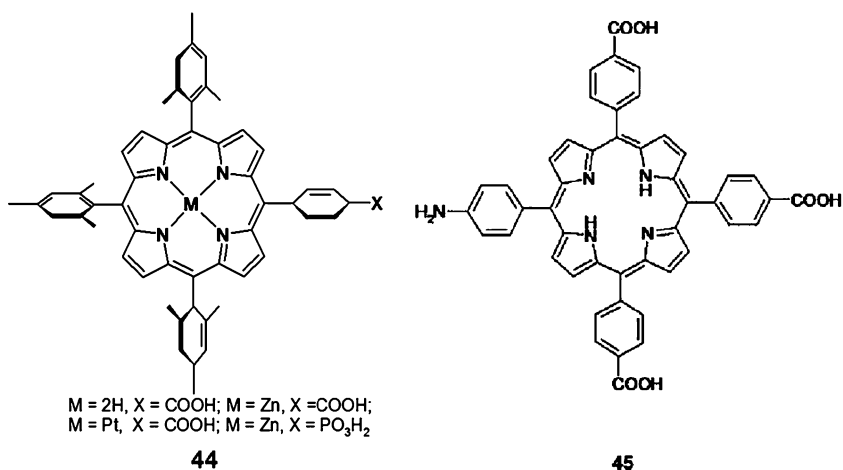


Among these five porphyrin sensitizers, **37b** is the best performer. The next is **39**, then **37a** and **38** behave similarly, and finally **28** is the worst performer. The better IPCE performance of **37b** with respect to **37a** was attributed to the hindered back electron transfer by the longer bridge. The lower performance of **28** could be linked to its lower extinction coefficient [78].



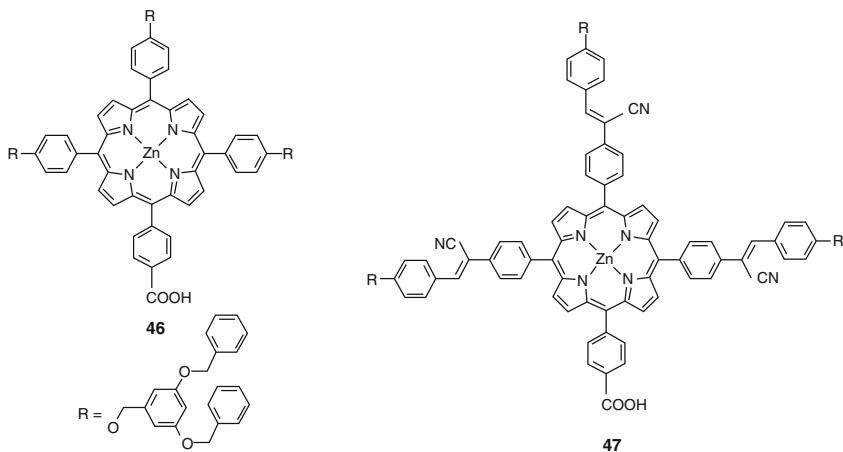
Very recently, the effects of distance between the sensitizer and the surface of  $\text{TiO}_2$  on the sensitization process were further addressed by Lin and co-workers. They prepared a series of porphyrin compounds (**40–43**) with only one anchoring group. The anchoring group was connected with the porphyrin ring by phenylethynyl bridges of different lengths [79]. The efficiencies of power conversion of the devices fabricated from these porphyrin dyes decreased systematically along with the increase in the length of the phenylethynyl bridges. But the transient absorption studies revealed that the kinetics of fluorescence quenching of porphyrin was not affected by the length of the bridges, suggesting similar electron injection rate for these porphyrins. It was the back electron transfer from the conduction band of  $\text{TiO}_2$  to the dye molecule that was responsible for the decreasing sensitization efficiency.

Meyer has tested the sensitization performance of porphyrins with only one functional group ( $-\text{COOH}$ ,  $\text{PO}_3\text{H}_2$ ) and different central metal ions (**44**). Methyl groups were introduced to the 2,4,6 positions of phenyl group which help to keep a perpendicular configuration for the four phenyl groups relative to the macrocycle plan. Their results indicate that all these porphyrins can anchor to the surface of  $\text{TiO}_2$  with high stability. The photocurrent and IPCEs were found to be not affected by the nature of anchoring groups. However, they were found to be pH dependent due to the variation on the  $\text{TiO}_2$  conduction band edge potential along with the changes of pH. The sensitization of porphyrin to  $\text{TiO}_2$  was “turn-off” when the electrolyte pH rose above 10. This finding is important because it reveals the origin of the pH-dependent behavior of the sensitizer for the first time [80].



Another interesting work conducted by Wamser and co-workers in the field of porphyrin monomer sensitizers is the functionalization of tetraphenylporphyrin at the *para* positions of *meso*-phenyl with one amino group and three carboxylic acid groups. The resulted asymmetrical porphyrin (**45**) can be successfully fabricated into a modified solid Grätzel type cell with polyaniline as the solid electrolyte. The overall energy conversion efficiency of this cell is about 2% with a number of opportunities to optimize the efficiency remaining [81].

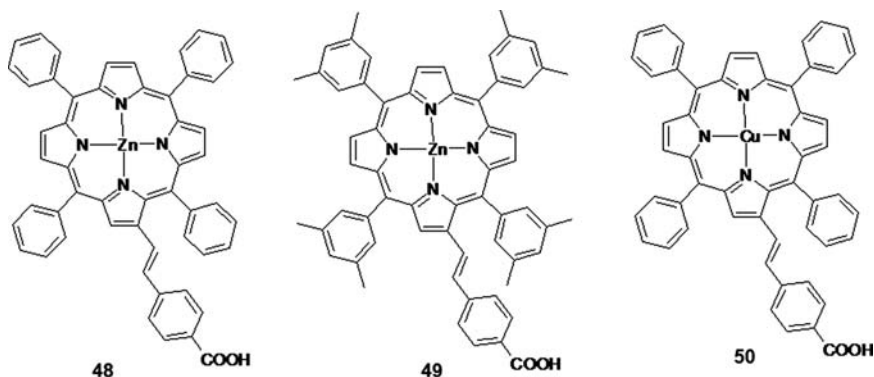
The sensitization properties of porphyrin compounds have also been improved by introducing dendron groups to the cyano substituted *meso*-stilbene moieties (**46**, **47**). The aggregation of porphyrin was efficiently suppressed by the bulky dendrons while the electron injection to the conduction band of  $TiO_2$  was improved by the cyano groups. The overall energy transfer efficiency was promoted remarkably to 2.76% for a solid DSSC. This is an encouraging result for a porphyrin dye and it offers the potential for porphyrins as alternatives to ruthenium-based dyes in the DSSC [82].

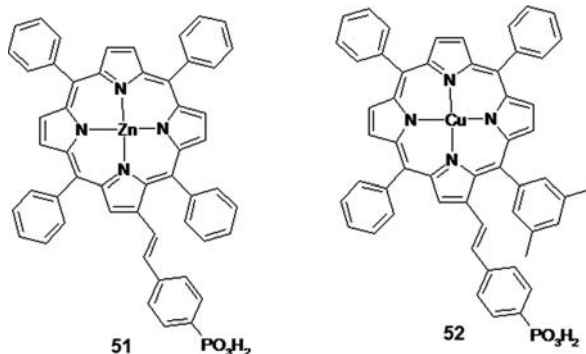


Another interesting attempt worth noting is the combination of porphyrin sensitized solar cell with a fuel cell made by Moore and Gust. The hybrid cell can realize an open circuit voltage of 1.2 V. The energy conversion efficiency of this photoelectrochemical biofuel cell can, in principle, produce more power than either a photoelectrochemical cell or a biofuel cell working individually [83].

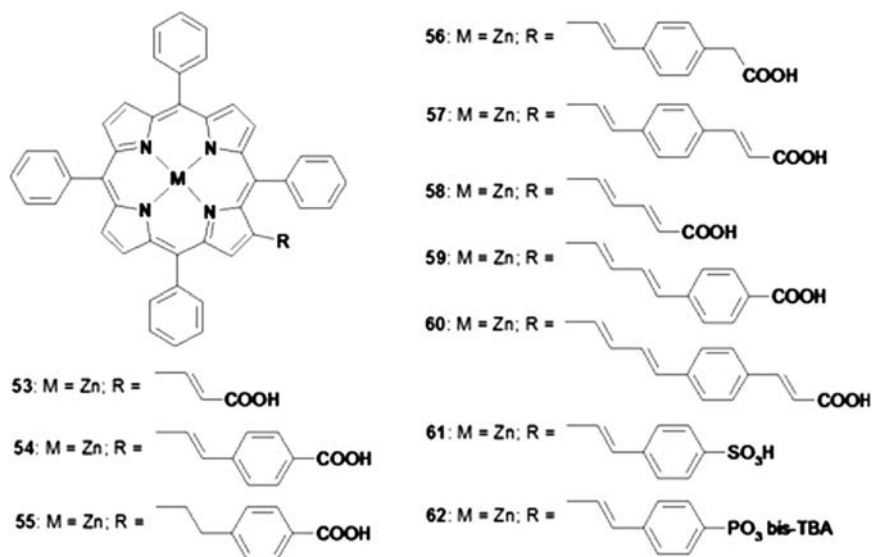
### 3.1.2 Porphyrins with Anchoring Groups Connected at $\beta$ -Pyrrolic Positions

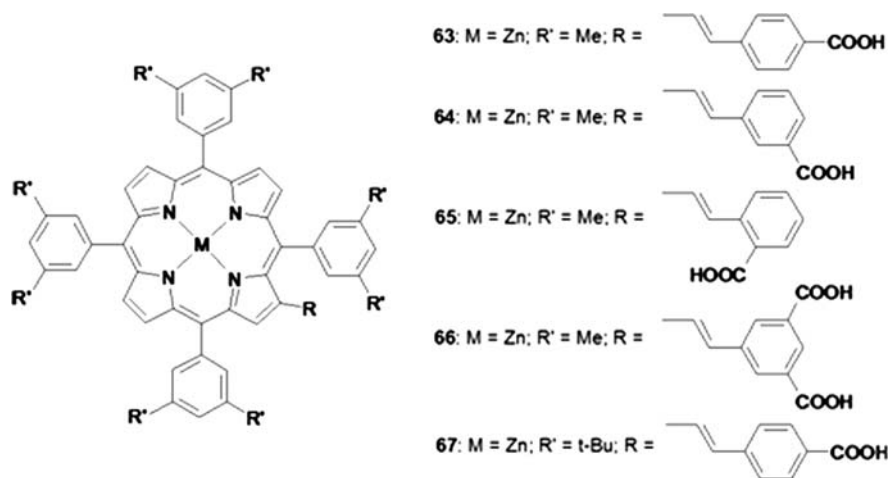
Anchoring groups of the porphyrin sensitizers mentioned above are exclusively connected at the *meso*-phenyl groups. Since the directionality of anchoring groups can change the electronic coupling between the porphyrin excited states and the conduction band of TiO<sub>2</sub>, synthetic research on connection of anchoring groups directly at different positions of the porphyrin macrocycle are attractive due to the perspective of tuning the electronic couplings. Nazeeruddin and co-workers have prepared a series of porphyrin sensitizers (**48–52**) with a benzoic acid or phenylphosphonic acid group connected at the  $\beta$ -pyrrolic position (2,3,7,8,12,13,17,18 positions) of porphyrin ring by a double bond. The binding of carboxylic acid group onto the surface of TiO<sub>2</sub> particle was confirmed by the ATR-FTIR spectra. The porphyrin with carboxylic acid group presents higher IPCEs than that with phosphoric acid probably because of the larger electronic coupling through carboxylic acid groups. The zinc porphyrins are better sensitizers than copper porphyrins as expected due to the longer lifetime of the excited state of zinc porphyrin with respect to copper porphyrin. The methyl groups at 3,5 positions also promote the IPCEs significantly by harnessing the aggregation of porphyrin molecules. The best sensitizer in this series of porphyrins was **49**, which presented IPCE at the Q band as high as 75% with an overall energy conversion efficiency of 4.8%. This finding opens up new avenues for improving further the efficiency of solar cells by engineering the structure of porphyrins [84].



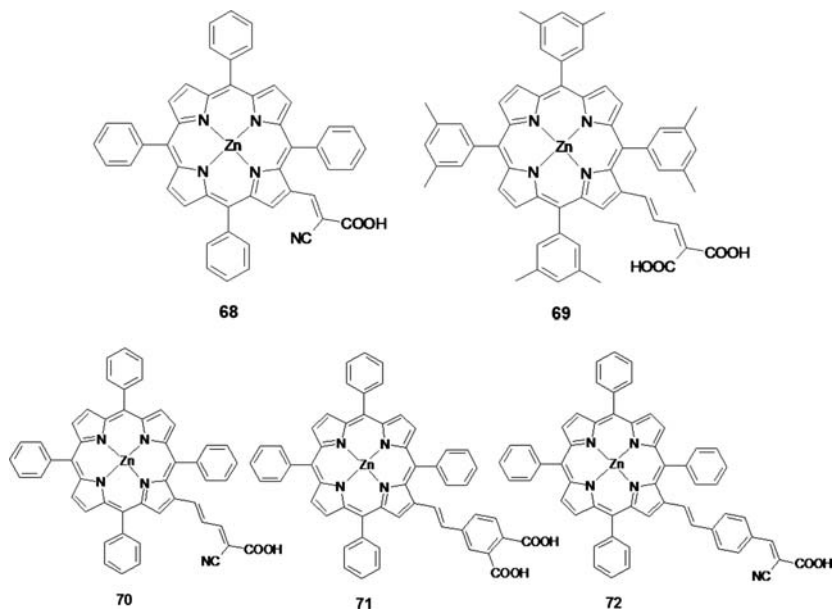


Systematic and comprehensive research on porphyrin sensitizers (**53–67**) with the anchoring group connected at  $\beta$ -pyrrolic positions have also been performed by Officer and co-workers [85]. Their results revealed that free acid form of the anchoring group exhibited the best adsorption on the surface of  $\text{TiO}_2$ , which is in accordance with the previous report [80]. The zinc porphyrins show more efficient sensitization than copper and metal free porphyrins. Their results also suggest that  $\beta$ -pyrrolic substituted porphyrin styryl carboxylic acids are superior to *meso*-aryl porphyrin carboxylic acids as light harvesters. Porphyrin **53** had been shown to be the most efficient porphyrin photosensitizer in this series of compounds with an overall energy conversion efficiency of 4.2%. Moreover, they found that the close proximity of porphyrins might not significantly diminish light harvesting. They had also demonstrated that either the sulphonic or phosphonic acid porphyrins bound to  $\text{TiO}_2$  tightly, but this stable binding did not bring better cell performance. This tends to suggest that electronic coupling between the dye and  $\text{TiO}_2$  surface through the binding group plays an important role in the efficiency of light harvesting. For the conjugated linkers, the number of double bonds, or the presence of the phenyl moiety, made no significant difference in overall cell performance. However, when the conjugation was interrupted, there is a significant fall in the cell performance [85].

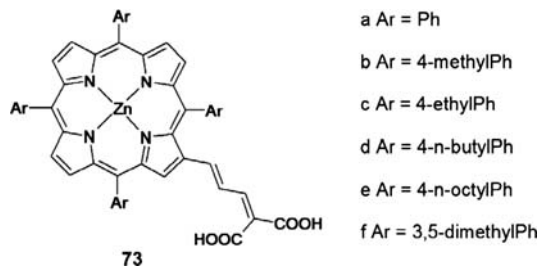




Officer and co-workers have also successfully connected carboxylic acid groups at the  $\beta$ -pyrrolic position of porphyrin with one or two double bonds (**68**, **69**) [86]. Compared with the tetraphenyl porphyrin (TPP), these two compounds show red shifted absorption spectra with larger extinction coefficient. The IPCEs of the liquid junction solar cell based on these sensitizers are 90% at Soret band and 60% at Q band. The overall energy conversion efficiency of the cell based on **68** and **69** are 2.44% and 3.0% respectively. It is worth noting that sensitizing efficiency seems not affected by the length of the linkage as also revealed in the previous research [85]. The nano-crystalline TiO<sub>2</sub> electrode sensitized by these sensitizers would remain transparent to the eye, while absorbing enough solar photons in the NIR region.

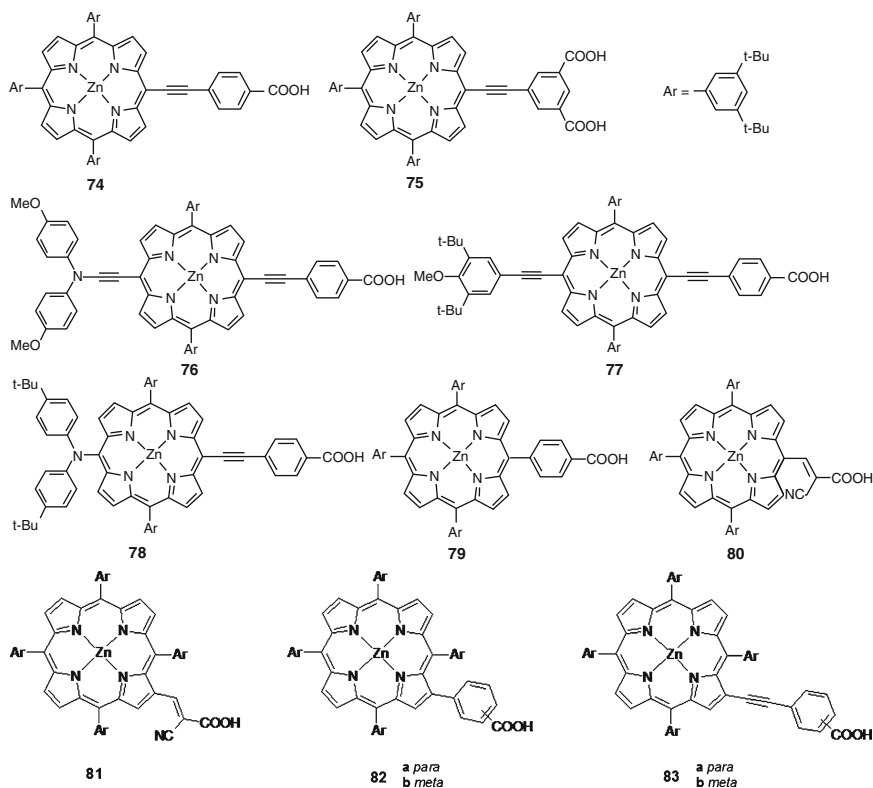


The same research group has also compared the sensitization properties of a series of novel green porphyrins (**70–72**) containing a  $\beta$ -pyrrolic substituent with that of **68** later. Because of the presence of electron withdrawing CN group at the substituent, the frontier molecular orbitals are stabilized and extended out onto the substituent by  $\pi$ -conjugation. The extension of the conjugation of porphyrin to the substituents provides the possibility of electron transfer from porphyrin to  $\text{TiO}_2$  through the substituent. Significant improvement on the solar cell performance had been achieved by using these porphyrins as sensitizers. The **72**-sensitized solar cell demonstrates an IPCE close to 85% and an overall conversion efficiency of 5.6% under standard AM 1.5 sunlight [87].



The effects of the substituent at the *para*-position of *meso*-phenyl on the sensitization properties of porphyrins (**73**) were also examined by the same group. All these novel darkgreen porphyrins yield IPCE values of up to 75% and overall power conversion efficiencies in the range of 5.1–7.1% under one sun in a liquid electrolyte cell. **73b** presented the best performance in this series of porphyrins. More impressively, a solid-state cell utilizing **73b** as the sensitizer performed a peak IPCE value as high as 63% and overall power conversion efficiency 3.6%. These record efficiencies demonstrate the exciting potential of porphyrins as light-harvesting green dyes [88].

Very recently, the effects of the connection position of anchoring groups on the sensitization performance of porphyrins (**74–83**) were further addressed in the research of Diao and co-workers. The carboxylic acid groups were selectively connected to the *meso* or  $\beta$ -pyrrolic positions by different conjugated linkages. Electron donating biaryl amino groups introduced onto the opposite *meso* position of the anchoring group tend to enhance the charge separation capability. The results indicate that both the position and nature of the linkages show significant influences on the spectral, electrochemical, and photovoltaic properties. However, the advantages of the  $\beta$ -pyrrolic position connection of anchoring groups over the *meso* position connection as revealed by the previous research was not exhibited by these series of porphyrin sensitizers. The phenylethynyl bridge at *meso* position could efficiently red-shift the absorption spectrum. The red shift became more pronounced when a conjugated electron donating group was connected at *meso* position opposite to the anchoring group. The DFT calculation revealed that the oxidized state was stabilized by the electron donating group and thus improved the sensitization performance dramatically. An overall energy conversion efficiency of 6.0% was achieved by compound **76**, which was comparable to the performance of the famous N3 dye [89].

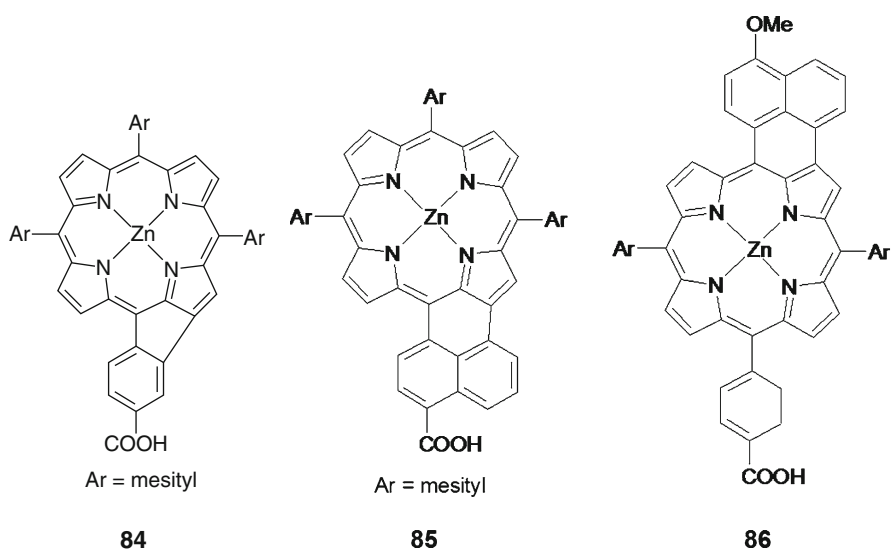


Although plenty of results support that the anchoring groups connected at the  $\beta$ -pyrrolic positions will benefit the sensitization of porphyrin to  $\text{TiO}_2$ , but there is also a few of researches which do not support this point. It is the overall electronic configuration of the porphyrin macrocycle that determines the coupling between the excited states of porphyrin and the conduction band of  $\text{TiO}_2$ , which then influences the sensitization performance of the dye. When the directionality of the anchoring group at  $\beta$ -pyrrolic position could enhance the coupling and stabilize the charge separated states, the sensitization will be promoted. In order to get a better sensitizer, the whole electronic configuration of the excited states of porphyrin must be taken into consideration.

### 3.1.3 Porphyrins Fused with Other Small Aromatic Rings

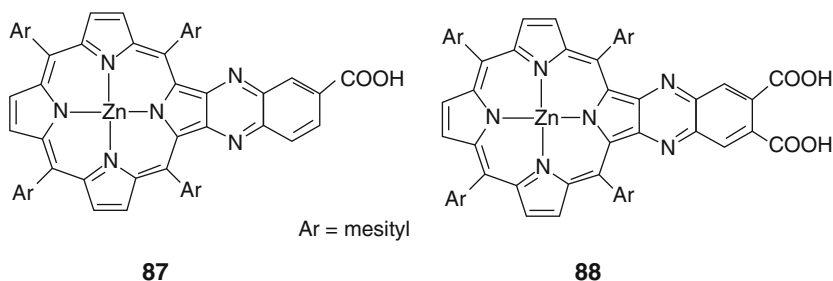
Besides to introduce substituents onto the *meso*-phenyl ring or the  $\beta$ -pyrrolic positions, modification of the molecular structures by fusing a small aromatic ring to the porphyrin ring has also been an attractive way to extend the absorption spectra and tune the electrochemical properties of porphyrins in the prospect of improving the sensitization behavior. Imahori has investigated the application of a fused five-membered porphyrin (**84**) as sensitizer in DSSC. Compared with the reference porphyrin, the fused porphyrin shows broaden and red-shifted absorption spectra

as expected and the photocurrent response extends to 800 nm for the first time. The oxidation potentials of the fused porphyrin have positive shifted for about 0.07 V relative to that of the standard porphyrin. However, the DSSC with this fused porphyrin as sensitizer show significantly lower IPCE and overall energy transfer efficiency relative to that made of the reference porphyrin. This has been attributed to the insufficient driving force for an efficient electron injection for this fused porphyrin [90].



Later, Imahori has synthesized a series of new porphyrins (**85**, **86**) fused in different ways with naphthyl moieties to improve the light-harvesting abilities in porphyrin sensitized solar cells. As the results of  $\pi$ -elongation with low symmetry, Soret and Q bands of the fused porphyrins were red-shifted and broadened, and the intensity of Q-band relative to that of Soret band was enhanced. The DSSC sensitized with **85** showed overall power conversion efficiency of 4.1% under standard AM 1.5 condition while the cell of **86** gave a power conversion efficiency of 1.1%. The better sensitization performance of **85** was attributed to the extension of the LUMO to the carboxylic acid group as revealed by the DFT calculation, which was not found for the LUMO of **86**. Accordingly, the larger electronic coupling between the porphyrin and the  $\text{TiO}_2$  surface in the **85**-sensitized cell may be responsible for the high cell performance. More interestingly, the performance of the **85**-sensitized solar cell can be further improved by co-sensitization of **85** and other porphyrins with complementary absorption properties. An overall power conversion efficiency of 5% under standard 1.5 AM condition was achieved by this co-sensitization method [91].





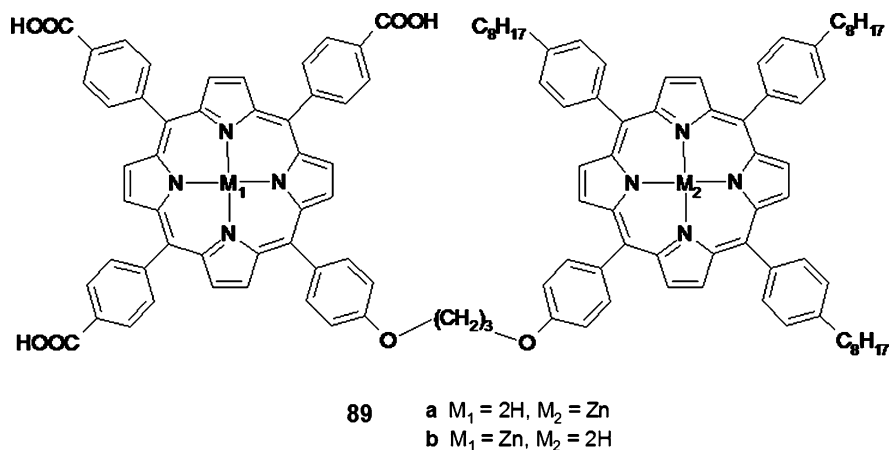
Another important work performed by the group of Imahori is the fusing of a quinoxaline ring with one or two carboxylic acid groups to the porphyrin ring (**87**, **88**). The XPS, FTIR spectroscopy, and cyclic voltammetry studies for the adsorbed porphyrins revealed that the carboxylic acid group in **87** employed bidentate binding mode to anchor itself onto the TiO<sub>2</sub> surface, whereas the two binding groups in **88** utilized one bidentate and one monodentate binding modes. The photovoltaic measurements on the DSSCs sensitized by **87** or **88** have revealed power conversion efficiencies of 5.2% and 4.0% respectively. Since the absorption spectra of these two porphyrins are similar, the difference on the power conversion efficiency is dominantly determined by the binding model [92].

### 3.2 Porphyrin Arrays

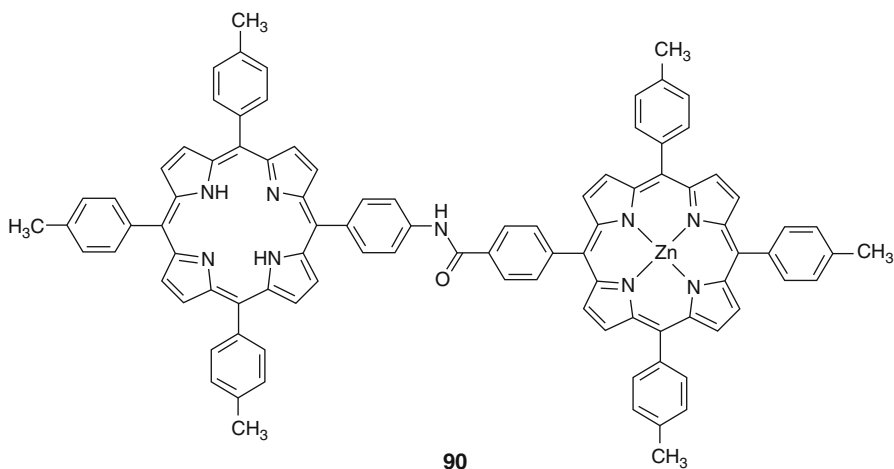
To harvest photons more efficiently in DSSCs, construction of chromophore arrays and attaching them to the semiconductor surface have been studied extensively. By connecting carefully designed series of chromophores in a branched or linear way, using appropriate spacers, the excited energy of chromophores can be tunneled to a selected chromophore, from which the electrons were injected into the conduction band of the semiconductor. The efficiency of the intramolecular energy and electron-transfer processes in chromophore arrays will depend on the bridge and the spatial orientation of individual chromophore units. The most popular chromophore arrays investigated so far are covalent bonded systems due to their high stabilities [93].

Koehorst and co-workers had tested the sensitizing properties of a porphyrin heterodimer (**89**) to TiO<sub>2</sub>, which represented the first example of the application of porphyrin arrays in DSSC [94]. This porphyrin heterodimer was composed of one free base porphyrin and one zinc porphyrin with one of them functionalized with carboxylic acid groups. Because of the binding of carboxylic acid groups at the surface of TiO<sub>2</sub>, the porphyrin unit functionalized with carboxylic acid groups was in direct contact with the substrate. For the DSSC fabricated from the porphyrin dimer with the carboxylic acid groups functionalized at metal free porphyrin (**89a**), the photocurrent action spectrum reproduced the absorption spectrum, i.e., both porphyrin units contributed to the photocurrent, indicating efficient energy transfer from zinc porphyrin to metal free porphyrin followed with efficient electron injection from the latter to TiO<sub>2</sub>. However, when the carboxylic acid groups

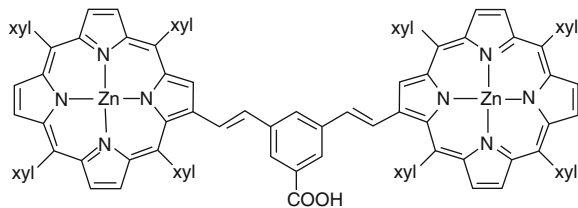
were functionalized at zinc porphyrin (**89b**), the photocurrent action spectrum of the solar cell presented only the contributions of zinc porphyrin. This is reasonable because the energy transfer from metal free porphyrin to zinc porphyrin was theoretically unfavorable. This result also suggested that the energy transfer from zinc porphyrin to metal free porphyrin was slower than that of the electron injection from zinc porphyrin to  $\text{TiO}_2$ . This research revealed a promising way to enhance the absorption of light and thus improve the performance of DSSC by constructing a supramolecular lighting antenna as sensitizer.



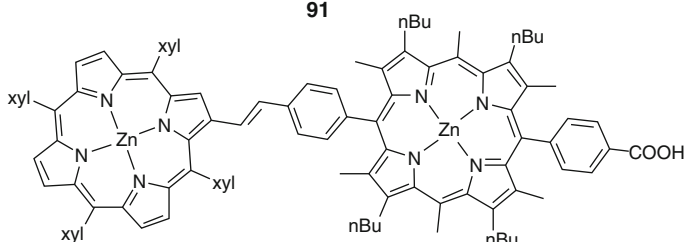
Sereno prepared a porphyrin dimer by connecting a metal free porphyrin to a zinc porphyrin with amid bond. The resulted porphyrin dimer was tested as a sensitizer for  $\text{SnO}_2$  electrode. Even without anchoring groups, this porphyrin dimer showed sensitization to  $\text{SnO}_2$  electrode with an IPCE value of 10% at 420 nm [95].



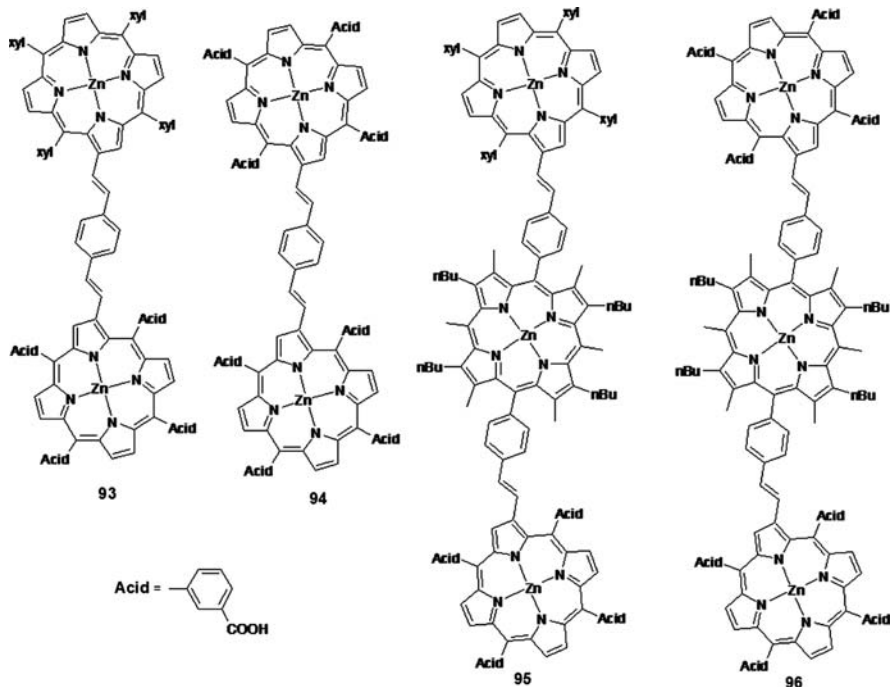
In a later research, Sereno and co-workers found efficient energy transfer from zinc porphyrin to metal-free porphyrin in the dyad (**90**) even in the adsorbed states. The fact that the dimer is less effective in comparison with metal free porphyrin monomer in the generation of photocurrent is explained as that the metallized porphyrin enhances the back electron-transfer process [96].

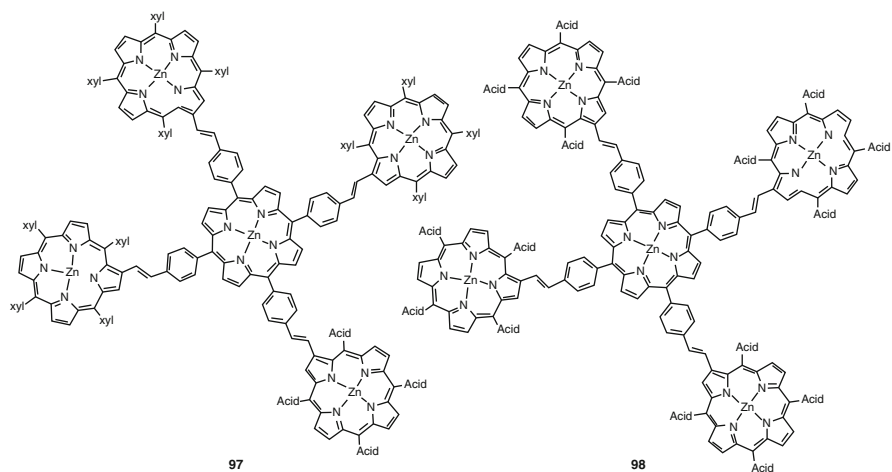


91



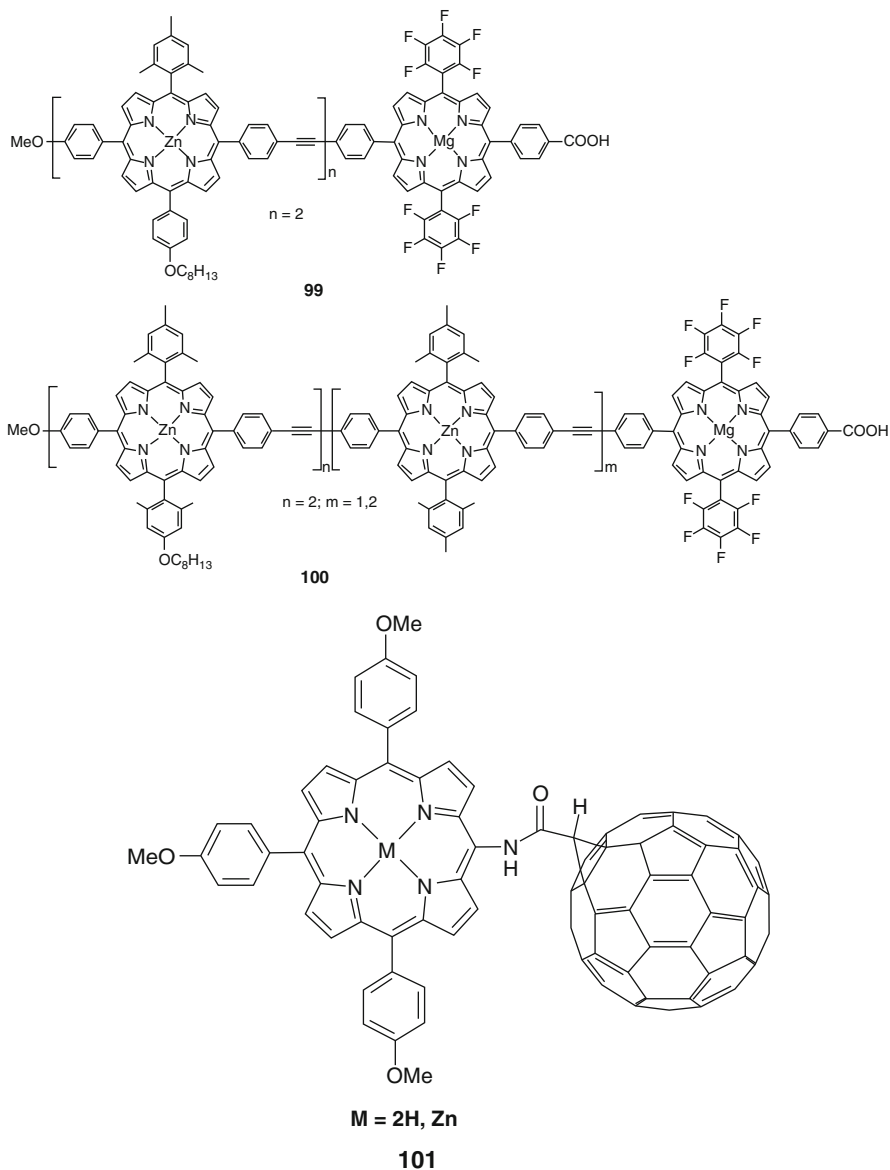
92





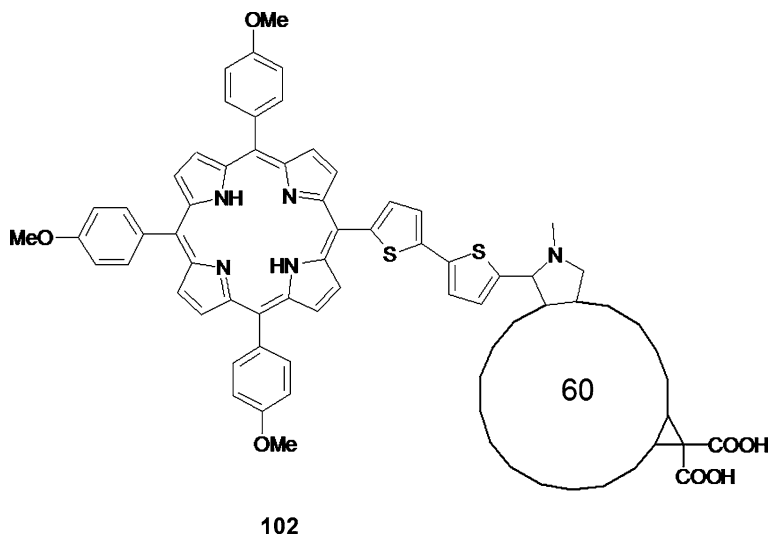
A comprehensive study on the photosensitization behavior of porphyrin arrays to  $\text{TiO}_2$  has been conducted by Campbell and co-workers. The porphyrin dimers (**91** and **92**) with one carboxylic acid group as binding site present weak surface adhesion and therefore low efficiency on sensitization. The DSSC with these two porphyrin arrays as sensitizers exhibit lower IPCEs relative to that with porphyrin monomer. To strengthen the adsorption of these porphyrin arrays on the surface of  $\text{TiO}_2$  nanoparticle, multi carboxylic acid groups were introduced to the porphyrin moieties and compounds **93–98** were prepared. The binding of these porphyrin arrays on the surface of  $\text{TiO}_2$  is indeed enhanced and stabilized. Yet here also the monomeric porphyrin outperforms these dyes, with no apparent antenna effect observed in spite of the strong binding. This result was attributed to the lack of directionality of the binding groups in the porphyrin arrays, but it is also highly likely that the small porosity of the  $\text{TiO}_2$  nanocrystalline layer may be preventing adsorption of these very bulky dyes [85].

Lindsey and co-workers have prepared a series of rod like porphyrin arrays (**99**) for the DSSC application. The triad, tetrad, and pentad porphyrin arrays, each is comprised of a terminal magnesium porphyrin bearing one carboxyl group (for surface attachment); the remaining porphyrins in each array are present as the zinc chelate. The steady absorption spectra reveal weak coupling between these porphyrins at ground state, while the fluorescence spectra indicate the obvious excited energy migration along the porphyrin array to the terminal magnesium porphyrin with the efficiency as high as 99%. These design and synthesis strategies should be useful for the construction of materials for molecular-based solar cells. Unfortunately, the sensitization properties of these porphyrin arrays to  $\text{TiO}_2$  nanoparticle electrode were not measured and no data on the photo to current conversion efficiency were reported so far [97].

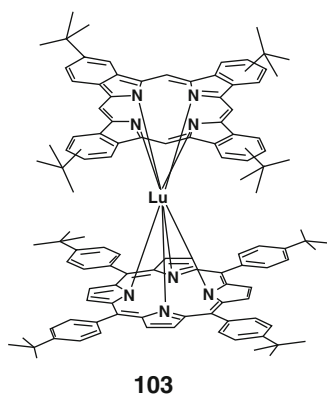


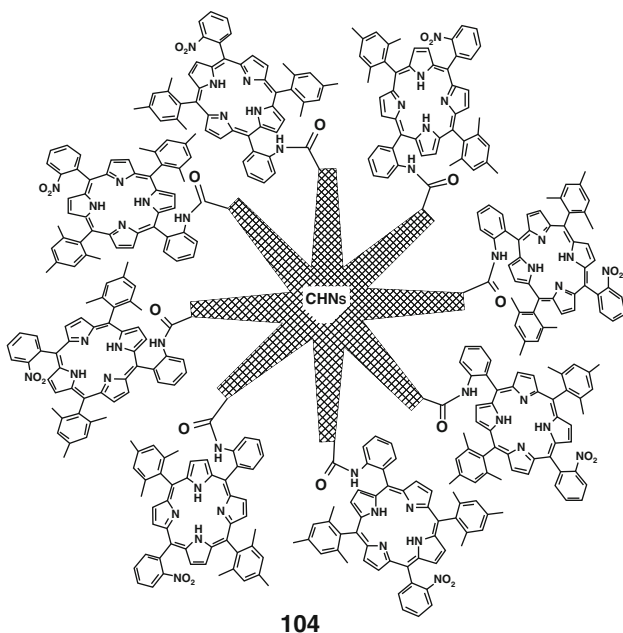
A porphyrin-C<sub>60</sub> dyad (**101**) has been used as a sensitizer in DSSC by Durantini and co-workers in 2002. The fluorescence quenching of porphyrin was observed in the dyad, indicating efficient electron transfer from porphyrin to C<sub>60</sub>. The test on the sensitization properties of this dyad to SnO<sub>2</sub> electrode revealed that the absorption of C<sub>60</sub> contributed to the photocurrent generation. The dyad produced a higher photoelectric effect than the corresponding amidoporphyrin model. An alternative photoelectric mechanism, which involves a charge separated state, other than direct electron injection from the excited porphyrin to SnO<sub>2</sub>, was suggested to be responsible for this improved photoelectrical response [98].

Another porphyrin–C<sub>60</sub> dyad (**102**) connected by a bithiophene bridge was prepared by Shiga very recently. Carboxylic acid groups were introduced to C<sub>60</sub> moiety as anchoring groups. The DSSC fabricated from this dye exhibited IPCEs at 420 nm larger than 40% with an overall photocurrent conversion efficiency over 0.53% at 100 mW cm<sup>-2</sup>. The contribution of C<sub>60</sub> to the photocurrent generation was obviously observed in the photocurrent action spectra. The introduction of C<sub>60</sub> between the porphyrin unit and TiO<sub>2</sub> is effective in improving photosensitization [99].



Liu prepared a sandwich type coordination compound (**103**) from porphyrin and phthalocyanine with the assistance of a microwave. The resulted compounds showed good solubility in conventional organic solvents. The photoelectric conversion properties have been tested with a Grätzel type cell. The results revealed that the sandwich type compound showed better photo-electric conversion efficiency than the corresponding monomeric porphyrin or phthalocyanine precursors. The short-circuit photocurrent of the solar cell with this sandwich type compound as sensitizer, was, as high as 691.31 A cm<sup>-2</sup>, which was much better, than those of porphyrin or phthalocyanine monomers [100].





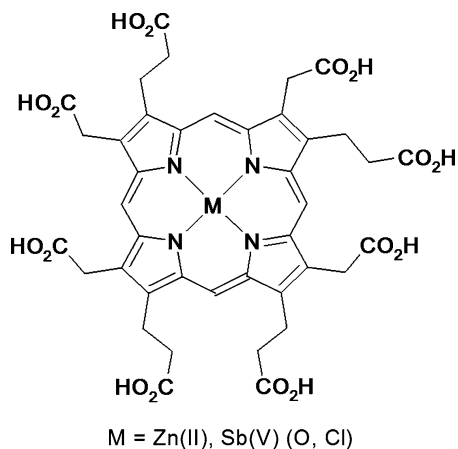
Very recently carbon nanohorns (CNHs) covalently functionalized at the conical tips with metal free porphyrin moieties (**104**) were tested as sensitizer in a photoelectrochemical solar cells. A nanostructured  $\text{SnO}_2$  electrode deposited with porphyrin functionalized CNH exhibited an IPCE of 5.8%; it is greater than the one observed for the sum of the single components. The fluorescence lifetime measurement reveals that photoinduced electron transfer from porphyrin to the nanohorns takes place followed by the direct electron injection from nanohorns to the conduction band of  $\text{SnO}_2$ . The results obtained demonstrate the potentiality and applied utility of CNHs in directing efficient charge transport in photoelectrochemical devices [101].

Controversial results have been deduced from the researches of different groups on the sensitization behavior of porphyrin arrays as mentioned above. Some of them revealed that porphyrin arrays have advantages over porphyrin monomers in the sensitization of wide band gap semiconductor while the rest showed the opposite results. The porphyrin dimer composed of a metal free porphyrin and a zinc porphyrin seems the most successful porphyrin array sensitizer so far. Programming the photoinduced energy and electron-transfer sequence in a porphyrin array is the key step toward a good porphyrin array sensitizer.

## 4 Natural Porphyrin Sensitizers

The important role of chlorophylls in photosynthesis inspired people looking for ways to apply these natural porphyrins in DSSC as light harvesting sensitizers. The use of zinc and antimony metallo-uroporphyrins **M-UP (105)** as photosensitizers

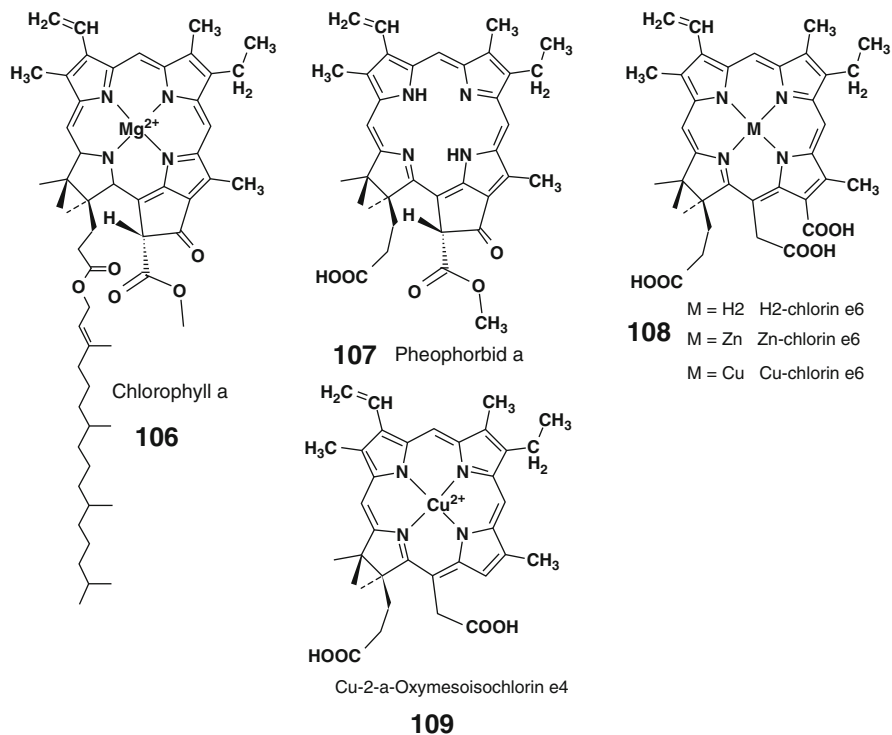
for  $\text{TiO}_2$  colloid was investigated by Kalyanasundaram et al. The flash photolysis studies revealed that the electron injection to  $\text{TiO}_2$  conduction band happened from both singlet and triplet excited states of Zn uroporphyrin [102].



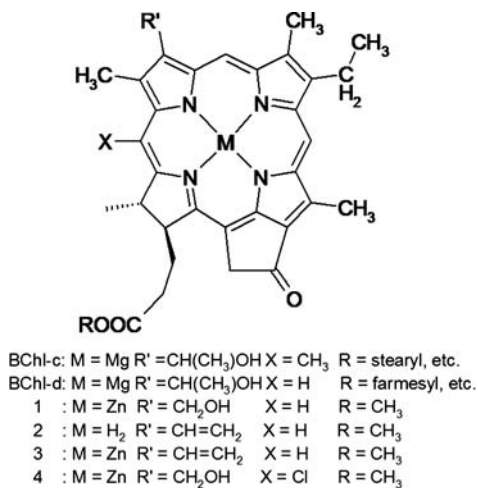
105

Grätzel has investigated the sensitization behavior of chlorophylls and related natural porphyrins to nano-crystalline  $\text{TiO}_2$  electrode. The natural porphyrins they employed include chlorophylls (**106**), Pheophorbids (**107**),  $\text{H}_2$ -, Zn-, or Cu-chlorin-e6 (**108**), Cu-2- $\alpha$ -Oxymesoisochlorine e4 (**109**) and  $\text{H}_2$ -, Zn-, Cu-Mesoporphyrin IX (**105**). The photosensitization of colloidal  $\text{TiO}_2$  electrodes by these chlorophyll derivatives gave high IPCEs, approaching the unity efficiency of primary charge separation in natural photosynthesis. More interestingly, even the nonfluorescent Cu chlorophyllin present efficient sensitization to  $\text{TiO}_2$  colloid electrode due to the fast electron injection from the excited states of Cu chlorophyllin into the conduction band of  $\text{TiO}_2$ . However, the realistic application of these chlorophyll derivatives is limited because of the low efficiency of the overall energy transfer as well as the low stability of these compounds [103]. The study on the mechanisms of the photosensitization by electrochemical and transient absorption studies revealed that the electron injection to the conduction band of  $\text{TiO}_2$  happened from singlet excited states for the fluorescent chlorine e6 and from triplet states for the non-fluorescent copper 2 $\alpha$ -oxymesoisochlorin e4. The recombination of the injected electron with the oxidized dye is relatively slow and leads to a high charge separation yield [104].

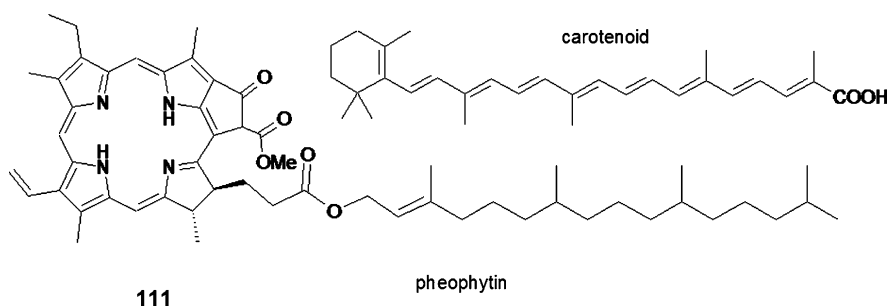




The sensitization of H<sub>2</sub>-chlorin e6 (**108**) was also tested by Amao and co-workers. Their results indicate that chlorine-e6 present efficient sensitization to TiO<sub>2</sub> with an overall energy transfer efficiency of 0.40% under light intensity of 100 mW cm<sup>-2</sup> [105, 106].

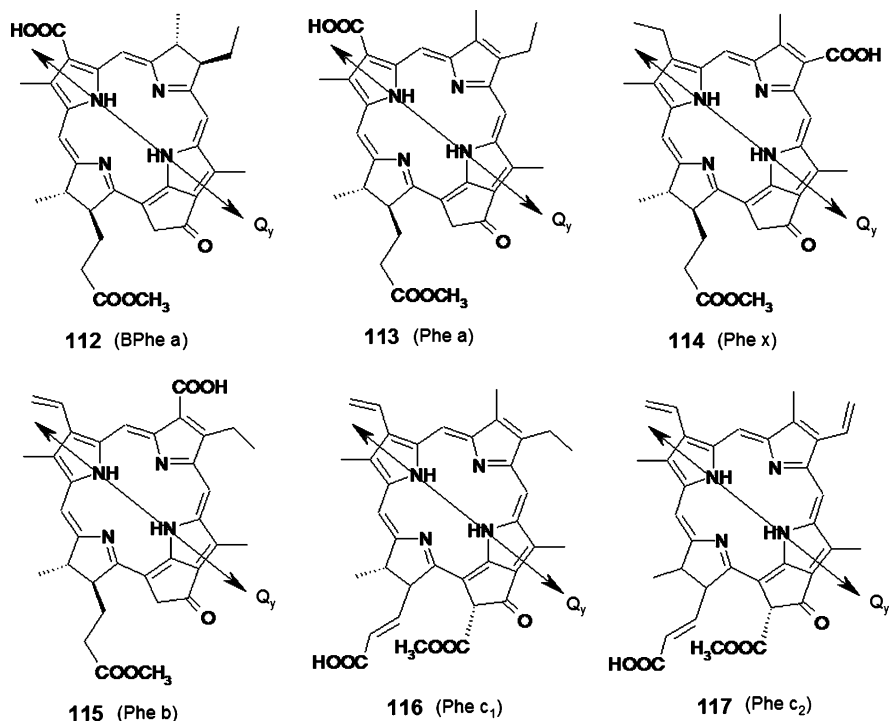


Tamiaki prepared a series of zinc chlorins with methyl carboxylate groups. The sensitization of these compounds to carbon past was investigated. The experimental results revealed surprisingly that the aggregates of zinc chlorin on the carbon past were responsible for the photocurrent generation, and even more surprising, the sensitization of chlorin aggregates was more efficient than that of zinc chlorin monomer. This result was opposite to most of the others obtained from porphyrin or phthalocyanines.  $O_2$  was suggested to get involved in the photocurrent generation [107].



Polívka had investigated the co-adsorption of carotenoid and pheophytin (**111**) on the surface of  $TiO_2$  electrode and the photophysical properties of pheophytin in this film. The results demonstrated that the fluorescence of **111** was efficiently reductively quenched by carotenoid in this co-assembled film, suggesting similar mechanisms to that in the natural photosynthetic systems. The radical anion of **111** formed during the electron transfer recovered to the neutral state quickly before the charge recombination between carotenoid cation and pheophytin anion took place. It is suspected that the electron injection from the pheophytin anion to the conduction band of  $TiO_2$  was responsible for this quick recovery. This result indicated that such a “self-assembling” strategy may be also considered for novel DSSC constructions [108].

Durrant have investigated the photoinduced electron-transfer reactions of zinc-substituted cytochrome c, ZnCyt-c, immobilized on the surface of nanocrystalline  $TiO_2$  electrodes. Efficient electron injection from the triplet state of ZnCyt-c into  $TiO_2$  electrodes is revealed by transient absorption studies, which resulted in a long-lived charge separated state. The previous research on the light-induced electron injection into  $TiO_2$  electrodes has typically focused on achieving strong electronic coupling between  $TiO_2$  nanoparticles and the dye molecules, this leading to fast electron injection into the conduction band of  $TiO_2$  from the singlet excited states of the dyes. In this ZnCyt-c sensitized system, the protein matrix acts as a spacer between the Zn-porphyrin and the nanoparticle surface, which hindered the fast electron injection from the singlet excited states. Due to the high efficiency of the intersystem crossing from singlet to triplet states of ZnCyt-c, the relative slow electron injection from the triplet states of ZnCyt-c presents a high efficiency too. This sensitization pathway requires only relatively weak electronic coupling between the sensitizer and the electrode surface and may be a promising way to improve the energy conversion efficiency in DSSCs [109].



Koyama has examined the sensitization behavior of a series of pheophorbide sensitizers (**112–117**) with similar structure. The results indicate that the short-circuit current density as well as the overall solar energy-to-electricity conversion efficiency increased with the increasing Q<sub>y</sub> absorption and with the decreasing one electron-oxidation potential. Two empirical models are built based on the experimental results. One model suggests a parallel electron injection from both excited and ground states to the conduction band of TiO<sub>2</sub> whereas the other one supports an electron injection via the excited state only, in which both the Q<sub>y</sub> absorption and the Q<sub>y</sub>-state one electron-oxidation potential can contribute [110].

## 5 Conclusion

Both phthalocyanines and porphyrins are very promising sensitizers for wide band gap semiconductors. DSSCs fabricated from these kind of sensitizers present overall power conversion efficiency as high as 7%, which is still smaller than that achieved by the ruthenium polypyridyl complexes though, but higher than most of other dyes. The multiplicity on the molecular structure modification of these compounds provides a great potential for further promotion on their sensitization properties. The research in this field is still far from systematic and comprehensive and quantitatively much less than the researches on polypyridyl ruthenium complexes. But

from the limited researches as mentioned above, several important aspects should be taken into account during the design of novel sensitizers.

1. To achieve an efficient sensitization of TiO<sub>2</sub> nanocrystalline electrode, anchoring groups connecting with phthalocyanine or porphyrin are necessary. The anchoring groups help not only to immobilize the dye molecule on the surface of the semiconductor electrode but also to keep a strong coupling between the excited states of the dye molecules and the conduction band of the semiconductor.
2. The electron injection from the excited states of the dyes to the conduction band of the electrode is predominately affected by the oxidation potential of the dye molecules as well the distribution of the LUMO over the whole molecule. Tuning the redox potentials and the LUMO distribution by functionalizing the aromatic ring asymmetrically with different groups at different positions seems a promising way towards a better sensitizer.
3. Aggregations of the porphyrin or phthalocyanine molecules on the surface of the nano-crystalline electrode always induce massive non-radioactive decay of the excited states and thus reduce the efficiency of the electron injection. Therefore, preventing the aggregation of the dye molecules on the electrode surface will be a foremost issue during the design of new sensitizers, which can be achieved normally by axial coordination, bulky substituents at peripheral positions or the co-adsorption with other materials.
4. Although with some disagreements, sensitization with two kinds of co-adsorbed dyes or with molecular arrays of different chromophores has proved to be advantageous to the overall power conversion efficiencies of DSSCs. New molecular arrays based on porphyrin or phthalocyanine molecules with carefully programmed photoinduced electron or energy transfer sequence are expected to be promising candidates for good sensitizers in DSSC.

The application of phthalocyanine or porphyrin analogs as sensitizers in DSSC has been explored for more than 10 years up to now. From the point of overall power conversion efficiency, these tetrapyrrole macrocyclic compounds are not as successful as polypyridyl ruthenium complexes. However, the recent great improvement on the performance of the phthalocyanine- or porphyrin-based DSSCs and the deeper understanding on the sensitization mechanisms revealed large potentials for further development for this kind of sensitizers. Given that many new porphyrin or phthalocyanine compounds exhibit excellent light-harvesting properties in artificial photosynthetic systems, we anticipate that many new sensitizers based on phthalocyanine or porphyrin will be forthcoming.

**Acknowledgements** Financial support from the Natural Science Foundation of China (Grant No. 20640420476, 207710666), Ministry of Education of China, and Shandong University are gratefully acknowledged.

## References

1. Armaroli N, Balzani V (2007) *Angew Chem Int Ed* 41:52
2. Balzani V, Credi A, Venturi M (2008) *ChemSusChem* 1:26
3. Special Section on "Sustainability and Energy" (2007) *Science* 315:781
4. Service RF (2005) *Science* 309:548
5. Balzani V, Moggi L, Manfrin MF, Bolletta F, Gleria M (1975) *Science* 189:852
6. Meyer TJ (1989) *Acc Chem Res* 22:163
7. Bard A J, Fox MA (1995) *Acc Chem Res* 28:141
8. Eisenberg R, Nocera DG (2005) *Inorg Chem* 44:6799
9. Lewis NU, Nocera DG (2006) *Proc Natl Acad Sci USA* 103:15729
10. Crabtree GW, Lewis NS (2007) *Phys Today* 60:37
11. Kamat PV (2007) *J Phys Chem C* 111:2834
12. Lewis NS (2007) *Science* 315:798
13. Lewis NS (2005) *Inorg Chem* 44:6900
14. Balzani V, Credi A, Venturi M (2003) *Molecular devices and machines – a journey into the nanoworld*. Wiley-VCH, Weinheim
15. Kay ER, Leigh DA, Zerbetto F (2007) *Angew Chem Int Ed* 46:72
16. Saha S, Stoddart JF (2007) *Chem Soc Rev* 36:77
17. Kay ER, Leigh DA (2006) *Nature* 440:286
18. O'Regan B, Grätzel M (1991) *Nature* 353:737
19. Kalyanasundaram K, Grätzel M (1998) *Coord Chem Rev* 77:347
20. Hagfeldt A, Grätzel M (2000) *Acc Chem Res* 33:269
21. Grätzel M (2005) *Inorg Chem* 44:6841
22. Nazeeruddin MK, Pechy P, Renouard T, Zakeeruddin SM, Humphry-Baker R, Comte P, Liska P, Cevey L, Costa E, Shklover V, Spiccia L, Deacon GB, Bignozzi CA, Grätzel M (2001) *J Am Chem Soc* 123:1613
23. Campbell WM, Burrell AK, Officer DL, Jolley KW (2004) *Coord Chem Rev* 248:1363
24. Claessens CG, Hahn U, Torres T (2008) *Chem Rec* 8:75
25. Kadish KM, Smith KM, Guillard R (2003) *The porphyrin handbook*, vols. 15–20. Academic, San Diego
26. de la Torre G, Vázquez P, Agulló-López F, Torres T (2004) *Chem Rev* 104:3723
27. Leznoff CC, Lever ABP (1989, 1993, 1996) *Phthalocyanines: properties and applications*, vols. 1–4. VCH Publishers, Cambridge
28. McKeown N B (1998) *Phthalocyanine materials. synthesis, structure and function*. Cambridge University Press, Cambridge
29. Shepard VR, Armstrong NR (1979) *J Phys Chem* 83:1268
30. Buttner WJ, Rieker PC, Armstrong NR (1985) *J Am Chem Soc* 107:3738
31. Rieke PC, Armstrong NR (1984) *J Am Chem Soc* 106:47
32. Klofta TJ, Danziger J, Lee P, Pankow J, Nebesny KW, Armstrong NR (1987) *J Phys Chem* 91:5646
33. Jaeger CD, Fan FRF, Bard AJ (1980) *J Am Chem Soc* 102:2592
34. Giraudeau A, Fan FRF, Bard AJ (1980) *J Am Chem Soc* 102:5137
35. Shen YC, Wang L, Lu ZH, Wei Y, Zhou QF, Mao HF, Xu HJ (1995) *Thin Solid Films* 257:144
36. Fang JH, Wu JW, Lu XM, Shen YC, Lu ZH (1997) *Chem Phys Lett* 270:145
37. Deng H, Lu ZH, Mao HF, Xu HJ (1997) *Chem Phys* 221:323
38. Deng H, Mao HF, Liang BJ, Shen YC, Lu ZH, Xu HJ (1996) *J Photochem Photobiol A Chem* 99:71
39. Deng H, Lu ZH, Shen YC, Mao HF, Xu HJ (1998) *Chem Phys* 231:95
40. Zhang J, Wang DJ, Chai XD, Li TI, Mao HF, Tian HJ, Zhou QF, Xu HJ (1997) *Synth Met* 86:1995
41. Mao HF, Tian HJ, Zhou QF, Xu HJ, Shen YC, Lu ZH (1997) *Chin Sci Bull* 42:833
42. Nazeeruddin MK, Humphry-baker R, Grätzel M, Wöhrle D, Schnurpfeil G, Schneider G, Hirth A, Trombach N (1999) *J Porphyr Phthalocyanines* 3:230

43. Hagfeldt A, Grätzel M (1995) *Chem Rev* 95:49
44. He JJ, Hagfeldt A, Lindquist S-E (2001) *Langmuir* 17:2743
45. He JJ, Benkő G, Korodi F, Polívka T, Lomoth R, Åkermark B, Sun L, Hagfeldt A, Sundström V (2002) *J Am Chem Soc* 124:4922
46. Liu GM, Jaegermann W, He JJ, Sundström V, Sun LC (2002) *J Phys Chem B* 106:5814
47. Clifford JN, Palomares E, Nazeeruddin MK, Grätzel M, Nelson J, Li X, Long NJ, Durrant JR (2004) *J Am Chem Soc* 126:5225
48. Reddy PY, Giribabu L, Lyness C, Snaith HJ, Vijaykumar C, Chandrasekharan M, Lakshmikantham M, Yum JH, Kalyanasundaram K, Grätzel M, Nazeeruddin MK (2007) *Angew Chem Int Ed* 46:373
49. Giribabu L, Kumar CV, Reddy VG, Reddy PY, Rao CS, Jang SR, Yum JH, Nazeeruddin MK, Grätzel M (2007) *Sol Energy Mater Sol Cell* 91:1611
50. Eu SH, Katoh T, Umeyama T, Matano Y, Imahori H (2008) *Dalton Trans* 5476
51. Yanagisawa M, Korodi F, Bergquist J, Holmberg A, Hagfeldt A, Åkermark B, Sun LC (2004) *J Porphyr Phthalocyanines* 8:1228
52. Yum JH, Jang SR, Humphry-Baker R, Grätzel M, Cid JJ, Torres T, Nazeeruddin MK (2008) *Langmuir* 24:5636
53. Cid JJ, Yum JH, Jang SR, Nazeeruddin MK, nez-Ferrero EM, Palomares E, Ko J, Grätzel M, Torres T (2007) *Angew Chem Int Ed* 46:8538
54. Robertson N (2008) *Angew Chem Int Ed* 47:1012
55. Chen Y, Zeng Z, Li C, Wang W, Wang X, Zhang B (2005) *New J Chem* 29:773
56. Nazeeruddin MK, Humphry-Baker R, Grätzel M, Murrer BA (1998) *Chem Comm* 719
57. Yanagisawa M, Korodi F, He J, Sundström V, Åkermark B (2002) *J Porphyr Phthalocyanines* 6:217
58. Liu G, Klein A, Thissen A, Jaegermann W (2003) *Surf Sci* 539:37
59. Morandeira A, López-Duarte I, Martínez-Díaz MV, O'Regan B, Shuttle C, Haji-Zainulabidin NA, Torres T, Palomares E, Durrant JR (2007) *J Am Chem Soc* 129:9250
60. O'Regan BC, López-Duarte I, Victoria M, Martínez-Díaz MV, Forneli A, Albero J, Morandeira A, Palomares E, Torres T, Durrant JR (2008) *J Am Chem Soc* 130:2906
61. Palomares E, Martínez-Díaz MV, Haque SA, Torres T, Durrant JR (2004) *Chem Commun* 2112
62. Aranyos V, Hjelm J, Hagfeldt A, Grennberg H (2001) *J Porphyr Phthalocyanines* 5:609
63. Amao Y, Komori T (2003) *Langmuir* 19:8872
64. Kalyanasundaram K, Vlachopoulos N, Krishnan V, Monnier A, Grätzel M (1987) *J Phys Chem* 91:2342
65. Dabestani R, Bard AJ, Campion A, Fox MA, Mallouk TE, Webber SE, White JM (1988) *J Phys Chem* 92:1872
66. Boschloo GK, Goossens A (1996) *J Phys Chem* 100:19489
67. Jasieniak J, Johnston M, Waclawik ER (2004) *J Phys Chem B* 108:12962
68. Cherian S, Wamser CC (2000) *J Phys Chem B* 104:3624
69. Chen DM, Dong Y, Geng JQ, Zhu JH, Jiang ZY (2008) *Appl Surf Sci* 255:2879
70. Tachibana Y, Haque SA, Mercer IP, Durrant JR, Klug DR (2000) *J Phys Chem B* 104:1198
71. Inoue K, Noma H, Yao K, Abe E (2002) *J Mater Sci Lett* 21:1013
72. Imahori H, Hayashi S, Umeyama T, Eu S, Oguro A, Kang S, Matano Y, Shishido T, Ngamsinlapasathian S, Yoshikawa S (2006) *Langmuir* 22:11405
73. Ma TL, Inoue K, Yao K, Noma H, Shuji T, Abe E, Yu JH, Wang XS, Zhang BW (2002) *J Electroanal Chem* 537:31
74. Ma TL, Inoue K, Noma H, Yao K, Abe E (2002) *J Photochem Photobiol A Chem* 152:207
75. Giribabu L, Kumar CV, Raghavender M, Somaiah K, Yella P, Rao PV (2008) *J Chem Sci* 120:455
76. Odobel F, Blart E, Lagree M, Villieras M, Boujtita H, Murr NE, Caramori S, Bignozzi CA (2003) *J Mater Chem* 13:502
77. Rochford J, Chu D, Hagfeldt A, Galoppini E (2007) *J Am Chem Soc* 129:4655
78. Tacconi NR, Chanmanee W, Rajeshwar K, Rochford J, Galoppini E (2009) *J Phys Chem C* 113:2996

79. Lin CY, Lo CF, Luo LY, Lu HP, Hung CS, Diau EW (2009) *J Phys Chem C* 113:755
80. Watson DF, Marton A, Stux AM, Meyer GJ (2004) *J Phys Chem B* 108:11680
81. Wamsler CC, Kim HS, Lee JK (2002) *Opt Mater* 21:221
82. Kang MS, Oh JB, Roh SG, Kim MR, Lee JK, Jin SH, Kim HK (2007) *Bull Korean Chem Soc* 28:33
83. Brune A, Jeong G, Liddell PA, Sotomura T, Moore TA, Moore AL, Gust D (2004) *Langmuir* 20:8366
84. Nazeeruddin MK, Humphry-Baker R, Officer DL, Campbell WM, Burrell AK, Grätzel M (2004) *Langmuir* 20:6514
85. Campbell WM, Burrell AK, Officer DL, Jolley KW (2004) *Coord Chem Rev* 248:1363
86. Schmidt-Mende L, Campbell WM, Wang Q, Jolley KW, Officer DL, Nazeeruddin MK, Grätzel M (2005) *ChemPhysChem* 6:1253
87. Wang Q, Campbell WM, Bonfantani EE, Jolley KW, Officer DL, Walsh PJ, Gordon K, Humphry-Baker R, Nazeeruddin MK, Grätzel M (2005) *J Phys Chem B* 109:15397
88. Campbell WM, Jolley KW, Wagner P, Wagner K, Walsh PJ, Gordon KC, Schmidt-Mende L, Nazeeruddin MK, Wang Q, Grätzel M, Officer DL (2007) *J Phys Chem C* 111:11760
89. Lee CW, Lu HP, Lan CM, Huang YL, Liang YR, Yen WN, Liu YC, Lin YS, Diau EW, Yeh CY (2009) *Chem Eur J* 15:1403
90. Hayashi S, Matsubara Y, Eu S, Hayashi H, Umeyama T, Matano Y, Imahori H (2008) *Chem Lett* 37:846
91. Hayashi S, Tanaka M, Hayashi H, Eu S, Umeyama T, Matano Y, Araki Y, Imahori H (2008) *J Phys Chem C* 112:15576
92. Eu S, Hayashi S, Umeyama T, Matano Y, Araki Y, Imahori H (2008) *J Phys Chem C* 112:4396
93. Bignozzi CA, Argazzi R, Kleverlaan CJ, Bignozzi CA, Argazzi R, Kleverlaan C (2000) *Chem Soc Rev* 29:87
94. Koehorst RBM, Boschloo GK, Savenije TJ, Gössens A, Schäfersma TJ (2000) *J Phys Chem B* 104:2371
95. Fungo F, Otero LA, Sereno L, Silber JJ, Durantini EN (2000) *J Mater Chem* 10:645
96. Fungo F, Otero L, Durantini EN, Silber JJ, Sereno LE (2000) *J Phys Chem B* 104:7644
97. Loewe RS, Lammi RK, Diers JR, Kirmaier C, Bocian DF, Holten D, Lindsey JL (2002) *J Mater Chem* 12:1530
98. Milanesio ME, Garvaldo M, Otero LA, Sereno L, Silber JL, Durantini EN (2002) *J Phys Org Chem* 15:844
99. Shiga T, Motohiro T (2008) *Thin Solid Films* 516:1204
100. Liu MO, Hu AT (2004) *J Organomet Chem* 689:2450
101. Pagona G, Sandanayaka ASD, Hasobe T, Charalambidis G, Coutsolelos AG, Yudasaka M, Iijima S, Tagmatarchis N (2008) *J Phys Chem C* 112:15735
102. Kalyanasundaram K, Shelnutt A, Grätzel M (1998) *Inorg Chem* 27:2820
103. Kay A, Grätzel M (1993) *J Phys Chem* 97:6272
104. Kay A, Humphry-Baker R, Grätzel M (1994) *J Phys Chem* 98:952
105. Amao Y, Yamada Y, Aoki K (2004) *J Photochem Photobiol A Chem* 164:47
106. Amao Y, Komori T (2004) *Biosens Bioelectron* 19:843
107. Kureishi Y, Shiraiishi H, Tamiaki H (2001) *J Electroanal Chem* 496:13
108. Pan JX, Xu YH, Sun LC, Sundström V, Polívka T (2004) *J Am Chem Soc* 126:3066
109. Astuti Y, Palomares E, Haque SA, Durrant JR (2005) *J Am Chem Soc* 127:15120
110. Wang XF, Koyama Y, Nagae H, Wada Y, Sasaki S, Tamiaki H (2008) *J Phys Chem C* 112:4418

# Organic Semiconductors of Phthalocyanine Compounds for Field Effect Transistors (FETs)

Yuexing Zhang, Xue Cai, Yongzhong Bian, and Jianzhuang Jiang

**Abstract** Various functional phthalocyanines as well as their tetrapyrrole analogs, porphyrins, have been extensively studied as organic semiconductors since the first report of organic field effect transistors (OFETs) in 1986. The large conjugated  $\pi$  system, excellent photoelectric characteristics, intriguing and unique optical properties, high thermal and chemical stability, and most importantly the easy functionalization of phthalocyanines render them ideal organic semiconductor materials as active layers for OFETs. In this chapter, the semiconducting properties of monomeric phthalocyanines as well as monomeric porphyrins, bis(phthalocyaninato) rare earth double-deckers, and tris(phthalocyaninato) rare earth triple-deckers in terms of their semiconducting nature (*p*-type, *n*-type, or ambipolar), carrier mobility, and current modulation reported in the past two decades have been summarized. Theoretical studies toward understanding the relationship between molecular structures as well as molecular electronic structures of phthalocyanines and their semiconducting properties have also been included.

**Keywords** Field effect transistors (FETs) · Organic semiconductor · Phthalocyanine · Porphyrin · Tetrapyrrole

## Contents

1	Introduction .....	277
2	Basics of Organic Field Effect Transistors (OFETs) .....	278
2.1	Device Structure .....	279
2.2	OFET Performance Characterization .....	281
3	Theoretical Studies on Phthalocyanine Semiconductors .....	282
4	<i>p</i> -Type Phthalocyanine Semiconductors .....	285
4.1	Monomeric Phthalocyanine Semiconductors .....	285
4.2	Sandwich Bis(Phthalocyaninato) Rare Earth Double-Decker Semiconductors .....	297
4.3	Sandwich Tris(Phthalocyaninato) Rare Earth Triple-Decker Semiconductors .....	298
4.4	Monomeric Porphyrin Semiconductors .....	300
5	<i>n</i> -Type Phthalocyanine Semiconductors .....	307

Y. Zhang, X. Cai, Y. Bian, and J. Jiang (✉)

Department of Chemistry, University of Science and Technology Beijing, Beijing 100083, China  
e-mail: jianzhuang@ustb.edu.cn



6	Ambipolar Phthalocyanine Semiconductors .....	311
7	Conclusion .....	317
	References .....	318

## Abbreviations

TC/BG	Top contact/bottom gate
BC/BG	Bottom contact/bottom gate
SC/BG	Sandwich contact/bottom gate
BC/TG	Bottom contact/top gate
PR-TRMC	Pulse-radiolysis time-resolved microwave conductivity technique
ITO	Indium tin oxide
OTS	Octadecyltrichlorosilane
GMA	Glycidyl methacrylate
PBMA	Poly(butyl methacrylate)
PMMA	Poly(methylmethacrylate)
P(MMA-co-GMA)	Poly(methylmethacrylate-co-glycidylmethacrylate)
PVP	Poly(4-vinylphenol)
C6	1,6-bis(trichlorosilyl)hexane
CPVP-C6	Poly[1,6-(4-vinylphenol)-bis(bichlorosilyl)hexane]
Parylene-C	Dichloro-[2,2]-paracyclophane
Parylene-N	[2,2]-paracyclophane
CyEPL	Cyanoethylpullulan
HMDS	Hexamethyldisilazane
PZT	$\text{PbZr}_{0.5}\text{Ti}_{0.5}\text{O}_3$
P1	Polyimide-1
P2	Poly(amic acid)
PI	Polyimide-2
PVC	Poly(vinylchloride)
PVDF	Poly(vinylidene fluoride)
PAN	Poly(acrylonitrile)
PNVP	Poly(N-vinylpyrrolidone)
PS	Poly(styrene)
PVPy	Poly(4-vinylpyridine)
PVK	Poly(N-vinylcarbazole)
<i>p</i> -6P	Para-sexiphenyl
MPc	Monomeric phthalocyaninate metal complex
H <sub>2</sub> Pc	Metal free phthalocyanine
VOPc	Vanadyl phthalocyanine
TiOPc	Titanyl phthalocyanine
H <sub>2</sub> PcAmBu	2(3)-amino-9(10),16(17),23(24)-tri( <i>tert</i> -butyl)-phthalocyanine
H <sub>2</sub> PcNT	2(3)-(1,8-naphthalimide)-9(10),16(17),23(24)-tri( <i>tert</i> -butyl)-phthalocyanine
CuPc-i-Pro	Tetra-iso-propoxy-phthalocyaninato copper (II)

CuPcTSNa	Copper phthalocyanine tetrasulfonic acid tetrasodium salt
ZnPcTO	Tetra-{4-[5-(4- <i>tert</i> -butyl-phenyl)-[1,3,4]oxadiazol-2-yl]-phenoxy}-zincphthalocyanine
H <sub>2</sub> PcT( <i>t</i> -Bu)(COOH)	2,9,16-tri( <i>tert</i> -butyl)-23-(10-hydroxydecyloxy) phthalocyanine
CuPcT( <i>t</i> -Bu)(COOH)	2,9,16-tri( <i>tert</i> -butyl)-23-(10-hydroxydecyloxy) copper phthalocyanine
M(Pc) <sub>2</sub>	Bis(phthalocyaninato) rare earth complex
MPc[Pc(OC <sub>8</sub> H <sub>17</sub> ) <sub>8</sub> ]	Heteroleptic (phthalocyaninato) [2,3,9,10,16,17,23,24-octakis(octyloxy)-phthalocyaninato] rare earth double-decker complex
MOEP	2,3,7,8,12,13,17,18-octaethyl-porphyrinate metal complex
H <sub>2</sub> OEP	2,3,7,8,12,13,17,18-ocataethyl-21H,23H-porphyrin
H <sub>2</sub> TPP	5,10,15,20-tetra-phenyl-21H,23H-porphyrin
H <sub>2</sub> TBP	Tetrabenzoporphyrin
NiTBP	Nickel tetrabenzoporphyrin
CuTBP	Copper tetrabenzoporphyrin
H <sub>2</sub> EP-I	Etioporphyrin-I
MEP-I	Metal etioporphyrin-I
H <sub>2</sub> TPrP	2,7,12,17-tetra-( <i>n</i> -propyl)-porphycene
PtTPrP	2,7,12,17-tetra-( <i>n</i> -propyl)-porphycene platinum
H <sub>2</sub> TBuP	5,10,15,20-tetra-( <i>n</i> -butyl)-porphyrin
PtTBuP	5,10,15,20-tetra-( <i>n</i> -butyl)-porphyrin platinum
MPcF <sub>16</sub>	Metal hexadecafluorophthalocyanine
FePcCl <sub>16</sub>	Iron hexadecachlorinphthalocyanine
FePc(CN) <sub>16</sub>	Copper hexadecacyanophthalocyanine
SnCl <sub>2</sub> Pc	Phthalocyanato tin(IV) dichloride
SnOPc	Tin (IV) phthalocyanine oxide
DH- $\alpha$ 6T	$\alpha$ , $\alpha'$ -dihexylsexithiophene
TCNQ	7,7,8,8-tetracyano- <i>p</i> -quinodimethane
BBL	Poly(benzobisimidazobenzophenanthroline)
BP2T	2,5-bis(4-biphenyl) bithiophene
AB	Copper(II) phthalocyanine tetrakis(methyl pyridinium) chloride

## 1 Introduction

Organic field effect transistors (OFETs) have attracted increasing research interests because of their great potential applications in the field of flexible displays, integrated circuits, and low-cost electronic devices since their first report in 1986 [1]. To achieve good OFET performance, organic semiconductor as the most important part of OFET devices should possess the following characteristics: large conjugated  $\pi$ -system, enough chemical purity, good film-forming properties, and good

intermolecular electronic overlap. In general, organic oligomers, polymers, and some small molecules with conjugated electronic structures are among the most intensively studied organic semiconductors for OFET applications.

Phthalocyanines and porphyrins, as the most common and important tetrapyrrole derivatives, have been at the focus of multidisciplinary interests for more than one century [2–7]. Both series of tetrapyrrole macrocycles are able to form complexes with almost all the metals in the Periodic Table. These tetrapyrrole macrocycles and their metal complexes have been emerging as an important class of novel advanced functional materials in molecular electronics, molecular magnet, molecular information storage, nonlinear optics, and OFET because of their unique electronic structures and properties. Associated with the large conjugated  $\pi$  system, excellent photoelectric characteristics, intriguing optical properties, high thermal and chemical stability, and the easy functionalization of tetrapyrrole compounds, both porphyrin and in particular phthalocyanine derivatives have been extensively studied for OFET applications since the first demonstration of organic semiconductors. The present chapter summarizes the progress made in the field of tetrapyrrole semiconductors with the emphasis on phthalocyanine complexes for OFETs.

Despite the extensive experimental studies of phthalocyanine semiconductors for OFETs since 1987, theoretical investigations on the OFET properties of these compounds are very scarce. Designing and synthesizing new semiconductor materials with high charge transfer mobility, high current modulation value, high ambient stability, and good solubility in common organic solvents as the active layer of OFETs is still a challenge for manufacturing OFETs, especially for those toward preparing ambipolar devices. Using theoretical scheme to predict the carrier mobility of phthalocyanine semiconductors is therefore carried out and included in this chapter.

Due to the great potential applications and the widespread interests of OFETs, several review articles with emphasis on different aspects of OFETs have been published [8–13]. However, despite the extensive studies and increasing research interests in phthalocyanine as well as porphyrin semiconductors, there is still no review article that systematically generalizes the research achievements in the field of tetrapyrrole organic semiconductors for OFETs. Thus, the present contribution should interest scientists in both industrial and theoretical fields. The main contents of this chapter is as follows: Firstly, some basic introduction of the structure and characteristics of OFET is provided; then theoretical factors that influence the performance of OFET devices is discussed; finally, the progress in phthalocyanine-based OFETs in the order of *p*-type, *n*-type, and ambipolar semiconductors is summarized.

## 2 Basics of Organic Field Effect Transistors (OFETs)

As the structures and current-voltage characteristic of OFETs have been well described in many other articles [8–13], herein we only give a very simple introduction on the basics of phthalocyanine-based OFET devices.

## 2.1 Device Structure

Figure 1 shows the structures of types of OFET devices arising from the relative position of the source-drain and gate electrodes in relation to the semiconductor layer. Most of the reported OFET devices have five components: substrate, gate electrode, insulator layer, semiconductor layer(s), and source-drain electrodes. Commonly, the substrate is at the bottom of the device as solid support, gate electrode is joined with the circuit to provide gate voltage, insulator layer locates between gate electrode and semiconductor layer to insulate the charge of gate electrode from injecting the semiconductor layers, semiconductor layer(s) is the active layer of OFET device in contact with the source-drain electrodes and separated from the gate electrode by the insulator layer, and the source and drain electrodes provide injection charge and drain voltage, respectively. As for the chemical composition, the gate electrode is often composed of highly doped silicon, which can also serve as substrate in some OFET devices. Some metals or conducting polymers can also work as gate electrode. The insulator layer is either an inorganic insulator such as  $\text{SiO}_2$  (thermally grown on Si),  $\text{Al}_2\text{O}_3$ ,  $\text{SiN}_x$ , and  $\text{Ta}_2\text{O}_5$  or some polymeric insulator such as PMMA and PVP. Figure 2 shows the molecular structures of some polymers used as insulator layer of phthalocyanine-based OFET devices. Multiple insulator layers composed of both inorganic and polymeric insulators are also used. The

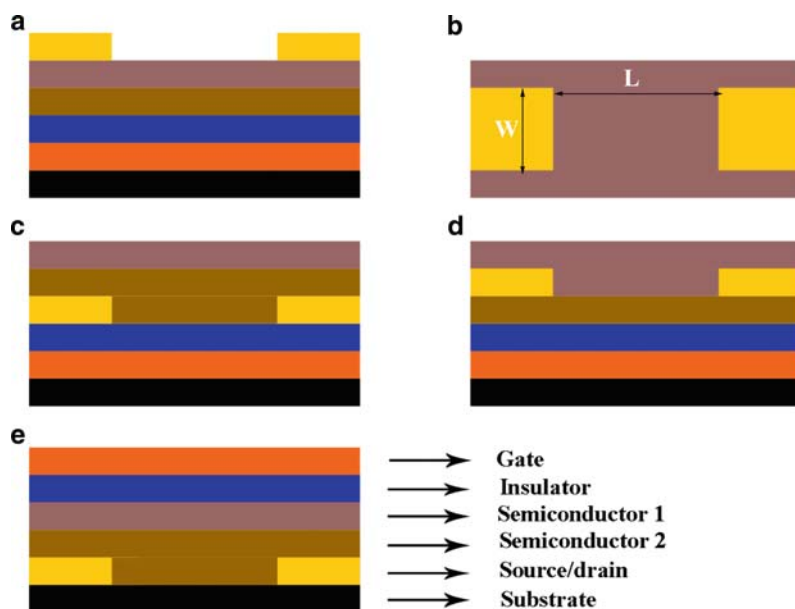


**Fig. 1** Schematic drawing of the structures of four kinds of typical OFET devices (a) Top contact/bottom gate (TC/BG); (b) Top view of (a),  $W$ : channel width,  $L$ : channel length; (c) bottom contact/bottom gate (BC/BG); (d) sandwich contact/bottom gate (SC/BG); and (e) bottom contact/top gate (BC/TG)

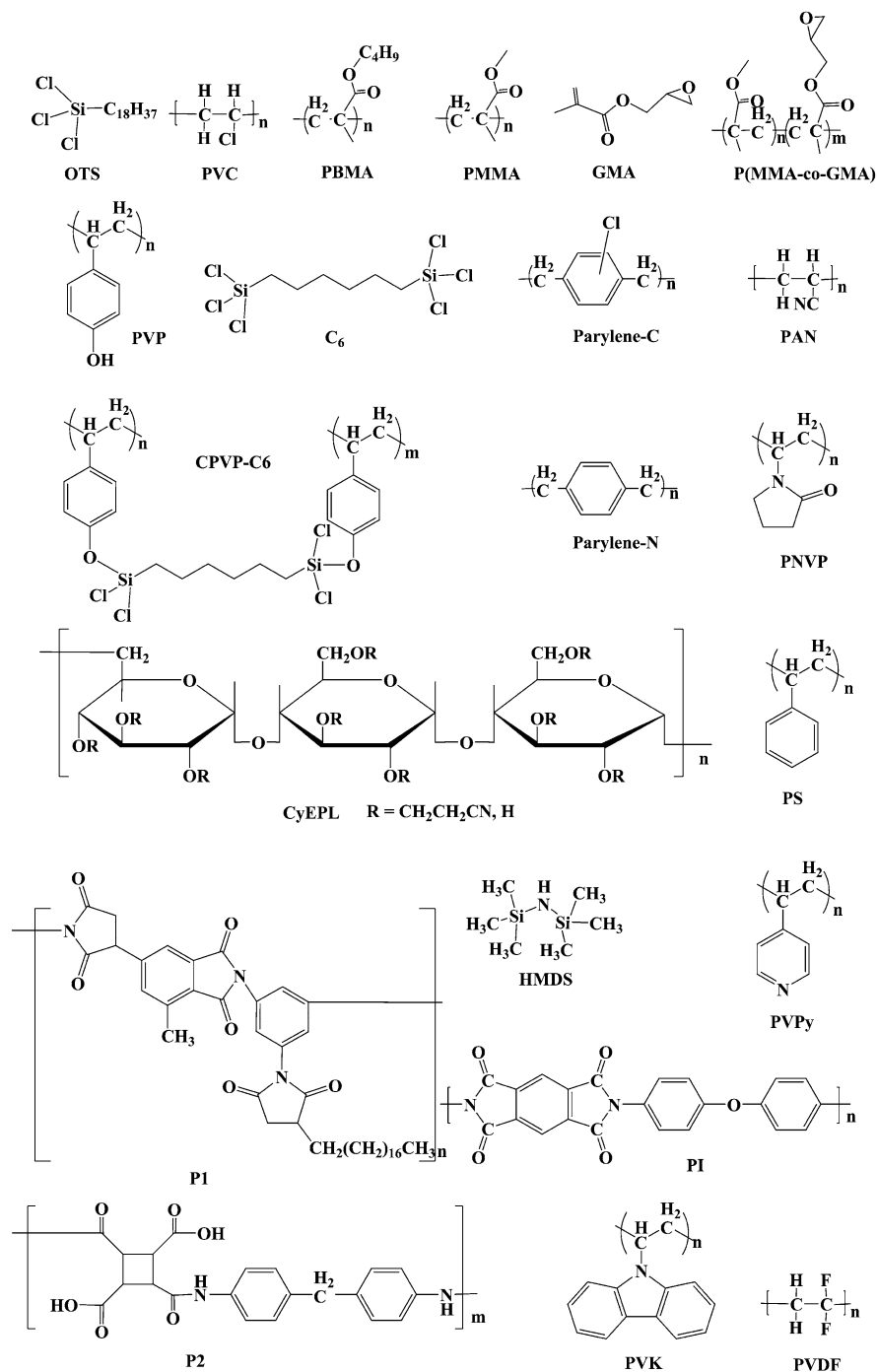


Fig. 2 Molecular structures of some polymers used as insulator layer in the reported phthalocyanine-based OFET devices

semiconductor layer can be made by vacuum depositing, spin-coating, drop-casting, or LB film technique depending on the properties of semiconductor materials. The source and drain electrodes are usually high work function metals such as gold, palladium, platinum, and silver, while conducting polymers are used as well. To achieve efficient charge injection, asymmetry electrodes (using different metals as source and drain electrodes respectively) and some low work function metals such as calcium are also used in OFET devices. Although top contact/bottom gate (TC/BG) OFET is most widely used because of the facility of fabrication, the choice of OFET device structure actually depends on the requirement of the physical nature of the semiconductor and insulator materials.

## 2.2 OFET Performance Characterization

The performance of OFET device is usually characterized by three important parameters: threshold voltage ( $V_T/V$ ), on/off current ratio ( $I_{\text{on}}/I_{\text{off}}$ ), and charge transfer mobility ( $\mu/\text{cm}^{-2} \text{V}^{-1} \text{s}^{-1}$ ). Threshold voltage reflects the minimum gate voltage applied to fill the deep traps in semiconductor layers in order to make the charge be mobile. It should be as small as possible. On/off current ratio is the ratio of the drain current in the on-state of a particular gate voltage and the drain current in the off-state. For clean switching behavior of the transistor, on/off current ratio should be as large as possible. Charge transfer mobility as the most important parameter in determining the performance of OFET devices quantifies the average charge carrier drift velocity per unit electric field, which should be as high as possible for OFET applications.

Usually, the source electrode is grounded while negative or positive voltage is applied to the drain electrode and gate electrode. By increasing the applied gate voltage and sweeping the drain voltage between some voltage region at a given gate voltage, one can get current-voltage characteristics as shown in Fig. 3. When negative gate and drain voltage is applied, the positive charge (hole) gathered at the insulator/semiconductor interface will work as charge carriers. If high drain current

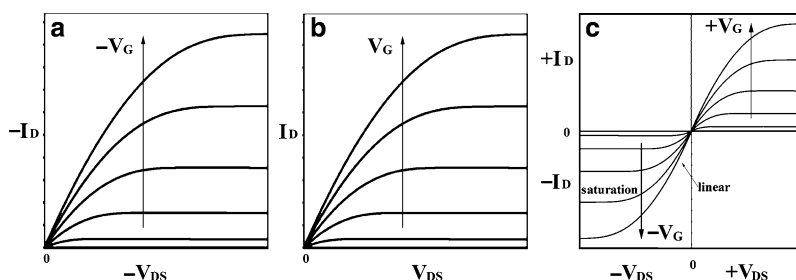


**Fig. 3** Schematic diagram of current-voltage characteristics of (a) *p*-type, (b) *n*-type, and (c) ambipolar OFET device

and field-effect behavior can be observed, this kind of OFET device is called *p*-type OFET and the corresponding semiconductor(s) is called *p*-type semiconductor(s) (Fig. 3a). In contrast, if positive gate and drain voltage is applied and negative charge (electron) works as charge carriers, *n*-type OFET is achieved (Fig. 3b). Nevertheless, if semiconductors display field-effect behavior in both negative and positive gate and drain voltage, that is, both hole and electron carriers can be observed, they are showing ambipolar semiconducting nature (Fig. 3c). As can be seen from Fig. 3, when gate voltage is low, only negligible drain current is detected, which almost does not change with increasing the drain voltage. The device is at off-state. When gate voltage ( $V_G$ ) is higher than the threshold voltage ( $V_T$ ), the device will be turned on. In this case, drain current ( $I_D$ ) firstly increases with increasing drain voltage ( $V_{DS}$ ) when  $V_{DS} < (V_G - V_T)$ . This region is called linear region. At the linear region with  $V_{DS} \ll V_G$ , current can be simply given by:

$$I_D = (WC_i/L)\mu_{\text{lin}}(V_G - V_T)V_{DS}$$

Where  $\mu_{\text{lin}}$  is the field-effect mobility in linear region,  $W$  and  $L$  are channel width and length (Fig. 1b), respectively, and  $C_i$  is the capacitance per unit area of the insulating layer. Thus the field-effect mobility in the linear region can be extracted from gradient of  $I_D$  versus  $V_G$  at constant  $V_{DS}$  (also applicable for gate voltage dependent mobility). When  $V_{DS} > (V_G - V_T)$ , the drain current will then keep almost unchanged with increasing drain voltage. This region is called saturation state. At the saturation region, current can be given by:

$$I_D = (WC_i/2L)\mu_{\text{sat}}(V_G - V_T)^2$$

Therefore, the device mobility can be calculated in the saturation region from the slope of a line drawn of an  $I_D^{1/2}$  vs.  $V_G$  plot through the linear part.

### 3 Theoretical Studies on Phthalocyanine Semiconductors

In addition to the intensive experimental studies over the preparation and fabrication techniques of OFET devices in the past two decades, great efforts have been paid in theoretical and computational aspects toward understanding the nature of organic semiconductors and the relationship between OFET performance and molecular as well as solid state structures and toward designing novel molecular materials with high OFET performance. For example, as early as in 1997, Demanze and co-workers have studied the effect of cyan substitution on tuning the electronic properties of oligothiophenes and the substitution pattern required for designing efficient electron-transporting (*n*-type) oligothiophene derivatives by calculating the reorganization energy [14]. On the basis of density functional theory (DFT) calculations, di-fluorinated boron substituted hexathienoacene was designed as ambipolar semiconductors recently by our group. The intrinsic charge transfer mobility was

calculated to be as high as 5.07 and 5.76 cm<sup>2</sup> V<sup>-1</sup> s<sup>-1</sup> for hole and electron, respectively [15].

Design and synthesis of new materials with high charge transfer mobility, high ambient stability, and good solubility in common organic solvents as the active layer of OFETs is still a great challenge, especially for those toward preparing ambipolar devices. Theoretically, (a) HOMO and LUMO energy, (b) ionization potential (IP) and electron affinity (EA), (c) reorganization energy for hole ( $\lambda_+$ ) and electron ( $\lambda_-$ ), (d) transfer integral for hole ( $t_+$ ) and electron ( $t_-$ ), and (e) corresponding charge transfer distance ( $r$ ) all have influence on the intrinsic semiconducting property of OFET materials. The first two factors (a and b) determine the easiness of charge injection from the source electrode to the semiconductors and thus the nature of semiconductor materials, while the last three factors (c–e) combine together to determine the charge transfer mobility of the organic semiconductors and thus the performance of the OFET device fabricated with these semiconductors. To ensure large charge transfer mobility, semiconductors should have small reorganization energy and/or large transfer integral even for far transfer distance. On the other hand, *p*- and *n*-type semiconductors should possess high HOMO and low LUMO energy, respectively, which in turn results in small ionization potential and large electron affinity (at least 3.0 eV). Both ionization potential and electron affinity should actually be close to the work function potential of the source-drain electrodes (5.1 eV for Au electrode) to yield small charge injection barrier for hole and electron, respectively and therefore ensure the effective charge injection from the source electrode. As expected, ambipolar semiconductors are those materials simultaneously with high HOMO and low LUMO energy as well as small ionization potential and large electron affinity. Among the five factors (a–e) mentioned above, the former three (a–c) are clearly determined by the intrinsic property of single molecule while the latter two factors (d and e) by interaction between neighbouring molecules and thus closely associated with the solid state structure of corresponding compounds. As a consequence, molecular design toward ambipolar organic semiconductors should aim for compounds with both high HOMO and low LUMO, small ionization potential and large electron affinity, and small intrinsic hole and electron reorganization energy in nature in terms of both injection barrier and charge transfer mobility. Functionalizing *p*-type semiconductors, including replacing the functional atom(s) and/or substituting the hydrogen atom(s) with electron-withdrawing group(s), has been revealed as one of the most effective methods in tuning the semiconductor nature from *p*-type to *n*-type or ambipolar semiconductors, as revealed by the groups of Chao and Jiang [15, 16].

In the two models treating carrier motion in solid state (coherent band model and incoherent hopping model), the hopping mechanism has been proved to be the dominant mechanism in organic semiconductors at high temperature and is advocated by Brédas and other scientists [17–20]. In the hopping model, charge transfer can be described as a self-exchange electron-transfer reaction between a neutral molecule and a neighboring radical cation (*p*-type) or radical anion (*n*-type). The rate constant for charge transfer ( $W$ ) thus can be modeled by classical Marcus theory [21, 22]:



$$W = (t^2/\hbar)(\pi/\lambda_{\pm}k_B T)^{1/2}\exp(-\lambda_{\pm}/4k_B T)$$

where  $t$  is the transfer integral,  $\lambda_{\pm}$  the reorganization energy,  $k_B$  the Boltzmann constant, and  $T$  the temperature. Neglecting the influence of intermolecular interaction on the molecular deformation, the reorganization energy  $\lambda_+$  or  $\lambda_-$  for hole or electron transfer, respectively, is calculated as the sum of the energy required for the reorganization of the vertically ionized neutral to the cation or anion geometry and the energy required to reorganize the cation or anion geometry back to the neutral equilibrium structure on the ground state potential energy surface. To achieve high charge carrier mobility, the reorganization energy needs to be minimized. The transfer integral  $t$  depends on the relative arrangement of the molecules in the solid state and describes the intermolecular electronic coupling which needs to be maximized to achieve high charge carrier mobility. The direct dimer Hamiltonian evaluation method [23] was used in evaluating charge transfer integrals:

$$t = \left\langle \Phi_{HOMO/LUMO}^{0,site1} \middle| F^0 \middle| \Phi_{HOMO/LUMO}^{0,site2} \right\rangle$$

which has been proved simple, efficient, and reliable [24] in comparison with the site energy and overlap corrected splitting scheme of Valeev and co-workers [25]. Given the rate constant for charge transfer ( $W$ ) between two neighboring molecules, the diffusion coefficient can be evaluated as [20, 26, 27]:

$$D = \frac{1}{2d} \frac{\langle x(t)^2 \rangle}{t} \approx \frac{1}{2d} \sum_i r_i^2 W_i P_i$$

In the above equation  $i$  represents a specific transfer path way with  $r_i$  being the transfer distance (intermolecular center to center distance),  $1/W_i$  the transfer time, and  $d$  the spatial dimension, which is equal to 3 for crystal, and  $P_i$  is the relative probability for the  $i$ th pathway:

$$P_i = W_i / \sum_i W_i$$

The basic assumption is that the charge transfer is a slow process in which the molecules have enough time to become equilibrium. This is pertinent for soft organic system. The drift charge transfer mobility,  $\mu$ , is then evaluated from the Einstein relation:

$$\mu = \frac{e}{k_B T} D$$

According to the above methodology, theoretical studies over bis(phthalocyaninato) metal complexes have been carried out in our group recently for further understanding the relationship between molecular structure and local charge transfer mobility and the rational designing of phthalocyanine-based organic semiconductor materials with good performance for OFET devices [28]. The results indicate

that the intrinsic delocalized hole in  $M(\text{Pc})_2$  ( $M = \text{Y, La}$ ) induces the high energy level of HOMO and low energy level of LUMO in the sandwich double-decker molecules as well as the small ionization potential and large electronic affinity, leading to very small injection barrier relative to Au source-drain electrode for both hole and electron and rendering these double-decker compounds as good potential ambipolar semiconductor. This is in line with the experimental findings by Simon and co-workers that bis(phthalocyaninato) rare earth complexes display both *p*- and *n*-type semiconducting properties [29]. Associated with the very small reorganization energy for hole and electron and large transfer integral in crystal, these two complexes  $M(\text{Pc})_2$  ( $M = \text{Y, La}$ ) are revealed to display charge transfer mobility of 0.034 and 0.17 cm<sup>2</sup> V<sup>-1</sup> s<sup>-1</sup> for hole and 0.031 and 0.088 cm<sup>2</sup> V<sup>-1</sup> s<sup>-1</sup> for electron in crystal, respectively, according to calculation results. In addition, the charge transfer mobility in the dimers composed of two  $\text{Y}(\text{Pc})_2$  molecules in terms of molecular packing mode is systematically studied, which rationalizes the good charge mobility for hole observed experimentally of sandwich-type heteroleptic phthalocyaninato rare earth complexes in thin solid films. Our theoretical studies on phthalocyanine semiconductors will be helpful in understanding the charge transfer properties of phthalocyanine materials and developing novel phthalocyanine-based semiconductor materials for OFET applications.

## 4 *p*-Type Phthalocyanine Semiconductors

Similar to the cases in other small molecules and polymers, most materials composed of phthalocyanine compounds are revealed to work as *p*-type semiconductors for OFET applications with only few phthalocyanine materials as *n*-type semiconductors and even less as ambipolar ones. Among the *p*-type tetrapyrrole semiconductors, monomeric phthalocyanine compounds hold all the trumps with only a few double- and triple-deckers together with some porphyrin derivatives having been reported.

### 4.1 Monomeric Phthalocyanine Semiconductors

Figure 4 shows the molecular structures of the monomeric phthalocyanines used as the active layer of *p*-type OFET devices, and Table 1 organizes the performance of these phthalocyanine-based OFETs. As can be seen, unsubstituted metal-free phthalocyanine and its metal complexes, axial substituted metal phthalocyanines, and peripheral tetra-substituted phthalocyanines all can work as *p*-type semiconductors for OFET devices. Most of the semiconductors composed of peripheral unsubstituted and axial substituted phthalocyanine derivatives are prepared through vacuum deposition method with a few exceptions being made of corresponding single

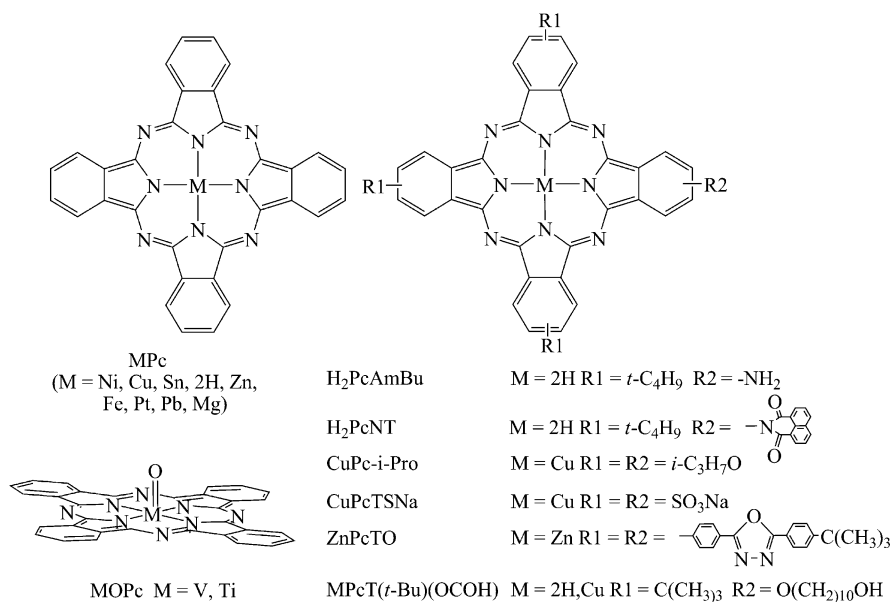


**Fig. 4** Molecular structures of the monomeric phthalocyanines used as semiconductors of *p*-type OFET

crystals, while the peripheral tetra-substituted phthalocyanine semiconductors are prepared through LB or spin-coating film-formation techniques.

The semiconducting behavior of metallo phthalocyanines was first observed in 1948 and then attracted research interest in advance of prototype organic semiconductors [30]. However, the transistor properties of these compounds have received less attention probably because of their low reported charge mobilities. Three years after the first report of OFET in 1986 [1], OFET devices with vacuum deposited NiPc thin film of different thickness as active layer and SiO<sub>2</sub> previously deposited on Si wafers (gate electrode) as insulator were fabricated by Guillaud and co-workers [31]. As the first reported monomeric phthalocyanine-based OFET, hole transfer mobility in the range of  $1.5\text{--}7.0 \times 10^{-4} \text{ cm}^2 \text{ V}^{-1} \text{ s}^{-1}$  and  $V_T$  ranging from  $-3$  to  $-10 \text{ V}$  were recorded for different thickness of NiPc films. The hole transfer mobility of NiPc-based OFETs was significantly improved (to  $0.02 \text{ cm}^2 \text{ V}^{-1} \text{ s}^{-1}$ ) through thermally activating the transistor at  $100^\circ \text{ C}$  [32]. The effect of room atmosphere on the OFET performance of NiPc-based OFET devices was also studied by Guillaud and co-workers in 1994 [33]. In 1995, they reported their NiPc-based OFETs with hole mobility of  $1.14 \times 10^{-3} \text{ cm}^2 \text{ V}^{-1} \text{ s}^{-1}$ , which was the highest mobility among all the reported NiPc-based thin-film transistors at that time [34]. Ben Chaabane and co-workers studied the effect of annealing on the properties of NiPc-based OFETs in 2003 and found that annealing could significantly improve the mobility from  $1.15 \times 10^{-5}$  to  $8.9 \times 10^{-3} \text{ cm}^2 \text{ V}^{-1} \text{ s}^{-1}$  [35].

**Table 1** Performance of some monomeric phthalocyanine-based *p*-type OFET devices (*mE<sub>n</sub>* means  $m \times 10^n$ )

Year	Mobility [ $cm^2V^{-1}s^{-1}$ ]	Material (deposition method)	$-V_T$ [V]	$I_{on}/I_{off}$	Source-drain electrode	Gate electrode	Insulator	Reference
1989	1.7–7E-4	NiPc (v)	3–10	NR	Au	Si	SiO <sub>2</sub>	[31]
1994	6.8E-4	NiPc (v)	24.7	> 1E3	Au	Si	SiO <sub>2</sub> -Si <sub>3</sub> N <sub>4</sub>	[32]
	0.02	NiPc (v, 100° C) <sup>a</sup>						
1995	1.14E-3	NiPc (v)	-31.6	NR	Au	Si	SiO <sub>2</sub> -Si <sub>3</sub> N <sub>4</sub>	[34]
2003	8.9E-3	NiPc (v)	17	NR	Au	Si	SiO <sub>2</sub> -Si <sub>3</sub> N <sub>4</sub>	[35]
1996	0.02	CuPc (v)	10	4E5	Au	Au	SiO <sub>2</sub>	[36]
2000	3E-4	CuPc (v)	NR	E7	Au (Pt)	Si	SiO <sub>2</sub> -SiN <sub>x</sub>	[38]
2001	4E-6	CuPc (v, ⊥) <sup>b</sup>	NR	NR	Au	Al	SiO <sub>2</sub>	[39]
2002	3.5E-3	CuPc (v, BC/BG) <sup>c</sup>	2.6	NR	Au	Si	SiO <sub>2</sub>	[41]
	1.4E-5	CuPc(E,BC/BG) <sup>d</sup>	NR	NR	Cr/Au	Si	SiO <sub>2</sub>	[42]
2003	3.75E-3	CuPc (v, 120° C) <sup>a</sup>	12	2.3E4	Au	Si	SiO <sub>2</sub>	[43]
	4.13E-3	CuPc (v)	4	E4	Au	Si	SiO <sub>2</sub>	[44]
	0.01	CuPc (v, BC/BG) <sup>c</sup>	12.5	NR	Au/Al	Ta	PMMA-Ta <sub>2</sub> O <sub>5</sub>	[45]
	0.01	CuPc (v)	12				Ta <sub>2</sub> O <sub>5</sub>	
2004	2.4E-2	CuPc (v, BC/BG) <sup>c</sup>	14	2E5	Au	Si	OTS-Ta <sub>2</sub> O <sub>5</sub>	[46]
	0.11	CuPc-Au-CoPc (v)	8.9	E5	Au	Si	Ta <sub>2</sub> O <sub>5</sub>	[47]
	0.04	CuPc (v)	13.8	E5				
	0.01	CoPc (v)	10.1	E5				
	0.043	CuPc-Au-CuPc	12.1	NR				
	0.094	(0.9CuPc:0.1CoPc)-CuPc(v)	NR	NR				
	0.015	CuPc(v)	NR	NR	Au	Si	HMDs-SiO <sub>2</sub>	[48]
	0.017		0.95	E3	Au	Nb/SrTiO <sub>3</sub>	PZT	
	3E-4 <sup>e</sup>	CuPc(DC, BC/BG) <sup>f,d</sup>	26	E4	Au	Si	SiO <sub>2</sub>	[49]
	1.1–2.0E-3	CuPc(TOP) <sup>g</sup>	NR	NR	NR	NR	NR	[50]

(continued)

**Table 1** (continued)

Year	Mobility [ $cm^2 V^{-1} s^{-1}$ ]	Material (deposition method)	$-V_T$ [V]	$I_{on}/I_{off}$	Source-drain electrode	Gate electrode	Insulator	Reference
2005	1.61E-2	CuPc (v)	NR	E3	Au	Si	SiO <sub>2</sub> (RW1) <sup>h</sup>	[51]
	1.21E-2		NR				SiO <sub>2</sub> (RW2) <sup>h</sup>	
	1.19E-2		NR				SiO <sub>2</sub>	
2006	1.48E-3	CuPc (v)	1	3.87E5	Au	Si	OTS-SiO <sub>2</sub>	[52]
	1.58E-2	(LuPc <sub>2</sub> buffer layer)-CuPc(v)	10	NR	Au	Ta	Ta <sub>2</sub> O <sub>5</sub>	[53]
	0.050	0.9CuPc:0.1NiPc (v)	9.5	E4	Au	Si	Ta <sub>2</sub> O <sub>5</sub>	[54]
	2E-5	CuPc (v)	6	E2	Au	Cr	PMMA	[55]
	4E-3	CuPc (v)	1.5	E5	Au	Cr-Au(Al)	Ta <sub>2</sub> O <sub>5</sub>	[56]
	9.3E-4	CuPc (v)	1.7	NR	Au	Al/Ta	Ta <sub>2</sub> O <sub>5</sub> + SiO <sub>2</sub>	[57]
	3.8E-3		1.8	> 1E4			Ta <sub>2</sub> O <sub>5</sub>	
	1.0E-3		4.2	NR			Al <sub>2</sub> O <sub>3</sub>	
	2.5E-3	CuPc (v)	18	NR	Au	ITO	P(MMA-co-GMA)	[58]
	4.2E-3	CuPc (v, A) <sup>j</sup>	10					
2007	3.2E-3	CuPc (v, ⊥) <sup>b</sup>	4.1	E4	Au-Au	Au	SiO <sub>2</sub> /SiN <sub>x</sub>	[59]
	3.6E-3	CuPc-V <sub>2</sub> O <sub>5</sub> <sup>j</sup>	NR	NR	Au	Si	SiO <sub>2</sub>	[60]
	6.3E-3	CuPc-V <sub>2</sub> O <sub>5</sub> <sup>j</sup>	NR	NR	Au	Si	SiO <sub>2</sub>	[61]
	1.51E-2	CuPc(v) <sup>k</sup>	8.15	5.96E3	Au	Si	Ta <sub>2</sub> O <sub>5</sub> -SiO <sub>2</sub>	[63]
	1.417E-2	CuPc(v) <sup>k</sup>	8.52	6.23E3				
	1.5E-3	CuPc (v)	6	E4	Al + MoO <sub>3</sub>	Si	OTS + SiO <sub>2</sub>	[64]
	1-6E-4	CuPcF <sub>16</sub> -CuPc	NR	NR	Au	Si	SiO <sub>2</sub>	[65]
	2-6E-4	TCNQ-CuPc						
	8.2E-3	CuPc(v)	15- 20	NR	Au	Si	SiO <sub>2</sub>	[66]
	2008	1.22E-2	CuPc (v)	8	7E3	Au	ITO	P(MMA-co-GMA)
2E-2		CuPc (v, 125° C) <sup>a</sup>	NR	NR	Au	Au	SiO <sub>2</sub>	[68]
3.4E-3		SnPc (v, 125° C) <sup>a</sup>						

(continued)

Table 1 (continued)

Year	Mobility [ $cm^2 V^{-1} s^{-1}$ ]	Material (deposition method)	$-V_T$ [V]	$I_{on}/I_{off}$	Source-drain electrode	Gate electrode	Insulator	Reference
	2.6E-3	H <sub>2</sub> Pc(v, 125° C) <sup>a</sup>						
	2.8E-3	ZnPc (v, 200° C) <sup>a</sup>						
	6.9E-4	FePc (v, 125° C) <sup>a</sup>						
	1.5E-4	PtPc (v, 30° C) <sup>a</sup>						
	5.4E-5	NiPc (v, 200° C) <sup>a</sup>						
1997	2.0E-6	H <sub>2</sub> Pc (BC/BG, v, 100° C) <sup>c,a</sup>	NR	NR	Cr/Au	Si	SiO <sub>2</sub>	[69]
	1.8E-6	CuPc (BC/BG, v, 100° C) <sup>c,a</sup>						
	4.4E-6	PbPc (BC/BG, v, 100° C) <sup>c,a</sup>						
2004	5E-3	VOPc (BC/BG, MBE) <sup>c,l</sup>	3	E3	ITO	(Sc <sub>0.7</sub> Y <sub>0.3</sub> ) <sub>2</sub> O <sub>3</sub>	ITO	[71]
2007	0.6–1.5	VOPc-(p-6P) (v)	8	E6	Au	Si	Al <sub>2</sub> O <sub>3</sub>	[73]
2007	3.31	TiOPc (v)	17.8	1.2E7	Au	Si	OTS-SiO <sub>2</sub>	[74]
2005	0.4–1	CuPc (C, BC/BG) <sup>m,c</sup>	6	10 <sup>4</sup>	Graphite	graphite	Parylene N	[76]
2006	0.1–0.2	CuPc (C)	2.4–2.9	NR	Au(Ti)	Si	SiO <sub>2</sub>	[77]
1999	5.2E-6	H <sub>2</sub> PcAmBu (LB)	3	100	Au	Au	PMMA	[79]
1999	2.05E-5	H <sub>2</sub> PcNT (LB)						[80]
2001	2.84E-5	H <sub>2</sub> PcAmBu (LB)	3	NR	Au	Au	PMMA	[81]
	4.42E-4	H <sub>2</sub> PcNT (LB)	0.4					
	3.25E-4	CuPc-i-Pro (LB)	1.6					

(continued)

Table 1 (continued)

Year	Mobility [ $\text{cm}^2 \text{V}^{-1} \text{s}^{-1}$ ]	Material (deposition method)	$-V_{\text{T}}$ [V]	$I_{\text{on}}/I_{\text{off}}$	Source-drain electrode	Gate electrode	Insulator	Reference
2003	4.8E-5	H <sub>2</sub> PcT ( <i>t</i> -Bu)(OCOH) (LB)	5	NR	Au	Si	SiO <sub>2</sub>	[82]
2006	1.1E-4	CuPcT ( <i>t</i> -Bu)(OCOH) (LB)	-2	NR	Au	Si	SiO <sub>2</sub>	[83]
2004	1.1E-8	ZnPcTO (LB)	NR	10 <sup>3</sup>	Au	Si	SiO <sub>2</sub>	[84]
2004	1-5E-6	CuPcTSNa spin-coated film	NR	NR	Au	Si	SiO <sub>2</sub>	[85]
2004	1-5E-6	Pc(R) <sub>8</sub> LC (LB)						[85]

<sup>a</sup>Deposition temperature

<sup>b</sup>L-, vertical type OFET device

<sup>c</sup>BC/BG, bottom contact/bottom gate OFET device

<sup>d</sup>E, electrophoretic deposition film

<sup>e</sup>mobility calculated with Shockley model

<sup>f</sup>DC, vacuum-deposited crystal in direct current electric field

<sup>g</sup>TOF, time of flight method

<sup>h</sup>RW, the SiO<sub>2</sub> insulator wafer was rubbed before depositing semiconductor

<sup>i</sup>A, film with annealing treatment

<sup>j</sup>the OFET device can be turned on by positive gate voltage

<sup>k</sup>measured after 13 months in air using cross-linked polyvinyl alcohol film as encapsulation

<sup>l</sup>MBE, molecular beam epitaxy

<sup>m</sup>C, crystal; <sup>n</sup>octa-substituted phthalocyanines liquid crystalline LB film

Despite the delayed investigation over CuPc-based OFET devices in comparison with NiPc-based ones, the much higher transfer mobility of CuPc-based OFETs makes CuPc among the most widely studied phthalocyanine semiconductor materials. In 1996, Bao et al. first manufactured CuPc into OFETs [36]. The mobility of these OFETs was found to strongly depend on the substrate temperature for depositing semiconductor films. The highest mobility of  $0.02 \text{ cm}^2 \text{ V}^{-1} \text{ s}^{-1}$  with on/off current ratio of  $4 \times 10^5$  was achieved when the material was deposited at  $125^\circ \text{C}$ . Antohe et al. prepared CuPc-based OFETs in 1998 and presented a model for obtaining the typical characteristics of the drain current versus drain voltage at different gate voltages [37]. In 2000, non-crystalline ordered CuPc films made by vacuum sublimation were used as active layers in OFET devices by ordering film in stacks parallel to the substrate through choosing proper substrate and annealing temperature as well as the thickness of the films [38]. The highest mobility achieved in those OFETs was  $3 \times 10^{-4} \text{ cm}^2 \text{ V}^{-1} \text{ s}^{-1}$  and on/off current ratio reached  $10^7$ , which were several orders of magnitude higher than those fabricated from unordered films. Kudo et al. comparatively fabricated lateral and vertical type OFETs using evaporated films of CuPc and recorded the basic static and dynamic characteristics of these OFETs in 2001 [39]. The vertical type OFETs showed high-frequency, high-current characteristics, and high hole transfer mobility under relatively low-voltage conditions compared with those of lateral type OFETs,  $4 \times 10^{-6}$  vs.  $6 \times 10^{-7} \text{ cm}^2 \text{ V}^{-1} \text{ s}^{-1}$ , because of the short length between the source-drain and gate electrodes in the vertical type device [39]. Gundlach et al. found that chemically modifying  $\text{SiO}_2$  insulator with vapor-deposited OTS monolayer can greatly improve the performance of thin-film OFET devices with small organic molecules such as CuPc as semiconductor materials [40]. Hoshino and co-workers studied the thickness dependence of semiconducting properties of CuPc-based OFET devices in 2002, and found that the devices with 80-nm thick of CuPc layer showed the highest hole mobility of  $3.5 \times 10^{-3} \text{ cm}^2 \text{ V}^{-1} \text{ s}^{-1}$  [41]. The electrical characteristics of OFET devices with CuPc film prepared by electrophoretic deposition as active layer was also studied by Takada et al. in 2002, which displayed *p*-type characteristic with mobility of  $1.4 \times 10^{-5} \text{ cm}^2 \text{ V}^{-1} \text{ s}^{-1}$  [42].

Seven years after the first report of CuPc-based OFET devices by Bao et al. [36], Liu and co-workers investigated again the influence of the substrate temperature during deposition on the characteristics of CuPc films and the OFET properties [43]. Hole mobility of  $3.75 \times 10^{-3} \text{ cm}^2 \text{ V}^{-1} \text{ s}^{-1}$  was obtained this time when the substrate temperature of  $120^\circ \text{C}$  was adopted. It is worth noting that despite the one order of magnitude smaller value of the highest mobility recorded by Liu than that measured by Bao and co-workers, the OFET device deposited at room temperature by Liu showed better OFET performance than that of Bao's because of the better film quality deposited at room temperature with a hole transfer mobility of  $4.13 \times 10^{-3} \text{ cm}^2 \text{ V}^{-1} \text{ s}^{-1}$  [44]. To further improve the OFET performance, Yan and co-workers introduced a low-dielectric PMMA polymer layer between gate insulator and source/drain electrodes in 2003 [45]. Due to the improved electric-field distribution between source-drain electrodes and semiconductor layer, the enhanced charge injection in the bottom-contact device, the improved growth behavior of



CuPc thin films, and the enhanced physical connection between source-drain electrodes and semiconductor channel associated with the PMMA polymer layer, the OFET performance of this bottom-contact device was significantly improved with leakage current being reduced by roughly one order of magnitude and on-state current enhanced by almost one order of magnitude. The hole mobility of this bottom-contact OFET device reached  $0.01 \text{ cm}^2 \text{ V}^{-1} \text{ s}^{-1}$ , which is comparable with that of top-contact device but much higher than that of normal bottom-contact device without polymer layer [45].

In 2004, Yan and co-workers further improved the performance of CuPc-based bottom-contact OFETs by introducing low dielectric constant OTS as second gate insulator on top of the first tantalum pentoxide ( $\text{Ta}_2\text{O}_5$ ) gate insulator [46]. The devices exhibited hole transfer mobility as high as  $0.024 \text{ cm}^2 \text{ V}^{-1} \text{ s}^{-1}$ , on/off current ratios as large as  $2.0 \times 10^5$ , and threshold voltage of only  $-14 \text{ V}$ , demonstrating the effectiveness of using inorganic/organic double insulator as the gate dielectric layer in improving the electric characteristics of OFET devices. By depositing CoPc layer on top of the CuPc semiconductor layer of normal top-contact OFET devices, Yan et al. fabricated sandwich type OFETs (Fig. 1d) with source-drain electrodes sandwiched between CuPc and CoPc layers. This sandwich type OFETs exhibited very high hole transfer mobility of  $0.11 \text{ cm}^2 \text{ V}^{-1} \text{ s}^{-1}$ , large on/off current ratios at the level of  $10^5$ , and low threshold voltage of  $-8.9 \text{ V}$  [47]. Okuda successively lowered the driving voltage of CuPc-based OFET to below  $2 \text{ V}$  by employing a  $\text{PbZr}_{0.5}\text{Ti}_{0.5}\text{O}_3$  film as a high-permittivity insulator layer [48]. The hole carrier mobility of this device was  $0.017 \text{ cm}^2 \text{ V}^{-1} \text{ s}^{-1}$  with an on/off current ratio of more than  $10^3$  and threshold voltage of only  $-0.95 \text{ V}$ . Sakai studied the OFET performance of thin-film transistors with oriented CuPc crystals fabricated by physical vapor deposition under DC electric field [49]. High current and a remarkable threshold for the drain voltage were achieved for this device, but the hole transfer mobility was relatively low ( $3 \times 10^{-4} \text{ cm}^2 \text{ V}^{-1} \text{ s}^{-1}$ ) because of the suppression of the drain current by a nonohmic junction [49].

Using time-of-flight measurement method, Kitamura got drift mobility of  $1.1 \times 10^{-3} - 2.0 \times 10^{-3} \text{ cm}^2 \text{ V}^{-1} \text{ s}^{-1}$  in CuPc film, which was comparable to the result in thin-film transistor [50]. In 2005, Ofuji and co-workers investigated the crystal-size effect on the hole mobility of uniaxially aligned CuPc-based OFETs by substrate rubbing treatment and revealed higher hole transfer mobility ( $0.02 \text{ cm}^2 \text{ V}^{-1} \text{ s}^{-1}$ ) in the rubbing treated OFET device than that of untreated ones [51]. Similar to the finding of Yan [46], Liu and co-workers revealed that self-assembling OTS monolayers on  $\text{SiO}_2$  substrate (between  $\text{SiO}_2$  insulator and CuPc semiconductor layers) can effectively enhance the performance of OFET devices because of the improvement in the quality of both the organic/dielectric interface and the evaporated CuPc thin films [52]. The mobility of this OFET device was  $1.48 \times 10^{-3} \text{ cm}^2 \text{ V}^{-1} \text{ s}^{-1}$ , 1–2 orders of magnitude higher than that of OFETs with bare  $\text{SiO}_2$  insulator. Using  $\text{Lu}(\text{Pc})_2$  as a buffer layer sandwiched between source-drain electrodes and organic semiconductor layer, Yan and co-workers fabricated top-contact CuPc-based OFETs with effectively enhanced performance in comparison with conventional top-contact ones due to the included difference of the Fermi level

and interface dipolar between  $\text{Lu}(\text{Pc})_2$  and Au electrode [53]. The on-state current and hole transfer mobility increased from 700 nA and  $0.7 \times 10^{-2} \text{ cm}^2 \text{ V}^{-1} \text{ s}^{-1}$  to 2.5  $\mu\text{A}$  and  $1.58 \times 10^{-2} \text{ cm}^2 \text{ V}^{-1} \text{ s}^{-1}$ , respectively, and threshold voltage downshifted from  $-21$  to  $-11$  V for the linear region with the on/off current ratio improved to a level of  $10^4$ , indicating the effectiveness of intrinsic molecular semiconductor with a high carrier density as a buffer layer in improving the linear region characteristics of the OFETs and thus making the device suitable for applications in flat panel display.

On the basis of the previous finding that CuPc–CoPc composites-based OFETs with source and drain electrodes sandwiched between CuPc and CoPc layers had different characteristics from that with pure materials [47], Yan and co-workers investigated the performance of OFET device with composite of CuPc and NiPc (CuPc:NiPc, 9:1 w/w) as the active layer [54]. The device exhibited high mobility, up to  $0.05 \text{ cm}^2 \text{ V}^{-1} \text{ s}^{-1}$ , which was probably due to the presence of a new crystalline phase consisting of two different molecules. In 2006, Puigdollers and co-workers fabricated CuPc thin-film transistors using PMMA as gate dielectric [55]. Despite the fact that the use of such organic dielectrics can allow the fabrication of OFETs on plastic substrates and thus open up the possibility to fabricate flexible devices, this device showed low mobility of  $2 \times 10^{-5} \text{ cm}^2 \text{ V}^{-1} \text{ s}^{-1}$ . Utilizing  $\text{Ta}_2\text{O}_5$  as the insulator layer, the mobility of CuPc-based top-contact OFETs achieved  $4 \times 10^{-3} \text{ cm}^2 \text{ V}^{-1} \text{ s}^{-1}$  [56], which is in the high-end of the reported values for CuPc-based OFETs. The effect of high dielectric constant gate oxide insulator, including  $\text{Ta}_2\text{O}_5/\text{SiO}_2$ ,  $\text{Al}_2\text{O}_3$ , and  $\text{Ta}_2\text{O}_5$ , on the electrical properties of CuPc-based OFETs was reported by Itoh and co-workers in 2006 [57]. The results suggested that  $\text{Ta}_2\text{O}_5$  was a more suitable material to obtain higher mobility and lower operating voltage in CuPc-based OFETs than other insulator materials. By applying the copolymer of methyl methacrylate and glycidyl methacrylate [P(MMA-co-GMA)] as a gate dielectric with a simple top-contact structure, Du and co-workers fabricated CuPc-based OFET device [58] exhibiting comparable performance with those devices with inorganic gate dielectric materials such as silicon dioxide under the same technical conditions but much higher performance than the previous reported device with PMMA gate dielectric materials [55]. After annealing, the highest mobility increased from  $2.5 \times 10^{-3}$  to  $4.2 \times 10^{-3} \text{ cm}^2 \text{ V}^{-1} \text{ s}^{-1}$  and threshold voltage decreased from  $-18$  to  $-10$  V [58]. In 2006, Liu and co-workers reported a method of fabricating noncoplanar channel OFETs by a conventional photolithographic technique, which was revealed suitable to obtain short channel transistors as well as transistors using two different metals as drain-source electrodes [59]. The fabricated OFET device with channel length of 6  $\mu\text{m}$  and Au source-drain electrodes showed hole transfer mobility of  $3.2 \times 10^{-3} \text{ cm}^2 \text{ V}^{-1} \text{ s}^{-1}$  and on/off current ratio of  $10^4$ . It is worth noting that when Al was used as source electrode and Au or Al as drain electrode, electron transfer behavior was also found in this kind of non-planar CuPc-based OFETs [59], *vide infra*.

By introducing Lewis-acid  $\text{V}_2\text{O}_5$  thin film between semiconductor and insulator layers, Minagawa et al. fabricated CuPc-based OFETs that can be turned on by positive gate voltage, which showed improved hole mobility in comparison

with traditional CuPc-based OFET,  $3.6 \times 10^{-3}$  vs.  $2.5 \times 10^{-4} \text{ cm}^2 \text{ V}^{-1} \text{ s}^{-1}$  [60]. The author further improved the hole transfer mobility of this kind of OFET to  $6.3 \times 10^{-3} \text{ cm}^2 \text{ V}^{-1} \text{ s}^{-1}$  in another work and attributed the interesting OFET behavior to the charge transfer complexes formed between CuPc layer and the  $\text{V}_2\text{O}_5$  Lewis-acid on the basis of the comparative results of XRD, UV-vis spectra, and ionization potential of CuPc monolayer,  $\text{V}_2\text{O}_5$  monolayer, and CuPc- $\text{V}_2\text{O}_5$  co-evaporated films [61]. Ikeda and co-workers studied the influence of active layer thickness on transport characteristics of a CuPc thin-film transistor by using the in situ FET measurement system, in which the film was continuously deposited up to several hundred nanometers in thickness [62]. It was found that the drain current and mobility showed maximum values in the early stage of film growth and then decreased with increasing the film thickness [62]. Yan et al. investigated the air stability of CuPc-based OFETs in 2006 [63]. It was found that the threshold voltage positive-shifted and the on/off current ratio lowered because of  $\text{O}_2$  doping to CuPc thin film assisted by water when the device was stored in water-humidified  $\text{O}_2$  and room air despite the almost unchanged mobility. However, the OFET devices were revealed to exhibit excellent stability when a cross-linked polyvinyl alcohol film was used as encapsulation layer to prevent the permeation of  $\text{O}_2$  and water, which would help to push the development of OFETs for practical applications.

Thin-film OFETs with  $\text{MoO}_3/\text{Al}$  electrode and  $\text{OTS}/\text{SiO}_2$  bilayer gate insulator were manufactured by Bai and co-workers in 2007 [64]. In line with the case in CuPc-based OFET with Au electrode and  $\text{OTS}/\text{Ta}_2\text{O}_5$  bilayer gate insulator reported by Yan and co-workers [46], the introduction of OTS significantly improved the performance of this device due to the low energy hydrophobic surface of OTS, from  $6 \times 10^{-4} \text{ cm}^2 \text{ V}^{-1} \text{ s}^{-1}$ ,  $10^3$ , and  $-9 \text{ V}$  for mobility, on/off current ratio, and threshold voltage, respectively, in the OFET device without OTS treatment to  $1.5 \times 10^{-3} \text{ cm}^2 \text{ V}^{-1} \text{ s}^{-1}$ ,  $10^4$ , and  $-6 \text{ V}$  in the OTS-treated OFET device [64]. In addition, the mobility in the OFET device with  $\text{OTS}/\text{SiO}_2$  bilayer gate insulator reported by Bai [64] was more than one order of magnitude lower than that in the device with  $\text{OTS}/\text{Ta}_2\text{O}_5$  obtained by Yan [46], corresponding well with the conclusion of Itoh et al. [57] that  $\text{Ta}_2\text{O}_5$  was a more suitable material to obtain higher mobility in CuPc-based OFETs than other insulator materials. Vidolot-Ackermann and co-workers fabricated heterojunction OFETs based on *p*-type CuPc and *n*-types CuPcF<sub>16</sub> or TCNQ and studied their OFET properties [65]. However, only *p*-type behavior was found in the device with hole transfer mobility in the range of  $1\text{--}6 \times 10^{-4} \text{ cm}^2 \text{ V}^{-1} \text{ s}^{-1}$  and non-ideal ohmic behavior was revealed, associated with the occurrence of a build-up electrical field self-bias at the CuPc/CuPcF<sub>16</sub> interface due to the charge transfer phenomenon between CuPc and CuPcF<sub>16</sub>.

The thickness dependence of mobility in CuPc-based OFETs on amorphous  $\text{SiO}_2$  substrate was investigated by Gao et al. in 2007 [66]. The results demonstrated that the mobility increased with increasing the thickness of CuPc layer and then was saturated at the thickness of 7.8 nm with mobility about  $0.008 \text{ cm}^2 \text{ V}^{-1} \text{ s}^{-1}$ . In 2008, Du and co-workers fabricated CuPc-based OFETs using PMMA and P(MMA-co-GMA) as gate insulators, and the difference between devices with different polymer gate insulators were explained with XRD, AFM, and SEM measuring

results [67]. The performance of the fabricated OFET devices with both PMMA and P(PMMA-co-GMA) was improved in comparison with the previously reported results [55, 58], showing mobility, on/off current ratio, and threshold voltage of  $5.89 \times 10^{-3} \text{ cm}^2 \text{ V}^{-1} \text{ s}^{-1}$ ,  $2 \times 10^3$ , and  $-15 \text{ V}$  for OFET with PMMA gate insulator and  $1.22 \times 10^{-2} \text{ cm}^2 \text{ V}^{-1} \text{ s}^{-1}$ ,  $7 \times 10^3$ , and  $-8 \text{ V}$  for device with P(PMMA-co-GMA) insulator, respectively [67].

In contrast to the widely conducted investigations of OFET devices with CuPc as active semiconductor layer, OFET devices based on thin solid films of other monomeric phthalocyanine compounds are very limited. Bao and co-workers had demonstrated OFETs using different metallophthalocyanines including CuPc, SnPc, H<sub>2</sub>Pc, ZnPc, FePc, PtPc, and NiPc [68]. It was found that the mobility of these materials changed significantly with substrate temperature and phthalocyanine species. For example, the mobility of ZnPc-based OFET increased from  $2.3 \times 10^{-4} \text{ cm}^2 \text{ V}^{-1} \text{ s}^{-1}$  for device fabricated at substrate temperature of  $30^\circ \text{C}$  to  $2.8 \times 10^{-3} \text{ cm}^2 \text{ V}^{-1} \text{ s}^{-1}$  for device fabricated at substrate temperature of  $200^\circ \text{C}$ , and that the mobility of OFET devices fabricated at substrate temperature of  $125^\circ \text{C}$  decreased from  $0.02 \text{ cm}^2 \text{ V}^{-1} \text{ s}^{-1}$  for CuPc semiconductor to  $3 \times 10^{-5} \text{ cm}^2 \text{ V}^{-1} \text{ s}^{-1}$  for NiPc semiconductor. Kudo et al. fabricated OFET devices with H<sub>2</sub>Pc, CuPc, and PbPc evaporated films as semiconductor layer and measured their OFET performance [69]. The mobility of these *p*-type OFETs was found to change significantly depending on the phthalocyanine semiconductor property and substrate temperature. Furthermore, the adsorption and desorption of oxygen molecule were also revealed to show marked effect on their electrical parameters [69]. The carrier mobility of TiOPc-based OFETs at the presence of electron acceptor gas (NO<sub>2</sub>) and electron donor gas (NH<sub>3</sub>) molecules was studied in 1999 by Touda et al. [70]. The results indicated that the adsorbed gas molecules played an important role on not only the carrier density but also the carrier transport. In 2004, Ohta and co-workers fabricated transparent OFETs using molecular-beam-deposited VOPc film as active layer and (Sc<sub>0.7</sub>Y<sub>0.3</sub>)<sub>2</sub>O<sub>3</sub> film heteroepitaxially grown on atomically epitaxial flat ITO film as gate insulator, which exhibited high carrier mobility of  $0.005 \text{ cm}^2 \text{ V}^{-1} \text{ s}^{-1}$  [71]. The applicability of different polymers (PVC, PVDF, PAN, PMMA, PVP, PS, PVPy, PVK, and PI) as dielectric layers for OFETs with phthalocyanines (ZnPc and VOPcF<sub>16</sub>) as the active semiconductor layers was discussed by Kelting and co-workers in 2006 in terms of the dielectric behavior and observed growth characteristics [72]. By growing VOPc on an ordered *p*-6P layer under a high substrate temperature, Yan and co-workers fabricated VOPc-based OFETs with improved mobility as high as  $1 \text{ cm}^2 \text{ V}^{-1} \text{ s}^{-1}$  due to the weak epitaxial growth behavior of VOPc on ordered *p*-6P layer [73]. In 2007, Liu and co-workers fabricated TiOPc-based OFET devices at substrate temperature of  $150^\circ \text{C}$  by using OTS-modified Si/SiO<sub>2</sub> substrates [74]. The OTS layer not only improved the contact between organic semiconductor and SiO<sub>2</sub> gate insulator but also induced the formation of ordered  $\alpha$ -TiOPc films, which together with the ultra close  $\pi$ -stack of  $\alpha$ -TiOPc and favorable “edge-on” molecular orientation with respect to substrates resulted in the good OFET performance, with the field effect mobility, on/off current ratio, and threshold voltage being  $3.31 \text{ cm}^2 \text{ V}^{-1} \text{ s}^{-1}$ ,  $1.2 \times 10^7$ , and  $-17.8 \text{ V}$ ,

respectively. The hole mobility of this device was among the highest ones for thin-film OFETs up to date, indicating the great potential of phthalocyanine compounds as semiconductor materials for OFET devices. Akazawa et al. fabricated top-contact OFETs using vacuum evaporated MgPc thin films as an active layer in 2007 [75], the on/off ratio and field-effect mobilities of which were revealed to be greatly improved by treating the MgPc semiconductor layer and the *n*-Si substrate surface with ethanol vapor and HMDS vapor respectively [75].

Molecular packing in single crystal usually reflects the most advantageous molecular arrangement of molecular materials in solid state. As a result, single crystal-based OFETs should exhibit the largest charge transfer mobility comparable with the intrinsic property of the semiconductor materials. However, due to the limitation of the experimental method and crystal size, only a few OFET devices with single-crystal of phthalocyanine compounds as semiconductors have been reported. Kloc and co-workers fabricated OFET with CuPc single crystals grown through physical vapor transport in 2005 [76]. As the first *p*-type OFET based on single-crystal of CuPc, this device exhibited hole transfer mobility up to  $1 \text{ cm}^2 \text{ V}^{-1} \text{ s}^{-1}$ , on/off current ratio larger than  $10^4$ , and lower threshold voltage around  $-6 \text{ V}$ . After 1 year, Hu and co-workers synthesized single-crystalline submicrometer-sized ribbons of CuPc and fabricated OFET devices based on individual submicrometer-sized ribbons [77]. These devices, as the first OFETs based on individual organic submicrometer-sized single crystals, showed very low threshold voltage lower than  $-3 \text{ V}$  and high carrier mobility in the range of  $0.1\text{--}0.2 \text{ cm}^2 \text{ V}^{-1} \text{ s}^{-1}$ .

The Langmuir–Blodgett (LB) technique allows fine control of both the structure and the thickness of the film at the molecular level and has been employed in building films for OFET studies. However, the mobility of LB film-based OFETs, usually in the range of  $10^{-7}\text{--}10^{-3} \text{ cm}^2 \text{ V}^{-1} \text{ s}^{-1}$ , is far behind those of vacuum deposited films. This, together with the fact that the LB technique is a difficult method for rapid manufacturing, has suppressed interest in using the LB technique for OFET studies. LB technique was firstly used to build film for OFETs in 1990 by the research group of Paloheimo [78]. Since then, several phthalocyanine-based OFET devices fabricated using LB technique have been reported by Liu's group [79–83]. In 2001, they fabricated OFETs with LB films of  $\text{H}_2\text{PcAmBu}$ ,  $\text{H}_2\text{PcNT}$ , and  $\text{CuPc-i-Pro}$  as the active semiconductor layer [81], which showed hole mobility of  $2.84 \times 10^{-5}$ ,  $4.42 \times 10^{-4}$ , and  $3.25 \times 10^{-4} \text{ cm}^2 \text{ V}^{-1} \text{ s}^{-1}$  for the three phthalocyanines, respectively. In 2003, they created OFET devices with the LB films of  $[\text{H}_2\text{PcT}(t\text{-Bu})(\text{OCOH})]$  and its copper complex  $[\text{CuPcT}(t\text{-Bu})(\text{OCOH})]$ . Hole transfer mobility of  $1.46 \times 10^{-5}$  and  $9.09 \times 10^{-4} \text{ cm}^2 \text{ V}^{-1} \text{ s}^{-1}$  were revealed for these two devices, respectively [82]. Recently, they synthesized  $\text{ZnPcTO}$  and studied their OFET properties [83]. Spin-coated single layer film of  $\text{CuPcTSNa}$  was revealed to exhibit semiconductor property for OFET by Nishimura and co-workers in 2004 [84]. However, the mobility for the OFET device with spin-coating films of  $\text{CuPcTSNa}$  was only  $1.1 \times 10^{-8} \text{ cm}^2 \text{ V}^{-1} \text{ s}^{-1}$ , much lower than common OFET device based on other solution processable methods. Donley et al. studied the direct current (dc) conductivities and OFET characteristics of a class of octa-substituted liquid crystalline (discotic mesophase) phthalocyanines in 2004 [85]. The OFETs

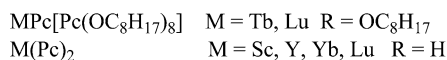
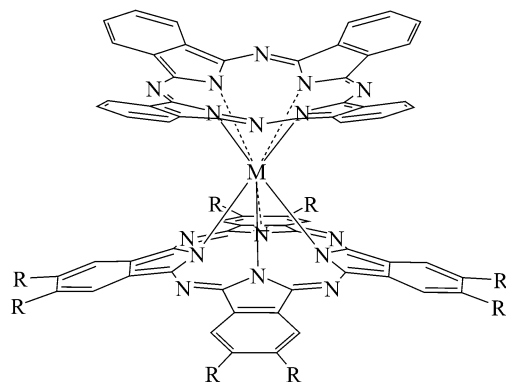


**Fig. 5** Molecular structures of sandwich bis(phthalocyaninato) rare earth double-decker complexes used as semiconductors of *p*-type OFET

prepared from the LB films of these phthalocyanines showed anisotropies in field effect mobility of approximately 10:1 in the direction of parallel and perpendicular to the column axis for a variety of W/L ratios (source/drain dimensions and spacing), which exhibited hole transfer mobility in the range of 1 to  $5 \times 10^{-6} \text{ cm}^2 \text{ V}^{-1} \text{ s}^{-1}$ .

#### 4.2 Sandwich Bis(Phthalocyaninato) Rare Earth Double-Decker Semiconductors

Figure 5 shows the molecular structures of sandwich bis(phthalocyaninato) rare earth double-decker complexes for *p*-type OFETs, and Table 2 organizes the performance of these OFETs. Probably due to the hardness in fabricating highly ordered films of bis(phthalocyaninato) rare earth complexes, OFETs based on double-deckers are much less than that on monomeric phthalocyanines. Clarisse and co-workers fabricated *p*-type OFET with mixture of NiPc and ScPc<sub>2</sub> as active layer in 1988, which exhibited hole mobility about  $10^{-3} \text{ cm}^2 \text{ V}^{-1} \text{ s}^{-1}$  and threshold of 1V [86]. In 1991, they reported the operation and characteristics of bis(phthalocyaninato) rare earth field effect transistors [87], which were fabricated with monomeric metal phthalocyanines (MPc, M = 2H, Cu, and Ni) as the first layer and bis(phthalocyaninato) rare earth complexes (MPc<sub>2</sub>, M = Sc, Y) as the active semiconducting layer using two successive sublimations method. The hole mobility of these OFET devices was revealed changing in the range of  $10^{-4}$ – $10^{-3} \text{ cm}^2 \text{ V}^{-1} \text{ s}^{-1}$  depending on different metallic ions in mono- and bis(phthalocyaninato) compounds. In 2005, Jiang et al. described the fabrication of heteroleptic bis(phthalocyaninato) rare earth complexes M(Pc)[Pc(OC<sub>8</sub>H<sub>17</sub>)<sub>8</sub>]

**Table 2** Performance of some bis(phthalocyaninato) rare earth double-decker-based *p*-type OFET devices (*mEn* means  $m \times 10^n$ )

Year	Mobility [ $\text{cm}^2 \text{V}^{-1} \text{s}^{-1}$ ]	Material (deposition method)	$-V_T$ [V]	$I_{\text{on}}/I_{\text{off}}$	Source-drain electrode	Gate electrode	Insulator	Reference
1988	1E-3	ScPc <sub>2</sub> -NiPc	-1	NR	Au	Si	SiO <sub>2</sub>	[86]
1991	1E-3	ScPc <sub>2</sub> -H <sub>2</sub> Pc (v)	-3	NR	Au	Ag	SiO <sub>2</sub>	[87]
	2E-4	ScPc <sub>2</sub> -CuPc (v)	0					
	1E-3	ScPc <sub>2</sub> -NiPc (v)	-1					
	1E-3	YPc <sub>2</sub> -NiPc (v)	NR					
2005	6.4E-4	TbPc[Pc(OC <sub>8</sub> H <sub>17</sub> ) <sub>8</sub> ] LB film	15	5.5E4	Au	Si	SiO <sub>2</sub>	[88] [88]
	1.7E-3	LuPc[Pc(OC <sub>8</sub> H <sub>17</sub> ) <sub>8</sub> ] LB film	NR	E2				

(M = Tb, Lu) into organic thin-film transistors by LB technique and reported their field effect mobility, which represented the first report for *p*-type OFETs based on bis(phthalocyaninato) rare earth complexes prepared via LB method [88]. Due to the highly ordered molecular arrangement of M(Pc)[Pc(OC<sub>8</sub>H<sub>17</sub>)<sub>8</sub>] (M = Tb, Lu) in LB films and the appropriate HOMO energy level of these double-deckers relative to the Au source-drain electrodes, the OFETs reported in that work exhibited higher hole transfer mobility of  $1.7 \times 10^{-3} \text{ cm}^2 \text{V}^{-1} \text{s}^{-1}$  in comparison with those fabricated from monomeric phthalocyanine LB films.

### 4.3 Sandwich Tris(Phthalocyaninato) Rare Earth Triple-Decker Semiconductors

Figure 6 shows the molecular structures of sandwich tris(phthalocyaninato) rare earth triple-decker complexes used as semiconductors of OFETs, and Table 3 organizes the performance of these OFETs. Similar to the case of bis(phthalocyaninato) rare earth complexes, OFETs based on tris(phthalocyaninato) rare earth triple-decker complexes are very scarce. The OFETs with LB films of amphiphilic tris(phthalocyaninato) rare earth triple-decker complexes (Pc')M(Pc')M[Pc(OC<sub>8</sub>H<sub>17</sub>)<sub>8</sub>] (M = Eu, Ho, Lu) as active semiconductor layers were fabricated recently by Jiang's group showing unexpectedly good OFET performance with carrier mobility reaching 0.24–0.60  $\text{cm}^2 \text{V}^{-1} \text{s}^{-1}$ . This is among the highest mobility achieved so far for LB film-based OFETs [89]. Such high hole transfer mobility was ascribed to the intramolecular  $\pi$ - $\pi$  stacking and the intermolecular *J* aggregation in the LB films, which had also been theoretically rationalized according to the DFT calculated results [28]. Excited by the high OFET performance of these triple-decker semiconductors, a series of amphiphilic heteroleptic tris(phthalocyaninato) europium complexes with different lengths of hydrophobic alkoxy substituents on one outer phthalocyanine ligand

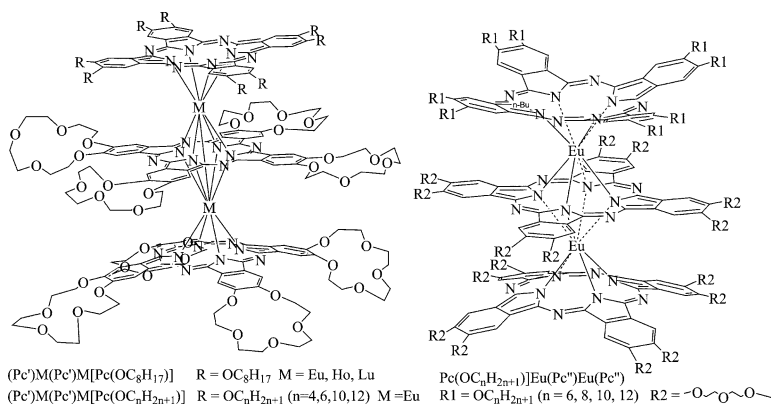


**Fig. 6** Molecular structures of sandwich tri(phthalocyaninato) rare earth triple-decker complexes used as semiconductors of *p*-type OFET

(Pc')Eu(Pc'')Eu[Pc(OC<sub>n</sub>H<sub>2n+1</sub>)<sub>8</sub>] (*n* = 4, 6, 10, 12) were designed and prepared, and the OFETs based on the LB films of these complexes were fabricated to investigate the effect of peripheral hydrophobic alkoxy substitution on the OFET performance [90]. These OFET devices displayed hole transfer mobility in the range of 0.0032–0.21 cm<sup>2</sup> V<sup>-1</sup> s<sup>-1</sup> in the direction parallel to the aromatic phthalocyanine rings depending on the length of the hydrophobic alkoxy substituents. At the same time, a series of amphiphilic heteroleptic tris(phthalocyaninato) europium complexes with hydrophilic poly(oxyethylene) heads and hydrophobic alkoxy tails [Pc(OC<sub>n</sub>H<sub>2n+1</sub>)<sub>8</sub>]Eu(Pc'')Eu(Pc') (*n* = 6, 8, 10, 12) were designed and prepared [91]. BC/BG OFETs fabricated using the LB films of this series of triple-deckers as semiconductor layers displayed good OFET performance with high carrier mobility for holes in the direction parallel to the aromatic phthalocyanine rings, which showed dependence on the length of the hydrophobic alkoxy side chains decreasing from 0.46 to 0.014 cm<sup>2</sup> V<sup>-1</sup> s<sup>-1</sup> along with the increase of the carbon number in the hydrophobic alkoxy side chains. Recently, two amphiphilic heteroleptic tris(phthalocyaninato) europium complexes with hydrophilic crown ether heads and hydrophobic octyloxy tails [Pc(*m*Cn)<sub>4</sub>]Eu[Pc(*m*Cn)<sub>4</sub>]Eu[Pc(OC<sub>8</sub>H<sub>17</sub>)<sub>8</sub>] (*m* = 12, *n* = 4; *m* = 18, *n* = 6) were designed, prepared, and then fabricated into TC/BG type OFET devices with bare SiO<sub>2</sub>/Si substrate, HMDS-treated SiO<sub>2</sub>/Si substrate, and OTS-treated SiO<sub>2</sub>/Si substrate, respectively, with the help of LB technique [92]. It was revealed that the device performance was dependent on the species of crown ether substituents and substrate surface treatment. The triple-decker substituted with 12-crown-4 [Pc(12C4)<sub>4</sub>]Eu[Pc(12C4)<sub>4</sub>]Eu[Pc(OC<sub>8</sub>H<sub>17</sub>)<sub>8</sub>] showed hole transfer mobility and current modulation of 0.03 cm<sup>2</sup> V<sup>-1</sup> s<sup>-1</sup> and 2.32 × 10<sup>3</sup> on the bare SiO<sub>2</sub>/Si substrate, 0.31 cm<sup>2</sup> V<sup>-1</sup> s<sup>-1</sup> and 8.59 × 10<sup>4</sup> on HMDS treated SiO<sub>2</sub>/Si substrate, and 0.33 cm<sup>2</sup> V<sup>-1</sup> s<sup>-1</sup> and 7.91 × 10<sup>5</sup> on OTS treated SiO<sub>2</sub>/Si substrate, respectively, while triple-decker substituted with 18-crown-6 [Pc(18C6)<sub>4</sub>]Eu[Pc(18C6)<sub>4</sub>]Eu[Pc(OC<sub>8</sub>H<sub>17</sub>)<sub>8</sub>] had hole



transfer mobility and current modulation of  $0.002 \text{ cm}^2 \text{ V}^{-1} \text{ s}^{-1}$  and  $5.5 \times 10^3$  on the bare  $\text{SiO}_2/\text{Si}$  substrate and of  $0.28 \text{ cm}^2 \text{ V}^{-1} \text{ s}^{-1}$  and  $1.73 \times 10^5$  on HMDS treated  $\text{SiO}_2/\text{Si}$  substrate [92]. By replacing the  $[\text{Pc}(\text{OC}_8\text{H}_{17})_8]$  ring of  $(\text{Pc}')\text{Eu}(\text{Pc}')\text{Eu}[\text{Pc}(\text{OC}_8\text{H}_{17})_8]$  with *meso*-5,10,15,20-tetra-*n*-decylporphyrin and *meso*-5,10,15,20-tetrakis(4-pentyloxyphenyl)porphyrin groups, the OFET performance fabricated from the LB films of these two novel sandwich triple-decker complexes  $\{\text{Eu}_2[\text{Pc}(15\text{C}5)_4]_2[\text{T}(\text{C}_{10}\text{H}_{21})_4\text{P}]\}$  and  $\text{Eu}_2[\text{Pc}(15\text{C}5)_4]_2[\text{TPOPP}]\}$  were found to be greatly improved [93]. The devices displayed good OFET performance with a carrier mobility in the range  $0.03\text{--}0.78 \text{ cm}^2 \text{ V}^{-1} \text{ s}^{-1}$  and showed a low threshold voltage ranging from  $-1.19$  to  $-4.34 \text{ V}$ . The mobility of the former compound reached  $0.78 \text{ cm}^2 \text{ V}^{-1} \text{ s}^{-1}$ , which was the highest value so far achieved for LB film-based OFETs, as a result of the narrow energy gap ( $1.04 \text{ eV}$ ) of this compound [93].

#### 4.4 Monomeric Porphyrin Semiconductors

As the natural analogs of phthalocyanines, porphyrin compounds have also been proposed for use in conducting materials and as conductive and capacitive elements in molecular electronic devices. However, in contrast to the most intensively studied phthalocyanine derivatives among various organic semiconductors, porphyrins as the most important tetrapyrrole derivatives occurring in nature have been relatively less investigated for their semiconducting properties. Despite the fact that Schouten and co-workers have studied the charge migration in supramolecular stacks of peripherally substituted porphyrins with PR-TRMC as early as in 1991 and maximum hole transfer mobility in the range of  $0.060\text{--}0.081 \text{ cm}^2 \text{ V}^{-1} \text{ s}^{-1}$  for the  $D_h$  phase and of  $0.27 \text{ cm}^2 \text{ V}^{-1} \text{ s}^{-1}$  for the K phase have been reported [94–96], fabrication of OFET devices from porphyrin compounds still remains rare, limited to very few types of porphyrins such as 2,3,7,8,12,13,17,18-octaethyl-porphyrin (OEP) and tetrabenzoporphyrin (TBP) derivatives with planar molecular structure. Figure 7 shows the molecular structures of monomeric porphyrins used as semiconductors of OFETs and their performance is organized in Table 4.

The first porphyrin-based OFETs characterized with electrical characteristics measurement was fabricated from metal free 2,3,7,8,12,13,17,18-octaethyl-porphyrin ( $\text{H}_2\text{OEP}$ ) and its metal derivatives MOEPs. Yase et al. grew PtOEP crystals on the surface of potassium bromide (KBr) or potassium chloride (KCl) crystals by thermal evaporation at various substrate temperatures and then fabricated the films into OFETs by wet-transferring method [97]. AFM and XRD analysis results on the morphology and crystal orientation of the films indicated that PtOEP molecules were deposited vertical and parallel to the substrates when the substrates were kept at room temperature and heated to  $50^\circ\text{C}$ , respectively, which resulted in the much higher charge transfer mobility of OFET devices with these films as active layers for the former than the latter,  $1.3 \times 10^{-4}$  vs.  $1.5 \times 10^{-6} \text{ cm}^2 \text{ V}^{-1} \text{ s}^{-1}$  [97]. The work of Yase et al. demonstrated that the molecular alignment of PtOEP crystals

**Table 3** Performance of some tris(phthalocyaninato) rare earth triple-decker complexes-based *p*-type OFET devices (*m*Eu means  $m \times 10^m$ )

Year	Mobility [ $cm^2V^{-1}s^{-1}$ ]	Material (deposition method)	$-V_T$ [V]	$I_{on}/I_{off}$	$W/L$ electrode	Source-drain electrode	Gate	Insulator	Reference
2005	0.6	(Pc')Eu(Pc')Eu [Pc(OC <sub>8</sub> H <sub>17</sub> ) <sub>8</sub> ] LB film	59	$1.4 \times 10^5$	119.2	Au	Si	SiO <sub>2</sub>	[89]
	0.4	(Pc')Ho(Pc')Ho [Pc(OC <sub>8</sub> H <sub>17</sub> ) <sub>8</sub> ] LB film	33	NR					
	0.24	(Pc')Lu(Pc')Lu [Pc(OC <sub>8</sub> H <sub>17</sub> ) <sub>8</sub> ] LB film	4	NR					
2007	3.2E-3	(Pc')Eu(Pc')Eu[Pc(OC <sub>4</sub> H <sub>9</sub> ) <sub>8</sub> ] LB film	NR	93	119.2	Au	Si	SiO <sub>2</sub>	[90]
	0.014	(Pc')Eu(Pc')Eu[Pc(OC <sub>6</sub> H <sub>13</sub> ) <sub>8</sub> ] LB film		8.2E3					
	0.21	(Pc')Eu(Pc')Eu[Pc(OC <sub>10</sub> H <sub>21</sub> ) <sub>8</sub> ] LB film		9.7E4					
	0.053	(Pc')Eu(Pc')Eu[Pc(OC <sub>12</sub> H <sub>25</sub> ) <sub>8</sub> ] LB film		39					
2007	0.46	[Pc(OC <sub>6</sub> H <sub>13</sub> ) <sub>8</sub> ]Eu(Pc'')Eu (P'') LB film bottom contact	NR	1.01E2	119.2	Au	Si	SiO <sub>2</sub>	[91]
	0.17	[Pc(OC <sub>8</sub> H <sub>17</sub> ) <sub>8</sub> ]Eu(Pc'')Eu (P'') LB film bottom contact		1.02E3					
	0.096	[Pc(OC <sub>10</sub> H <sub>21</sub> ) <sub>8</sub> ]Eu(Pc'')Eu (P'') LB film bottom contact		3.85E4					
	0.014	[Pc(OC <sub>12</sub> H <sub>25</sub> ) <sub>8</sub> ]Eu(Pc'')Eu (P'') LB film bottom contact		1.15E2					

(continued)

Table 3 (continued)

Year	Mobility [ $cm^2 V^{-1} s^{-1}$ ]	Material (deposition method)	$-V_T$ [V]	$I_{on}/I_{off}$	$W/L$ electrode	Source-drain electrode	Gate	Insulator	Reference
2009	0.03	[Pc(12C4) <sub>4</sub> ]Eu[Pc(12C4) <sub>4</sub> ] Eu[Pc(OC <sub>8</sub> H <sub>17</sub> ) <sub>8</sub> ]		2.3eE3				SiO <sub>2</sub> /Si	[92]
	0.31			8.59E4				HMDS-treated SiO <sub>2</sub> /Si	
	0.33			7.91E5				OTS-treated SiO <sub>2</sub> /Si	
	0.002	[Pc(18C6) <sub>4</sub> ]Eu[Pc(18C6) <sub>4</sub> ] Eu[Pc(OC <sub>8</sub> H <sub>17</sub> ) <sub>8</sub> ]		5.5E3				SiO <sub>2</sub> /Si	
	0.28			1.73E5				HMDS-treated SiO <sub>2</sub> /Si	
2009	0.78	[Pc(15C5) <sub>4</sub> ]Eu[Pc(15C5) <sub>4</sub> ] Eu[T(C <sub>10</sub> H <sub>21</sub> ) <sub>4</sub> P]	3.84	2.20E4				HMDS-treated SiO <sub>2</sub> /Si	[93]
	0.04	[Pc(15C5) <sub>4</sub> ]Eu[Pc(15C5) <sub>4</sub> ] Eu[T(C <sub>10</sub> H <sub>21</sub> ) <sub>4</sub> P]	4.02	4.94E3				OTS-treated SiO <sub>2</sub> /Si	
	0.05	[Pc(15C5) <sub>4</sub> ]Eu[Pc(15C5) <sub>4</sub> ] Eu[TPOPP]	1.19	1.48E4				HMDS-treated SiO <sub>2</sub> /Si	
	0.03	[Pc(15C5) <sub>4</sub> ]Eu[Pc(15C5) <sub>4</sub> ] Eu[TPOPP]	4.34	1.03E4				OTS-treated SiO <sub>2</sub> /Si	

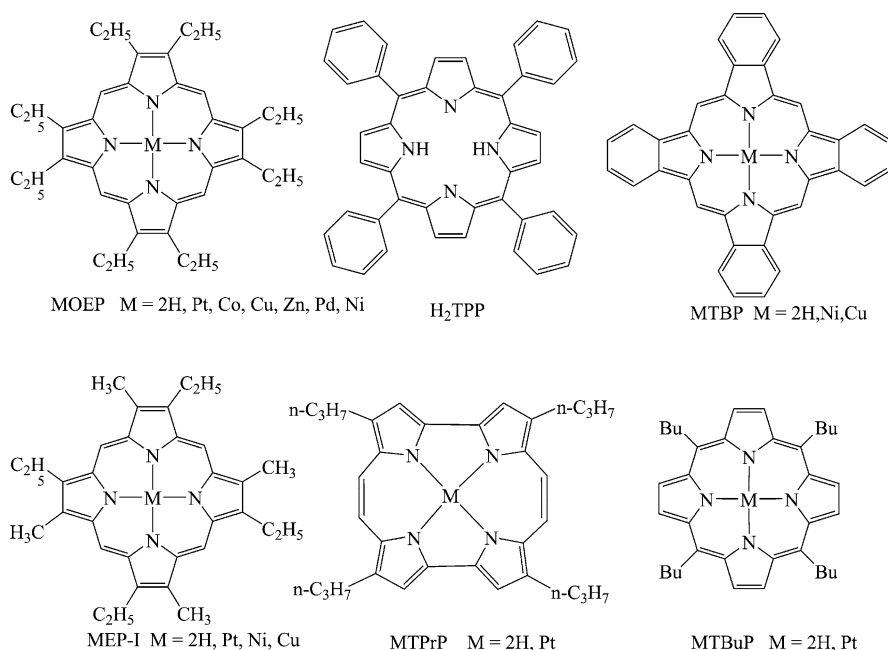


**Fig. 7** Molecular structures of monomeric porphyrins used as semiconductor of OFETs

and thus the mobility of the fabricated OFET devices with these crystals can be reasonably tuned by changing the substrate temperature [97]. They further reported the preparation and characteristics of OFETs from the epitaxially grown film of PtOEP crystals at room temperature fabricated by a wet-transferring process [98]. In 2007, Minari et al. fabricated OFET devices with single crystal of a series of MOEP ( $M = \text{Co}, \text{Cu}, \text{Zn}, \text{Pd}$ ) and studied the effect of crystal structures on the performance of these OFETs [99]. It was found that the charge transfer mobility increased with decreasing intermolecular distance due to the increased overlap of  $\pi$  orbitals among close-packed molecules and the consequent promotion of charge transport in the crystals, from  $0.014 \text{ cm}^2 \text{ V}^{-1} \text{ s}^{-1}$  for PdOEP to  $0.036 \text{ cm}^2 \text{ V}^{-1} \text{ s}^{-1}$  for ZnOEP,  $0.068 \text{ cm}^2 \text{ V}^{-1} \text{ s}^{-1}$  for CuOEP, and  $0.200 \text{ cm}^2 \text{ V}^{-1} \text{ s}^{-1}$  for CoOEP.

OFETs with spin coated film of H<sub>2</sub>TPP from a chloroform solution as active semiconductor layers, Al as gate electrode, and Cd as source-drain electrodes were fabricated by Checcoli and co-workers in 2003 [100]. This device exhibited zero-bias hole transfer mobility of  $0.007 \text{ cm}^2 \text{ V}^{-1} \text{ s}^{-1}$  with a threshold of  $-7.5 \text{ V}$  and field-dependent mobility, as high as  $0.012 \text{ cm}^2 \text{ V}^{-1} \text{ s}^{-1}$ .

In comparison with MOEP and H<sub>2</sub>TPP, the increased planarity and  $\pi$  conjugate system associated with the attached benzene rings on the pyrroles of porphyrin core render tetrabenzoporphyrins (TBPs) the most widely studied molecules among porphyrin derivatives for OFET devices. In 2004, Ono and co-workers

**Table 4** Performance of some monomeric porphyrin-based *p*-type OFET devices (*mEn* means  $m \times 10^n$ )

Year	Mobility [ $cm^2 V^{-1} s^{-1}$ ]	Material (deposition method)	$-V_T$ [V]	$I_{on}/I_{off}$	$W/L$ electrode	Source-drain electrode	Gate	Insulator	Reference
2003	1.3E-4	PtOEP <sup>a</sup>	NR	E4-E5	250	Au	Si	SiO <sub>2</sub>	[97]
	2.2E-4								
2003	1.3E-4	PtOEP <sup>a</sup>	NR	E4-E5	250	Au	Si	SiO <sub>2</sub>	[98]
	2.2E-4								
	1.4E-4	PtOEP (v)		E4-E5					
	3.6E-4								
2007	0.200	CoOEP <sup>b,c</sup>	NR	NR	0.08	Au	Si	SiO <sub>2</sub>	[99]
	0.068	CuOEP <sup>b,c</sup>			0.22				
	0.036	ZnOEP <sup>b,c</sup>			0.20				
	0.014	PdOEP <sup>b,c</sup>			0.036				
2003	0.007	H <sub>2</sub> TPP <sup>d</sup>	7.5	NR	3600	Cr	Al	SiO <sub>2</sub>	[100]
2004	0.017	H <sub>2</sub> TBP <sup>e</sup>	3.4	E5	50	Au/Cr	Si	SiO <sub>2</sub>	[101]
2005	(3.6, 9.9, 2, 1.1)E-3	H <sub>2</sub> TBP <sup>e</sup>	18.4, 14.7; 17, 10.8	NR	26.7	Au	Si	SiO <sub>2</sub>	[102]
2005	9.9E-3	H <sub>2</sub> TBP <sup>e</sup>	14.7	E5	26.7	Au	Si	SiO <sub>2</sub>	[103]
2007	2.5, 20E-4	H <sub>2</sub> TBP <sup>e</sup>	15.4, 15.3	NR	NR	Au	Si	SiO <sub>2</sub>	[104]
2006	0.13, 0.22	NiTBP <sup>e</sup>	18.9, 13	E3	20.8	Au	Si	SiO <sub>2</sub>	[105]
2007	0.1, 0.13	CuTBP <sup>e</sup>	-5, -7.5	E4	32	Au	Si	SiO <sub>2</sub>	[106]
2008	0.11	PtEP-1 <sup>c</sup>	-9	E3	25/3	Ti/Au	Si	SiO <sub>2</sub>	[108]
	0.32	PtEP-1 <sup>f</sup>	-9	E3					
	8.3E-4	CuEP-1 <sup>c</sup>	-10	E4					
	2.7E-3	NiEP-1 <sup>c</sup>	7	E2					
	8.7E-6	H <sub>2</sub> EP-1 <sup>c</sup>	-27	10					

(continued)

Table 4 (continued)

Year	Mobility [ $cm^2 V^{-1} s^{-1}$ ]	Material (deposition method)	$-V_T$ [V]	$I_{on}/I_{off}$	$W/L$ electrode	Source-drain electrode	Gate	Insulator	Reference
	1.2E-4	PtOEP	-11	E4					
	2.0E-4	CuOEP	-4	E3					
	6.0E-3	NiOEP	-20	E3					
	3.0E-6	H <sub>2</sub> OEP	-24	10					
	6.3E-5	PrTPrP	-21	E2					
	1.9E-4	H <sub>2</sub> TPrP	-17	E4					
	1.1E-4	PrTBuP	-12	E3					

<sup>a</sup>Wet transferred vertically aligned film<sup>b</sup>Crystal<sup>c</sup>BT/BC<sup>d</sup>Spin-coated film<sup>e</sup>Films obtained by heating the spin coated CP film<sup>f</sup>Top contact

fabricated H<sub>2</sub>TBP-based OFETs by spin-coating the chloroform solution of 1,4:8,11:15,18:22,25-tetraethano-29H,31H-tetrabenzo[b,g,l,q]porphine (H<sub>2</sub>TCP) onto the channel region of SiO<sub>2</sub> substrate and then heating the obtained film at 210°C for 5 min to convert H<sub>2</sub>TCP into H<sub>2</sub>TBP [101]. The device exhibited good *p*-type OFET properties with the mobility of 0.017 cm<sup>2</sup> V<sup>-1</sup> s<sup>-1</sup>, threshold voltage of -3.4 V, and on/off ratio of 1 × 10<sup>5</sup>. They also fabricated H<sub>2</sub>TBP-based OFET device with staggered source and drain electrode using the same method as described above and characterized the devices using linear and nonlinear best-fit methods [102]. A possible relation between a thin-film microstructure and behavior of a thin-film OFET device was discussed in terms of nonlinearity in the extraction of the electrical parameters of the device [102]. At the same time, the electrical performance of these solution-processed polycrystalline H<sub>2</sub>TBP OFETs with staggered source and drain contacts was also characterized and analyzed [103]. The device showed saturation field-effect mobility about 10<sup>-2</sup> cm<sup>2</sup> V<sup>-1</sup> s<sup>-1</sup> with threshold voltage of -15 V and on/off current ratio exceeding 10<sup>5</sup> [103]. Furthermore, Ono et al. fabricated solution-processed OFETs of H<sub>2</sub>TBP on a thermal silicon oxide gate insulator patterned with nanometer-scale trenches in 2007 [104]. The results revealed that the field-effect mobility with channels parallel to trench growth direction was about one order of magnitude higher than that with the channel oriented perpendicular to trench growth direction, 2.0 × 10<sup>-3</sup> vs. 2.5 × 10<sup>-4</sup> cm<sup>2</sup> V<sup>-1</sup> s<sup>-1</sup> [104]. Additionally, nickel and copper complexes of H<sub>2</sub>TBP were also fabricated into OFET devices. Using similar method in fabricating H<sub>2</sub>TBP-based OFETs, they successfully fabricated NiTBP thin-film field-effect transistors from spin coated films in 2006, which demonstrated hole transfer mobility around 0.1 and 0.2 cm<sup>2</sup> V<sup>-1</sup> s<sup>-1</sup> and accumulation threshold voltages of -19 and -13 V in the linear and saturation regions, respectively [105]. In 2007, they fabricated OFETs using polycrystalline CuTBP thin films by thermal converting the precursor (CuTCP) film at 165°C in vacuum [106]. The device exhibited charge transfer mobility about 0.1 cm<sup>2</sup> V<sup>-1</sup> s<sup>-1</sup>, accumulation threshold voltages around -5 V, and on/off current ratio of approximately 10<sup>4</sup>. Meanwhile, the low-temperature carrier transport properties of CuTBP-based OFET devices were also studied by Dhoot et al., using a four-probe measurement in order to separate the channel resistance from any contact resistance [107].

Recently, Che and co-workers described a series of field-effect transistors made from thin films of metal-free porphyrins and related macrocyclic compounds together with their metal complexes including MEP-I, MOEP, MTPrP, and MTBuP [108]. The peripheral substituents on porphyrin core were revealed to have a significant effect on the film structure and charge mobility. The OFET made from annealed PtEP-I film exhibited excellent overall charge transport properties with mobility as high as 0.32 cm<sup>2</sup> V<sup>-1</sup> s<sup>-1</sup>, low threshold voltage of -9 V, and on/off current ratio of 10<sup>3</sup>, due to the robust and efficient molecular packing with extensive lateral aggregation and π-π stacking interaction caused by the unique molecular shape and peripheral substituents of PtEP-I.

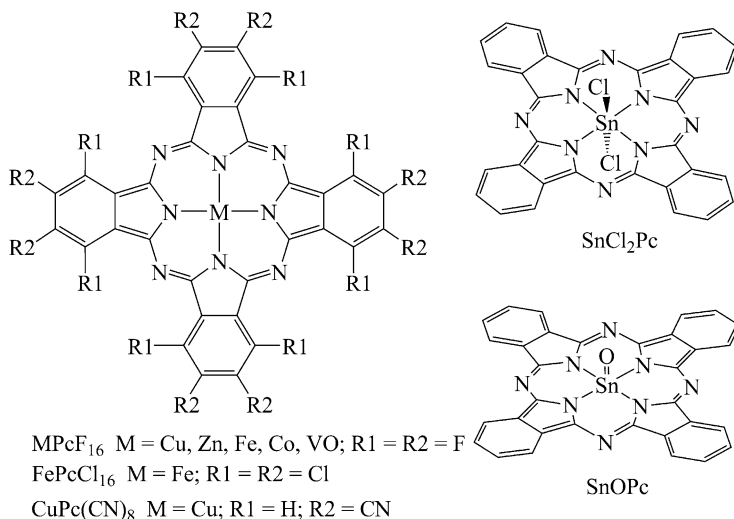


**Fig. 8** Molecular structures of some phthalocyanines used as semiconductors of *n*-type OFETs

## 5 *n*-Type Phthalocyanine Semiconductors

Air-stable *n*-channel semiconductor materials are important components in fabricating *p*-*n* junction diodes, bipolar transistors, and complementary circuits. However, despite the extensive studies of phthalocyanine semiconductors for OFETs, only very few phthalocyanine compounds have been found to function as *n*-channel semiconductors, most of which are molecules with strong electron-withdrawing groups at the peripheral and non-peripheral positions. Figure 8 shows the molecular structures of some phthalocyanines used as *n*-type semiconductors for OFETs and Table 5 summarizes the performance of these *n*-type OFET devices. The earliest reported *n*-type semiconductors for phthalocyanine-based OFETs are hexadeca-halogenated metallophthalocyanines MPcR (M = Cu, Zn, Fe, Co; R = F<sub>16</sub>, Cl<sub>16</sub>, (CN)<sub>8</sub>, Py) by Bao and co-workers in 1998 [109]. A maximum electron field-effect mobility of 0.03 cm<sup>2</sup> V<sup>-1</sup> s<sup>-1</sup> was achieved for the OFET device with CuPcF<sub>16</sub> as semiconductor layer, which was deposited at substrate temperature of 125°C with a 12 μm channel. In 1999, Tada and co-workers investigated the electron mobility of CuPcF<sub>16</sub> film-based OFETs in vacuum and various gas atmospheres including NH<sub>3</sub>, NO<sub>2</sub>, and O<sub>2</sub> [110]. The results revealed that the electron mobility increased when measured in NH<sub>3</sub> while it decreased in O<sub>2</sub>. However, the performance of the OFET device recovered quickly when gas molecules were evacuated, indicating the low capability of gas adsorption. By using Teflon as dielectric material, indium-tin-oxide as source-drain electrode, and Ag as gate electrode, the vacuum deposited CuPc-based OFET was found to show *n*-type characteristic with electron mobility of 1.1 × 10<sup>-6</sup> cm<sup>2</sup> V<sup>-1</sup> s<sup>-1</sup> and on/off current ratio of 500 according to Qiu et al. [111]. Yuan and co-workers investigated the effects of positive and negative



**Table 5** Performance of some phthalocyanine-based *n*-type OFET devices (*mE<sub>l</sub>* means  $m \times 10^l$ )

Year	Mobility [ $cm^2V^{-1}s^{-1}$ ]	Material (deposition method)	$-V_T$ [V]	$I_{on}/I_{off}$	$W/L$ electrode	Source-drain electrode	Gate	Insulator	Reference
1998	0.03	CuPcF16 (v, 125° C)	NR	5E4	NR	Au	Au	SiO <sub>2</sub>	[109]
	5E-3	CuPcF16 (v, 30° C)		NR					
	0.02	CuPcF16 (v, 215° C)							
	1.7E-5	ZnPcF16 (v, 30° C)							
	4.6E-4	ZnPcF16 (v, 125° C)							
	1.2E-3	ZnPcF16 (v, 215° C)							
	1.8E-6	CoPcF16 (v, 30° C)							
	4.5E-5	CoPcF16 (v, 125° C)							
	4.3E-5	CoPcF16 (v, 215° C)							
	5.5E-4	FePcF16 (v, 30° C)							
5.8E-3	FePcF16 (v, 125° C)								
2.1E-3	FePcF16 (v, 215° C)								
NR	FePcCl16 (v, 30° C)								
2.7E-5	FePcCl16 (v, 125° C)								
1999	2E-3	CuPcF16 (v, vacuum)	NR	NR	240	Au/Cr	Si	SiO <sub>2</sub>	[110]
	5.7E-3	CuPcF16 (v, NH3)							
2002	5E-4	CuPcF16 (v, O <sub>2</sub> )							
	1.1E-6	CuPc (TG BC, v)	NR	500	1,620	ITO	Ag	teflon	[111]
2004	0.017	CuPcF16 (v)				Al	Ta	Ta <sub>2</sub> O <sub>5</sub>	[112]
	5E-3	CuPcF16 (v)	0.5	E3	NR	Au	Si	CPVP-C6	[113]
2005	3E-3		20	E4				SiO <sub>2</sub>	
	0.082	CuPcF16 (v, 125° C)	-23	3.5E5				SiO <sub>2</sub>	[114]
2006	0.03		21	3.3E5		Au			
	4.5E-3	CuPcF16 (v, 25° C)	29	4.4E4		Au soft contact lamination			
	5.6E-3		34	1.2E5		Au soft contact lamination			

(continued)

**Table 5** (continued)

Year	Mobility [ $cm^2 V^{-1} s^{-1}$ ]	Material (deposition method)	$-V_T$ [V]	$I_{on}/I_{off}$	$W/L$ electrode	Source-drain electrode	Gate	Insulator	Reference
2006	6.6E-2	CuPc (buffer layer)-CuPcF16 (v)	5.48	2.44E5	6.25	Au	Si	OTS-SiO <sub>2</sub>	[115]
	4.2E-2	CuPcF16 (v)	7.31	1.63E5					
2006	1.0E-6	CuPc (v, nonplanar)		E2	x/6 $\mu m$	Al-Cu	Au	SiO <sub>2</sub> /SiN <sub>x</sub>	[59]
	1.2E-6			E2	x/6 $\mu m$	Al-Al			
2006	6E-3	CuPcF16 (v)	14.8	5.4E3	10	Au	Si	P1-P2	[116]
	1.8E-3		7.7	8.1E2				HMDS SiO <sub>2</sub>	
	1E-3		9.1	4.2E2				SiO <sub>2</sub>	
2006 <sup>a</sup>	4.25E-3	CuPcF16 (v, 100° C)					Si	SiO <sub>2</sub>	[117]
2008	0.3	SnCl <sub>2</sub> Pc	NR	E6	NR	Au	Si	<i>p</i> -6P-SiO <sub>2</sub>	[118]
2008	0.44	SnOPc	NR	E3	26.7	Au	Si	<i>p</i> -6P-SiO <sub>2</sub>	[119]
2000	1.7a	CuPcF16 crystal	NR	NR	NR	Au	Au	SiO <sub>2</sub>	[120]
2006	0.2	CuPcF16 single crystal	-5.5	6E4	0.035	Ag-Au	Si	SiO <sub>2</sub>	[121]

<sup>a</sup>Estimated from the trap-free space charge limited current (SCLC) method

gate-bias stress on the performance of CuPcF<sub>16</sub>-based OFETs with Ta<sub>2</sub>O<sub>5</sub> as the insulator at various stress time, stress voltage, and temperature in 2004 [112], revealing that changing deposition method or optimizing deposition condition was beneficial in reducing gap trap site concentration and hence improving the stability of OEFT devices. Using ultrathin cross-linked polymers as gate dielectrics, the CuPcF<sub>16</sub>-based OFETs exhibited very low threshold voltage of only 0.5 V with electron mobility of  $5 \times 10^{-3} \text{ cm}^2 \text{ V}^{-1} \text{ s}^{-1}$  and on/off current ratio of  $10^4$  [113]. Enhanced field-effect mobility of CuPcF<sub>16</sub> transistors made by soft contact lamination was reported in 2006 [114]. Due to the avoidance of the damage to organic semiconductor during conventional vacuum deposition of metal electrodes and the improvement for the injection of charge carrier from metal electrodes into semiconductor layer together with the surface chemical treatment of the dielectric layer in soft contact lamination method, the CuPcF<sub>16</sub>-based OFET device showed greatly enhanced electron transfer mobility of  $0.08 \text{ cm}^2 \text{ V}^{-1} \text{ s}^{-1}$  in comparison with devices made by direct metal deposition method. At the same time, Yan and co-workers reported another way to improve the performance of CuPcF<sub>16</sub>-based *n*-type OFET devices [115]. By adding *p*-type CuPc as buffer layer between the CuPcF<sub>16</sub> semiconductor layer and the Au source-drain electrodes during the fabricating process, the electron transfer mobility was improved to  $0.076 \text{ cm}^2 \text{ V}^{-1} \text{ s}^{-1}$  for this kind of sandwich type OFET. This provides an effective way to improve the performance of *n*-type OFET devices. Using Al as source electrode and Au or Al as drain electrode, the non-planar CuPc-based OFETs also exhibited electron transfer behavior with the mobility of  $1.0 \times 10^{-6}$ – $1.2 \times 10^{-6} \text{ cm}^2 \text{ V}^{-1} \text{ s}^{-1}$  and on/off current ratio of  $10^2$  [59]. Pyo and co-workers fabricated *n*-type OTFTs with CuPcF<sub>16</sub> as active semiconductor and polymeric blend as gate insulator [116]. This device exhibited improved performance with electron transfer mobility of  $0.006 \text{ cm}^2 \text{ V}^{-1} \text{ s}^{-1}$  and on/off current ratio of  $5.4 \times 10^3$  in comparison with the device with bare SiO<sub>2</sub> and HMDS treated SiO<sub>2</sub> as insulator. Ye et al. reported the correlation between morphology and electronic properties of CuPcF<sub>16</sub> thin films deposited on SiO<sub>2</sub>/Si substrate at different substrate temperatures [117]. It was found that the mobility was strongly dependent on the substrate temperature and the maximum mobility of  $4.25 \times 10^{-3} \text{ cm}^2 \text{ V}^{-1} \text{ s}^{-1}$  was obtained when deposition of CuPcF<sub>16</sub> was conducted at a substrate temperature of 100°C. In addition to the peripheral substituted phthalocyanines with electron-withdrawing groups, Yan et al. showed that the axial oxygen and axially dichloro substituted tin phthalocyanines also exhibited high *n*-type OFET performance with good air stability [118, 119]. An electron mobility of  $0.30 \text{ cm}^2 \text{ V}^{-1} \text{ s}^{-1}$  along with a current on/off ratio of  $10^6$  was realized in air for SnCl<sub>2</sub>Pc-based device with *p*-6P modified substrate [118]. The SnOPc-based OFET device fabricated on *p*-6P modified substrate exhibited high electron transfer mobility of  $0.44 \text{ cm}^2 \text{ V}^{-1} \text{ s}^{-1}$  and excellent air stability, rendering SnOPc a good candidate for widely applicable *n*-type material [119]. Furthermore, the work provided a new way to design *n*-type semiconductors by incorporating a suitable metal connected with electron-withdrawing group into  $\pi$ - $\pi$  conjugated system.

As expected, *n*-type OFET devices fabricated from single crystals display higher performance than those made from thin solid films because of the more

close-grained structures in crystals than in solid films. Schön and co-workers investigated the electrical properties of CuPcF<sub>16</sub> single crystals in air as functions of time and temperature, and the mobility in thin-film devices as functions of gate bias and temperature [120]. Mobility as high as  $1.7 \text{ cm}^2 \text{ V}^{-1} \text{ s}^{-1}$  estimated from the trap-free space charge limited current (SCLC) regime at room temperature was found for CuPcF<sub>16</sub> single crystals. High-performance air-stable *n*-type OFETs based on single-crystalline submicro- and nanometer ribbons of CuPcF<sub>16</sub> were fabricated by Liu et al. in 2006 [121]. The intimate contact between the crystal and the insulator surface generated by the “in situ” growing process and the asymmetrical drain/source (Au/Ag) electrode configuration rendered the OFET device displaying air stable and reproducible high performance with electron mobility of  $0.2 \text{ cm}^2 \text{ V}^{-1} \text{ s}^{-1}$  and on/off ratio of  $6 \times 10^4$ .

## 6 Ambipolar Phthalocyanine Semiconductors

The development of *p*- and *n*-type OFETs together with their potential application in organic integrated circuits makes ambipolar OFETs become the research focus of this field recently. In fact, the first reported phthalocyanine-based OFETs by Simon and co-workers in 1987 showed ambipolar properties [122]. Ambipolar OFETs can be divided into two types according to the composition of semiconductor layer: (a) those with a single semiconductor material having high charge transfer mobility for both hole and electron as active layer and (b) those with separate *p*-type and *n*-type semiconductor materials with balanced high mobility combined together as semiconductor layers (Fig. 9 and Table 6).

Despite the intrinsic ambipolar nature for both hole and electron transfer of the organic materials in terms of theory, few single-component organic semiconductors have been found to exhibit ambipolar transfer property because of the high injection barrier for at least one charge carrier, either hole or in particular electron, of general organic OFET materials relative to the work function potential of source-drain electrodes. Among all the phthalocyanine semiconductors, only LuPc<sub>2</sub>, SmPc<sub>2</sub>, TiOPc, CuPc, and PbPc have been reported to show ambipolar property. Simon et al. described the electrical characteristics of the field effect transistor based on LuPc<sub>2</sub> in 1988 [123]. The OFET device showed *p*-type characteristic in the negative source-drain voltage region with mobility of  $10^{-4} \text{ cm}^2 \text{ V}^{-1} \text{ s}^{-1}$  and threshold voltage of  $-2 \text{ V}$ , while space-charge-limited current (SCLC) behavior was observed in the positive source-drain voltage region with mobility calculated from SCLC model of  $6 \text{ cm}^2 \text{ V}^{-1} \text{ s}^{-1}$ . In 1990, they fabricated OFETs with the intrinsic semiconductors LuPc<sub>2</sub> and SmPc<sub>2</sub> as active layer and purely inorganic materials as insulating layers [29]. Both *p*- and *n*-type electronic properties were found ranging from  $2 \times 10^{-4} \text{ cm}^2 \text{ V}^{-1} \text{ s}^{-1}$  to  $1.5 \times 10^{-2} \text{ cm}^2 \text{ V}^{-1} \text{ s}^{-1}$  depending on the ambient atmosphere. In 2000, Tada and co-workers found that the *n*-type OFET of TiOPc could converse to *p*-type when the film was exposed to oxygen, with the mobility for electron of  $9 \times 10^{-6} \text{ cm}^2 \text{ V}^{-1} \text{ s}^{-1}$  conversed to hole mobility of  $1 \times 10^{-5} \text{ cm}^2 \text{ V}^{-1} \text{ s}^{-1}$  [124]. On the contrary, the *p*-type conduction was found to disappear in an NH<sub>3</sub>

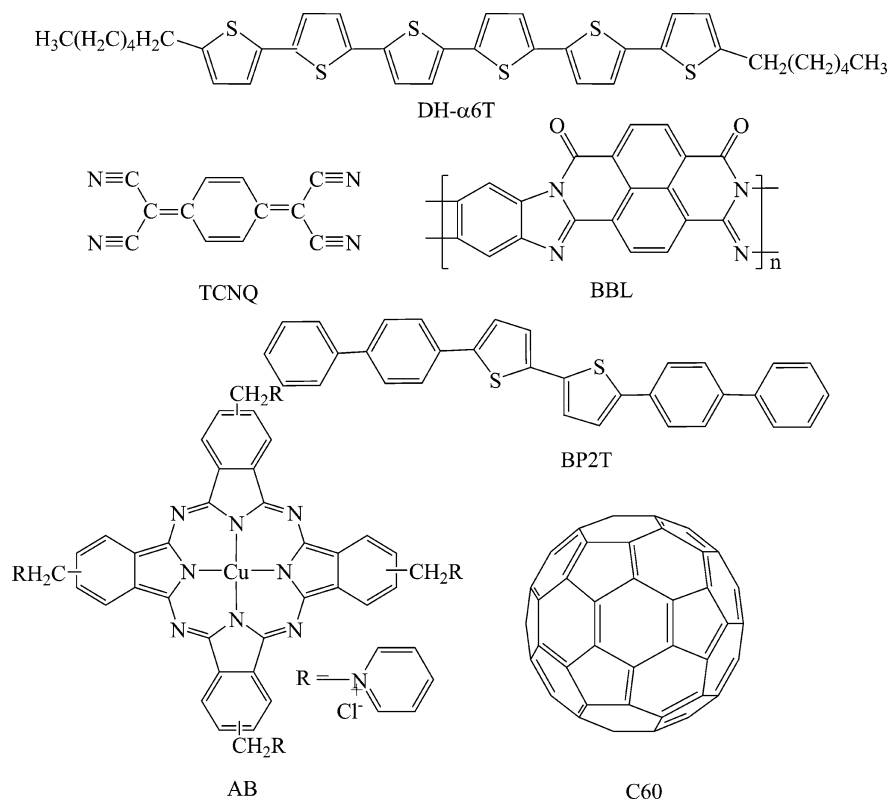


**Fig. 9** Molecular structures of the reported compounds forming ambipolar OFETs with phthalocyanines

atmosphere. Strict control of atmosphere made it possible to obtain a quasi-intrinsic state where both *p*- and *n*-type conduction appeared simultaneously, and hole and electron mobilities of  $2.0 \times 10^{-6}$  and  $2.7 \times 10^{-6} \text{ cm}^2 \text{ V}^{-1} \text{ s}^{-1}$ , respectively, were evaluated using SCLC method [124].

By using the insulator hysteresis method, Mizuno et al. fabricated ambipolar OFET with the common reported *p*-type CuPc as semiconducting layer and cyanoethylpullulan as insulating layer in 2005, and the temperature dependence of the mobility was studied [125]. The OFET devices exhibited field-effect mobility of  $4.1 \times 10^{-3}$  and  $3.5 \times 10^{-6} \text{ cm}^2 \text{ V}^{-1} \text{ s}^{-1}$  for hole and electron, respectively, with the on/off ratio of  $6 \times 10^4$  and 70 at  $V_{\text{SG}} = \pm 10 \text{ V}$ . Ambipolar OFETs based on vacuum-evaporated CuPc film were also reported by Yasuda and co-workers in 2005 [126]. Different from the strategy of Mizuno et al., Yasuda and co-workers attained the ambipolar properties by reducing the electron injection barrier through using low work functional Ca instead of Au as source-drain electrodes and at the same time by eliminating extrinsic traps in CuPc through avoiding ambient air. The hole mobility of  $2.5 \times 10^{-4} \text{ cm}^2 \text{ V}^{-1} \text{ s}^{-1}$  and electron mobility of  $1.0 \times 10^{-3} \text{ cm}^2 \text{ V}^{-1} \text{ s}^{-1}$

**Table 6** Performance of some phthalocyanine-based ambipolar OFET devices (*mEn* means  $m \times 10^4$ )

Year	Mobility [ $\text{cm}^2 \text{V}^{-1} \text{s}^{-1}$ ]	Material (deposition method)	$-V_T$ [V]( <i>p/n</i> )	$I_{\text{on}}/I_{\text{off}}$ ( <i>p/n</i> )	<i>W/L</i> electrode	Source-drain electrode	Gate	Insulator	Reference
1988	1E-4/6 <sup>a</sup>	LuPc <sub>2</sub> -ZnPc(v)	NR/-2	NR	NR	Au	Au	SiO <sub>2</sub>	[123]
1990	/2E-4	LuPc <sub>2</sub> (v)	/8	NR	NR	Au	Si	SiO <sub>2</sub> -(SiN <sub>x</sub> )	[29]
	2E-3/	LuPc <sub>2</sub> (v, 150° C)	1.5/						
	3E-3/	LuPc <sub>2</sub> (v, 150° C, air)	1/						
	/3E-4	SmPc <sub>2</sub> (v)	/10						
	/1.4E-3	SmPc <sub>2</sub> (v, 150° C)	/10						
	5E-3/	SmPc <sub>2</sub> (v, 150° C, air)	4/						
	1.5E-2/	SmPc <sub>2</sub> (v, 150° C, air, annealing 150° C 2 days)	4/						
2000	/9E-6	TiOPc (v, ultrahigh vacuum)	NR	NR	240	Au/Cr	Si	SiO <sub>2</sub>	[124]
	1E-5/	TiOPc (v, O <sub>2</sub> )							
	2E-6/2.7E-6 <sup>a</sup>	TiOPc (v, little O <sub>2</sub> )							
2005	4.1E-3/3.5E-6	CuPc (v)	-0.1/0.9	6E4/70	102.6	Au	Au/Ti	CyEPL	[125]
2005	2.5E-4/1.0E-3	CuPc (v)	-60/36	5.1- 220/45- 1,000	66.7	Ca/Ag	Au	Parylene-C	[126]
2005	0.3/0.03	FePc crystal	NR	NR	NR	Au	Si	SiO <sub>2</sub>	[127]
	0.3/E-3	CuPc crystal							
2006	7.1E-4/8.3E-4	PbPc (v, glove box)	-58/31	NR	66.7	Au	Au	Parylene-C	[128]
	4.7E-4/1.3E-3		-60/36			Ca-Ag			
	4.2E-3/1.3E-3	PbPc (v, glove box, annealing)	-27/45			Au			
	1.8E-3/2.0E-3		-22/31			Ca-Ag			
2003	1.41-16.0E-5/4.4-111E-6	CuPcTSSNa/AB <sup>b</sup>	NR	NR	10-167,5.5	Au	Si	SiO <sub>2</sub>	[129]
2004	6-200E-6/6-30E-6	BBL-CuPc <sup>c</sup>	NR	NR	20	Au	Si	SiO <sub>2</sub>	[130]

(continued)

Table 6 (continued)

Year	Mobility [ $\text{cm}^2 \text{V}^{-1} \text{s}^{-1}$ ]	Material (deposition method)	$-V_T$ [V]( $p/n$ )	$I_{\text{on}}/I_{\text{off}}$ ( $p/n$ )	$W/L$ electrode	Source-drain electrode	Gate	Insulator	Reference
2005	0.042/NR	CuPcF <sub>16</sub> -Au-CuPc	19/NR	NR	7.5	Au	Si	Ta <sub>2</sub> O <sub>5</sub>	[131]
2005	E-6/E-6(1.47E-2)	CuPc-Au-CuPcF <sub>16</sub> (v)	NR/-29	NR	7.2	Au	Si	SiO <sub>2</sub>	[132]
2005	1.44E-3/9.97E-4	CuPc-CuPcF <sub>16</sub>	NR	NR	71.4	Au	Si	SiO <sub>2</sub>	[133]
2005	3.26E-3/3.34E-3	CuPc-CuPcF <sub>16</sub>	-1.25/3.25	NR	71.4	Au	Si	SiO <sub>2</sub>	[134]
2006	3.8-7.8E-4/1.4-4.6E-4	25° CCuPcF <sub>16</sub> - -Au-250° CCuPc	NR	NR	7.2	Au	Si	SiO <sub>2</sub>	[135]
2006	/6.2-11.2E-3	CuPc-Au-CuPcF <sub>16</sub>	/-33	NR	NR	Au	Si	SiO <sub>2</sub>	[136]
2006	0.04/0.036	CuPcF <sub>16</sub> -BP2T	-12/7	NR	7.5	Au	Si	SiO <sub>2</sub>	[137]
2007	1E-4/3.1E-4	CuPc-C <sub>60</sub> <sup>d</sup>	-17.7/35.1	NR	250,500	Ti/Au	Si	SiO <sub>2</sub>	[138]
2007	3E-3/3E-3 /2.6E-2	CuPc-CuPcF <sub>16</sub> (5 nm, v) CuPc-CuPcF <sub>16</sub> (12 nm, v)	-2/2 /-7.4	NR	71.4	Au	Si	SiO <sub>2</sub>	[139]
2008	1.77E-3/8.18E-3	DH- $\alpha$ 6T-CuPcF <sub>16</sub>	3.3/6.82	NR	71.4	Au	Si	SiO <sub>2</sub>	[140]

<sup>a</sup>Measured with the pulse-radiolysis time-resolved microwave conductivity (PR-TRMC) technique

<sup>b</sup>Layer by layer film aqueous solution, BC/BG

<sup>c</sup>Spin-coated film, BC/BG

<sup>d</sup>Ring-type geometry device, CuPc:C<sub>60</sub> = 3 : 1

were estimated from the saturation currents above the threshold voltage [126]. In 2005, Morpurgo et al. reported the observation of ambipolar transport in FETs fabricated with single crystals of CuPc and FePc, using gold as a high work-function metal for the fabrication of source and drain electrodes [127]. Room temperature mobility for hole as high as  $0.3 \text{ cm}^2 \text{ V}^{-1} \text{ s}^{-1}$  for both FePc and CuPc was achieved, while the highest electron transfer mobility was about  $0.03 \times 10^{-3} \text{ cm}^2 \text{ V}^{-1} \text{ s}^{-1}$  for FePc and CuPc, respectively. Another promising way to reduce injection barriers for both carriers and thus achieve ambipolar properties with single semiconductor was demonstrated by Yasuda et al. in 2006 [128]. They fabricated high-performance ambipolar OFETs with PbPc as active layer and Parylene-C as insulator layer. Both Ca and Au were used as source and/or drain electrodes. Due to the low band gap energy of PbPc (1.2 eV) and the usage of polymer insulator, the devices with Au source-drain electrodes showed hole mobility of  $7.1 \times 10^{-4} \text{ cm}^2 \text{ V}^{-1} \text{ s}^{-1}$  at threshold voltage of  $-58 \text{ V}$  and electron mobility of  $8.3 \times 10^{-4} \text{ cm}^2 \text{ V}^{-1} \text{ s}^{-1}$  at threshold voltage of  $31 \text{ V}$ , while those with Ca source-drain electrodes exhibited charge mobility of  $4.7 \times 10^{-4}$  and  $1.3 \times 10^{-3} \text{ cm}^2 \text{ V}^{-1} \text{ s}^{-1}$  for hole and electron, respectively. After annealing the device for 12 h at  $100^\circ \text{ C}$ , the mobility was improved to the order of magnitude of  $10^{-3} \text{ cm}^2 \text{ V}^{-1} \text{ s}^{-1}$  for both hole and electron [128].

Fabricating ambipolar OFET devices with combined *p*-type and *n*-type semiconducting materials as active layers is a more common and widely used method than that with single molecular material as semiconductor. In 2003, Bao et al. fabricated ambipolar OFETs for the first time by layer-by-layer depositing water-soluble cationic and anionic phthalocyanine derivatives [129]. Although the mobility of this kind of devices was only in the range of  $10^{-5} - 10^{-4} \text{ cm}^2 \text{ V}^{-1} \text{ s}^{-1}$  for both hole and electron, the unusual “ambipolar” transistor-like behavior due to an ion-modulated electrical conduction mechanism which relied on the assistance of mobile ions to stabilize the oxidized or reduced species in the channel region proved the effectiveness of fabricating phthalocyanine-based ambipolar OFETs using this method [129]. Due to the nice *p*-type and *n*-type properties of CuPc and CuPcF<sub>16</sub>, respectively, most of ambipolar OFETs fabricated with this method are based on CuPc and/or CuPcF<sub>16</sub>. Ambipolar OFETs based on a series of air-stable, solution-processed blends of a *p*-type small molecule CuPc and a *n*-type polymer (BBL) were reported by Babel and co-workers in 2004, which exhibited high stability under ambient conditions [130]. Depending on the blend composition of BBL and CuPc, the devices showed hole mobility ranging from  $6.0 \times 10^{-6}$  to  $2.0 \times 10^{-4} \text{ cm}^2 \text{ V}^{-1} \text{ s}^{-1}$  and electron mobility in the region of  $2.0 \times 10^{-6}$  and  $3.0 \times 10^{-5} \text{ cm}^2 \text{ V}^{-1} \text{ s}^{-1}$  [130]. The results also demonstrated that ambipolar charge transport and carrier mobility in multicomponent organic semiconductors were intricately related to the phase-separated nano-scale and crystalline morphology. Yan et al. fabricated heterojunction OFET based on *p*-type CuPc and *n*-type CuPcF<sub>16</sub> in 2005 [131]. This device not only showed increased hole mobility of  $0.042 \text{ cm}^2 \text{ V}^{-1} \text{ s}^{-1}$  in comparison with CuPc single-layered OFET with mobility of  $0.017 \text{ cm}^2 \text{ V}^{-1} \text{ s}^{-1}$  but also exhibited ambipolar electric characteristics. At the same time, by depositing CuPcF<sub>16</sub> on the SiO<sub>2</sub> gate insulator and CuPc on CuPcF<sub>16</sub> as the second active layers, the fabricated OFET device exhibited typical *n*-type semiconductor



characteristic with electron mobility of  $1.47 \times 10^{-2} \text{ cm}^2 \text{ V}^{-1} \text{ s}^{-1}$  [132]. However, ambipolar properties were found with mobility at the level of  $10^{-6} \text{ cm}^2 \text{ V}^{-1} \text{ s}^{-1}$  for both hole and electron by tuning the thickness of the two-layer thin film, probably because of comparable concentrations of the two carriers under various gate voltages. These results indicate that combining *p*- and *n*-type semiconductors with balanced mobility is an effective method toward ambipolar OFETs. In 2005, Ye and co-workers fabricated ambipolar OFET with CuPcF<sub>16</sub> as the first layer and CuPc as the second layer, which showed high performance air-stable ambipolar characteristics with hole mobility of  $1.44 \times 10^{-3} \text{ cm}^2 \text{ V}^{-1} \text{ s}^{-1}$  and electron mobility of  $9.97 \times 10^{-4} \text{ cm}^2 \text{ V}^{-1} \text{ s}^{-1}$  [133]. They reported afterward improved OFET property with hole mobility of  $3.26 \times 10^{-3} \text{ cm}^2 \text{ V}^{-1} \text{ s}^{-1}$  and electron mobility of  $3.34 \times 10^{-3} \text{ cm}^2 \text{ V}^{-1} \text{ s}^{-1}$  in another work [134]. By carefully controlling the morphology of the interpenetrating network structure, the fabricated ambipolar OFET with 5-nm thick CuPc deposited at high temperature (250°C) as the first *p*-type component layer and 25-nm thick CuPcF<sub>16</sub> deposited at room temperature as the second *n*-type component layer exhibited typical ambipolar charge transport with symmetric hole and electron mobility of the order of magnitude of  $10^{-4} \text{ cm}^2 \text{ V}^{-1} \text{ s}^{-1}$  [135], which was two order of magnitude higher than the previous reported results of the same group [132]. This group also studied the interfacial electric structures of OFETs with CuPc and CuPcF<sub>16</sub> as active layers and determined the thickness of the charge accumulation at both sides of the heterojunction interface by varying the thickness of the active layer in OFETs in 2006, which supplied a physical method by utilizing the heterojunction-effect to optimize the threshold voltage of organic transistors in order to meeting different requirements [136]. The ambipolar OFETs based on the organic heterojunction of CuPcF<sub>16</sub> and 2,5-bis(4-biphenyl)thiophene (BP2T) were fabricated in 2006 by Yan's group, which were revealed to show high air stability, high mobility, and balanced transport. High field-effect mobility of  $0.04 \text{ cm}^2 \text{ V}^{-1} \text{ s}^{-1}$  for hole and  $0.036 \text{ cm}^2 \text{ V}^{-1} \text{ s}^{-1}$  for electron were obtained, and the hole and electron were revealed to transport at BP2T and CuPcF<sub>16</sub> layers, respectively [137]. In 2007, Opitz et al. studied the ambipolar properties of OFETs with mixed layers of CuPc and C<sub>60</sub> in different ratio as active layers [138]. Hole and electron transport was observed for all analyzed mixing ratios and deposition temperature, which decreased exponentially with decreasing volume percentage of the respective conducting material. The variation of mobility and threshold voltage along with the mixing ratio and ambipolar inverters as a leadoff application were discussed. A mixing ratio of CuPc to C<sub>60</sub> of 3:1 was found to yield balanced hole and electron mobility with the value of  $1.0 \times 10^{-4}$  and  $3.1 \times 10^{-4} \text{ cm}^2 \text{ V}^{-1} \text{ s}^{-1}$ , respectively [138]. Ye and co-workers found that CuPcF<sub>16</sub>/CuPc-based OFETs exhibited ambipolar transport performance at the thickness between 4 and 12 nm of CuPcF<sub>16</sub> film layer and showed balanced transport mobility for hole and electron of about  $3 \times 10^{-3} \text{ cm}^2 \text{ V}^{-1} \text{ s}^{-1}$  at CuPcF<sub>16</sub> thickness of 5 nm, which however displayed enhanced *n*-type operating characteristics but suppressed *p*-type behavior with the increase of the thickness for CuPcF<sub>16</sub> layer above 12 nm. Electron mobility as high as  $2.6 \times 10^{-2} \text{ cm}^2 \text{ V}^{-1} \text{ s}^{-1}$  and threshold voltage of  $-7.4 \text{ V}$  was shown at CuPcF<sub>16</sub> thickness of 15 nm [139]. Ambipolar OFETs with hetero-structured

thin films of CuPcF<sub>16</sub> and  $\alpha$ ,  $\alpha'$ -dihexylsexithiophene (DH- $\alpha$ 6T) were also fabricated by the same group recently. The devices showed highly air-stable ambipolar characteristics with hole and electron field-effect mobility of  $1.77 \times 10^{-3}$  and  $8.18 \times 10^{-3} \text{ cm}^2 \text{ V}^{-1} \text{ s}^{-1}$ , respectively [140].

## 7 Conclusion

We have reviewed the progress in OFETs with various tetrapyrrole materials including monomeric phthalocyanines, bis(phthalocyaninato) rare earth complexes, tris(phthalocyaninato) rare earth complexes, and monomeric porphyrins as the active semiconductors in terms of the semiconducting nature (*p*-type, *n*-type, or ambipolar), carrier mobility, and current modulation reported in the past two decades. Since the first phthalocyanine-based OFET reported in 1987, about 55 *p*-type monomeric phthalocyanine semiconductors, 3 *p*-type bis(phthalocyaninato) rare earth double-decker semiconductors, 15 *p*-type tris(phthalocyaninato) rare earth triple-decker semiconductors, 14 *p*-type monomeric porphyrin semiconductors, 13 *n*-type phthalocyanine semiconductors, and 19 ambipolar phthalocyanine semiconductors have been reported so far. The highest hole transfer mobility of  $3.31 \text{ cm}^2 \text{ V}^{-1} \text{ s}^{-1}$  for vacuum-deposited film of TiOPc,  $1 \text{ cm}^2 \text{ V}^{-1} \text{ s}^{-1}$  for single crystal of CuPc, and  $0.78 \text{ cm}^2 \text{ V}^{-1} \text{ s}^{-1}$  for LB film of tris(phthalocyaninato) rare earth complexes, electron transfer mobility of  $0.44 \text{ cm}^2 \text{ V}^{-1} \text{ s}^{-1}$  for vacuum-deposited film of SnOPc and  $0.2 \text{ cm}^2 \text{ V}^{-1} \text{ s}^{-1}$  for single-crystalline submicro- and nanometer ribbons of CuPcF<sub>16</sub>, and ambipolar charge transfer mobility in the order of magnitude of  $10^{-3} \text{ cm}^2 \text{ V}^{-1} \text{ s}^{-1}$  have been achieved. Altering and modifying the insulator layer, source-drain electrodes, and gate electrode and tuning the fabricating condition of semiconductor layers were demonstrated useful methods in improving the OFET performance. Theoretical studies toward understanding the relationship between the molecular and electronic structures of phthalocyanines and their semiconducting properties in the viewpoint of OFETs have also been included.

Despite the vast amount of reported OFETs with tetrapyrrole compounds as active semiconductors, the OFET performance of tetrapyrrole semiconductors is still very poor compared with the traditional inorganic semiconductors. On the basis of great potential applications of OFETs and the high theoretical charge transfer mobility of phthalocyanines, improving the OFET performance of existing phthalocyanine semiconductors and fabricating OFETs with novel phthalocyanine compounds will continue to draw the interests of scientists in future.

**Acknowledgements** The authors thank the National Natural Science Foundation of China, Education Ministry of China, University of Science and Technology Beijing, and Shandong University for financial support.

## References

1. Tsumura A, Koezuka H, Ando T (1986) *Appl Phys Lett* 49:1210
2. Lever ABP, Leznoff CC *Phthalocyanine: properties and applications*. VCH, New York, 1989, Vol. 1; 1993, Vols. 2 and 3; 1996, Vol. 4
3. McKeown NB *Phthalocyanines materials-synthesis, structure and function*. Cambridge University Press, New York, 1998
4. Kadish KM, Smith KM, Guillard R *The porphyrin handbook*, Vols. 1–20. Academic, San Diego, 2000–2003
5. Jiang J, Kasuga K, Arnold DP (2001) Sandwich-type phthalocyaninato and porphyrinato metal complexes. In: Nalwa HS (ed) *Supramolecular photo-sensitive and electroactive materials*. Academic, New York, pp 113–210
6. Ng DKP, Jiang J (1997) *Chem Soc Rev* 26:433
7. Jiang J, Ng DKP (2009) *Acc Chem Res* 42:79
8. Zaumseil J, Siringhaus H (2007) *Chem Rev* 107:1296–1323
9. Veres J, Ogier S, Lloyd G, de Leeuw D (2004) *Chem Mater* 16:4543
10. Newman CR, Frisbie CD, da Silva Filho DA, Brédas J-L, Ewbank PC, Mann KR (2004) *Chem Mater* 16:4436
11. Forrest SR (2004) *Nature* 428:911
12. Dimitrakopoulos CD, Malenfant PRL (2002) *Adv Mater* 14:99
13. Roncali J, Leriche P, Cravino A (2007) *Adv Mater* 19:2045
14. Demanze F, Cornil J, Garnier F, Horowitz G, Valat P, Yassar A, Lazzaroni R, Brédas JL (1997) *J Phys Chem B* 101:4553
15. Zhang Y, Cai X, Bian Y, Li X, Jiang J (2008) *J Phys Chem C* 112:5148
16. Chen HY, Chao I (2006) *ChemPhysChem* 7:2003
17. Coropceanu V, Cornil J, da Silva Filho, DA, Olivier Y, Silbey R, Brédas JL (2007) *Chem Rev* 107:926
18. Brédas JL, Calbert JP, da Silva Filho DA, Cornil J (2002) *Proc Natl Acad Sci USA* 99:5804
19. Hutchison GR, Ratner MA, Marks TJ (2005) *J Am Chem Soc* 127:16866
20. Deng WQ, Goddard WA III (2004) *J Phys Chem B* 108:8614
21. Marcus RA (1964) *Annu Rev Phys Chem* 15:155
22. Marcus RA (1993) *Rev Mod Phys* 65:599
23. Troisi A, Orlandi G (2001) *Chem Phys Lett* 344:509
24. Yang X, Wang L, Wang C, Long W, Shuai Z (2008) *Chem Mater* 20:3205
25. Valeev EF, Coropceanu V, da Silva Filho DA, Salman S, Brédas JL (2006) *J Am Chem Soc* 128:9882
26. Song Y, Di C, Yang X, Li S, Xu W, Liu Y, Yang L, Shuai Z, Zhang D, Zhu D (2006) *J Am Chem Soc* 128:15940
27. Schein LB, McGhie AR (1979) *Phys Rev B* 20:1631
28. Zhang Y, Cai X, Qi D, Bian Y, Jiang J (2008) *J Phys Chem C* 112:14579
29. Guillaud G, Al Sadoun M, Maitrot M, Simon J, Bouvet M (1990) *Chem Phys Lett* 167:503
30. Vartanyan AT (1948) *Zh Fiz Khim* 22:769
31. Guillaud G, Madru R, Al Sadoun M, Maitrot M (1989) *J Appl Phys* 66:4554
32. Guillaud G, Simon J (1994) *Chem Phys Lett* 219:123
33. Guillaud G, Ben Chaabane R, Gamoudi M (1994) *L'Onde Electrique* 74:14
34. Guillaud G, Ben Chaabane R, Jouve C, Gamoudi M (1995) *Thin Solid Films* 258:279
35. Ben Chaabane R, Ltaief A, Dridi C, Rahmouni H, Bouazizi A, Ben Ouada H (2003) *Thin Solid Films* 427:371
36. Bao Z, Lovinger AJ, Dodabalapur A (1996) *Appl Phys Lett* 69:3066
37. Antohe S, Ruxandra V, Ion L (1998) *Balk Phys Lett* 16:290
38. Schauer F, Zhivkov I, Nespurek S (2000) *J Non-Cryst Solids* 266:999
39. Kudo K, Iizuka M, Kuniyoshi S, Tanaka K (2001) *Thin Solid Films* 393:362
40. Gundlach DJ, Kuo CCS, Sheraw CD, Nichols JA, Jackson TN (2001) Organic field effect transistors. In: Fichou D, Bao Z (eds) *Proceedings of the Society of Photo-Optical Instrumentation Engineers (SPIE)* 4466:54–64

41. Hoshino S, Kamata T, Yase K (2002) *J Appl Phys* 92:6028
42. Takada M, Yoshioka H, Tada H, Matsushige K (2002) *Jpn J Appl Phys* 41:L73
43. Xiao K, Liu Y, Yu G, Zhu D (2003) *Appl Phys A* 77:367
44. Xiao K, Liu Y, Yu G, Zhu D (2003) *Synth Met* 137:991
45. Yuan J, Zhang J, Wang J, Yan X, Yan D, Xu W (2003) *Appl Phys Lett* 82:3967
46. Wang J, Yan X, Xu Y, Zhang J, Yan D (2004) *Appl Phys Lett* 85:5424
47. Zhang J, Wang J, Wang H, Yan D (2004) *Appl Phys Lett* 84:142
48. Okuda T, Shintosh S, Terada N (2004) *J Appl Phys* 96:3586
49. Sakai M, Iizuka M, Nakamura M, Kudo K (2004) *Jpn J Appl Phys* 43:2362
50. Kitamura M, Imada, T, Kako S, Arakawa Y (2004) *Jpn J Appl Phys* 43:2326
51. Ofuji M, Ishikawa K, Takezoe H, Inaba K, Omote K (2005) *Appl Phys Lett* 86:062114
52. Xiao K, Liu Y, Guo Y, Yu G, Wan L, Zhu D (2005) *Appl Phys A* 80:1541
53. Wang J, Wang H, Zhang J, Yan X, Yan D (2005) *J Appl Phys* 97:026106
54. Zhang J, Wang H, Yan X, Wang J, Shi J, Yan D (2005) *Adv Mater* 17:1191
55. Puigdollers J, Voz C, Fonrodona M, Cheylan S, Stella M, Andreu J, Vetter M, Alcubilla R (2006) *J Non-Cryst Solids* 352:1778
56. Itoh E, Miyairi K (2006) *Thin Solid Films* 499:95
57. Higuchi T, Murayama T, Itoh E, Miyairi K (2006) *Thin Solid Films* 400:374
58. Jiang W, Du G, Yu S, Wang W, Chang Y, Wang X (2006) *Chin Phys Lett* 23:1939
59. Di C, Yu G, Liu Y, Xu X, Song Y, Wang Y, Sun Y, Zhu D, Liu H, Liu X, Wu D (2006) *Appl Phys Lett* 88:121907
60. Minagawa M, Shinbo K, Usuda K, Iwasaki M, Kato K, Kaneko F (2006) *Jpn J Appl Phys* 45:L99
61. Minagawa M, Shinbo K, Usuda K, Takahashi T, Iwasaki M, Kato K, Kaneko F (2006) *Jpn J Appl Phys* 45:8890
62. Ikeda S, Yamakawa H, Kiguchi M, Nakayama M, Saiki K, Shimada T, Miyadera T, Tsutsui K, Wada Y (2006) *Mol Cryst Liq Cryst* 455:347
63. Yan X, Wang H, Yan D (2006) *Thin Solid Films* 515:2655
64. Bai Y, Liu X, Chen L, Khizar-ul-Haq, Khan M, Zhu WQ, Jiang XY, Zhang ZL (2007) *Microelectron J* 38:1185
65. Videlot-Ackermann C, Ackermann J, Fages F (2007) *Synth Met* 157:551
66. Gao J, Xu JB, Zhu M, Ke N, Ma D (2007) *J Phys D Appl Phys* 40:5666
67. Yu S, Wang X, Cheng C, Zhang D, Ji D, Xia D, Jiang W, Li W, Guan H, Fan Z, He W, Chang Y, Du G (2008) *J Non-Cryst Solids* 354:1516
68. Bao Z, Lovinger AJ, Dodabalapur A (1997) *Adv Mater* 9:42
69. Kudo K, Sumimoto T, Hiraga K, Kuniyoshi S, Tanaka K (1997) *Jpn J Appl Phys* 36:6994
70. Touda H, Tada H, Matsushige K (1999) *Mol Cryst Liq Cryst* 327:287
71. Ohta H, Hambayashi T, Nomura K, Hirano M, Ishikawa K, Takezoe H, Hosono H (2004) *Adv Mater* 16:312
72. Kelting C, Michaelis W, Hirth A, Wöhrlé D, Schlettwein D (2006) *J Porphyr Phthalocyanines* 10:1179
73. Wang H, Song D, Yang J, Yu B, Geng Y, Yan D (2007) *Appl Phys Lett* 90:253510
74. Li L, Tang Q, Li H, Yang X, Hu W, Song Y, Shuai Z, Xu W, Liu Y, Zhu D (2007) *Adv Mater* 19:2613
75. Akazawa T, Takatsuka Y, Ohdaira Y, Shinbo K, Kato K, Kaneko F (2007) *Mol Cryst Liq Cryst* 471:213
76. Zeis R, Siegrist T, Kloc Ch (2005) *Appl Phys Lett* 86:022103
77. Tang Q, Li H, He M, Hu W, Liu C, Chen K, Wang C, Liu Y, Zhu D (2006) *Adv Mater* 18: 65
78. Paloheimo J, Kuivalainen P, Stubb H, Vuorimaa E, Yli-Lahti P (1990) *Appl Phys Lett* 56:1157
79. Hu W, Liu Y, Xu Y, Liu S, Zhou S, Zhu D (1999) *Synth Met* 104:19
80. Hu W, Liu Y, Xu Y, Liu S, Zhou S, Zhu D (1999) *Mol Cryst Liq Cryst* 337:511
81. Liu Y, Hu W, Qiu W, Xu Y, Zhou S, Zhu D (2001) *Sens Actuators B Chem* 80:202
82. Xiao K, Liu Y, Huang X, Xu Y, Yu G, Zhu D (2003) *J Phys Chem B* 107:9226
83. Chen S, Liu Y, Xu Y, Sun Y, Qiu W, Sun X, Zhu D (2006) *Synth Met* 156:1236

84. Nishimura H, Iizuka M, Kuniyoshi S, Nakamura M, Kudo K, Tanaka K (2004) *Electron Commun Jpn* 287:18
85. Donley CL, Zangmeister RAP, Xia W, Minch B, Drager A, Cherian SK, LaRussa L, Kippelen B, Domercq B, Mathine DL, O'Brien DF, Armstrong NR (2004) *J Mater Res* 19:2087
86. Clarisse C, Riou MT, Gauneau M, Le Contellec M (1988) *Electron Lett* 24:674
87. Clarisse C, Riou MT, (1991) *J Appl Phys* 69:3324
88. Su W, Jiang J, Xiao K, Chen Y, Zhao Q, Yu G, Liu Y (2005) *Langmuir* 21:6527
89. Chen Y, Su W, Bai M, Jiang J, Li X, Liu Y, Wang L, Wang S (2005) *J Am Chem Soc* 127:15700
90. Chen Y, Li R, Wang R, Ma P, Dong S, Gao Y, Li X, Jiang J (2007) *Langmuir* 23:12549
91. Li R, Ma P, Dong S, Zhang X, Chen Y, Li X, Jiang J (2007) *Inorg Chem* 46:11397
92. Gao Y, Ma P, Chen Y, Zhang Y, Bian Y, Li X, Jiang J (2009) *Inorg Chem* 48:45
93. Ma P, Chen Y, Sheng N, Bian Y, Jiang J (2009) *Eur J Inorg Chem* 2009:954
94. Schouten PG (1994) Charge carrier dynamics in pulse-irradiated columnar aggregates of mesomorphic porphyrins and phthalocyanines. Delft University of Technology, The Netherlands. ISBN: 90-73861-22-5 (available from Warman JM on request)
95. van de Craats AM, Schouten PG, Warman JM (1998) *EKISHO, J Jpn Liq Cryst Soc* 2/1:12
96. Schouten PG, Warman JM, de Haas MP, Fox MA, Pan HL (1991) *Nature* 353:736
97. Noh YY, Kim JJ, Yoshida Y, Yase K (2003) *Adv Mater* 15:699
98. Noh YY, Kim JJ, Yase K, Nagamatsu S (2003) *Appl Phys Lett* 83:1243
99. Minari T, Seto M, Nemoto T, Isoda S, Tsukagoshi K, Aoyagi Y (2007) *Appl Phys Lett* 91:123501
100. Checcoli P, Conte G, Salvatori S, Paolesse R, Bolognesi A, Berliocchi M, Brunetti F, D'Amico A, Di Carlo A, Lugli P (2003) *Synth Met* 138:261
101. Aramaki S, Sakai Y, Ono N (2004) *Appl Phys Lett* 84:2085
102. Shea PB, Kanicki J, Ono N (2005) *J Appl Phys* 98:014503
103. Shea PB, Johnson AR, Ono N (2005) *IEEE T Electron Dev* 52:1497
104. Shea PB, Chen C, Kanicki J, Pattison LR, Petroff P, Yamada H, Ono N (2007) *Appl Phys Lett* 90:233107
105. Shea PB, Kanicki J, Pattison LR, Petroff P, Kawano M, Yamada H, Ono N (2006) *J Appl Phys* 100:034502
106. Shea PB, Pattison LR, Kawano M, Chen C, Chen J, Petroff P, Martin DC, Yamada H, Ono N, Kanicki J (2007) *Synth Met* 157:190
107. Dhoot AS, Aramaki S, Moses D, Heeger A (2007) *Adv Mater* 19:2914
108. Che CM, Xiang HF, Chui SS-Y, Xu ZX, Roy VAL, Yan JJ, Fu WF, Lai PT, Williams ID (2008) *Chem Asian J* 3:1092
109. Bao Z, Lovinger AJ, Brown J (1998) *J Am Chem Soc* 120:207
110. Tada H, Touda H, Takada M, Matsushige K (1999) *J Porphyr Phthalocyanines* 3:667
111. Qiu Y, Hu Y, Dong G, Wang L, Gao Y (2002) *Chin Sci Bull* 47:1529
112. Yuan J, Zhang J, Wang J, Yan D, Xu W (2004) *Thin Solid Films* 450:316
113. Yoon M-H, Yan H, Facchetti A, Marks TJ (2005) *J Am Chem Soc* 127:10388
114. Ling M-M, Bao Z (2006) *Org Electron* 7:568
115. Yan X, Wang J, Wang H, Wang He, Yan D (2006) *Appl Phys Lett* 89:053510
116. Oh Y, Pyo S, Yi MH, Kwon SK (2006) *Org Electron* 7:77
117. Ye R, Baba M, Ohishi Y, Mori K, Suzuki K (2006) *Mol Cryst Liq Cryst* 444:203
118. Song D, Wang H, Zhu F, Yang J, Tian H, Geng Y, Yan D (2008) *Adv Mater* 20:2142
119. Song D, Zhu F, Yu B, Huang L, Geng Y, Yan D (2008) *Appl Phys Lett* 92:143303
120. Schon JH, Kloc C, Bao Z, Batlogg B (2000) *Adv Mater* 12:1539
121. Tang Q, Li H, Liu Y, Hu W (2006) *J Am Chem Soc* 128:14634
122. Madru M, Guillaud G, Al Sadoun M, Maitrot M, Clarisse C, Le Contellec M, André JJ, Simon J (1987) *Chem Phys Lett* 142:103
123. Madru R, Guillaud G, Al Sadoun M, Maitrot M, André JJ, Simon J, Even R (1988) *Chem Phys Lett* 145:343
124. Tada H, Touda H, Takada M, Matsushige K (2000) *Appl Phys Lett* 76:873
125. Mizuno E, Taniguchi M, Kawai T (2005) *Appl Phys Lett* 86:143513

126. Yasuda T, Tsutsui T (2005) *Chem Phys Lett* 402:395
127. de Boer RWI, Stassen AF, Craciun MF, Mulder CL, Molinari A, Rogge S, Morpurgo AF (2005) *Appl Phys Lett* 86:262109
128. Yasuda T, Tsutsui T (2006) *Jpn J Appl Phys* 45:L595
129. Lochlin J, Shinbo K, Onishi K, Kaneko F, Bao Z, Advincula RC (2003) *Chem Mater* 15:1404
130. Babel A, Wind JD, Jenekhe SA (2004) *Adv Funct Mater* 14:891
131. Wang J, Wang H, Yan X, Huang H, Yan D (2005) *Appl Phys Lett* 87:093507
132. Wang J, Wang H, Yan X, Huang H, Yan D (2005) *Chem Phys Lett* 407:87
133. Ye R, Baba M, Oishi Y, Mori K, Suzuki K (2005) *Appl Phys Lett* 86:253505
134. Ye R, Baba M, Mori K (2005) *Jpn J Appl Phys* 44:L581
135. Wang J, Wang H, Yan X, Huang H, Jin D, Shi J, Tang Y, Yan D (2006) *Adv Funct Mater* 16:824
136. Wang H, Wang J, Huang H, Yan X, Yan D (2006) *Org Electron* 7:369
137. Wang H, Wang J, Yan X, Shi J, Tian H, Geng Y, Yan D (2006) *Appl Phys Lett* 88:133508
138. Opitz A, Bronner M, Brütting W (2007) *J Appl Phys* 101:063709
139. Ye R, Baba M, Suzuki K, Mori K (2007) *Jpn J Appl Phys* 46:2878
140. Ye R, Baba M, Suzuki K, Mori K (2008) *Solid State Electron* 52:60

# Index

- Absorption spectral properties 51  
Adlayers 25  
    phthalocyanine/porphyrin 147  
Aggregation 62  
Anthracenocyanine (Ac) 46  
Anthraquinone 11  
Axial coordination 169  
Axial ligand coordination, self-assembly of porphyrins 156
- Ball-type Pcs 105  
Benzobis(1,3-diimino pyrroline) 100  
Benzodiguanamine (BDG) 140  
Benzohelicenocyanine (BHc) 46  
Bimolecular arrays, controlled 147  
Bis(phthalocyaninato) rare earth double-decker semiconductors 297  
Bis(phthalocyaninato)dysprosium anions 218  
Bis(phthalocyaninato)lanthanide anions 219  
    quantum tunneling of magnetization 221  
Bis(phthalocyaninato)terbium(III) 27, 218  
Bis(phthalocyanine) 6  
Bisphthalocyaninates, rare-earth 110  
Bisphthalonitrile 114  
5-Bromo-2,2'-bipyridine 7  
Bulk heterojunction (BHJ) solar cell 34  
*tert*-Butylphthalonitrile 5
- Calix[4]arene 108  
Carbon nanohorns (CNHs) 265  
Carbon nanotubes (CNTs) 14  
    precursors, phthalocyanine 30  
    supramolecular interactions 31  
Carotenoids 268  
Central metal 63  
Chemosensors 105  
Chlorophylls 266  
Chromium(II) phthalocyanine 215
- Clathrates, phthalocyanines, nanostructuration 31  
Cobalt(II) coordinated “picket-fence” porphyrin (CoTpivPP) 144  
Cobalt(II) hexadecafluoro-phthalocyanine 147  
Cobalt(II) octaethylporphyrin (CoOEP) 144  
Cobalt(II) phthalocyanine 216  
Cobalt(II) tetraphenylporphyrin (CoTPP) 144, 173  
Conjugated systems/assemblies 3  
Connection on surface, direct 154  
Copper(II) phthalocyanine 216  
CuPc wire-like nanostructures 29  
Cyclic voltammetry 105
- Dendrimers 20–24  
4,9-Diaminoperylenequinone-3,10-diimine (DPDI) 152  
Diaza[2.2.2]bicyclooctane (DABCO) 157  
(3,5-Di-*t*-butylphenyl)porphyrin (TBPP) 146  
1,2-Dicyano-bis(trimethyl-3-thiophenyl) ethane 100  
Diiminoisoindoline 4  
Dipyridyldiphenylporphyrinate zinc(II) 157  
Dithienylethenes 89  
    bridged porphyrins 90  
Dithiophenes-fused phthalocyanines, photochromic 97  
Dodecaphenylporphyrin 19  
Donor–acceptor bis(phthalocyanine) 201  
Double-decker complexes 159  
Dye-sensitized solar cells (DSSCs) 35
- Electrocatalysis 45  
Electrocatalytic behavior 75  
Electrocatalytic detection, analytes 78  
Electrochemical interface, single-component adlayers 143

- Electrochemistry 45, 65  
Electrode modification 78  
Electronic absorption spectra 45  
Electronic structure 211  
Ethynyltri-*tert*-butylphthalocyaninatozinc(II) 7
- Ferromagnets 211  
Field effect transistors (FETs) 275  
Fullerenes 4, 8, 94, 149  
Fulleropyrrolidine–Pc conjugate 13  
Functional materials/devices 32, 89
- Gas-sensing properties, ball-type Pcs 130
- Helicenocyanine (Hc) 46  
Highly oriented pyrolytic graphite (HOPG) 27, 142  
Host–guest complexes 169  
Hydrogen-bonding architectures 145
- Iodophthalocyanines 200  
4-Iodophthalonitrile 6  
Ionic self-assembly 16  
Iron(II) phthalocyanine 214  
Isopropylidendioxydiphenyl 114
- Langmuir–Blodgett (LB) technique 32  
Light-emitting devices (LEDs) 33  
Lithium phthalocyanine,  $\pi$ -radical 216  
Lu(Pc)<sub>2</sub> 110, 293
- Macromolecular structures 1  
Manganese(II) phthalocyanine 213  
Mass spectroscopy 105  
Metal phthalocyanines 5  
    magnetism 212, 217  
Metallation on surface, direct 152  
Metallo-uroporphyrins 265  
Mn<sub>III</sub>Pc complexes 67  
Molecular assembly, two-dimensional 139  
Monomeric complexes 156  
Multicomponent assemblies 1  
Multi-walled CNTs (MWCNTs) 30
- Nanoapplications 160  
Nanoparticles, phthalocyanine-based 28  
Nanostructuring 1
- Nanostructures, direct formation on surface 152  
    phthalocyanine-based 24  
Nanowires, phthalocyanine-based 28  
Naphthalene tetracarboxylic diimide (NTCDI) 140  
Naphthalocyanines 46  
Nickel naphthalocyanine 28  
Nickel(II) phthalocyanine 17, 216  
4-Nitrophthalonitrile 5  
Nonlinear optics (NLO) 47, 105  
    ball-type Pcs 126
- Octaphenyl Zn(II) phthalocyaninate 19  
Oligo(phenyleneethynylene) spacer 10  
Optical information recording media 33  
Organic field effect transistors (OFETs) 32, 278  
    performance characterization 281  
Organic light emitting devices (OLEDs) 33  
Organic semiconductors 275  
Organic vapor-phase deposition (OVPD) 29  
Oxo-vanadium(IV) phthalocyanine 216
- Pentaerythritol 112  
Perylene tetra-carboxylic di-imide (PTCDI) 152  
Perylenes 4  
Phenathralocyanine (Pa) 46  
Phenyl-C-butyric acid methyl ester (PCBM) 34  
Pheophorbids 266  
Pheophytin 268  
Photochromism 89  
Photocurrents 229  
Phthalocyanine adlayers 25  
Phthalocyanine aggregates, hydrogen-bonded 193  
Phthalocyanine dimers, self-coordinated 186  
Phthalocyanine semiconductors 282  
    ambipolar 311  
    monomeric 285  
    n-type 307  
    p-type 285  
Phthalocyanine–fullerene hetero-arrays 177  
    hydrogen-bonded 190  
Phthalocyanine–oligothiophene hetero-arrays 184  
Phthalocyanine–perylene diimide hetero-arrays 182  
Phthalocyanine–polypyridyl ruthenium(II) hetero-arrays 184  
Phthalocyanine–porphyrin hetero-arrays 171



- Phthalocyanine–squinone hetero-array 185  
Phthalocyanine–subphthalocyanine hetero-arrays 177  
Phthalocyanines 1ff  
  anchoring groups, axial direction 240  
  peripheral positions 231  
  without 244  
  ball-type 105  
  functional 1  
  monofunctionalized 3  
  self-organization 27  
  sensitizers 231  
  supramolecular organization 14  
   $\pi$ -radical 216  
    double-decker 217  
Phthalonitriles 50  
Poly(3-hexylthiophene) (P3HT) 34  
Polymers, phthalocyanine-based 20  
Polynorborene, fullerene-containing 23  
Polysiloxane Pc polymer 21  
Polythiophenes 22  
Porphyrin arrays 259  
Porphyrin semiconductors, monomeric 300  
Porphyrin–Ru(II) phthalocyanine 20  
Porphyrins 229, 275  
  dithienylethene-bridged 90  
  monomers 246  
  sensitizers 245, 265  
Porphyrins/fullerene supramolecular assembly 149  
Pyridyl subphthalocyanines 177
- Q band 51  
Quantum confined effects 26
- Rare-earth bisphthalocyaninates 110  
Ring expansion 52  
Ring substitution 56  
Ru(II) phthalocyaninate 19
- Sandwich semiconductors 297  
Self-assembled monolayer (SAM) 75  
Self-assembly 169  
  ionic 16  
Self-organization 27  
Semiconductors, sandwich 297  
Sensitizers 229
- Sensors 33  
Silicon(IV) phthalocyanine 203  
Single-molecule magnets (SMM) 27, 211  
Single-walled carbon nanotubes (SWNTs) 13  
Solar cells 34, 229  
Solution-processable techniques 27  
Subphthalocyanines 177  
  Kobayashi ring opening 5  
Supramolecular arrays, axial coordination 171  
  donor–acceptor interactions 200  
  electrostatic interactions 198  
  host–guest interactions 203  
  hydrogen bonding 190  
Supramolecular chemistry 169  
Supramolecular organization 1  
Surfaces 27  
Synthesis 105
- Tetraazaporphyrin 98  
Tetrakis(3,5-di-*tert*-butylphenyl)porphyrin (CoTBPP) 139, 173  
Tetramesitylporphyrin 154  
Tetra(perylene*di*imide)phthalocyanine 17  
Tetrapyrrole 275  
Tetrathiafulvalene 15  
Titanylphthalocyanine (TiOPc) 73, 141  
Tribenzotetraazachlorin 206  
Triple-decker complexes 159  
Tris(10-carboxydecyloxy) benzene (TCDB) 148  
Tris(phthalocyaninato) rare earth triple-decker semiconductors 298  
Tris(phthalocyaninato)bislanthanide 224  
Tris-Pc-benzene 11
- UHV, single-component adlayers 139
- VPc complexes 73
- Zn(II) 5,15-bis(3-cyanophenyl)-10,20-bis[3,5-di(*tert*-butyl)phenyl] porphyrin 160  
Zn(II) tetra(perylene*di*imide)Pc 15  
ZnOEP 153  
ZnPc–fullerene 18